Larry A. Viehland

Gaseous Ion Mobility, Diffusion, and Reaction



Springer Series on Atomic, Optical, and Plasma Physics

Volume 105

Editor-in-chief

Gordon W. F. Drake, Department of Physics, University of Windsor, Windsor, ON, Canada

Series editors

James Babb, Harvard-Smithsonian Center for Astrophysics, Cambridge, MA, USA Andre D. Bandrauk, Faculté des Sciences, Université de Sherbrooke, Sherbrooke, QC, Canada

Klaus Bartschat, Department of Physics and Astronomy, Drake University, Des Moines, IA, USA

Philip George Burke, School of Mathematics and Physics, Queen's University, Belfast, UK

Robert N. Compton, Knoxville, TN, USA

Tom Gallagher, University of Virginia, Charlottesville, VA, USA

Charles J. Joachain, Faculty of Science, Université Libre Bruxelles, Bruxelles, Belgium

Michael Keidar, School of Engineering and Applied Science, George Washington University, Washington, DC, USA

Peter Lambropoulos, FORTH, IESL, University of Crete, Iraklion, Crete, Greece Gerd Leuchs, Institut für Theoretische Physik I, Universität Erlangen-Nürnberg, Erlangen, Germany

Pierre Meystre, Optical Sciences Center, University of Arizona, Tucson, AZ, USA

The Springer Series on Atomic, Optical, and Plasma Physics covers in a comprehensive manner theory and experiment in the entire field of atoms and molecules and their interaction with electromagnetic radiation. Books in the series provide a rich source of new ideas and techniques with wide applications in fields such as chemistry, materials science, astrophysics, surface science, plasma technology, advanced optics, aeronomy, and engineering. Laser physics is a particular connecting theme that has provided much of the continuing impetus for new developments in the field, such as quantum computation and Bose-Einstein condensation. The purpose of the series is to cover the gap between standard undergraduate textbooks and the research literature with emphasis on the fundamental ideas, methods, techniques, and results in the field.

More information about this series at http://www.springer.com/series/411

Gaseous Ion Mobility, Diffusion, and Reaction



Larry A. Viehland Science Department Chatham University Pittsburgh, PA, USA

ISSN 1615-5653 ISSN 2197-6791 (electronic) Springer Series on Atomic, Optical, and Plasma Physics ISBN 978-3-030-04493-0 ISBN 978-3-030-04494-7 (eBook) https://doi.org/10.1007/978-3-030-04494-7

Library of Congress Control Number: 2018962124

© Springer Nature Switzerland AG 2018

This work is subject to copyright. All rights are reserved by the Publisher, whether the whole or part of the material is concerned, specifically the rights of translation, reprinting, reuse of illustrations, recitation, broadcasting, reproduction on microfilms or in any other physical way, and transmission or information storage and retrieval, electronic adaptation, computer software, or by similar or dissimilar methodology now known or hereafter developed.

The use of general descriptive names, registered names, trademarks, service marks, etc. in this publication does not imply, even in the absence of a specific statement, that such names are exempt from the relevant protective laws and regulations and therefore free for general use.

The publisher, the authors and the editors are safe to assume that the advice and information in this book are believed to be true and accurate at the date of publication. Neither the publisher nor the authors or the editors give a warranty, express or implied, with respect to the material contained herein or for any errors or omissions that may have been made. The publisher remains neutral with regard to jurisdictional claims in published maps and institutional affiliations.

This Springer imprint is published by the registered company Springer Nature Switzerland AG The registered company address is: Gewerbestrasse 11, 6330 Cham, Switzerland

Acknowledgements

It is a pleasure to acknowledge the major contributions of Rainer Johnsen (Chaps. 1, 2, and 7), William F. Siems (Chap. 3), Timothy G. Wright (Chap. 6), Alexei A. Buchachenko (Chap. 6), and Claudia K. Viehland (figures and photos). Contributions that are of smaller extent but perhaps equal significance were made by Douglas E. Goeringer and Robert E. Robson. This book is devoted to all of these people and to the memory of Isadore Amdur, Charles F. Curtiss, Edward A. Mason, and Earl W. McDaniel.

Notation and Abbreviations

$\mathbf{a}(\mathbf{r},t)$	Acceleration vector as a function of \mathbf{r} and t , Sect. 4.1
$a^{(1,t)}$ $a^{(2T)}_{r,s}$	
	2T Matrix elements of \mathfrak{J}_j for one gas in a mixture, Sect. 5.6
$a_j^{(MT)}(\cdots)$	MT Matrix elements of \mathfrak{J}_i for one gas in a mixture, Sect. 5.7
a_0	Atomic unit of distance, the bohr, Sect. 6.3
A	Vector potential in Maxwell's equations, Sect. 6.16
$\overline{\mathbf{A}}$	Vector representation of area, Sect. 1.9
$A^{''}$	Constant used to extract $\overline{\Omega}^{(1,1)}$ from mobility data, Sect. 2.8.4
aug-cc	cc basis set augmented to include diffuse functions,
	Sect. 6.11.1
b	Impact parameter of a collision, Sect. 1.11
b_1	Ions in a pulse entering the drift tube, Sect. 2.4
$b_{r,s}^{(2T)}$	2T Matrix elements of \mathfrak{J}_j for one gas or a mixture, Sect. 5.6
$b^{(MT)}(\ldots)$	MT Matrix elements of \mathfrak{J}_j for one gas or a mixture, Sect. 5.7
B	Magnetic field strength, Sect. 2.11
В	Magnetic field vector, Sect. 1.15
B(km; pqst)	Basis functions of a 2T treatment of molecules, Sect. 8.7
BMM	Beyond Monchick–Mason approximation, Sect. 8.10
BSSE	Basis set superposition error, Sect. 6.11.3
c	Speed of light in a vacuum, Sect. 6.16
\overline{c}	Constant term in various equations
$c_{l,m,r}$	Expansion coefficient for $f(\mathbf{r}, \mathbf{v}, t)$, Sect. 5.4
c_2, c_4	Correction terms in Eq. (1.9), Sect. 1.8
C_3	Coefficient of r^{-3} in long-range potential, Sect. 8.11
C_4	Coefficient of r^{-4} in long-range potential, Sect. 6.22
\widehat{C}_4	Value of C_4 in atomic units, Sect. 6.22
C_6	Coefficient of r^{-6} in long-range potential, Sect. 9.1
C_n	Coefficient of r^{-n} in short-range potential, Sect. 9.1.3
cc	Family of correlation consistent basis functions, Sect. 6.11.1
сс-р	cc basis set with polarized orbitals
	*

cc-pC.. cc basis set with polarized core orbitals, Sect. 6.11.1 cc basis set with polarized, weighted core orbitals, Sect. 6.11.1 cc-pwC.. CAS Complete active space, Sect. 6.13 **CASSCF** Complete active space SCF method, Sect. 6.13 Complete basis set, Sect. 6.11.1 **CBS** CC Coupled-cluster method, Sect. 6.12.1 CI Configuration interaction, Sect. 6.12.1 CP Counterpoise correction, Sect. 6.11.3 d Rigid sphere diameter, Sect. 1.11 Dimensionless ratio in $f_{rel}(\mathbf{g})$, Sect. 7.2 d_L Dimensionless ratio in $f_{rel}(\mathbf{g})$, Sect. 7.2 d_T D Ion diffusion coefficient (a scalar), Sect. 1.9 D Ion diffusion tensor, Sect. 1.9 D_L Ion diffusion coefficient along E or B, Sect. 1.9 Hall component of **D**, Sect. 1.15 D_H D_T Ion diffusion coefficient perpendicular to E, Sect. 1.9 D_r Same as D_T , Sect. 6.23 D_7 Same as D_L , Sect. 6.23 D_{\parallel} Same as D_L , Sect. 1.15 D_{\perp} Same as D_T , Sect. 1.15 cc.. basis set doubly augmented with diffuse functions, d-aug-cc.. Sect. 6.11.1 D Doubles in a CI calculation, Sect. 6.10 Differential IMS, Sect. 2.8.4 **DMS DTMS** Drift-tube mass spectrometer, Sect. 2.2 Fundamental charge, Sect. 2.8.2 e E Electric field strength, Sect. 1.1 \overline{E} Average excess energy in a ping-pong experiment, Sect. 2.9.1 \tilde{E} Time-independent total energy, Sect. 6.3 \mathbf{E} Electric field vector, Sect. 1.8 E_{h} Atomic unit of energy, the hartree, Sect. 6.3 $E_{\rm ion}$ Ion kinetic energy in swarm frame, Sect. 4.5 $E_{\mathbf{k}}$ Ion kinetic energy in laboratory frame, Sect. 4.5 E_n Energy of nth state in perturbation theory, Sect. 6.18 $E_{\mathfrak{p}}$ Electrical potential energy, Sect. 1.3 Total energy, Sect. 6.3 E_{tot} $E^{(0)}$ Energy for a simpler problem in perturbation theory, Sect. 6.18 Energy dyadic in laboratory frame, Sect. 4.5 ÊÊ E/n_0 Reduced field strength, Sect. 1.1 **ECP** Effective core potential, Sect. 6.4.6 Ion distribution function of many variables, Sect. 8.1 f f_c Fraction of collisions that cool an ion, Sect. 3.5.2 Fraction of collisions that heat an ion, Sect. 3.5.2 f_h Ion speed distribution function, Sect. 1.8 f(v)

Notation and Abbreviations

$f(\mathbf{v})$	Ion velocity distribution function, Sect. 5.1
	·
$f(\mathbf{r}, \mathbf{v}, t)$	Ion distribution as a function of \mathbf{r} , \mathbf{v} and t , Sect. 4.1
$f^{(2T)}(km;.)$	Expansion coefficient for f of molecular ions, Sect. 8.7
$f_0(\mathbf{v})$	Zero-order ion velocity distribution function, Sect. 5.4
$f_0^{(1T)}(\mathbf{v})$	Zero-order ion vdf in 1T theory, Sect. 5.5
$f_0^{(2T)}(\mathbf{v}) \ f_0^{(MT)}(\mathbf{v})$	Zero-order ion vdf in 2T theory, Sect. 5.6
$f_0^{(MT)}(\mathbf{v})$	Zero-order ion vdf in MT theory, Sect. 5.7
$f_{GC}(\mathbf{v})$	Gram-Charlier ion vdf, Sect. 7.2
$f_j(\mathbf{v}_j)$	Velocity distribution function of neutral <i>j</i> , Sect. 5.2
$f_R(\mathbf{v}_R)$	Velocity distribution function of reactive neutral R, Sect. 7.1
$f_j(\mathbf{r},\mathbf{v}_j,t)$	Distribution as a function of \mathbf{r} , \mathbf{v}_i and t of neutral j , Sect. 4.2
$f_{rel}(\mathbf{g})$	Relative vdf for an ion–reactive neutral pair, Sect. 7.2
$f_R^{(eta_R)}(\mathbf{v}_R)$	Vdf of reactive R in state β_R as a function of \mathbf{v}_R , Sect. 3.4.3
$f_R(\mathbf{r}, \mathbf{v}_R, t)$	Distribution of reactive R as a function of \mathbf{r} , \mathbf{v}_R and t , Sect. 4.3
F	Electrical force, Sect. 1.3
\mathfrak{F}	Functional operator, Sect. 5.2
$F(\mathbf{r},t)$	External force as a function of \mathbf{r} and t , Sect. 4.1
F_{\parallel}	Full width at half height, Sect. 2.4
FAIMS	Field-asymmetric ion mobility spectrometer, Sect. 2.9
	Relative speed before collision, Sect. 3.2
$g \\ g'$	Relative speed after collision, Sect. 3.2 Relative speed after collision, Sect. 3.3
	-
g	Relative velocity before collision, Sect. 3.3
$egin{array}{c} \mathbf{g}' \ \mathbf{G} \end{array}$	Relative velocity after collision, Sect. 3.4
\mathbf{G}'	Center of mass velocity before collision, Sect. 3.3
	Center-of-mass velocity after collision, Sect. 3.3
GC	Gram-Charlier, Sect. 5.9
GER	Generalized Einstein Relation, Sect. 1.19
h	Planck's constant, Sect. 6.3
H	Hamiltonian operator, Sect. 6.3
H'	Difference operator in perturbation theory, Sect. 6.18
$H^{(0)}$	H for a simpler problem in perturbation theory, Sect. 6.18
$H_{ m int}$	Internal Hamiltonian for molecules, Sect. 8.1
$H_p(x)$	Hermite polynomial of order p for variable x , Sect. 5.7
HF	Hartree–Fock method, Sect. 6.8
HPCCS	High Performance Collision Cross Section, Sect. 9.7
i	Base of the imaginary numbers, $\sqrt{-1}$, Sect. 6.3
I	Electric current (in Ch. 1 only), Sect. 1.4
I	Moment of inertia of a molecular ion, Sect. 8.7
I_{j}	Moment of inertia of a molecule of type j , Sect. 8.5
ICR	Ion cyclotron resonance, Sect. 2.12
IMS	Ion mobility spectrometer, Sect. 2.7
IMS/MS	IMS with a mass spectrometer 2.8
IMoS	Computer program for mobility simulation, Sect. 9.7

IOS	Infinite-order sudden approximation, Sect. 8.10
ITSIM	Computer program for ion trap simulation, Sect. 2.13
j	Ion (or current density) flux vector, Sect. 1.9
j	Index labeling non-reactive gases, Sect. 1.8
J	Pre-collision ion angular momentum vector, Sect. 8.5
$\mathbf{J}^{'}$	Post-collision ion angular momentum vector, Sect. 8.5
\mathbf{J}_{j}	Pre-collision angular momentum vector of j , Sect. 8.5
$\mathbf{J}_{j}^{'}$	Post-collision ion angular momentum vector, Sect. 8.5
\mathbf{J}_0	Angular momentum of a pure neutral gas, Sect. 8.8
\mathbf{J}_R	Pre-collision angular momentum vector of <i>R</i> , Sect. 8.5
	Boltzmann collision operator for neutral j , Sect. 4.2
<i>₹</i> ,	Collision operator for reactive neutral <i>R</i> , Sect. 4.3
k	Reaction rate coefficient, Sect. 1.9
\mathfrak{I}_{j} \mathfrak{I}_{R} k \widetilde{k}	Parameter in $V(r)$, Sect. 6.15.3
$k \choose k(\mathbf{r},t)$	Reaction rate coefficient as a function of \mathbf{r} and t , Sect. 4.8
k_{B}	Boltzmann's constant, Sect. 1.9
K	Ion mobility (a scalar), Sect. 1.8
K	Ion mobility (a tensor), Sect. 1.15
$K^{'}$	Logarithmic derivative of K, Sect. 1.19
$K_{ m H}$	Hall component of K , Sect. 1.15
K_L	Ion mobility along a magnetic field, Sect. 1.15
K_0	Standard ion mobility (a scalar), Sect. 1.8
$K_{0,n}$	Nominal value of K_0 , Sect. 2.2.5
K_T	Ion mobility perpendicular to magnetic field, Sect. 1.15
$KE_{\rm cm}$	Kinetic energy in the center-of-mass frame, Sect. 7.3
L	Length of apparatus, Sect. 1.1
\mathbf{L}_0	Relative angular momentum, Sect. 8.8
$L_r^{(l+1/2)}$	Associated Laguerre polynomial, Sect. 5.5
LCAO	Linear combination of atomic orbitals, Sect. 6.7
LDA	Local density approximation, Sect. 6.2
m	Ion mass, Sect. 1.7
\widehat{m}	Ion mass fraction, Sect. 2.7.1
m_j	Mass of neutral j in a mixture, Sect. 5.2
m_0	Neutral mass, Sect. 2.6.1
m_1	Mass of neutral isotope 1, Sect. 2.6.1
m_2	Mass of neutral isotope 2, Sect. 2.6.1
m_R	Mass of reactive neutral R, Sect. 5.2
\widehat{m}_0	Neutral mass fraction, Sect. 2.7.1
M	Molar mass of ion, Sect. 1.13
M_R	Molar mass of reactive neutral gas R, Sect. 1.17
$\frac{M_0}{M}$	Molar mass of neutral gas molecules, Sect. 1.1
\overline{M}	Weighted average of neutral masses, Sect. 2.6.3
MBPT	Many-body perturbation theory, Sect. 6.12.1

MC	Monte Carlo calculation, Sect. 9.4
MCA	Multichannel analyzer, Sect. 2.2.1
MCSCF	Multiconfiguration SCF, Sect. 6.13
MET	Many-electron theory, Sect. 6.20
MMA	Monchick–Mason approximation, Sect. 8.10
MOBCAL	Computer program for mobility calculations, Sect. 9.7
MOBDIF	Computer program for mobility & diffusion, Sect. 6.22.3
MP	Moller–Plesset theory, Sect. 6.19
MP2	Second-order Moller–Plesset theory, Sect. 6.19
MRCI	Multi-reference CI, Sect. 6.14
MS	Mass spectrometer
n	Ion number density, Sect. 1.1
$n(\mathbf{r},t)$	Ion number density as a function of \mathbf{r} and t , Sect. 4.1
n_j	Number density of gas j in a mixture, Sect. 3.2
n_0	Gas number density, Sect. 1.1
n_R	Number density of reactive gas R, Sect. 4.2
N_G	Normalization factor for Gaussian orbital, Sect. 6.4.1
N_0	Loschmidt's constant, Sect. 1.8
N_S	Normalization factor for Schrodinger orbital, Sect. 6.4.1
$N_{l,m,r}$	Normalization factor for $\Psi_{l,m,r}(\mathbf{v})$, Sect. 5.4
$N_{l,m,r}^{(2T)}$	Normalization factor for $\Psi_{l,m,r}^{(2T)}(\mathbf{v})$, Sect. 5.4
NTE	Nernst–Townsend–Einstein equation, Sect. 1.9
OMEGA	Computer program for collision integrals, Sect. 9.1.3
p	Linear momentum vector, Sect. 6.3
$\stackrel{\leftrightarrow}{\mathbf{p}}$	Four-vector version of p , Sect. 6.17.1
p_j	Component of p along Cartesian axis j, Sect. 6.3
$P_l^{(m)}$	Associated Legendre polynomial, Sect. 5.5
P_0^{ι}	Gas pressure, Sect. 1.1
\widehat{P}_0	Gas pressure in torr, Sect. 4.7
$P_{0,n}$	Nominal gas pressure, Sect. 2.2.9
PC PC	Computer program for cross sections, Sect. 5.9
PES	Potential energy surface, Sect. 6.15.1
PUHF	Projected UHF method, Sect. 6.12.3
q	Ion charge, Sect. 1.1
Q	Molar ion charge, Sect. 1.9
Q	Skewness tensor of order three, Sect. 2.4
\mathbf{Q}_{H}	Heat flux vector in laboratory frame, Sect. 4.5
\mathbf{Q}_{ion}	Heat flux vector in swarm frame, Sect. 4.5
$Q_{ m RCT}$	Cross section of resonant charge transfer, Sect. 6.22.3
Q_R^*	Ion reactive cross section with reactive gas R , Sect. 1.17
Q_R^* $\overline{Q}^{(l)}$ $\overline{Q}^{(l)}_{\mathrm{eff}}$	Normalized transport cross section, Sect. 1.11
$\overline{Q}_{ m eff}^{(l)}$	Effective $\overline{Q}^{(l)}$ for molecular systems, Sect. 8.11
Qex	Computer program for charge exchange, Sect. 6.22.3
	-

QED	Quantum electrodynamics, Sect. 6.17.1
r	Separation (a scalar), Sect. 1.3
r	Separation vector, Sect. 1.9
$\overset{\leftrightarrow}{\mathbf{r}}$	Four-vector version of r , Sect. 6.17.1
\widetilde{r}	True minimum of $V(r)$, Sect. 6.15.3
$\mathbf{r}^{(n)}$	Separation vector in space for n electrons, Sect. 6.3
r_A	Separation above which there are no interactions, Sect. 4.2
r_o	Turning point in a collision, Sect. 1.11
r_1	Radius of entrance hole into drift tube, Sect. 2.4
r_2	Radius of exit hole from drift tube, Sect. 2.4
R	Molar gas constant, Sect. 1.9
$ ilde{R}$	Radius of a circular loop, Sect. 6.16
R	Index labeling a reactive neutral, Sect. 1.17
R_t	Resolving power, Sect. 2.5
RASSCF	Restricted active space SCF method, Sect. 6.13
RCC	Restricted coupled-cluster method, Sect. 6.20
RCT	Resonant charge transfer, Sect. 6.22.3
RHF	Restricted Hartree–Fock method, Sect. 6.12.1
S	Total spin quantum number, Sect. 6.12.1
S	Spin angular momentum operator, Sect. 6.6
$S_{l+1/2}^{(r)}$	Sonine polynomial, Sect. 5.5
S	Singles in a CI or CC calculation, Sect. 6.10
SD	S plus doubles, Sect. 6.10
SDT	SD plus triples, Sect. 6.10
SD(T)	SD plus non-perturbative triples, Sect. 6.10
SDTQ	SDT plus quadruples, Sect. 6.10
t	Time, Sect. 1.1
$t^{'}$	Time needed to reverse an electrostatic field, Sect. 2.9.1
t_d	Time to move from shutter to mass spectrometer, Sect. 2.3.1
$\langle t \rangle$	Average time in drift region, Sect. 1.8
$\langle t \rangle_n$	Nominal average time in drift region, Sect. 2.2.9
T	Ion temperature (a scalar), Sect. 1.13
T	Ion temperature tensor in laboratory frame, Sect. 4.5
T_x, T_y, T_z	Ion temperatures along x, y, and z, Sect. 5.7
T_L	Ion temperature along the field, Sect. 1.19
T_T	Ion temperature perpendicular to the field, Sect. 1.19
$T_{\mathrm{eff},L}$	Effective temperature along the field, Sect. 7.2
$T_{\mathrm{eff},T}$	Effective perpendicular temperature, Sect. 7.2
$T_{ m int}$	Internal ion temperature of molecules, Sect. 1.20
$\mathbf{T}_{\mathrm{ion}}$	Ion temperature tensor in swarm frame, Sect. 4.5
T_0	Gas temperature, Sect. 1.1
\widehat{T}_0	Gas temperature in kelvin, Sect. 4.7
$T_{0,n}$	Nominal gas temperature, Sect. 2.2.9

$T_{ m eff}$	Effective temperature of collisions, Sect. 1.13
$T_{\rm kin}$	Kinetic ion temperature for molecular ions, Sect. 8.7
T_R	Ion–reactive neutral effective temperature, Sect. 1.17
TM	Trajectory model in MOBCAL, Sect. 9.7
TRAJECK	Computer program for classical trajectories, Sect. 8.9
UHF	Unrestricted Hartree–Fock, Sect. 6.12.3
v	Ion speed (a scalar), Sect. 1.8
V	Ion velocity (a vector), Sect. 1.14
$v_{ m d}$	Ion drift speed (a scalar), Sect. 1.8
\mathbf{v}_{d}	Ion drift velocity (a vector), Sect. 1.8
v_i	Ion speed along axis i (a scalar), Sect. 3.2
v_{j}	Molecular speed of neutral gas j in a mixture, Sect. 4.2
\mathbf{v}_j	Velocity vector of neutral gas j in a mixture, Sect. 4.2
v_0	Neutral speed (a scalar), Sect. 3.3
\mathbf{v}_0	Neutral velocity vector, Sect. 3.3
\mathbf{v}_R	Velocity vector of reactive neutral R, Sect. 7.1
$\mathbf{v}_{R,i}$	Component of \mathbf{v}_R along axis i , Sect. 7.2
$\langle \mathbf{v} \rangle$	Average ion velocity vector, Sect. 1.9
$\langle v \rangle$	Average ion speed before collision, Sect. 3.5.1
$\langle v^{'} angle$	Average ion speed after collision, Sect. 3.5.1
\overline{v}_d	Average ion drift speed in a ping-pong expt., Sect. 2.9.1
$\overline{\mathbf{v}}_d$	Average ion drift velocity (a vector), Sect. 2.8.1
v_r	Ion speed in the radial direction, Sect. 7.2
v_z	Ion speed along the field, Sect. 3.2
$v_{ m eff}$	Effective thermal speed, Sect. 3.4.2
$v_{ m dis}$	Displacement of the ion velocity along E, Sect. 5.7
v_{th}	Thermal Speed, Sect. 2.7.1
V(r)	Interaction potential energy as a function of r, Sect. 1.11
$V(\mathbf{r})$	V as a function of r , per unit charge, Sect. 6.3
$V(\mathbf{r},t)$	V as a function of \mathbf{r} and t , per unit charge, Sect. 6.3
$\stackrel{V_0}{\widehat{}}$	Gas volume, Sect. 1.1
\widehat{V}_0	Gas volume bounded by a surface, Sect. 1.9
vdf	velocity distribution function, Sect. 1.14
VDZ	Valence double zeta basis set, Sect. 6.4.2
VXZ	Valence basis set with $X = D$, T , Q , S , G , Sect. G .
VXZ-PP	A specific version of VXZ, Sect. 6.21
\mathbf{W}_{1T}	Dimensionless ion velocity in 1T Theory, Sect. 5.5
\mathbf{W}_{2T}	Dimensionless ion velocity in 2T Theory, Sect. 5.6 Proposition ion speed in a special frame. Sect. 3.5.2
\widehat{W}	Pre-collision ion speed in a special frame, Sect. 3.5.2
$\widehat{W}^{'} \ \widehat{W}_{0}$	Post-collision ion speed in a special frame, Sect. 3.5.2
\dot{W}_0	Pre-collision neutral speed in a special frame, Sect. 3.5.2
$\widehat{W}_{0}^{'}$	Post-collision neutral speed in a special frame, Sect. 3.5.2
WUB	Wang Chang-Uhlenbeck-de Boer equation, Sect. 1.20

**	Integration variable, Sect. 1.11
x	
X_j	Mole fraction of gas j , Sect. 1.8
$Y_l^m(\theta,\phi)$	Spherical harmonic function, Sect. 6.4.1
Z	Cartesian axis defined by E, Sect. 1.8
z_1	Distance along z, Sect. 2.4
\widehat{z}	Dimensionless charge number, Sect. 2.8.2
<i>Z</i> 0	Gas compressibility, Sect. 2.2
Z	Partition function of molecular ions, Sect. 1.20
\widetilde{Z}	Nuclear charge, Sect. 6.21
Z_0	Partition function of neutral gas molecules, Sect. 3.4.2
Z_R	Partition function of reactive molecules, Sect. 1.20
α	Pre-collision internal state of an ion, Sect. 3.2
$\alpha^{'}$	Post-collision internal state of an ion, Sect. 8.2
α	Vector in Dirac equation, Sect. 6.17.1
$\overset{\leftrightarrow}{\alpha}$	Four-vector version of α , Sect. 6.17.1
\widetilde{lpha}	Parameter for even-tempered basis set, Sect. 6.4.4
$\alpha(\xi_s)$	First eigenfunction of S in spin space, Sect. 6.6
$lpha(\xi_s)$ \widetilde{lpha}_i	Determinant coefficients in CI method, Sect. 6.9
$\widehat{lpha_0}$	Neutral polarizability in cubic Angstroms, Sect. 1.11
α_c	Correction in fundamental ion mobility equation, Sect. 1.11
$lpha_j$	Cartesian component of α along axis j, Sect. 6.17.1
α_{T}	Townsend's first ionization coefficient, Sect. 1.10
$lpha_{ m MT}$	Momentum-transfer coefficient, Sect. 3.6
α_{\parallel}	Skewness of Gram-Charlier vdf, Sect. 7.2
	Scalar in Dirac equation, Sect. 6.17.1
$rac{eta}{\widetilde{eta}}$	Parameter for even-tempered basis set, Sect. 6.44
β_c	Correction factor in Wannier equation, Sect. 1.13
β_0	Pre-collision internal state of a neutral, Sect. 3.2
$eta_0 \ eta_0'$	Post-collision internal state of a neutral, Sect. 8.2
$\beta_{\rm B}$	Pre-collision internal state of a reactive neutral, Sect. 8.2
$eta_R eta(\xi_s)$	Second eigenfunction of S in spin space, Sect. 6.6
β_{\parallel}	Excess kurtosis of the GC vdf along the field, Sect. 7.2
β_{\perp}	Excess kurtosis perpendicular to the field, Sect. 7.2
$egin{array}{c} eta_{\perp} \ \widetilde{\gamma} \end{array}$	Parameter for well-tempered basis set, Sect. 6.44
γ	Dimensionless relative velocity vector, Sect. 3.4.2
$\stackrel{\centerdot}{\gamma}_i$	Component of γ along axis i , Sect. 7.2
$\stackrel{\prime}{\gamma}_1^{\imath}$	Correlation of speed and energy in GC vdf, Sect. 7.2
γ_2	Correlation of two energies in GC vdf, Sect. 7.2
$\widetilde{\widetilde{\gamma}}_1$	First momentum-transfer coefficient, Sect. 3.5.3
$\widetilde{\widetilde{\gamma}}_2$	Second momentum-transfer coefficient, Sect. 3.5.3
$\overset{'}{\widetilde{\gamma}}_{2}^{2}$	Third momentum-transfer coefficient, Sect. 3.5.3
δ_i	Mixture factor for mobility, Sect. 2.5
$egin{array}{l} \widetilde{\gamma}_1 \ \widetilde{\gamma}_2 \ \widetilde{\gamma}_3 \ \delta_j \ \delta_{ m P} \end{array}$	Error in gas pressure, Sect. 2.2.9
~ r	Suo pressure, Seen 2.27

Notation and Abbreviations xv

$\delta_{ m s}$	Skewness parameter, Sect. 6.23.5
$\delta_{ m T}$	Error in gas temperature, Sect. 2.2.9
δ_ϵ	Error in electromotive force, Sect. 2.2.9
$\delta_ au$	Error in average time in drift region, Sect. 2.2.9
$<\gamma_{z}(\gamma_{z}-\gamma_{z}^{'})>$	Momentum-transfer collision integral (molecules), Sect. 8.7
$\overline{\epsilon}$	Angle of rotation in a collision, Sect. 4.2
$\epsilon_{ m cm}$	Center-of-mass collision energy, Sect. 3.3
$\epsilon_{ m d}$	Potential well depth, Sect. 9.1.4
3	Collision energy, Sect. 1.11
$arepsilon_V$	Electromotive force (emf), Sect. 1.4
$\varepsilon_{V,n}$	Nominal electromotive force, Sect. 2.2.9
ε_0	Electric constant, Sect. 1.3
$\epsilon^{(lpha)}$	Internal energy of ions in state α , Sect. 1.20
$\epsilon_0^{(eta)}$	Internal energy of neutrals in state β , Sect. 3.3
ε_R	$\epsilon_{\rm cm}$ with reactive neutral R, Sect. 1.17
$\epsilon_R^{(eta)}$	Internal energy of reactive neutrals in state β , Sect. 1.20
$\epsilon_{ m rot}$	Pre-collision rotational energy, Sect. 8.8
ζ	Dimensionless orbital exponent (zeta parameter), Sect. 6.4.1
ζ_i	Value of ζ for orbital <i>i</i> , Sect. 6.4.4
ζ_{MT}	Momentum-transfer correlation coefficient, Sect. 3.2
$\zeta(v)$	Druyvesteyn distribution function for electrons, Sect. 1.14
η_l	Phase shift for quantum number <i>l</i> , Sect. 6.22.2
θ	Polar scattering angle of an ion, Sect. 1.11
θ_0	Polar scattering angle of a neutral, Sect. 3.5.3
κ	Correction factor for gas temperature, Sect. 2.2.5
$\widetilde{\kappa}$	Wave number, Sect. 6.22.2
$\widehat{\kappa}$	Anisotropy of ion-dipole potential, Sect. 8.11
μ_j	Reduced mass for ions with a molecule of type j , Sect. 5.8.2
μ_0	Reduced mass for ions with a pure neutral gas, Sect. 1.11
$\widehat{\mu}_0$	Ion-neutral reduced mass in Da (g/mole), Sect. 1.11
μ_R	Reduced mass of ion-reactive neutral system, Sect. 1.17
$v^{(1)}$	Microscopic version of $\widetilde{v}^{(1)}$, Sect. 2.6.3
$\widetilde{v}^{(1)}$	Collision frequency for momentum transfer, Sect. 1.14
ξ ξ_s	Effective collision frequency, Sect. 2.13
ξ_s	Coordinate for spin space, Sect. 6.6
ξ_s $\xi^{(1T)}$	Collision frequency for ions in 1T theory, Sect. 5.8
$\xi_j^{(1T)}$	Collision frequency for ions in gas j in 1T theory, Sect. 5.8
$\xi^{(2T)}$	Collision frequency for ions in 2T theory, Sect. 5.8
$\xi_{:}^{(2T)}$	Collision frequency for ions in gas j in 2T theory, Sect. 5.8
$\xi^{(3T)}$	Collision frequency for ions in 3T theory, Sect. 5.8
$\xi_j^{(3T)}$	Collision frequency for ions in gas j in 3T theory, Sect. 5.8
J	

```
Kinetic momentum vector, Sect. 6.17.1
\pi
                        Charge or electron density, Sect. 6.2
ρ
                        Differential scattering cross section, Sect. 1.13
σ
                        Standard deviation of pulse entering drift tube, Sect. 2.4
\sigma_1
                        Standard deviation of arrival times along field, Sect. 2.4
\sigma_{\parallel}
\sigma^{(\lambda,v)}
                        Cross section of atomic ions in diatoms, Sect. 8.8
\tau
                        Collection of four variables: x, y, z, t, Sect. 6.18
                        Mean time between collisions, Sect. 1.8
\tau_c
                        Azimuthal scattering angle of an ion, Sect. 3.4.1
φ
                        Azimuthal scattering angle of a neutral, Sect. 3.5.3
\phi_0
                        Phase angle of J, Sect. 8.8
\phi_{\rm I}
                        Phase angle of L, Sect. 8.8
\phi_{\rm L}
                        Index specifying one nucleus in a molecule, Sect. 6.3
φ
                        Dimensionless center-of-mass velocity vector, Sect. 3.4.2
χ
                        Frequency of an ac field, Sect. 2.11
ω
\omega_i
                        Weighting factor in MMA and BMM, Sect. 8.11
                        Weighting factor for average mass, Sect. 2.6.3
\omega_i
Γ
                        Gamma function, Sect. 1.14
\Gamma^{(+)}
                        Rate of gain of ions in phase space, Sect. 4.1
\Gamma^{(-)}
                        Rate of loss of ions in phase space, Sect. 4.1
                        Change in ion momentum along the field, Sect. 3.2
\Delta p_{\tau}
                        Period of time, Sect. 1.4
\Delta t
                        Change in energy, Sect. 1.4
18
                        Change in internal energy, Sect. 3.3
\Delta \varepsilon_{\rm int}
                        Ratio of molecular collision integrals, Sect. 8.7
\Delta_1
\Delta_L
                        Correction term in GER for D_L/K, Sect. 1.19
\Delta_T
                        Correction term in GER for D_T/K, Sect. 1.19
                        Change in ion speed along the field, Sect. 3.2
\Delta v_{z}
                        Momentum-transfer correction factor, Sect. 3.6
\Upsilon_{\mathrm{MT}}
Φ
                        Ratio of collision integrals for molecular systems, Sect. 1.20
                        Slater or Gaussian orbital, Sect. 6.4.1
\psi_{n,l,m}
                        Wave function for a simpler problem, Sect. 6.18
\psi^{(0)}
\Psi(\mathbf{r},t)
                        Position and time-dependent wave function, Sect. 6.3
\Psi(\mathbf{r})
                        Position-independent wave function, Sect. 6.3
\Psi(\mathbf{r}^{(n)})
                        \Psi(\mathbf{r}) for n electrons, Sect. 6.3
\Psi_{l,m,r}(\mathbf{v})
                        Generalized basis function of velocity, Sect. 5.4
\varPsi_{l,m,r}^{(1T)}(\mathbf{v})
                        \Psi_{l,m,r}(\mathbf{v}) in 1T Theory, Sect. 5.5
\Psi_{l,m,r}^{(2T)}(\mathbf{v})
                        \Psi_{l,m,r}(\mathbf{v}) in 2T Theory, Sect. 5.6
\Psi_{l,m,r}^{(MT)}(\mathbf{v})
                        \Psi_{l,m,r}(\mathbf{v}) in MT Theory, Sect. 5.7
Ω
                        Molecular momentum-transfer collision integral, Sect. 1.20
                        Structure factor, Sect. 2.8.2
\Omega_d/\widehat{z}
                        Normalized collision integral for atoms, Sect. 1.11
\overline{O}^{(l,s)}
```

Notation and Abbreviations xvii

$\overline{\Omega}^{(1,1)}$	Momentum-transfer collision integral for atoms, Sect. 1.11
$\overline{\Omega}_{ m mol}^{(l,s)}$	Normalized collision integral for molecules, Sect. 3.4.2
∇	Gradient operator (vector) in space, Sect. 1.9
$\nabla_{\mathbf{v}}$	Gradient operator (vector) in velocity space, Sect. 4.1
∇_{x}	Component of ∇ along direction x , Sect. 1.9
∇^2	Laplacian operator (scalar), Sect. 1.9
\mathfrak{N}	Number of collisions, Sect. 3.5.1
\odot	Contraction operator for two tensors, Sect. 1.15
$\stackrel{\longleftrightarrow}{\mathbf{\cdot}}$	Four-vector version of ∇ and $\frac{\partial}{\partial t}$, Sect. 6.17.1
$\frac{\partial}{\partial x}$	Partial derivative with respect to any quantity, x , Sect. 1.9
•	Scalar product of two vectors (dot product), Sect. 1.9
×	Cross product of two vectors (vector product), Sect. 5.1
$[\;,\;]$	Commutator or Poisson bracket, Sect. 8.1
$[p;q]^{(l)}$	Irreducible collision integrals of 3T theory, Sect. 5.7
[p,q,r s,t,u]	Irreducible collision integrals of MT theory, Sect. 5.8
$\binom{k'}{k} \cdots$	Matrix element for diatomic systems, Sect. 8.7

Figure Credits

Graphical figures were prepared by the author, with the assistance of Claudia K. Viehland. The paintings, sketches, and photos of deceased scientists are from the online addresses (initial http:// omitted) in the table below.

Allis upclosed.com/people/william-allis/

Anderson www.nobelprize.org/nobel_prizes/physics/laureates/1936/

anderson postcard.jpg

Arrhenius www.nobelprize.org/nobel_prizes/chemistry/laureates/1903/

arrhenius.jpg

Aston www.biografiasyvidas.com/biografia/a/fotos/aston_francis.jpg Bailey www.science.org.au/files/userfiles/fellowship/memoirs/images/

bailey.jpg

Beenakker https://upload.wikimedia.org/wikipedia/commons/thumb/3/38/

JJMBeenakker.jpg/1200px-JJMBeenakker.jpg

Bethe https://upload.wikimedia.org/wikipedia/commons/5/5f/Hans

Bethe.jpg

Blackett collectionimages.npg.org.uk/large/mw49543/mw49543.jpg

Bohr www.jewoftheday.com/Ulpan/Images/NeilsBorh.jpg

Boltzmann www.thefamouspeople.com/profiles/images/ludwig-boltzmann-1.

ipg

Born upload.wikimedia.org/wikipedia/commons/f/f7/Max_Born.jpg
Cannizzaro www.chemistryexplained.com/images/chfa_01_img0161.jpg
Carlisle upload.wikimedia.org/wikipedia/commons/3/3c/Anthony_Carlisle_

by_Henry_Bone.jpg

Cavendish www.argia.eus/astekaria/docs/2358/argazkiak/cavendish-300.jpg

Chapman apprendre-math.info/history/photos/Chapman_3.jpeg

Charlier https://sok.riksarkivet.se/sbl/bilder/14793_7_008_00000373_2.jpg Cook upload.wikimedia.org/wikipedia/en/e/e7/William_Richard_Joseph_

Cook.jpg

Coulomb www.tayabeixo.org/biografias/images/Coulomb.jpg

 $Cowling \\ www.phys-astro.sonoma.edu/BruceMedalists/Cowling/cowling.jpg$

xx Figure Credits

Crookes api.ning.com/files/vRWi3e17RGo7u0-6VqhffF1v*Kc AznnHzhH-

ltjVJgrpo*l*c6lrrmdHYJDHMgDp3E

wsIGdEGK7dB6TMQhEJoVS9-iBP98kQ/Croo.gif

Curtiss www.chem.wisc.edu/deptfiles/docs/badger-chemist/BChemist_08.

pdf

Davy www.wikigallery.org/paintings/201501-202000/201847/painting1.

jpg

Dempster sciencenotes.org/wp-content/uploads/2014/08/Arthur Jeffrey

Dempster.jpg

Dirac www.nobelprize.org/nobel_prizes/physics/laureates/1933/dirac_

postcard.jpg

Drift Tube www.indiana.edu/~clemmer/Research/Early%20Work/

Instruments/highresdt_pic.gif

Druyvesteyn http://members.home.nl/arjen.boogaard/images/druyvesteyn.jpg
Du Fay images.fineartamerica.com/images-medium-large/charles-dufay-du-

fay1698-1739-sheila-terry.jpg

Einstein 3.bp.blogspot.com/ 2BiG4q7GCqk/TTHot-b6 mI/

AAAAAAAAB2M/Lq1m4BvikII/s1600/Albert Einstein Photo

+II.jpg

Enskog www-history.mcs.st-and.ac.uk/PictDisplay/Enskog.html Eyring upload.wikimedia.org/wikipedia/commons/5/54/Henry_B._

Eyring2.jpg

Faraday media.gettyimages.com/photos/portrait-of-michael-faraday-british-

chemist-and-physicist-painting-by-picture-id164083627

Feynman upload.wikimedia.org/wikipedia/en/4/42/Richard_Feynman_

Nobel.ipg

Fick upload.wikimedia.org/wikipedia/commons/b/b3/Adolf Fick 8bit

korr_klein1.jpg

Fock en.wikipedia.org/wiki/File:Vladimir_Fock_-_photo.jpg

Franck www.britannica.com/biography/James-Franck Franklin postalmuseum.si.edu/outofthemails/franklin.jpg Gaede www.converter.cz/fyzici/images/gaede-39.jpg

Galerkin upload.wikimedia.org/wikipedia/commons/3/35/Boris_Galerkin_

01.jpg

Galilei www-history.mcs.st-and.ac.uk/PictDisplay/Galileo.html

Galvani upload.wikimedia.org/wikipedia/commons/3/39/Luigi_galvani.jpg Geissler www.browsebiography.com/images/4/14783-heinrich_geissler.jpg Gerlach upload.wikimedia.org/wikipedia/en/9/9e/Walther_Gerlach.jpg

Gilbert cdn.quotationof.com/images/william-gilbert-3.jpg

Goldstein www.100ciaquimica.net/images/biografias/ima/Golstein.jpg
Goudsmit https://upload.wikimedia.org/wikipedia/commons/6/68/

UhlenbeckKramersGoudsmit_%28cropped%29.jpg

Graham www.famousbirthdays.com/faces/graham-thomas-image.jpg
Gram https://upload.wikimedia.org/wikipedia/commons/e/e7/J%C3%

B8rgen_Pedersen_Gram_by_Johannes_Hauerslev.jpg

Figure Credits xxi

Guericke cdn.britannica.com/668x448/48/11348-004-56C944AA.jpg

Hall www.universetoday.com/wp-content/uploads/2011/10/Edwin-H.-

Hall.jpg

Hamilton todayinsci.com/H/Hamilton_WmRowan/HamiltonWmRowanThm.

ipg

Harkins www.radjournal.com/articles/History/March/Harkins.jpg

Hartree www.converter.cz/fyzici/images/hartree.jpg

Heisenberg www.thefamouspeople.com/profiles/images/werner-heisenberg-1.

jpg

Hertz upload.wikimedia.org/wikipedia/commons/5/50/Heinrich_Rudolf_

Hertz.jpg

Hirschfelder https://s3.amazonaws.com/photos.geni.com/p13/ff/e1/7a/b4/

5344483c5c3ed03f/dud46hez_medium.jpg

Hittorf upload.wikimedia.org/wikipedia/commons/c/c4/Johann_Wilhelm_

Hittorf_01.jpg

Hund http://www.nndb.com/people/155/000099855/friedrich-hund-1-

sized.jpg

Huxley www.asap.unimelb.edu.au/bsparcs/aasmemoirs/gifs/huxley.jpg

Kato https://opc.mfo.de/photoNormal?id=5377

Kaufmann upload.wikimedia.org/wikipedia/commons/1/1d/Walter_kaufmann.

png

Kohn www.physique.usherbrooke.ca/tremblay/professeurs/kohn.jpg

Kronig tse2.mm.bing.net/th?id=OIP.

xdaGHpxeYr25w5N7lGOJDQHaK2&pid=15.1&P=0&w=300&h=

300

Lamb upload.wikimedia.org/wikipedia/commons/7/77/Willis Lamb

1955.jpg

Landau www-history.mcs.st-andrews.ac.uk/BigPictures/Landau_Lev_9.

jpeg

Langevin upload.wikimedia.org/wikipedia/commons/c/cd/Paul_Langevin_

Wellcome.jpg

Lenard upload.wikimedia.org/wikipedia/commons/1/1d/Phillipp_Lenard_

in 1900.jpg

Lifshitz www-history.mcs.st-and.ac.uk/BigPictures/Lifshitz.jpeg

Loeb en.wikipedia.org/w/index.php?curid=53508692 Loschmidt www.converter.cz/fyzici/images/loschmidt.jpg

Mack chemistry.osu.edu/sites/chemistry.osu.edu/files/styles/full_width/

public/Edward%20Mack%20Jr.jpg?itok=tTT-dKAH

Massey www.phys.ucl.ac.uk/department/history/BFox3.html#Fox332 Maxwell upload.wikimedia.org/wikipedia/commons/e/ec/James_clerk_

maxwell.jpg

McDaniel http://gtalumni.org/Apps/livinghistory/faculty.php?id=23
Millikan media1.britannica.com/eb-media/95/19595-004-A80924D0.jpg

Moseley www.scientificlib.com/en/Physics/Biographies/images/

HenryMoseley.jpg

xxii Figure Credits

Mott nobelprize.org/nobel_prizes/physics/laureates/1977/mott-bio.html

Nernst www.nernst.de/nernst.jpg

Nicholson https://upload.wikimedia.org/wikipedia/commons/1/13/William

Nicholson_b1753.jpg

Occhialini upload.wikimedia.org/wikipedia/commons/0/05/Occhialini.jpg Ohm www.shodor.org/refdesk/Resources/Activities/OhmsLaw/Ohm_2.

jpeg

Oppenheimer upload.wikimedia.org/wikipedia/commons/0/03/JROppenheimer-

LosAlamos.jpg

Pascal www.catholiceducation.org/en/images/authos/pascal3.jpg Pasteur ebooks.adelaide.edu.au/p/pasteur/louis/portrait.jpg

Paul www.nobelprize.org/nobel_prizes/physics/laureates/1989/paul.jpg

Pauli upload.wikimedia.org/wikipedia/commons/4/43/Pauli.jpg
Penning upload.wikimedia.org/wikipedia/en/3/35/FMPenning.jpg
Perrin www.nndb.com/people/720/000099423/jean-perrin-1.jpg
Plesset https://s3.amazonaws.com/photos.geni.com/43/79/89/f7/

327789384330007946/tab63nug/437989f77a03062f medium.jpg

Plücker www.inovatifkimyadergisi.com/wp-content/uploads/2017/07/

julius-plucker.jpg

Pohl www.dpg-physik.de/preise/pix/wichard-pohl.jpg

Poisson https://upload.wikimedia.org/wikipedia/commons/thumb/b/b7/

Simeon_Poisson.jpg/800px-Simeon_Poisson.jpg

Polanyi manwithoutqualities.files.wordpress.com/2016/03/screen-shot-

2016-03-05-at-1-27-56-pm.png

Powell www.kakophone.com/kakorama/images/nobel/powell.jpg

Ramsauer www.enciklopedija.hr/Ilustracije/HE9 0064.jpg

Ritz upload.wikimedia.org/wikipedia/commons/5/5e/Walter Ritz

Physicist.gif

Roentgen http://images.fineartamerica.com/images-medium-large/2-wilhelm-

konrad-roentgen-german-science-source.jpg

Rutherford www.ihep.ac.cn/kejiyuandi/zhishi/070627-cosmic/Rutherford.gif http://cache.boston.com/resize/bonzai-fba/Globe_Photo/2008/11/

28/1227931370 3037/300h.jpg

Schrödinger upload.wikimedia.org/wikipedia/commons/2/2e/Erwin_

Schrödinger_%281933%29.jpg

Schuster upload.wikimedia.org/wikipedia/commons/thumb/9/9d/Arthur_

Schuster.jpg/220px-Arthur_Schuster.jpg

Schwinger upload.wikimedia.org/wikipedia/commons/3/3c/Schwinger.jpg

Sinanoglu www.itusozluk.com/image/oktay-sinanoglu_17444.jpg

Slater web.mit.edu/physics/images/history/slater.jpg

Stern upload.wikimedia.org/wikipedia/commons/6/6e/Otto Stern 1950s.

jpg

Stoney www.ssplprints.com/image.php?imgref=10309421

Strutt www.nobelprize.org/nobel_prizes/physics/laureates/1904/strutt_

postcard.jpg

Figure Credits xxiii

Thomson www.wired.com/images_blogs/thisdayintech/2012/04/jj_

thompson_400px.jpg

Tizard collectionimages.npg.org.uk/large/mw50701/mw50701.jpg
Tomonaga upload.wikimedia.org/wikipedia/commons/3/3a/Tomonaga.jpg
Torricelli www.thefamouspeople.com/profiles/images/evangelista-torricelli-

1.jpg

Townsend upload.wikimedia.org/wikipedia/commons/a/a8/John_Sealy_

Townsend.jpg

Tyndall teara.govt.nz/files/large_images/t278-tyndall-arthur-atl-1.jpg
Uhlenbeck www.100ciaquimica.net/images/biografias/ima1/Uhlenbeck.jpg
Unsőld upload.wikimedia.org/wikipedia/id/2/2a/T1820_unsoeld.gif
Urey upload.wikimedia.org/wikipedia/commons/2/29/Urey.jpg

Van de Graaf tvdg10.phy.bnl.gov/vandegraaff.html

Varley upload.wikimedia.org/wikipedia/ru/c/c9/Cromwell_Fleetwood_

Varley.jpg

Volta techstory.in/wp-content/uploads/2016/02/Alessandro-Volta.jpg Waldmann https://www.mpic.de/uploads/pics/Waldmann_Ludwig_web2.jpg

Wang Chang www.ias.edu/ideas/2015/hu-studying-physics

Wannier fr.cdn.v5.futura-sciences.com/builds/images/rte/RTEmagicC_

wannier_gregory_AIP_Emilio_Segre_Visual_Archives_Physics_

Today_Collection.jpg

Watson cdn.quotationof.com/images/william-watson-5.jpg nuclearplanet.com/Final2%20Emil_Wiechert.jpg

Wien https://upload.wikimedia.org/wikipedia/commons/d/dd/Wilhelm

Wien_1911.jpg

Zeleny history.aip.org/phn/Photos/zeleny john al.jpg

Preface

This book is about the drift, diffusion, and reaction of ions moving through gases under the influence of an external electric field, the gas temperature, and the number density. Late in the nineteenth century, research in this area helped to establish the existence of electrons and ions and laid the foundation of modern physics and chemistry. Experimental and theoretical studies of ion and electron swarms continue to be important in such varied fields as atomic and molecular physics, aeronomy and atmospheric chemistry, gaseous electronics, plasma processing, and laser physics. In short, there is more that unites all of these research and application areas than the emphases, terminology, and details that separate them. This book is directed toward graduate students and researchers new to this research field, particularly those involved with ion mobility spectrometry and the use of ion transport coefficients to test and improve ab initio ion—neutral interaction potentials.

Surveys of the early history of charged particle transport in gases are given by Loeb (1955), Beynon and Morgan (1978), and others. The early literature is covered so thoroughly by Loeb that in most places in this book the original literature will be cited only if it was published after 1950.

There are three books that may be considered predecessors of the present work, since they are similar in spirit to it. They are by McDaniel and Mason (1973), Huxley and Crompton (1974), and Mason and McDaniel (1988). The titles of these books reflect the unfortunate fact that the transport of electrons and ions has been treated separately for many years. Although there are both theoretical and experimental reasons for this, the two subdisciplines have more in common than is generally appreciated. Accordingly, this book was originally going to treat electrons and ions on an equal basis, similar to the approach used by Kumar et al. (1980), Robson (2006), and Konovalov et al. (2017) in works that can be considered as introductions to the present book. However, this work quickly grew beyond acceptable limits. In addition, a recent book by Robson et al. (2018) treats the transport of any type of charged particle in both gases and condensed matter, albeit

xxvi Preface

with less detail and from a more advanced starting point than we propose to use here. Therefore, we reluctantly had to limit the majority of this book to swarms of atomic and molecular ions.

Chapter 1 of the book expands upon an encyclopedia article (Viehland 2003) to give a history of swarm research, including information about electron swarms. At the same time, it introduces the basic concepts, physical relationships, and mathematical equations that will be used in the remaining sections. This history emphasizes swarm research connected to physical chemistry and chemical physics. The history of swarm research of interest to analytical chemists is covered by Eiceman et al. (2014).

Chapter 2 discusses the experimental techniques used to study gaseous ion transport, paying more attention to the techniques presently being used than to the older techniques discussed at length in the books mentioned above and focusing more on the theoretical implications of the equipment used. Here too, it was necessary to limit the focus, not only because of space limitations but also because the author's expertise is more in the realm of theory.

Chapter 3 presents momentum-transfer theory, an elementary theory of ion mobility. This introduces the reader to the thinking that undergirds the kinetic theory of swarms and makes clear some of the limitations of the fundamental low-field ion mobility equation.

The kinetic theory of gases is the subset of statistical mechanics that uses the Boltzmann kinetic equation to describe the nonequilibrium properties of a dilute gas. Chapter 4 discusses the Boltzmann equation for atomic ions in atomic gases, thus deferring treatment of molecular ions and neutrals until later in the book.

Solving the Boltzmann equation exactly can be done only for models of the ion motion in gases, not for the general cases of interest here. We begin the process of successive approximations to its solution in Chap. 5, by discussing moment theories. These methods are based on Maxwell's equations of change that are equivalent to Boltzmann's equation. This chapter includes a discussion of what is now considered the standard approach to gaseous ion mobility and diffusion, here called the two-temperature (2T) theory.

The big problem with the 2T theory is that it cannot handle situations that are inherently anisotropic. This problem led to the development of the three-temperature (3T) and Gram–Charlier (GC) theories that are described in Chap. 5. Both use three temperatures: the gas temperature, an ion temperature characterizing the average kinetic energy along the direction of the electrostatic field, and a different ion temperature characterizing the average energy perpendicular to the field. They allow the ion mobility and diffusion coefficients to be calculated from an ion–neutral interaction potential in a series of successive approximations.

Chapter 6 discusses how ion-neutral interaction potentials for atomic ion-atom systems can be calculated ab initio, and how from such potentials the transport coefficients can be calculated ab initio using GC theory. These calculations proceed in a systematic series of approximations starting from a guess for the ion velocity

Preface xxvii

distribution function (vdf). This guess (called a zero-order approximation of the vdf) involves not only the ion velocity and temperatures but also quantities that in statistics are called skewness and kurtosis. In addition, it allows for correlation between ion properties parallel and perpendicular to the field.

Chapter 7 first discusses the application of the 2T theory to the analysis and understanding of gaseous ion–neutral reaction. It then considers how the vdf for atomic ions moving through atomic gases can be visualized from GC theory and used to compute rate coefficients for chemical reactions of the ions with small amounts of a reactive molecular gas that are included with the neutral buffer gas. It ends by showing that in some cases the reaction cross sections inferred in the past from swarm studies are in error by more than 30%.

Chapter 8 is devoted to changes that occur when either the ion or neutral is molecular. It moves then to a discussion of various extensions of the Boltzmann equation that have been proposed. Only the fully classical extension is presently useful for swarm studies, because the matrix elements of the collision operators used in the other extensions are too difficult to compute. Ab initio calculations are then described for atomic ions in diatomic neutrals and for diatomic ions in atomic neutrals. While such calculations are feasible, they are still so difficult that alternative methods are desirable. The chapter ends with a discussion of the MMA approximation (Monchick and Mason 1961) and the extension of it (Viehland and Chang 2012) that is known as the BMM, for beyond Monchick–Mason. Although still in its infancy, the BMM shows promise of being simple (hence using small amounts of computer power) and accurate enough to test interaction potential energy surfaces.

Chapter 9 starts by describing atomic models that have been used to describe molecular systems. All such models have significant weakness, so this chapter also describes Monte Carlo and molecular dynamics calculations for molecular systems. The final chapter contains a short summary of this book, along with a prediction for the things that lie ahead in a research area that already is more than 120 years old.

It is essential in this book to use a fair amount of mathematics. When calculus is used, the derivations are done slowly so that readers whose calculus skills have weakened with time can have their memories refreshed. In this regard, Appendix A is particularly important, as it explains the mathematical terminology, particularly the terminology of vector calculus, that is crucial to the understanding of swarm experiments but may be unfamiliar to some readers. Appendix B discusses atomic term symbols that are used throughout this book to specify a particular state of an atomic ion or neutral. Unless specifically indicated otherwise, the neutral gases are assumed to be the naturally occurring mixture of the various isotopes. Appendix C discusses the method of weighted residuals that can be used to solve the time-independent Schrödinger equation, the Boltzmann equation, or indeed any mathematical equation involving a linear operator.

xxviii Preface

References

- J.H. Beynon, R.P. Morgan, Int. J. Mass Spectr. Ion Phys. 27, 1 (1978)
- G.A. Eiceman, Z. Karpas, H.H. Hill, Jr., Ion Mobility Spectrometry, 3rd edn. (CRC Press, Boca Raton, Florida 2014)
- L.G.H. Huxley, R.W. Crompton, *The Diffusion and Drift of Electrons in Gases* (Wiley, New York, 1974)
- D.A. Konovalov, D.G. Cocks, R.D. White, Eur. Phys. J. D 71, 258 (2017)
- K. Kumar, H.R. Skullerud, R.E. Robson, Aust. J. Phys. 33, 343 (1980)
- L.B. Loeb, *Basic Processes of Gaseous Electronics* (University of California Press, Oakland, 1955)
- E.A. Mason, E.W. McDaniel, Transport Properties of Ions in Gases (Wiley, New York, 1988)
- E.W. McDaniel, E.A. Mason, *The Mobility and Diffusion of Ions in Gases* (Wiley, New York, 1973)
- L. Monchick, E.A. Mason, J. Chem. Phys. 35, 1676 (1961)
- R.E. Robson, *Introductory Transport Theory for Charged Particles in Gases* (World Scientific, Singapore, 2006)
- R.E. Robson, R. White, M. Hildebrandt, Fundamentals of Charged Particle Transport in Gases and Condensed Matter (CRC Press, Boca Raton, Florida, 2018)
- L.A. Viehland, Transport Properties, in *The Encyclopedia of Mass Spectrometry: Vol. 1. Theory and Ion Chemistry*, ed. by P.B. Armentrout (Elsevier, Amsterdam, 2003) pp. 491–498
- L.A. Viehland, Y. Chang, Mol. Phys. 110, 2596 (2012)

Contents

1	Intro	duction	1
	1.1	Definition and Importance of Swarms	1
	1.2	Air and Vacuum Pumps	2
	1.3	Static Electricity	5
	1.4	Current Electricity	7
	1.5	Faraday's Laws of Electrochemistry	9
	1.6	Electrical Conduction	1
	1.7	Ions	3
	1.8	Ion Swarms, 1896–1928	6
	1.9	Ion Diffusion, 1855–1926	1
	1.10	Electron Swarms, 1900–1922	4
	1.11	Early Kinetic Theory, 1905–1931	7
	1.12	Mass Spectrometers	0
	1.13	Ion Swarms, 1928–1960	2
	1.14	Electron Swarms, 1922–1965	6
	1.15	Electron and Ion Swarms, 1960–1975	8
	1.16	Atomic Ion–Atom Kinetic Theory	2
	1.17	Ion–Neutral Reactions	3
	1.18	Improved Kinetic Theories	4
	1.19	Generalized Einstein Relations	5
	1.20	Transport with Molecular Systems	6
	Refer	ences	8
2	Evno	rimental Techniques	1
_	2.1		Т
			_
	2.2	<u> </u>	
		2.2.1 Illustration	
		2.2.2 Basics	-
		2.2.3 Ion Mobility	_
		2.2.4 Effects of Drift-Tube Length	Ó

xxx Contents

	2.2.5	Effects of Gas Temperature	
	2.2.6	Effects of Gas Pressure	
	2.2.7	Effects of Electromagnetic Field	
	2.2.8	Effects of Time Measurements	
	2.2.9	Calibration of the Entire DTMS	
2.3	Ion An	rival Time Distributions	
2.4		on in Drift-Tube Mass Spectrometers	
2.5		es of Buffer Gases	
2.6		es of Ions	
	2.6.1	Mixtures of Atomic Isotopes	
	2.6.2	Separation of Ions	
2.7		bility Spectrometers	
2.,	2.7.1	Low-Field Limits	
	2.7.2	Effects of Ion–Neutral Mass Ratio	
	2.7.3	Effects of Charge State	
	2.7.4	Effects of Chemical Reactions	
	2.7.4	False Negatives and False Positives	
2.8		[S	
2.0	2.8.1		
		Basics	
	2.8.2	Effects of Ion Mass in Atomic Systems	
	2.8.3	Effects of Structure–Molecular Systems	
2.0	2.8.4	High Accuracy IMS/MS	
2.9		ntial IMS (DMS)	
	2.9.1	Ping-Pong Experiments	
	2.9.2	Basics of DMS	
	2.9.3	Higher Order DMS	
2.10		ng-Wave IMS	
2.11		d-Ion IMS	
2.12		clotron Resonance	
2.13		aps	
2.14		Probing of Drift Tubes	
Refer	ences		
Mom	entumT	Fransfer Theory	
3.1		ative Momentum-Transfer Theories	
3.2		als of Momentum-Transfer Theory	
3.3		e Speed	
3.4		Sections	
J. +	3.4.1	Momentum Transfer in a Collision	
	3.4.1	Average Momentum Transfer	1
3.5]
5.5	_	ge Ion Momentum Lost in a Collision	
	3.5.1	Average Drift Speed Between Collisions	1
	3.5.2	Classification of Collisions	1

3

Contents xxxi

		3.5.3 Archetype Collisions	106
	3.6	Fundamental Ion Mobility Equation	110
	3.7	Discussion	113
	Refer	rences	114
4	The 1	Boltzmann Equation	117
	4.1	General Form	117
	4.2	The Nonreactive Collision Term	119
	4.3	Reactive Collision Terms	120
	4.4	Equilibrium Velocity Distribution Function	121
	4.5	Properties of an Ion Ensemble	122
	4.6	Quantum-Mechanical Effects	124
	4.7	The Maxwell Model	124
	4.8	Rate Equation of Continuity	125
	Refer	rences	126
5	Mom	ent Methods for Solving the Boltzmann Equation	127
	5.1	Introduction	127
	5.2	General Moment Equations	128
	5.3	Successive Approximations	132
	5.4	Basis Functions in General	132
	5.5	One-Temperature Basis Functions	133
	5.6	Two-Temperature Basis Functions	134
	5.7	Three-Temperature Basis Functions	137
	5.8	Multi-temperature Basis Functions	139
	5.9	Gram-Charlier Basis Functions	141
	5.10	Moment Equation for Ion Velocity	144
		5.10.1 First Approximation of 2T Equation	144
		5.10.2 First Approximation of 1T and MM Equations	146
		5.10.3 First Approximation of MT Equation	147
		5.10.4 Higher Approximations	149
	5.11	Moment Equations for Energy	150
	5.12	Final Comments	152
	Refer	rences	153
6	Ab Iı	nitio Calculations of Transport Coefficients	155
	6.1	Introduction	155
	6.2	Density Functional Theory	156
	6.3	The Time-Independent Schrödinger Equation	157
	6.4	Basis Functions for Solution of the TISE	162
		6.4.1 Slater and Gaussian Orbitals	162
		6.4.2 Classification of Basis Sets by Size	163
		6.4.3 Polarization and Correlation in Basis Sets	164
		6.4.4 Balanced, Even- and Well-Tempered Basis Sets	165

xxxii Contents

	6.4.5	Contracted Basis Sets	166		
	6.4.6	Pseudopotentials	167		
6.5	Variation Method				
6.6	Electron Spin				
6.7	Slater Determinants				
6.8	The Self-consistent-Field and Hartree–Fock Methods 1				
6.9	Configuration Interaction				
6.10	Excited	Slater Determinants	177		
6.11		About Basis Sets	178		
		Correlation-Consistent and Complete Basis Sets	178		
	6.11.2	Frozen Core and Frozen Virtuals Approximations	179		
	6.11.3	Basis Set Superposition Error	180		
6.12	Electro	n Correlation Calculations	180		
	6.12.1	Overview	180		
	6.12.2	Truncated Configuration Interaction	182		
	6.12.3	Restricted and Unrestricted CI	182		
6.13	Multico	onfiguration SCF	184		
6.14		eference CI	185		
6.15		al Energy Surfaces	185		
	6.15.1	Basic Features	185		
	6.15.2	Stationary Points	187		
	6.15.3	Geometry Optimization and Energy Minimization	187		
6.16	Maxwe	ell's Equations in a Vacuum	189		
6.17		rac Equation	191		
	6.17.1	Introduction	191		
	6.17.2	The Dirac-Fock Method	196		
6.18	The Per	rturbation Method	197		
6.19	Moller-	-Plesset Perturbation Method	197		
6.20	Couple	d Cluster Methods	198		
6.21	The Breit–Pauli Hamiltonian				
6.22	Transpo	ort Cross Sections	200		
	6.22.1	Classical Calculations	200		
	6.22.2	Quantum Calculations	204		
	6.22.3	Resonant Charge Transfer	206		
6.23	Gaseou	s Ion Transport Coefficients	207		
	6.23.1	Computer Program GC	207		
	6.23.2	Field-Dependent Mobilities	207		
	6.23.3	Zero-Field Mobilities	209		
	6.23.4	Diffusion Coefficients	210		
	6.23.5	Other Transport Coefficients	211		
6.24	Summa	ıry	216		
Refer			216		

Contents xxxiii

7	React	tions in Drift Tubes	219		
	7.1	Importance of Drift Tubes for Ion–Molecule Reactions	219		
	7.2	The Ion VDF	220		
	7.3	Reaction of ${}^{16}O^+({}^4S_{3/2})$ with $N_2(v=0)$	225		
	7.4	Convergence Problems	229		
	7.5	Summary	231		
	Refer	rences	231		
8	Kinetic Theory for Molecules				
	8.1	Basics	233		
	8.2	Quantum Collision Operators	234		
	8.3	Semiclassical Collision Operators	236		
	8.4	Taxman's Classical Theory	236		
	8.5	The Curtiss Equation for Gaseous Ion Transport	238		
	8.6	Density-Gradient-Independent Moment Equations	240		
	8.7	Extension of the 2T Theory to Molecules	240		
	8.8	Atomic Ions in Diatomic Gases	242		
	8.9	Diatomic Ions in Atomic Gases	244		
	8.10	Monchick–Mason Approximation	245		
	8.11	Beyond the MMA	249		
	8.12	Future Calculations with the MMA and BMM	251		
	Refer	rences	252		
9	Model Calculations for Molecules				
	9.1	Atomic Models of Molecular Systems	255255		
	7.1	9.1.1 Maxwell Model	255		
		9.1.2 Rigid-Sphere Model	255		
		9.1.3 (n, 6, 4) Model	257		
		9.1.4 Core Models	258		
	9.2	Site-Site Models	260		
	9.3	Exact Hard Spheres Model	262		
	9.4	Early Monte Carlo Calculations	263		
	9.5	Molecular Dynamics Calculations	264		
	9.6	Recent Monte Carlo Calculations	264		
	9.7	Software for Modeling Mobilities	265		
		rences	267		
10	Sumr	nary and Prognosis	269		
Apr		es	271		
Ind	Index				

Chapter 1 Introduction



1

1.1 Definition and Importance of Swarms

This chapter introduces the reader to the history and basic concepts of swarm research, along with the physical relationships and mathematical equations that will be used in the chapters to follow.

A swarm is defined here as a group of microscopic particles present in trace amounts in a neutral gas that is dilute (not influenced by three-body collisions) but of much larger number density. The particles may or may not be charged, and there may or may not be external electric or magnetic fields. Since so few swarm particles are present, mutual interaction between them is negligible and the properties of the gas are not affected by their presence. The properties of the swarm particles are, however, strongly affected by their collisions with the gas molecules.

The definition above should be compared to that of Kumar et al. (1980):

a swarm is defined as an ensemble of independent charged test particles moving in a neutral background gas. The motion of the particles is determined by the forces exerted by external electric and magnetic fields and collisions with the gas molecules, which may lead to reactions. The ensemble is to be interpreted as arising from a large number of identically prepared gas systems, each with one test particle.

Although there are exceptions, we will mostly be considering charged swarm particles in this book, so this difference in the two definitions generally is unimportant. Our assumption of trace amounts of the swarm particles means that space-charge and other collective phenomena (such as discharges, plasma oscillations and magnetohydrodynamics) are negligible. The definition of Kumar et al. (1980) allows for the study of such phenomena, but in most swarm experiments they are not included, so once again the difference in the definitions generally is unimportant.

The ergodic hypothesis is equivalent to the final sentence of the second definition of a swarm, since no real experiment is done with a single swarm particle. On the other hand, real experiments are conducted with only $10^3 - 10^6$ swarm particles, which is still so few (in comparison to the gas number density, n_0) that they can be treated

© Springer Nature Switzerland AG 2018 L. A. Viehland, *Gaseous Ion Mobility, Diffusion, and Reaction*, Springer Series on Atomic, Optical, and Plasma Physics 105, https://doi.org/10.1007/978-3-030-04494-7_1 2 1 Introduction

as if they do not interact with one another. Thus, the two definitions are consistent if the systems are studied over long periods of time, t, or over many repetitions of the same experiment.

In the language of plasma physics, our definition of a swarm means that we are looking at the test particle problem and the free diffusion regime of a weakly ionized plasma. The criterion (Mason and McDaniel 1988) for being in this regime is that

$$n << \frac{E}{4\pi L |q|},\tag{1.1}$$

where n is the ion number density, E is the electric field strength, q is the ion charge, and L is the length of the apparatus. Typical experimental values are E=200 V/m and L=0.010 m, so (1.1) predicts significant space-charge effects when there are more than about 10^{11} singly charged ions per cubic meter. Thus, charge–charge interactions are not generally a problem in swarm experiments, and we note that larger n can be tolerated in experiments at higher fields or in apparatus with smaller dimensions.

The first definition of a swarm lends itself to the description of a broader class of phenomena than is ordinarily considered to be part of swarm physics. Thus, we may include under the umbrella definition the following natural and laboratory phenomena: diffusion in the ionosphere; hot atom chemistry; multi-wire drift tubes in high-energy accelerators; the foreign-gas perturber problem in spectroscopy; muon-catalyzed cold fusion; neutron transport; positron annihilation in gases; ion traps used in mass spectrometry; ion mobility spectrometry; the Franck–Hertz experiment; the motion of hot charge carriers in semiconductors; and the dispersion of a passive additive in a turbulent atmosphere.

The above list is not complete, particularly since we have omitted the traditional area of swarm physics and chemistry: the drift, diffusion, and reaction of charged particles moving through a neutral gas with molar mass M_0 , pressure P_0 , volume V_0 and temperature T_0 as functions of T_0 and the reduced field strength, E/n_0 . Studies late in the nineteenth century of the motion of charged particles through dilute gases helped establish the existence of electrons and ions and laid the foundation of modern physics and chemistry. Experimental and theoretical studies of ion and electron swarms continue to be important, since a thorough understanding of charged particle motion through gases is important in such varied fields as atomic and molecular physics, aeronomy and atmospheric chemistry, gaseous electronics, plasma processing and laser physics. In short, there is more that unites all of these research and application areas than the emphases, terminology, and details that separate them.

1.2 Air and Vacuum Pumps

We start with a discussion of pumps, since they are essential to the study of gases at low pressure and hence to the study of gaseous ion mobility, diffusion and reaction. The predecessor to the modern pump was the suction pump known to the Romans;

dual-action suction pumps have been found in the ruins of Pompeii. Arab engineer Abu al-'Iz Ibn Isma'il ibn al-Razaz al-Jazari (1136–1206) described suction pumps in the early thirteenth century; he said that his model was a version of the siphons the Byzantines used to discharge "Greek fire". The suction pump reappeared in Europe in the fifteenth century.

By the seventeenth century, pump designs had improved to the point that they could produce a measurable vacuum, but this was not immediately understood. What was known was that suction pumps could not pull water beyond a certain height: 18 Florentine yards (about 10 m) according to a measurement taken around 1635. The explanation from the days of the ancient Greeks was that nature abhors a vacuum, so she would not allow you to create a perfect vacuum.

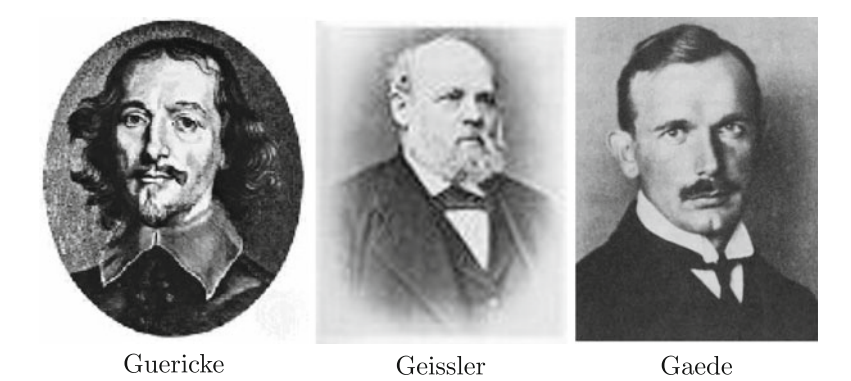


This limit was a concern for the irrigation and mine drainage projects, as well as the decorative water fountains, planned by the Duke of Tuscany, so the Duke commissioned Galileo Galilei (1564–1642) to investigate the problem. Galilei advertised the puzzle to other scientists, including Gasparo Berti (ca.1600–1643) who replicated it by building the first water barometer, in Rome in 1639. Berti's barometer produced a vacuum above the water column, but he did not recognize this. The breakthrough was made by Evangelista Torricelli (1608–1647) in 1643. Based upon Galilei's notes, he built the first mercury barometer and wrote a convincing argument in 1644 (not published until years later) that the space at the top was a vacuum. The height of the column was then limited to the maximum weight per unit area that the atmosphere could support.

Torricelli's experiments were repeated a little later in France by Blaise Pascal (1623–1662). In addition, Pascal showed that the variation of the atmosphere's pressure with altitude was consistent with a fixed height for the air surrounding the Earth. Nature does not abhor a vacuum; instead, most of nature is a vacuum!

Otto von Guericke (1602–1686) invented the first vacuum pump (an air pump that creates a near vacuum). He used it to show that sound will not travel in a vacuum. In 1654, before the leading figures of the German states at Magdeburg, Guericke placed two hemispheres together along a greased flange, removed the air within by using an air pump, and demonstrated that two teams of horses could not pull the pieces apart!

4 1 Introduction



In 1855, Heinrich Geissler (1814–1879) invented the mercury displacement pump and achieved a record low pressure of about 10 Pa. This pump consisted of a column of mercury that could be raised and lowered to decrease gradually the pressure in a closed container, until it reached the pressure of the mercury vapor. Geissler used his vacuum pump to investigate electrical discharges through a low-pressure gas. He found that light was emitted in such discharge tubes, with the color depending upon which gas was in the tube and the type of glass from which the tube was constructed.

Modern vacuum pumps are of three distinct types, although there are many variations of each type. A mechanical or reciprocating pump typically contains meshed gears that draw in gas from the region being evacuated and push it out into the atmosphere. To achieve high vacuums, a mechanical pump must be used as a roughing pump for either a diffusion pump or a turbomolecular pump.

The diffusion pump was invented in 1915 by Wolfgang Max Paul Gaede (1878–1945). It boils oil in a reservoir open to the region being evacuated, and the oil vapor and gas molecules escape through small holes into a reservoir that is externally cooled. The oil condenses and is pushed back into the first reservoir to be recycled. The gas is directed through an one-way valve into a region that is maintained at a reduced pressure by a mechanical pump.

In 1947, several people at Aerojet (now Aerojet Rocketdyne) in California invented the turbomolecular pump. In this device, a rapidly spinning fan moves gas molecules from the low-pressure inlet into a region that is maintained at a reduced pressure by a mechanical pump. Its advantages over the diffusion pump are that it does not consume as much energy (since no oil is being boiled), it avoids possible contamination from oil vapors, and it can achieve pressures lower than the vapor pressure of the oil; the disadvantage is that it is not as rugged, since the bearing for the spinning fan may not last long.

Although the equipment is somewhat expensive, it is now rather easy to obtain a high vacuum, i.e., pressures of 10^{-8} Torr (about 10^{-6} Pa). A leak valve can then be used to allow a steady flow of neutral gas into the apparatus, leading to a steady-state situation where gas is leaking into the drift tube at the same time the pumps are eliminating it. The steady-state value of P_0 is usually between 0.1 and 1 Torr (or 10-100 Pa) in a drift-tube mass spectrometer (DTMS) (see Sect. 2.2). This is the

first step in creating a low-pressure drift tube to measure the mobility, diffusion, and reaction rate coefficients of trace amounts of ions moving through a dilute gas.

In ion mobility spectrometry (IMS, see Sect. 2.8), one usually works with gases near atmospheric pressure. In such cases, only a mechanical pump may be needed.

1.3 Static Electricity

The ancient Greeks knew that rubbing amber with wool or fur causes the amber to attract lightweight objects. Not much was done about investigating this phenomenon scientifically until about 1600, when William Gilbert (1540–1603), an English physician, performed a series of experiments analogous to the following:



Gilbert

- 1. If we suspend a light object by a thread and then hold it near a piece of amber that has been rubbed with fur, the amber attracts the object. However, if the amber is allowed to touch the object, it will thereafter repel it.
- 2. A rubbed glass rod will behave the same way as a rubbed piece of amber. However, a light object that is repelled by rubbed amber will be attracted by rubbed glass, and vice versa.
- 3. If we suspend the rubbed amber and bring the rubbed glass rod near it (or vice versa), we observe an attraction between the two. On the other hand, two rubbed glass rods will repel each other, and two pieces of rubbed amber will also repel each other.

Gilbert concluded that rubbing some objects gives them what we now call an electrical charge, that there seem to be two kinds of electrical charge, that we can produce both kinds by rubbing the appropriate materials, and that the following law is experimentally true: like charges of electricity repel each other, while unlike charges attract each other.

The experiments showed that electric charges can be transferred from one object to another by contact. Furthermore, the amount of electric charge is finite, since rubbed amber gradually can have its charge depleted by touching it to enough other objects (although it can be restored by rubbing the amber again). Additional experimentation

showed that objects possessing opposite kinds of electric charge, if allowed to touch, will neutralize each other, and that some materials (called insulators) will not allow electricity to pass while others (called conductors) will.



The experiments described above led naturally to the two-fluid theory of electricity proposed in 1733 by the French chemist Charles Francis de Cisternay Du Fay (1698–1739). According to this theory, there are two types of electricity on a microscopic level, which we now call positive and negative.

A one-fluid theory of electricity was proposed in 1746 by Benjamin Franklin (1706–1790), the first American scientist to gain worldwide fame (through his work with electricity). It was proposed independently by William Watson (1715–1787), the first person to describe the continuous discharge of electricity through a rarefied gas. According to this theory, there is only one kind of electric fluid, and the behavior we describe as "positive" results from having an excess of this fluid while "negative" behavior results from having a deficiency.

Which of the above theories of static electricity is correct? Both have some convenient features, so we currently use whichever best fits a particular application that we have in mind. We usually talk in terms of two types of electricity, positive and negative charge, whereas we usually solve problems in electricity by ignoring the positive charge and pretending that only one fluid (the negative one) flows through a circuit. Moreover, we usually express the law of conservation of charge in terms of the two-fluid theory by stating that the creation of a certain amount of positive charge is always accompanied by the simultaneous creation of an equal amount of negative charge; this law is more easily justified in terms of the one-fluid theory.

The flexibility in describing electricity in terms of either theory above is similar to the flexibility used in describing light. In some circumstances, we treat light as particles (photons) and in others we treat it as waves.

1.3 Static Electricity 7





Cavendish

Coulomb

Experiments show that the attractive and repulsive forces due to electric charges are experienced between objects "at a distance", that is, between objects that are not in direct contact. The fact that the electrical forces are inversely proportional to the square of the distance was discovered by the English scientist Henry Cavendish (1731–1810), the discoverer of hydrogen. However, his results were not published during his lifetime, so the credit of discovery is given to the French physicist Charles Augustin Coulomb (1736–1806), who discovered it independently in 1785. The law is

$$F = \frac{q_1 q_2}{4\pi \varepsilon_0 r^2},\tag{1.2}$$

where F is the electrical force and where q_1 and q_2 are the charges of the two objects that are separated by a the distance r. The 2014 CODATA value of the electric constant is $\varepsilon_0 = 8.854187817 \times 10^{-12} \, \mathrm{C}^2/\mathrm{Nm}^2$.

The electrical potential energy, E_p , is the negative of the integral of the electrical force with respect to distance. It can be shown from (1.2) to be given by the formula

$$E_p = \frac{q_1 q_2}{4\pi \varepsilon_o r}. (1.3)$$

The electrostatic potential energy is zero when the charges are infinitely far apart, it is always positive when two charges of the same sign interact, and it is always negative when charges of the opposite sign interact.

1.4 Current Electricity

Until about 1780, all studies of electricity involved static electricity. Although successive improvements were made in devices for generating, storing, and using electricity, experimenters were limited by the characteristics of static charges. Current electricity was discovered at the end of the eighteenth century as the outgrowth of research by Luigi Galvani (1737–1798) and Alessandro Giuseppe Antonio Anastasio Volta (1745–1827). Galvani experimented with frog legs, showing that a powerful contrac-

tion could be caused by contact of the nerves and muscles with a circuit composed of dissimilar metals. Galvani's explanation, consistent with the dominant thought of the time that the world could be separated into living and nonliving things, was that this twitching was a manifestation of animal electricity.





Galvani Volta

At first, Volta accepted Galvani's idea of animal electricity. However, he soon found it necessary to modify this theory because dissimilar metals (more precisely, dissimilar metal–metal oxide layers, e.g., Cu-CuO with $Al-Al_2O_3$) when brought into contact with each other and touched to the tongue, cause a bitter taste. More spectacularly, when brought into contact and touched to the eye, dissimilar metals cause a sensation of light.

Further studies by Volta demonstrated that an electrical force is generated when two dissimilar metal disks are separated by a moist conductor and brought into contact with a wire. Eventually, he developed a "Voltaic pile", the first battery, shown along with his picture. When such a battery delivers a direct current, I, for a period of time, Δt , the amount of charge that travels through the circuit is $q = I \Delta t$. The units of electrical charge, electric current, and time are therefore related, with 1 C = 1 As. Finally, if the electromotive force (emf, measured in volts) of the battery is ε_V , then the change in energy experienced by the battery is $\Delta \varepsilon = q \varepsilon_V$, where the units are such that 1 J = 1 CV.

Volta also studied a somewhat more sophisticated source of current electricity, one that is now often an experiment in first-year chemistry labs. Suppose one has a piece of zinc metal partially immersed in a ZnSO₄ solution contained in one beaker and a piece of copper metal partially immersed in a CuSO₄ solution contained in a second beaker. A U-shaped tube filled with a gelatin made from an aqueous solution of either ZnSO₄ or CuSO₄ is used to connect the two beakers, thus connecting the solutions electrically but keeping them separate physically. When wires are used to connect dry spots on the two pieces of metal of this galvanic cell to the two leads of an electroscope (thereby completing the circuit), the electroscope indicates that current is flowing. Zinc metal disappears into its solution (which becomes more concentrated in zinc sulfate), while copper metal is plated out onto the copper electrode (the copper solution becomes less concentrated in copper sulfate). A galvanic cell like this makes it possible to obtain electric energy directly from a chemical reaction!

As a result of his studies, Volta announced in 1800 that a flow of electric charge can be generated by chemical as well as physical means such as rubbing. If so, can an electric current produce a chemical reaction? The answer to this question was provided within weeks of Volta's announcement, through an accidental discovery by two English chemists, William Nicholson (1753–1815) and Anthony Carlisle (1768–1840). While experimenting with a Voltaic pile, they added a drop of water to get better contact between the two metals. They noticed the immediate formation of a gas at the juncture. Chemical tests revealed some of the gas to be hydrogen. More precise measurements disclosed that water decomposes to yield two volumes of hydrogen and one volume of oxygen if the gases are compared at the same T_0 and P_0 . Thus, they found that water is not an element, and that its formula must be H_2O .

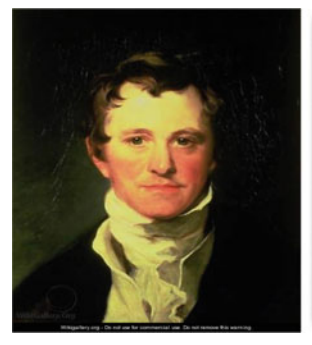


The story in the previous paragraph illustrates the role of accidental discovery in science. It should be noted, however, that in the hands of untrained, unobservant, or less astute people, the formation of gas might have been ignored. As Louis Pasteur (1822–1895) has pointed out, chance favors the mind that is prepared! The story also illustrates that scientific discoveries are not made in a technological and cultural vacuum. Nicholson and Carlisle could not have made their discovery without the source of current electricity provided by Volta, and their work would not have been appreciated except that the "climate" was just right for these ideas. Almost immediately, practical use was made of electrolysis by the English chemist Humphry Davy (1778–1829), who in 1807 isolated two new elements (sodium and potassium) through electrolysis of their molten hydroxides.

1.5 Faraday's Laws of Electrochemistry

The work of Galvani and Volta showed that chemistry and electricity are intimately connected. Much effort was devoted in the early 1800s to trying to understand this connection. This research led Michael Faraday (1791–1867) to suspect that there was a quantitative relationship between the amount of substance decomposed in a battery and the quantity of current that passed through the external circuit. The discovery of this relationship was not easy because side reactions frequently complicated the results. However, Faraday's work proceeded smoothly after he developed

the coulometer, an electrolytic cell designed so that the gases evolved in the decomposition of water could be collected and measured.





Davy

Faraday

Faraday's findings can be summarized by two laws that he presented in 1833:

- 1. The mass of a given material deposited at (or removed from) an electrode by a given amount of electricity is always the same.
- 2. The masses of different materials deposited at (or removed from) an electrode by a fixed amount of electricity have a ratio that is proportional by small integers to the ratio of the molar masses of these substances.

Faraday's laws of electrochemistry should have assisted the chemists of that day in solving their big problem—the simultaneous determination of molar masses for the elements and molecular formulas for the compounds. It did not, primarily because establishing the second law of electrochemistry required the use of previously known molar masses for particular compounds, so circular reasoning seemed to be involved.

Faraday's second law of electrochemistry is analogous to the law of definite proportions, which originally suggested the existence of atoms. If a fixed number of atoms react with only a fixed amount of electricity, it seems reasonable to suppose that electricity itself is composed of particles. An elementary electrode process must therefore involve each molecule combining with or losing a small, integer number of these electrical particles. Only after the work of Stanislao Cannizzaro (1826–1910) in 1858 was it possible to draw this implication. In 1875, George Johnstone Stoney (1826–1911) suggested the existence of fundamental particles of electricity.







Stoney

1.6 Electrical Conduction 11

1.6 Electrical Conduction

Many people had observed in the early 1800s that two wires carrying electric current produce a spark when separated, and that this spark jumps further when the air is at a reduced pressure. In 1838, Faraday decided to see how the spark would behave in the absence of air. He sealed two wires into opposite ends of a glass tube, removed the air with a vacuum pump and noticed that the gas began to conduct electricity while a greenish glow appeared inside the tube.





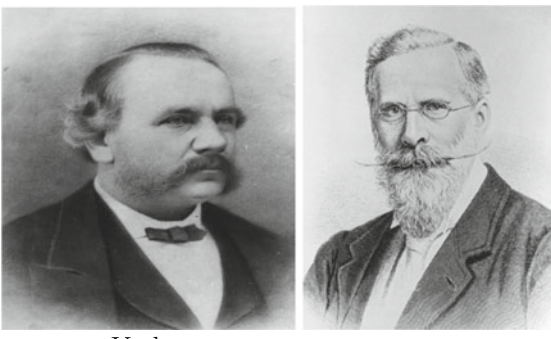
Plücker

Hittorf

Julius Plücker (1801–1868) discovered that electrical conduction created by an induction coil persists as the gas pressure is lowered from 1 kPa to 10 Pa, but that the luminosity of the gas decreases. He showed in 1858 that the conduction is influenced by a magnet, and in 1865 that the glow on the walls of the tube can be affected by an external magnet. In 1869, this green glow was shown by Johann Wilhelm Hittorf (1824–1919) to be the result of the bombardment of the glass by "rays" that originate at the cathode and travel in straight lines until they strike the anode or the walls.

Cromwell Fleetwood Varley (1828–1883) was the first person to publish the suggestion that cathode rays are composed of particles. In the same year, 1871, William Crookes (1832–1919) proposed, incorrectly, that they are molecules that have picked up a negative charge from the cathode and are repelled by it.

In 1874, Stoney used the Faraday constant and Avogadro's number (2014 CODATA values, $96485.33289~C~mole^{-1}$ and $6.022140857 \times 10^{23}~mole^{-1}$, respectively) to estimate the charge on each cathode ray particle. Stoney proposed the name "electrine" for the negatively charged part of a hydrogen ion, but in 1891 he changed the word to electron.



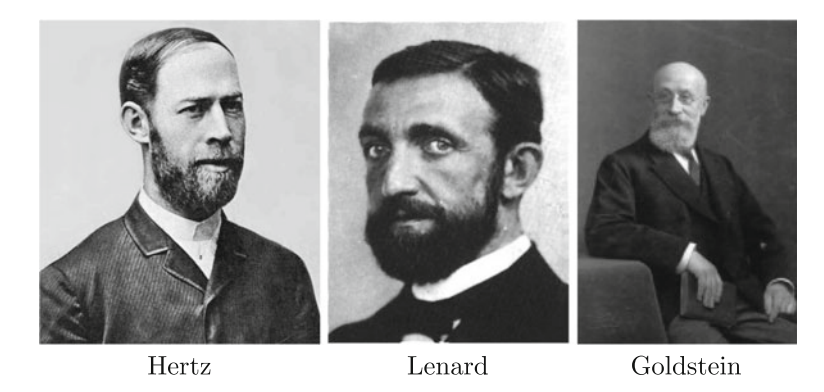
Varley Crookes

The purposeful investigation of cathode rays began in 1879 by Crookes, whose name is most often associated with cathode ray tubes. He reasoned that if cathode rays could be stopped before they reached the end of the tube, the intense green glow would disappear. He therefore introduced barriers into the tube and studied their shadows and the influence that magnets had on the shadows. In this way, Crookes obtained or confirmed the following experimental results:

- 1. At very high vacuum, cathode rays travel in straight lines.
- 2. Flat cathodes produce more clearly defined shadows than point cathodes, as would be expected from projected, mutually repelling particles coming from the cathode.
- 3. A magnet causes deflection of the cathode rays, like a magnet causes on a loose wire carrying an electrical current.
- 4. When cathode rays are focused, an intense heating effect is observed, implying that cathode rays are composed of particles with appreciable mass.
- 5. The cathode rays produced have the same properties, regardless of the composition of the cathode or what gas is used.

From these results, Crookes hypothesized that cathode rays consist of streams of negatively charged particles emanating at high speed from the cathode of the tube. The implication of Crookes' fifth point is that these particles lie inside every atom. This violation of the basic premise of atomic theory led many other people to argue that these were instead "aether waves", some new form of electromagnetic radiation. Among the latter were Heinrich Rudolph Hertz (1857–1894) and Philipp von Lenard (1864–1947). In 1892, Lenard developed a cathode ray tube with a thin aluminum window that permitted the rays to escape into the open air. Hertz also showed that cathode rays can penetrate thin metal foils, a fact that he used as support for his belief that cathode rays were really light waves. The exact nature of cathode rays remained unknown until they could be related to canal rays and ions.

1.7 Ions 13



1.7 Ions

In 1886, Eugen Goldstein (1850–1930) experimented with a gas discharge tube that had a perforated cathode. When a high electrical potential (several thousand volts) is applied between the cathode and anode, faint luminous "rays" are seen extending from the holes in the back of the cathode. These rays are beams moving in a direction opposite to the cathode rays. Goldstein called these positive rays "canal rays" because of the holes (canals) that he bored in the cathode in order to discover them.



Wien

In 1898, Wilhelm Wien (1864–1928) showed that canal rays are the positive equivalent of the negatively charged cathode rays. He measured their deviation due to magnetic and electric fields and concluded that they are composed of heavy, positively charged particles. In 1907, a study of how canal rays are deflected in a magnetic field showed that the particles making up the rays were not all the same mass. The lightest ones, formed when there was some hydrogen gas in the tube, are 1836.15267389 (2014 CODATA value) times as massive as a cathode ray particle; they are now called protons.

If we assume that positively charged atoms or molecules exist, then the process by which canal rays are formed in a gas discharge tube can be described as follows. When a high voltage is applied to the cathode ray tube, the electric field accelerates the small

number of electrons or ions that may be present in the gas due to natural processes such as radioactivity. These collide with atoms of the gas, knocking negative particles off them and creating more positive ions. These ions in turn strike more atoms, creating more ions in a chain reaction. The negative particles are attracted to the positive anode; these are the cathode rays moving from the cathode to the anode. The positive ions are attracted to the negative cathode, and some pass through the holes in the cathode; these are the canal rays moving from the anode toward the cathode.

Before they reach the cathode, the cathode rays have been accelerated to a fast enough speed that when they collide with other atoms in the gas they excite the atoms to a higher energy level. When these atoms return to their former energy levels, they release the excess energy as light.

Using such a device, Joseph John Thomson (1856–1940) announced in 1894 that the speed of cathode rays is 1.9×10^5 m/s, thus finally proving that they are not a form of light, which has a much higher speed in air. A similar conclusion was reached in 1895 by Jean-Baptiste Perrin (1870–1942), who showed that cathode rays deposit a negative electric charge where they impact, a result never obtained with light.







Thomson

Perrin

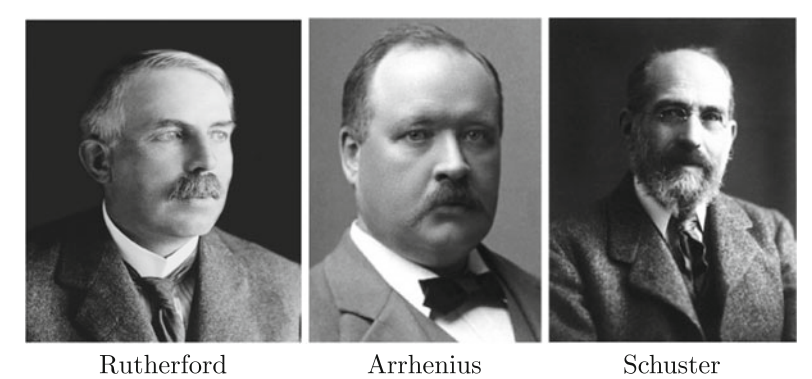
Roentgen

On November 8, 1895, Wilhelm Konrad Roentgen (1845–1923) was experimenting with cathode rays. According to the biography by Glasser (1934): "He had covered the [cathode ray] tube with pieces of black cardboard and had darkened the room in order to test the opacity of the black paper cover. Suddenly, about a yard from the tube, he saw a weak light that shimmered on a little bench he knew was nearby ... Highly excited, Roentgen lit a match and, to his great surprise, discovered that the source of the mysterious light was a little barium platinocyanide screen lying on the bench." Barium platinocyanide was known to fluoresce under ultraviolet light, but no such light was present. Cathode rays were known to be stopped by only a few centimeters of air. Therefore, the glow must be a new source of radiation, named X-rays.

Soon after Roentgen's discovery, several scientists observed that X-rays also make gases become electrical conductors. In 1896, Thomson and Ernst Rutherford (1871–1937) showed that the gas conduction produced by X-rays behaved very similarly to

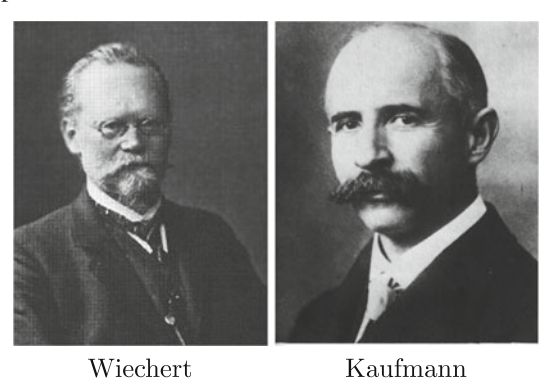
1.7 Ions 15

cathode rays. All of these results could be explained by assuming that the conduction was due to the production of small charged particles in the gas.



Thomson and Rutherford soon established that the conductivity produced by X-rays is due to the movement of electrical charges of both signs. The electrical conductivity decays with time after the radiation is stopped, which they attributed to recombination of the positive and negative carriers of electricity that were present in the apparatus, and to diffusion of these charge carriers from the gas to the walls.

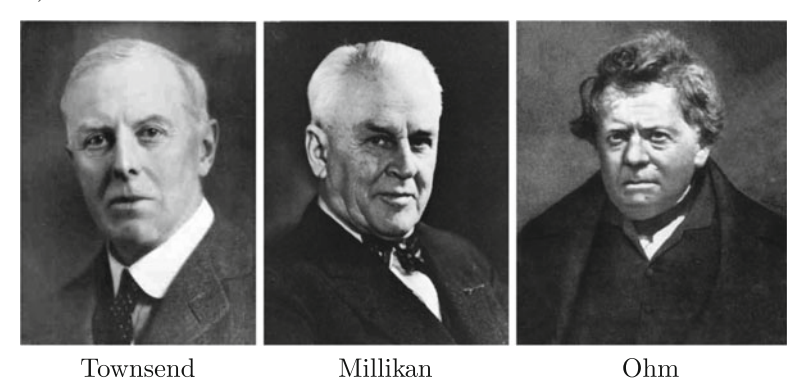
Because of the pioneering work of Svante August Arrhenius (1859–1927), the charge-to-mass ratio, q/m, of most of the ions commonly found in aqueous solutions had been obtained by the mid-1890s, from electrolysis experiments. Franz Arthur Friedrich Schuster (1851–1934) determined an imprecise value of this ratio for cathode ray particles in 1890.



Thomson, Emil Johann Wiechert (1861–1928) and Walter Kaufmann (1871–1947) recognized that an accurate determination of q/m would help identify the cathode ray particles. Accordingly, they each, independently, measured it in 1897 by using what would now be called a swarm apparatus in which a magnetic field bent the rays. The 2014 CODATA value of this ratio is $1.758820024 \times 10^{11}\,\mathrm{C\,kg^{-1}}$. This value is 1.836.15267389 times larger than that for H⁺, which has the largest value for any atomic or molecular ion. These results from swarm experiments led Thomson to announce, on April 30, 1897, that cathode rays are not charged atoms but instead are

small charged objects (electrons) that are contained in all atoms. More information about the discovery of the electron is given by Pais (1997).

The first direct determination of the charge of the electron was made in 1898 by John Sealy Edward Townsend (1868–1957). An accurate value was finally determined in the famous oil-drop experiment of Robert Andrew Millikan (1868–1953) in 1909; the 2014 CODATA value is $1.6021766208 \times 10^{-19}$ C.



1.8 Ion Swarms, 1896–1928

Thomson and Rutherford discovered in 1896 that gaseous ions whose identity does not change drift under the influence of an electrostatic field with an average velocity, called the drift velocity, that is proportional to the field. Thus,

$$\mathbf{v}_d = K\mathbf{E},\tag{1.4}$$

where \mathbf{v}_d is the ion velocity vector, \mathbf{E} is the electric field vector, and the scalar, K, is the ion mobility. Equation (1.4) is equivalent to Ohm's Law, named after George Simon Ohm (1789–1854), with 1/K playing the role of the electrical resistance. This vector equation indicates that the drift velocity lies along z, the Cartesian axis that lies along direction of the electric field, and that the basic SI unit for K is $\mathbf{m}^2/\mathbf{V}\mathbf{s}$. This unit for K is of appropriate size for electron mobilities, but ions move through gases so much more slowly that it is customary to report their mobilities in $\mathbf{cm}^2/\mathbf{V}\mathbf{s}$.

The magnitude of \mathbf{v}_d is often called the drift velocity, even though v_d is technically the average speed of the ions as they drift along the field whose magnitude is E. It may be noted in passing that some people, especially those involved with electron mobilities, use the symbol μ rather than K.

The transit time of an ion through a gas is controlled by the huge number of collisions that it makes with the atoms or molecules of the neutral gas. If we ignore end and injection effects that will be discussed later, this transit time must be inversely proportional to v_d and hence, by (1.4), inversely proportional to K. Consequently, the mobility of ions of unchanging identity as they move through a gas must be related

to the fundamental physics of ion–neutral collisions, which accounts for much of the interest in drift tubes among theoretical chemists and physicists for more than 100 years.

This is an appropriate point to mention that there are two ways to calculate v_d . The experimental way assumes that there are no end or injection effects and uses the formula,

$$v_d = L/\langle t \rangle, \tag{1.5}$$

where $\langle t \rangle$ is the average time that it takes an ion to move through the drift tube. The theoretical way is to compute it as the integral,

$$v_d = \int_0^\infty v f(v) dv, \tag{1.6}$$

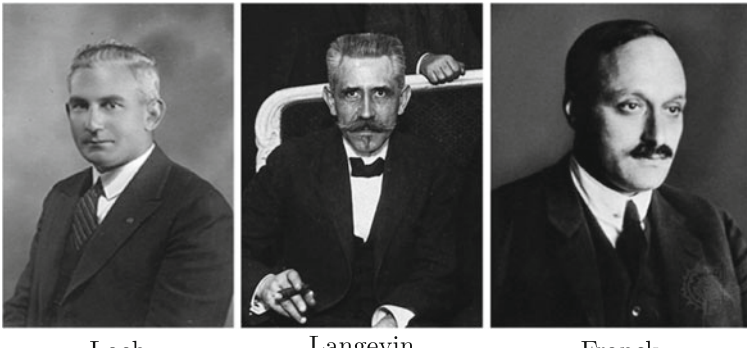
where f(v) is the ion speed distribution function, i.e., the fraction of ions that have a particular speed, v, along the field, within the interval from v to v+dv. The difference between these definitions is sometimes referred to as arising from non-hydrodynamic contributions that add to the other end effects in the drift tube. The difference can be written as a power series in 1/L (England and Elford 1987; Standish 1987; Kondo and Tagashira 1993). This means that correction factors must be incorporated into the analysis of small drift tubes, but this topic will not be covered in this book, where we assume that L is large enough ($L \gtrsim 0.01$ m) that there is no difference.



Zeleny Tyndall

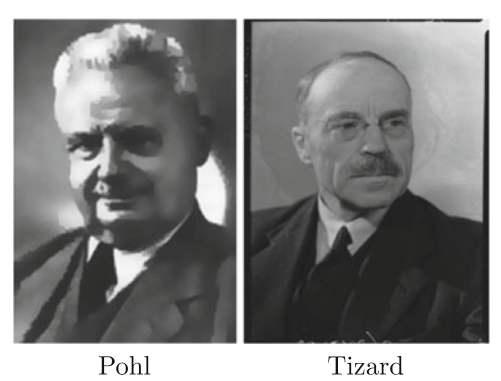
In 1897, Rutherford published the first table of ion mobilities. These values were superseded by the more accurate results that John Zeleny (1872–1951) published in 1898 and 1900. Zeleny was the first to establish conclusively that the charge carriers in an ionized gas move at different velocities and hence have different mobilities. For the next 30 years, there was slow but steady progress in measuring mobilities for more ion–neutral systems and with greater accuracy, and in measuring the recombination

rates of ions and electrons. A detailed description of the many problems encountered, and the apparatus developed to overcome them, is given in the 1938 book by Arthur Mannering Tyndall (1881–1961) and in the (1955) book by Leonard Benedict Loeb (1891-1979).



Langevin Loeb Franck

The dependence of the mobility upon the gas pressure was first investigated by Rutherford in 1898. In the more extensive experiments of Paul Langevin (1872–1946) in 1902, it was found that the mobilities of positive ions are inversely proportional to the pressure, except at low pressures. The inverse relationship between K and P_0 is not surprising, given that collisions control the transit time of ions through the gas.



The studies of James Franck (1882–1964) and Robert Wichard Pohl (1884–1976) in 1910, of Robert Tabor Lattey (1881–1967) in 1910, and of Lattey and Henry Thomas Tizard (1885-1959) in 1912 established that low-pressure deviations are due to the influence of small amounts of contaminant gases, in particular, the ability of these contaminants to react chemically with the ions and/or cause negative ions to transform to free electrons. Much of the interest in drift tubes among experimental chemists and atomic physicists is due to the fact that they can be used to study such reactions in considerable detail.

The inverse proportionality between K and P_0 implies that there is a similar relationship between K and n_0 . This in turn allows a standard mobility, K_0 , to be defined by the equation

$$K_0 = \frac{n_0 K}{N_0},\tag{1.7}$$

where N_0 is the number density (2014 CODATA value is 2.6867811 \times 10²⁵ m⁻³) of an ideal gas at $P_0 = 101.325$ Pa and $T_0 = 273.15$ K. N_0 is called the Loschmidt constant in honor of Johann Joseph Loschmidt (1821–1895).

Note that in this book, we put 0 subscripts on properties of the neutral gas or on quantities that involve both the charged particles and the neutrals. It is worth noting that experimenters often calculate the standard mobility from the measured values of P_0 and T_0 , via the equation

$$K_0 = K \left(\frac{P_0}{101.325 \,\text{kPa}} \right) \left(\frac{273.15 \,\text{K}}{T_0} \right). \tag{1.8}$$

The two equations give identical results if the gas obeys the ideal gas equation; it is possible to incorporate the compressibility factor into (1.8) if one is going to work at pressures where the ideal gas equation is not accurate enough.



Loschmidt

Huxley

Equation (1.7) takes care of the pressure dependence of the mobility, but the standard mobility turns out to depend upon the experimental parameters that affect the average energy of the ion swarm. Therefore, it is now customary to report values of K_0 as a function of E/n_0 and T_0 , either in the form of graphs such as Fig. 1.1 or in the more usual form of tables (Ellis et al. 1976, 1978, 1984; Viehland and Mason 1995; Viehland database 2018). Because of its importance in swarm research, the basic unit for E/n_0 has been given a special name by Leonard George Holden Huxley (1902–1988) et al. (1966); it is the Townsend, with 1 Td = 10^{-21} V m².

The reason that E/n_0 is an important parameter for swarm experiments can be seen from the following argument from the 1973 book by Earl Wadsworth McDaniel (1926–1997) and Edward Allen Mason (1926–1994). The electrical force on an ion of charge q and mass m is qE, and the resulting acceleration is qE/m. If τ_c is

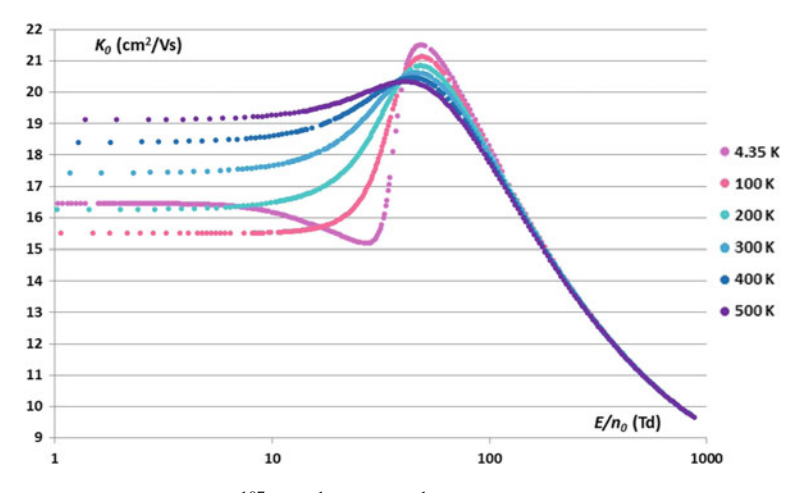


Fig. 1.1 Standard mobility of ${}^{107}\text{Ag}^+({}^{1}\text{S}_0)$ in $\text{He}({}^{1}\text{S}_0)$ at various T_0

the mean free time between collisions, the additional speed acquired just before a collision is $q E \tau_c/m$ and the additional kinetic energy acquired is $(q E \tau_c)^2/2m$. Since τ_c is inversely proportional to n_0 , the additional energy required is proportional to $(E/n_0)^2$. More generally, gaseous ion transport coefficients depend upon the ratio E/n_0 , not separately upon E and E/n_0 .

At fixed T_0 and low E/n_0 , K_0 can be written as a power series in the square of E/n_0 :

$$K_0(E/n_0, T_0) = K_0(0, T_0) \left[1 + c_2(E/n_0)^2 + c_4(E/n_0)^4 + \ldots \right]$$
 (1.9)

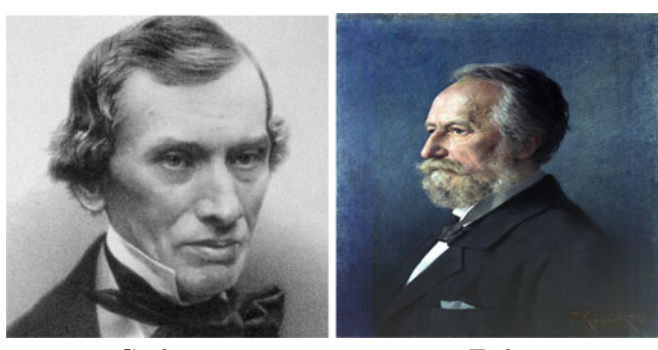
The reason that only even powers of E/n_0 appear in (1.9) is easy to see. Suppose the electric field originally defined the +z axis but that we decide to change the coordinate system so that +z becomes -z. Since nothing changes about the physical apparatus, this requires the electric field vector to change from \mathbf{E} to $-\mathbf{E}$ and the drift velocity vector to change from \mathbf{v}_d to $-\mathbf{v}_d$. Equation (1.4) shows that the mobility is the proportionality constant between these vectors, so its value cannot change. In order for K_0 to remain unchanged when \mathbf{E}/n_0 changes sign, only even powers of E/n_0 can occur in (1.9). It should be noted, however, that (1.9) has a limited radius of convergence (see Appendix A). At intermediate and high E/n_0 , it is generally better to give the mobility as a table or graph than to try to relate it to $K_0(0, T_0)$.

The zero-field mobilities at room temperature of relatively stable ions in mixtures of hydrogen, air, and carbon dioxide were measured by Blanc (1908), as functions of the gas composition. The result now known as Blanc's law is that

$$\frac{1}{K_{0,mix}(0,T_0)} = \sum_{j} \frac{x_j}{K_{0,j}(0,T_0)},$$
(1.10)

where x_j is the mole fraction of pure gas j and where subscripts have been added to the standard mobility to indicate whether it is for the gas mixture or a pure gas. This formula is easily understood by remembering that the reciprocal of the mobility is proportional to the electrical resistance of the gas, that the molecules in a gas act so independently that a mixture can be thought of as a succession of pure gases present in amounts proportional to the mole fractions, and that the resistance in a series circuit is the sum of the individual resistances.

1.9 Ion Diffusion, 1855–1926



Graham Fick

The first systematic study of diffusion was that of Thomas Graham (1805–1869) between 1828 and 1833. It involved the diffusion of one neutral gas through another. However, the fundamentals of diffusion (Philibert 2006) were established in 1855 by Adolf Eugen Fick (1829–1901).

Fick observed that the flux of mass in a nonequilibrium system that was not influenced by an external field is directly proportional to the density gradient. The gradient of the ion number density is written as ∇n and defined so that it has components along each of the three Cartesian axes. Thus,

$$\nabla_z n = \frac{\partial n}{\partial z} \tag{1.11}$$

along z, and similarly for $\nabla_x n$ and $\nabla_y n$. Therefore, Fick's First Law for ion diffusion is

$$\mathbf{j} = n \langle \mathbf{v} \rangle = -D \nabla n, \tag{1.12}$$

where **j** is the ion flux vector, D is the scalar diffusion coefficient, and $\langle \mathbf{v} \rangle$ is the average velocity vector of the ion swarm.

When applied to a moving ion swarm in three dimensions, Fick's first law relates the space and time dependences of \mathbf{j} to ∇n and the ion drift velocity, \mathbf{v}_d . If we let \mathbf{r} be the separation vector that locates the ion swam with reference to some arbitrary origin and then assume that n depends upon \mathbf{r} and t while t0 do not, then

$$\mathbf{j}(\mathbf{r},t) = \mathbf{v}_d n(\mathbf{r},t) - D \nabla n(\mathbf{r},t) = K \mathbf{E} n(\mathbf{r},t) - D \nabla n(\mathbf{r},t). \tag{1.13}$$

Note by comparing (1.12) and (1.13) that $\langle \mathbf{v} \rangle$ and \mathbf{v}_d differ because of the gradient of the ion number density.

To proceed further, we need the equation of continuity. To obtain this equation, consider an ensemble of ions diffusing through an infinite medium that contains no sources of sinks for the ions. By definition of $\mathbf{j}(\mathbf{r},t)$, the net leakage outward through an arbitrary, three-dimensional closed surface within the medium is $\int \mathbf{j}(\mathbf{r},t) \cdot d\mathbf{\tilde{A}}$, where $d\mathbf{\tilde{A}}$ is a vector (pointing outward) whose magnitude is the infinitesimal area of the surface being considered and \cdot indicates the scalar product of the two vectors it connects. Gauss' Law from vector calculus (see Appendix A) shows that this leakage may also be expressed as $\int \nabla \cdot \mathbf{j}(\mathbf{r},t) d\hat{V}_0$, where \hat{V}_0 is the volume bounded by the surface. Since this leakage must create a decrease in n within \hat{V}_0 , it follows that

$$\int \nabla \cdot \mathbf{j}(\mathbf{r}, t) d\widehat{V}_0 = -\int \left[\frac{\partial}{\partial t} n(\mathbf{r}, t) \right] d\widehat{V}_0$$
 (1.14)

or

$$\frac{\partial}{\partial t}n(\mathbf{r},t) + \nabla \cdot \mathbf{j}(\mathbf{r},t) = 0, \qquad (1.15)$$

where $\frac{\partial}{\partial t}$ represents the partial derivative with respect to time (see Appendix A). Equation (1.15) indicates that the number of ions is conserved because there is no source or sink (i.e., there is no term on the right-hand side).

In an experiment with a weak, uniform electrostatic field, \mathbf{v}_d and D are independent of time and position. Then (1.13) and (1.15) can be combined to give the left-hand side of the equation,

$$\frac{\partial}{\partial t}n(\mathbf{r},t) + \mathbf{v}_d \cdot \nabla \cdot n(\mathbf{r},t) - D\nabla^2 n(\mathbf{r},t) = -n(\mathbf{r},t)n_0 k, \qquad (1.16)$$

a result known as Fick's second law or the diffusion equation for a weak, uniform electrostatic field. The right-hand side describes the rate of loss of ions due to reactions with neutral molecules. The loss is proportional to the first powers of the ion and neutral number densities, so it is called a second-order reaction overall. The reaction rate coefficient, k, must be independent of position and time, since we have assumed this to be true of the transport coefficients on the left of (1.16). Finally, $\nabla^2 = \nabla \cdot \nabla$ is the Laplacian (Laplace operator) discussed in Appendix A.





Maxwell

Boltzmann

The practical application of (1.16) requires that it be supplemented with terms describing the gain and loss of ions from external sources and sinks, with initial conditions, and with boundary conditions describing the influence of the walls. In the early days of swarm research, little information was available about these supplementary terms and conditions, so it was not possible to extract values of \mathbf{v}_d , D and k by matching the solution of this partial differential equation (see Appendix A) to the observed values of $n(\mathbf{r}, t)$. We will return to this topic in Sect. 2.4.

The problem of how to measure the diffusion coefficients of ions in gases was first solved by Townsend in 1899. He obtained the diffusion coefficients at low E/n_0 from the loss of ions to the walls as an ionized gas flowed through narrow metal tubes. In the same 1899 paper, Townsend also deduced from the kinetic theories of James Clerk Maxwell (1831–1879) and Ludwig Edward Boltzmann (1844–1906) an important relationship between the mobility and the diffusion coefficient of a gaseous ion. The formula had been obtained previously by Hermann Walther Nernst (1864–1941) in 1889 for ions in solution, and it was used later by Albert Einstein (1879–1955) in his 1905 investigation of Brownian motion. It is now known as the Nernst–Townsend–Einstein equation, or more simply as the NTE equation.







Einstein



Mack

The two forms of the NTE are

$$K_0(0, T_0) = \frac{qD(0, T_0)}{k_B T_0} = \frac{QD(0, T_0)}{RT_0},$$
 (1.17)

where R is the molar gas constant (2014 CODATA value 8.3144598 J/mole K), k_B is Boltzmann's constant (2014 CODATA value 1.68064852 \times 10⁻²³ J/K) and Q is the molar ion charge. The notation used in (1.17) indicates that it applies to the standard mobility and the diffusion coefficient at any T_0 but only in the limit $E/n_0 \rightarrow 0$. Townsend found in 1900 that D is inversely proportional to P_0 , as predicted by the kinetic theories of Maxwell and Boltzmann.

It is often overlooked that Edward Mack, Jr. (1893–1956) and colleagues (Mack 1925; Melaven and Mack 1932; Everhart et al. 1932) made surprisingly accurate measurements of the diffusion coefficients of neutral molecules in gases and extracted structural information (the momentum-transfer collision integral discussed in Sect. 1-11) from their data. Unfortunately, such experiments were not conducted for gaseous ions until many years later.

Combining (1.10) and (1.17) shows that in mixtures of neutral gases the ion diffusion coefficient at low E/n_0 also obey Blanc's law. Thus,

$$\frac{1}{D_{mix}(0, T_0)} = \sum_{j} \frac{x_j}{D_j(0, T_0)}.$$
 (1.18)

It is crucial to note that (1.17) and (1.18) are applicable only in the limit of vanishingly small values of E/n_0 . At intermediate and high E/n_0 , the diffusion coefficient becomes a diagonal tensor, \mathbf{D} , of rank two (see Appendix A) with two independent components, D_L and D_T , that characterize diffusion parallel and perpendicular to the electric field. It is now customary (Ellis et al. 1978, 1984; Viehland and Mason 1995) to report values of n_0D_L and n_0D_T as a function of E/n_0 and T_0 . Finally, it is possible to make expansions of n_0D_L and n_0D_T at fixed T_0 in even powers of E/n_0 , equivalent to (1.9), but we will not make use of such expansions in this book.

1.10 Electron Swarms, 1900–1922

Electrons may be produced by thermionic emission from filaments, by photoemission from surfaces, or by beta decay of radioactive elements. The production of ions, on the other hand, is much more difficult, usually being achieved by electron bombardment of neutral precursors, photoionization, electrical discharge, or by ion—neutral reactions in a source region separated from the drift tube. In addition to being easier to produce, electrons are easier to identify—their high speeds are almost a unique signature, whereas ions can be conclusively identified only with mass spectrometers. Therefore, it is somewhat surprising that the drift velocities (and hence mobilities) of electrons in gases were not measured until 15 years after the discovery of electrons.

The first reason for the belated study of electron transport is that the drift velocities and diffusion coefficients of electrons in gases are three orders of magnitude larger than those for ions, due to the very small electron mass. Accurate measurement of these large values was difficult in the early 1900s.

The second reason also is due to the small mass of electrons, since this means that electrons are accelerated much more rapidly by an external field than are ions. In turn, this means that small imperfections in the electrodes present in an apparatus, small contact potentials, and weak magnetic fields can have larger effects on the measured transport properties of electrons than of ions.

The third reason is that charged particles lose kinetic energy, when colliding with a neutral, in a manner that depends on the ratio of their mass to that of the neutrals. Hence, electrons lose energy by collisions at a much slower rate than do ions. This means that electrons can easily achieve kinetic energies at which inelastic collisions with molecular contaminants are critical determinants of their motion.

The final reason is that the ion–neutral reactions that occur in swarm experiments are qualitatively different from two special electron-neutral reactions that are frequently observed. The first of these was discovered in 1900, when Townsend used an apparatus in which the electrode separation could be varied and showed that, at fixed E/n_0 , the current increases as the separation increases. He proposed a qualitative explanation that has since been provided a solid theoretical foundation: in drifting through a gas at high E/n_0 , the electrons gain enough energy that ionization occurs when they subsequently collide with gas molecules. The new electrons behave similarly, ionizing molecules at the same linear rate that is proportional to Townsend's first ionization coefficient. Experimental measurements of this ionization coefficient are now reported (Huxley and Crompton 1974) as values of α_T/n_0 as a function of E/n_0 and T_0 .

Townsend's second ionization coefficient accounts for the fact that, at high E/n_0 , the positive ions created by an electron-neutral collision can liberate electrons during their subsequent collisions with other molecules or with the cathode. It is the foundation for Townsend's theory of electrical breakdown in gases. However, this topic is beyond the scope of this book, and the interested reader should consult the text by Huxley and Crompton (1974).

In 1912, Townsend and his students made the first quantitative measurements of electron mobilities in low-pressure gases. They found that the mobility is not inversely proportional to n_0 at high E/n_0 . It is now understood that this is a result of electron runaway (Cavalleri and Paveri-Fontona 1972), a process that sets in when the momentum-transfer cross section is so small that the electrons, on the average, cannot lose momentum by collisions as fast as they gain it from the electric field. Only many years later was it discovered that runaway is not unique to electrons, occurring most notably (Lin et al. 1979a; Howorka et al. 1979) for H⁺ and D⁺ in helium.





Ramsauer

Bailey

In effect, a drift tube in which electron or ion runaway occurs is functioning as a (poor) particle accelerator. This fact was not appreciated in the early 1900s, so it became widely believed that the mobility depends upon E/n_0 for ions but not for electrons. As a consequence, electron swarms came to be described only in terms of the drift velocity while ion swarms continued to be described in terms of the mobility. This is unfortunate because:

- 1. it helped separate these two similar research areas;
- 2. the mobility is a transport coefficient relating the flux of charged particles to the force of the electric field, whereas the drift velocity is technically not a transport coefficient; and,
- 3. it led to the presentation of electron transport data at constant T_0 in the form of log-log plots of v_d versus E/n_0 . These are much more difficult to use for accurate estimations than are semilog plots of K_0 versus E/n_0 , such as Fig. 1.1.





Mott

Bohr

The transparency of the heavier rare gas atoms (Ar, Xe, Kr) to electrons with an energy of about 1 eV was discovered independently by Carl Wilhelm Ramsauer (1879–1955) and by Townsend and Victor Albert Bailey (1895–1964) in 1921. This transparency, now known as the Ramsauer–Townsend effect, corresponds to a very high electron drift velocity and a very low momentum-transfer cross section. Its explanation in terms of the scattering of matter waves, was first suggested by Niels Henrik David Bohr (1885–1962) and worked out in detail (Mott and Massey 1965)

by Neville Francis Mott (1905–1996) and others. This was one of the early successes of quantum mechanics.

In 1922, Loeb studied electron transport in gases at atmospheric pressure. Such measurements, although made with drift tubes that by modern standards leave much to be desired, established that the equations in the previous subsections apply to both ion and electron swarms. We note again that there is more that connects electron and ion transport in gases than there is that differentiates them.

1.11 Early Kinetic Theory, 1905–1931

The kinetic theory of gaseous ion transport will be treated in more detail in Chaps. 4 and 5, so we will only point out highlights in this chapter. Only atomic ions moving in atomic gases are considered here; molecular systems are considered in Chap. 8.

In 1905, Langevin published a paper "in which he treated the problem of diffusion and applied it to mobility. As pointed out by Sydney Chapman (1888–1970), this paper forms the basis of the strictly rigorous treatment of the kinetic theory which he, Enskog and others ... developed, though at the time the paper did not attract the attention it deserved." (Tyndall 1938). An English translation of Langevin's paper is given by McDaniel (1964).

With the aid of (1.17), Langevin derived the fundamental low-field ion mobility equation for an atomic ion in an atomic neutral gas. In modern notation, this equation is

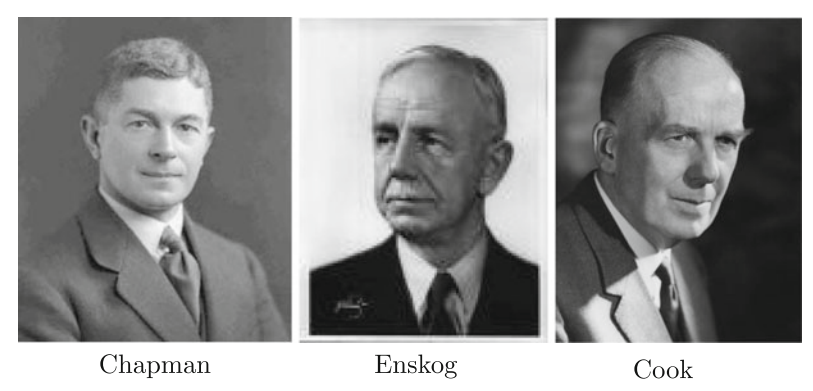
$$K_0(0, T_0) = \left(\frac{2\pi}{\mu_0 k_B T_0}\right)^{1/2} \frac{3q}{16N_0} \frac{1 + \alpha_c}{\overline{\Omega}^{(1,1)}(T_0)},\tag{1.19}$$

where μ_0 is the ion–neutral reduced mass, the dimensionless quantity α_c represents correction terms that are generally small (see Sect. 2.7), and $\overline{\Omega}^{(1,1)}(T_0)$ is the momentum-transfer collision integral discussed below. This equation is limited to ions whose diameters are small compared to their mean free paths; extensions to macro-ions that do not satisfy this restriction are summarized by Revercomb and Mason (1975).

An important special case is when the ion–neutral interaction potential is like that between a point charge and a perfectly elastic sphere that becomes polarized in the electric field of the ion. This potential corresponds precisely to the longest ranged component of the interaction between an atomic ion and a neutral atom in a 1 S₀ ground state, so for such systems the so-called Langevin mobility (or, polarization mobility) must be the value of the mobility in the double limit of low E/n_0 and low T_0 . As a result of some slight improvements over the years, most notably by Henry Ronald Hassé (1884–1955) in (1926), it is now known that

$$K_0(0,0) = \frac{13.853 \text{ cm}^2 \text{V}^{-1} \text{s}^{-1}}{\sqrt{\widehat{\alpha}_0 \, \widehat{\mu}_0}},\tag{1.20}$$

when $\widehat{\alpha}_0$ is the value in cubic Angstroms of the neutral polarizability and $\widehat{\mu}_0$ is the value of μ_0 in g/mole (or Da). Unfortunately, T_0 values well below 1 K are often needed (see Fig. 1.1) before (1.20) provides an accurate estimate of the low-field mobility actually measured.



Langevin's 1905 work established that the mobility is inversely proportional to the square root of the ion–neutral reduced mass. This was verified experimentally, and was confirmed by the kinetic theory work of Chapman in 1916 and 1917, of David Enskog (1884–1947) in 1917, and of Hassé and William Richard Joseph Cook (1905–1987) in (1931). Since α_c depends slightly on the ion and neutral masses, Langevin's prediction is an approximation, albeit a very good one (Gardner et al. 2010; see Sect. 2.8.2).

The important quantity in (1.19) is $\overline{\Omega}^{(1,1)}(T_0)$. This is the simplest of a set of collision integrals that depend upon T_0 and are defined by the equation

$$\overline{\Omega}^{(l,s)}(T_0) = [(s+1)!]^{-1} \int_0^\infty \exp(-x) \, x^{s+1} \overline{Q}^{(l)}(x k_B T_0) \, dx. \tag{1.21}$$

These are not cross sections, even though they have the units of m^2 , since the term cross section is restricted here to microscopic properties of a system. Instead, $\overline{\mathcal{Q}}^{(1,1)}(T_0)$ is an average over translational energy, $\varepsilon = xk_BT_0$, of the momentum-transfer cross section, $\overline{\mathcal{Q}}^{(1)}(\varepsilon)$, and a Maxwellian distribution of the ion–neutral collision energy.

When classical mechanics provides an adequate description of the ion-neutral interactions, then the transport cross sections may be calculated from the expression

$$\overline{Q}^{(l)}(\varepsilon) = 2\pi \left[1 - \frac{1 + (-1)^l}{2(l+1)} \right]^{-1} \int_0^\infty \left[1 - \cos^l\left(\theta\left(\varepsilon, b\right)\right) \right] b db, \tag{1.22}$$

where b is the impact parameter. We note in passing that some people prefer to use Legendre polynomials (see Appendix A) rather than powers of the cosine; the

relationship between these two kinds of transport cross sections is given in Viehland and Mason (1978) and in Viehland et al. (2016).

The new quantity in (1.22) is the polar scattering angle,

$$\theta(\varepsilon, b) = \pi - 2b \int_{r_0}^{\infty} \frac{dr}{r^2 \sqrt{1 - (b/r)^2 - V(r)/\varepsilon}}.$$
 (1.23)

Here, V(r) is the ion–neutral interaction potential energy as a function of separation and r_o is the turning point, the largest, positive, real root of the quantity under the square root sign. Hence, the zero-field mobility given by (1.19) is related to the ion–neutral interaction potential through the three layers of integration in (1.21)–(1.23).

Consider the situation where the ion–neutral interaction potential is that of rigid spheres of diameter d, i.e.,

$$V(r) = \begin{cases} 0 & r \ge d \\ \infty & r < d \end{cases}$$
 (1.24)

With this interaction potential, the turning point in (1.23) is

$$r_o = \begin{cases} b & b \ge d \\ d & b < d \end{cases}$$
 (1.25)

Putting this into (1.23) gives

$$\theta(\varepsilon, b) = \begin{cases} 0 & b \ge d \\ 2\cos^{-1}(b/d) & b < d \end{cases}$$
 (1.26)

Then (1.21) and (1.22) give

$$\overline{\Omega}^{(l,s)}(T_0) = \overline{Q}^{(l)}(\varepsilon) = \pi d^2. \tag{1.27}$$

The bars on the quantities in (1.21)–(1.27) serve as reminders that normalization factors have been included so that both $\overline{Q}^{(l)}(\varepsilon)$ and $\overline{\Omega}^{(l,s)}(T_0)$ are equal to πd^2 for the interaction of classical-mechanical rigid spheres of diameter d.

Like many equations to be developed in this text from detailed consideration of the Boltzmann equation, the basic features of (1.19) can be obtained from momentum-transfer theory or mean-free-path theory. Both of these theories were introduced by Maxwell in 1860. Mean-free-path theory is the standard version of elementary kinetic theory appearing in textbooks. Momentum-transfer theory has a stronger theoretical pedigree, since there are no approximations about the physics behind its main idea: the momentum and energy gained by the ion from the field must, at steady state, be balanced by losses through collisions with the neutral molecules. More information about both mean-free-path and momentum-transfer theory is contained

in the books by McDaniel and Mason (1973) and by Mason and McDaniel (1988), and momentum-transfer theory will be discussed in detail in Chap. 3.

Equation (1.19) was given by Hassé and Cook (1931) and by Allen Vincent Hershey (1910–2004) in (1939); in both cases, Langevin was properly cited. Although it was given explicitly in modern notation by Mason and Schamp (1958), and is often referred to as the Mason–Schamp equation, it should instead be called the fundamental low-field ion mobility equation.

Equation (1.19) gives another explanation for the validity of Blanc's law: it arises because of the additivity of transport cross sections in dilute gases, where only binary collisions affect the motion. So great now is our confidence in Blanc's law, because of experimental tests (Schultz et al. 1977) as well as theoretical arguments, that significant deviations are often taken as evidence that chemical reactions are occurring in the swarm experiments. It should be noted, however, that α_c in (1.19) leads to small but non-negligible deviations from Blanc's law.

1.12 Mass Spectrometers

In 1912–1913, Thomson invented an instrument, called a mass spectrograph, that used a photographic plate to record the motions of ions passing through combined electrostatic and magnetic fields. When the plate is placed in a plane perpendicular to the axis of the canal rays, the ions of equal mass are spread into a parabola whose Cartesian coordinates can be used to give the energy and momentum of the particles. More simply, the range of ion energies contained in the ion beam could be measured by the lengths of the parabolic curves. With this device, Thomson discovered that the canal rays generated in neon gas are split into two beams, with masses corresponding to 20 and 22 g/mole. In other words, he identified two isotopes of neon.





Aston

Dempster

A somewhat similar device that is a more direct forerunner of modern mass spectrometers was devised by Francis William Aston (1877–1945) in 1918, based on a design of Arthur Jeffrey Dempster (1886–1950). In a mass spectrometer, a gas sample at very low pressure is bombarded by a stream of high-energy electrons,

X-rays or gamma rays. A few of the gas particles are converted into positive ions. These are focused into a narrow beam and accelerated toward a magnet by a set of accelerating plates. The magnetic field deflects the ions from their straight-line path, toward a collector. By measuring the strength of the magnetic and accelerating fields, it is possible to determine accurately the charge-to-mass ratio (sometimes called the mass-to-charge ratio) since the amount of deflection is precisely controlled by:

- 1. the strength of the magnetic field (stronger fields give greater deflection).
- 2. the strength of the accelerating field (stronger fields give smaller deflection).
- 3. the charge-to-mass ratio of the ions (larger ratios give greater deflection).

When a mass spectrometer is used with hydrogen gas, two types of positive "anode rays" are observed, indicating that there are two positively charged particles. Type 1 rays are deflected more than the other type, so they must have the larger value of q/m. Since the charge on a positive ion must be some integer multiple of the electron charge, the simplest possibility for the type 1 rays is that they consist of protons (singly charged hydrogen ions, H^+).

The type 2 rays observed in a mass spectrometer containing hydrogen gas have a q/m value that is almost exactly half that found for the type 1 rays. Since one unit of charge (positive or negative) is the smallest amount of charge possible for an atom or molecule, the simplest model for the type 2 rays is a singly charged particle having almost exactly twice the mass of the proton. Although it is seldom found in drift tubes used to study gaseous ion mobility, diffusion, and reaction, the existence of diatomic hydrogen ion, H_2^+ , as a stable particle in a mass spectrometer is of great significance to the theory of chemical bonds. (The small difference between twice the mass of the proton and the mass of the diatomic hydrogen ion is now known to be a reflection of the energy required to hold the two nuclei together.)

When a mass spectrometer is used with helium gas, two other types of positive rays are observed. Type 3 rays have q/m approximately one-half that of the proton but not exactly equal to that of H_2^+ . The logical conclusion is that they are doubly charged helium ions (alpha particles, ${}^4\mathrm{He}^{2+}$). Type 4 rays have q/m approximately one-fourth that of the proton, and hence are ${}^4\mathrm{He}^+({}^2\mathrm{S}_{1/2})$.

The mass spectrometer results with helium present us with a problem. One possible model of a helium atom has four times the mass of a hydrogen atom and consists of four protons and four electrons. This model predicts that the type 3 and type 4 positive ions could be produced in a mass spectrometer, but it also predicts the existence of two other ions, corresponding to a helium atom that has been stripped of three and four electrons, respectively. These ions have never been observed, despite many attempts to find them in a mass spectrometer. Moreover, this model of the helium atom conflicts with the conclusion reached by Henry Gwyn-Jeffreys Moseley (1887–1915) that the atomic number of an element is equal to the number of protons in the nucleus of each atom of that element results. The conflict between theory and experiment leads us to discard this model.



If we believe the mass spectrometer results using helium gas and Moseley's results, then a neutral helium atom contains only two electrons and two protons. To have four times the mass of a hydrogen atom, it must also contain one or more neutral particles, called neutrons. Further support for the existence of neutrons can be found by a more careful analysis of mass spectrometer results. Thus, Harold Clayton Urey (1893–1981) found in 1932 that there are really two components to the type 2 signal for hydrogen; the second signal has nearly but not exactly the same q/m as H_2^+ , but it is much weaker (indicating an abundance of only 0.0115%).

Painstaking efforts revealed that the extra peak is not due to a small amount of impurity in the hydrogen, and lent support to the suggestion in 1920 by William Draper Harkins (1873–1951) that there is a second type of hydrogen, chemically identical to the first but with a composition of one electron, one proton, and one neutron. We now call this deuterium. Further experiments indicated a very tiny amount of a third type of hydrogen, called tritium, which has 1 electron, 1 proton, and 2 neutrons per atom.

1.13 Ion Swarms, 1928–1960

The precision and reliability of gaseous ion mobility data were advanced considerably in 1928 by the introduction into mass spectrometry of time-of-flight methods by Robert Jemison Van de Graaff (1901–1967). Significant advances were made in the next decade by Tyndall, Cecil Frank Powell (1903–1969) and their collaborators at the University of Bristol, England, who developed powerful new techniques and used them for accurate measurements of the mobility of alkali ions in simple gases. The general conclusion is that all mobility data obtained prior to 1930 are subject to doubt because of impurities in the gas samples used. Such impurities can be preferentially ionized or can attach by chemical reactions to the ions of interest, so that ions of unknown composition can be drifting and diffusing in the apparatus.





Van de Graaf

Powell

The new measurements obtained by the Bristol group between 1932 and 1941 verified the accuracy of the equations presented above except in two situations. First, at high enough E/n_0 the mobility begins to depend on this experimental parameter, as shown in Fig. 1.1. This was qualitatively explained as resulting from the gain of energy by the ions from the electric field, such additional energy being negligible at low E/n_0 compared to thermal energy. The second exception is the transport of atomic or molecular ions through their parent gases, where resonant charge transfer of an electron causes a substantial increase in the momentum-transfer collision integral. This, in turn, leads to a substantial decrease in the measured mobility. Quantitative explanations for this effect require quantum-mechanical calculations.

If the interaction be between an atomic ion and a neutral atom must be described quantum-mechanically, then the transport cross sections can be calculated from a generalization of (1.22):

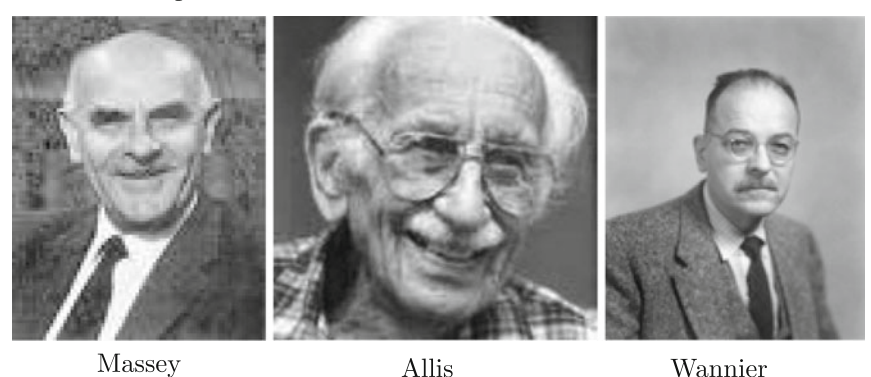
$$\overline{Q}^{(l)}(\varepsilon) = 2\pi \left[1 - \frac{1 + (-1)^l}{2(l+1)} \right]^{-1} \int_0^{\pi} \left[1 - \cos^l(\theta) \right] \sigma(\theta, \varepsilon) \sin(\theta) d\theta. \quad (1.28)$$

Here, $\sigma(\theta, \varepsilon)$ is the differential cross section for scattering through polar angle θ when the translational energy is ε .

 $\overline{Q}^{(l)}(\varepsilon)$ has the dimensions of area and may be calculated (Wood 1971; Hirschfelder et al. 1964) directly from the phase shifts in the radial wave function caused by the ion–neutral interaction potential. It is also possible to use (1.28) to develop semiclassical expressions for the transport cross sections as sums involving differences between phase shifts of various orders (Mason and McDaniel 1988; Viehland et al. 2016).

The earliest theoretical investigation of ion transport in gases that was based on quantum mechanics was that of Harrie Stewart Wilson Massey (1908–1983) and Courtney Balthazar Oppenheim Mohr (1906–1986) in 1934. They computed $K_0(0, 300 \text{ K})$ to be $12 \text{ cm}^2 \text{V}^{-1} \text{s}^{-1}$ for $^4\text{He}^+(^2\text{S}_{1/2})$ in He, whereas the experimental value of Tyndall and Powell was $21.4 \text{ cm}^2 \text{V}^{-1} \text{s}^{-1}$. Considerable effort finally established that the experimental value was for $^4\text{He}_2^+$, and that the quantum-mechanical calculations were accurate. These investigations established for electrons and atomic

ions that the translational degrees of freedom can always be treated classically, that relativistic effects are negligible, and therefore that an effective approach is to use quantum cross sections obtained from (1.28) in the classical Boltzmann equation discussed in Chap. 4.



After World War II, microwave breakdown studies in very pure, inert gases were initiated by Sanborn Conner Brown (1913–1981) and William Phelps Allis (1901–1999). The use of microwaves had the advantages that the ion number densities were reasonably high and quite uniform over relatively large volumes, there were no electrodes to bring boundary conditions into question, and there were no asymmetries such as are produced by electric currents. The disadvantage was that the plasma of ions and electrons had to be allowed to "cool" through dissociation, recombination and other chemical processes. This disadvantage was turned into an advantage with the theoretical analyses by Allis and Rose (1954) of electron and ion motions under the influence of ac fields. Experimental advances made microwave breakdown a useful swarm method for studying dissociative recombination and other reactive processes.

Gregory Hugh Wannier (1911–1983) published a landmark paper in (1953) that dealt mainly with the motion of gaseous ions at high E/n_0 . Although this work did not contain a general solution of the problem of how to relate the measured macroscopic properties to the microscopic details of the ion–neutral interactions, it gave solutions for some theoretical models and provided much insight into the high E/n_0 situation. For example, it made explicit reference to diffusion coefficients parallel and perpendicular to the electric field, although this concept did not spread to other workers in swarms at that time.

Of special importance is the expression that Wannier was able to deduce for the mean ion energy at high E/n_0 , based on a special model of the ion–neutral interaction potential. Written in terms of the ion temperature, T, the Wannier equation is

$$\frac{3}{2}RT = \frac{3}{2}RT_0 + \frac{1}{2}Mv_d^2 + \frac{1}{2}M_0v_d^2.$$
 (1.29)

Here, M and M_0 are the molar masses of the ions and neutral molecules, respectively. The first term on the right of (1.29) represents the thermal energy that is always

available to the ions. The second term represents energy that the ions have gained from the electric field and are exhibiting as directed motion along the direction of the electric field. Finally, the third term represents energy gained from the field but transformed into random ion motion as a result of collisions between the ions and the neutral molecules.

When atomic ions move in their parent gases and experience resonant charge transfer, (1.29) is apparently inaccurate. A better equation is (Heimerl et al. 1969)

$$\frac{3}{2}RT = \frac{3}{2}RT_0 + \frac{\pi}{4}Mv_d^2. \tag{1.30}$$

By transforming the ion energy given by (1.29) and the thermal energy of the neutral from the laboratory frame into the center-of-mass frame, we obtain a simple formula for the average collision energy of a charged particle and a neutral molecule. In terms of an effective temperature, T_{eff} , that characterizes both the ion and the neutral in a collision, this formula is

$$\frac{3}{2}RT_{eff} = \frac{3}{2}RT_0 + \frac{1}{2}M_0v_d^2 [1 + \beta_c].$$
 (1.31)

Here we have incorporated β_c , a small correction factor (Viehland et al. 1974) that is equal to zero for the special model considered by Wannier but is more generally on the order of \pm 0.1. For many years following Wannier's work, (1.29) and (1.31) were believed to be only crude approximations. Monte Carlo (Skullerud 1973) and kinetic theory (Viehland et al. 1974) studies in the 1970s confirmed their general applicability and high accuracy for electrons and atomic ions moving through atomic gases; these studies will be discussed later in this book.

Equation (1.29) also allows us to estimate how low E/n_0 must be in order to be in the low-field region. Requiring the last two terms to be small compared to the first means that

$$v_d \ll \left(\frac{3RT_0}{M+M_0}\right)^{1/2}.$$
 (1.32)

Combining this with (1.4) and (1.7) gives

$$E/n_0 < \frac{1}{5N_0K_0} \left(\frac{3RT_0}{M+M_0}\right)^{1/2}.$$
 (1.33)

The number 5 in (1.33) comes from numerical simulations (Yousef et al. 2007) and many comparisons between theoretical and experimental values (Viehland et al. 2017). Equation (1.33) is easy to use, since it involves only experimental quantities; alternative equations (Revercomb and Mason 1975; Mason and McDaniel 1988; Eiceman et al. 2014) involve the mean-free-path or the sum of the radii of the ion and neutral, quantities that are difficult to estimate.

In the 1950s, experimental work on gaseous ion transport turned to the temperature dependence of the low-field mobility. This is because (1.19) shows that such data provide information about the temperature dependence of the momentum-transfer collision integral, which in turn is related in well-established ways to the ion–neutral interaction potential. Indeed, Geltman (1953) used the $K_0(0, T_0)$ measurements of the Bristol group for ${}^4\text{He}_2^+$ in He to yield an effective spherical potential for the He $_2^+$ -He system. Similar analyses of the temperature variations of the standard mobility continued until the early 1990s (von Helden et al. 1992), when they were replaced by analyses of the E/n_0 variations.

1.14 Electron Swarms, 1922–1965

Important simplifications are possible in the theoretical description of electron swarms that are not possible for general ion swarms. The smallness of the electron mass means that even a weak electric field causes the electrons to have so much energy that thermal energy is negligible, so we may as well assume that T_0 is 0 K. Moreover, the smallness of M/M_0 means that electron scattering by neutral atoms and molecules is nearly isotropic in velocity space, so velocity distribution function (vdf) of the electrons may be expanded in a series of spherical harmonics (Appendix A) in velocity. When the electric field is static, this collapses to being an expansion in Legendre polynomials(Appendix A) of the angle with respect to E. Mari Johan Druyvesteyn (1901–1995) in (1930), and Druyvesteyn and Frans Michel Penning (1894–1953) in (1940), showed that the first coefficient in this expansion could be determined by retaining only two terms and assuming that $\overline{Q}^{(1)}(\varepsilon)$ is independent of ε . The result (McDaniel et al. 1993) is that the zero-order vdf depends only upon the ion speed, v, and is given by the equation,







Penning

$$f_0(\mathbf{v}) = \frac{\exp(-v^4/\zeta^4(v))}{\pi \Gamma(3/4)\zeta^3(v)},$$
(1.34)

where Γ is the gamma function (i.e., $\Gamma(3/4) = 1.2254$; see Appendix A). Using $\overline{Q}^{(1)}$ to represent the constant value of the momentum-transfer cross section, the new function in (1.34) is

$$\zeta^4(v) = \frac{4M_0}{3M} \left(\frac{QE}{Mn_0\overline{Q}^{(1)}}\right)^2.$$
 (1.35)

In terms of $\zeta(v)$, the mobility and diffusion coefficients are (McDaniel et al. 1993):

$$K(E/n_0, 0) = -\frac{4\pi}{3} \frac{Q}{M} \int_{0}^{\infty} \frac{v^3}{\widetilde{\nu}^{(1)}(v)} \frac{df_0(v)}{dv} dv,$$
 (1.36)

$$D_T(E/n_0, 0) = \frac{4\pi}{3} \int_0^\infty \frac{v^4}{\widetilde{\nu}^{(1)}(v)} f_0(v) dv, \tag{1.37}$$

and

$$D_L(E/n_0, 0) = D_T(E/n_0, 0) - \frac{4\pi}{3} \frac{qE}{M} \int_{0}^{\infty} b_1(v) f_0(v) \left(\frac{d}{dv} \frac{v^3}{\widetilde{\nu}^{(1)}(v)}\right) dv, \quad (1.38)$$

where

$$\widetilde{\nu}^{(1)}(v) = n_0 v \overline{Q}^{(1)} \left(\frac{1}{2} m v^2\right) \to n_0 v \overline{Q}^{(1)}. \tag{1.39}$$

The first equality in (1.39) is the general expression for the collision frequency for momentum transfer, while the second assumes a constant $\overline{Q}^{(1)}$. The expression for $b_1(v)$ is too involved to give here, especially since more general expressions are given by Kumar et al. (1980) for collision frequencies derived from momentum-transfer cross sections that do vary with velocity.

Time-of-flight methods were successfully adapted by Bradbury and Nielsen (1936) to the measurement of drift velocity of electrons in gases. This led to electron mobility data as accurate as the ion mobilities measured by the Bristol group.

The electrons in a swarm that is in contact with an absorbing boundary may be significantly cooled by two distinct processes. First, an ambipolar potential well may be set up, which allows only the more energetic electrons to pass to the wall and leaves the remaining electrons with a lower mean energy. Biondi (1954) studied this "ambipolar diffusion cooling" effect in the afterglow of a microwave discharge. The second diffusional cooling effect occurs when the neutral gas acts as a selective filter. Depending upon the nature of $\nu^{(1)}(v)$, the neutral gas may allow only the high-energy electrons to diffuse to the walls, leaving the bulk of the electrons with a lower average energy. Parker (1965) investigated this "free diffusion cooling" effect.

1.15 Electron and Ion Swarms, 1960–1975



Drift Tube for DTMS

An important experimental advance came about between 1960 and 1963 with the development of the drift-tube mass spectrometer. A DTMS is a drift tube that incorporates mass analysis of the ion exiting the drift region (and preferably at the entrance also). These apparatus were developed at Georgia Tech (Barnes et al. 1961; McDaniel et al. 1962) and the Bell Telephone Laboratories (McAfee and Edelson 1963; Edelson and McAfee 1964). More recent versions have been reviewed by McDaniel and Mason (1973) and by Mason and McDaniel (1988), and more information will be given in Sect. 2-2.

Improvements in the DTMS apparatus made it important to reexamine the basic equations presented above. It was shown by Wannier (1952) that at high values of E/n_0 the diffusion coefficient in (1.12) must be replaced by a diffusion tensor. Thus, Fick's first law was generalized to become

$$\mathbf{j}(\mathbf{r},t) = \mathbf{v}_d n(\mathbf{r},t) - \mathbf{D} \cdot \nabla n(\mathbf{r},t). \tag{1.40}$$

It should be noted that (1.40) serves to define the diffusion tensor in strong but uniform electrostatic fields so, as before, theoretical calculations of diffusion coefficients must be based on consideration of density gradients in space.

When (1.40) is used in (1.13), we get a generalization of Fick's second law, a diffusion equation for strong, uniform electrostatic fields,

$$\frac{\partial}{\partial t}n(\mathbf{r},t) + \mathbf{v}_d \cdot \nabla n(\mathbf{r},t) - \mathbf{D} \odot \nabla \nabla n(\mathbf{r},t) = -n(\mathbf{r},t)n_0k. \tag{1.41}$$

The \odot symbol in (1.41) represents the complete contraction of the tensors it connects (see Appendix A), in this case, the tensor of rank two, **D**, and two copies of the gradient, ∇ , i.e., two tensors of rank one.

In most DTMS experiments, the apparatus is cylindrical, with an external electrostatic field parallel to the axis of the cylinder, which determines the z-axis. In this situation, the ion drift velocity lies entirely along z with magnitude v_d , and the diffusion tensor is diagonal, with identical values along x and y (labeled D_T or D_\perp , with the subscripts indicating that the direction is transverse or perpendicular to the electric field) but a different value (labeled D_L or D_\parallel), when the diffusion is longitudinal or parallel to the electric field.

In the absence of sources or sinks of ions, (1.41) reduces to the simpler diffusion equation for ion motion in a strong, uniform electrostatic field in a cylindrical device,

$$\frac{\partial}{\partial t}n(\mathbf{r},t) + v_d \frac{\partial}{\partial z}n(\mathbf{r},t) - D_T \left(\frac{\partial^2}{\partial x^2} + \frac{\partial^2}{\partial y^2}\right)n(\mathbf{r},t)
-D_L \frac{\partial^2}{\partial z^2}n(\mathbf{r},t) = -n(\mathbf{r},t)n_0k.$$
(1.42)

Discussions of the mathematical solution of (1.42) are given by Moseley et al. (1969), by Gatland (1974) and in Sect. 2-6 of Mason and McDaniel (1988).

For later purposes, we note that (1.42) contains no terms involving third- or higher order derivatives of $n(\mathbf{r}, t)$. It has been shown (Lovass et al. 1987) that this omission can lead to significant errors in values of D_L and D_T . We will return to this topic in Sect. 2.4.

Measurements of D_T were reported by Miller et al. (1968) for H⁺ and H₃⁺ ions in H₂. (Since it has no electrons, H⁺ cannot be given an atomic term symbol of the type discussed in Appendix B.) Rough estimates for D_L for $^{14}\text{Ne}^+(^2\text{P}_{3/2})$ ions in Ne were made by Beaty and Patterson (1968) and both D_L and D_T were reported for massidentified $^{14}N^+(^2P_{3/2})$ and N_2^{2+} ions in N_2 by Moseley et al. (1968). As an illustration of such results, Fig. 1.2 shows theoretical values for n_0D_L from the same calculations that gave the standard mobilities in Fig. 1.1. The local maximum in n_0D_L at low T_0 and intermediate E/n_0 has been found in many calculations involving atomic ions in He, but has yet to be demonstrated experimentally. As T_0 increases, the maximum on the log-log plot becomes a shoulder and eventually cannot be seen. There is no similar structure on a plot of n_0D_T , as can be seen in Fig. 1.3. As expected from the NTE, (1.17), n_0D_L and n_0D_T are identical at low E/n_0 . Generally, n_0D_T values are smaller than n_0D_L values at intermediate and high E/n_0 . Although theoretical calculations for some systems show this inequality being reversed at very high E/n_0 , no experimental support for this prediction has yet been reported, due to the difficulty in reaching high enough E/n_0 .

Although anisotropy in the diffusion coefficients was described by Wannier in (1953) and was incorporated into (1.40) and (1.41), most researchers were surprised when anisotropic diffusion of electrons in gases was first observed by Hurst and Parks (1966) and by Wagner et al. (1967). This is because the electron distribution function

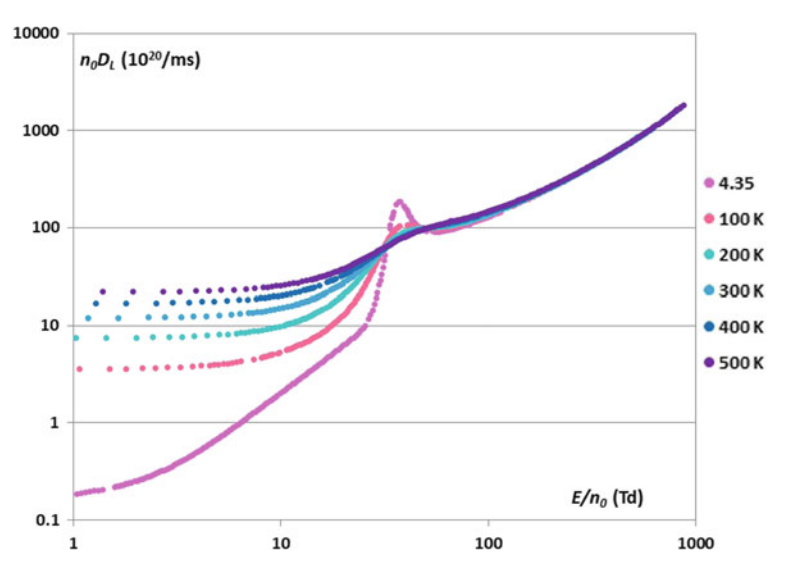


Fig. 1.2 Same as Fig. 1.1, for the product n_0D_L

must be nearly isotropic in velocity space, and it is easy to confuse this distribution with its distribution in physical space. Anisotropic electron diffusion was explained theoretically, within the context of two-term, spherical harmonic solutions of the Boltzmann equation, by Skullerud (1969), Parker and Lowke (1969), Lowke and Parker (1969), Francey (1969), Huxley (1972) and Lowke (1973). An explanation in terms of nonequilibrium thermodynamics was given by Robson (1972). More information about these developments is contained in the review by Skullerud (2017) and the book by Robson (2006).



Cowling

It should be mentioned that the presence of a strong magnetic field also renders an ionized gas anisotropic. In this case, both the mobility and diffusion coefficient become second rank tensors and Fick's Second Law as given by (1.42) no longer

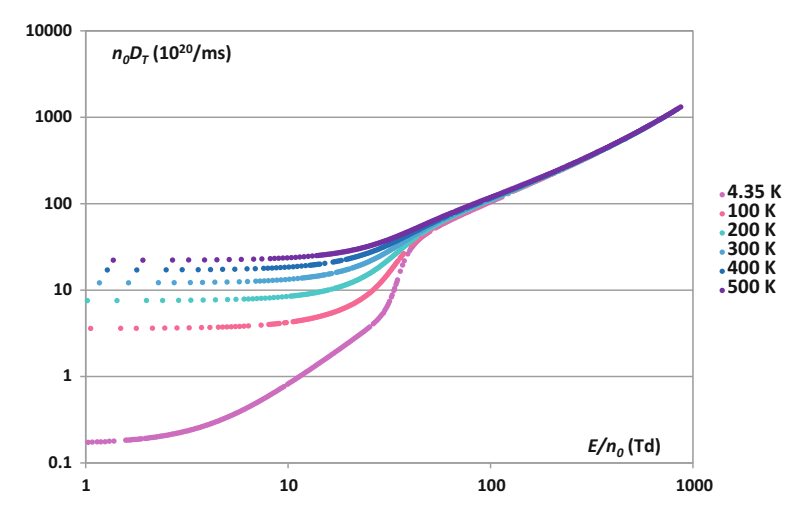


Fig. 1.3 Same as Fig. 1.1, for the product n_0D_T

applies. When the *z*-axis lies along the electric field, **E**, and the *x*-axis lies along the magnetic field, **B**, then the work of Chapman and Thomas George Cowling (1906–1990) shows that these tensors must have the forms (McDaniel 1964):

$$\mathbf{K} = \begin{vmatrix} K_T & K_H & 0 \\ -K_H & K_T & 0 \\ 0 & 0 & K_L \end{vmatrix}$$
 (1.43)

and

$$\mathbf{D} = \begin{vmatrix} D_T & D_H & 0 \\ -D_H & D_T & 0 \\ 0 & 0 & D_L \end{vmatrix}. \tag{1.44}$$

Here the T and L subscripts indicate the components transverse and longitudinal to the magnetic field, while the H subscripts indicate the Hall component, named after Edwin Herbert Hall (1855–1938) who discovered a similar effect in 1879 for electrons moving in metals. Note that the terms transverse and longitudinal mean something completely different here than in the cases where there is a strong electrostatic field. To prevent confusion we will restrict our attention hereafter to those situations where there is no external magnetic field present, unless specifically stated otherwise.

42 1 Introduction

1.16 Atomic Ion–Atom Kinetic Theory



Hall

Monte Carlo methods for simulating the motion of atomic ions through atomic gases became feasible with the development by Skullerud (1968) of the "null-collision" method. As indicated in Chap. 9, the method allows velocity moments (such as the ion mobility and diffusion coefficients) to be calculated (Skullerud 1973; Lin and Bardsley 1975, 1977, 1978) with known standard deviations at any value of E/n_0 . A Monte Carlo method that takes into account rotational degrees of freedom for molecular systems was developed by Koutselos (1995). An extension of the null-collision method was developed by Yousfi et al. (1998) to overcome the problem of incident ions that vanish at relatively high E/n_0 due to asymmetric charge transfer or electron detachment. However, large amounts of computing time are needed with any Monte Carlo scheme to get accuracies better than about 1% for the mobility and 5% for the diffusion coefficients.

Prior to 1975, kinetic theory treatments of the Boltzmann equation for gaseous ion transport were one-temperature methods, so called because the ions and neutrals were both assumed to be characterized by the same temperature. These had always yielded power series or ratios of polynomials in E/n_0 . Such expressions diverge at large E/n_0 and thus have only limited usefulness in relating the measured transport coefficients to the fundamental, microscope interaction between the ions and neutrals.

The first kinetic theory of gaseous ion transport that was valid for arbitrary E/n_0 without restriction on the ion–neutral mass ratio or interaction potential energy was presented by Viehland and Mason (1975, 1978). The key point in this two-temperature approach to the Boltzmann equation was the use of basis functions that involved the ion temperature, T, and the gas temperature, T_0 . Since the ions are present only in trace amounts in a drift tube, T can be substantially larger than T_0 at intermediate and high values of E/n_0 , as shown by (1.29).

The two-temperature kinetic theory gives a theoretical foundation for an expression for the ion mobility that can be obtained by combining (1.19) and (1.31),

$$K_0\left(\frac{E}{n_0}, T_0\right) = \left(\frac{2\pi}{\mu_0 k_B T_{eff}}\right)^{1/2} \frac{3q}{16N_0} \frac{1 + \alpha_c}{\overline{\Omega}^{(1,1)}(T_{eff})}.$$
 (1.45)

Note that there is no justification for allowing $\overline{\Omega}^{(1,1)}(T_{eff})$ to depend upon the effective temperature without simultaneously using T_{eff} in the square root term of the fundamental ion mobility equation, which is the name we shall use for (1.45).

The higher order terms in (1.31) and (1.45) are α_c and βc , both of which are functions of T_o and T_{eff} as well as the ion and neutral masses. If we ignore them, we see that theory predicts that the mobility does not vary separately with E/n_0 and T_0 , but is instead a function of the single variable, T_{eff} , that characterizes the average kinetic energy of an ion-neutral collision in the center-of-mass frame. This prediction has been verified experimentally (Viehland and Mason 1975; Ellis et al. 1976), within approximately 10%, which is the magnitude of α_c and βc . Both the two-temperature theory and momentum-transfer theory have been used (Viehland and Mason 1975; Viehland and Robson 1989) to obtain equations that allow α_c and β_c to be evaluated entirely from quantities that can be measured in a drift-tube experiment, i.e., the mobility, reaction rate coefficients and diffusion coefficients parallel and perpendicular to the direction of the electric field.

1.17 Ion-Neutral Reactions

Since increasing the value of E/n_0 in a drift tube is qualitatively similar to increasing T_0 , drift tube measurements of ion–neutral reaction rate coefficients have been made in such apparatus for many years. This research focus intensified in the late 1970s and early 1980s, after the first approximation of the two-temperature kinetic theory led (Viehland and Mason 1977) to a relatively simple expression for k. For the reaction between the trace ions in a swarm and the reactive molecules that are contained in small amounts in a nonreactive (buffer) gas that is atomic and dilute, each collision conserves charge and the ions collide so seldom with reactive neutrals that their vdf is determined entirely by interactions with the buffer gas. Then the second-order reaction rate coefficient is

$$k = \left(\frac{1}{k_B T_R}\right) \left(\frac{8}{\pi \mu_R k_B T_R}\right)^{1/2} \int_0^\infty \exp\left(-\frac{\varepsilon_R}{k_B T_R}\right) Q_R^*(\varepsilon_R) \varepsilon_R d\varepsilon_R, \tag{1.46}$$

where the ion–reactive neutral effective temperature, T_R , is given by the equation,

$$\frac{3}{2}k_{B}T_{R} = \frac{3}{2}k_{B}T_{0} + \frac{1}{2}M_{R}v_{d}^{2}\left(\frac{M+M_{0}}{M+M_{R}}\right) \approx \varepsilon_{R}.$$
(1.47)

Here, M_R is the molar mass of the reactive gas molecules, μ_R is the reduced mass for the ion and reactive neutral pair, and $Q_R^*(\varepsilon_R)$ is the energy-dependent, integral cross section for the reaction. In higher approximations, terms appear that are equivalent to α_c and β_c in (1.45) and (1.31), respectively. These equations provide a method

44 1 Introduction

(Viehland and Mason 1977) for extracting thermal rate coefficients at elevated temperatures, T_R , from swarm measurements at low T_0 and high E/n_0 .

The two-temperature treatment of the Boltzmann equation is not adequate for treating ion diffusion through gases, a process that is inherently anisotropic. Another problem is more important in treating ion—neutral reactions: the 2T treatment assumes the ion vdf is spherically symmetric and centered at zero velocity in the laboratory frame, while physical arguments indicate that it must be centered at \mathbf{v}_d and different along the field than perpendicular to it.

To overcome these problems, a three-temperature (3T) treatment of the Boltzmann equation was developed (Lin et al. 1979c; Viehland and Lin 1979). Here, the ions are characterized by two temperatures, one related to the average kinetic energy parallel to the electric field and the other perpendicular to it, and the ion vdf is displaced from the origin by an amount, v_d , along the electric field. Although the equations obtained from the three-temperature treatment of the Boltzmann equation are not as physically transparent as those of the two-temperature treatment, the result is again a prescription for calculating the transport and reaction rate coefficients from an assumed ion–neutral interaction potential.

More information about theoretical treatments of the Boltzmann equation is given in the next section and in Chap. 5. The implications for k are given in Chap. 7.

1.18 Improved Kinetic Theories

The 2T and 3T treatments of atomic systems suffer from a common problem: at sufficiently low gas temperatures there is a region of intermediate E/n_0 where convergence of the calculated mobility is very slow or nonexistent. This appears to be related to partial ion runaway (Mason and McDaniel 1988), where the ions gain more energy, on the average, during the time between collisions than they can transfer to the neutral atoms during the collisions, so they accelerate. Based on this idea, a bimaxwellian treatment of the Boltzmann equation was presented by Ness and Viehland (1990).

Skullerud (1984) pointed out that the 2T and 3T methods can never be absolutely convergent, because the tail of the ion vdf falls off more slowly with increasing energy than any Gaussian. He advocated solving the Boltzmann equation by a Galerkin method of weighted residuals (see Appendix C) with a nonanalytic zero-order distribution function. Larsen et al. (1988) showed that the calculations are much easier if this method is supplemented by a Kramers–Moyal expansion of the collision operator. The advantage of this approach is that it allows the mobility and other transport properties to be calculated from the ion–neutral interaction potential even at E/n_0 values where partial ion runaway occurs. The disadvantage is that it is not based on an explicit expression for a zero-order approximation to the ion vdf.

A different method of weighted residuals for solving the Boltzmann equation was introduced by Viehland (1994). It is based on a Gram-Charlier distribution function, specifically the three-temperature distribution function multiplied by an expression

that contains five new parameters. They are the coefficient of skewness along the field, kurtosis parallel to the field, kurtosis perpendicular to the field, correlation between parallel velocity and perpendicular energy, and correlation between parallel and perpendicular energy. Choosing these coefficients so that they are consistent with the low-approximation results for the appropriate moments of the distribution gives more rapid convergence to accurate transport coefficients. Since the assumed zero-order distribution is not Gaussian, Skullerud's arguments do not apply to the GC method for solving the Boltzmann equation.

The situation at present is that it is possible to calculate transport coefficients for atomic ions moving through atomic gases at arbitrary values of E/n_0 and T_0 from knowledge of the ion–neutral interaction potential, with equal or greater accuracy than they can be measured. Such calculations can best be performed using the Kramers–Moyal or Gram–Charlier techniques. The ability to make such calculations means that gaseous ion transport coefficients can serve as discriminating tests of the accuracy of potential energy functions calculated by ab initio methods (Chap. 6), inferred from spectroscopy or other experimental techniques, or obtained by adjusting the parameters in some model function.

1.19 Generalized Einstein Relations

Generalizations of (1.17) to nonvanishing values of E/n_0 have become known as generalized Einstein relations, or GER. They have been obtained from the two-temperature theory (Viehland and Mason 1975, 1978), Wannier's theory (Skullerud 1976), momentum-transfer theory (Robson 1976), and the three-temperature theory (Waldman and Mason 1981). The most crucial feature in these derivations is that D_L and D_T are related to the differential mobility rather than to the mobility itself. For elastic collisions such as those that characterize atomic ions and atoms, the GER can be written in the forms.

$$\frac{D_L}{K} = \frac{k_B T_L}{q} \left[1 + (1 + \Delta_L) K \right]$$
 (1.48)

and

$$\frac{D_T}{K} = \frac{k_B T_T}{q} \left(1 + \frac{\Delta_T K'}{1 + K'} \right),\tag{1.49}$$

where the logarithmic derivative of the mobility is

$$K' = \frac{d \ln(K)}{d \ln(E/n_0)}.$$
 (1.50)

Here T_L and T_T are the ion temperatures that characterize the average kinetic energy of the ion motion along and perpendicular to the direction of the electric field, while

46 1 Introduction

 Δ_L and Δ_T are specified by the particular theory being used. The numerical calculations of Waldman and Mason (1981) have led to recommended parameters (Mason and McDaniel 1988) for estimating all of the quantities on the right-hand sides of (1.48) and (1.49). The GERs are in good agreement with experimental data for ion mobilities and diffusion coefficients reported in a series of papers from Georgia Institute of Technology. Unfortunately, these data were shown later (Lovass et al. 1987) to be inaccurate when the ion arrival distribution function is skewed, and little attention has been paid to ion diffusion and the GER since then.

1.20 Transport with Molecular Systems

There are few differences between swarm experiments with atomic ions in atomic neutrals and those where the ion, the neutral or both species are molecular. The theory, however, is completely different because the collisions are governed by interaction potential energy surfaces that depend on both distances and angles and because the molecular species can absorb (or release) energy during inelastic (or superelastic) collisions involving their internal energy states.

In principle, transport experiments with molecular systems must be described by a quantum-mechanical extension of Boltzmann's equation (see Chap. 8). The interference effects that can occur when the internal energy states are degenerate (i.e., with rotational levels) are best treated with the Waldmann–Snider equation (Snider 1960; Waldmann 1964). Fortunately, such effects on gaseous ion transport coefficients are small (Lin et al. 1979b), and it is possible to use the WUB equation (Wang Chang et al., 1964) of Cheng-shu Wang Chang (1912–1999), George Eugene Uhlenbeck (1900–1988), and Jan de Boer (1911–2010). In this kinetic equation, ions in different internal states are treated as if they were completely different ions.





Wang Chang

Uhlenbeck

A two-temperature-like treatment (Viehland et al. 1981) of the WUB equation gives first-approximation results that are very similar to (1.31) and (1.45) with $\alpha_c = \beta_c = 0$:

$$K_0\left(\frac{E}{n_0}, T_0\right) = \left(\frac{2\pi}{\mu k_B T_{eff}}\right)^{1/2} \frac{3q}{16N_0} \frac{1}{\Omega(T_{eff})}$$
(1.51)

with

$$\frac{3}{2}k_B T_{eff} = \left[1 + \frac{M_0 \Phi}{M}\right]^{-1/2} \left[\frac{3}{2}k_B T_0 + \frac{1}{2}M_0 v_d^2\right]. \tag{1.52}$$

The ion temperature is given by

$$\frac{3}{2}k_BT = \left[1 + \frac{M_0\Phi}{M}\right]^{-1/2} \left[\frac{3}{2}k_BT_0(1-\Phi) + \frac{1}{2}Mv_d^2 + \frac{1}{2}M_0v_d^2\right].$$
 (1.53)

As discussed in Chaps. 3 and 8, the momentum-transfer collision integral in (1.51) is slightly different from the atomic one defined by (1.21). More important, however, is the presence in (1.52) and (1.53) of Φ , the dimensionless ratio of the collision integral for inelastic energy loss to that for momentum-transfer. Because Φ is multiplied by M_0/M in these equations, the presence of anisotropic interaction potentials and inelastic collisions for molecular systems is expected to be most important for the mobility in the case of light ions in heavy neutral gases. It should be noted, however, that there have been few experimental tests of this prediction (Viehland and Fahey 1983) and no theoretical calculations to show that the higher order corrections to these first-approximation equations of the two-temperature theory are as small as they are for atomic ion—atom systems.

Ion–neutral systems with molecular species must be characterized by at least three temperatures: the gas temperature, the temperature characterizing the kinetic energy of the ions, and the temperature characterizing the average energy possessed by the internal states of the molecule. The internal temperature, T_{int} , will generally depend upon the collision cross sections in a complicated way. However, there is one special case that is of particular importance: molecular ions in an atomic gas. In this special case, energy is fed into the internal degrees of freedom of the ions by collisions with the structureless neutrals and it leaks out of both the internal and translational degrees of freedom of the ions only through the translational motion of the neutrals. Since the outward leak is the same for both forms of energy, and since the source of the internal energy is the translational energy, T_{int} must be equal to T at steady state for this special case (Viehland et al. 1981).

The two-temperature-like kinetic theory for molecular systems leads to a first-approximation expression for the rate coefficient for the reaction between the molecular ions in a swarm and a small amount of reactive molecules immersed in a large amount of nonreactive, buffer gas. It is a generalization of (1.46),

48 1 Introduction

$$k = \left(\frac{1}{k_B T_R}\right) \left(\frac{8}{\pi \mu_R k_B T_R}\right)^{1/2} \frac{1}{Z Z_R} \sum_{\alpha, \beta} \int_0^\infty \exp\left(-\frac{\varepsilon}{k_B T_R}\right) \left(\frac{\varepsilon^{(a)}}{k_B T_{int}} - \frac{\varepsilon_R^{(\beta)}}{k_B T_0}\right) Q^* \left(\alpha, \beta; \varepsilon + \varepsilon^{(a)} + \varepsilon_R^{(\beta)}\right) \varepsilon d\varepsilon,$$
(1.54)

with T_R still given by (1.47). Here the ion and reactive neutral partition functions are given in terms of the respective internal energy levels, $\varepsilon^{(\alpha)}$ and $\varepsilon^{(\beta)}_R$, of ion and neutral states α and β by

$$Z = \sum_{\alpha} \exp\left(-\frac{\varepsilon^{(\alpha)}}{k_B T}\right) \tag{1.55}$$

and

$$Z_R = \sum_{\alpha} \exp\left(-\frac{\varepsilon_R^{(\beta)}}{k_B T_0}\right). \tag{1.56}$$

Note that the reactive cross section, Q^* , depends upon the internal states and upon the total collision energy, $\varepsilon + \varepsilon^{(a)} + \varepsilon_R^{(\beta)}$, where ε is the relative translational energy.

References

W.P. Allis, D.J. Rose, Phys. Rev. 93, 84 (1954)

W.S. Barnes, D.W. Martin, E.W. McDaniel, Phys. Rev. Lett. 6, 110 (1961)

E.C. Beaty, P.L. Patterson, Phys. Rev. 170, 116 (1968)

M.A. Biondi, Phys. Rev. 93, 1136 (1954)

A. Blanc, J. Phys. (Paris) 7, 825 (1908)

N.E. Bradbury, R.A. Nielsen, Phys. Rev. 49, 388 (1936)

G. Cavalleri, S.L. Paveri-Fontona, Phys. Rev. A 6, 327 (1972)

M.J. Druyvesteyn, Physica 10, 61 (1930)

M.J. Druyvesteyn, E.M. Penning, Rev. Mod. Phys. 12, 87 (1940)

D. Edelson, K.B. McAfee, Rev. Sci. Instrum. 35, 187 (1964)

G.A. Eiceman, Z. Karpas, H.H. Hill Jr., Ion Mobility Spectrometry, 3rd edn. (CRC Press, Boca Raton, 2014)

H.W. Ellis, R.Y. Pai, E.W. McDaniel, E.A. Mason, L.A. Viehland, At. Data Nucl. Data Tables 17, 177 (1976)

H.W. Ellis, E.W. McDaniel, D.L. Albritton, L.A. Viehland, S.L. Lin, E.A. Mason, At. Data Nucl. Data Tables 22, 17 (1978)

H.W. Ellis, M.G. Thackston, E.W. McDaniel, E.A. Mason, At. Data Nucl. Data Tables 31, 113 (1984)

J.P. England, M.T. Elford, Aust. J. Phys. 40, 355 (1987)

W.A. Everhart, W.A. Hare, E. Mack Jr., J. Am. Chem. Soc. 54, 888 (1932)

J.L.A. Francey, J. Phys. B 2, 680 (1969)

A.M. Gardner, C.D. Withers, J.B. Graneek, T.G. Wright, L.A. Viehland, W.H. Breckenridge, J. Phys. Chem. A 114, 7631 (2010)

I.R. Gatland, Case Stud. Atom. Phys. 4, 369 (1974)

References 49

- S. Geltman, Phys. Rev. 90, 808 (1953)
- O. Glasser, William Conrad Roentgen and the Early History of the Roentgen Rays (Charles C. Thomas, Springfield, Illinois, 1934)
- H.R. Hassé, Phil. Mag. 1, 139 (1926)
- H.R. Hassé, W.R. Cook, Phil. Mag. 12, 554 (1931)
- J.M. Heimerl, R. Johnsen, M.A. Biondi, J. Chem. Phys. 51, 5041 (1969)
- A.V. Hershey, Phys. Rev. 56, 916 (1939)
- J.O. Hirschfelder, C.F. Curtiss, R.B. Bird, Molecular Theory of Gases and Liquids (Wiley, New York, Corrected with Notes, 1964)
- F. Howorka, F.C. Fehsenfeld, D.L. Albritton, J. Phys. B 12, 4189 (1979)
- G.S. Hurst, J.E. Parks, J. Chem. Phys. 45, 242 (1966)
- L.G.H. Huxley, Aust. J. Phys. 25, 43 (1972)
- L.G.H. Huxley, R.W. Crompton, *The Diffusion and Drift of Electrons in Gases* (Wiley, New York, 1974)
- L.G.H. Huxley, R.W. Crompton, M.T. Elford, Br. J. Appl. Phys. 17, 1237 (1966)
- K. Kondo, H. Tagashira, J. Phys. D: App. Phys. 26, 1948 (1993)
- A.D. Koutselos, J. Chem. Phys. 102, 7216 (1995)
- K. Kumar, H.R. Skullerud, R.E. Robson, Aust. J. Phys. 33, 343 (1980)
- P.-H. Larsen, H.R. Skullerud, T.H. Lovaas, Th Stefansson, J. Phys. B 21, 2519 (1988)
- S.L. Lin, J.N. Bardsley, J. Phys. B 8, L461 (1975)
- S.L. Lin, J.N. Bardsley, J. Chem. Phys. 66, 435 (1977)
- S.L. Lin, J.N. Bardsley, Comp. Phys. Comm. 15, 161 (1978)
- S.L. Lin, I.R. Gatland, E.A. Mason, J. Phys. B. 12, 4179 (1979a)
- S.L. Lin, R.E. Robson, E.A. Mason, J. Chem. Phys. 71, 3483 (1979b)
- S.L. Lin, L.A. Viehland, E.A. Mason, Chem. Phys. 37, 411 (1979c)
- L.B. Loeb, Basic Processes of Gaseous Electronics (University of California Press, Oakland, 1955)
- T.H. Løvass, H.R. Skullerud, D.-H. Kristensen, D. Linhjell, J. Phys. D 20, 1465 (1987)
- J.J. Lowke, Aust. J. Phys. 28, 489 (1973)
- J.J. Lowke, J.H. Parker, Phys. Rev. 181, 302 (1969)
- E. Mack Jr., J. Am. Chem. Soc. 47, 2468 (1925)
- E.A. Mason, E.W. McDaniel, Transport Properties of Ions in Gases (Wiley, New York, 1988)
- E.A. Mason, H.W. Schamp Jr., Ann. Phys. 4, 233 (1958)
- K.B. McAfee, D. Edelson, Proc. Phys. Soc. London 81, 382 (1963)
- E.W. McDaniel, Collision Phenomena in Ionized Gases (Wiley, New York, 1964)
- E.W. McDaniel, E.A. Mason, The Mobility and Diffusion of Ions in Gases (Wiley, New York, 1973)
- E.W. McDaniel, D.W. Martin, W.S. Barnes, Rev. Sci. Instrum. 33, 2 (1962)
- E.W. McDaniel, J.B.A. Mitchell, M.E. Rudd, *Atomic Collisions: Heavy Particle Projectiles* (Wiley, New York, 1993)
- R.M. Melaven, E. Mack Jr., J. Am. Chem. Soc. 54, 888 (1932)
- T.M. Miller, J.T. Moseley, D.W. Martin, E.W. McDaniel, Phys. Rev. 173, 115 (1968)
- J.T. Moseley, R.M. Snuggs, D.W. Martin, E.W. McDaniel, Phys. Rev. Lett. 21, 873 (1968)
- J.T. Moseley, I.R. Gatland, D.W. Martin, E.W. McDaniel, Phys. Rev. 178, 234 (1969)
- N.F. Mott, H.S.W. Massey, The Theory of Atomic Collision (Clarendon Press, Oxford, 1965)
- K.F. Ness, L.A. Viehland, Chem. Phys. 148, 255 (1990)
- A. Pais, Beam Line **27**, 4 (1997)
- J.H. Parker, Phys. Rev. **139**, A1792 (1965)
- J.H. Parker, J.J. Lowke, Phys. Rev. 181, 290 (1969)
- J. Philibert, Diffus. Fundam. **4**, 6.1 (2006)
- H.E. Revercomb, E.A. Mason, Anal. Chem. 47, 970 (1975)
- R.E. Robson, Aust. J. Phys. 25, 685 (1972)
- R.E. Robson, J. Phys. B 9, L337 (1976)
- R.E. Robson, *Introductory Transport Theory for Charged Particles in Gases* (World Scientific, Singapore, 2006)

50 1 Introduction

- G. Schultz, G. Charpak, F. Sauli, Rev. Phys. Appl. 12, 67 (1977)
- H.R. Skullerud, J. Phys. D 1, 1567 (1968)
- H.R. Skullerud, J. Phys. B 2, 696 (1969)
- H.R. Skullerud, J. Phys. B 6, 728 (1973)
- H.R. Skullerud, J. Phys. B 9, 535 (1976)
- H.R. Skullerud, J. Phys. B 17, 913 (1984)
- H.R. Skullerud, Plasma Sources Sci. Tech. 26, 045003 (2017)
- R.F. Snider, J. Chem. Phys. 32, 1051 (1960)
- R.K. Standish, Aust. J. Phys. 40, 519 (1987)
- A.M. Tyndall, The Mobility of Positive Ions in Gases (Cambridge Physical Tracts, Cambridge University Press, Cambridge, 1938)
- L.A. Viehland, Chem. Phys. 179, 71 (1994)
- Viehland database (2018), www.lxcat.net
- L.A. Viehland, D.W. Fahey, J. Chem. Phys. 78, 435 (1983)
- L.A. Viehland, S.L. Lin, Chem. Phys. 43, 135 (1979)
- L.A. Viehland, E.A. Mason, Ann. Phys. (N.Y.) 91, 499 (1975)
- L.A. Viehland, E.A. Mason, J. Chem. Phys. **66**, 422 (1977)
- L.A. Viehland, E.A. Mason, Ann. Phys. (N.Y.) 110, 287 (1978)
- L.A. Viehland, E.A. Mason, At. Data Nucl. Data Tables 60, 37 (1995)
- L.A. Viehland, R.E. Robson, Int. J. Mass Spectrom. Ion Proc. 90, 167 (1989)
- L.A. Viehland, E.A. Mason, J.H. Whealton, J Phys. B 7, 2433 (1974)
- L.A. Viehland, S.L. Lin, E.A. Mason, J. Chem. Phys. 54, 341 (1981)
- L.A. Viehland, R. Johnsen, B.R. Gray, T.G. Wright, J. Chem. Phys. 144, 074306 (2016)
- L.A. Viehland, T. Skaist, C. Adhikari, A. Landin, W.F. Siems, Int. J. Ion Mobility Spectrom. 20, 1 (2017)
- G.P. von Helden, P.R. Kemper, M.-T. Hsu, M.T. Bowers, J. Chem. Phys. 96, 6591 (1992)
- E.B. Wagner, F.J. Davis, G.S. Hurst, J. Chem. Phys. 47, 4138 (1967)
- M. Waldman, E.A. Mason, Chem. Phys. 58, 121 (1981)
- L. Waldmann, Quantum-theoretical transport equations for polyatomic gases, in *Statistical Mechanics of Equilibrium and Non-equilibrium*; Proc. Int. Symp. Stat. Mech. Thermodyn. at Aachen, Germany, June 15-20, 1964, ed. by J. Meixner. (North-Holland, Amsterdam 1965)
- C.S. Wang Chang, G.E. Uhlenbeck, J. de Boer, in *Studies in Statistical Mechanics*, ed. by J. de Boer, G.E. Uhlenbeck (North-Holland, Amsterdam, 1964)
- G.H. Wannier, Phys. Rev. 87, 795 (1952)
- G.H. Wannier, Bell Syst. Tech. J. 32, 170 (1953)
- H.T. Wood, J. Chem. Phys. 54, 977 (1971)
- A. Yousef, S. Shrestha, L.A. Viehland, E.P.F. Lee, B.R. Gray, V.L. Ayles, T.G. Wright, W.H. Breckenridge, J. Chem. Phys. 127, 154309 (2007)
- M. Yousfi, A. Hennad, O. Eichwald, J. Appl. Phys. 84, 107 (1998)

Chapter 2 Experimental Techniques



2.1 General Assumptions

This chapter will discuss experimental techniques that have used drift tubes to study ion motion in gases, but primarily from the viewpoint of what implications the theories discussed in Chap. 1 (and later in this book) have for the experiments. This means, in particular, that little or no attention will be given to applications, particular instrumental problems and advancements, or similar things. Some of the material omitted here can be found in the books by Mason and McDaniel (1988), Shvartsburg (2009) and Eiceman et al. (2014). However, much of it will have to be pursued in the original research.

The experiments of primary interest in this book are those in which a trace amount of ions moves through a dilute gas under the influence of electrical fields external to or on the boundaries of the drift tube containing the ions and buffer gas molecules. We are specifically excluding plasmas in which both positive and negative charges are present, and hence we are not concerned with ambipolar diffusion (see Sect. 1.14).

All of the instruments that use drift tubes to study ion motion in gases satisfy a number of restrictions (Ness and Viehland 1990). In order to encompass a wide variety of experimental techniques, we impose only the most general of restrictions, as follows.

- 1. The velocities of all particles (except the electrons within the atoms and molecules involved) are much smaller than the speed of light in a vacuum.
- 2. The dilute neutral gas can be a mixture, but the entire gas is in equilibrium. The vdf for each neutral species therefore has the usual Maxwellian form for atoms, given by (4.18) below, or the Maxwell–Boltzmann form for molecules with internal degrees of freedom, given by (3.19).
- 3. The ion number densities are small, so only trace amounts of ions are present at any time. Since a mixture of trace ions (all cations or all anions) can be treated as a superposition of separate swarms, in theoretical discussions we need consider only one ion species at a time. An ion mobility spectrum observed experimentally,

for cations only or for anions only, is just a superposition of the arrival time spectra that could be observed for each separate ion.

4. The effects of the apparatus walls are negligible, so the ion swarm can be given a hydrodynamic description involving a stationary vdf and small gradients of the ion number density.

It is beyond the scope of this book to discuss the short-time development of swarms, i.e., how a swarm approaches its large-time, hydrodynamic behavior; readers interested in this topic should consult the specialized papers devoted it (Kumar 1981, 1984; Robson et al. 2002). It is also beyond the scope to consider the many types of instruments which contain drift tubes and their applications, particularly in analytical chemistry. Below we will consider several such instruments, but for more complete introductions to these the reader is referred to the books by Eiceman et al. (2014) and Shvartsburg (2009).

2.2 Drift-Tube Mass Spectrometers

2.2.1 Illustration

To illustrate a DTMS we will describe the Pittsburgh DTMS that was moved in late 2016 from the University of Pittsburgh to Chatham University. A schematic diagram of this instrument is given in Fig. 2.1.

The neutral gas in the drift tube is kept at a pressure of between 0.1 and 10 torr (10-1000 Pa) by the combined action of the two diffusion pumps indicated by the large arrows in Fig. 2.1 and a slow leak from the gas manifold. The gas temperature and pressure are measured with gauges connected to the device and shown schematically

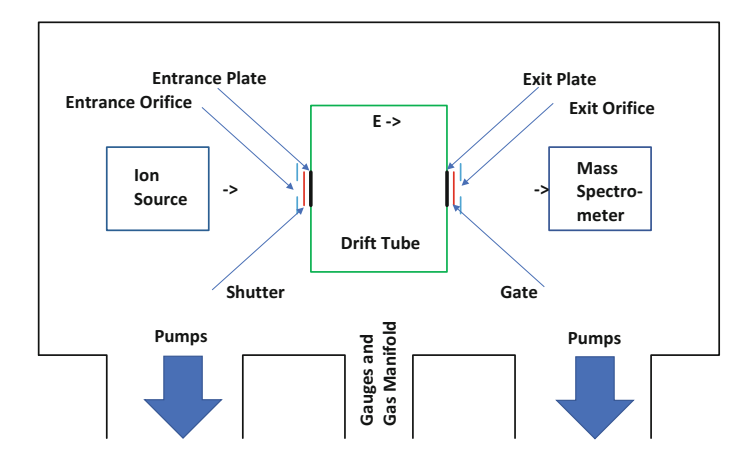


Fig. 2.1 Schematic diagram of the Pittsburgh DTMS

at the center of the bottom of Fig. 2.1. All of the electrical connections discussed below are also made through this port.

The ion source is indicated by a box in Fig. 2.1, since different DTMS have sources of various kinds. In working with cations in the Pittsburgh DTMS, an appropriate gas is admitted through a capillary into the source region, where it is ionized by electrons emitted from a hot filament (a Thoria-coated iridium ribbon). The ions are accelerated by applying the appropriate voltages to electrodes in the source, and they are guided with other small electrical fields into the drift tube through a small (25 μm diameter) entrance orifice. They next encounter a shutter, a pair of wire grids that are usually maintained at a voltage difference sufficient (about 2 V) to keep the ions out of the drift tube. The shutter is connected to a pulse generator that can counteract the shutter voltage for a variable period of time, typically one μs . This causes a pulse of ions to move into the drift tube through a small hole in the entrance plate.

The drift tube is about 0.3 m long and contains twelve guard rings made from stainless steel. All of the ring electrodes are wired via a vacuum feed-through to a small box that contains a resistor chain made from precision, $2~k\Omega$ resistors. Great care is taken to make sure that the resulting electric field in the drift tube, indicated as E in Fig. 2.1, is static and highly uniform, except very close to the entrance and exit plates. Nonuniformities cannot be avoided there, and they cause so-called end effects that are discussed below. In addition, the electric fields used to guide the ions into the drift tube lead to what are called injection effects, where the ions are moving with an average velocity and energy different than the ones that will be attained in the main portion of the drift tube. Note that the pulse generator can cause additional end and injection effects.

After leaving the drift tube through a small hold in the exit plate, the ions encounter another pair of wire grids that is called the gate. When the shutter is closed but the pulse generator allows ions to enter the drift tube, the gate is kept open in order to record data about the ion pulses as they move from the shutter all the way to the ion detector. After data collection from the shutter if finished, the shutter is kept open but the gate is closed unless the pulse generator opens it for a brief period of time. Hence this gives data about the ion pulses as they move from the gate to the detector.

The ion detector or analyzer section of the Pittsburgh DTMS contains the mass spectrometer indicated in Fig. 2.1, a Channeltron, and electrical connections to a multichannel analyzer (MCA). The quadrupole mass spectrometer is differentially pumped, i.e., the second diffusion pump is used to lower the gas pressure from the "high" value in the drift tube down to 10^{-7} torr (10^{-5} Pa) or less. As the name implies, it has four cylindrical rods, and these are surrounded by a boron nitride yoke that is biased to accelerate the ions from the exit orifice into the quadrupole.

Ions with the proper q/m (equivalently, m/q) ratio are passed by the mass spectrometer and detected by a Channeltron multiplier. This has a gain of about 10^8 , which means that about 10^8 electrons leave the Channeltron for each ion that strikes its entrance funnel. These electrons form a negatively charged pulse (about 10 mV into a 50 Ω resistor) that is detected by a preamplifier and discriminator. The discriminator selects pulses that exceed an adjustable threshold, thus rejecting small

pulses due to electrical noise and RF signals that can arise from the Channeltron or other electrical devices in the laboratory.

The output pulses from the discriminator are fed to an MCA that accumulates and stores the counts received in a given time window that is automatically reset to t=0 whenever it senses that the pulse generator has started moving towards the voltage that it is set to provide to the shutter or gate. Being able to set the channel widths to 0.1-1.0 ns is important, as will be shown below.

The MCA is connected to a computer, and the software supplied by the MCA manufacturer allows the experimenter to watch the arrival time spectrum of the ions as it develops. When the displayed counts reach about 1000 in the channel where it is at a maximum, the experiment is stopped and the data transferred to a separate computer where it can be analyzed.

2.2.2 Basics

As illustrated above, a drift tube is a cylinder made of closely spaced and appropriately biased ring electrodes. There is an ion source that delivers ions along the axis of the drift tube, where the rings establish an electrostatic field that is highly uniform. Unless specifically indicated otherwise, we will assume that there are no external magnetic fields and that the ions are introduced into the drift-tube in pulses.



McDaniel

Using a mass spectrometer as the ion detector at the end of a drift tube produces a compound instrument known as a DTMS. The first DTMS were developed under the leadership of Earl Wadsworth McDaniel (1926–1997) at the Georgia Institute of Technology (Barnes et al. 1961; McDaniel et al. 1962) and by a team at Bell Telephone Laboratories (McAfee and Edelson 1963; Edelson and McAfee 1964).

Mason and McDaniel (1988) have given complete but reasonably concise descriptions of low-pressure DTMS, variable-temperature instruments, a reversible-field (ping-pong) DTMS, a selected-ion drift apparatus, and a selected-ion flow-drift tube. Although some of those instruments are no longer in service, others have since

been placed into operation that differ only slightly from each other and from the Pittsburgh DTMS. However, the operation of the various instruments will be much easier to understand if the basics of DTMS are described carefully.

We define a DTMS for measuring ion mobilities as a device with all or most of the following features:

1. A cylindrical enclosure containing a dilute gas at constant T_0 and P_0 such that

$$n_0 = \frac{P_0}{k_B T_0 z_0}. (2.1)$$

Here z_0 is the compressibility factor that accounts for deviations of (2.1) from the ideal gas equation. In most DTMS, $z_0 = 1$. If the gas is near or above atmospheric pressure, however, the value of z_0 must be determined by independent measurements. The dilute gas is ordinarily the naturally occurring mixture of the isotopes of a inert gas like Ar or N_2 , or a gas mixture (like purified air) whose composition is well characterized.

- 2. A source (external or internal) that produces ions in trace amounts, i.e., *n* is so low that space charge has no appreciable effect on the ion motion.
- A thermalization region following the source in which the ions achieve a steadystate distribution by means of collisions with the dilute gas atoms or molecules.
- 4. Where necessary, bias voltages that guide the ions so that they are moving along the axis of the cylinder when they reach the entrance to the drift tube, which is usually a small hole in a metal plate.
- 5. Where necessary, a mass spectrometer before the drift tube that ensures that only specific ions get into the drift region.
- 6. Two wire grids, together known as the shutter, that have a sufficiently high voltage difference to keep all the ions in the thermalization region but that can be pulsed to admit a small number of ions into the drift region; the pulses typically are 0.5–2 μs in duration.
- 7. A drift region of precisely and accurately known length that contains a set of ring electrodes that establish a highly uniform, axial, electrostatic field whose magnitude is $E = \varepsilon_V/L$.
- 8. Another pair of wire grids, together known as the gate. The gate is kept open when one is measuring the ions' arrival at the detector after they have started at the shutter. It is kept closed but pulsed open when one is measuring the ions' arrival at the detector after they start from the gate.
- 9. A mass spectrometer that serves as the detector because it senses the arrival of ions with the correct mass-to-charge ratio as they pass through the shutter and the gate (or just the gate).
- 10. A multichannel analyzer (MCA) that produces data from which the arrival times from the shutter and the gate can be determined and then analyzed to give $\langle t \rangle$.

2.2.3 Ion Mobility

In the drift tube, ions quickly acquire an average drift velocity as a result of a balance between the momentum gained from the electric field and that lost by collisions with the neutral gas atoms or molecules. This drift velocity must lie along **E**. If we ignore injection and end effects until later in this chapter, then (1.5) indicates that the magnitude of the drift velocity can be determined from measurements of L and $\langle t \rangle$. After v_d has been measured at particular values of ε_V , P_0 and T_0 , the mobility, K, is computed from (1.4) and then converted to a value of K_0 by means of (1.7). The working equations are

$$K_0(E/n_0, T_0) = \frac{L}{(E/n_o)N_0 \langle t \rangle}$$
 (2.2)

and

$$E/n_0 = \frac{\varepsilon_V z_0}{L N_0} \left(\frac{101325 \,\text{Pa}}{P_0}\right) \left(\frac{T_0}{273.15 \,\text{K}}\right).$$
 (2.3)

Values of K_0 are then reported as functions of T_0 and E/n_0 ; the functional dependence upon two variables is indicated by the notation on the left-hand side of (2.2). The value of T_0 affects both E/n_0 and $\langle t \rangle$.

It is straightforward to combine (2.2) and (2.3) to give

$$K_0(E/n_0, T_0) = \frac{L^2}{\varepsilon_V \langle t \rangle z_0} \left(\frac{P_0}{101325 \text{ Pa}} \right) \left(\frac{273.15 \text{ K}}{T_0} \right).$$
 (2.4)

At low E/n_0 , the product $\varepsilon_V \langle t \rangle$ becomes constant, so $K_0(E/n_0, T_0)$ becomes equal to the low-field standard mobility, $K_0(0, T_0)$.

2.2.4 Effects of Drift-Tube Length

Equation (2.4) shows that $K_0(E/n_0, T_0)$ and $K_0(0, T_0)$ depend on the square of L. One power arises from determining E/n_0 from (2.3) and the other from then determining $K_0(E/n_0, T_0)$ from (2.2). Therefore, considerable care must be exercised to determine this distance if one hopes to get accurate mobility data. Unfortunately, no matter how accurately the length of the drift tube is determined before the DTMS is constructed, it is not obvious whether the widths of the grids constituting the shutter and gate should be incorporated into the value of L.

A careful comparison (Viehland et al. 2017) of ${}^{4}\text{He}^{+}({}^{2}\text{S}_{1/2})$ mobilities in ${}^{4}\text{He}({}^{1}\text{S}_{0})$ at 300 K with values computed ab initio led to a value of L for the Pittsburgh DTMS that was only slightly larger than the sum of the measured distances between the top and bottom of the drift tube and between the wires constituting the shutter (both measured when the instrument was disassembled). It is best if L is determined for

each DTMS or IMS by similar methods, but at the very least L should not be assumed to be equal to the measured length of the drift tube alone.

2.2.5 Effects of Gas Temperature

The gas temperature affects the measured mobility in three ways. The first effect arises because T_0 appears in (2.3) and (2.4); this potential source of error can be overcome by using a calibrated thermometer, such as those used in calorimetric studies of chemical reactions. The second effect is more difficult to account for, since it arises because the average energy of an ion–neutral collision depends upon T_0 . As shown in Fig. 2.2, sometimes this dependence has a weak effect on $K_0(0, T_0)$ and sometimes it is significant. The third effect is that ion–neutral reactions can be quite sensitive to small changes in T_0 ; since reactions have only a small influence on mobility and diffusion coefficients, we will defer consideration of this effect until Chap. 7.

Most of the currently operating DTMS work at room temperature, since there is no advantage to increasing T_0 when high energies can more easily be probed by increasing E/n_0 and since lowering T_0 is difficult and expensive. There is a problem in working at room temperature, however. When setback thermostats are used to control building and laboratory temperatures, which therefore may not be

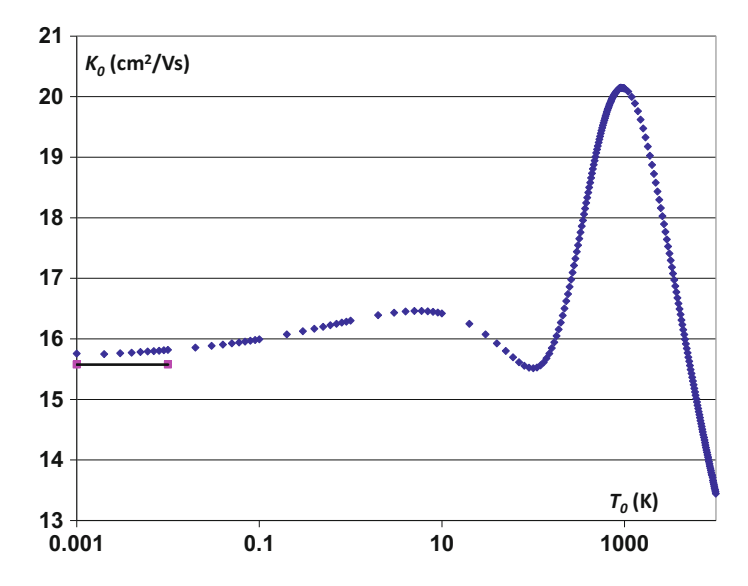


Fig. 2.2 Zero-field standard mobility as a function of T_0 for $^{107}{\rm Ag}^+(^1{\rm S}_0)$ in ${\rm He}(^1{\rm S}_0)$, as computed from the potential of Viehland and Yang (2015). The short horizontal line at the left indicates the limit as $T_0 \to 0$

under the control of the experimenter, the measured T_0 can vary during a series of measurements, particularly those conducted over several or many days. The question is then how to determine $K_0(E/n_0, T_0)$ as a function of E/n_0 at the same, fixed value of T_0 .

Let's assume that we want to report mobilities at 300.00 K. If there are theoretical values of the ion mobility to compare against, then one can determine the difference between the theoretical values at T_0 and 300.00 K and add (or subtract) this small amount from the experimental value at T_0 . This is what was done by Viehland et al. (2017). In most case, however, theoretical values are not available. In such cases, the nominal value, K_n , of K_0 at T_0 should be used to obtain T_0 at 300.00 K from the equation

$$K_0 = K_n - \kappa \left(\frac{300.00 \text{ K} - T_0}{T_0} \right). \tag{2.5}$$

The value of κ can be obtained experimentally from a few values of K_n near 300.00 K, or from tabulated values (Ellis et al. 1976, 1978, 1984; Viehland and Mason 1995) near 300.00 K of the logarithmic derivative of the mobility with respect to the effective temperature. In the cases examined so far, the correction due to (2.5) was never larger than 0.01 cm²/Vs for differences of a few Kelvin between T_0 and 300.00 K; corrections of this magnitude are important only in attempts to make highly accurate measurements of $K_0(E/n_0, T_0)$.

2.2.6 Effects of Gas Pressure

The gas pressure also affects the measured mobility in three ways. The first is because P_0 appears in (2.3) and (2.4), while the second arises because the average energy of an ion–neutral collision depends upon E/n_0 and hence, from (2.1) or (2.3), upon P_0 . The third arises from its influence on the total chemical reaction rate; once again, this will be deferred to Chap. 7.

In contrast to the second effect of T_0 , the second effect of P_0 can be ignored. This is because one is ordinarily interested in determining $K_0(E/n_0, T_0)$ as a function of E/n_0 at the same, fixed value of T_0 , so variations in n_0 can be considered along with variations in ε_V that lead to E/n_0 from (2.3). The first effect of P_0 is minimal because modern instruments for measuring P_0 come with built-in calibration procedures that allow values to be obtained that are accurate to 0.001%. Hence we can defer consideration of the effects of pressure errors to Sect. 2.2.9.

2.2.7 Effects of Electromagnetic Field

It is important that an experimenter using a DTMS makes accurate measurements of ε_V . It is okay to use a multimeter for this purpose, as long as it has been separately

calibrated to give results near 100 V that are accurate to four or more significant figures (Viehland et al. 2017). Any remaining inaccuracies in either n_0 or ε_V can be considered to be errors in E/n_0 and treated as described in Sect. 2.2.9.

2.2.8 Effects of Time Measurements

A MCA usually includes computer programs to determine the centroid, average, standard deviation, and other properties of the ion arrival time distribution. It is important to check this software, for example by moving raw data from the MCA to an Excel spreadsheet and reanalyzing it. Our experience (Viehland et al. 2017) is that the time differences are accurate to about 0.03% when the signal-to-noise ratio of the arrival time spectrum is large. We will discuss later the mean, standard deviation, and skewness of the arrival time distributions, while considering how to compensate for even the small errors in $\langle t \rangle$ in the next subsection.

2.2.9 Calibration of the Entire DTMS

The five effects just described have been recognized for many years, and considerable effort has been expended trying to minimize them in order to obtain highly accurate mobilities. Nevertheless, with few exceptions, experimental results have had estimated errors of 2% or more for the last 40 years. Since it is presently possible to make ab initio calculations for atomic ion—atom systems that are more accurate than this (if the ion—neutral interaction potential is correct), it is time that experimenters begin using theoretical results to calibrate their DTMS as a whole.

The purpose of this calibration step is to compensate for errors due to interactions between the measurements of L, T_0 , P_0 , ε_V and $\langle t \rangle$ and for errors due to things that indirectly affect the measured mobilities (such as the emf and the duration of the pulses delivered to the shutter and gate, voltages used as signal conditioners to remove much of the random noise delivered to the mass spectrometer, etc.) It also can calibrate systematic errors due to improper calibration of the devices mentioned above, for systematic but poor choices for when a signal begins and ends its arrival at the mass spectrometer, for the use of pulse voltages sent to the shutter or gate that do not properly overcome the bias voltages keeping these grids closed, and for other things cited by Viehland et al. (2017).

It will be assumed in the rest of this subsection that any of the indirect influences just discussed cause a small but constant error when experiments are performed in the same manner each time. It will also be assumed that errors in L are constant; this assumption is necessary because it is not possible to make changes in L without disassembling the instrument, and even this might not help because the distances between the wire grids in the shutter and gate may change during reassembly. However, the true values of the four remaining variables $(T_0, P_0, \varepsilon_V)$ and $\langle t \rangle$ may be

slightly different than the nominal values (indicated by a subscript n) shown by the instruments attached to the apparatus. Equation (2.4) gives

$$\frac{K_0(E/n_0, T_0)}{K_{0,n}(E/n_0, T_0)} = (1 + \widetilde{c}) \left(\frac{\varepsilon_V}{\varepsilon_{V,n}}\right)^{-1} \left(\frac{\langle t \rangle}{\langle t \rangle_n}\right)^{-1} \left(\frac{P_0}{P_{0,n}}\right) \left(\frac{T_0}{T_{0,n}}\right)^{-1} \tag{2.6}$$

where \tilde{c} indicates the effect of all of the errors that we have assumed to be constant. It should be noted that the emf in (2.6) and in similar equations below is often called the drift voltage.

We now let

$$\langle t \rangle = \langle t \rangle_n + \delta_t, \tag{2.7}$$

and similarly for the other three quantities. This converts (2.6) into the equation,

$$\frac{K_0(E/n_0, T_0)}{K_n(E/n_0, T_0)} = (1 + \widetilde{c}) \left(1 + \frac{\delta_{\varepsilon}}{\varepsilon_n} \right)^{-1} \left(1 + \frac{\delta_t}{\langle t \rangle_n} \right)^{-1} \times \left(1 + \frac{\delta_P}{P_{0,n}} \right) \left(1 + \frac{\delta_T}{T_{0,n}} \right)^{-1} \tag{2.8}$$

Multiplying the terms on the right-hand side gives a simple result if we assume that \widetilde{c} and the ratios involving the various δ are small, use Taylor series expansions (see Appendix A), and drop terms that are the products of two or more small quantities. We get

$$\frac{K_0(E/n_0, T_0)}{K_n(E/n_0, T_0)} = 1 + \widetilde{c} - \frac{\delta_{\varepsilon}}{\varepsilon_{V,n}} - \frac{\delta_t}{\langle t \rangle_n} + \frac{\delta_P}{P_{0,n}} - \frac{\delta_T}{T_{0,n}}.$$
 (2.9)

Equation (2.9) is in a form suitable for least-square determination (see Appendix A) of \widetilde{c} and the δ quantities after at least 15 measurements of the ratio on the left-hand side, i.e., the ratio of the theoretical mobility at the given E/n_0 and T_0 to the experimental value obtained by using the nominal values of the five variables in the right-hand side of (2.4) After determining \widetilde{c} and the δ quantities, it is important to make an additional 15 or more measurements of $K_n(E/n_0, T_0)$, convert them to values of $K_0(E/n_0, T_0)$ by using (2.9), and compare the results to the appropriate theoretical values. After such a calibration (Viehland et al. 2017), the Pittsburgh DTMS was found to give mobilities precise (reproducible) within $\pm 0.6\%$. A least-squares determination of the best fit through such reproducible data gave mobilities accurate within $\pm 0.4\%$ when compared to ab initio values calculated as described in Chap. 6.

2.3 Ion Arrival Time Distributions

The data analysis described in the previous section assumes that it is easy to determine $\langle \tau \rangle_n$ in a particular experiment. That this is not always the case can be illustrated by considering the Pittsburgh DTMS. (Each separate DTMS and IMS should be analyzed by methods similar to those described below.)

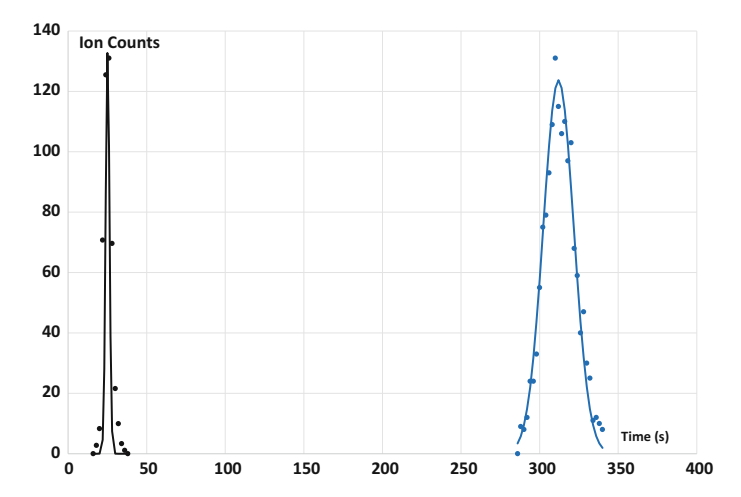


Fig. 2.3 Arrival time distributions for ${}^{4}\text{He}^{+}$ ions in ${}^{4}\text{He}$ at T_{0} =301.5 K and E/n_{0} =45 Td. The blue points at large times are experimental values obtained when the ions start at the shutter. The black points at small times are when they arrive from the gate. The curves are Gaussian fits to the data

Figure 2.3 shows the arrival time distributions from the shutter and gate when each is opened by a pulse 2 μs in duration. This was the minimum bin width in the MCA in use at that time. The background has been determined by averaging the $^4\text{He}^+(^2S_{1/2})$ counts in bins far away from those included in the peaks, and this small background has been subtracted from the counts recorded in each of the bins. There are very few points in the peak arriving from the gate, making it difficult to identify the peak time with an accuracy better than 1 μs . There are more points in the peak arriving from the shutter, but statistical fluctuations still limit the accuracy with which the peak time can be determined. Therefore the value $\langle \tau \rangle_n$ obtained by subtracting the times of the two maxima is uncertain by about 1%, even when Gaussian fits to the data are made; this was perhaps the biggest source of uncertainty in measuring the mobility when these data were obtained.

To overcome this problem, we acquired a modern MCA, one with bin widths as small as 0.1 μs . Figure 2.4 shows the measured arrival time distributions (after removal of the small background count) when the shutter and gate are pulsed by 1 μs and the bin widths are 0.5 μs ; the values obtained from the gate have been adjusted so the two peak heights are identical. The increased number of data points (four times as many) means that the arrival time distributions from the gate and shutter are more precisely determined. This in turn means that the value of $\langle \tau \rangle_n$, obtained by subtracting the times of the maxima, has an uncertainty of less than 0.1%, greatly reducing the imprecision of the mobility data (Viehland et al. 2017).

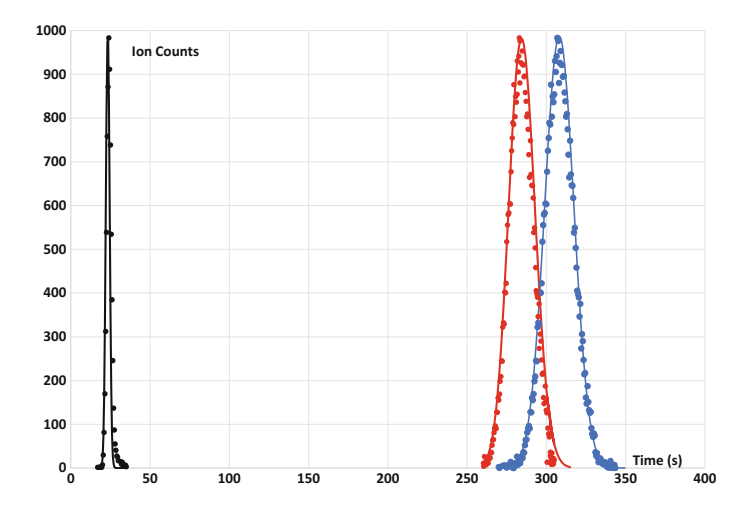


Fig. 2.4 Same as Fig. 2.3, but obtained with a modern multichannel analyzer. The red points are obtained by subtracting a Gaussian distribution of the gate points from the shutter points. The red curve is discussed in Sect. 2.4

2.4 Diffusion in Drift-Tube Mass Spectrometers

The arrival time distributions in Fig. 2.4 show tails, particularly when the ions arrive from the gate. There are no excited states of ${}^{4}\text{He}^{+}$ in these experiments, but the tails indicate that the arrival time distributions still are not Gaussian. If we ignore this, then values of D_L can be determined (Viehland et al. 2017) from the equation

$$\frac{D_L}{K} = \frac{\varepsilon_V}{2} \frac{\sigma_{\parallel,1}^2 - \sigma_{\parallel,2}^2}{\langle t \rangle_n^2},\tag{2.10}$$

where $\sigma_{\parallel,1}$ and $\sigma_{\parallel,2}$ are the standard deviations of the arrival times along the field when the ions have started at the shutter and gate, respectively. Moreover, if the distributions are Gaussian then there is a well-known relationship between the standard deviation and the full width at half-height, F_{\parallel} :

$$\sigma_{\parallel} = \frac{F_{\parallel}}{2\sqrt{2\ln(2)}} \approx \frac{F_{\parallel}}{2.355}.$$
 (2.11)

It is more accurate to measure F_{\parallel} than σ_{\parallel} when the arrival time spectrum has a poor signal-to-noise ratio, a moderate degree of skewness or kurtosis, two or more overlapping peaks, or is so sharply peaked that only a few points on a peak can be measured. In favorable situations, we have measured F_{\parallel} and computed values of D_L/K that are within 2–5% of values computed ab initio.

Unfortunately, a Gaussian distribution does not satisfy the diffusion equation, (1.42). There is a long history of determining distributions that do satisfy this equation, as discussed by Orient (1974) and in Sect. 2-6 of Mason and McDaniel (1988). The following assumptions can be made in order to solve this equation (Orient 1974):

- the ions enter the drift space through a circular hole of radius r_1 lying in a plane perpendicular to and centered on the axis of the drift tube;
- a pulse generator is used to create "instantaneously" a thin disk of b_1 ions with a Gaussian distribution along the field that has a standard deviation of σ_1 ;
- there are no ion sources within the drift tube, but ions can be removed by secondorder chemical reactions with the neutral gas;
- the radii of the rings determining the drift region are so much larger than the radius of the entrance hole that a negligible number of ions reach the rings by diffusion;
- T_0 and E/n_0 have constant values, which means that the transport and reaction rate coefficients have constant values in one particular experiment; and
- the ions leave the drift tube through a circular hole of radius r_2 lying in a plane perpendicular to and on the axis of the drift tube.

Then the analytical solution of the generalized diffusion equation in Cartesian coordinates, (1.42), considering motion only along the field, gives an expression for the ion flux density at distance z_1 along the axis. After correcting misprints in the paper by Orient (1974), this expression is

$$j(z_1, t) = \frac{r_2 b_1}{4\pi r_1^2 \sqrt{2\pi}} \frac{(z_1 + v_d t) D_L + \sigma_1^2 v_d}{\left(\sigma_1^2 + 2D_L t\right)^{3/2}} \left[1 - \exp\left(-\frac{r_0^2}{4D_T t}\right) \right] \times \exp\left(-kt - \frac{(z - v_d t)^2}{2\left(\sigma_1^2 + 2D_L t\right)}\right).$$
(2.12)

In the limit $\sigma_1 \to 0$, this result agrees with that of Moseley et al. (1969) for an initial pulse of uniform density.

In principle, v_d (or equivalently, K_0), D_L , D_T and k can be determined by a multiparameter fit of (2.12) to the experimental data for the arrival time of the ions at the detector. In practice, the effects of each of the transport and reaction coefficients on $j(\mathbf{r},t)$ are first closely approximated by separate analyses and then confirmed by such a fit.

Before discussing the separate analyses, it is important to note that v_d is not equal to $\langle v \rangle$ when diffusion is considered, as indicated in Sect. 1.9. Moreover, (2.12) does not take into account end effects, such as the ion motion from the end of the drift tube through the mass spectrometer. It also does not take into account injection effects that arise because the apparatus cannot possibly deliver repeated pulses in which every ion is moving with exactly the same velocity at time t=0, or even a Gaussian distribution with a constant σ_1 . The end and injection effects can best be minimized by subtracting the ion arrival time distributions with the same maximum number of counts from the shutter and the gate, as shown by the red points in the middle of Fig. 2.4. Specifically, the time when a specific fraction of the maximum

number of counts arrive from the shutter is decreased by the time that it takes the same fraction of counts to arrive from the gate, as obtained by a Gaussian or other fit to the normalized data from the gate. (It is important to note that the Gaussian fit shown in Fig. 2.3 for the arrival time distribution from the shutter is not used in this data analysis, but are shown there only as a guide to the eye.) The red points should then be described by (2.12).

The diffusion coefficient perpendicular to the field appears in (2.12) only in the term that is enclosed in square brackets. Determining this transport coefficient therefore requires that measurements be made as a function of the size of the entrance hole, which is a virtually impossible task. Instead, one should consider the solution of the diffusion equation in all three spatial dimensions and then measure the arrival time distribution as a function of how far the detector is from the axis of the drift tube. The interested reader should consult Sect. 2-6 of Mason and McDaniel (1988).

The reaction rate coefficient appears in (2.12) only as the customary exponential decay. Hence extracting its value from DTMS data involves an experimental technique that can be viewed as equivalent to adding a small amount (compared to the nonreactive, buffer gas) of a reactive neutral near the middle of the drift tube and observing the decrease in the flux of the reactant ions (or an increase in the flux of product ions) as a function of the amount of reactive gas added. A further generalization is to study two or more ion species that are in dynamic equilibrium during their motion through the drift tube. Analysis (Iinuma 1991; Iinuma et al. 1993, 1994) of an extension of the diffusion equation to this situation leads to a generalization of (2.12) that agrees with experimental results (McKnight et al. 1967) for the reaction of N_4^+ with N_2 . Further discussion of reactive studies in DTMS will be deferred until Chap. 7.

Setting k and r_0 equal to zero in (2.12) gives the ion flux arriving at the detector as

$$j(z_1, t) = \tilde{c} \frac{(z_1 + v_d t) D_L + \sigma_1^2 v_d}{(\sigma_1^2 + 2D_L t)^{3/2}} \exp\left(-\frac{(z_1 - v_d t)^2}{2(\sigma_1^2 + 2D_L t)}\right), \tag{2.13}$$

where \tilde{c} is a normalization constant. For a slab pulse, where $\sigma_1 = 0$, this reduces to

$$j(z_1, t) = \tilde{c} \, \frac{(z_1 + v_d t)}{D_L^{1/2} t^{3/2}} \exp\left(-\frac{(z_1 - v_d t)^2}{4D_L t}\right),\tag{2.14}$$

where \tilde{c} has a slightly different value than in (2.13). This expression for the ion flux density should not be confused with the similar equation (when the same approximations are made) for the axial ion number density, which is

$$n(z_1, t) = \frac{\tilde{c}}{(4\pi D_L t)^{1/2}} \exp\left(-\frac{(z_1 - v_d t)^2}{4D_L t}\right). \tag{2.15}$$

The difficulty with (2.13) is that it is unclear what values should be used for z_1 and σ_1 . A first guess is that $\sigma_1 = 0$ and that z_1 is equal to the measured length of the drift

tube without including the shutter widths. The red curve in Fig. 2.4 has been obtained using these values in (2.13) along with ab initio values of v_d and D_L ; adjusting the value of \widetilde{c} to give the proper maximum count clearly gives excellent agreement with the measured arrival time distribution. Work is now underway to verify that the same values of z_1 and σ_1 will bring agreement at all values of T_0 and T_0 and for all ion–neutral systems measured in the same apparatus.

Another comment is in order at this point. Løvass et al. (1987) generalized the diffusion equation to include second (and higher, as necessary) order gradients of n. They did this by replacing Fick's First Law, (1.40), by

$$\mathbf{j}(\mathbf{r},t) = \mathbf{v}_d n(\mathbf{r},t) - \mathbf{D} \cdot \nabla n(\mathbf{r},t) + \mathbf{Q} : \nabla \nabla n(\mathbf{r},t) + \dots, \tag{2.16}$$

where \mathbf{Q} is a transport coefficient called the skewness tensor of order three, and where the ellipses indicate higher order gradients that will not be considered here. When (2.16) is used in (1.15), a generalization of Fick's second law, (1.41), is obtained. If it is again assumed that the transport coefficients do not depend upon \mathbf{r} or t but a term is added for ion–neutral reactions, this generalized diffusion equation is

$$\frac{\partial}{\partial t}n(\mathbf{r},t) + \mathbf{v}_d \cdot \nabla n(\mathbf{r},t) - \mathbf{D} \odot \nabla \nabla n(\mathbf{r},t) - \mathbf{Q} \odot \nabla \nabla \nabla n(\mathbf{r},t) + \dots$$

$$= -n(\mathbf{r},t)n_0k. \qquad (2.17)$$

Løvass et al. (1987) showed how to solve the one-dimensional version of this equation, e.g., the equation in which there are no gradients perpendicular to the field, and applied their solution to analyze new experimental measurements for the motion of $^7\text{Li}^+(^1\text{S}_0)$ ions in $\text{He}(^1\text{S}_0)$ at 296.0 K, They compared their results with several other sets of experimental results. They found that below E/n_0 =40 Td, there was excellent agreement ($\pm 0.3\%$) with the mobility data of Cassidy and Elford (1985). These results supported the conclusion of the Australian group that previous results from the Georgia Tech group (Gatland et al. 1977) for the mobility were 1–2% too high at low E/n_0 . There was an increasing and significant discrepancy as E/n_0 increased, presumably because the Australian and Georgia Tech results were based on using the original diffusion equation rather than (2.17). Although it was not specifically stated, this implied that the values of D_L and D_T obtained by the Georgia Tech group for this and many other ion–neutral systems were probably considerably less accurate than had been claimed. Since then, many (but not all) ab initio calculations have found those diffusion coefficients to be inaccurate.

It is the author's opinion that graphs equivalent to Fig. 2.4 should be examined for evidence of significant skewness. If not found, then (1.41) can be used to determine the mobility and parallel diffusion coefficient. If there is significant skewness, then the procedure of Løvass et al. (1987) should be used to determine these transport coefficients along with appropriate components of the skewness tensor, **Q**.

2.5 Mixtures of Buffer Gases

Mixtures of buffer gases are straightforward to treat theoretically. Since the ions are present in trace amounts and the gas is dilute, the effects of each microscopic ion-neutral collision add in proportion to the mole fraction (x_j) of each neutral gas j. For a gas mixture, the transport cross sections are therefore computed from the separate quantities for each pure gas, i.e.

$$\overline{Q}^{(l)}(\varepsilon) = \sum_{i} x_{j} \overline{Q_{j}}^{(l)}(\varepsilon). \tag{2.18}$$

However, the fact that the neutral atoms or molecules have different masses means that a similar expression is not accurate for the transport coefficients, so calculations of the type discussed in Chaps. 6–9 must be carried out for both the pure gases and then the particular gas mixtures of interest. Avoiding this additional effort therefore has been of theoretical interest, and the results are of experimental interest when they allow accurate transport coefficients in mixtures to be estimated entirely from the corresponding values in the various pure gases.

As discussed in Sects. 1.8 and 1.9, Blanc's law shows that the mobilities and diffusion coefficients can be easily calculated from the mole fractions and the values of the same transport coefficients in the pure gases. It is also possible (Petrović 1986) to use Blanc's law in reverse, i.e., to use initial data for the mobility in mixtures as a function of composition in order to obtain data for other mixtures or even pure gases. Both uses assume, however, that the T_0 and T_0 values are all the same and that the transport coefficients are in the low-field limit ($E/n_0 \rightarrow 0$).

The generalization of Blanc's law to higher values of E/n_0 appears not to have been attempted until the work of Mason and Hahn (1972). They used the qualitative momentum-transfer theory discussed in Sect. 3.1 and an approximate calculation of the partitioning of the ion energy in the mixture based on the assumption that the transport cross sections are constant. After the correction of an error (Whealton et al. 1974), this gives the same result obtained by Milloy and Robson (1973) and by Robson (1973). This extension of Blanc's Law is

$$\frac{1}{K_{0,mix}} = \sum_{j} \frac{x_{j}}{K_{0,,j}} \left[1 + \frac{K_{0,,j}^{\prime}}{2} (1 - \delta_{j}) \right], \tag{2.19}$$

where the prime on the standard mobility indicates the logarithmic derivative, as in Sect. 1.19, and where

$$\delta_j^{-1} = \left(m_1 + m_j\right) K_{0,,j}^2 \left(\sum_i \frac{x_i}{K_{0,i}}\right) \left(\sum_i \frac{x_i}{(m_1 + m_i) K_{0,i}}\right). \tag{2.20}$$

Note that (2.19) requires knowledge of more than just the $K_{0,,j}$ at the same values of T_0 and E/n_0 ; one must also know $K_{0,,j}$ over at least a small range of E/n_0 in order to calculate $K_{0,,j}^{'}$.

An alternate derivation of the generalization of Blanc's Law was given by Iinuma et al. (1987), starting from the Boltzmann equation rather than momentum-transfer theory. It leads to the equation,

$$\frac{1}{K_{0,mix}} = \sum_{j} \frac{x_{j}}{K_{0,,j}} \left[1 + \frac{1}{2} \left(\frac{K'_{0,j}}{1 + K'_{0,j}} \right) (1 - \delta_{j}) \right]. \tag{2.21}$$

Since the $K_{0,j}'$ are often small, the slight difference between (2.19) and (2.21) is often negligible. It is worth noting that mixture formulas that are generalization of Blanc's Law for the diffusion coefficients have also been derived (Iinuma et al. 1987), as have formulas for the mobility and diffusion of electrons in mixtures (Petrović 1986; Chiflikian 1995, 1997, 1999; Wang and Van Brunt 1997, Jovanović et al. 2004, Šašić et al. 2005).

Equations (2.21) and (2.20) give results in moderate to good agreement with the measurements of Milloy and Robson (1973) for $^{39}K^+(^1S_0)$ ions in He, Ne, Ar and mixtures of these gases, as well as in H_2 , N_2 and their mixtures. They also give good agreement for the mobility of rare-gas ions in mixtures of rare gases (Piscitelli et al. 2003). Unfortunately, they give erroneous and even unphysical results (Iinuma et al. 1987) in some cases, whereupon it is necessary to use an implicit set of equations and solve them iteratively. The implicit equations of Iinuma et al. (1987) are equivalent to those obtained by Takata (1985).

A new feature that can arise with a mixture of molecular neutral gases is negative differential conductivity (Petrović et al. 1984; de Urquijo 2004; Hernández-Ávila et al. 2004). Here the drift velocity at fixed T_0 , not just the mobility, decreases with increasing E/n_0 . Although this effect can have important experimental consequences, especially for electron transport, it will not be discussed further in this book

More information about gas mixtures and more recent results with extended versions of Blanc's Law are given in Sect. 2.4 of Shvartsburg (2009). Unfortunately, the use of these extensions of Blanc's laws has been slow to move into experimental plasma physics (Robson et al. 2008).

2.6 Mixtures of Ions

2.6.1 Mixtures of Atomic Isotopes

Suppose we want to obtain the unknown standard mobility, $K_{0,2}$, for isotope 2 of a particular atomic ion from known values, $K_{0,1}$, at the same value of T_0 and the same

effective temperature, T_{eff} , for isotope 1. Following Viehland (2016b), we use the fundamental ion mobility equation, (1.45), with $\alpha_c = 0$ to show that:

$$K_{0,2} = f K_{0,1} , (2.22)$$

where

$$f = \left(\frac{m_1}{m_2} \frac{m_0 + m_2}{m_0 + m_1}\right)^{1/2} \tag{2.23}$$

in terms of the masses m_0 , m_1 and m_2 of the neutral atom, ion isotope 1 and ion isotope 2, respectively.

The problem now is how to ensure that the T_{eff} values are the same. The Wannier equation, (1.29) gives the effective temperatures for each isotope-neutral system, so equating two such expressions with the same gas temperature and with $\beta_c = 0$ in each gives

$$\left(\frac{E}{n_0}\right)_2 = \frac{1}{f} \left(\frac{E}{n_0}\right)_1. \tag{2.24}$$

If we view the standard mobility as a function of T_0 and E/n_0 , then (2.22) and (2.24) indicate that

$$K_{0,2}(E/n_0, T_0) = f K_{0,1}\left(\frac{E/n_0}{f}, T_0\right).$$
 (2.25)

Therefore, in order to calculate the standard mobility of isotope 2 at particular values of T_0 and E/n_0 , one should look up the standard mobility of isotope 1 at the same T_0 but at the reduced field strength of E/n_0 divided by f, and then multiply that value by f.

Equation (2.25) was first obtained by Robson et al. (2012), who called it an aliasing method. Neither the title of this paper nor the applications in it indicated its applicability to using different isotopes in DTMS and IMS experiments, and it appears to have been overlooked by researchers using these methods. Viehland (2016b) showed that, even when two isotopes have mobilities that differ by 10%, the aliasing method represented by (2.25) is accurate within 0.05% at zero field (i.e., in IMS experiments) and within 1.5% at any E/n_0 (i.e., in DTMS experiments).

A generalization (Viehland 2016a) of the arguments just given leads to expressions allowing the mobility of a mixture of isotopes of the same atomic ion in a mixture of atomic gases to be obtained directly from the mobilities of a single isotope of the ion and one isotope of each neutral species. At low E/n_0 , these equations are a combination of the aliasing procedure in (2.25) and Blanc's law, (1.10). At intermediate and high E/n_0 , they combine the aliasing procedure with the extended version of Blanc's Law given by (2.19) and (2.21). Tests have shown (Viehland 2016a) that the expressions are so accurate that they obviate the necessity in future work of making measurements or calculations for more than one isotope of each atomic ion and each atomic neutral.

2.6 Mixtures of Ions 69

2.6.2 Separation of Ions

A mixture of cations or anions (but not both) studied in a drift tube without mass analysis can be understood as a superposition of results for each of the ions involved, since the number density of each ion is extremely small and there are no space-charge effects. The problem this presents to analytical chemists is determining the resolution or resolving power, R_m , of the instrument. The analysis of Revercomb and Mason (1975) allows this to be written as

$$R_m \approx \left(\frac{LEq}{16k_B T_0 \ln(2)}\right)^{1/2}.$$
 (2.26)

Equation (2.26) indicates that R_m can be increased by lowering T_0 , but this is ordinarily difficult and expensive. It can also be increased by increasing L, another difficult and expensive solution after the apparatus has already been built. The most practical procedure for increasing R_m is to use larger ε_V and hence larger E. For example, R_m values more than an order of magnitude higher that in conventional drift tubes were achieved (Dugourd et al. 1997) by constructing an apparatus with L=0.63 m and using it at nearly atmospheric pressure and with ε_V values up to 14 kV.

If the widths of the electrical pulses applied to the shutter and gate are small compared to the time it takes a pulse to move between them, the resolving power for the ion masses in a drift tube is given by the equation (Rokushika et al. 1985; Siems et al. 1994; Spangler 2002; Kanu et al. 2008),

$$R_m = \frac{2\langle t \rangle}{F_{\parallel}}. (2.27)$$

This allows R_m to be estimated from a single peak. The formulas for calculating R_m from two neighboring peaks are given by Spangler (2002), who provided an expanded theory for the resolving power of a drift tube. He also identified a variety of possible sources of additional peak broadening.

It should be noted that careful attention to the design and construction of an ion mobility spectrometer (IMS, see Sect. 2.7) can give a more uniform electrostatic field within the drift tube, resulting in improved resolution (Sappart and Baumbach 2000). Another technique is to use a so-called shift reagent that changes the buffer gas composition and leads to new ion identities (Fernandez-Maestre 2018). More information about IMS resolving power is given in Chap. 8 of Eiceman et al. (2014).

Using larger ε_V values to increase R_m can lead to another problem–electrical breakdown of the gas (see Sect. 1.3.3 of Shvartsburg 2009). Since electrical breakdown is less important at high n_0 , analytical chemists use drift tubes at or near atmospheric pressure in order to obtain a high R_m . Physical chemists and chemical physicists are less interested in resolving power than in covering a wide range of E/n_0 , which leads them to use low n_0 . The differing demands lead to two main types of drifts tubes. Hereafter we shall refer to a drift apparatus with a low gas pressure

that can be used over wide ranges of E/n_0 , but with a low R_m , as a DTMS, even in the rare cases where a mass spectrometer is not used. We will refer to a drift tube used at moderate or near atmospheric pressure with a high R_m , but a low E/n_0 , as an IMS. There is, of course, no sharp distinction been the two experimental techniques according to this definition, so other definitions have been used (Eiceman et al. 2014) to distinguish them. For example, what is here called a DTMS is sometimes referred to as an injected-ion drift tube or even as an injected-ion IMS.

2.7 Ion Mobility Spectrometers

2.7.1 Low-Field Limits

The development of the plasma chromatograph introduced a new method of chromatography into analytical chemistry (Cohen and Karasek 1970). The name plasma chromatography was suggested by the formation of an equal number of positive and negative charges (a plasma) by a radioactive source, followed by sequential generation of individual cation (or anion, but not both) peaks from each chemical species of the sample as it exits the device after having been pulled through a neutral gas by an electrostatic field. The arrival time of a peak therefore measures the drift speed or mobility of a particular ion species, and the width and shape of the distribution contain information about the diffusion coefficient, rate coefficients for chemical reaction and other transport properties.

Plasma chromatography is simply electrophoresis in the gas phase; hence its alternative name as gaseous electrophoresis. Its advantage over other types of electrophoresis is that, since the electric field is kept as small as practical while still extracting and separating the ions, a theoretical explanation of plasma chromatography (Revercomb and Mason 1975; Mason 1984) can be based on the kinetic theory that led to (1.19).

Over time, the names gaseous electrophoresis and plasma chromatography have come to be replaced by ion mobility spectrometry (IMS), since that name emphasizes the physical quantity (the ion mobility) that is being measured (Hill et al. 1990). From this point on, we will use the more modern term.

IMS is an important analytical tool due to its high sensitivity, instrumental simplicity, low cost, flexibility, real-time monitoring capability, amenability to miniaturization and ruggedness in operation (Snyder et al. 1993). Many of these advantages come from the absence of a mass spectrometer. An extensive treatment of the development of IMS and its application to the detection of explosives, chemical weapons, illegal drugs, pharmaceuticals and chemicals of industrial importance is given by Eiceman et al. (2014). Here we will highlight some points that may be overlooked when using an IMS; the combination of IMS with MS will be discussed in the next section.

Modern IMS instruments are designed and operated so as to maximize the resolving power (see Sect. 2.6.2) or to maximize the rate of ion transmission and hence increase the signal and/or the signal-to-noise ratio. To achieve such goals, IMS researchers frequently employ E/n_0 values that are high enough to bring into question whether they are operating at low field strengths. The field strength is sometimes judged to be low if the ion mobility does not vary noticeably with E/n_0 , but this can be in error if the operating conditions happen to be near a mobility minimum or maximum (see Fig. 1.1). A better classification of field strength is based on the degree to which the average collision energy is increased above the thermal value. One natural metric is the comparison of v_d to the zero-field, average, relative ion–neutral speed,

$$v_{th} = \left(\frac{8k_b T_0}{\pi \mu_0}\right)^{1/2},\tag{2.28}$$

which will be referred to simply as the thermal speed. If it is assumed that the quantities measured in IMS possess three significant digits, then in a general sense we may expect all of the measured quantities to begin changing simultaneously when v_d grows to within two orders of magnitude of v_{th} . Due to the interrelationships among the quantities, it is thus possible for the fundamental low-field ion mobility equation, (1.19), to become untrustworthy before a dependence of K_0 on E/n_0 becomes noticeable.

A low-field criterion based on experimentally determined quantities is given by (1.33). Written in terms of the thermal velocity, this criterion becomes

$$\frac{v_d}{v_{th}} \le \frac{1}{5} \left(\frac{3\pi}{8}\right)^{1/2} \left(\frac{M}{M+M_0}\right)^{1/2} \left(\frac{M_0}{M+M_0}\right)^{1/2} = 0.21708\sqrt{\widehat{m}\widehat{m}_0}, \quad (2.29)$$

where \widehat{m} and \widehat{m}_0 are the mass fractions of the ions and neutrals, respectively. It is easy to show from (1.4) and (1.7) that when \widehat{K}_0 is the standard mobility in cm²/Vs, \widehat{E}/n_0 is the density-reduced field strength in Td, and \widehat{v}_{th} is the thermal speed in m/s, then (2.29) gives

$$\widehat{K}_0 \ \widehat{E}/n_0 \le 0.080796 \ \widehat{v}_{th} \sqrt{\widehat{m}\widehat{m}_0} \ . \tag{2.30}$$

An equivalent expression when T_0 is in K is obtained directly from (1.33):

$$\widehat{K}_0 \ \widehat{E}/n_0 \le 11.756 \left(\frac{T_0}{\widehat{M} + \widehat{M}_0}\right)^{1/2},$$
 (2.31)

where \widehat{M} and \widehat{M}_0 are the ion and neutral masses in g/mole (Da).

Equation (2.31) has been checked against theoretical calculations (Viehland et al. 2017) for many atomic ion–atom systems at 300.00 K. The criterion is obeyed within 0.5% for 330 of the 332 systems examined. The exceptions are $^{11}B^+(^1S_0)$ in Ne(1S_0) (0.66%) and $^{19}F^-(^1S_0)$ in Ar(1S_0) (0.52%), so even in those cases the inequality is moderately accurate.

It has been claimed (Siems et al. 2012) that the mass dependence shown in (2.30) makes the low-field criterion more difficult to satisfy when the ion and neutral masses differ greatly from one another. However, this claim assumes that the thermal velocities are all the same, i.e., it ignores the reduced mass in (2.28). The claim is therefore wrong, as is clear from (2.31).

Siems et al. (2012) went on to state that two specific experimental studies were actually conducted at low fields but not in the low-field limit, and that most of the IMS measurements being made today do not come from deep within the low-field region but from the border between the low- and high-field regimes. In light of the error in the claim based on (2.30), these statements still must be verified experimentally. Until then, IMS experimenters need to check the inequality in (2.31) before asserting that they are working in the low-field limit.

2.7.2 Effects of Ion-Neutral Mass Ratio

It is possible to use ab initio calculations (see Chap. 6) to separately address the effects of the ion–neutral mass ratio and the interaction potential in DTMS or IMS. Figure 2.5 gives results obtained from ab initio potentials (Buchachenko and Viehland 2018) for 138 Ba $^{+}(^{2}S_{1/2})$ and 138 Ba $^{2+}(^{1}S_{0})$ in He at 300.00 K. It also shows results calculated from the same potentials for barium-like ions, ones whose masses have been artificially changed by factors of ten, as indicated, but without making any changes in the neutral mass or the transport cross sections calculated from the potentials. The calculated mobilities have been rescaled in Fig. 2.5 so that the values at low E/n_0 all match the value for 138 Ba $^{+}(^{2}S_{1/2})$, which is 17.274 cm 2 Vs.

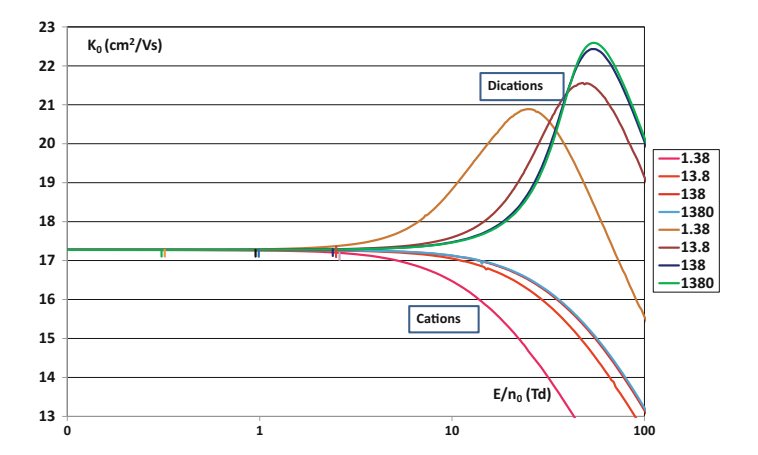


Fig. 2.5 Standard mobilities of barium-like ions in He at 300.00 K. The legend indicates the ion masses in g/mole (Da)

Figure 2.5 shows that there are large changes in the mobility when the ion/neutral mass ratio is small, but there is very little difference between the mobility when the mass is between 138 and 1380 g/mole (Da) for either cation. A good cut-off appears to be about $M/M_0=30$. Since most IMS measurements are made with air as the buffer gas, this means that ions with molar masses above about 900 Da will be insensitive to the mass changes for different isotopes. This insensitivity threshold can extend to even lower ion–neutral mass ratios if the accuracy of the measured mobility becomes worse or one demands a higher degree of separation between the ion mobility spectra of ions that differ by only 1 Da. This insensitivity can be overcome by using IMS/MS, as shown in the next section.

Figure 2.5 has small vertical lines at the E/n_0 values obtained from the low-field criterion, (2.31). As expected, the values at E/n_0 smaller than those indicated by the vertical lines are essentially constant, while the values at slightly higher E/n_0 begin to vary.

2.7.3 Effects of Charge State

Another feature of Fig. 2.5 is the large difference between the behavior of the singly charged and dications, regardless of the ion–neutral mass ratio. Comparison with the 300 K values in Fig. 1.1, and with many other experimental and theoretical values between 300 and 600 K, shows that the behavior of the dications is the typical one.

Variations with E/n_0 like those shown for the singly charged cations occur near 300 K only when the buffer gas is helium or neon, although they may arise at higher temperatures when other neutral gases are used. This is because a mobility maximum arises when the values of T_0 and E/n_0 lead to an average ion–neutral collision energy that is approximately equal to the well depth of the interaction potential energy function (or surface, for molecules) governing the collision. Helium and neon atoms are very small and have small electric polarizabilities. Hence, ion–He and ion–Ne interactions often have well depths smaller than the thermal energy at 300 K, at least when the ion is singly charged. Consequently, ion mobilities in He and Ne often begin to decrease as E/n_0 increases at fixed T_0 .

Dications of course have twice the charge of singly charged cations, which means that the ion-induced dipole portion of the interaction potential (the portion that governs the forces between the ion and neutral when they are far apart) is four times as large. Since this attractive part of the interaction is so large, even in He and Ne, the colliding particles can get much closer together before the repulsive force between the nuclei become comparable to the attractive force. This smaller bond length corresponds to a larger well depth, and hence larger values of T_0 and/or E/n_0 are needed before the mobility maximum is reached for dications in the lighter rare gases; the variation with E/n_0 therefore is the same in this case as it is for atomic ions of any charge in the heavier rare gases.

A final point about Fig. 2.5 is that one must anticipate that a change in the charge state of an ion causes the potential energy of the ion–neutral interaction to change

so much that one might as well be looking at a completely different ion. This is true even for molecular ions (Karpas et al. 1986; Canzani et al. 2018), or if the ion is the same but the neutral gas is changed (Bleiholder et al. 2015). In other words, IMS without a mass spectrometer often is insensitive or only slightly sensitive to the ion mass but is, or at least can be, a sensitive probe of the charge state of the ion.

2.7.4 Effects of Chemical Reactions

The reason many IMS are operated at temperatures of 400 K or above is that high temperatures minimize the influence that ion–molecule clustering reactions have on the measurements made at or near atmospheric pressure. These effects are described in some detail in Sect. 11.3 of Eiceman et al. (2014). Briefly, one must be concerned with reactions of the ion with small amounts of water vapor, forming cluster ions that have drift times in the instrument that are reasonably correlated with the average degree of hydration. Similar effects can also occur with CO₂ or other components in "dirty" air. Finally, one must be careful that the higher gas temperatures do not result in fragmentation of the ions of interest.

2.7.5 False Negatives and False Positives

An important use of IMS is as part of a swab test at airports and similar places where security is a concern. Here a cotton swab is rubbed over skin, clothing or other material that may have come in contact with explosives, illegal drugs or other contraband chemicals. Vapors from the swab are then injected into an IMS, resulting in a spectrum corresponding to the various chemicals absorbed onto the swab.

A false negative in airport applications is when a swab test reports negative results, e.g., that the passenger has not been using explosives or other contraband chemicals, even though he or she has been doing so. Since the consequences of a false negative can be disastrous, the operating parameters of the IMS used for such applications are usually chosen so that the chances of a false negative are remote. Unfortunately, this causes an increase in the chances of a false positive, where a red light indicates that the passenger has been working with explosives, illegal drugs, etc., when in fact they have not.

The trend toward miniaturization of an IMS used for security purposes makes it difficult if not impossible to distinguish ion mobilities that differ by more than 1%, while false positives result in considerable expense (in time and money) and poor passenger relations. Two methods for minimizing false positives that have been proposed are combining IMS with MS (Hill et al. 2006) and replacing the IMS with a secondary electrospray ionization-ion mobility-time-of-flight mass spectrometer (Crawford and Hill 2013). Given the large number of IMS presently in use for security purposes and the cost of adding a mass spectrometer, these are expensive propositions

that are unlikely to be implemented. A simpler method (Viehland 2015) would be to add a switch to the IMS so that it ordinarily works at the low E/n_0 values presently used but, when a suspect ion is identified, then the switch can be activated to deliver a larger ε_V to the drift tube and thus to increase E/n_0 by a factor of 10-100. Two ions with essentially the same K_0 at low E/n_0 are unlikely to have the same K_0 at the higher E/n_0 , so they can be distinguished quickly.

2.8 IMS/MS

2.8.1 *Basics*

It was shown in Sect. 2.6.2 that a drift tube by itself cannot separate ions very well. Therefore, it is essential to combine mass spectrometry with IMS if one hopes to obtain accurate information about one particular ion. The MS separates ions by their molar mass while the IMS separates them by their size and structure, i.e., by their ionneutral interaction potential energy surface. IMS/MS separation based on structure as well as mass provides a 2D analysis of each ion; the findings in the next subsections mean, however, that the separations by IMS and MS are not entirely independent. Another advantage of combining IMS with MS is that the IMS provides a rapid pre-separation step prior to the MS.

In order to focus on the basics of IMS/MS, this section is limited to atomic ions and to molecular ions that are not too large. The reader interested in large biochemical or biological ions is directed to the review by Bohrer et al. (2008) and to Chap. 18 of Eiceman et al. (2014).

2.8.2 Effects of Ion Mass in Atomic Systems

Since $\overline{\Omega}^{(1,1)}(T_0)$ is an energy-average of the momentum-transfer cross section, it is frequently (but not always) the case that it increases with the size (and hence the mass) of the ion. Therefore one expects that $1/K_0$ should increase with m_1 . This was illustrated long ago by Tyndall (1938), in a paper that is overlooked by most IMS researchers.

Here it is assumed that both the ions and neutrals are atomic, that there are no chemical reactions, and that (2.31) is satisfied, so one is working in the low-field regime. It is also assumed that one is interested only in theoretical calculations and experimental measurements at the same value of T_0 . Then the terms in (1.19) involving the ion mass can be isolated, to get

$$\sqrt{\frac{\mu_0}{m_0}} \frac{\overline{\Omega}^{(1,1)}}{\widehat{z}(1+\alpha_c)} = \left(\frac{2\pi}{m_0 k_B T_0}\right)^{1/2} \frac{3e}{16N_0 K_0},\tag{2.32}$$

where $|q| = \widehat{z}e$. Here e is the magnitude of the fundamental charge (2014 CODATA value, 1.6021766297 \times 10¹⁹ C), so \widehat{z} is the dimensionless charge number for the ion. Note that both $\overline{\Omega}^{(1,1)}$ and K_0 are constant in the low-field limit when T_0 is fixed, so the notation used here for them is simpler than before. The quantity, $\overline{\Omega}^{(1,1)}/\widehat{z}$ is often called the size-to-charge ratio, but here we shall anticipate the results in the next subsection and define a low-field structure factor, Ω_d/\widehat{z} , as the left-hand side of (2.32). Then that equation can be rewritten as

$$\frac{\Omega_d}{\widehat{z}} = \left(\frac{2\pi}{m_0 k_B T_0}\right)^{1/2} \frac{3e}{16N_0 K_0}.$$
 (2.33)

If $\alpha_c = 0$, Ω_d/\widehat{z} is equal to the size-to-charge ratio for ions that are much heavier than the neutral molecules ($\mu_0 \approx m_0$); in all situations, the low-field structure factor is inversely proportional to the zero-field mobility.

This is an appropriate place to discuss α_c . It has been stated many times in the literature that $|\alpha_c| \leq 0.02$ in the limit $E/n_0 \to 0$, but it appears that all of these assertions trace back to calculations made by the author and colleagues at Brown University in the 1970s, for atomic systems. Not only was the kinetic theory of gaseous ions in a more primitive state in those days (see Chap. 1), so were ab initio calculations of atomic ion—atom interaction potentials; consequently model systems were studied in low orders of solution of the Boltzmann equation.

New calculations in the limit of low E/n_0 for T_0 between 300 and 600 K were performed during the writing of this book using the ab initio methods discussed in Chap. 6. These gave $|\alpha_c| \leq 0.0036$ for all 186 state-specific atomic ions considered in He(1S_0) and 130 of the 140 considered in Ar(1S_0). The exceptions are the six isotopes of Ca⁺($^2S_{1/2}$) and the three isotopes of Mg⁺($^2S_{1/2}$), where $|\alpha_c| \leq 0.0060$ for all nine, and $^{19}F^{-}(^{1}S_0)$, where $|\alpha_c| = 0.0123$. Better yet, the vast majority of the $|\alpha_c|$ are less than 0.001 in both gases. Thus, setting α_c equal to zero in low-field IMS experiments is a better approximation than has previously been recognized.

Figure 2.6 shows Ω_d/\widehat{z} values calculated with the techniques discussed in Chap. 6 for atomic ion-He and atomic ion-Ar systems at 300 K. The results are very similar at the higher temperatures more commonly used in IMS. There are five things to note from this graph.

- 1. The structure factor does not say anything about the structure of an atomic ion. The important thing is that it is a function of the ion mass (usually called a trendline) that is never zero.
- 2. The only system shown that has resonant charge transfer is ⁴He⁺ in ⁴He, which is clearly distinct from the other ions in He. Thus, when ion–neutral interactions are sufficiently different, the structure factor can distinguish them.
- 3. Ar atoms are larger and heavier than He atoms, so the Ω_d/\widehat{z} values in Ar are much larger than those in He. This shows the effect that a change in buffer gas can sometimes have in IMS (Karpas and Berant 1989; Fernandez-Maestre 2018).

2.8 IMS/MS 77

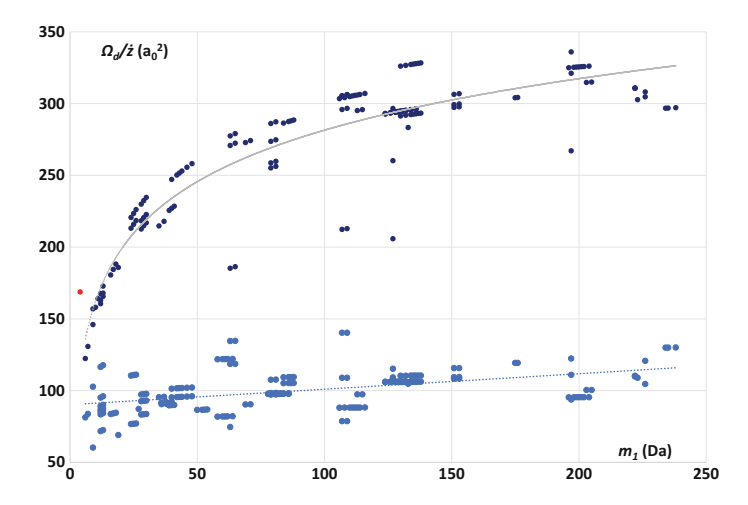


Fig. 2.6 Structure factors for atomic ions in He (light blue circles) and in Ar (dark blue) at 300.00 K. The red point is ${}^4\text{He}^+$ in ${}^4\text{He}$

- 4. The steeply rising region at low m_1 in Ar arises because of the factor $\sqrt{\mu_0/m_0}$ in the definition of Ω_d/\widehat{z} . When the ion mass becomes much larger than the mass of Ar, the trend line is nearly linear, like it is in He.
- 5. Some outliers are as far as 50% away from the appropriate trend line; one clearly needs both m_1/\widehat{z} and Ω_d/\widehat{z} in order to identify the particular ion and isotope being used in an IMS/MS experiment.

2.8.3 Effects of Structure-Molecular Systems

The previous subsection suggests that IMS/MS can give information about both Ω_d/\widehat{z} and m/\widehat{z} , and that identification of the electronic or vibrational state of an ion might be possible using such a 2D analysis. Experimental tests have confirmed this (Karpas et al. 1988). However, to make this at least semi-quantitative for molecular systems one must have theoretical values of Ω_d/\widehat{z} . The state of theory is such that this cannot be done rigorously for molecular ions or neutrals (see Chaps. 8 and 9). Hence researchers have had to resort to rather primitive ways of estimating Ω_d/\widehat{z} , and a quick review of this long history is in order.

Melaven and Mack (1932) calculated Ω_d/\widehat{z} by a shadow-graphic method in which the areas along various axes of the molecular ion were averaged as the molecule was rotated; this model is not satisfactory for long-chain molecules, since they are not rigid. Kihara (1963) calculated Ω_d/\widehat{z} with a convex-core model. Patterson (1972) used models of ion–He interactions to compute Ω_d/\widehat{z} values for six polyatomic anions; it was concluded that the mobilities were dominated by the ion–neutral repul-

sive interaction term rather than the (ion-induced dipole) attractive term, a result that is not too surprising given the very small size and polarizability of He. Lin et al. (1974) used a static model where the polyatomic ion was assumed stationary (non-rotating) during collisions and a kinetic model where it was assumed to be rotating rapidly. The static model gave Ω_d/\widehat{z} values that were too small, while the dynamic model gave values that were too large. Harland et al. (1986) made experimental measurements of the mobility of polyatomic ions drifting in helium and used atomic transport theory to rationalize their differences in terms of structural differences; similar work in air and He for a much larger collection of ions was reported by Berant and Karpas (1989), Jarrold (1995), Mesleh et al. (1996) and others.

It was noted in Sect. 1.11 that $\overline{\Omega}^{(1,1)}(T_0) = \pi d^2$ for rigid spheres of diameter d. The ion mass, on the other hand, should increase with its volume (i.e., as d^3) when the ion is large enough that its mass density is approximately constant. Hence the previous subsection indicates that $1/K_0$ should be proportional to $m^{2/3}$ for large ions that interact with the buffer gas as rigid, atomic-like spheres whose combined radii are equal to d. Unfortunately, large ions (and especially biochemical or biological ions) are generally "floppy" rather than rigid, so the best one can hope is that a class of generally similar ions will follow a trend line, where Ω_d/\widehat{z} is a nonanalytical function of m/\widehat{z} . This is discussed in more detail by Griffin et al. (1973) and by Revercomb and Mason (1975). Indeed, Griffin et al. (1973) showed that such a plot has a standard error of $\pm 20\%$ when structurally unrelated ions are considered, but only $\pm 2\%$ for a series of similar polynuclear hydrocarbons. The residual small errors can be attributed to their assumptions that $\mu_0 = m_0$ and $\alpha_c = 0$ or, equivalently, that $\Omega_d/\widehat{z} = \overline{\Omega}^{(1,1)}/\widehat{z}$. Note that the first assumption should be excellent for large ions with masses much greater than the mass of the neutral gas through which the ions move.

Recent work has continued to use the right-hand side of (2.33) to extract Ω_d/\widehat{z} from mobility data for many ions moving through the same neutral gas at the same T_0 , and to plot the results as a function of m/\widehat{z} . What are obtained are "trend lines" similar to those in Fig. 2.6 but different for different classes of molecular ions. Such trend lines were observed by Karasek et al. (1978) and later described in more detail by Karpas (1989). Chapter 9 of Eiceman et al. (2014) illustrates that lipids, peptides, carbohydrates, and nucleotides form four distinct trend lines, as long as one realizes that not every ion in one of these groups will fall exactly on the trend line for the group. This exception was of course shown for atomic systems in Fig. 2.6.

It is often argued that the values of Ω_d/\widehat{z} extracted from mobility data are cross sections that can be compared to values estimated from structural considerations about the molecular ions involved. One problem with this interpretation is that $\overline{\Omega}^{(1,1)}$ is an energy average of the microscopic, momentum-transfer cross sections, and so varies because different ion–neutral systems average in slightly different ways, particularly when there is internal energy of rotation (and sometimes vibration) that must be considered. Another problem was pointed out long ago, when Revercomb and Mason (1975) showed that molecular geometry cannot account for all molecular structure effects since some of the effects are of a dynamical nature. The example used

2.8 IMS/MS 79

by Revercomb and Mason (1975) was the motion of loaded spheres through smooth spheres, where $\overline{\Omega}^{(1,1)}$ (and hence Ω_d) decreases as the mass eccentricity increases, even though the rotationally averaged geometric cross section increases (Sandler and Mason 1967). Thus, a wobbling sphere is more likely to suffer a collision than a smoothly rotating one, but it is also harder to deflect; the deflection effect dominates. Hence Ω_d/\widehat{z} , while it is a useful identifying characteristic, cannot serve alone to identify an ion, any more than m/\widehat{z} alone can.

There is another thing that effects the structure of molecular systems more than atomic systems, clustering reactions (Berant et al. 1989). Not only do these often change the identity (and hence the mass) of the drifting ion, they are highly sensitive to the temperature used in the IMS. In fact, it is the common finding that polyatomic ions cluster with small amounts of water vapor that has led IMS experimenters routinely to use temperatures as high as 600 K, where such clusters are usually absent. The interested reader should consult the book by Eiceman et al. (2014).

2.8.4 High Accuracy IMS/MS

As was the case for DTMS, the accuracy claimed for IMS or IMS/MS measurements has been 2% or worse for many years (Lubman 1984). Partly this is due to the effects of clustering reactions, particularly ion—water clustering. More significantly, it results from the common practice of working only with polyatomic ions and gases and determining their relative mobilities, whereby some particular ion—neutral system is assigned a particular mobility value. The danger with the latter is illustrated by Hauck et al. (2018) who found that in air and under essentially the same conditions, the average K_0 value from the available literature for the proton-bound dimer of dimethyl methylphosphonate (DMMP) is 1.42 ± 0.04 cm² V⁻¹s⁻¹. This shows a variation of $\pm 2.8\%$ even for this often-studied and well-characterized ion, and means that the mobilities of other ions obtained by using this as a reference system are likely to be even less accurate.

To the best of the author's knowledge, the only atomic ion–atom systems that have been studied by IMS/MS are the lanthanide cations in He (Manard and Kemper 2017) and Ar (Laatiaoui et al. 2012). These ion–neutral systems satisfy (2.31) and their experimentally measured mobilities do not change with E/n_0 ; hence the measurements were made in the low-field limit. The mobilities of three ions in He were within 2% of the ab initio results of Buchachenko and Viehland (2014). Those in Ar were similarly consistent with unpublished, theoretical calculations for five ions. However, the agreement was poor for Gd^+ in both gases. Recently (Buchachenko and Viehland 2018b) it has been found that this failure is due to the fact that the interaction potentials were obtained using spin-orbit calculations (see Chap. 6) that were only approximate. We will return to the lanthanide cations in Sect. 6.23.3. However, the essential point is that IMS/MS measurements can give accurate mobility values,

even though they still are not as highly accurate as a physical chemist or chemical physicist would like.

With this as background, the usual procedure used to infer zero-field Ω_d/\widehat{z} values is based on the following line of reasoning (Smith et al. 2009):

1. The fundamental low-field ion mobility equation, (1.19), is combined with (2.32) to get

$$\overline{\Omega}^{(1,1)} = \frac{\widehat{z}e}{\sqrt{\mu_0}} A'' \langle t \rangle, \qquad (2.34)$$

where

$$A'' = \left(\frac{2\pi}{k_B T_0}\right)^{1/2} \frac{3}{16N_0} \frac{\varepsilon_V z_0}{L^2} (1 + \alpha_c) \left(\frac{101325 \text{ Pa}}{P_0}\right) \left(\frac{T_0}{273.15 \text{ K}}\right). \quad (2.35)$$

- 2. It is assumed that A'' is constant in a particular series of experiments.
- 3. It is assumed that $\langle t \rangle$ is the drift time, so no corrections are made for end effects, injection effects, etc.

For molecular ions and neutrals, it is assumed that (2.34) can be generalized to

$$\overline{\Omega}^{(1,1)} = \frac{\widehat{z}e}{\sqrt{\mu_0}} A' \langle t \rangle^b , \qquad (2.36)$$

where $A^{'}$ and b are constants whose values can be determined by comparison with values of $\overline{\Omega}^{(1,1)}$ obtained for known calibrants (Forsythe et al. 2015).

Stow et al. (2017) reported studies from four different laboratories that were all taken with the same commercially available IMS/MS. The measured mobilities of more than 120 ions in N₂ at room temperature were converted to values of $\overline{\Omega}^{(1,1)}(T_0)$ by using (1.19) with $\alpha_c=0$. They reported a relative standard deviation of only 0.29% for all ion species measured in three of the labs, when compared to those obtained in the fourth (the reference). However, they appear to have made no attempt to determine whether E/n_0 was low enough that (1.19) could be used rather than the more general (1.45), whether α_c was close enough to zero that its influence could be neglected, whether their mobilities could be obtained in other types of IMS/MS instruments, or whether the measured values agreed with theoretical values for simple systems like the lanthanides in the rare gases. Hence the 0.29% figure is a reliability (or precision) estimate and not an accuracy estimate.

Other attempts to increase the accuracy of IMS/MS have been discussed by Shvartsburg et al. (1997), Crawford et al. (2012), Fernandez-Maestre (2017) and Hauck et al. (2018). The latter reported zero-field mobilities in air with a claimed accuracy of $\pm 0.1\%$ for the ammoniated monomer and dimer of DMMP and ions produced from three explosives: 2,4,6-trinitrotoluene, 1,3,5-trinitroperhydro-1,3,5-triazine and pentaerythritol tetranitrate. They pointed out that many considerations, other than the accuracy of the instrumental parameters, need to be taken into account

2.8 IMS/MS 81

when striving to measure mobilities with high accuracy. They also recommended that "other researchers should confirm these K_0 values on multiple accurate instruments to verify agreement within the literature". To this we add the advice that IMS/MS practitioners should confirm that their instruments are operating in the low-field limit given by (2.31) and give the same values for atomic ions in atomic gases that are obtained by measurements in DTMS and by ab initio calculations (see Sect. 6.23.3)

2.9 Differential IMS (DMS)

2.9.1 Ping-Pong Experiments

Although there are notable exceptions (Robson et al. 1995, 1997; White et al. 1995; White 1996), ac fields have seldom been considered for use in drift tubes. More often, ac fields are used in drift tubes when they are paired with and perpendicular to dc fields (Vidal-de-Miguel et al. 2012). In contrast, asymmetrical time-dependent fields are used in field asymmetric ion mobility spectrometer (FAIMS), also known as differential ion mobility spectrometry and abbreviated as DIMS (although here we use DMS).

A good place to start the discussion of DMS is with an earlier and simpler technique that goes by the name of ping-pong experiments (Heimerl et al. 1969; Johnsen and Biondi 1972). In a ping-pong experiment, the direction of the electric field is quickly reversed while the ions are in the drift tube. Repeated reversals result in the ion swarm moving through the neutral gas as if the drift-tube length was much larger than its real value. If the total path length followed by the swarm could have been determined, this could have been used to improve the resolving power of the apparatus and result in more precise measurements of transport coefficients. In practice, however, it was used to improve the accuracy of measured reaction rate coefficients, based on the assumption that the transients that occur during the reversals are negligible.

Phenomenological and rigorous kinetic theories were used (Lin et al. 1977) to investigate the persistence of transient effects after abrupt changes in the field are applied to a drift tube. Comparison of the theoretical results to Monte Carlo calculations for special cases showed that the transfer of energy into directions perpendicular to the field is slower than into the parallel direction, and that the transient effects on the ion energy last about ten times longer than those on the mobility. In general, the persistence depends upon the details of the ion–neutral interaction potential. Lin et al. (1977) indicate that neglect of transient effects results in a fractional error no greater than given by the following equations:

$$\frac{\overline{v}_d - v_d(\infty)}{v_d(\infty)} \approx \frac{\overline{E} - E(\infty)}{E(\infty)} \approx -\frac{2m_1\overline{v}_d}{qEt'},$$
(2.37)

where \overline{v}_d and \overline{E} are the average speed and excess energy (above thermal) of the ions during the short time, t', that it takes to reverse the fields. Note that the unchanging magnitude of the field, E, should not be confused with \overline{E} or the excess energy long after the field reversal, $E(\infty)$, and that $v_d(\infty)$ is the drift speed at infinite after the field reversal.

2.9.2 Basics of DMS

More complicated time-varying but asymmetric electric fields are the basis of DMS. This experimental technique was invented in the former USSR (Gorshkov 1982; Shvartsburg 2009), but politics and the cold war prevented it from spreading to the West for more than a decade. A U.S. patent was issued to Carnahan and Tarrasov (1995) for such an instrument. It was incorporated into practical devices soon after (Purves et al. 1998; Krylov 1999; Guevremont and Purves 1999).

The difference between IMS and DMS is indicated by the following definitions (Shvartsburg et al. 2014).

- "Conventional IMS includes methods based on absolute ion transport properties that could be measured using a time-independent electric field."
- "Differential IMS comprises methods dependent on a change of some ion transport property as a function of electric field and thus requiring a time-dependent field that substantially varies during the measurement."

Thus DMS separates ions not by their absolute mobility but by the difference in mobility values, ΔK , between a strong field and a relatively weak field (or, equivalently, by the ratio of the mobilities at high and low E/n_0). Indeed, as indicated in Sect. 2.7.5, ΔK has been proposed (Viehland 2015) as a way to avoid false positives in IMS.

In practice, the ions in a DMS are carried by a flowing buffer gas between two closely spaced electrodes across which a weak dc field and a strong, time-dependent field are applied. The high field is applied for a short time but the weak field (in the opposite direction) is always present. The time-dependent field has a magnitude that is usually called the dispersion voltage (DV). The magnitude of the weak, constant field is said to be the compensating voltage (CV), and it is tuned so that its influence precisely opposes the influence of the strong field, allowing the ions to pass completely through the device and thus be detected (Guevremont 2004). Scanning the CV allows for the detection of different cations (or anions, but not both) that may be present in the experiment. A key feature of DMS is that it is a continuous technique for separating ions, so its duty cycle is high compared to those for DTMS and IMS; however, there is a trade-off between resolution and sensitivity due to the high duty cycle (Shvartsburg et al. 2004).

The principles of operation of DMS were described for a parallel plate geometry by Buryakov et al. (1993) and for concentric cylinders by Guevremont and Purves (1999) and by Purves et al. (1998) and Purves and Guevremont (1999). The cylindrical

geometry better focuses and traps the ions, but of course it is harder to construct. A cylindrical apparatus with an electrospray ionization source was tested (Viehland et al. 2000) by comparing the mobility of $^{35}Cl^{-}(^{1}S_{0})$ ions in air measured by DMS to values obtained with E/n_{0} varying from 10 to 60 Td in a DTMS (Bohringer et al. 1987). The results were in excellent agreement, even though the DMS used atmospheric pressure air while the DTMS used much lower pressures.

Equation (2.37) applies when the dc and the time-dependent asymmetric fields are applied parallel to the axis along which the ions move, while the fields are generally applied in perpendicular directions in DMS, as described above. Nevertheless, this equation has been used (Guevremont 1999) to show that the transients that occur due to changing fields in DMS are negligible, even when square waves are used. A possible exception occurs for ions with a molar mass above 10⁵ Da. This was not a concern in 2000, but recent efforts have extended DMS to large biochemical and biological ions. It is time for someone to consider how transient effects in the field perpendicular to the ion motion may be interfering with such measurements. Another area just beginning to be investigated (Shvartsburg 2009) is the extent to which the extended Blanc's laws discussed in Sect. 2.5 can be used for DMS studies with mixtures of neutral gases.

More information about DMS has been given by Schneider et al. (2016). In particular, that paper indicates the important role that ion—neutral reactions can have in DMS experiments in which even a trace amount of water vapor are present.

2.9.3 Higher Order DMS

Early DMS measurements were made at E/n_0 values below about 60 Td, so the power series expansion in (1.9) was often used to interpret the data in terms of a so-called alpha function,

$$\alpha(E/n_0) = 1 + c_2(E/n_0)^2 + c_4(E/n_0)^4 + \dots$$
 (2.38)

This assumes, of course, that T_0 is at some fixed, known value. Guevremont et al. (2001) truncated (2.38) at the c_4 term and showed that interpretation of the data is easy when the asymmetric electric field is delivered as a square wave, but that it can still be carried out when the electrical wave form is a combination of a sinusoidal wave and its harmonic. As a note of practical importance, this paper showed that DMS could separate leucine and isoleucine ions, which cannot be done by MS or ordinary IMS (Asbury and Hill 2000).

Shvartsburg et al. (2006) described a higher order DMS (HODMS) technique in which the asymmetric field has more than two intensity levels. In their notation, MS is considered zeroth order since it is independent of ion mobility. DTMS and conventional IMS are first order, since they depend on the absolute value of K_0 . DMS experiments that measure ΔK are second order. HODMS allows methods as high as fourth or fifth order to be used in air, with still higher orders possible

in insulating gases. Although no consideration has yet been given to the effect of transients in HODMS, calculations suggest that higher order separations should be largely orthogonal to each other and to separations using techniques of lower order. More information about HODMS is given in Sect. 5.2 of Shvartsburg (2009).

2.10 Traveling-Wave IMS

DTMS and IMS experiments have a low duty cycle because a shutter is used to create a pulse of ions in the drift tube. This means that about 99% of the ions that could have been studied are deliberately excluded from the drift tube. Similar low duty cycles occur in ordinary DMS. This can be overcome with a newer version of IMS (Giles et al. 2004; Ruotolo et al. 2005; Pringle et al. 2007) involving an asymmetric time-dependent electric field, known as traveling-wave IMS (TW-IMS); the instrument is usually combined with time-of-flight mass spectrometry.

In TW-IMS methods, a set of 25–50 rings is placed in a low-pressure chamber. Ions are injected into this drift tube from an ion trap (see Sect. 2.11) that accumulates the ions. As a pulse of ions is introduced, the electrical potential is raised on the first ring, establishing an electric field and initiating ion movement characterized by the mobility along the field. At the appropriate time, the potential is then lowered on the first ring while simultaneously raised on the second. The process of raising and lowering the electrical potential between the rings establishes a wave of ions moving down the drift tube. Once the first wave (pulse of ions) is initiated and begins moving along the drift tube, a second and then subsequent waves are introduced. The ion waves are usually about five rings apart, and the duty cycle is enhanced because multiple waves are moving through the drift tube at the same time and because ions not in the drift tube are stored in the ion trap until needed.

The resolving power of the TW-IMS is not large, but when used in conjunction with a time-of-flight MS the combined instrument becomes analytically powerful. TW-IMS/MS is particularly useful for investigating large ions, e.g., biological ions. Commercial availability of a TW-IMS/MS has made this instrument widely accepted within the biomolecular ion research community. The unusual control of electrical fields inside the device is discussed in the original papers and in Sect. 6-5 of Eiceman et al. (2014), while Sun et al. (2016) have shown that the type of ion source has little influence on the TW-IMS/MS results and, in particular, that exposure of native proteins to electrospray conditions can generate trapped ions that retain their solution-like structures.

The fundamentals of TW-IMS are described by Shvartsburg and Smith (2008). Their analysis does not consider transient effects due to time-dependent fields, and these would be expected to be much more significant in this device than in DTMS or IMS, particularly since a TW-IMS/MS is used ordinarily for ions of high molar mass. In addition, their analysis ignores the influence of the ion trap, especially the fact that the ions must be accelerated in order to be ejected from the trap in order to enter the drift tube. Finally, they estimated that other experimental parameters

in TW-IMS might cause the ions to have effective temperatures as high as 7000 K. This means that the mobility values determined from TW-IMS measurements (Giles et al. 2010) are not constant and there may be fragmentation or distortion of macromolecular ion structures. Such things do not affect the use of the TW-IMS/MS for separations with high resolution (Shvartsburg and Smith 2008) or for estimates of the large collision integrals that occur when biochemical or biological ions interact with small gas molecules (Ruotolo et al. 2005; Sivalingam et al. 2013), but they make highly questionable the extent to which absolute mobilities of high accuracy may be inferred from the data.

An improved estimate of the ion heating in TW-IMS was provided by Merenbloom et al. (2012), using so-called thermometer ions, i.e., ions for which the dissociation energies are known, as are the energies at which particular fragment ions appear. They found that dissociation occurred during injection into the TW-IMS, presumably due to ejection from the ion trap, but little if any dissociation occurs during the ion motion through the drift tube. With careful attention to detail, they were able to hold the effective ion temperature to 449–470 K, which is lower than the 7000 K estimate of Shvartsburg and Smith (2008) and even slightly lower than a previous finding by Morsa et al. (2011). Nevertheless, they concluded that "ion heating and conformational changes induced by TW-IMS ... can complicate attempts to relate gas phase and solution-phase structure for small proteins or similar size molecules".

Technical improvements have led (Giles et al. 2010) to a second-generation TW-IMS instrument that has a resolving power four times larger than before. The instrument measured Ω_d/\widehat{z} values that were within about 5% of previously obtained values for doubly charged reverse peptides and singly charged terphenyl complexes, and the latter were in agreement with theoretical values obtained using the methods described and critiqued in Chap. 9.

2.11 Trapped-Ion IMS

Another IMS device with time-dependent fields is a trapped-ion IMS (TI-IMS), whose big advantage over other forms of IMS is its high resolving power. In this device (Fernandez-Lima et al. 2011; Hernandez et al. 2014), a pressure differential between the entrance and exit of the drift tube induces a stream of neutral gas molecules to move through it with a constant speed. A pulse of ions is then introduced into the drift tube with a very small electric field, and it is carried down the drift tube by the flowing gas. A resistor chain connects the 25 or more electrodes in the drift tube, and the electrical resistance between the plates at the start and end of the drift tube increases for a while but is kept constant near the gate. In a TI-IMS, the potential difference is set so that the force created by the electric field counteracts the force due to collisions with the moving gas molecules. Also, each ring is composed of electrically isolated segments that create a radially confining quadrupolar field.

A theory has been presented (Bleiholder 2016) for TI-IMS. This theory treats an ensemble of ions as if it was a single ion at the center of the swarm. The single, average ion moves according to Newton's laws of motion under two separate forces. One is the electrical force describing the interaction of a single ion with the external, time-dependent electric field. The other is a "drag" force acting on the ion due to momentum-transfer because of ion collisions with the buffer gas molecules; Bleiholder (2016) used the Boltzmann equation (see Chaps. 4 and 5) to evaluate this second force. From the viewpoint of the author of this book, it would have been better to analyze the TI-IMS entirely using the Boltzmann equation.

Although the theory of Bleiholder (2016) takes into account the fact that both the gas and the ion swarm are moving and that the axial electric field is neither uniform nor static, it does not appear to consider that changes in both the gas pressure and the electric field strength can lead to changes in E/n_0 that are sufficiently large that the ions are not always moving in the low-field limit assumed in the theory. Although this theory indicates that it is feasible to determine ion mobilities directly from measurements in a TI-IMS, the only such results to appear so far are those of Manard and Kemper (2017) for lanthanide cations in He, as discussed briefly in Sect. 2.8.4 and in more detail in Chap. 6.

Recent work with a cyclic drift tube (Merenbloom et al. 2009) and nonlinear scanning functions (Silvira et al. 2016) brings us, in a sense, back to the ping-pong experiments discussed at the beginning of this section. A cyclotron-type geometry is constructed from four curved drift-tubes and four ion funnels, and electrostatic fields are applied to move an ion pulse around the cyclotron many times. The effective length of the drift tube can exceed 180 m, giving the device a high resolving power. The advantage of the cyclic drift tube is that the changes in the applied external fields are not as abrupt as in a ping-pong experiment, so transient effects may be unimportant even for very heavy ions. The precision of the measured mobilities is better than 1%, but the overall accuracy is unclear, for reasons cited by Merenbloom et al. (2009).

2.12 Ion Cyclotron Resonance

Ion cyclotron resonance (ICR) is the name given to experiments based on the principal that an ion moving under the influence of a constant magnetic field of magnitude B will rotate in the plane perpendicular to B with a sharp cyclotron frequency,

$$\omega_c = \frac{qB}{m}.\tag{2.39}$$

At pressures low enough that only one or a few ion-neutral collisions occur during the observation time, the application of a sinusoidal electric field with frequency ω causes the ion(s) to absorb energy when $\omega = \omega_c$. A finite linewidth of the absorption frequencies arises from instrumental effects. Early ICR experiments were

conducted in this manner, but Fourier transform ICR (FT-ICR) is now the preferred method. "This has produced the world's highest mass resolution and highest mass measurement accuracy" (Marshall and Chen 2015). However, it is essential to avoid ion–neutral collisions in order to do this, which means that most ICR work is not directly related to the subject of this book. The interested reader is referred to the paper by Comisarow and Marshall (1976) and to the many papers on ICR that have appeared in the past 40 years.

When the ions in an ICR apparatus undergo many collisions with neutrals during the observation time, but with a collision frequency much less than ω , they absorb energy over a range of frequencies near ω_c . The finite linewidth arises primarily because of collisions. Because almost any ion can be used in an ICR, collision-dominated ICR experiments offer the possibility (Wobschall et al. 1963) of obtaining information about the ion–neutral interactions similar to that which can be obtained from DTMS and IMS experiments.

A kinetic theory of the collision broadening of ICR lines was presented by Viehland et al. (1975). It is similar to the two-temperature theory outlined in Sect. 1.16. Since there has been little or no experimental work involving collision-dominated ICR in recent years, no theoretical work has reported using the other kinetic theory methods discussed in Chap. 5. Therefore, we will pay no further attention to ICR in this book, except to note that Fourier transform ICR can be coupled to IMS and a time-of-flight mass spectrometer (Bluhm et al. 2000) to produce mobilities in excellent agreement with literature values.

2.13 Ion Traps

The radio-frequency (rf) quadrupole ion trap was patented by Wolfgang Paul (1913–1993) and Helmut Steinwedel (1921–2004) in Paul and Steinwedel (1956). Practical operation of a quadrupole ion trap, and more complicated traps involving direct-current (dc) and magnetic fields, requires the presence of neutral molecules within the apparatus. This is because, even if the neutrals were present in amounts as small as the ions, each ion–neutral collision would scatter an ion to the wall and thus prevent the device from acting as a trap. When there is a small but nonnegligible amount of neutral gas present, there are enough ion–neutral collisions to keep most of the ions near the center of the device, and hence they can be trapped by electric fields (static or time-dependent) and/or magnetic fields. This means that ion–neutral collisions must be considered before the ion trap can be useful as a tool for mass spectrometry (March and Todd 1995).



Paul

The approach most often employed to understand ion motion in complicated electric and magnetic fields is to use Newton's equations of motion to describe the motion of a single, average ion. Collision effects are introduced ad hoc, by adding a constant damping term. The general equation of motion is thus

$$\frac{d\mathbf{v}}{dt} = \frac{q}{m} \left[\mathbf{E} + \mathbf{v} \times \mathbf{B} \right] - \xi \mathbf{v},\tag{2.40}$$

where \mathbf{v} is the ion velocity and ξ is called the effective collision frequency since it has the dimensions of reciprocal seconds. For a pure quadrupole ion trap, there is no magnetic field and the ion velocity can be replaced by the derivative of the ion position. This gives a second-order differential equation governing the ion position, namely

$$\frac{d^2\mathbf{r}}{dt^2} + \xi \frac{d\mathbf{r}}{dt} - \frac{q\mathbf{E}}{m} = 0. \tag{2.41}$$

If the applied electric potential varies as $U + V \cos(\omega t)$, then (2.41) becomes Mathieu differential equations (March and Todd 1995), one for ion motion in each direction in the apparatus. It is possible to solve the equations using the ITSIM program (Julian et al. 1993). The weakness of this approach is that it treats ionneutral collisions in an ad hoc manner, even though such collisions are crucial for the operation of these devices.

The advantage of using the Boltzmann equation is that it treats collisions properly, with the same level of sophistication and detail as is used to treat the external fields. The disadvantage is that the results are difficult to apply, except in special cases such as the Maxwell model of constant collision frequency, where \mathcal{E} is indeed constant.

As an intermediary between the two approaches just described, one can use moments of the Boltzmann equation to provide an approximate kinetic theory. It is now known that the simplest approximation to the moment equations, known as momentum-transfer theory (see Chap. 3), is accurate within 15–20% (and in most cases within a few per cent) for electrostatic fields. It gives results in agreement with the 2T kinetic theory described in detail in Chap. 5, and both lead (Viehland and Goeringer 2004) to a more general form of (2.40)

2.13 Ion Traps 89

$$\frac{d\langle \mathbf{v} \rangle}{dt} = \frac{q}{m} \left[\mathbf{E} + \langle \mathbf{v} \rangle \times \mathbf{B} \right] - \xi \langle \mathbf{v} \rangle, \qquad (2.42)$$

where

$$\xi = \frac{8n_0}{3} \frac{m_0}{m_0 + m_1} \left(\frac{2k_B T_{eff}}{\pi \mu}\right)^{1/2} \overline{\Omega}^{(1,1)}(T_{eff}). \tag{2.43}$$

Note that that (2.42) cannot be turned into a second-order differential equation for the position of a single ion, since ξ is not constant. This means that a proper treatment of collisions in ion traps requires reconsideration of most of the results that have been obtained (or approximated) during the last four or five decades, since those are based on (2.41). Work using (2.42) has been published (Viehland and Goeringer 2005, 2008; Viehland et al. 2005, 2006a, b; Goeringer and Viehland 2005) but much still remains to be done.

Increasingly often, the original quadrupole ion trap is being replaced by linear ion traps (Kenny et al. 2010). This is because the latter have an increased capacity for ions (Campbell et al. 1998).

The first publication concerning the use of ion traps with IMS, called trapped IMS (TIMS), was by Benigni and Fernandez-Lima (2016). Briefly, the concept behind TIMS is the use of an electrostatic field to hold ions stationary while the neutral gas in which they were originally immersed flows through the drift tube. TIMS has a high resolving power, up to 400. In addition, the ions can be gated from a TIMS into a FT-ICR (Fernandez-Lima 2016).

2.14 Laser Probing of Drift Tubes

Since they are not directly related to transport and reaction properties of ions in gases, we have left to last the topic of energy distributions in drift tubes. Attempts to measure or model the distribution of electron or ion energy date to the 1960s and 1970s (Frost and Phelps 1962; Lucas 1969; Whealton and Woo 1972; Rebentrost 1972). The measurements primarily involved retarding potential studies (Moruzzi and Harrison 1974; Kosmider and Hasted 1975; Ong et al. 1981; Fhadil et al. 1982; Naveed-Ullah et al. 1978; Khatri 1984, 1985; Makabe and Shinada 1985; Ong and Hogan 1985; Hogan and Ong 1986) in which ions sampled through a small hole are passed through a retarding lens system. Despite such considerable effort, it was eventually found (Hogan and Ong 1985; Braglia et al. 1985; Skullerud and Holmstrom 1985) that the presence of the metal plates making up the lens system disturbed the distribution so much that accurate values could not be obtained in this manner.

The first measurements obtained by laser-induced fluorescence were by Dressler et al. (1987a). They also reported optically determined values of the standard mobility and the ion temperatures parallel and perpendicular to the electric field, for $^{138}\mathrm{Ba}^+(^2\mathrm{S}_{1/2})$ in He at 330±5 K; these will be compared to theoretical calculations in Chap. 6. In subsequent papers, they used the same techniques to study the

rotational alignment that develops when N_2^+ ions drift in $He(^1S_0)$ at intermediate and high E/n_0 (Dressler et al. 1987b) and the rotationally resolved vdf for $CO^+(v=0)$ (Lauenstein et al. 1991) and $NO^+(v=0)$ (Anthony et al. 2000) in $He(^1S_0)$. Alignment is caused by collisions that cause the angular momentum vectors of the ions to become preferentially aligned perpendicular to E. Such alignment for larger ions could significantly affect the energy distribution of the ions, and cause a large effect on ion–molecule reaction rates measured in drift tubes (Meyer and Leone 1988).

There has been a lull in laser probing of drift-tube experiments, primarily because the use of drift tubes to study ion—neutral reactions became uncommon. As discussed in Chap. 7, this situation is likely to change in the near future.

References

- E.B. Anthony, M.J. Bastian, V.M. Bierbaum, S.R. Leone, J. Chem. Phys. 112, 10269 (2000)
- G.R. Asbury, H.H. Hill Jr., J. Microcolumn Sep. 12, 172 (2000)
- W.A. Barnes, D.W. Martin, E.W. McDaniel, Phys. Rev. Lett. 6, 110 (1961)
- P. Benigni, F. Fernandez-Lima, Anal. Chem. 88, 7404 (2016)
- Z. Berant, Z. Karpas, J. Am. Chem. Soc. 111, 3819 (1989)
- Z. Berant, Z. Karpas, O. Shahal, J. Phys. Chem. 93, 7529 (1989)
- C. Bleiholder, Int. J. Mass Spectrom. **399–400**, 1 (2016)
- C. Bleiholder, N.R. Johnson, S. Contreras, T. Wyttenbach, M.T. Bowers, Anal. Chem. 87, 7196 (2015)
- B.K. Bluhm, K.J. Gillig, D.H. Russell, Rev. Sci. Instrum. 11, 4078 (2000)
- B.C. Bohrer, S.I. Merenbloom, S.L. Koeniger, A.E. Hilderbrand, D.E. Clemmer, Annu. Rev. Anal. Chem. 1, 10.1 (2008)
- H. Bohringer, D.W. Fahey, W. Lindinger, F. Howorka, F.C. Fehsenfeld, D.L. Albritton, Int. J. Mass Spectrom. Ion Proc. 81, 45 (1987)
- G.L. Braglia, L. Romanò, M. Diligenti, Il Nuovo Cim. B 85, 193 (1985)
- A.A. Buchachenko, L.A. Viehland, J. Chem. Phys. 140, 114309 (2014)
- A.A. Buchachenko, L.A. Viehland, J. Chem. Phys. 148, 154304 (2018a)
- A.A. Buchachenko, L.A. Viehland, unpublished (2018b)
- I.A. Buryakov, E.V. Krylov, E.G. Nazarov, U, K., Rasulev, Int. J. Mass Spectrom. Ion Proc. 128, 143 (1993)
- J.M. Campbell, B.A. Collings, D.J. Douglas, Rapid Commun. Mass Spectrom. 12, 1463 (1998)
- D. Canzani, K.J. Laszlo, M.F. Bush, J. Phys. Chem. A 122, 5625 (2018)
- B.L. Carnahan, A.S. Tarrasov, U. S. Patent No. 5420424 (1995)
- R.A. Cassidy, M.T. Elford, Aust. J. Phys. 38, 587 (1985)
- R.V. Chiflikian, Phys. Plasmas 2, 3902 (1995); Errata in Phys. Plasmas 3, 1477 (1996)
- R.V. Chiflikian, Phys. Plasmas 4, 551 (1997)
- R.V. Chiflikian, Phys. Plasmas **6**, 4794 (1999)
- M.J. Cohen, F.W. Karasek, J. Chromatogr. Sci. 8, 330 (1970)
- M.B. Comisarow, A.G. Marshall, J. Chem. Phys. 64, 110 (1976)
- C.L. Crawford, B.C. Hauck, J.A. Tufariello, C.S. Harden, V. McHugh, W.F. Siems, H.H. Hill Jr., Talanta 101, 161 (2012)
- C.L. Crawford, H.H. Hill Jr., Anal. Chim. Acta 795, 36 (2013)
- R.A. Dressler, H. Meyer, A.O. Langford, V.M. Bierbaum, S.R. Leone, J. Chem. Phys. 87, 5578 (1987a)
- R.A. Dressler, H. Meyer, S.R. Leone, J. Chem. Phys. 87, 6029 (1987b)
- R.R. Ph Dugourd, D.E. Hudgins, M.F. Jarrold Clemmer, Rev. Sci. Instrum. 68, 1122 (1997)

References 91

- D. Edelson, K.B. McAfee, Rev. Sci. Instrum. 35, 1887 (1964)
- G.A. Eiceman, Z. Karpas, H.H. Hill Jr., *Ion Mobility Spectrometry*, 3rd edn. (CRC Press, Boca Raton, 2014)
- H.W. Ellis, R.Y. Pai, E.W. McDaniel, E.A. Mason, L.A. Viehland, At. Data Nucl. Data Tables 17, 177 (1976)
- H.W. Ellis, E.W. McDaniel, D.L. Albritton, L.A. Viehland, S.L. Lin, E.A. Mason, At. Data Nucl. Data Tables 22, 179 (1978)
- H.W. Ellis, M.G. Thackston, E.W. McDaniel, E.A. Mason, At. Data Nucl. Data Tables 31, 113 (1984)
- F. Fernandez-Lima, Int. J. Ion Mobil. Spectrom. 19, 65 (2016)
- F. Fernandez-Lima, D.A. Kaplan, M.A. Park, Rev. Sci. Instrum. 82, 126106 (2011)
- R. Fernandez-Maestre, Int. J. Mass. Spectrom. 421, 8 (2017)
- R. Fernandez-Maestre, J. Mass Spectrom. 53, 1 (2018)
- H.A. Fhadil, D. Mathur, J.B. Hasted, J. Phys. B 15, 1443 (1982)
- J.G. Forsythe, A.S. Petrov, C.A. Walker, S.J. Allen, J.S. Pellissier, M.F. Bush, N.V. Hud, F.M. Fernandez, Analyst 140, 6853 (2015)
- L.S. Frost, A.V. Phelps, Phys. Rev. 127, 1621 (1962)
- I.R. Gatland, W.F. Morrison, H.W. Ellis, M.G. Thackston, E.W. McDaniel, M.H. Alexander, L.A. Viehland, E.A. Mason, J. Chem. Phys. **66**, 5121 (1977)
- K. Giles, S.D. Pringle, K.R. Worthington, D. Little, J.L. Wildgoose, R.H. Bateman, Rapid Commun. Mass Spectrom. 18, 2401 (2004)
- K. Giles, J.L. Wildgoose, D.J. Langridge, I. Campuzano, Int. J. Mass Spectrom. 298, 10 (2010)
- D.E. Goeringer, L.A. Viehland, J. Phys. B 38, 4027 (2005)
- M.P. Gorshkov, USSR Inventors certificate 966583 (1982)
- G.W. Griffin, I. Dzidic, D.I. Carroll, R.N. Stillwell, E.C. Horning, Anal. Chem. 45, 1204 (1973)
- R. Guevremont, private communications with L. A. Viehland (1999)
- R. Guevremont, J. Chromatogr. 1058, 3 (2004)
- R. Guevremont, R.W. Purves, Rev. Sci. Instrum. **70**, 1370 (1999)
- R. Guevremont, D.A. Barnett, R.W. Purves, L.A. Viehland, J. Chem. Phys. 114, 10270 (2001)
- P.W. Harland, B.J. McIntosh, R.W. Simpson, N.R. Thomas, J. Chem. Soc. Faraday Trans. 2, 2039 (1986)
- B.C. Hauck, W.F. Siems, C.S. Harden, V.M. McHugh, Anal. Chem. 90, 4578 (2018)
- J. Heimerl, R. Johnsen, M.A. Biondi, J. Chem. Phys. **51**, 5041 (1969)
- D.R. Hernandez, J.D. DeBord, M.E. Ridgeway, D.A. Kaplan, M.A. Park, F. Fernandez-Lima, Analyst 139, 1913 (2014)
- J.L. Hernández-Ávila, E. Basurto, J. de Urquijo, J. Phys. D 37, 3088 (2004)
- H.H. Hill Jr., W.F. Siems, R.H. St, Louis, D.G. McMinn, Anal. Chem. 62, 1201A (1990)
- H.H. Hill Jr., P. Dwivedi, A.B. Kanu, Bull. Laser Spectrosc. Soc. India 14, 92 (2006)
- M.J. Hogan, P.P. Ong, Int. J. Mass Spectrom. Ion Process. 65, 119 (1985)
- M.J. Hogan, P.P. Ong, J. Phys. D 19, 2123 (1986)
- K. Iinuma, Can. J. Chem. 69, 1090 (1991)
- K. Iinuma, E.A. Mason, L.A. Viehland, Mol. Phys. 61, 1131 (1987)
- K. Iinuma, T. Hamano, M. Takebe, J. Chem. Phys. 101, 2949 (1994)
- K. Iinuma, N. Sasaki, M. Takebe, J. Chem. Phys. 99, 6907 (1993)
- M.F. Jarrold, J. Phys. Chem. 99, 11 (1995)
- R. Johnsen, M.A. Biondi, J. Chem. Phys. 57, 1975 (1972)
- J.V. Jovanović, S.B. Vrhovac, Z.Lj. Petrović, Eur. Phys. J. D 28, 91 (2004)
- R.K. Julian Jr., H.-P. Reiser, R.G. Cooks, Int. J. Mass Spectrom. Ion Proc. 123, 85 (1993)
- A.B. Kanu, M.M. Gribb, H.H. Hill Jr., Anal. Chem. 80, 6610 (2008)
- F.W. Karasek, S.H. Kim, S. Rokushika, Anal. Chem. 50, 2013 (1978)
- Z. Karpas, Anal. Chem. 61, 684 (1989)
- Z. Karpas, Z. Berant, J. Phys. Chem. 93, 3021 (1989)
- Z. Karpas, M.J. Cohen, R.M. Stimac, R.F. Wenlund, Int. J. Mass Spectrom. Ion Proc. 74, 153 (1986)

- Z. Karpas, R.M. Stimac, Z. Rappoport, Int. J. Mass Spectrom. Ion Proc. 83, 163 (1988)
- D.J. Kenny, K.R. Worthington, J.B. Hoyes, J. Am. Soc. Mass Spectrom. 21, 1061 (2010)
- M.H. Khatri, J. Phys. D 17, 273 (1984)
- M.H. Khatri, J. Phys. D 18, 395 (1985)
- T. Kihara, Adv. Chem. Phys. 5, 147 (1963)
- R.G. Kosmider, J.B. Hasted, J. Phys. B 8, 273 (1975)
- E.V. Krylov, Tech. Phys. 44, 113 (1999)
- K. Kumar, J. Phys. D: Appl. Phys. 14, 2199 (1981)
- K. Kumar, Phys. Rep. 112, 319 (1984)
- M. Laatiaoui, H. Backe, D. Habs, P. Kunz, W. Lauth, M. Sewtz, Eur. Phys. J. D 66, 232 (2012)
- C.P. Lauenstein, M.J. Bastian, V.M. Bierbaum, J. Chem. Phys. 94, 7810 (1991)
- S.N. Lin, G.W. Griffin, E.C. Horning, W.E. Wentworth, J. Chem. Phys. 60, 4994 (1974)
- S.N. Lin, L.A. Viehland, E.A. Mason, J.H. Whealton, J.N. Bardsley, J. Phys. B 10, 3567 (1977)
- T.H. Lovass, H.R. Skullerud, D.-H. Kristiensen, D. Linhjell, J. Phys. D. 20, 1465 (1987)
- D.M. Lubman, Anal. Chem. 56, 1298 (1984)
- J. Lucas, Int. J. Electron. 27, 201 (1969)
- T. Makabe, H. Shinada, J. Phys. D 18, 2385 (1985)
- M.J. Manard, P.R. Kemper, Int. J. Mass Spectrom. 412, 14 (2017)
- R.E. March, J.F.J. Todd, Fundamentals of Ion Trap Mass Spectrometry. Volume 1. Florida, Practical Aspects of Ion Trap Mass Spectrometry (CRC, Boca Raton, 1995)
- A.G. Marshall, T. Chen, Int. J. Mass Spectrom. 377, 410 (2015)
- E.A. Mason, Ion mobility: its role in plasma chromatography, in *Plasma Chromatography*, ed. by T.W. Carr ((Plenum, New York, 1984)
- E.A. Mason, E.W. McDaniel, Transport Properties of Ions in Gases (Wiley, New York, 1988)
- E.A. Mason, H. Hahn, Phys. Rev. A 5, 438 (1972)
- K.B. McAfee, D. Edelson, Proc. Phys. Soc. Lond. 81, 382 (1963)
- E.W. McDaniel, D.W. Martin, W.S. Barnes, Rev. Sci. Instrum. 33, 2 (1962)
- L.G. McKnight, K.B. McAfee, D.P. Sipler, Phys. Rev. 164, 62 (1967)
- R.M. Melaven, E. Mack Jr., J. Am. Chem. Soc. 54, 888 (1932)
- S.I. Merenbloom, R.S. Glaskin, Z.B. Henson, D.E. Clemmer, Anal. Chem. 81, 1482 (2009)
- S.I. Merenbloom, T.G. Flick, E.R. William, J. Am. Soc. Mass Spectrom. 23, 553 (2012)
- M.F. Mesleh, J.M. Hunter, A.A. Shvartsburg, G.C. Schatz, M.F. Jarrold, J. Phys. Chem. 100, 16082 (1996)
- H. Meyer, S.R. Leone, Mol. Phys. 63, 705 (1988)
- H.B. Milloy, R.E. Robson, J. Phys. B 6, 1139 (1973)
- D. Morsa, V. Gabelica, E. De Pauw, Anal. Chem. 83, 5775 (2011)
- J.L. Moruzzi, L. Harrison, Int. J. Mass Spectrom. Ion Phys. 13, 163 (1974)
- J.T. Moseley, I.R. Gatland, D.W. Martin, E.W. McDaniel, Phys. Rev. 178, 234 (1969)
- K. Naveed-Ullah, D. Mathur, J.B. Hasted, Int. J. Mass Spectrom. Ion Phys. 26, 91 (1978)
- K.F. Ness, L. A. Viehland, **148**, 255 (1990)
- P.P. Ong, M.J. Hogan, J. Phys. B 18, 1897 (1985)
- P.P. Ong, D. Mathur, M.H. Khatri, J.B. Hasted, M. Hamdan, J. Phys. D 14, 633 (1981)
- O.J. Orient, Phys. Acad. Sci. Hung. 35, 247 (1974)
- P.L. Patterson, J. Chem. Phys. 56, 3943 (1972)
- W. Paul, H. Steinwedel, German Patent 944900 (1956); U.S. Patent 2939952 (1960)
- Z.Lj. Petrović, Aust. J. Phys. 39, 237 (1986)
- Z.Lj. Petrović, R.W. Crompton, G.N. Haddad, Aust. J. Phys. 37, 23 (1984)
- D. Piscitelli, A.V. Phelps, J. de Urquijo, E. Basurto, L.C. Pitchford, Phys. Rev. E 68, 046408 (2003)
- S.D. Pringle, K. Giles, J.L. Wildgoose, J.P. Williams, S.E. Slade, K. Thalassinos, R.H. Bateman, M.T. Bowers, J.H. Scrivea, Int. J. Mass Spectrom. 261, 1 (2007)
- R.W. Purves, R. Guevremont, Anal. Chem. 71, 2346 (1999)
- R.W. Purves, R. Guevremont, S. Day, C.W. Pipich, M.S. Matyjaszczyk, Rev. Sci. Instrum. 69, 4094 (1998)

References 93

- F. Rebentrost, Chem. Phys. Lett. 17, 486 (1972)
- H.E. Revercomb, E.A. Mason, Anal. Chem. 47, 970 (1975)
- R.E. Robson, Aust. J. Phys. 26, 203 (1973)
- R.E. Robson, K. Mada, T. Makabe, R.D. White, Aust. J. Phys. 48, 335 (1995)
- R.E. Robson, R.D. White, T. Makabe, Ann. Phys. **261**, 74 (1997)
- R.E. Robson, R. Winkler, F. Sigeneger, Phy. Rev. E 65, 056410 (2002)
- R.E. Robson, P. Nicoletopoulos, B. Li, R.D. White, Plasma Sources Sci. Technol. 17, 024020 (2008)
- R.E. Robson, P. Nicoletopoulos, M. Hildebrandt, R.D. White, J. Chem. Phys. 137, 214112 (2012)
- S. Rokushika, H. Hatano, M.A. Baim, H.H. Hill Jr., Anal. Chem. 57, 1902 (1985)
- B.T. Ruotolo, K. Giles, I. Campuzano, A.M. Sandercock, R.H. Bateman, C.V. Robinson, Science 310, 1658 (2005)
- S.I. Sandler, E.A. Mason, J. Chem. Phys. 47, 4653 (1967)
- O. Sappart, J.I. Baumbach, Meas. Sci. Technol. 11, 1473 (2000)
- O. Šašić, J. Jovanović, Z. Lj, J. de Petrović, J.R. Urquijo, J.L. Castrejó-Pita, E. Basurto Hernández-Ávilla, Phys. Rev. E **71**, 046408 (2005)
- B.B. Schneider, E.G. Nazarov, F. Londry, P. Vouras, T.R. Covey, Mass Spectrom. Rev. 35, 687 (2016)
- A.A. Shvartsburg, Differential Ion Mobility Spectrometery: Nonlinear Ion Transport and Fundamentals of FAIMS (CRC Press, Boca Raton, 2009)
- A.A. Shvartsburg, Differential Ion Mobility Spectrometry (CRC Press, Boca Raton, 2009)
- A.A. Shvartsburg, R.D. Smith, Anal. Chem. 80, 9689 (2008)
- A.A. Shvartsburg, R.R. Hudgins, P. Dugourd, M.F. Jarrold, J. Phys. Chem. A 101, 1684 (1997)
- A.A. Shvartsburg, K. Tang, R.D. Smith, J. Am. Soc. Mass Spectrom. 15, 1487 (2004)
- A.A. Shvartsburg, S.V. Mashkevich, R.D. Smith, J. Phys. Chem. A 110, 2663 (2006)
- A.A. Shvartsburg, Y.M. Ibrahim, R.D. Smith, J. Am. Soc. Mass Spectrom 25, 480 (2014)
- W.F. Siems, L.A. Viehland, H.H. Hill Jr., Anal. Chem. 84, 9782 (2012)
- W.F. Siems, C. Wu, E.E. Tarver, H.H. Hill Jr., P.R. Larsen, G.D. McMinn, Anal. Chem. **66**, 4195 (1994)
- J.A. Silvira, W. Danielson, M.E. Ridgeway, M.A. Park, Int. J. Ion Mobil. Spectrom. 19, 87 (2016)
- G.N. Sivalingam, J. Yan, H. Sahota, K. Thalassinos, Int. J. Mass Spectrom. 345-347, 54 (2013)
- H.R. Skullerud, S. Holmstrom, J. Phys. D 18, 2375 (1985)
- D.P. Smith, T.W. Knapman, I. Campuzano, R.W. Malham, J.T. Berryman, S.E. Radford, A.E. Ashcroft, Eur. J. Mass Spectrom. 15, 113 (2009)
- A.P. Snyder, C.S. Harden, A.H. Brittain, M.-G. Kim, N.S. Arnold, H.L.C. Meuzelaar, Anal. Chem. 65, 299 (1993)
- G.E. Spangler, Int. J. Mass Spectrom. 220, 399 (2002)
- S.M. Stow, T. Causon, X. Zheng, R.T. Kurulugama, T. Mairinger, J.C. May, E.E. Rennie, E.S. Baker, R.D. Smith, J.A. McLean, S. Hann, J.C. Fjeldsted, Anal. Chem. 89, 9048 (2017)
- Y. Sun, S. Vahidi, M.A. Sowole, L. Konermann, J. Am. Soc. Mass Spectrom. 27, 31 (2016)
- N. Takata, J. Phys. D 18, 1795 (1985)
- A.M. Tyndall, *The Mobility of Positive Ions in Gases* (Cambridge University Press, London, 1938). Ch. 5
- J. de Urquijo, AIP Conf. Proc. 740, 33 (2004)
- G. Vidal-de-Miguel, M. Macia, J. Cuevas, Anal. Chem. 84, 7831 (2012)
- L.A. Viehland, Int. J. Mass Spectrom. **18**, 171 (2015)
- L.A. Viehland, Int. J. Mass Spectrom. 19, 1 (2016a)
- L.A. Viehland, Int. J. Mass Spectrom. 19, 11 (2016b)
- L.A. Viehland, D.E. Goeringer, J. Chem. Phys. **120**, 9090 (2004)
- L.A. Viehland, D.E. Goeringer, J. Phys. B 38, 3987 (2005)
- L.A. Viehland, D.E. Goeringer, J. Phys. Conf. Ser. 115, 012011 (2008)
- L.A. Viehland, E.A. Mason, At. Data Nucl. Data Tables 60, 37 (1995)
- L.A. Viehland, C.-L. Yang, Mol. Phys. **113**, 3874 (2015)
- L.A. Viehland, E.A. Mason, J.H. Whealton, J. Chem. Phys. **82**, 4715 (1975)

- L.A. Viehland, R. Guevremont, R.W. Purves, D.A. Barnett, Int. J. Mass Spectrom. 197, 123 (2000)
- L.A. Viehland, E.A. Kabbe, V.V. Dixit, J. Phys. B 38, 4011 (2005)
- L.A. Viehland, D.M. Danailov, D.E. Goeringer, J. Phys. B 39, 3993 (2006a)
- L.A. Viehland, D.M. Danailov, D.E. Goeringer, J. Phys. B 39, 4015 (2006b)
- L.A. Viehland, A. Lutfullaeva, J. Dashdorj, R. Johnsen, Int. J. Ion Mobil. Spectrom 20, 95 (2017)
- Y. Wang, R.J. Van Brunt, Phys. Plasmas **4**, 551 (1997) J.H. Whealton, S.B. Woo, Phys. Rev. A **6**, 2319 (1972)
- J.H. Whealton, E.A. Mason, R.E. Robson, Phys. Rev. A **9**, 1017 (1974)
- R.D. White, Time-dependent multi-term soltuion of Boltzmann's equation for charged particle swarms in temporally-varying electric fields. Ph.D. thesis, James Cook University of North Oueensland, Australia (1996)
- R.D. White, R.E. Robson, K.F. Ness, Aust. J. Phys. 48, 925 (1995)
- D. Wobschall, J.R. Graham, Jr., D.P. Malone, Phys. Rev. 131 (1565) (1963)

Chapter 3 Momentum-Transfer Theory



3.1 Qualitative Momentum-Transfer Theories

Chapter 2 presented a somewhat rapid review of various types of drift-tube experiments that have been and are being used to study gaseous ion mobility, diffusion, and reaction. In the remainder of this book, we consider the theories behind such experiments.

We start with momentum-transfer theory because it primarily relies on algebra, trigonometry, and classical mechanics. The term momentum-transfer theory is used for "bottom-up" justifications of the fundamental ion mobility equation based on repetitions of a single average collision and general conservation principles (Revercomb and Mason 1975; Mason and McDaniel 1988). However, it is incorrect to refer to early bottom-up treatments as theories because two crucial inaccuracies were knowingly permitted for the sake of simplicity. The resulting expressions have the expected dependences on experimental variables and physical constants but differ from (1.45) in the numerical coefficient that appears; the correct numerical value was thus grafted on at the end from the top-down derivations based on the Boltzmann equation (Chaps. 4 and 5). This is why they are referred to here as qualitative momentum-transfer theories.

One of the two inaccuracies of the qualitative momentum-transfer theories, use of the root mean square speed instead of the average speed, is easily remedied. But it is more difficult to correct the second inaccuracy: use of \mathbf{v}_d as an approximation for the ion velocity immediately before a collision. Obviously, ions must be traveling with an average velocity less than the pre-collision velocity, since they are continually accelerated between collisions and reach their largest velocity just before the next collision. This second approximation is less defective for massive ions in low-mass drift gases, but it is always somewhat wrong and becomes seriously so with ions of low mass in a massive drift gas.

In the qualitative momentum-transfer treatments (Revercomb and Mason 1975; Mason and McDaniel 1988), not only were the constants adjusted to agree with

(1.45) from kinetic theory, but α_c was implicitly set equal to zero by using the first approximation solution of the Boltzmann equation to correct the numerical coefficient. It is fortunate that, as shown in Sect. 2.8.2, α_c is very small for atomic ions and neutrals in the low-field limit. This is not the case at intermediate and high E/n_0 , i.e., where the low-field criterion, (2.31), is not obeyed. It also may not be true at any E/n_0 for molecules, since few ab initio calculations have been made to test its value for such systems.

Analytical practitioners of IMS usually employ no follow-up adjustment after using (2.33) to calculate the structure factor (Ω_d/\bar{z}) for comparison with values estimated by geometrical approximations (see Chap. 9). This is acceptable for atomic ions in atomic gases at low E/n_0 , as long as it is remembered that Ω_d/\widehat{z} involves the momentum-transfer collision integral, which is an energy average of the cross section and cannot possibly be exactly the same as a geometrical cross section. For molecular systems, it will be shown below, and more rigorously in Chap. 8, that there is an additional problem: the molecular collision integral involved is expressed in terms of several collision integrals, the most important of which is only approximately the same as $\overline{\Omega}^{(1,1)}(T_{eff})$. Experimental values of Ω_d/\widehat{z} are, therefore, not as easily related to the microscopic interactions of molecule ion-neutral systems than many researchers expect. This motivated Siems et al. (2012) to create a proper momentum transfer derivation of the fundamental low-field ion mobility equation for atomic and molecular systems. Here we will present an alternate but somewhat more rigorous momentum-transfer theory, valid for molecular as well as atomic systems and for any value of E/n_0 . For convenience in notation, we assume that the neutral gas is composed of a single chemical species, so we only need to use 0 subscripts to refer to the neutrals.

3.2 Essentials of Momentum-Transfer Theory

The momentum-transfer theory in this chapter will build on the principles that mass, momentum, and energy are conserved in every ion–neutral collision and that, after transient effects have died out and steady-state behavior has been achieved, ions do not accumulate momentum or energy on the average. Instead, they transfer them to the neutrals at the same steady rate that they gain them from the electrostatic field.

The axiom that reflects the existence of a terminal (steady-state) drift speed is that the force on an ion, $q\mathbf{E}$, must (by Newton's laws of motion) equal the rate of increase of the ion's linear momentum. In order for momentum to not be accumulated, $q\mathbf{E}$ must be equal to the rate at which the ions lose momentum by transferring it to the neutrals. Thus "momentum balance" along the field direction may always be written as

$$qE = \langle \Delta p_z \ \nu^{(1)} \rangle, \tag{3.1}$$

where $\Delta p_z = m \Delta v_z$ is the ion momentum along the field that is lost in a single collision, $\nu^{(1)}$ is the momentum-transfer collision frequency whose dependence on

experimental variable must still be determined, and the brackets indicate an average over collisions.

The first step needed to arrive at an equation for ion mobility from momentumbalance considerations is to replace the average of products by the product of averages. Thus,

$$\langle \Delta p_z \ \nu^{(1)} \rangle \approx \langle \Delta p_z \rangle \langle \nu^{(1)} \rangle.$$
 (3.2)

The second is to make a standard approximation of kinetic theory (Present 1958): the collision frequency for transfer of some physical quantity is the product of the number density, the relative speed, g, before collision, and the cross section for this transfer. Thus, for trace amounts of an ion motion moving in a pure neutral gas,

$$u^{(1)} \approx n_0 \, g \, \overline{Q}^{(1)}(\varepsilon) \,.$$
(3.3)

The cross section for momentum transfer, $\overline{Q}^{(1)}(\varepsilon)$, has yet to be defined, but it must have the units of area. Note that it depends upon the total energy, ε , in the center-of-mass frame for a single collision, so it must depend upon the energy that the ions and neutrals have when they are in pre-collision internal states α and β (with internal energies $\varepsilon^{(\alpha)}$ and $\varepsilon^{(\beta)}_0$, respectively) as well as the initial relative kinetic energy of the colliding ion and neutral.

We can use a correlation coefficient, designated as ζ_{MT} , to change the approximations above into an equality. Thus,

$$qE = \zeta_{MT} \, n_0 \, \langle \Delta p_z \rangle \, \left\langle g \overline{Q}^{(1)} \left(\varepsilon \right) \right\rangle. \tag{3.4}$$

Determining ζ_{MT} will be discussed later in this chapter.

3.3 Relative Speed

The natural descriptors for experiments are the ion and neutral velocities in the laboratory frame of reference, \mathbf{v} and \mathbf{v}_0 , respectively. However, the relative and center-of-mass velocities before a collision,

$$\mathbf{g} = \mathbf{v} - \mathbf{v}_0 \tag{3.5}$$

and

$$\mathbf{G} = \widehat{m}\mathbf{v} + \widehat{m}_0\mathbf{v}_0,\tag{3.6}$$

respectively, are more convenient for treating conservation of energy and linear momentum in a single collision. Note that \widehat{m} and \widehat{m}_0 are the mass fractions of the ions and neutrals, respectively, so $\widehat{m} + \widehat{m}_0 = 1$.

Because \mathbf{g} is a difference vector, it is unchanged by Galilean transformations of the frame of reference. Therefore, it may be shifted unchanged between laboratory, center of mass, and other uniformly translating frames of reference. This invariance makes \mathbf{g} the key descriptor of collisions and of moments of the ion vdf in the laboratory frame.

The first moment is the ion speed, so in the absence of gradients of n_0 , we must have

$$v_d = \langle v_z \rangle \,, \tag{3.7}$$

where the angular brackets represent the same average as in (3.1). Since the entire neutral gas is assumed to be at rest, $\langle \mathbf{v}_0 \rangle = 0$ and (3.5) and (3.7) give

$$v_d = \langle g_z \rangle. \tag{3.8}$$

The second moment of the ion vdf can be used to define an ion temperature in the laboratory frame, as follows:

$$\frac{3}{2}k_B T = \left\langle \frac{1}{2}mv^2 \right\rangle = \frac{m}{2} \sum_{i=x,y,z} \left\langle (g_i + v_{0i})^2 \right\rangle
= \frac{m}{2} \sum_{i=x,y,z} \left\langle (g_i^2 + 2g_i v_{0i} + v_{0i}^2) \right\rangle = \frac{m}{2} \left\langle g^2 \right\rangle + \frac{m}{m_0} \left(\frac{3}{2} k_B T_0 \right).$$
(3.9)

Note that we have assumed that there are no correlations between the ion and neutral speeds along any direction, so $\langle g_i v_{0i} \rangle = 0$, and that the average neutral energy in the laboratory frame is

$$\left\langle \frac{1}{2}m_0v_0^2 \right\rangle = \frac{3}{2}k_BT_0. \tag{3.10}$$

The process of identifying moments can be continued indefinitely, with the third moment describing the skewness of the distribution, the fourth moment its kurtosis, etc. In this chapter, however, we are concerned only with the first two moments.

For conservation of linear momentum in a collision, it is necessary and sufficient that G = G', where the lack of a prime indicates pre-collision values and its presence indicates post-collision values. Conservation of total energy requires

$$\varepsilon = \frac{1}{2}mv^{2} + \frac{1}{2}m_{0}v_{0}^{2} + \varepsilon^{(\alpha)} + \varepsilon_{0}^{(\beta)} = \frac{1}{2}\mu_{0}g^{2} + \frac{1}{2}(m + m_{0})G^{2} + \varepsilon^{(\alpha)} + \varepsilon_{0}^{(\beta)}$$
$$= \frac{1}{2}\mu_{0}(g')^{2} + \frac{1}{2}(m + m_{0})G^{2} + \varepsilon^{(\alpha')} + \varepsilon_{0}^{(\beta')}, \tag{3.11}$$

where we have replaced $G^{\prime 2}$ by G^2 in the final equality. Therefore, the center-of-mass energy must remain constant, i.e.,

3.3 Relative Speed 99

$$\epsilon_{cm} = \frac{1}{2}\mu_0 g^2 + \varepsilon^{(\alpha)} + \varepsilon_0^{(\beta)} = \frac{1}{2}\mu_0 \left(g'\right)^2 + \varepsilon^{(\alpha')} + \varepsilon_0^{(\beta')}. \tag{3.12}$$

This equation can be rewritten as

$$g' = g \left[1 - \tilde{\gamma}_1 \right]^{1/2}. \tag{3.13}$$

Here the first dimensionless coefficient,

$$\widetilde{\gamma}_1 = \frac{2\Delta\varepsilon_{int}}{\mu_0 q^2},\tag{3.14}$$

is the ratio of the change in internal energy,

$$\Delta \varepsilon_{int} = \varepsilon^{(\alpha')} + \varepsilon_0^{(\beta')} - \varepsilon^{(\alpha)} - \varepsilon_0^{(\beta)}, \tag{3.15}$$

to the pre-collision relative kinetic energy. Thus, g' = g when only elastic collisions occur, such as with the atomic ion and neutral systems considered by Siems et al. (2012).

3.4 Cross Sections

3.4.1 Momentum Transfer in a Collision

Suppose that a randomly selected ion is initially approaching a stationary neutral with relative velocity \mathbf{g} ; we will account later for the fact that only half of the randomly selected ions can be approaching the neutral. The total linear momentum is clearly $m\mathbf{g}$. In spherical polar coordinates, the collision will result in the ion moving away from the neutral at a polar angle, $0 \le \theta \le \pi$, and an azimuthal angle, $0 \le \phi \le 2\pi$, with respect to \mathbf{g} but with a new velocity, \mathbf{g}' , whose magnitude is given by (3.13). Thus, the final linear momentum of the ion along \mathbf{g} will be $mg' \cos \theta$. Nothing in the differential scattering cross section or the change in linear momentum requires information about what happens to the position of the neutral after the ion collides with it. Therefore, the loss of linear momentum of the ion is

$$\Delta \mathbf{p} = m\mathbf{g} \left[1 - \left(\frac{g'}{g} \right) \cos \theta \right] \tag{3.16}$$

in any frame of reference where θ is the angle between **g** and **g**'.

The cross section for momentum transfer is the fraction of the initial momentum in the center-of-mass frame that is lost by the ions. Therefore, the cross section for all scattering angles and for all final states of the ion and neutral is

$$\overline{Q}^{(1)}(\varepsilon) = \sum_{a'\beta'} \int_{0}^{2\pi} \int_{0}^{\pi} \left[1 - \left(\frac{g'}{g} \right) \cos \theta \right] \sigma \sin \theta d\theta d\phi. \tag{3.17}$$

Note that $\overline{Q}^{(1)}(\varepsilon)$ has the units of area and depends upon ε through its dependence upon σ and its separate dependence upon the relative speeds.

It is instructive to consider what happens to (3.17) when the ions and neutrals are atomic. The sums vanish and conservation of energy requires g'=g, which means that the cross section depends only upon the relative kinetic energy. The differential scattering cross section depends upon θ but not ϕ , so the integral over ϕ can be evaluated to give a factor of 2π . Finally, the integral of $\sigma \sin \theta d\theta$ can be written as the integral of bdb (Robson 2006), where b is the impact parameter. Therefore,

$$\overline{Q}^{(1)}(\varepsilon) = 2\pi \int_{0}^{\infty} [1 - \cos \theta] b db; \qquad (3.18)$$

this is the usual expression for the momentum-transfer (or diffusion) cross section (Hirschfelder et al. 1964) for atomic ions moving through atomic gases, with $\varepsilon = \mu g^2/2$.

3.4.2 Average Momentum Transfer

In (3.4), $\langle g\overline{Q}^{(1)}(\varepsilon)\rangle$ is a weighted average of $g\overline{Q}^{(1)}(\varepsilon)$ over the energy distributions that arise in real mobility experiments. These distributions are, of course, unknown so approximate distribution functions must be introduced. This is equivalent to solutions of the Boltzmann equation like those discussed in Chap. 5; they each start with a guess for the (zero-order) ion vdf, construct basis functions that are orthogonal with respect to this vdf, and then use the method of weighted residuals (Finlayson 1972; Appendix C) to determine successively more accurate results for the vdf and the mobility, diffusion and reaction rate coefficients calculated from it.

The Maxwell–Boltzmann distribution for a pure gas designated by 0 subscripts, with a known set of internal states labeled by β with energies $\varepsilon_0^{(\beta)}$, is

$$f_0^{(\beta)}(\mathbf{v}_0) = \frac{1}{Z_0} \left(\frac{m_0}{2\pi k_B T_0} \right)^{3/2} \exp\left(-\frac{m_0 v_0^2}{2k_B T_0} - \frac{\varepsilon_0^{(\beta)}}{k_B T_0} \right). \tag{3.19}$$

It is known (Hirschfelder et al. 1964; Mason and McDaniel 1988) that (3.19) is an excellent approximation for the neutral vdf when the partition function is

3.4 Cross Sections 101

$$Z_0 = \sum_{\beta} \exp\left(-\frac{\varepsilon_0^{(\beta)}}{k_B T_0}\right). \tag{3.20}$$

A similar distribution is accurate for the ions at low E/n_0 . However, the ions in a swarm experiment are present in trace amounts, so at intermediate and high values of E/n_0 , the average energy of the ions can be far above that of the neutrals without influencing the gas temperature. Therefore, it is plausible that the ions have a Maxwell–Boltzmann distribution characterized by a much higher ion temperature, T. Thus for applicability over a wide range of E/n_0 , we assume that

$$f^{(\alpha)}(\mathbf{v}) = \frac{1}{Z} \left(\frac{m}{2\pi k_B T} \right)^{3/2} \exp\left(-\frac{mv^2}{2k_B T} - \frac{\varepsilon^{(\alpha)}}{k_B T} \right), \tag{3.21}$$

where

$$Z = \sum_{\alpha} \exp\left(-\frac{\varepsilon^{(\alpha)}}{k_B T}\right). \tag{3.22}$$

Note that we have assumed a relatively easy exchange of ion energy between translational and internal modes, by assuming that T characterizes both the kinetic and internal energy distributions of the ions; the result is equivalent to a two-temperature kinetic theory for atomic ions and neutrals (see Chap. 5).

The change of variables needed to simplify the product ff_0 is more complicated than simply changing variables to **g** and **G**. Instead, we use the vectors introduced by Viehland and Mason (1975):

$$\gamma = \left(\frac{\mu}{2k_B T_{eff}}\right)^{1/2} (\mathbf{v} - \mathbf{v}_0) \tag{3.23}$$

and

$$\chi = \left(\frac{mT_0 + m_0 T}{2k_B T T_0}\right)^{1/2} \left[\frac{mT_0 \mathbf{v} + m_0 T \mathbf{v}_0}{mT_0 + m_0 T}\right],\tag{3.24}$$

where

$$T_{eff} = \frac{mT_0 + m_0T}{m + m_0} = \widehat{m}T_0 + \widehat{m}_0T.$$
 (3.25)

These quantities have been constructed so that

$$\gamma^2 + \chi^2 = \frac{mv^2}{2k_B T} + \frac{m_0 v_0^2}{2k_B T_0}.$$
 (3.26)

Then it can be shown that

$$ff_0 = \frac{1}{ZZ_0\pi^3} \exp\left(-\gamma^2 - \chi^2 - \frac{\varepsilon^{(\alpha)}}{k_B T} - \frac{\varepsilon_0^{(\beta)}}{k_B T_0}\right),\tag{3.27}$$

which is dimensionless and normalized to one when integrated over all γ and χ and summed over all α and β .

Since σ depends upon the velocities only through the magnitude of \mathbf{g} , it does not depend upon χ or the angles of γ . Therefore, we first integrate (3.27) over all χ to get

$$ff_0 = \frac{1}{ZZ_0\pi^{3/2}} \exp\left(-\gamma^2 - \frac{\varepsilon^{(\alpha)}}{k_B T} - \frac{\varepsilon_0^{(\beta)}}{k_B T_0}\right). \tag{3.28}$$

Then we change to spherical polar coordinates for γ and integrate over the angles of this vector to get a factor of 4π . Since the change in coordinates introduces a factor of γ^2 , we get

$$ff_0 = \frac{4\gamma^2}{ZZ_0\pi^{1/2}} \exp\left(-\gamma^2 - \frac{\varepsilon^{(\alpha)}}{k_B T} - \frac{\varepsilon_0^{(\beta)}}{k_B T_0}\right); \tag{3.29}$$

this product is dimensionless and normalized to one when integrated over all γ from 0 to ∞ .

How should we use (3.29) to average $g\overline{Q}^{(1)}(\varepsilon)$? Since $\overline{Q}^{(1)}(\varepsilon)$ is the fraction of the linear momentum that is transferred, it describes the transfer of momentum in velocity space, but as a function of the energies involved. Using (3.29) involves averaging over the dimensionless relative kinetic energy in velocity space. Hence, we should multiply $\overline{Q}^{(1)}(\varepsilon)$ by γ^2 to have the amount of dimensionless kinetic energy that is involved in momentum transfer; it is this quantity that it is appropriate to average using ff_0 . We also must divide (3.29) by 2 since only half of the ions are approaching the ion (see above). Thus we get

$$\left\langle g\overline{Q}^{(1)}\left(\varepsilon\right)\right\rangle = \sum_{\alpha\beta} \int_{0}^{\infty} \left(\frac{2\gamma^{2}}{ZZ_{0}\pi^{1/2}}\right) \exp\left(-\gamma^{2} - \frac{\varepsilon^{(\alpha)}}{k_{B}T} - \frac{\varepsilon_{0}^{(\beta)}}{k_{B}T_{0}}\right) \times \gamma^{2}g\overline{Q}^{(1)}\left(\varepsilon\right) d\gamma = v_{eff}\overline{\Omega}_{mol}^{(1,1)}\left(T_{0}, T_{eff}\right), \quad (3.30)$$

where the effective thermal speed,

$$v_{eff} = \left(\frac{8k_B T_{eff}}{\pi \mu_0}\right)^{1/2},\tag{3.31}$$

comes from the factor of $2/\pi^{1/2}$ and from using (3.5) and (3.23) to convert g to γ . Note that v_{eff} differs from v_{th} because it involves T_{eff} rather than T_0 .

3.4 Cross Sections 103

Combining (3.17) and (3.30) gives the momentum-transfer collision integral for molecular systems,

$$\overline{\Omega}_{mol}^{(1,1)}\left(T_{0}, T_{eff}\right) = \frac{1}{ZZ_{0}} \sum_{\alpha\beta\alpha'\beta'} \int_{0}^{\infty} \int_{0}^{2\pi} \int_{0}^{\pi} \exp\left(-\gamma^{2} - \frac{\varepsilon^{(\alpha)}}{k_{B}T} - \frac{\varepsilon_{0}^{(\beta)}}{k_{B}T_{0}}\right) \times \gamma^{5} \left[1 - \frac{\gamma'}{\gamma} \cos\theta\right] \sigma \sin\theta d\theta d\phi d\gamma.$$
(3.32)

It is worth noting that there are five powers of γ ; two arise from the transformation into spherical polar coordinates, one comes from the factor of g involved in computing $\langle g\overline{\mathcal{Q}}^{(1)}(\varepsilon)\rangle$, and the other two arise from multiplying $\overline{\mathcal{Q}}^{(1)}(\varepsilon)$ by $\gamma^2/2$ when moving from a fraction (cross section) to an average dimensionless energy lost due to momentum transfer.

Although $\overline{\Omega}^{(1,1)}\left(T_0,T_{eff}\right)$ involves three temperatures, T, T_0 , and T_{eff} , (3.25) relates them and so only two are independent. As indicated by the notation, we have chosen the independent ones to be T_0 and T_{eff} . Note that T_{eff} is given in terms of v_d by (1.31), an equation that has been obtained by Revercomb and Mason (1975) by algebraic methods based on momentum-transfer theory.

Suppose we specialize to atomic ions and neutrals applying the methods used previously. Then (3.32) reduces to

$$\overline{\Omega}_{mol}^{(1,1)}\left(T_{0}, T_{eff}\right) \to \int_{0}^{\infty} \exp\left(-\gamma^{2}\right) \gamma^{5} \overline{Q}\left(k_{B} T_{eff}\right) d\gamma = \overline{\Omega}^{(1,1)}\left(T_{eff}\right). \tag{3.33}$$

Here $\overline{Q}^{(1)}\left(k_BT_{eff}\right)$ and $\overline{\Omega}^{(1,1)}\left(T_{eff}\right)$ are the usual (Mason and McDaniel 1988) momentum-transfer cross section and momentum-transfer collision integral, normalized as in Sect. 1.11, whose interactions are described by classical mechanics. Equation (3.33) is the same result obtained by Siems et al. (2012), although they obtained it by assuming in advance that $\left\langle g\overline{Q}^{(1)}\left(\varepsilon\right)\right\rangle$ was equal to $\left\langle g\right\rangle\left\langle \overline{Q}^{(1)}\left(\varepsilon\right)\right\rangle$. These results will be derived in Chap. 5 for atomic ion—atom systems from a top-down solution of the Boltzmann equation using the two-temperature theory. Note that, at low E/n_0 , it is rigorously true that only half of the ions can be approaching the chosen neutral at any given time, T_{eff} becomes equal to T_0 and the equations reduce to the expressions given in Chap. 1 for the low-field situation.

An important point is that (3.32) extends the definition of the momentum-transfer collision integral for atomic systems at arbitrary E/n_0 to the case of molecular ions and neutrals. In particular, the molecular collision integral involves $1 - (\gamma'/\gamma) \cos(\theta)$ rather than $1 - \cos(\theta)$. The only previous derivation (Viehland et al. 1981) of this expression for molecular systems was obtained by a top-down solution of the appropriately modified Boltzmann equation (see Chap. 8).

3.5 Average Ion Momentum Lost in a Collision

3.5.1 Average Drift Speed Between Collisions

According to the definitions in Sect. 3.2, the quantity

$$\langle \Delta p_z \rangle = m \left\langle \left(v - v' \right)_z \right\rangle \tag{3.34}$$

must be directly proportional to v_d if (3.4) and (3.30) are going to turn into an equation for the mobility. Solving (3.5) for \mathbf{v}_0 and inserting the result into (3.6) gives

$$\mathbf{g} = (\mathbf{v} - \mathbf{G})/\widehat{m}_0. \tag{3.35}$$

Solving this equation for \mathbf{v} and inserting the result into (3.34) gives

$$\langle \Delta p \rangle = \mu_0 \langle g_z - g_z' \rangle, \tag{3.36}$$

since $G_z^{'} = G_z$ by conservation of linear momentum. Our task therefore is to quantify the relationship between (3.36) and v_d . In order to do this, we must carefully consider the average speed between collisions.

A gaseous ion under the influence of a constant T_0 and E/n_0 moves along the direction of the field in the manner represented by the blue line in Fig. 3.1. The collisions occur after different time intervals, but they are instantaneous events in this figure, as they are in the Boltzmann equation. Hence, the ion speed abruptly changes from a pre-collision value, v_z , to a post-collision value, v_z' , and then smoothly increases at a rate of qE/m until the next collision. For a strong graphical presentation, the

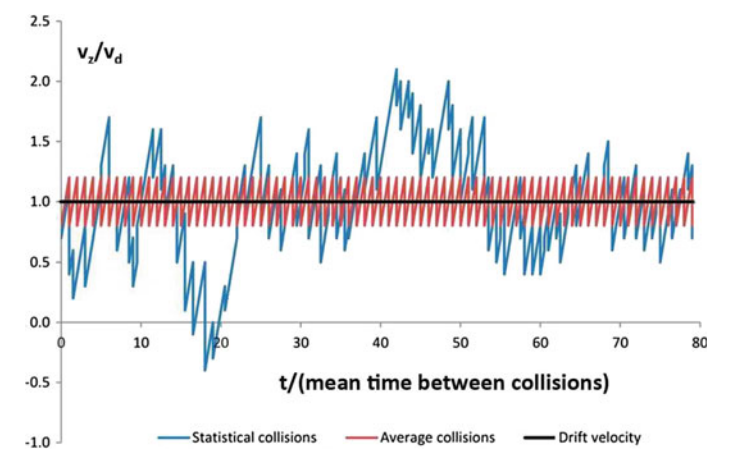


Fig. 3.1 Movement of a gaseous ion at fixed T_0 and E/n_0

figure depicts the case of a massive ion, $m\gg m_0$, in a high field, where the average drift speed of the ions (the constant, black line) is large in comparison to the relative thermal speed, i.e., $v_d>v_{th}$. In such a case, v_d is larger than the average change in ion speed during a collision, and there are correspondingly few instances (but there are some!) in Fig. 3.1 of the instantaneous drift speed having negative values after collision (i.e., the ions are temporarily moving against the field) or where $v_z'>v_d$. The latter type of collision would become much more prevalent as $E/n_0\to 0$; in this limit, the fraction of these collisions approaches 0.5 and the ion path along the field becomes nearly indistinguishable from a random walk, as it always is in directions perpendicular to the field.

Because an ion's speed along the field always increases linearly with time during the interval between collisions, the average speed between the kth and the (k+1)th collision is $(v_k + v_{k+1})/2$. Therefore, the average over \mathfrak{N} collisions (counting from 0 to $\mathfrak{N}-1$) must be given by the expressions

$$\langle v \rangle = \frac{1}{2\mathfrak{N}} \sum_{k=0}^{\mathfrak{N}-1} (v_k + v_{k+1}).$$
 (3.37)

If we ignore transient effects and density gradients of n_0 , the first and last velocities of the ion's path do not significantly affect the averages and from (3.7), we have

$$v_d = \frac{1}{2} \langle v + v' \rangle = \frac{1}{2} (\langle v \rangle + \langle v' \rangle). \tag{3.38}$$

where $\langle v \rangle$ is the average ion speed before collision and $\langle v' \rangle$ is the average ion speed after collision. Equation (3.38) tells us that we may think of the average drift speed as the average formed from the starting and ending speeds of a single collision, and to suppose the mobility experiment equivalent to the result of such an average collision repeated \mathfrak{N} times, as shown by the regularly varying lines in Fig. 3.1.

3.5.2 Classification of Collisions

By creating a preferred direction for ion motion, the electric field becomes the basis for classifying collisions. A collision will be called \mathbf{r}^+ if $\mathbf{g} \cdot \mathbf{E} > 0$, \mathbf{r}^- if $\mathbf{g} \cdot \mathbf{E} < 0$, \mathbf{cm}^+ if $\mathbf{G} \cdot \mathbf{E} > 0$, and \mathbf{cm}^- if $\mathbf{G} \cdot \mathbf{E} < 0$. These collision classes are summarized in Fig. 3.2, where the first of the two signs inside brackets indicates whether the collisions are \mathbf{r}^+ or \mathbf{r}^- and the second indicates whether they are \mathbf{cm}^+ or \mathbf{cm}^- . Although this figure depicts the colliding molecules as hard spheres (circles in two dimensions), the relationships among the vectors are independent of the nature of the ion–neutral interaction potential, assuming the local approximation that is also used in the Boltzmann equation, i.e., that the distances being considered are much larger than the separations at which there are appreciable ion–neutral interactions.

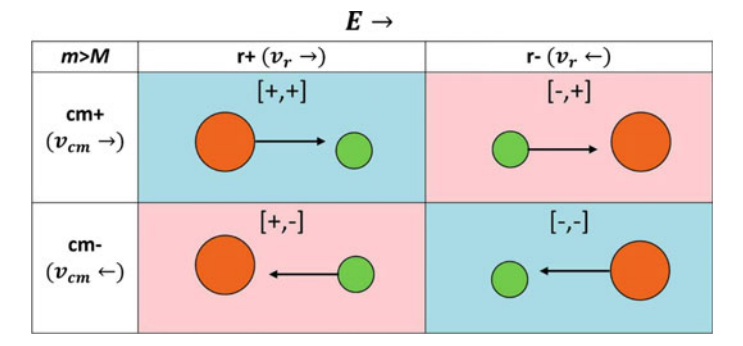


Fig. 3.2 Collision classes

Finally, the vectors start at the center of one particle but do not necessarily point at the center of the other; this offset represents the impact parameter of the collision.

The collisions in Fig. 3.1 may be related to the classes in Fig. 3.2. Cooling collisions (blue background in Fig. 3.2) move the speed of the ion (orange circle) toward $v_z = 0$, either from $v_z > 0$ for [+, +] collisions or from $v_z < 0$ for [-, -] collisions. Heating collisions (pink background) move the ion's speed away from $v_z = 0$, either from a positive value to a more positive value for [-, +] collisions, or from a negative value to a more negative value for [+, -] collisions. It is clear that velocity changes due to collisions depend on m, m_0 , E/n_0 , and T_0 , as well as upon the details of the ion–neutral interactions.

A [+,+] cooling encounter can be viewed as a [-,-] cooling collision if the directions of ${\bf g}$ and ${\bf g}'$ are reversed and the positions of the pre- and post-collision particles are switched. With similar changes, a [+,-] heating collision can be viewed as a [-,+] heating collision. Consequently, there are really only two types of collisions that need to be examined in general terms: [+,+] cooling collisions and [-,+] heating collisions. However, the fact that there are two types means that we must change (3.38) to have separate contributions from them:

$$v_d = \frac{1}{2} \langle v + v' \rangle_c f_c + \frac{1}{2} \langle v + v' \rangle_h f_h.$$
 (3.39)

Here and below, the subscripts c and h designate quantities that differ for the two types of collisions, while the fraction of ions having each type obviously must obey the equation $f_c + f_h = 1$.

3.5.3 Archetype Collisions

We first analyze [+, +] cooling collisions in a frame of reference where the precollision neutral is at rest and in internal state β . We assume that the ion is in internal state α and that its velocity before collision lies entirely along one of the Cartesian axes (call it \widehat{z}). We will denote the speed by \widehat{W} so that it is not confused with the speed in the laboratory frame of reference. To describe the situation after collision, we use spherical polar coordinates, $(\widehat{W}', \theta, \phi)$ and $(\widehat{W}'_0, \theta_0, \phi_0)$ with respect to \widehat{z} , for the ion and neutral, respectively.

Conservation of linear momentum and energy require

$$m\widehat{W} = m\widehat{W}'\cos\theta + m_0\widehat{W}_0'\cos\theta_0, \tag{3.40}$$

$$0 = m\widehat{W}'\sin\theta\cos\phi + m_0\widehat{W}'_0\sin\theta_0\cos\phi_0 \tag{3.41}$$

$$0 = m\widehat{W}'\sin\theta\sin\phi + m_0\widehat{W}'_0\sin\theta_0\sin\phi_0 \tag{3.42}$$

and

$$\frac{1}{2}m\widehat{W}^{2} + \varepsilon^{(\alpha)} + \varepsilon_{0}^{(\beta)} = \frac{1}{2}m\widehat{W}^{2} + \frac{1}{2}m_{0}\widehat{W}_{0}^{2} + \varepsilon^{(\alpha')} + \varepsilon_{0}^{(\beta')}.$$
 (3.43)

There are four equations relating six post-collision quantities, since four quantities $(W, m, m_0, \varepsilon^{(\alpha)})$ and $\varepsilon_0^{(\beta)}$ are known. Therefore, we can solve for W', W'_0, θ and ϕ as functions of θ_0 and ϕ_0 and the other four quantities.

We first solve (3.41) and (3.42) to get

$$m_0 \widehat{W}_0' \cos \phi_0 = -\frac{\sin \theta \cos \phi}{\sin \theta_0} m \widehat{W}'$$
 (3.44)

and

$$m_0 \widehat{W}_0' \sin \phi_0 = -\frac{\sin \theta \sin \phi}{\sin \theta_0} m \widehat{W}'. \tag{3.45}$$

By dividing these equations, we see that

$$\tan \phi_0 = \tan \phi \tag{3.46}$$

or $\phi_0 = \phi \pm n\pi$, where *n* is an integer whose value will turn out to be irrelevant for our purposes. Equations (3.44)–(3.46) can be used to show that

$$m_0 \widehat{W}_0' = -(-1)^n \frac{\sin \theta}{\sin \theta_0} m \widehat{W}'.$$
 (3.47)

We next use (3.47) to eliminate \widehat{W}'_0 and ϕ_0 from (3.40) and (3.43), getting

$$\widehat{W} = \widehat{W}' \left[\cos \theta - (-1)^n \frac{\cos \theta_0}{\sin \theta_0} \sin \theta \right]$$
 (3.48)

and

$$\frac{1}{2}m\widehat{W}^{2} = \frac{1}{2}m\widehat{W}^{2} \left[1 + \frac{m\sin^{2}\theta}{m_{0}\sin^{2}\theta_{0}} \right] + \Delta\varepsilon_{int}.$$
 (3.49)

We square (3.48) and multiply (3.49) by 2/m to get two equations for W^2 . Equating these gives

$$\left[\cos\theta - (-1)^n \frac{\cos\theta_0}{\sin\theta_0} \sin\theta\right]^2 = 1 + \frac{m\sin^2\theta}{m_0\sin^2\theta_0} + \frac{2\Delta\varepsilon_{int}}{m\widehat{W}^2}.$$
 (3.50)

Analysis of this equation involves: writing out the square term; multiplying by $\sin^2 \theta_0$; replacing $\cos^2 \theta$ by $1 - \sin^2 \theta$; and, grouping the terms proportional to $\sin^2 \theta$. Since the neutral was initially not moving in our archetype collision, we can write (3.14) as

$$\widetilde{\gamma}_1 = \frac{2\Delta\varepsilon_{int}}{\mu_0 \widehat{W}^2} \tag{3.51}$$

and use (3.48) to end up with a quadratic equation for $\sin \theta / \cos \theta$. The solution of this equation is

$$\frac{\sin \theta}{\cos \theta} = \frac{(-1)^n \sin(2\theta_0) (1 - \widehat{m}_0 \widetilde{\gamma}_1)}{2 \cos^2(\theta_0) - 1/\widehat{m}_0 - \widehat{m}_0 \widetilde{\gamma}_1 \cos^2(\theta_0)} \widetilde{\gamma}_2 \tag{3.52}$$

where the second dimensionless coefficient is

$$\widetilde{\gamma}_2 = \frac{1}{2} \left\{ 1 + \left[1 - \frac{1 - 2\widehat{m}_0 \cos^2 \theta_0 + \widehat{m}_0^2 \widetilde{\gamma}_1 \cos^2 \theta_0}{\cos^2 \theta_0 (1 - \widehat{m}_0 \widetilde{\gamma}_1)^2} \widetilde{\gamma}_1 \right]^{1/2} \right\}.$$
(3.53)

When we insert (3.52) into (3.48), we find that

$$W = W' \cos \theta \left[1 - (-1)^n \frac{\cos \theta_0}{\sin \theta_0} \frac{\sin \theta}{\cos \theta} \right] = \frac{W' \cos \theta}{\widetilde{\gamma}_3} , \qquad (3.54)$$

where the third dimensionless coefficient, $\tilde{\gamma}_3$, is defined by the second equality in (3.54) but can be simplified using (3.52) to become

$$\widetilde{\gamma}_{3} = \frac{1 - (2 - \widehat{m}_{0}\widetilde{\gamma}_{1})\,\widehat{m}_{0}\cos^{2}\theta_{0}}{1 - [2\,(1 - \widetilde{\gamma}_{2}) - (1 - 2\widetilde{\gamma}_{2})\,\widehat{m}_{0}\widetilde{\gamma}_{1}]\,\widehat{m}_{0}\cos^{2}\theta_{0}}.$$
(3.55)

For atomic ions and neutrals, $\widetilde{\gamma}_1=0$ and $\widetilde{\gamma}_2=1$, so (3.55) may be written as

$$\widetilde{\gamma}_3 = 1 - 2\widehat{m}_0 \cos^2 \theta_0. \tag{3.56}$$

This means that

$$\widehat{W}'_{z} = \widehat{W}' \cos \theta = \widehat{W} c_{3} = \widehat{W} \left[1 - 2\widehat{m}_{0} \cos^{2} \theta_{0} \right]$$
(3.57)

for such systems. This is the same result as obtained previously (Siems et al. 2012) for atomic ion–neutral systems.

Equations (3.54) and (3.55) apply for all values of θ_0 and ϕ_0 , even though they do not depend upon the latter. Averaging the results over these angles is equivalent in classical mechanics to averaging the results over all impact parameters, which are shown as the offsets between the centers of the circles in Fig. 3.2. To see this, suppose for the moment that the ion and neutral are hard spheres of radii r and r_0 , respectively. When b=0, the ion rebounds after hitting the neutral, and the neutral moves away from the point of collision with an angle $\theta_0=0$. When b is infinitesimally smaller than $d=r+r_0$, the ion just grazes the neutral and $\theta_0=\pm\pi/2$, with the sign depending upon whether the ion hits the bottom of the neutral or the top. Then it is easy to calculate an average value for any function that depends only on θ_0 ; in particular,

$$\frac{1}{\cos^2 \theta_0} = \frac{\int_0^d (1 - b^2/d^2) (2\pi b) db}{\int_0^d (2\pi b) db} = \frac{1}{2}.$$
(3.58)

Here, the factors of $2\pi b$ in the integrands arise because of the rotational symmetry around the direction of the electric field, i.e. the irrelevance of the angle ϕ_0 .

For real ions and neutrals, the upper limits of the integrals in (3.58) are ∞ and both the numerator and the denominator appear to become infinite. However, ion–neutral interactions at large separation always decrease so rapidly with distance that there is an effective cut-off distance to the integrals. Therefore, we can assume that (3.58) applies in all circumstances, whether one uses classical, semiclassical or quantal methods to determine σ .

It was assumed above that the initial ion speed along \widehat{z} was the relative speed, i.e., $\widehat{W}_z = g$. We can evaluate $\overline{\widehat{W}_z'}$ by computing $\overline{\widetilde{\gamma}_3}$ from (3.55) and assuming again that the average of a product is the product of an average. This gives

$$\overline{\left(\widehat{W}_z + \widehat{W}_z'\right)_c} = \overline{\left(g + g\widetilde{\gamma}_3\right)_c} = \overline{g_c} \left(1 + \overline{\widetilde{\gamma}_{3c}}\right) , \qquad (3.59)$$

where

$$\overline{\widetilde{\gamma}_{3c}} = \frac{2\widehat{m} + \widehat{m}_0^2 \overline{\gamma_1}}{2\widehat{m} + \widehat{m}_0^2 \overline{\widetilde{\gamma}_1} + 2\widehat{m}_0 \overline{\widetilde{\gamma}_2} \left(1 - \widehat{m}_0 \overline{\widetilde{\gamma}_1}\right)}$$
(3.60)

and

$$\overline{\widetilde{\gamma}_2} = \frac{1}{2} \left\{ 1 + \left[1 - \frac{2\widehat{m} + \widehat{m}_0^2 \overline{\widetilde{\gamma}_1}}{\left(1 - \widehat{m}_0 \overline{\widetilde{\gamma}_1}\right)^2} \overline{\widetilde{\gamma}_1} \right]^{1/2} \right\},\tag{3.61}$$

and $\overline{\gamma}_1$ is given by the right-hand side of (3.14). Note that we have added c subscripts to indicate that the results hold only for cooling collisions.

Equations (3.59)–(3.61) apply in every frame of reference because the final results involve only the relative velocity. They also apply to the [-, -] cooling collisions because we have used general angles in the derivation above. However, they do not apply to heating collisions. For [-, +] and [+, -] heating collisions, the analysis is similar to that given above, except that the frame of reference is the one where the ion is initially at rest. The final result is similar to the equation for cooling collisions; all one must do is interchange the neutral and ion masses and replace c subscripts by b subscripts. Thus

$$\overline{\left(\widehat{W}_z + \widehat{W}_z'\right)_h} = \overline{g_h} \left(1 + \overline{\widetilde{\gamma}_{3h}}\right),$$
(3.62)

where

$$\overline{\widetilde{\gamma}_{3h}} = \frac{2\widehat{m}_0 + \widehat{m}^2 \overline{\widetilde{\gamma}_1}}{2\widehat{m}_0 + \widehat{m}^2 \overline{\widetilde{\gamma}_1} + 2\widehat{m} \overline{\widetilde{\gamma}_2} \left(1 - \widehat{m} \overline{\widetilde{\gamma}_1}\right)}.$$
(3.63)

Note that $\overline{c_{3c}}$ becomes \widehat{m} and $\overline{c_{3h}}$ becomes \widehat{m}_0 when inelastic collisions cannot occur. The large number of collision in a DTMS or IMS/MS experiment means that the averaging over impact parameters will automatically occur. Consequently, we can drop the overbars used in (3.59)–(3.63). The final result is that (3.39) can be written as

$$v_d = \frac{1}{2} \left(1 + \widetilde{\gamma}_{3c} \right) \langle g \rangle_c \ f_c + \frac{1}{2} \left(1 + \widetilde{\gamma}_{3h} \right) \langle g \rangle_h \ f_h. \tag{3.64}$$

There is admittedly a large amount of algebra involved in obtaining this result, but we have not found a simpler or more elegant method for deriving it.

3.6 Fundamental Ion Mobility Equation

The techniques used above can also be applied to (3.36). The initial relative velocity in the previous section was $g_z = \widehat{W}_z$, while the final relative velocity after an archetype cooling collision was

$$g_z' = \widehat{W}' \cos \theta - \widehat{W}_o' \cos \theta_0. \tag{3.65}$$

Making use of (3.47) gives

$$g_z' = \widehat{W}' \cos \theta \left[1 + (-1)^n \frac{m}{m_0} \frac{\sin \theta}{\cos \theta} \frac{\cos \theta_0}{\sin \theta_0} \right]. \tag{3.66}$$

Next, (3.52) and (3.54) can be used to write this as

$$g_z' = g\widetilde{\gamma}_{3c} \left[1 + \frac{\widehat{m}}{\widehat{m}_0} \frac{2\cos^2\theta_0 (1 - \widehat{m}_0\widetilde{\gamma}_1)}{2\cos^2\theta_0 - 1/\widehat{m}_0 - \widehat{m}_0\widetilde{\gamma}_1 \cos^2\theta_0} \widetilde{\gamma}_2 \right]. \tag{3.67}$$

Averaging over impact parameters gives

$$g_z' = g\gamma_{3c} \left[1 - \frac{2\widehat{m} \left(1 - \widehat{m}_0 \widetilde{\gamma}_1 \right)}{2\widehat{m} + \widehat{m}_0^2 \widetilde{\gamma}_1} \widetilde{\gamma}_2 \right]$$
(3.68)

for cooling collisions and similarly for heating collision. Therefore when averaged over a very large number of collisions (3.36) becomes

$$\langle \Delta p_z \rangle = \mu_0 \left[1 - \widetilde{\gamma}_{3c} + \frac{2\widehat{m} \left(1 - \widehat{m}_0 \widetilde{\gamma}_1 \right)}{2\widehat{m} + \widehat{m}_0^2 \widetilde{\gamma}_1} \widetilde{\gamma}_2 \widetilde{\gamma}_{3c} \right] \langle g \rangle_c f_c + \mu_0 \left[1 - \widetilde{\gamma}_{3h} + \frac{2\widehat{m}_0 \left(1 - \widehat{m} \widetilde{\gamma}_1 \right)}{2\widehat{m}_0 + \widehat{m}^2 \widetilde{\gamma}_1} \widetilde{\gamma}_2 \widetilde{\gamma}_{3h} \right] \langle g \rangle_h f_h.$$
 (3.69)

This can be written as

$$\langle \Delta p_z \rangle = \frac{4}{3} \alpha_{MT} \mu_0 v_d = \frac{4}{3} \alpha_{MT} \mu_0 K E, \qquad (3.70)$$

if (3.69) is used to define the momentum-transfer coefficient as

$$\alpha_{MT} = \frac{3}{2} \left\{ \left[1 - \widetilde{\gamma}_{3c} + \frac{2\widehat{m} \left(1 - \widehat{m}_{0} \widetilde{\gamma}_{1} \right)}{2\widehat{m} + \widehat{m}_{0}^{2} \widetilde{\gamma}_{1}} \widetilde{\gamma}_{2} \widetilde{\gamma}_{3c} \right] \langle g \rangle_{c} f_{c} \right.$$

$$+ \left[1 - \widetilde{\gamma}_{3h} + \frac{2\widehat{m}_{0} \left(1 - \widehat{m} \widetilde{\gamma}_{1} \right)}{2\widehat{m}_{0} + \widehat{m}^{2} \widetilde{\gamma}_{1}} \widetilde{\gamma}_{2} \widetilde{\gamma}_{3h} \right] \langle g \rangle_{h} f_{h} \right\}$$

$$\times \left[\left(1 + \widetilde{\gamma}_{3c} \right) \langle g \rangle_{c} f_{c} + \left(1 + \widetilde{\gamma}_{3h} \right) \langle g \rangle_{h} f_{h} \right]^{-1} .$$
 (3.71)

Consider now the low-field limit, where both fractions become 1/2 and the average relative speeds are both thermal. Therefore, in this limit

$$\alpha_{MT} = \frac{3}{2} \left[2 + \widetilde{\gamma}_{3c} + \widetilde{\gamma}_{3h} \right]^{-1} \times \left\{ \left[1 - \widetilde{\gamma}_{3c} + \frac{2\widehat{m} \left(1 - \widehat{m}_0 \widetilde{\gamma}_1 \right)}{2\widehat{m} + \widehat{m}_0^2 \widetilde{\gamma}_1} \widetilde{\gamma}_2 \widetilde{\gamma}_{3c} \right] + \left[1 - \widetilde{\gamma}_{3h} + \frac{2\widehat{m}_0 \left(1 - \widehat{m} \widetilde{\gamma}_1 \right)}{2\widehat{m}_0 + \widehat{m}^2 \widetilde{\gamma}_1} \widetilde{\gamma}_2 \widetilde{\gamma}_{3h} \right] \right\}.$$
(3.72)

For atomic systems in the low-field limit, we have

$$\alpha_{MT} = 1; \tag{3.73}$$

obtaining this simple result is why (3.70) contains the factor of 4/3.

In the high-field limit, $f_h = 0$ and $f_c = 1$, so (3.71) becomes

$$\alpha_{MT} = \frac{3}{2(1+\widetilde{\gamma}_{3c})} \left[1 - \widetilde{\gamma}_{3c} + \frac{2\widehat{m}(1-\widehat{m}_0\widetilde{\gamma}_1)}{2\widehat{m} + \widehat{m}_0^2\widetilde{\gamma}_1} \widetilde{\gamma}_2 \widetilde{\gamma}_{3c} \right]$$
(3.74)

in general, or

$$\alpha_{MT} = \frac{3}{2} \frac{1}{(1+\widehat{m})} \tag{3.75}$$

for atomic systems.

Making use of (2.1), (3.30), (3.31) and (3.70) allows (3.4) to be written as

$$\Upsilon_{MT} \frac{\Omega_{mol}^{(1,1)} \left(T_0, T_{eff} \right)}{\widehat{z}} = \frac{3eE}{16v_d} \left(\frac{2\pi}{\mu_0 k_B T_{eff}} \right)^{1/2} \frac{k_B T_0}{P_0},$$
(3.76)

where the momentum-transfer correction factor is

$$\Upsilon_{MT} = \frac{\alpha_{MT} \zeta_{MT}}{z_0}. (3.77)$$

Note that a modified momentum-transfer collision integral, (3.32), and a higher order correction factor, Υ_{MT} , have to be taken into account not only here but in top-down solutions of a modified Boltzmann equation, with the modifications accounting for internal energy states, inelastic collisions and angle-dependent forces between molecular ions and neutrals. The limited calculations that have been reported to date (Viehland 1984, 1994a; Viehland and Dickinson 1995; Viehland et al. 1992, 1996; Maclagan et al. 1999) indicate that these modifications and corrections are small but not negligible.

When specialized to atomic systems, (3.76) is the same equation as in the paper by Siems et al. (2012),

$$\gamma_{MT} \frac{\overline{\Omega}^{(1,1)} (T_{eff})}{\widehat{z}} = \frac{3eE}{16v_d} \left(\frac{2\pi}{\mu_0 k_B T_{eff}} \right)^{1/2} \frac{k_B T_0}{P_0},$$
(3.78)

at intermediate and high E/n_0 . This is exactly the same as the fundamental ion mobility equation, (1.45), if the small correction terms are related by the equation

$$\Upsilon_{MT} z_0 = \alpha_{MT} \zeta_{MT} = 1 + \alpha_c. \tag{3.79}$$

In the limit of low E/n_0 , (3.78) and (3.79) reduce to the fundamental low-field ion mobility equation, (1.19). On the other hand, the approximate MT theory of Mason and McDaniel (1988) gives (1.19) only if one assumes that in (3.79) we have

$$\zeta_{MT} = 1 + \alpha_c \tag{3.80}$$

and that

$$\alpha_{MT} = \frac{3}{4} \left(\frac{3\pi}{8} \right)^{1/2} = 0.814. \tag{3.81}$$

Equation (3.81) is in conflict with (3.78) and (3.80), which means that the qualitative momentum-transfer theory is off by nearly 20% at low E/N, a fact acknowledged by Revercomb and Mason (1975) and by Mason and McDaniel (1988) when they indicated that they obtained a numerical value of $3^{-1/2}$ rather than $(3/16)(2\pi)^{1/2}$. In the high-field limit, the error depends upon \widehat{m} , as shown by a comparison of (3.73) and (3.75). At intermediate E/n_0 , the error depends upon the ion–neutral mass ratio and the other factors in (3.78).

3.7 Discussion

The preceding arguments allow (1.19) and (1.45) to be derived by reasoning upward from a single collision rather than downward from the Boltzmann equation. It is clear for atomic systems that any discrepancy between theory and experiment is due to Υ_{MT} ; such discrepancies must not be ignored or absorbed into $\overline{\Omega}^{(1,1,)}(T_0)$, since that would invalidate the connection that the momentum-transfer collision integral has with the ion–neutral interactions that undergird IMS and DTMS experiments. Estimating Υ_{MT} is a subject of current research.

It is more significant, however, that we have arrived at the fundamental low-field ion mobility equation via a more general result, (3.76), that can be tested over a range of field strengths for a variety of approximate or exact ion–neutral interaction potentials describing atomic ions and neutrals. Given the success of the 2T kinetic theory (Viehland and Mason 1975) for such systems, it is expected that Υ_{MT} will be in the range 0.9–1.1 for all values of T_0 and E/n_0 . This justifies calling (3.76) the fundamental ion mobility equation and (3.78) the fundamental low-field ion mobility equation for molecular systems.

From the viewpoint of analytical IMS measurements, the values of (3.76) and (3.78) arise from the prevalence of measurements made on the borderline between the low- and high-field regimes, coupled with the need for accurate collision integrals (energy-averaged cross sections), comparable across a range of instruments and operating conditions. Hence, practical implementations of these equations require computation or estimation of Υ_{MT} . As indicated above, such considerations have begun.

Some comments have been made (Mason and McDaniel 1988) suggesting that the effort put into deriving (3.76) and (3.78), here and from top-down procedures, may have little practical impact. It is worth paraphrasing these comments before trying to counter them. The first point is that inelastic collisions enter $\overline{\Omega}^{(1,1)}$ (T_0, T_{eff}) through the differential scattering cross section in (3.32) but also through the term $1 - (\gamma'/\gamma)\cos\theta$. Since vibrational and electronic levels are separated by large amounts of energy, compared to the average kinetic energies in IMS and DTMS experiments, γ' can differ from γ only if there is a large transfer of rotational energy during the average collision.

A second, related point is that one can expect that γ' can be written as γ plus some terms in $\Delta \varepsilon_{int}$, by using a Taylor series expansion (see Appendix A) of (3.13). Inelastic correction terms are then of the form of collisions integrals involving $\gamma \Delta \varepsilon_{int} \cos \theta$. These collision integrals would vanish for isotropic scattering, and even for anisotropic scattering would be expected to be small unless some special correlation existed between θ and $\Delta \varepsilon_{int}$.

A third point is that the difference between γ (1 – $\cos \theta$) and $\gamma - \gamma' \cos \theta$ appears to be minor based on experimental measurements of the diffusion coefficients of atomic gases and those of molecular gases, where the same collision integrals appear.

The response is essentially the same to all three points: the comments do not necessarily apply to IMS and DTMS experiments at intermediate and high E/n_0 . In such cases, the values of T_{eff} and T are no longer equal to T_0 , the average total energy is so far above thermal energy that inelastic collisions become highly likely and highly dependent upon the angles with which the ion and neutral approach one another, and hence the momentum-transfer collision integral for molecules may depend strongly on inelastic collisions and angle-dependent interaction potential energies. There is some experimental evidence (Viehland and Fahey 1983) supporting this counterclaim.

The main weakness in the present momentum-transfer theory is the choice of (3.21) for the ion distribution function at intermediate and high E/n_0 . For atomic systems, better results have been achieved by the three-temperature kinetic theory (Lin et al. 1979; Viehland and Lin 1979) in which the exponential has one ion temperature along the electric field and a different one perpendicular to the field; here "better" means more rapid convergence to stable values for γ_{MT} . Even better results have been achieved by using a Gram-Charlier kinetic theory (Viehland 1994b) in which the three-temperature distribution is multiplied by terms that take into account skewness of the distribution along the field, kurtosis both parallel and perpendicular to it, correlation between the ion velocity parallel and the ion energy perpendicular to the field, and the coefficient of correlation between the ion energies parallel and perpendicular to the electric field. Both of these approaches are discussed in Chap. 5. They give fundamental ion mobility equations of the same form as the equations above, but involving a collision integral that differs from (3.69) and, because of the asymmetry of the energy distributions, cannot be expressed as an energy average of a transport cross section, either for atomic nor molecular systems.

References

B.A. Finlayson, *The Method of Weighted Residuals and Variational Principles* (Academic Press, New York, 1972)

J.O. Hirschfelder, C.F. Curtiss, R.B. Bird, Molecular Theory of Gases and Liquids (Wiley, New York, corrected edition 1964)

S.L. Lin, L.A. Viehland, E.A. Mason, Chem. Phys. 37, 411 (1979)

R.G.A.R. Maclagan, L.A. Viehland, A.S. Dickinson, J. Phys. B 32, 4947 (1999)

E.A. Mason, E.W. McDaniel, Transport Properties of Ions in Gases (Wiley, New York, 1988)

References 115

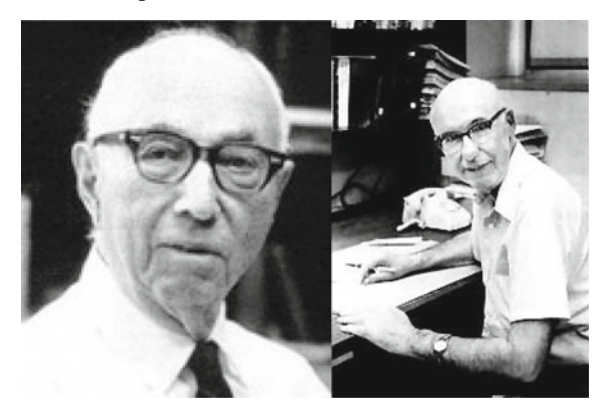
- R.D. Present, Kinetic Theory of Gases (McGraw-Hill, New York, 1958)
- H. Revercomb, E.A. Mason, Anal. Chem. 47, 970 (1975)
- R.E. Robson, *Introductory Transport Theory for Charged Particles in Gases* (World Scientific, Singapore, 2006)
- W.F. Siems, L.A. Viehland, H.H. Hill Jr., Anal. Chem. 84, 9782 (2012)
- L.A. Viehland, Internal-energy distribution of molecular ions in drift tubes, in *Swarms of Ions and Electrons in Gases*, ed. by W. Lindinger, T.D. Mark, F. Howorka (Springer, New York, 1984)
- L.A. Viehland, Phys. Scripta **T53**, 53 (1994a)
- L.A. Viehland, Chem. Phys. 179, 71 (1994b)
- L.A. Viehland, A.S. Dickinson, Chem. Phys. 193, 255 (1995)
- L.A. Viehland, D.W. Fahey, J. Chem. Phys. 78, 435 (1983)
- L.A. Viehland, S.L. Lin, Chem. Phys. 43, 135 (1979)
- L.A. Viehland, E.A. Mason, Ann. Phys. (N. Y.) 91, 499 (1975)
- L.A. Viehland, S.L. Lin, E.A. Mason, Chem. Phys. 54, 341 (1981)
- L.A. Viehland, S.T. Grice, R.G.A.R. Maclagan, A.S. Dickinson, Chem. Phys. 165, 11 (1992)
- L.A. Viehland, A.S. Dickinson, R.G.A.R. Maclagan, Chem. Phys. 211, 1 (1996)

Chapter 4 The Boltzmann Equation



4.1 General Form

We are concerned with experiments in which the effects of collisions must be treated on an equal basis with the effects of external fields. Hence, we cannot simply add a collisional damping term to Newton's equations of motion for a single particle. Instead, we take the 1872 equation of Ludwig Edward Boltzmann (1844–1906) as the fundamental kinetic equation for an ion swarm.



Hirschfelder

Curtiss

Over the years, many derivations of the Boltzmann equation have been presented (Cercignani 1988; Colonna 2016). Since each of them involves one or more approximations, it suffices here to present a physical derivation based on that of Joseph Oakland Hirschfelder (1911–1990), Charles C. Curtiss (1921–2007), and Robert Byron Bird in 1964. It is similar to the original derivation by Boltzmann, but it is specialized here to the case of trace amounts of atomic ions (or electrons) moving through a dilute, atomic gas. Molecular systems will be considered in Chap. 8.

Although the neutral gas may be pure or a mixture, it is assumed to be sufficiently dilute that collisions of three particles at a time may be completely neglected compared to the effects of two-body collisions. In addition, we need to consider only ions of a single species since their presence in trace amounts means that we can neglect the possibility of ion—ion collisions. This means that the Boltzmann equation will end up being linear and hence much easier to work with.

We suppose that the ions are subject to an external force, $\mathbf{F}(\mathbf{r}, t)$, that may be a function of \mathbf{r} and t but is not a function of \mathbf{v} . We further assume that $\mathbf{F}(\mathbf{r}, t)$ is much smaller than the forces that act during a collision, and that $\mathbf{F}(\mathbf{r}, t)$ causes an ion to experience an acceleration, $\mathbf{a}(\mathbf{r}, t) = \mathbf{F}(\mathbf{r}, t)/m$, during the time between collisions.

The Boltzmann equation is an equation of continuity for the ion distribution function, $f(\mathbf{r}, \mathbf{v}, t)$, that is normalized so that the ion number density as a function of \mathbf{r} and t is

$$n(\mathbf{r},t) = \int f(\mathbf{r}, \mathbf{v}, t) d\mathbf{v}.$$
 (4.1)

This gives $f(\mathbf{r}, \mathbf{v}, t)d\mathbf{r}d\mathbf{v}$ a physical interpretation as the number of ions that, at time t, are contained in a small volume $d\mathbf{r}d\mathbf{v}$ surrounding the point (\mathbf{r}, \mathbf{v}) in the six-dimensional phase space where \mathbf{r} and \mathbf{v} are independent, three-dimensional vectors.

In the absence of collisions, the ions in the volume $d\mathbf{r}d\mathbf{v}$ move in such a way that at time t + dt their position vectors are $\mathbf{r} + \mathbf{v}dt$ and their velocity vectors are $\mathbf{v} + \mathbf{a}(\mathbf{r}, \mathbf{t})dt$. Conservation of mass in the absence of collisions thus requires that

$$f(\mathbf{r} + \mathbf{v}dt, \mathbf{v} + \mathbf{a}(\mathbf{r}, t)dt, t + dt)d\mathbf{r}d\mathbf{v}dt = f(\mathbf{r}, \mathbf{v}, t)d\mathbf{r}d\mathbf{v}dt. \tag{4.2}$$

When there are collisions, not all of the ions that start near the point (\mathbf{r}, \mathbf{v}) in phase space arrive near the point $(\mathbf{r} + \mathbf{v}dt, \mathbf{v} + \mathbf{a}(\mathbf{r}, t)dt)$. Similarly, some of the ions that arrive near $(\mathbf{r} + \mathbf{v}dt, \mathbf{v} + \mathbf{a}(\mathbf{r}, t)dt)$ did not start near (\mathbf{r}, \mathbf{v}) . Let the number of ions lost due to collisions with atoms of neutral species j be represented by $\Gamma_j^{(-)}d\mathbf{r}d\mathbf{v}dt$ and the number gained be represented by $\Gamma_j^{(+)}d\mathbf{r}d\mathbf{v}dt$. When (4.2) is modified to take into account the effects of collisions, it becomes

$$f(\mathbf{r} + \mathbf{v}dt, \mathbf{v} + \mathbf{a}(\mathbf{r}, t)dt, t + dt)d\mathbf{r}d\mathbf{v}dt = f(\mathbf{r}, \mathbf{v}, t)d\mathbf{r}d\mathbf{v}dt + \sum_{j} \left(\Gamma_{j}^{(+)} - \Gamma_{j}^{(-)}\right)d\mathbf{r}d\mathbf{v}dt.$$
(4.3)

The term on the left-hand side of (4.3) may be expanded in a Taylor series (see Appendix A). If we truncate the expansion after the linear gradients in time, position, and velocity, we obtain the formal form of the Boltzmann equation,

$$\left[\frac{\partial}{\partial t} + \mathbf{v} \cdot \nabla + \mathbf{a}(\mathbf{r}, t) \cdot \nabla_{\mathbf{v}}\right] f(\mathbf{r}, \mathbf{v}, t) = \sum_{j} \left(\Gamma_{j}^{(+)} - \Gamma_{j}^{(-)}\right), \tag{4.4}$$

where ∇ is the spatial gradient operator and ∇_v is the gradient operator in velocity space. It should be mentioned that the right-hand side does not include contributions

4.1 General Form 119

resulting from collisions of the ions with the walls, nor does it include an external source or sink of ions; these contributions are taken into account in the initial and boundary conditions that have to be imposed when solving the Boltzmann equation.

4.2 The Nonreactive Collision Term

The formal Boltzmann equation is useless unless we have explicit expressions for the Γ quantities. To develop such expressions, we consider the classical-mechanical description of a collision between an atomic ion with laboratory velocity \mathbf{v} and an atom of species j with laboratory velocity \mathbf{v}_j . We assume that the intermolecular force is negligible for separations greater than some value, r_A , that is small compared to the mean free path of the ions in the apparatus. The question then is how many neutral atoms with relative velocity

$$\mathbf{g}_i = \mathbf{v} - \mathbf{v}_i \tag{4.5}$$

start at a separation larger than r_A but come closer than r_A to the ion in a small time interval dt.

During dt, any atom that is initially a distance r_A away from the ion will come close enough to be said to have collided (or to have begun a collision) if it lies within a small cylindrical shell of height g_jdt and area $2\pi bdb$. Here, b is the impact parameter, the smallest distance between the colliding particles that would have occurred had there been no interaction forces at work on them. The factor of 2π arises because of the rotational symmetry, i.e., the collisions are the same at any angle, $\overline{\epsilon}$, so long as the impact parameter is the same; from here on, we will replace 2π by $d\overline{\epsilon}$ when only a small angle is meant.

The probable number of atoms in that part of the cylindrical shell corresponding to $d\bar{\epsilon}$ is

$$f_j(\mathbf{r}, \mathbf{v}_j, t)g_jbdbd\bar{\epsilon}dt, \tag{4.6}$$

where $f_j(\mathbf{r}, \mathbf{v}_j, t)$ is the distribution function at \mathbf{r} and t for neutral atoms of species j with velocity \mathbf{v}_j . The total number of collisions experienced by the ion is obtained by adding together the number of collisions characterized by all values of b, $\bar{\epsilon}$ and g_j . Since \mathbf{g}_j is directly proportional to \mathbf{v}_j , the result is

$$dt \iiint f_j(\mathbf{r}, \mathbf{v}_j, t) g_j b db d\overline{\epsilon} d\mathbf{v}_j. \tag{4.7}$$

Now the probable number of ions in the volume element $d\mathbf{r}$ about \mathbf{r} with velocities in the range $d\mathbf{v}$ about \mathbf{v} is $f(\mathbf{r}, \mathbf{v}, t)d\mathbf{r}d\mathbf{v}$. It follows therefore from (4.7) that

$$\Gamma_{j}^{(-)}d\mathbf{r}d\mathbf{v}dt = f(\mathbf{r}, \mathbf{v}, t)d\mathbf{r}d\mathbf{v}dt \iiint f_{j}(\mathbf{r}, \mathbf{v}_{j}, t)g_{j}bdbd\overline{\epsilon}d\mathbf{v}_{j}, \tag{4.8}$$

so

$$\Gamma_{j}^{(-)} = \iiint f(\mathbf{r}, \mathbf{v}, t) f_{j}(\mathbf{r}, \mathbf{v}_{j}, t) g_{j} b db d\overline{\epsilon} d\mathbf{v}_{j}. \tag{4.9}$$

The expression for $\Gamma_j^{(+)}$ is obtained by similar arguments, expressed in terms of what happens after rather than before the collision. After making use of conservation of linear momentum and kinetic energy to equate the differential involving the post-collision quantities to the one involving the pre-collision quantities, the result is that

$$\Gamma_j^{(+)} = \iiint f(\mathbf{r}, \mathbf{v}', t) f_j(\mathbf{r}, \mathbf{v}'_j, t) g_j b db d\bar{\epsilon} d\mathbf{v}_j, \tag{4.10}$$

where \mathbf{v}' and \mathbf{v}'_j are the post-collision velocities of the ion and neutral, respectively. The post-collision velocities are related to the pre-collision velocities and the impact parameter by the laws of classical mechanics and the interaction potential energy function; more will be said about this later.

Combining (4.4), (4.9), and (4.10) gives the classical-mechanical Boltzmann equation

$$\left[\frac{\partial}{\partial t} + \mathbf{v} \cdot \nabla + \mathbf{a}(\mathbf{r}, t) \cdot \nabla_{\mathbf{v}}\right] f(\mathbf{r}, \mathbf{v}, t) = \sum_{j} \mathfrak{J}_{j} f(\mathbf{r}, \mathbf{v}, t), \tag{4.11}$$

where

$$\mathfrak{J}_{j}f(\mathbf{r},\mathbf{v},t) = \iiint \left[f(\mathbf{r},\mathbf{v}',t)f_{j}(\mathbf{r},\mathbf{v}'_{j},t) - f(\mathbf{r},\mathbf{v},t)f_{j}(\mathbf{r},\mathbf{v}_{j},t) \right] g_{j}bdbd\epsilon d\mathbf{v}_{j}.$$
(4.12)

The left-hand side of (4.11) describes how the ion distribution function changes during its streaming (collisionless) motion through phase space. The collision operators on the right-hand side describe how it changes due to collisions that are local in position (compared to the size of the apparatus) and that occur instantaneously (compared to the time between collisions). It should be noted also that each \mathfrak{J}_j is a scalar operator (does not change the angles of any vector or tensor quantities upon which it acts) and is linear because the ions are present in such small amounts that ion—ion interactions and space-charge effects can be ignored. It is the linear nature of \mathfrak{J}_j that makes the present study of gaseous ion transport in weakly ionized plasmas so different from other studies of plasmas (Colonna 2016).

4.3 Reactive Collision Terms

In most of this book, ion–neutral reactions are assumed to be infrequent, so the difference between bulk and flux transport coefficients (Robson et al. 2018) is assumed to be negligible. The chemical reactions of interest in this book may be assumed to be irreversible, since the product ion and product neutral are immersed in such

large amounts of other ions and neutrals that the chances of them encountering one another and back-reacting are negligible. Moreover, these chemical reactions are what chemists call second order, i.e., the reaction rate is proportional to the first power of the ion number density and the first power of the neutral number density. The proportionality constant is the reaction rate coefficient.

The assumptions just given mean that reactive collision terms in the Boltzmann collision operator can be ignored except in those few cases where the nonreactive collision terms vanish. This in turn means (Viehland and Mason 1977) that (4.11) can be generalized to the form

$$\left[\frac{\partial}{\partial t} + \mathbf{v} \cdot \nabla + \mathbf{a}(\mathbf{r}, t) \cdot \nabla_{\mathbf{v}}\right] f(\mathbf{r}, \mathbf{v}, t) = \left[\sum_{j} n_{j} \mathfrak{J}_{j} - \sum_{k} n_{k} \mathfrak{J}_{k}\right] f(\mathbf{r}, \mathbf{v}, t),$$
(4.13)

where the new sum is over the neutral species, R, with which the ion can react.

The negative sign in (4.13) in front of the reactive collision operator,

$$\mathfrak{J}_R = \int f_R(\mathbf{r}, \mathbf{v}_R, t) Q_R^*(\varepsilon_R) |\mathbf{v} - \mathbf{v}_R| d\mathbf{v}_R, \tag{4.14}$$

indicates that ion–neutral reactions remove ions from the swarm but that no reactions produce ions. The signs in (4.12) indicate that \mathfrak{J}_j represents the difference between ion–neutral collisions that scatter ions into the region of interest in phase space and those that scatter them out, so the signs are consistent with the fact that the streaming terms on the left of (4.13) are positive when $f(\mathbf{r}, \mathbf{v}, t)$ increases.

Note that the distribution functions for each of the reactive and nonreactive neutral gases, $f_R(\mathbf{r}, \mathbf{v}_R, t)$ and $f_j(\mathbf{r}, \mathbf{v}_j, t)$, respectively, is normalized to one, which is why (4.13) explicitly incorporates the number densities, n_R and n_j . Finally, $Q_R^*(\varepsilon_R)$ is assumed to known (from ab initio calculations, for example) as a function of the relative kinetic energy,

$$\varepsilon_R = \frac{1}{2}\mu_R |\mathbf{v} - \mathbf{v}_R|^2. \tag{4.15}$$

4.4 Equilibrium Velocity Distribution Function

By definition, the streaming terms in the Boltzmann equation are zero at equilibrium, the ions and neutrals must have the same temperature, T_0 , and there can be no chemical reactions. Thus at equilibrium, (4.12) and (4.13) reduce to

$$0 = \iiint \left[f(\mathbf{r}, \mathbf{v}', t) f_j(\mathbf{r}, \mathbf{v}'_j, t) - f(\mathbf{r}, \mathbf{v}, t) f_j(\mathbf{r}, \mathbf{v}_j, t) \right] g_j b db d\epsilon d\mathbf{v}_j.$$
(4.16)

It is easy to verify that the solution of this equation is that both the ions and neutrals have a Maxwellian vdf. Thus, if we insert

$$f(\mathbf{r}, \mathbf{v}, t) = \left(\frac{m}{2\pi k_B T_o}\right)^{3/2} \exp\left(-\frac{mv^2}{2k_B T_o}\right) n(\mathbf{r}, t)$$
(4.17)

and

$$f_j(\mathbf{r}, \mathbf{v}_j, t) = \left(\frac{m_j}{2\pi k_B T_o}\right)^{3/2} \exp\left(-\frac{m_j v_j^2}{2k_B T_o}\right) n_j(\mathbf{r}, t)$$
(4.18)

into (4.16), we get

$$\iiint \left[\exp\left(-\frac{mv^{2}}{2k_{B}T_{o}} - \frac{m_{j}v_{j}^{2}}{2k_{B}T_{o}}\right) - \exp\left(-\frac{mv^{2}}{2k_{B}T_{o}} - \frac{m_{j}v_{j}^{2}}{2k_{B}T_{o}}\right) \right] g_{j}bdbd\epsilon d\mathbf{v}_{j}. \tag{4.19}$$

The quantity in square brackets vanishes because conservation of energy for atomic ions and neutrals guarantees that

$$\frac{1}{2}mv^2 + \frac{1}{2}mv_j^2 = \frac{1}{2}mv^2 + \frac{1}{2}mv_j^2; \tag{4.20}$$

this is sometimes said to indicate that energy, like number density and linear momentum, is a collisional invariant.

It is shown in most undergraduate courses in modern physics and physical chemistry that the Maxwellian vdf can be derived from equilibrium statistical mechanics. This gives us some degree of confidence in the validity of the Boltzmann equation, confidence that is greatly strengthened by the good agreement between measured transport properties for nonequilibrium gases and values calculated by methods such as those described in Chap. 6. Our task in the rest of this chapter is to describe solutions of the Boltzmann equation in the nonequilibrium situations present in drift-tube measurements.

4.5 Properties of an Ion Ensemble

After solving (4.13) for $f(\mathbf{r}, \mathbf{v}, t)$, the properties of an ensemble of ions can be determined. The properties discussed later in this book are listed below, where the theoretical quantities indicated by the decorations are implicitly dependent upon \mathbf{r} and t.

1. The ion flux vector, $\hat{\mathbf{j}}$, and the drift velocity vector, $\hat{\mathbf{v}}_d$, in the laboratory frame are given by the equation

$$\widehat{\mathbf{j}} = n(\mathbf{r}, t)\widehat{\mathbf{v}}_{\mathbf{d}} = \int f(\mathbf{r}, \mathbf{v}, t)\mathbf{v}d\mathbf{v}.$$
 (4.21)

2. The drift velocity in the frame of reference of the ion swarm must be zero, because

$$\int f(\mathbf{r}, \mathbf{v}, t) (\mathbf{v} - \widehat{\mathbf{v}}_{\mathbf{d}}) d\mathbf{v} = \int f(\mathbf{r}, \mathbf{v}, t) \mathbf{v} d\mathbf{v} - \widehat{\mathbf{v}}_{\mathbf{d}} \int f(\mathbf{r}, \mathbf{v}, t) d\mathbf{v}$$

$$= n(\mathbf{r}, t) \widehat{\mathbf{v}}_{\mathbf{d}} - \widehat{\mathbf{v}}_{\mathbf{d}} n(\mathbf{r}, t) = 0. \tag{4.22}$$

3. The average ion kinetic energy in the laboratory frame is

$$\widehat{E}_k = \int f(\mathbf{r}, \mathbf{v}, t) \left(\frac{1}{2} m v^2\right) d\mathbf{v}.$$
 (4.23)

4. The average ion kinetic energy in the frame of the ion swarm is

$$\widehat{E}_{ion} = \int f(\mathbf{r}, \mathbf{v}, t) \left[\frac{1}{2} m \left(\mathbf{v} - \widehat{\mathbf{v}}_{\mathbf{d}} \right)^{2} \right] d\mathbf{v} = \widehat{E}_{k} - \frac{1}{2} m \widehat{\mathbf{v}}_{\mathbf{d}}^{2}.$$
(4.24)

5. The ion temperature in the laboratory frame is a tensor of order two given by the equation

$$\frac{k_B}{m}\widehat{\mathbf{T}}(\mathbf{r},t) = \int f(\mathbf{r},\mathbf{v},t)\mathbf{v}\mathbf{v}d\mathbf{v}.$$
 (4.25)

6. The ion temperature tensor in the swarm frame is

$$\frac{k_B}{m}\widehat{\mathbf{T}}_{ion}(\mathbf{r},t) = \int f(\mathbf{r},\mathbf{v},t) \left(\mathbf{v} - \widehat{\mathbf{v}}_{\mathbf{d}}\right) \left(\mathbf{v} - \widehat{\mathbf{v}}_{d}\right) d\mathbf{v} = \frac{k_B}{m}\widehat{\mathbf{T}} - \widehat{\mathbf{v}}_{\mathbf{d}}\widehat{\mathbf{v}}_{\mathbf{d}}.$$
 (4.26)

7. The heat flux vector in the laboratory frame is

$$\widehat{\mathbf{Q}}_{H} = \int f(\mathbf{r}, \mathbf{v}, t) \left(\frac{1}{2} m v^{2}\right) \mathbf{v} d\mathbf{v}.$$
 (4.27)

8. The heat flux vector in the swarm frame is

$$\widehat{\mathbf{Q}}_{ion}(\mathbf{r},t) = \int f(\mathbf{r},\mathbf{v},t) \left[\frac{1}{2} m \left(\mathbf{v} - \widehat{\mathbf{v}}_{\mathbf{d}} \right)^{2} \right] \left(\mathbf{v} - \widehat{\mathbf{v}}_{\mathbf{d}} \right) d\mathbf{v}$$

$$= \widehat{\mathbf{Q}}_{H} - k_{B} \widehat{\mathbf{T}} \cdot \widehat{\mathbf{v}}_{\mathbf{d}} - \left[\widehat{E}_{k} - m \widehat{v}_{d}^{2} \right] \widehat{\mathbf{v}}_{\mathbf{d}}(\mathbf{r},t). \tag{4.28}$$

9. The energy dyadic in the laboratory frame is a tensor of rank two that has Cartesian components given by

$$(\widehat{\mathbf{E}}\widehat{\mathbf{E}})_{i,j} = \int f(\mathbf{r}, \mathbf{v}, t) \left(\frac{1}{2}mv_i^2\right) \left(\frac{1}{2}mv_j^2\right) d\mathbf{v}.$$
 (4.29)

For future reference, note that the theoretical quantities in (4.21)–(4.29) are not necessarily the same as the quantities measured experimentally and described in Chap. 1. As an example, (4.21) defines the drift velocity without consideration of the effects of ion density gradients, while those gradients are essential in using one of the

various forms of the diffusion equation, each with its own build-in assumptions, to extract both the drift velocity and diffusion coefficients from experiment data. Such problems arise because experimental quantities rely for their definition on some theory of the instrument, i.e., one or more equations relating the quantities that are being measured (the raw data) with the more basic quantities that can presumably be calculated theoretically. It is the responsibility of experimenters to clearly indicate how their reported results were extracted from the raw data, and it is the responsibility of theorists to include the same set of assumptions in their calculations of the experimental quantities from microscopic properties of the ion motion in gases.

4.6 Quantum-Mechanical Effects

It is outside the scope of this book to give the details of how quantum-mechanical effects should be incorporated into the Boltzmann equation for atomic systems. It suffices to note that the translational degrees of freedom can be treated classically and that the only difference is that the nonreactive collision operator has the form

$$\mathfrak{J}_{j}f(\mathbf{r},\mathbf{v},t) = \iiint \left[f(\mathbf{r},\mathbf{v}',t)f_{j}(\mathbf{r},\mathbf{v}'_{j},t) - f(\mathbf{r},\mathbf{v},t)f_{j}(\mathbf{r},\mathbf{v}_{j},t) \right] \times g_{j}\sigma_{j}(\theta,g_{j})\sin(\theta)d\theta d\varphi d\mathbf{v}_{j}.$$
(4.30)

Here, $\sigma_j(\theta,g_j)$ is the quantum-mechanical, differential scattering cross section. The collision causes scattering through a polar scattering angle, θ , and an azimuthal scattering angle, φ , but $\sigma_j(\theta,g_j)$ is independent of φ . This means that the correspondence between the quantum and classical kinetic theories for atomic ions and electrons moving through atomic gases is that (Robson 2006)

$$\sigma_i(\theta, g_i) \sin(\theta) d\theta = b db.$$
 (4.31)

Hereafter, we shall use (4.30) to represent the collision operator in the classical and quantum-mechanical Boltzmann equations, relying on (4.31) to make the conversion when classical calculations are in order. When quantum calculations are necessary, the differential scattering cross section must be calculated from phase shifts in the wave function; this will be described at the appropriate place in Chap. 6.

4.7 The Maxwell Model

The special case that most easily allows the Boltzmann equation to be solved was introduced by Maxwell in 1867, i.e., before the Boltzmann equation was given. In terms of the quantities introduced above, Maxwell assumed that $n_i g_i \sigma_i(\theta, g_i)$

4.7 The Maxwell Model 125

was constant. Since this quantity has the dimensions of an inverse time, the Maxwell model is also referred to as the model of constant collision frequency. It is now known (Mason and McDaniel 1988) that the Maxwell model corresponds to collisions that are governed by an ion-induced dipole interaction potential that varies as the inverse fourth power of the separation between the colliding particles, with a small rigid core to keep the attractive forces from pulling the colliding particles together even at very small distances.

The eigenfunctions and eigenvalues of \mathfrak{J} are known (Ferrari 1978) for the Maxwell model. For a single-component neutral gas, the most important eigenfunction is the ion velocity, i.e.,

$$\mathfrak{J}\mathbf{v} = \xi\mathbf{v},\tag{4.32}$$

whose constant eigenvalue,

$$\xi = n_0 g \overline{Q}^{(1)}, \tag{4.33}$$

is called the effective collision frequency for momentum transfer in the Maxwell model.

For the Maxwell model, the classical-mechanical expression for $\overline{Q}^{(1)}$ given by (1.22) is exact and independent of kinetic energy. It leads (Viehland and Goeringer 2005) to the result that

$$\xi = \left(6.96467 \times 10^{10} \text{ Hz}\right) \left(\frac{\widehat{P}_0}{760}\right) \left(\frac{273.15}{\widehat{T}_0}\right) \frac{m_1}{m_0 + m_1} \left(\frac{\widehat{\alpha}_0}{\widehat{\mu}_0}\right)^{1/2}, \tag{4.34}$$

where \widehat{P}_0 is the gas pressure in Torr, \widehat{T}_0 is the gas temperature in K, $\widehat{\mu}$ is the reduced mass in Dalton (g/mole), and $\widehat{\alpha}_0$ is the dipole polarizability of the neutral atom in cubic Angstrom. Note that the eigenvalue is not affected by the external fields, so neither will any of the transport properties of the ions; these conclusions are valid only for the Maxwell model.

4.8 Rate Equation of Continuity

If we integrate the Boltzmann equation (4.13) over all velocities, the right-hand side vanishes because mass is a collisional invariant of the Boltzmann collision operator, which is equivalent to saying that it vanishes due to conservation of mass in the absence of chemical reaction (see the general assumptions in Chap. 1). The term involving the acceleration vanishes after integrating by parts. The remaining terms constitute the rate equation of continuity:

$$\frac{\partial}{\partial t}n(\mathbf{r},t) + \nabla \cdot n(\mathbf{r},t)\mathbf{v_d}(\mathbf{r},t) = -n(\mathbf{r},t)\sum_{R}n_Rk_R(\mathbf{r},t). \tag{4.35}$$

Here the rate coefficient for the reactions between the ions and reactive neutrals of type R is

$$k_R(\mathbf{r},t) = \iint f(\mathbf{r},\mathbf{v},t) f_R(\mathbf{r},\mathbf{v}_R,t) Q_R^*(\varepsilon_R) |\mathbf{v} - \mathbf{v}_R| d\mathbf{v}_R d\mathbf{v}.$$
(4.36)

It is important to note that $f(\mathbf{r}, \mathbf{v}, t)$ appears in (4.36), so a solution of (4.13) is still needed. Note also that the various number densities are explicitly indicated in (4.35) and hence should be omitted from the distribution functions used in (4.36); in other words, the distribution functions are now normalized to one, not the number densities.

References

- C. Cercignani, The Boltzmann Equation and Its Applications, vol. 67, Applied Mathematical Sciences (Springer, New York, 1988)
- G. Colonna, Boltzmann and Vlasov equations in plasma physics, in *Plasma Modeling Methods and Applications*, ed. by G. Colanna, A. D'Angola (IOP Publishing, Bristol, 2016)
- L. Ferrari, Phys. A **93**, 531 (1978)
- J.O. Hirschfelder, C.F. Curtiss, R.B. Bird, Molecular Theory of Gases and Liquids (Wiley, New York, 1964)
- E.A. Mason, E.W. McDaniel, The Transport Properties of Ions in Gases (Wiley, New York, 1988)
- R.E. Robson, *Introductory Transport Theory for Charged Particles in Gases* (World Scientific, Singapore, 2006)
- R.E. Robson, R. White, M. Hildebrandt, Fundamentals of Charged Particle Transport in Gases and Condensed Matter (CRC Press, Boca Raton, 2018)
- L.A. Viehland, D.E. Goeringer, J. Phys. B 38, 3987 (2005)
- L.A. Viehland, E.A. Mason, J. Chem. Phys. 66, 422 (1977)

Chapter 5 Moment Methods for Solving the Boltzmann Equation



5.1 Introduction

In swarm studies, one generally is less interested in $f(\mathbf{r}, \mathbf{v}, t)$ than in its moments, i.e., integrals of particular functions of \mathbf{v} multiplied by the ion vdf, $f(\mathbf{v})$. In this case, one is better off converting the Boltzmann equation to an equation governing the moments themselves and then solving the resulting moment equations. We shall do this in the rest of this chapter, after first reviewing moment methods that have been suggested previously.

Whealton (1975) used moment equations obtained from the Boltzmann equation to consider the problem of a weakly ionized gas in a uniform electrostatic field. No restrictions were placed on the smoothness of the initial data or on the ion–neutral mass ratio, and an expansion in terms of density gradients was not made. In principle, this means that Whealton's work should contain a complete solution for moments when the electrostatic field is constant. Unfortunately, the basis functions he used to form moments of the ion vdf involved the gas temperature, even though the ions are present in trace amounts in a weakly ionized gas and hence can have, at large E/n_0 , an average kinetic energy considerably greater than the thermal energy of the neutral molecules. The radius of convergence (see Appendix A) of such one-temperature approaches is limited to small E/n_0 (Milloy et al. 1974).

It is tempting to think that the work of Whealton (1975) could be modified by including an ion temperature so as to provide a general, two-temperature solution to the moment equations. However, Berge and Skullerud (1976) pointed out that it is not appropriate when truncating the infinite sums that arise in Whealton's approach to replace the highest order, time-dependent moments that are retained by their steady-state values, because the highest moments are those which have the largest effect on the high-energy tail of the ion vdf. Whealton (1976) himself pointed out that replacing the highest moments by their steady-state values mean that the moments are no longer independent of the time origin. This approach to moment methods came to an abrupt end.

The two-temperature kinetic theory of gaseous ion transport (Viehland and Mason 1975, 1978) discussed in Sect. 1.16 is a moment method that uses an ion temperature in the basis functions rather than the gas temperature. This greatly increases the radius of convergence, allowing the mobility in a swarm experiment to be calculated accurately at high E/n_0 from knowledge of the ion–neutral interaction potential. Subsequent improvements were the three-temperature and biMaxwellian approaches discussed in Sects. 1.17–1.18.

Skullerud (1984) showed that eventually the expansions used in the one-, two-, and three-temperature moment methods will fail because the basis functions are orthogonal with respect to a Gaussian weighting function and the tail of the true ion vdf must fall off more slowly than any Gaussian. A decade later, Skullerud's objections became moot when the Gram-Charlier method was introduced (Viehland 1994). This approach was described briefly in Sect. 1.18 and will be discussed in detail later in this chapter. A noteworthy point is that when mathematical arguments prove that something cannot be done in the ways currently in use, this does not rule out the possibility of finding a slightly different approach that is not subject to the assumptions made in the mathematics.

5.2 General Moment Equations

Based on the arguments given in Chap. 4, the Boltzmann equation for a system composed of trace amounts of atomic ions (with charge q and mass m) moving through a dilute gas that is composed of large amounts of nonreactive, atomic gases labeled by j subscripts and small amounts of a variety of reactive gases labeled by R is

$$\left[\frac{\partial}{\partial t} + \mathbf{v} \cdot \nabla + \mathbf{a}(\mathbf{r}, t) \cdot \nabla_{\mathbf{v}}\right] f(\mathbf{r}, \mathbf{v}, t)$$

$$= \left[\sum_{j} n_{j} \mathfrak{J}_{j} - \sum_{R} n_{R} \mathfrak{J}_{R}\right] f(\mathbf{r}, \mathbf{v}, t). \quad (5.1)$$

Here, the unknown is the ion distribution function, $f(\mathbf{r}, \mathbf{v}, t)$, and the acceleration vector is

$$\mathbf{a}(\mathbf{r},t) = \frac{q}{m} \left(\mathbf{E} + \mathbf{v} \times \mathbf{B} \right), \tag{5.2}$$

where **E** and **B** are the external electric and magnetic fields that are (implicitly) known functions of **r** and *t*. The gradient operators in time, position, and velocity are $\frac{\partial}{\partial t}$, ∇ , and $\nabla_{\mathbf{v}}$, respectively, while \cdot and \times represent dot and cross products (see Appendix A) of the two vectors that they connect. Note that, the number densities in the experiment are assumed to be such that

$$n_0 = \sum_j n_j \tag{5.3}$$

is the total number density of the neutral gas and that, for any R and j,

$$n(\mathbf{r}, t) << n_R << n_i \le n_0.$$
 (5.4)

The number densities of the reactive and nonreactive neutral gases are assumed to be independent of \mathbf{r} and t.

Some attention needs to be given to the neutral vdf that are implicit in the collision operators, \mathfrak{J}_j and \mathfrak{J}_R . Because the number densities have been explicitly written in (5.1) and because they satisfy (5.4), the distribution function for the atomic buffer gases must have the equilibrium, Maxwellian form (Chapman and Cowling 1970; Mason and McDaniel 1988; Cercignani 1988),

$$f_j(\mathbf{v}_j) = \left(\frac{m_j}{2\pi k_B T_0}\right)^{3/2} \exp\left(-\frac{m_j v_j^2}{2k_B T_0}\right),$$
 (5.5)

where m_j and \mathbf{v}_j are the mass and velocity of species j, k_B is Boltzmann's constant, and T_0 is the common temperature of all of the neutral gases. A similar Maxwellian form applies to the reactive gas if it is atomic, although we will allow for the possibility that the reactive neutrals are molecular and hence have a Maxwell–Boltzmann distribution (Mason and McDaniel 1988),

$$f_R^{(\beta)}(\mathbf{v}_j) = \frac{1}{Z_R} \left(\frac{m_R}{2\pi k_B T_0} \right)^{3/2} \exp\left(-\frac{m_R v_R^2}{2k_B T_0} - \frac{\varepsilon_R^{(\beta)}}{k_B T_0} \right), \tag{5.6}$$

when they are in internal state β with energy $\varepsilon_R^{(\beta)}$. Here, the internal partition function for neutral species R is

$$Z_R = \sum_{\beta} \exp\left(-\frac{\varepsilon_R^{(\beta)}}{k_B T_0}\right). \tag{5.7}$$

Note that, the notation in (5.5) and (5.6) indicates that the neutral distribution functions are independent of time or position in the apparatus, i.e., they are vdf.

If we multiply (5.1) from the left by any function, $\psi(\mathbf{v})$, of the ion velocity alone, and then integrate over all \mathbf{v} , we get five terms that can be expressed in terms of moments of $f(\mathbf{r}, \mathbf{v}, t)$ defined by the relation,

$$\langle \psi(\mathbf{v}) \rangle = \frac{1}{n(\mathbf{r}, t)} \int f(\mathbf{r}, \mathbf{v}, t) \psi(\mathbf{v}) d\mathbf{v}.$$
 (5.8)

Here, the dependence of the moments upon \mathbf{r} and t has been left implicit. This notation reflects (but is not limited to) the most common situation, where the other moments of

 $f(\mathbf{r}, \mathbf{v}, t)$ vary much less rapidly with position and time than does $n(\mathbf{r}, t)$. Because we have introduced $n(\mathbf{r}, t)$ into (5.8), the ion number density will be indicated explicitly in the rest of the equations in this chapter, just as n_R and n_i are.

The first and second terms obtained from (5.1) are easy to write in terms of (5.8) because the time derivative and spatial gradient are independent of velocity and can be taken out of the integrals. The third term can be written in terms of moments after integration by parts (see Appendix A). The fourth term can also be written this way by introducing the adjoint (see Appendix A) of the Boltzmann collision operator (Kumar et al. 1980). However, it is simpler for atomic ions and atomic buffer gases to make use of the fact (Chapman and Cowling 1970; Viehland and Mason 1975) that inverse collisions exist for atomic systems, i.e., those without internal degrees of freedom. Thus,

$$\int \psi(\mathbf{v}) \mathfrak{J}_j f(\mathbf{r}, \mathbf{v}, t) d\mathbf{v} \equiv -\left\langle \mathfrak{J}_j \psi(\mathbf{v}) \right\rangle = -\int f(\mathbf{r}, \mathbf{v}, t) f_j(\mathbf{v}_j) \\
\times \left[\psi(\mathbf{v}) - \psi(\mathbf{v}') \right] g\sigma \left(g, \theta_c \right) \sin \left(\theta_c \right) d\theta_c d\phi_c d\mathbf{v}_j d\mathbf{v}, \quad (5.9)$$

where g is the relative speed, $|\mathbf{v} - \mathbf{v}_j|$, and where the negative sign reflects a preference for having the difference in the integrand be between the pre-collision value and the post-collision value, rather than the reverse. The final term can be written in terms of moments because \mathfrak{J}_R is self-adjoint; thus

$$\int \psi(\mathbf{v}) \mathfrak{J}_R f(\mathbf{r}, \mathbf{v}, t) d\mathbf{v} \equiv \langle \mathfrak{J}_R \psi(\mathbf{v}) \rangle$$

$$= \sum_{\beta} \int f(\mathbf{r}, \mathbf{v}, t) f_R^{(\beta)}(\mathbf{v}_j) \psi(\mathbf{v}) Q_R^*(\varepsilon_R) |\mathbf{v} - \mathbf{v}_R| d\mathbf{v}_R d\mathbf{v}.$$
 (5.10)

The dependence of the integral cross section, $Q_R^*(\varepsilon_R)$, for ion reaction with a molecule of species R is explicitly indicated as a function of the relative kinetic energy, ε_R , but its dependence (if any) upon the internal state of the reactive neutral is left implicit.

Putting all of the pieces together gives the general equation for any moment,

$$\frac{\partial}{\partial t} n(\mathbf{r}, t) \langle \psi(\mathbf{v}) \rangle + \nabla \cdot n(\mathbf{r}, t) \langle \psi(\mathbf{v}) \mathbf{v} \rangle - n(\mathbf{r}, t) \langle \mathbf{a} \cdot \nabla_v \psi(\mathbf{v}) \rangle
= -n(\mathbf{r}, t) \sum_j n_j \langle \mathfrak{J}_j \psi(\mathbf{v}) \rangle - n(\mathbf{r}, t) \sum_R n_R \langle \mathfrak{J}_R \psi(\mathbf{v}) \rangle.$$
(5.11)

This equation is equivalent to the equation of change of Maxwell (1867), which is an alternative approach to the Boltzmann equation for the description of the transport properties of gases. In the absence of reactions, it is identical to the equation obtained by Kihara (1953), although his derivation required that the collision operator be symmetric and positive definite. A derivation starting from the Boltzmann equation

that does not include this requirement was given by Viehland and Mason (1975) using essentially the procedure used here.

If we set ψ (**v**) = 1, (5.11) simplifies greatly, because a constant is one of the so-called collision invariants (Chapman and Cowling 1970), i.e., $\langle \mathfrak{J}_j 1 \rangle = 0$ because of conservation of mass for nonreactive collisions (Cercignani 1988). Hence, we get the rate equation of continuity that was derived more generally in Sect. 4.8:

$$\frac{\partial}{\partial t}n(\mathbf{r},t) + \nabla \cdot n(\mathbf{r},t) \langle \mathbf{v} \rangle = -n(\mathbf{r},t) \sum_{R} n_{R} k_{R}(\mathbf{r},t), \qquad (5.12)$$

where

$$k_R(\mathbf{r},t) = \langle \mathfrak{J}_R 1 \rangle \tag{5.13}$$

is the two-body (or second order) rate coefficient for ion reactions with molecules of neutral species R. Note that, the reactive terms differ from the expression in Chap. 1 because we have put $n(\mathbf{r}, t)$ into (5.8).

Before the rate equation of continuity can be solved for $n(\mathbf{r}, t)$, it is necessary to know the dependence of $\langle \mathbf{v} \rangle$ and the $k_R(\mathbf{r}, t)$ upon space and time. Note also that (5.12) does not contain an ion source term, which according to the assumptions in the Boltzmann equation must be added empirically, along with boundary conditions. To avoid these difficulties, we use (5.12) to eliminate the time derivative of the ion number density from (5.11). After minor rearrangement, we get

$$\frac{\partial}{\partial t} \langle \psi (\mathbf{v}) \rangle - \langle \mathbf{a} \cdot \nabla_v \psi (\mathbf{v}) \rangle + \sum_j n_j \langle \mathfrak{J}_j \psi (\mathbf{v}) \rangle = \mathfrak{F}(\psi (\mathbf{v})), \tag{5.14}$$

where we have introduced the functional operator,

$$\mathfrak{F}(\psi(\mathbf{v})) = [\langle \psi(\mathbf{v}) \rangle \langle \mathbf{v} \rangle - \langle \psi(\mathbf{v}) \mathbf{v} \rangle] \cdot \nabla \ln n(\mathbf{r}, t) + [\langle \psi(\mathbf{v}) \rangle \nabla \cdot \langle \mathbf{v} \rangle - \nabla \cdot \langle \psi(\mathbf{v}) \mathbf{v} \rangle] + \langle \psi(\mathbf{v}) \rangle \sum_{R} n_{R} k_{R}(\mathbf{r}, t) - \sum_{R} n_{R} \langle \mathfrak{J}_{R} \psi(\mathbf{v}) \rangle.$$
(5.15)

It should be noted that (5.14) is exact for atomic systems, which means that it has the same level of mathematical rigor as the Boltzmann equation from which it was derived. It also shares the general disadvantage of any moment method: the equation for a simple moment involves moments of more complicated functions, so the hierarchy must somehow be truncated before it can be put to practical use. This was the stumbling block for the solution methods discussed in Sect. 5.1. What we will do here is use the successive approximation scheme of Viehland and Siems (2012) and Viehland (2015), generalized to the case of gas mixtures. We will find that this scheme is equivalent to a method of weighted residuals discussed in Appendix C and used for decades to study gaseous ion transport.

5.3 Successive Approximations

The first term in $\mathfrak{F}(\psi(\mathbf{v}))$ involves $\nabla \ln n(\mathbf{r},t)$, which is the ratio of the gradient of the ion number density to $n(\mathbf{r},t)$ itself. Not only is this ratio small in most situations, in swarm experiments, it is many times smaller yet when compared with n_0 . This term also involves another small quantity, the difference between the product of two average quantities and the average of their product. Hence, we will ignore this term in the first of our series of successive approximation. This has one important consequence: the ion diffusion coefficients will not be treated until the second approximation is considered.

The second term in $\mathfrak{F}(\psi(\mathbf{v}))$ is ordinarily neglected in analyzing swarm data, i.e., spatial gradients are ignored in the theory of the instrument being used, except for $\nabla \ln n(\mathbf{r},t)$. Alternately, this second term is approximated following careful consideration (Robson 2006) of the heat flux vector, the temperature tensor and the like. We will neglect this term in the first approximation and treat it in subsequent steps in the hierarchy of systematic approximations.

The other terms on the right-hand side of (5.15) incorporate the effects upon the transport properties of chemical reactions that lead to nonconservation of ions. Neglection of these terms is justified when such reactions are slow enough that $k_R(\mathbf{r}, t)$ and $\langle \mathfrak{J}_R \psi(\mathbf{v}) \rangle$ are small compared with the nonreactive terms in (5.14). Although it is possible to treat situations with fast reactions (Robson 2006), we will assume that these terms can be neglected in the first approximation.

We note before proceeding that there is no requirement that each of the three types of terms in $\mathfrak{F}(\psi(\mathbf{v}))$ have the same degree of "smallness". It is therefore possible to specialize the final equations obtained in second approximation by retaining any or all of these terms, with similar procedures being allowed in the higher approximations (Viehland 2015) that are not considered here. Finally, we have not yet specified how to treat, in the successive approximations, the nonreactive collision terms on the left-hand side of (5.14).

5.4 Basis Functions in General

Since the Boltzmann equation of interest here is linear, the method of weighted residuals discussed in Appendix C can be used to solve it. In this method, it is assumed that the ion distribution function can be written as

$$f(\mathbf{r}, \mathbf{v}, t) = n(\mathbf{r}, t) f_0(\mathbf{v}) \sum_{l,m,r} c_{l,m,r}(\mathbf{r}, t) \Psi_{l,m,r}(\mathbf{v}), \qquad (5.16)$$

where three indices are needed because of the three-dimensional nature of \mathbf{v} . In order to use a three-dimensional method of weighted residuals, it is customary to choose basis functions, $\Psi_{l,m,r}(\mathbf{v})$, that are orthogonal with respect to $f_0(\mathbf{v})$ as weighting function, i.e.,

$$(\Psi_{l,m,r}, \Psi_{l',m',r'}) = \delta_{l,l'} \delta_{m,m'} \delta_{r,r'} N_{l,m,r} , \qquad (5.17)$$

where

$$(A, B) = \int f_0(\mathbf{v}) A^*(\mathbf{v}) B(\mathbf{v}) d\mathbf{v}, \qquad (5.18)$$

the asterisk indicates a complex conjugate (see Appendix A), and the normalization constants, $N_{l,m,r}$, depend upon the particular basis functions being used. There is no error introduced by making these assumptions, so long as we use all possible values of the indices and so long as the basis functions form a complete set in velocity space, i.e., as long as the difference between the right-hand side of (5.16) and any piecewise continuous function of the velocity converges to zero as the upper limit on the sums becomes infinite (Kaplan 1959).

It is easy to show from (5.8) and (5.16)–(5.18) that

$$\langle \Psi_{l,m,r}^*(\mathbf{v}) \rangle = N_{l,m,r} c_{l,m,r}(\mathbf{r},t), \tag{5.19}$$

so techniques based on (5.16) are equivalent to moment methods, assuming that the same basis functions are used. Our problems then are to decide what basis functions or, equivalently, what zero-order ion vdf, $f_0(\mathbf{v})$, to use and then how to truncate the sums in (5.16) in a way that is consistent with our treatment of $\mathfrak{F}(\psi(\mathbf{v}))$.

5.5 One-Temperature Basis Functions

For many years, it was customary to assume that the ion vdf was approximately Maxwellian, i.e., that

$$f_0^{(1T)}(\mathbf{v}) = \left(\frac{m}{2\pi k_B T_0}\right)^{3/2} \exp\left(-\frac{mv^2}{2k_B T_0}\right).$$
 (5.20)

The corresponding basis functions that satisfy (5.17) and (5.18) are the one-temperature (1T) Burnett functions (Burnett 1935a,b),

$$\Psi_{l,m,r}^{(1T)}(\mathbf{v}) = W_{1T}^l S_{l+1/2}^{(r)}(W_{1T}^2) P_l^{(m)}(\cos \theta) e^{im\phi}, \tag{5.21}$$

where

$$\mathbf{W}_{1T} = \left(\frac{m}{2k_B T_0}\right)^{1/2} \mathbf{v}.\tag{5.22}$$

The l and r indices are nonnegative integers that indicate a particular Sonine polynomial, $S_{l+1/2}^{(r)}(W_{1T}^2)$; these are the same as the associated (generalized) Laguerre polynomials (see Appendix A) when those are written as $L_r^{(l+1/2)}(W_{1T}^2)$. The angles θ and ϕ are the polar and azimuthal angles describing the vector \mathbf{W}_{1T} in spherical

polar coordinates with respect to some space-fixed axis, usually **E**. The $P_l^{(m)}$ are the associated Legendre polynomials (see Appendix A) of degree l and order m. Finally, the normalization constants are the same as given below for the 2T basis functions.

The eigenfunctions (see Appendix A) of the Boltzmann collision operator are known (Ferrari 1978) for the Maxwell model of constant mean free time, and they can be expressed in terms of the 1T Burnett functions. However, results obtained using the 1T Burnett functions can be obtained easily from those obtained with the 2T Burnett functions described in the next section, by setting the ion temperature equal to T_0 . Thus, there is no point in discussing separately the details of their use in solving the 1T moment equations.

Instead of the Burnett functions, it is sometimes more convenient to use equivalent functions that involve the spherical harmonics of \mathbf{W}_{1T} . Our reasons for not doing this will be given in the next section.

The special case that is the foundation of momentum-transfer theory in Chap. 3 is the Maxwell model discussed in Sect. 4.7. Since the results for the Maxwell model, which shall be indicated with an MM subscript or superscript, are independent of the strengths of the external electric or magnetic fields, it does not matter for this model what temperature is used in (5.22). This, along with the lack of inspiration about what else could be done, led people to ignore the fact that the 1T basis functions involve the ion mass and the ion velocity but the temperature of the *neutral* gas.

All 1T results are valid only in the limit of small E/n_0 , which is why 1T basis functions are no longer in use for solving the Boltzmann equation or the equivalent moment equations.

5.6 Two-Temperature Basis Functions

Good success has been obtained in describing ion mobility in IMS and DTMS experiments (Viehland and Mason 1975, 1978) by using a zero-order approximation to the ion vdf that contains an ion temperature, T. At steady state, T can be substantially larger than T_0 , since the ions are present only in trace amounts. Thus, in the 2T approach one assumes that

$$f_0^{(2T)}(\mathbf{v}) = \left(\frac{m}{2\pi k_B T}\right)^{3/2} \exp\left(-\frac{mv^2}{2k_B T}\right),$$
 (5.23)

and uses 2T Burnett functions,

$$\Psi_{l,m,r}^{(2T)}(\mathbf{v}) = W_{2T}^{l} S_{l+1/2}^{(r)}(W_{2T}^{2}) P_{l}^{(m)}(\cos \theta) e^{im\phi}, \tag{5.24}$$

where

$$\mathbf{W}_{2T} = \left(\frac{m}{2k_B T}\right)^{1/2} \mathbf{v}.\tag{5.25}$$

The ion temperature is defined by requiring that the equation,

$$\frac{3}{2}k_BT = \left\langle \frac{1}{2}mv^2 \right\rangle,\tag{5.26}$$

be imposed as a constraint at each step in the solution of the Boltzmann equation or the moment equations equivalent to it. Finally, it can be shown from (5.17) and (5.18) that

$$N_{l,m,r}^{(2T)} = (\Psi_{l,m,r}^{(2T)}(\mathbf{v}), \Psi_{l,m,r}^{(2T)}(\mathbf{v})) = \frac{\Gamma(l+r+3/2)}{4\pi r! \Gamma(3/2)},$$
 (5.27)

where Γ indicates a gamma function (see Appendix A). This normalization factor is independent of the m index.

Since the 2T basis functions are complex rather than real functions, careful treatment is required at times. For example, this is why the complex conjugate, $A^*(\mathbf{v})$, appears in (5.18). Such care, when combined with the properties of the collision operator (it is local, instantaneous, scalar and linear) leads to a representation of the collision terms in (5.14) as

$$\sum_{j} n_{j} \left\langle \mathfrak{J}_{j} \Psi_{l,m,r}^{(2T)}(\mathbf{v}) \right\rangle = n_{0} \sum_{s=0}^{\infty} b_{r,s}^{(2T)}(l) \left\langle \Psi_{l,m,s}^{(2T)}(\mathbf{v}) \right\rangle, \tag{5.28}$$

where we can use the mole fraction, x_i , of buffer gas j to write

$$b_{r,s}^{(2T)}(l) = \sum_{j} x_j a_{r,s}^{(2T)}(l)$$
 (5.29)

and

$$a_{r,s}^{(2T)}(l) = \frac{(\Psi_{l,m,s}^{(2T)}(\mathbf{v}), \mathfrak{J}_j \Psi_{l,m,r}^{(2T)}(\mathbf{v}))}{N_{l,s}^{(2T)}}.$$
 (5.30)

with the j index for the $a_{r,s}^{(2T)}(l)$ being left implicit. Note that, $b_{r,s}^{(2T)}(l)$ and $a_{r,s}^{(2T)}(l)$ are the same no matter what value of the index m is used on the right-hand sides of (5.29) and (5.30).

After considerable mathematical effort (Viehland and Mason 1975), the reducible matrix elements, $a_{r,s}^{(2T)}(l)$ for ions in gas j can be expressed as a linear combination of the (irreducible) collision integrals, $\overline{\Omega_j}^{(l,s)}(T_{eff,j})$, defined by (1.21)–(1.23), with the effective temperature given by

$$T_{eff,j} = \frac{mT_0 + m_j T}{m + m_j}. (5.31)$$

Fortunately, this mathematical work does not need to be repeated and the available expression can be put into 2T computer programs by straightforward programming methods.

Analytical expressions for a few of the matrix elements with small values of the indices ones are given by Mason and McDaniel (1988), who correct a misprint in the similar table of Viehland and Mason (1975). Note again that quantities with a 2T superscript apply to the 1T theory when one passes to limit $T \rightarrow T_0$.

There are five important points to note about the use of the ion temperature in (5.25):

- 1. It is this seemingly small change that allows the solution of the Boltzmann equation to be valid for intermediate and large E/n_0 . The limited radius of convergence observed with the 1T functions does not arise with the 2T functions, or at least it is large enough compared to experimental values of E/n_0 that it can be ignored.
- 2. The ion temperature is not defined by the Wannier equation discussed in Chap. 1. Indeed, as demonstrated below, the Wannier equation comes from (5.26) and (5.31), along with small correction factors.
- 3. It is possible (Kumar et al. 1980; Ness and Robson 1985; Robson and Ness 1986) to construct a series of increasing values of T, each of which allows the Boltzmann equation or the moment equations to be solved over a range of E/n_0 . However, this technique cannot handle situations where the average kinetic energy of the ions changes rapidly due to time-varying or position-dependent external fields. Moreover, the steady increase in computer speed over the years has obviated the slight advantage of this technique.
- 4. Moments of the 2T basis functions can depend upon space and time, and (5.8) and (5.26) show that this is true of *T*. When *T* is a function of **r** and t, one cannot apply the mathematical machinery (the algebra of irreducible tensors) developed over many years (Kumar 1966, 1967, 1976, 1980; Weinert 1982, 1984; Ender et al. 2009) to solve (5.14). This is because the goal is to determine moments, averages of functions of **v**, that can be compared to experiment, rather than averages of functions of **W**_{2T}.
- 5. There is no reason for using spherical harmonics if the algebra of irreducible tensors cannot be applied. It is better to work in Cartesian tensors since they are the way in which we ordinarily think about our physical world and the way we ordinarily describe swarm experiments.

For the Maxwell model, all of the $b_{rs}(l)$ with s > r are zero (Mason and McDaniel 1988). For other ion–neutral interactions, it is expected (Viehland and Mason 1975, 1978) that they become progressively smaller as s increases above r. Hence, we define our first approximation for any moment using 1T or 2T basis functions as occurring when we neglect $\mathfrak{F}(\psi(\mathbf{v}))$ and all matrix elements $b_{r,s}(l)$ with s > r in (5.14). In approximation k > 1, we keep $\mathfrak{F}(\psi(\mathbf{v}))$ for moment equations with $s + k - 1 \le r$, but neglect it and the matrix elements when s + k > r. This series of successive approximations automatically truncates the set of moment equations. Although other methods of truncation can and have been devised, this one has the advantage of leading, in every order of approximation, to a closed set of coupled equations that

numerical tests have demonstrated to have good accuracy for the ion mobility when k = 1, and even better accuracy as k increases.

Unfortunately, the 2T basis functions are not a good set to use for gaseous ion diffusion at intermediate and high E/n_0 . This is because they are inherently isotropic and not well-suited for describing properties that are inherently anisotropic. Moreover, the convergence obtained for the mobility and other isotropic properties is slower than for the multi-temperature basis function described below.

One approach to overcoming these problems is to assume (Ness and Viehland 1990) that the zero-order ion vdf is a biMaxwellian, i.e., contains two terms like the one in (5.23). The two terms have different ion temperatures, reflecting the physical argument that most of the ions cluster around a low ion velocity but some cluster around a higher velocity as a result of partial ion runaway.

The 2T and bi-Maxwellian approaches are no longer in use for numerical calculations, since the methods still to be discussed converge more quickly. However, the 2T theory is useful for understanding the fundamental ion mobility equation, the Wannier equation, and corrections to them. We will therefore return to it in Sect. 5.10.

5.7 Three-Temperature Basis Functions

To treat accurately situations that are intrinsically anisotropic (ion diffusion, for example), it is necessary to go beyond the two-temperature theory. As originally developed (Lin et al. 1979; Viehland and Lin 1979), the three-temperature (3T) theory applied to a drift tube with a uniform electrostatic field; the three temperatures were the gas temperature, an ion temperature, T_{\parallel} , characterizing motion along the direction of the electric field, and another ion temperature, T_{\perp} , characterizing motion perpendicular to the field. This means that the zero-order vdf is

$$f_0^{(3T)}(\mathbf{v}) = \left(\frac{m}{2\pi k_B T_{\parallel}}\right)^{1/2} \left(\frac{m}{2\pi k_B T_{\perp}}\right) \times \exp\left(-\frac{m\left(v_x^2 + v_y^2\right)}{2k_B T_{\perp}} - \frac{m\left(v_z - v_{dis}\right)^2}{2k_B T_{\parallel}}\right)$$
(5.32)

and the basis function are the products of three Hermite polynomials (see Appendix A),

$$\Psi_{p,q,r}^{(MT)}(\mathbf{v}) = H_p \left(\left(\frac{m}{2k_B T_\perp} \right)^{1/2} v_x \right) H_q \left(\left(\frac{m}{2k_B T_\perp} \right)^{1/2} v_y \right) \times H_r \left(\left(\frac{m}{2k_B T_\parallel} \right)^{1/2} (v_z - v_{dis}) \right). \tag{5.33}$$

The normalization factor is the same as that given in (5.40) for the multi-temperature basis functions.

The velocity displacement, v_{dis} , is a parameter that can be adjusted to speed up the convergence of 3T moments, although it is expected on physical grounds that it should be close in value to v_d . However, if it is set exactly equal to v_d , two problems arise. First, in drift-tube experiments involving time- or space-dependent fields, the drift velocity must depend upon \mathbf{r} and t, and this violates the assumption in (5.32) that $f_0^{(3T)}(\mathbf{v})$ depends only upon \mathbf{v} , i.e., is an ion vdf. Second, even in the first-approximation solution of the moment equations for DTMS and IMS experiments, the results are implicit equations for v_d that must be solved by iteration starting from an initial guess. This makes it impossible to give a closed form, analytical solution equivalent to the fundamental ion mobility equation.

One important consequence of the 3T theory is that matrix elements of the collision operator can be expressed as linear combinations of the irreducible collision integrals defined by the equation (Lin et al. 1979; Viehland and Lin 1979),

$$[p;q]^{(l)} = 2\pi^{-1/2} \int_0^\infty d\gamma_r \gamma_r^{p+1} \exp\left(-\gamma_r^2\right) \times \int_{-\infty}^\infty d\gamma_z \gamma_z^q \exp\left(-\gamma_z^2\right) g \overline{Q}^{(l)}(g). \tag{5.34}$$

Here, $\overline{Q}^{(l)}(g)$ is the usual transport cross section of order l given by (1.23), but the relative velocity is given by the following expression for a pure neutral gas:

$$\frac{1}{2}\mu_0 g^2 = \gamma_r^2 k_B T_{\perp}^{(eff)} + (\gamma_z - \widetilde{v}_d)^2 k_B T_{\parallel}^{(eff)}$$
 (5.35)

with

$$\tilde{v}_d^2 = \frac{\mu_0 v_{dis}^2}{2k_B T_{\parallel}^{(eff)}} \tag{5.36}$$

$$T_{\parallel}^{(eff)} = \frac{mT_0 + m_0 T_{\parallel}}{m + m_0} \tag{5.37}$$

and similarly for $T_{\perp}^{(eff)}$ in terms of T_{\perp} . These equations mean that the transport coefficients cannot be expressed in terms of the usual collision integrals defined by (1.22). Instead, the $[p;q]^{(l)}$ are inherently two-dimensional integrals over the components of the collision energy that are parallel and perpendicular to the electrostatic field.

Since the 3T approach to solving the Boltzmann equation is no longer is use, we will not give any more specifics about it. The interested reader should consult the original papers (Lin et al. 1979; Viehland and Lin 1979) or the book by Mason and McDaniel (1988).

5.8 Multi-temperature Basis Functions

In order to study ion traps (Viehland and Goeringer 2004, 2005; Goeringer and Viehland 2005; Viehland et al. 2005), the 3T method was modified to include, in addition to T_0 , three ion temperatures that may differ because they characterize ion motion along three mutually perpendicular directions in the apparatus. Such a multi-temperature (MT) kinetic theory reduces to the 3T theory (without a velocity distribution, i.e., setting $v_{dis} = 0$) when the ion temperatures perpendicular to z are set equal to one another.

The zero-order vdf used in a multi-temperature kinetic theory is thus

$$f_0^{(MT)}(\mathbf{v}) = \left(\frac{m}{2\pi k_B T_x}\right)^{1/2} \left(\frac{m}{2\pi k_B T_y}\right)^{1/2} \left(\frac{m}{2\pi k_B T_z}\right)^{1/2} \times \exp\left(-\frac{m v_x^2}{2k_B T_x} - \frac{m v_y^2}{2k_B T_y} - \frac{m v_z^2}{2k_B T_z}\right), \tag{5.38}$$

where the superscript represents "multi-temperature". The basis functions that correspond to (5.38) are

$$\Psi_{p,q,r}^{(MT)}(\mathbf{v}) = H_p \left(\left(\frac{m}{2k_B T_x} \right)^{1/2} v_x \right) H_q \left(\left(\frac{m}{2k_B T_y} \right)^{1/2} v_y \right) \times H_r \left(\left(\frac{m}{2k_B T_z} \right)^{1/2} v_z \right), \tag{5.39}$$

and their normalization is such that

$$N_{p,q,r}^{(MT)} = 2^{p+q+r} \ p! \ q! \ r! \tag{5.40}$$

Note that, the velocity along the field is not displaced like it is for the 3T theory; the reasons for this were discussed above.

For the MT basis functions, the representation of the collision terms in (5.14) is

$$\sum_{j} n_{j} \left\langle \mathfrak{J}_{j} \Psi_{p,q,r}^{(MT)}(\mathbf{v}) \right\rangle = n_{0} \sum_{s,t,u=0}^{\infty} b^{(MT)}(p,q,r|s,t,u) \left\langle \Psi_{s,t,u}^{(MT)}(\mathbf{v}) \right\rangle, \tag{5.41}$$

where

$$b^{(MT)}(p,q,r|s,t,u) = \sum_{j} x_{j} a_{j}^{(MT)}(p,q,r|s,t,u)$$
 (5.42)

and

$$a_j^{(MT)}(p,q,r|s,t,u) = \frac{(\Psi_{s,t,u}^{(MT)}(\mathbf{v}), \mathfrak{J}_j \Psi_{p,q,r}^{(MT)}(\mathbf{v}))}{N_{s,t,u}^{(MT)}}.$$
 (5.43)

The matrix elements defined by (5.43) are the same as those used by Viehland and Goeringer (2005), and they are expressed as a linear combination of irreducible collision integrals in the supplementary material for that paper.

The irreducible collision integrals in the MT theory are defined as

$$[p, q, r|s, t, u]_{j} = \pi^{-3/2} \int \exp\left(-\gamma_{x}^{2} - \gamma_{y}^{2} - \gamma_{z}^{2}\right) \gamma_{x}^{p} \gamma_{y}^{q} \gamma_{z}^{r}$$

$$\times \left[(\gamma_{x})^{s} (\gamma_{y})^{t} (\gamma_{z})^{u} - (\gamma_{x}')^{s} (\gamma_{y}')^{t} (\gamma_{z}')^{u} \right]$$

$$\times g\sigma(g, \theta_{C}) \sin(\theta_{C}) d\theta_{C} d\phi_{C} d\gamma_{x} d\gamma_{y} d\gamma_{z}. \tag{5.44}$$

Here, the post-collision (primed) dimensionless velocities are related to the precollision (unprimed) velocities and the scattering angles (θ_C and ϕ_C) by the following equations:

$$\gamma_{x}' = \gamma_{x} \cos(\theta_{C}) + \left(\frac{\gamma_{z}^{2} T_{z}^{(eff)}}{\gamma_{x}^{2} T_{x}^{(eff)} + \gamma_{y}^{2} T_{y}^{(eff)}}\right)^{1/2} \gamma_{x} \sin(\theta_{C}) \cos(\phi_{C}) + \left(1 - \frac{\gamma_{z}^{2} T_{z}^{(eff)}}{\gamma_{x}^{2} T_{x}^{(eff)} + \gamma_{y}^{2} T_{y}^{(eff)}}\right)^{1/2} \left(\frac{T_{y}^{(eff)}}{T_{x}^{(eff)}}\right)^{1/2} \gamma_{y} \sin(\theta_{C}) \sin(\phi_{C})$$
 (5.45)

$$\gamma_{y}' = \gamma_{y} \cos(\theta_{C}) + \left(\frac{\gamma_{z}^{2} T_{z}^{(eff)}}{\gamma_{x}^{2} T_{x}^{(eff)} + \gamma_{y}^{2} T_{y}^{(eff)}}\right)^{1/2} \gamma_{y} \sin(\theta_{C}) \cos(\phi_{C})$$

$$- \left(1 - \frac{\gamma_{z}^{2} T_{z}^{(eff)}}{\gamma_{x}^{2} T_{x}^{(eff)} + \gamma_{y}^{2} T_{y}^{(eff)}}\right)^{1/2} \left(\frac{T_{x}^{(eff)}}{T_{y}^{(eff)}}\right)^{1/2} \gamma_{y} \sin(\theta_{C}) \sin(\phi_{C})$$
(5.46)

and

$$\gamma_z' = \gamma_z \cos(\theta_C) - \left(\frac{\gamma_x^2 T_x^{(eff)} + \gamma_y^2 T_y^{(eff)}}{\gamma_z^2 T_z^{(eff)}}\right)^{1/2} \sin(\theta_C) \cos(\phi_C).$$
 (5.47)

The relationship between g and these dimensionless velocities is that

$$\frac{1}{2}\mu_0 g^2 = \gamma_x^2 k_B T_x^{(eff)} + \gamma_y^2 k_B T_y^{(eff)} + \gamma_z^2 k_B T_z^{(eff)}, \tag{5.48}$$

where the relationships between the three effective temperatures and the equivalent ion temperatures is equivalent to that given by (5.37).

Equation (5.47) corrects a misprint in the supplement to Viehland and Goeringer (2005), but the analytical expressions given there are correct for matrix elements with small values of the indices. Note that in classical mechanics, the integral represented

as $\sigma(g, \theta_C) \sin(\theta_C) d\theta_C d\phi_C$ can be written (Robson 2006) as $2\pi b db$, where b is the impact parameter.

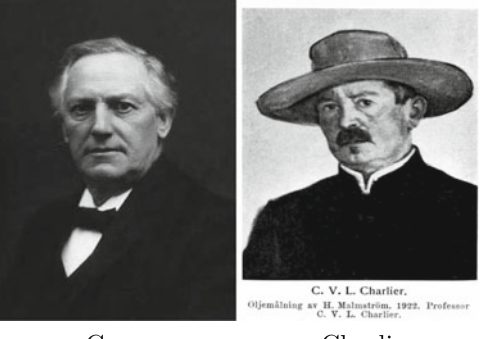
The key point is that (5.44) can be expressed (Viehland and Goeringer 2005) as a linear combination of integrals involving the usual transport cross sections defined by (1.23). However, the integrals are three-dimensional rather than one, i.e., they are over the energies along each of the three space-fixed axes rather than over only the total kinetic energy of the collision. The irreducible collision integrals are not "omega integrals" defined by (1.22). In addition, they depend upon three effective temperatures.

All of the $b^{(MT)}(p',q',r'|p,q,r)$ with p+q+r>p'+q'+r' are zero for the Maxwell model, while for other ion–neutral interactions they become progressively smaller as p+q+r increases above p'+q'+r'. Hence we define our first approximation for any moment using the MT basis functions as occurring when we neglect $\mathfrak{F}(\psi(\mathbf{v}))$ and all matrix elements $b^{(MT)}(p,q,r|p',q',r')$ with p+q+r>p'+q'+r' when (5.41) is used in (5.14). In approximation k>1, we keep $\mathfrak{F}(\psi(\mathbf{v}))$ when $p+q+r+k-1\leq p'+q'+r'$ but neglect it and matrix elements with p+q+r+k>p'+q'+r'. This series of successive approximations automatically truncates the set of moment equations, leading in every order of approximation to a closed set of coupled partial differential equations that have good accuracy when k=1 and even better accuracy as k increases.

The MT basis functions have proven useful in kinetic theory studies of ion traps, as described in Sect. 2.13. We will not consider them further in this book, in order to focus on DTMS and IMS experiments with no external magnetic fields and an electric field that is static and uniform.

5.9 Gram-Charlier Basis Functions

The Gram–Charlier (GC) approach to solving the Boltzmann equation (equivalently, the moment equations obtained from it) for atomic ions in atomic neutrals was developed (Viehland 1994) in order to bypass the arguments by Skullerud (1984) that eventually the 1T, 2T, 3T, and MT theories should fail because their basis functions are orthogonal with respect to a Gaussian weighting function and the tail of the true ion vdf must fall off more slowly than any Gaussian. This was done by modifying the three-temperature expression for the ion vdf, $f_0^{(3T)}(\mathbf{v})$. Although we will demonstrate in Chap. 6 that the GC approach converges to accurate values for the transport coefficients, this method shares a weakness with the 3T approach: it leads to implicit equations that can only be solved numerically.



Gram Charlier

The Gram–Charlier type A series is named in honor of Jørgen Pedersen Gram (1850–1916) and Carl Vilhelm Ludwig Charlier (1862–1934). It is used in statistics to approximate a probability distribution, which suggested that it could be used for solving the moment equations obtained from Boltzmann equation, after generalization to three dimensions and allowing for correlation of the ion behavior in different directions. The zero-order vdf used in a GC kinetic theory is thus

$$f_0^{(GC)}(\mathbf{v}) = f_0^{(3T)}(\mathbf{v}) \left[1 + \frac{\sqrt{2}}{6} \widetilde{\alpha}_L W_z \left(2W_z^2 - 3 \right) + \frac{1}{24} \left(\widetilde{\beta}_L - 3 \right) \left(4W_z^4 - 12W_z^2 + 3 \right) + \frac{1}{24} \left(\widetilde{\beta}_T - 3 \right) \left(4W_x^4 - 12W_x^2 + 3 + 4W_y^4 - 12W_y^2 + 3 \right) + \sqrt{2} \widetilde{\gamma}_1 \left(W_x^2 + \frac{1}{2} + W_y^2 + \frac{1}{2} \right) W_z + \left(\widetilde{\gamma}_2 - 1 \right) \left(W_x^2 + \frac{1}{2} + W_y^2 + \frac{1}{2} \right) \left(W_z^2 + \frac{1}{2} \right) \right], \quad (5.49)$$

where

$$f_0^{(3T)}(\mathbf{v}) = \left(\frac{m}{2\pi k_B \tilde{T}_L}\right)^{1/2} \left(\frac{m}{2\pi k_B \tilde{T}_T}\right) \exp\left(-W_x^2 - W_y^2 - W_z^2\right),\tag{5.50}$$

$$W_{i} = \left(\frac{m}{2\pi k_{B}\tilde{T}_{T}}\right)^{1/2} v_{i} \quad i = x, y,$$
 (5.51)

and

$$W_z = \left(\frac{m}{2\pi k_B \widetilde{T}_L}\right)^{1/2} (v_z - \widetilde{v}_d). \tag{5.52}$$

It is easy to show from (5.49) that

$$\int f_0^{(GC)}(\mathbf{v})d\mathbf{v} = 1,\tag{5.53}$$

$$\int f_0^{(GC)}(\mathbf{v})v_z d\mathbf{v} = \widetilde{v}_d, \tag{5.54}$$

$$\int f_0^{(GC)}(\mathbf{v}) (v_z - \widetilde{v}_d)^2 d\mathbf{v} = k_B \widetilde{T}_L / m, \tag{5.55}$$

$$\int f_0^{(GC)}(\mathbf{v}) (v_z - \widetilde{v}_d)^3 d\mathbf{v} = \left(k_B \widetilde{T}_L / m\right)^{3/2} \widetilde{\alpha}_L, \tag{5.56}$$

$$\int f_0^{(GC)}(\mathbf{v}) (v_z - \widetilde{v}_d)^4 d\mathbf{v} = \left(k_B \widetilde{T}_L / m\right)^2 \widetilde{\beta}_L, \tag{5.57}$$

$$\int f_0^{(GC)}(\mathbf{v})v_x d\mathbf{v} = \int f_0^{(GC)}(\mathbf{v})v_y d\mathbf{v} = 0,$$
(5.58)

$$\int f_0^{(GC)}(\mathbf{v}) v_x^2 d\mathbf{v} = \int f_0^{(GC)}(\mathbf{v}) v_y^2 d\mathbf{v} = k_B \widetilde{T}_T / m,$$
 (5.59)

$$\int f_0^{(GC)}(\mathbf{v})v_x^3 d\mathbf{v} = \int f_0^{(GC)}(\mathbf{v})v_y^3 d\mathbf{v} = 0,$$
(5.60)

$$\int f_0^{(GC)}(\mathbf{v})v_x^4 d\mathbf{v} = \int f_0^{(GC)}(\mathbf{v})v_x^4 d\mathbf{v} = \left(k_B \widetilde{T}_T./m\right)^2 \widetilde{\beta}_T, \tag{5.61}$$

$$\int f_0^{(GC)}(\mathbf{v}) v_x^2 (v_z - \widetilde{v}_d) d\mathbf{v} = \int f_0^{(GC)}(\mathbf{v}) v_y^2 (v_z - \widetilde{v}_d) d\mathbf{v}$$
$$= (k_B \widetilde{T}_T / m) (k_B \widetilde{T}_L / m)^{1/2} \widetilde{\gamma}_1, \qquad (5.62)$$

and

$$\int f_0^{(GC)}(\mathbf{v})v_x^2 (v_z - \widetilde{v}_d)^2 d\mathbf{v} = \int f_0^{(GC)}(\mathbf{v})v_y^2 (v_z - \widetilde{v}_d)^2 d\mathbf{v}$$
$$= (k_B \widetilde{T}_T/m) (k_B \widetilde{T}_L/m) \widetilde{\gamma}_2. \tag{5.63}$$

It is therefore expected that the eight parameters indicated with decorations in (5.53)–(5.63) should be approximately equal to the true (undecorated) values of the ion drift speed (v_d) along the field, the parallel ion temperature (T_L) , the perpendicular ion temperature (T_T) , the parallel skewness (α_L) , the parallel excess kurtosis (β_L) , the perpendicular excess kurtosis (β_T) , the correlation (γ_1) between the parallel velocity and the perpendicular energy, and the correlation (γ_2) between the parallel and perpendicular energies. Note that by construction, the ion drift speeds perpendicular to the field, the perpendicular skewness, and other possible correlations are all zero, as expected on physical grounds.

The basis functions in the GC method are exactly the same as those in the 3T method and given by (5.33). In addition, matrix elements of the collision operator can be expressed (Viehland 1994) as linear combinations of the collision integrals defined by (5.34)–(5.37), although the linear combinations are different than for the 3T theory.

Equations for numerically evaluating (5.34)–(5.37) have been incorporated into a computer program called GC (Yousef et al. 2007), which uses as input values of the transport cross sections obtained from the computer program named PC (Viehland and Chang 2010). Also built into program GC are the equations from Viehland (1994) for forming matrix elements of the collision operator from the $[p;q]^{(l)}$ and iterating the equations in each successive order of approximation to get converged values for v_d (equivalent to values of K_0), α_L , β_L , β_T , γ_1 and γ_2 as functions of T_0 and E/n_0 . Programs PC and GC are available upon request to the author. Their use will be illustrated in the last few sections of Chap. 6.

5.10 Moment Equation for Ion Velocity

5.10.1 First Approximation of 2T Equation

In the rest of this chapter, we will consider the analytical results that can be obtained from the basis functions discussed above that do not include velocity displacement. We first consider (5.14) for the special function $\psi(\mathbf{v}) = \mathbf{v}_z$:

$$\frac{\partial}{\partial t} \langle \mathbf{v}_z \rangle - \langle a_z \rangle + \sum_j n_j \langle \mathfrak{J}_j v_z \rangle = \mathcal{F}(v_z). \tag{5.64}$$

Making use of (5.24) and (5.28), we find that in terms of the 2T basis functions,

$$\sum_{j} n_{j} \langle J_{j} v_{z} \rangle = \sum_{j} n_{j} \left(\frac{2k_{B}T}{m} \right)^{1/2} \langle \mathfrak{J}_{j} \Psi_{1,0,0}^{(2T)}(\mathbf{v}) \rangle$$

$$= n_{0} \left(\frac{2k_{B}T}{m} \right)^{1/2} \sum_{s=0}^{\infty} b_{0,s}^{(2T)}(1) \langle \Psi_{1,0,s}^{(2T)}(\mathbf{v}) \rangle$$

$$= n_{0} \sum_{s=0}^{\infty} b_{0,s}^{(2T)}(1) \langle v_{z} S_{3/2}^{(s)}(W^{2}) \rangle. \tag{5.65}$$

Because the Boltzmann collision operator is a scalar operator, this equation becomes

$$\sum_{j} n_{j} \langle J_{j} \mathbf{v} \rangle = n_{0} \sum_{s=0}^{\infty} b_{0,s}^{(2T)}(1) \langle \mathbf{v} S_{3/2}^{(s)}(W^{2}) \rangle.$$
 (5.66)

If we insert (5.66) into (5.64) and separate the r=0 term from the others terms, we get

$$\frac{\partial}{\partial t} \langle \mathbf{v} \rangle - \frac{q}{m} \left(\mathbf{E} + \langle \mathbf{v} \rangle \times \mathbf{B} \right) + n_0 b_{0,0}^{(2T)}(1) \langle \mathbf{v} \rangle
= \mathcal{F}(\mathbf{v}) - n_0 \sum_{s>0} b_{0,s}^{(2T)}(1) \left\langle \mathbf{v} S_{3/2}^{(s)}(W^2) \right\rangle.$$
(5.67)

In the first approximation, we neglect the right-hand side of (5.67) for reasons described above. This gives the first approximation, 2T equation for ion velocity as

$$\frac{\partial}{\partial t} \langle \mathbf{v} \rangle - \frac{q}{m} (\mathbf{E} + \langle \mathbf{v} \rangle \times \mathbf{B}) + \xi^{(2T)}(T) \langle \mathbf{v} \rangle = 0, \tag{5.68}$$

where the 2T collision frequency for momentum transfer can be written as

$$\xi^{(2T)}(T) = n_0 b_{0,0}^{(2T)}(1)$$

$$= \sum_{j} \left(\frac{8n_j}{3}\right) \left(\frac{m_j}{m + m_j}\right) \left(\frac{2k_B T_j^{(eff)}}{\pi \mu_j}\right)^{1/2} \overline{\Omega}_j^{(1,1)}(T_j^{(eff)}). \tag{5.69}$$

We define the 2T collision frequency for momentum transfer with species j by

$$\xi_j^{(2T)}(T_j^{(eff)}) = \left(\frac{8}{3}\right) \left(\frac{m_j}{m + m_j}\right) \left(\frac{2k_B T_j^{(eff)}}{\pi \mu_j}\right)^{1/2} \overline{\Omega}_j^{(1,1)}(T_j^{(eff)}), \tag{5.70}$$

where the effective temperatures is given by (5.37). Then for a mixture,

$$\xi^{(2T)}(T) \equiv \sum_{j} n_{j} \xi_{j}^{(2T)}(T_{j}^{(eff)}) = n_{0} \sum_{j} x_{j} \xi_{j}^{(2T)}(T_{j}^{(eff)}).$$
 (5.71)

It is particularly important to note that $\xi_j^{(2T)}(T_j^{(eff)})$ has a microscopic definition, since it is shown in Chap. 1 how the momentum-transfer collision integral, $\overline{\Omega}_j^{(1,1)}(T_j^{(eff)})$, can be calculated as a function of $T_j^{(eff)}$ from knowledge only of the ion and neutral masses and the ion–neutral interaction potential energy as a function of internuclear separation.

In a DTMS or IMS experiment, there is no magnetic field and $\langle \mathbf{v} \rangle$ is not a function of time. Then for these experiments, (5.68) reduces to

$$\langle \mathbf{v} \rangle = \frac{q\mathbf{E}}{m\xi^{(2T)}(T)}.$$
 (5.72)

Since density gradients are specifically ignored in first approximation, $\langle \mathbf{v} \rangle = \mathbf{v}_d$ and, as expected, \mathbf{v}_d lies entirely along \mathbf{E} .

Combining (5.72) with (1.4) and (1.7) gives

$$K_0 = \frac{n_0}{N_0} \frac{q}{m\xi^{(2T)}(T)}. (5.73)$$

Then inserting (5.70) and (5.71) into (5.73) gives an extension of Blanc's law, (A.10), to arbitrary E/n_0 :

$$\frac{1}{K_{0,mix}} = \sum_{j} \frac{x_j}{K_{0,j}},\tag{5.74}$$

where

$$K_{0,j} = \left(\frac{2\pi}{\mu_j k_B T_j^{(eff)}}\right)^{1/2} \frac{3q}{16N_0} \frac{1}{\overline{\Omega}_j^{(1,1)} (T_j^{(eff)})}.$$
 (5.75)

The high-field extension of Blanc's law given in Sect. 2.5 includes the contribution of the correction terms, which come from the higher order approximations discussed below.

If there is only a single nonreactive gas instead of a mixture, the j subscripts in (5.75) can be dropped and we obtain the fundamental ion mobility equation, (1.45), except that the correction term, α_c , is equal to zero here since we are working only in the first approximation.

5.10.2 First Approximation of 1T and MM Equations

In the low-field limit where T and each $T_j^{(eff)}$ becomes equal to T_0 , the first approximation moment equation for ion velocity obtained from (5.68) is

$$\frac{\partial}{\partial t} \langle \mathbf{v} \rangle - \frac{q}{m} (\mathbf{E} + \langle \mathbf{v} \rangle \times \mathbf{B}) + \xi^{(1T)} (T_0) \langle \mathbf{v} \rangle = 0, \tag{5.76}$$

where the 1T collision frequency for momentum transfer is

$$\xi^{(1T)}(T_0) = \sum_{j} \left(\frac{8n_j}{3}\right) \left(\frac{m_j}{m + m_j}\right) \left(\frac{2k_B T_0}{\pi \mu_j}\right)^{1/2} \overline{\Omega}_j^{(1,1)}(T_0)$$

$$= \sum_{j} x_j \xi_j^{(1T)}(T_0). \tag{5.77}$$

Note that the last equality in (5.77) serves to define the $\xi_j^{(1T)}(T_0)$, that the gas number densities are included in this definition, and that $\xi^{(1T)}(T_0)$ is a function only of the gas temperature, the ion and neutral masses, and the ion–neutral interaction potentials.

For the Maxwell model, and only for this model, $\xi^{(1T)}(T_0)$ become independent of T_0 . Generalizing to a mixture of neutral gases the expression of Viehland and Goeringer (2004, 2005) gives

$$\xi^{(MM)} = (6.96467 \times 10^{10} \text{ Hz}) \left(\frac{P_0}{101325 \text{ Pa}}\right) \left(\frac{273.15 \text{ K}}{T_0}\right) \times \sum_j \frac{x_j m_j}{m + m_j} \left(\frac{\widehat{\alpha}_j}{\widehat{\mu}_j}\right)^{1/2}$$
(5.78)

where $\widehat{\alpha}_j$ is the polarizability of gas j in cubic Angstrom and $\widehat{\mu}_j$ is the reduced mass in g/mole (Da) for an ion and an atom of gas j. Thus, for ion–neutral systems whose interactions follow the Maxwell model, the moment equation for ion velocity involves a constant collision frequency.

Equation (5.76) with constant $\xi^{(MM)}$ is equivalent to the damped Mathieu equation so often studied in the context of quadrupole ion traps (March and Todd, 1955). There are two important differences. The first is that (5.76) is a first-order differential equation for the average velocity rather than for the velocity of a single ion. As discussed previously (Viehland and Goeringer 2005; Viehland et al. 2005; Goeringer and Viehland 2005), this means that it cannot be converted to a second-order differential equation for the position. The second difference is that the collision frequency for momentum transfer in the two-temperature theory is, except for the Maxwell model, a function of the effective temperatures (equivalently, the average ion–neutral kinetic energies). We, therefore, need a moment equation that describes how the ion energy changes; this is given in Sect. 5.11.

5.10.3 First Approximation of MT Equation

We now consider what happens to the moment equation for ion velocity when we use the MT basis functions defined by (5.39). In terms of those functions we have

$$\sum_{j} n_{j} \langle J_{j} v_{z} \rangle = \sum_{j} n_{j} \left(\frac{2k_{B} T_{z}}{m} \right)^{1/2} \langle \mathfrak{J}_{j} \Psi_{0,0,1}^{(MT)}(\mathbf{v}) \rangle$$

$$= n_{0} \left(\frac{2k_{B} T_{z}}{m} \right)^{1/2} \sum_{p,q,r=0}^{\infty} b^{(MT)}(0,0,1|p,q,r) \langle \Psi_{p,q,r}^{(MT)}(\mathbf{v}) \rangle, \qquad (5.79)$$

SO

$$\frac{\partial}{\partial t} \langle v_z \rangle - \frac{q}{m} \left(\mathbf{E} + \langle \mathbf{v} \rangle \times \mathbf{B} \right)_z + n_0 b^{(MT)}(0, 0, 1 | 0, 0, 1) \langle v_z \rangle = \mathcal{F}(v_z)
- n_0 \left(\frac{2k_B T_z}{m} \right)^{1/2} \sum_{p \ge 0} \sum_{q \ge 0} \sum_{r > 0} b^{(MT)}(0, 0, 1 | p, q, r) \left\langle \Psi_{p,q,r}^{(MT)}(\mathbf{v}) \right\rangle,$$
(5.80)

where the p = q = 0, r = 1 term is omitted from the sum.

We can define a MT collision frequency for momentum transfer along the z direction as

$$\xi_z^{(MT)}(T_x, T_y, T_z) = n_0 b^{(MT)}(0, 0, 1|0, 0, 1).$$
 (5.81)

Goeringer and Viehland (2005) show that this becomes

$$\xi_{z}^{(MT)}(T_{x}, T_{y}, T_{z}) = n_{0} \sum_{j} x_{j} \left(\frac{8}{3}\right) \left(\frac{m_{j}}{m + m_{j}}\right) \left(\frac{3}{4\pi^{3/2}}\right)$$

$$\iiint \exp\left(-\gamma_{x}^{2} - \gamma_{y}^{2} - \gamma_{z}^{2}\right) \gamma_{z}^{2} g Q^{(1)} \left(\frac{1}{2}\mu_{j}g^{2}\right) d\gamma_{x} d\gamma_{y} d\gamma_{z}$$

$$= n_{0} \sum_{j} x_{j} \xi_{j,z}^{(MT)}(T_{x}, T_{y}, T_{z}), \qquad (5.82)$$

where the last equality defines, $\xi_{j,z}^{(MT)}(T_x, T_y, T_z)$ the MT collision frequency for momentum transfer between the ions and the atoms of species j along the z direction. In (5.82), g (equivalently, the relative kinetic energy) is given by (5.48) and the three effective temperatures (one along each Cartesian axis, i = x, y, z) are defined in terms of the three ion temperatures by (5.37).

Equation (5.82) is a generalization of (5.70) and (5.71), the main difference being that a single energy integral that occurs in $\overline{\Omega}_j^{(1,1)}(T_j^{(eff)})$ becomes a triple integral because the ions have three temperatures that do not necessarily have to be the same, rather than a single temperature as they do in the 2T basis functions. To be absolutely clear, the energy average of the transport cross sections that arise in the MM, 1T, and 2T theories are the familiar "omega integrals" that involve integration over a single variable, while those that arise in the 3T, MT, and GC theories involve a triple integral and hence cannot be expressed in terms of the omega integrals, even though they do involve the same transport cross sections.

In the first approximation of the MT approach, we neglect the right-hand side of (5.80). Then, we can write the equation in the form

$$\frac{\partial}{\partial t} \langle \mathbf{v} \rangle - \frac{q}{m} (\mathbf{E} + \langle \mathbf{v} \rangle \times \mathbf{B}) + \xi_i^{(MT)} (T_x, T_y, T_z) \langle \mathbf{v} \rangle = 0, \tag{5.83}$$

where the subscript i on $\xi_i^{(MT)}(T_x, T_y, T_z)$ implies that one must use i = x, y, z when considering the x, y, z components of this vector equation. Note that for $\xi_i^{(MT)}(T_x, T_y, T_z)$, one must replace the separate γ_z^2 in (5.82) by γ_i^2 .

In a DTMS or IMS experiment where the ion moves only along the z axis defined by the electric field, (5.83) reduces to

$$v_d = \frac{qE}{m\xi_z^{(MT)}(T_x, T_y, T_z)}. (5.84)$$

Proceeding as in Sect. 5.10.1 gives (5.74) with

$$K_{0,j} = \frac{q}{4N_0} \left(\frac{2\pi^3}{\mu_j k_B T_{z,j}^{(eff)}} \right)^{1/2} \frac{1}{\Omega_{MT} \left(T_{x,j}^{(eff)}, T_{y,j}^{(eff)}, T_{z,j}^{(eff)} \right)}, \tag{5.85}$$

where the momentum-transfer collision integrals is

$$\Omega_{MT} \left(T_{x,j}^{(eff)}, T_{y,j}^{(eff)}, T_{z,j}^{(eff)} \right) = \iiint \exp\left(-\gamma_x^2 - \gamma_y^2 - \gamma_z^2 \right) \gamma_z^2 \\
\times \left(\gamma_x^2 \frac{T_{x,j}^{(eff)}}{T_{z,j}^{(eff)}} + \gamma_y^2 \frac{T_{y,j}^{(eff)}}{T_{z,j}^{(eff)}} + \gamma_z^2 \right)^{1/2} Q^{(1)} \left(\frac{1}{2} \mu_j g^2 \right) d\gamma_x d\gamma_y d\gamma_z \tag{5.86}$$

Note that the relative kinetic energy, $\frac{1}{2}\mu_j g^2$, is given by (5.48), and that the MT subscript is doing double duty, as it indicates both momentum transfer and multi-temperature.

As expected, (5.82) reduces to (5.65) when the three ion temperatures are set equal to T. In particular, $\left(T_{z,j}^{(eff)}\right)^{1/2} \Omega_{MT}\left(T_{x,j}, T_{y,j}, T_{z,j}\right)$ reduces to $\left(T_{j}^{(eff)}\right)^{1/2} \overline{\Omega}^{(1,1)}$ $\left(T_{j}^{(eff)}\right)$. If T is set equal to T_{0} , the equations reduce exactly to the 1T equations. Finally, if one specializes to the Maxwell model, the equations reduce to the MM equations.

5.10.4 Higher Approximations

The second approximations to the 2T and MT moment equations for ion velocity have been given by Viehland and Goeringer (2005). The analytical expressions have some use in studies of ion traps (March and Todd, 1955; Viehland and Goeringer 2005; Viehland et al. 2005; Goeringer and Viehland 2005), but their convergence in DTMS and IMS experiments are too slow to be investigated by anything except for numerical techniques. If one is going to switch to numerical studies only, then one might as well use the GC method described above and illustrated in Chap. 6.

5.11 Moment Equations for Energy

There is one more thing that can and should be studied with analytical moment equations, ion kinetic energy. We first note that it is always true that

$$\left\langle (\mathbf{E} + \mathbf{v} \times \mathbf{B}) \cdot \nabla_v \left(\frac{1}{2} m v^2 \right) \right\rangle = m \left\langle (\mathbf{E} + \mathbf{v} \times \mathbf{B}) \cdot \mathbf{v} \right\rangle = m \mathbf{E} \cdot \langle \mathbf{v} \rangle, \qquad (5.87)$$

with the final equality arising because $\mathbf{v} \times \mathbf{B}$ must be perpendicular to \mathbf{v} . This means that a magnetic field cannot affect the ion energy in a drift tube.

For the special function, $\psi(\mathbf{v}) = \frac{1}{2}mv^2$, (5.14) then gives

$$\frac{\partial}{\partial t} \left\langle \frac{1}{2} m v^2 \right\rangle - q \mathbf{E} \cdot \langle \mathbf{v} \rangle + \sum_{j} n_j \left\langle \mathfrak{J}_j \left(\frac{1}{2} m v^2 \right) \right\rangle = \mathcal{F} \left(\frac{1}{2} m v^2 \right)$$
(5.88)

Now we note from (5.24) that, in terms of the 2T basis functions,

$$\frac{1}{2}mv^2 = k_B T W_{2T}^2 = k_B T \left(\frac{3}{2} \Psi_{0,0,0}^{(2T)}(\mathbf{v}) - \Psi_{0,0,1}^{(2T)}(\mathbf{v})\right). \tag{5.89}$$

Hence from (5.28) we find that

$$\sum_{j} n_{j} \left\langle \Im_{j} \left(\frac{1}{2} m v^{2} \right) \right\rangle = n_{0} k_{B} T \sum_{s=0}^{\infty} \left[\frac{3}{2} b_{0,s}^{(2T)}(0) - b_{1,s}^{(2T)}(0) \right] \left\langle \Psi_{0,0,s}^{(2T)}(\mathbf{v}) \right\rangle. \tag{5.90}$$

Since $b_{0.s}^{(2T)}(0)$ is shown in Table 6-2-1 of Mason and McDaniel (1988) to be identically zero, we can combine (5.88) and (5.90) to get

$$\frac{\partial}{\partial t} \left\langle \frac{1}{2} m v^{2} \right\rangle - q \mathbf{E} \cdot \langle \mathbf{v} \rangle
- n_{0} k_{B} T \left[b_{1,0}^{(2T)}(0) \left\langle \Psi_{0,0,0}^{(2T)}(\mathbf{v}) \right\rangle + b_{1,1}^{(2T)}(0) \left\langle \Psi_{0,0,1}^{(2T)}(\mathbf{v}) \right\rangle \right]
= \mathcal{F} \left(\frac{1}{2} m v^{2} \right) + n_{0} k_{B} T \sum_{s>1} b_{1,s}^{(2T)}(0) \left\langle \Psi_{0,0,s}^{(2T)}(\mathbf{v}) \right\rangle.$$
(5.91)

From Sects. 8.753 and 8.973 of Gradshteyn and Ryzhik (1980) and (5.24) and (5.25), we find that

$$\left\langle \Psi_{0,0,0}^{(2T)}(\mathbf{v}) \right\rangle = \langle 1 \rangle = 1$$
 (5.92)

and

$$\left\langle \Psi_{0,0,1}^{(2T)}(\mathbf{v}) \right\rangle = \left\langle \frac{3}{2} - W^2 \right\rangle = \frac{3}{2} - \frac{m}{2k_B T} \left\langle v^2 \right\rangle = 0.$$
 (5.93)

Therefore (5.91) simplifies to

$$\frac{\partial}{\partial t} \left\langle \frac{1}{2} m v^2 \right\rangle - q \mathbf{E} \cdot \langle \mathbf{v} \rangle - n_0 k_B T b_{1,0}^{(2T)}(0)
= \mathcal{F} \left(\frac{1}{2} m v^2 \right) + n_0 k_B T \sum_{s>1} b_{1,s}^{(2T)}(0) \left\langle \Psi_{0,0,s}^{(2T)}(\mathbf{v}) \right\rangle.$$
(5.94)

Now (5.29) and Table 6-2-1 of Mason and McDaniel (1988) can be used to show that

$$b_{1,0}^{(2T)}(0) = \sum_{j} x_{j} a_{0,0}^{(2T)}(1) \left[-\frac{3m}{m+m_{j}} \left(1 - \frac{T_{0}}{T} \right) \right], \tag{5.95}$$

with the j index for the $a_{0,0}^{(2T)}(1)$ being left implicit. Combining (5.26), (5.29), (5.69) and (5.95) gives

$$\frac{\partial}{\partial t} \left(\frac{3}{2} k_B T \right) - q \mathbf{E} \cdot \langle \mathbf{v} \rangle
+ \sum_{j} x_j \left(\frac{2m}{m + m_j} \right) \xi_j^{(2T)} (T_{eff,j}) \left[\frac{3}{2} k_B (T - T_0) \right]
= \mathcal{F} \left(\frac{1}{2} m v^2 \right) + n_0 k_B T \sum_{r>1} b_{1,s}^{(2T)} (0) \left\langle \Psi_{0,0,s}^{(2T)}(\mathbf{v}) \right\rangle.$$
(5.96)

In the first approximation, (5.96) becomes

$$\frac{\partial}{\partial t} \left(\frac{3}{2} k_B T \right) - q \mathbf{E} \cdot \langle \mathbf{v} \rangle
+ \sum_{j} x_j \left(\frac{2m}{m + m_j} \right) \xi_j^{(2T)} \left(\frac{m T_0 + m_j T}{m + m_j} \right) \left[\frac{3}{2} k_B \left(T - T_0 \right) \right] = 0. \quad (5.97)$$

This is a generalization to mixtures of the result obtained by Viehland and Goeringer (2005) for the situation where there is only one buffer gas. The result was used there to show that when the ions are much heavier than the neutral atoms, the influence of the electric field term is slight and the rate of change of the effective temperature is dominated by the 2T collision frequency for momentum transfer. The reverse is true when the ions are much lighter than the neutral atoms.

If we limit ourselves to DTMS and IMS experiments in which there is only a single neutral gas and no time dependence of the ion temperature, we can drop the first term on the left of (5.97), use (5.72) to replace $q\mathbf{E}$ by its first approximation equivalent $m\xi^{(2T)}(T^{(eff)})\langle \mathbf{v}\rangle$, set $\langle \mathbf{v}\rangle \cdot \langle \mathbf{v}\rangle$ equal to v_d^2 , and reduce (5.97) to

$$m\xi^{(2T)}(T^{(eff)})v_d^2 = \left(\frac{2m}{m+m_0}\right)\xi^{(2T)}\left(\frac{mT_0 + m_0T}{m+m_0}\right)\left[\frac{3}{2}k_B(T-T_0)\right]. \quad (5.98)$$

This of course is the Wannier equation discussed in Sect. 1.13:

$$\frac{3}{2}k_BT = \frac{3}{2}k_BT_0 + \frac{1}{2}(m+m_0)v_d^2.$$
 (5.99)

In the first approximation of the 2T theory, therefore, we have obtained Blanc's law, the fundamental ion mobility equation and Wannier's equation!

5.12 Final Comments

Several alternatives to moment methods have been developed previously for swarm experiments. One is to use Monte Carlo methods, as pioneered by Skullerud (1973) and by Lin and Bardsley (1977). This method has been improved and extended by Yousfi et al. (1998). The second method is molecular dynamics simulation (Koutselos 1997; Balla and Koutselos 2003); this method in essence reproduces the experiment on a computer, and it can be applied to a wide variety of different experiments. The third method is based on time-correlation functions (Kumar et al. 1980), from which one can make contact with the path integral methods (Reif 1965) and integral equation approaches (Paveri-Fontana 1974; Cavalleri and Paveri-Fontana 1972; Braglia 1977, 1978). We will discuss the first two methods again in Chap. 9, but discussing the third would lead us too far astray from the main topic in this book.

There are several other methods that can be useful in certain circumstances but are not helpful in describing experiments with ions of arbitrary mass and with external fields that vary with both position and time. The first of these Sato and Tagashira (1985) use numerical techniques that start from the Boltzmann equation and generate the vdf without using a density gradient expansion. The second method (French and Darcie 1986) calculates spatial moments of the electron distribution function by a propagator method that is based on a series of simultaneous equations and the use of Hermite polynomials. The third method (Francey and Jones 1976) uses a Green's function technique and the assumption that the electron-neutral collision frequencies vary as a power of the collision energy. A similar method that did not involve the assumption about the collision frequencies was provided by Tagashira et al. (1978) and later extended (Kitamori et al. 1980) to different experimental techniques for measuring the transport coefficients; these methods are difficult to use, since they involve inverse Fourier transforms that cannot be performed analytically. The use of Fourier transforms led Yachi et al. (1991) and Date et al. (1992a, b, 1993) to consider calculating electron transport coefficients in gases from a Fourier-transformed Boltzmann equation. They showed that such coefficients could be inferred with the same accuracy as they could be obtained from the untransformed equation. However, in order to get a good agreement with results calculated from the untransformed equation, it was necessary for them to postulate a new equation of continuity, one for which there appears to be no experimental support.

References 153

References

- G. Balla, A.D. Koutselos, J. Chem. Phys. 119, 1137 (2003)
- T. Berge, H.R. Skullerud, Phys. Rev. A 13, 1975 (1976)
- G.L. Braglia, Phys. C 92, 91 (1977)
- G.L. Braglia, in Theory of Electron Motion in Gases. I. Stochastic Theory of Homogeneous Systems (IFPR Report no. 174, Univ (Parma, Italy, 1978)
- D. Burnett, Proc. Lond. Math. Soc. 39, 385 (1935a)
- D. Burnett, Proc. Lond. Math. Soc. 40, 382 (1935b)
- G. Cavalleri, S.L. Paveri-Fontana, Phys. Rev. A 6, 327 (1972)
- C. Cercignani, The Boltzmann Equation and Its Applications (Springer, New York, 1988)
- S. Chapman, T.G. Cowling, The Mathematical Theory of Non-uniform Gases, 3rd edn. (Cambridge Mathematical Library, Cambridge, 1970), pp. 62–64
- H. Date, S. Yachi, K. Kondo, H. Tagashira, J. Phys. D 25, 42 (1992a)
- H. Date, S. Yachi, K. Kondo, H. Tagashira, J. Phys. D 25, 1330 (1992b)
- H. Date, K. Kondo, H. Tagashira, J. Phys. D 26, 1211 (1993)
- A.Y. Ender, I.A. Ender, A.B. Gerasimenko, Open plasma. Phys. J. 2, 24 (2009)
- L. Ferrari, Phys. A 93, 531 (1978)
- J.L.A. Francey, D.A. Jones, J. Phys. D 9, 457 (1976)
- J.B. French, T.E. Darcie, J. Chem. Phys. 84, 1764 (1986)
- D.E. Goeringer, L.A. Viehland, J. Phys. B 38, 4027 (2005)
- I.S. Gradshteyn, I.M. Ryzhik, Table of Integrals, Series, and Products (Academic, New York, 1980)
- W. Kaplan, Advanced Calculus (Addison-Wesley, Reading, 1959), pp. 417–424
- T. Kihara, Rev. Mod. Phys. 25, 844 (1953)
- K. Kitamori, H. Tagashira, Y. Sakai, J. Phys. D 13, 535 (1980)
- A.D. Koutselos, J. Chem. Phys. 106, 7117 (1997)
- K. Kumar, Ann. Phys. (N.Y.) 37, 113 (1966)
- K. Kumar, Aust. J. Phys. **20**, 205 (1967)
- K. Kumar, Aust. J. Phys. 23, 505 (1976)
- K. Kumar, Aust. J. Phys. 33, 449 (1980)
- K. Kumar, H.R. Skullerud, R.E. Robson, Aust. J. Phys. 33, 343 (1980)
- S.L. Lin, J.N. Bardsley, J. Chem. Phys. 66, 43 (1977)
- S.L. Lin, L.A. Viehland, E.A. Mason, Chem. Phys. 37, 411 (1979)
- E.A. Mason, E.W. McDaniel, Transport Properties of Ions in Gases (Wiley, New York, 1988)
- J.C. Maxwell, Philos. Trans. R. Soc. Lond. 157, 49 (1867). A reprint is available in S.G. Brush, Kinetic Theory, Vol. 2, Irreversible Processes (Pergamon, Oxford, 1966)
- H.B. Milloy, R.O. Watts, R.E. Robson, M.T. Elford, Aust. J. Phys. 27, 787 (1974)
- K.F. Ness, R.E. Robson, Transp. Theory Stat. Phys. 14, 257 (1985)
- K.F. Ness, L.A. Viehland, Chem. Phys. 148, 255 (1990)
- S.L. Paveri-Fontana, The moment method applied to the validation of Davydov's approximate results for weakly ionized gases, in *Proceedings of 9th International Symposium on Rarified Gas Dynamics*, ed. by M. Becker, M. Fiebig (DFVLR, Porz-Wahn, 1974)
- R. Reif, Fundamentals of Statistical and Thermal Physics (McGraw-Hill, New York, 1965)
- R.E. Robson, *Introductory Transport Theory for Charged Particles in Gases* (World Scientific, Singapore, 2006)
- R.E. Robson, K.F. Ness, Phys. Rev. A 33, 2068 (1986)
- N. Sato, H. Tagashira, J. Phys. D 18, 2451 (1985)
- H.R. Skullerud, J. Phys. D 6, 728 (1973)
- H.R. Skullerud, J. Phys. B 17, 913 (1984)
- H. Tagashira, T. Taniguchi, K. Kitamori, Y. Sakai, J. Phys. D 11, L43 (1978)
- L.A. Viehland, Chem. Phys. **179**, 71 (1994)
- L.A. Viehland, J. Stat. Phys. 163, 175 (2015)
- L.A. Viehland, Y. Chang, Comput. Phys. Commun. 181, 1687 (2010)

- L.A. Viehland, D.E. Goeringer, J. Chem. Phys. 120, 9090 (2004)
- L.A. Viehland, D.E. Goeringer, J. Phys. B 38, 3987 (2005)
- L.A. Viehland, S.L. Lin, Chem. Phys. 43, 135 (1979)
- L.A. Viehland, E.A. Mason, Ann. Phys. (N.Y.) 91, 499 (1975)
- L.A. Viehland, E.A. Mason, Ann. Phys. (N.Y.) 110, 287 (1978)
- L.A. Viehland, W.F. Siems, J. Am. Soc. Mass Spectrom. 23, 1841 (2012)
- L.A. Viehland, E.A. Kabbe, V.V. Dixit, J. Phys. B 38, 4011 (2005)
- U. Weinert, Phys. Rep. 91, 297 (1982)
- U. Weinert, Physica 125A, 498 (1984)
- J.H. Whealton, Phys. Rev. A 11, 2 (1975)
- J.H. Whealton, Phys. Rev. A 13, 1977 (1976)
- S. Yachi, H. Date, K. Kitamori, N. Tagashira, J. Phys. D 24, 573 (1991)
- A. Yousef, S. Shrestha, L.A. Viehland, E.P.F. Lee, B.R. Gray, V.L. Ayles, T.G. Wright, W.H. Breckenridge, J. Chem. Phys. 127, 154309 (2007)
- M. Yousfi, A. Hennad, O. Eichwald, J. Appl. Phys. 84, 107 (1998)

Chapter 6 Ab Initio Calculations of Transport Coefficients



6.1 Introduction

There are two main philosophies behind theoretical calculations . The one illustrated in Chap. 9 is to use models of physical phenomenon, specifically mathematical models, that can be solved exactly, either analytically or by numerical methods. Such models often involve adjustable parameters whose values are fit by comparing model results to experimental values; once the parameters are determined, the models are then used to make similar calculations for other situations, ones that were not part of the set used to determine the parameters. The philosophy illustrated in this chapter is to start from our best theories and, as necessary, make approximations to reduce the equations to forms that are practical to solve, again either analytically or numerically. The hope is that, with time, the approximations will improve such that the calculated values match experimental results without using adjustable parameters. In short, the first philosophy is to make exact calculations with approximate theories, while the second is to make approximate calculations with theories that one believes to be exact.

The reason that this chapter is rather long is that most readers of this book are assumed to have good knowledge of part, but only part, of what is discussed. They are urged to skim the parts that they understand but read the others in detail, in hopes that by the end of the chapter they will have developed a deeper understanding of the approximate calculations used to compute gaseous ion transport coefficients from the theories that at present are believed to be correct. Such theories include the Boltzmann equation presented in Chap. 4, which can be turned into moment equations and solved by the techniques discussed in Chap. 5. We will start with what is missing so far in this book, the theories that allow one to calculate transport cross sections from information about the ion-neutral interaction potentials.

This chapter will focus on ab initio calculations of gaseous ion transport coefficients for atomic ions moving in atomic gases, leaving reactions for Chap. 7 and molecular systems for Chap. 8. Since ab initio means from the beginning, without

input from experiment, we must start with the basics of quantum mechanics, show how the properties of one ion-neutral pair are determined, and then show how solutions of the Boltzmann equation can be used to calculate the transport coefficients that can be measured. Along the way, we will leave out many important topics of quantum mechanics and computational chemistry, focusing only on the direct line from the beginning to the calculated transport coefficients.

6.2 Density Functional Theory



Kohn

The informed reader may wonder why density functional theory (DFT) is ignored in this book. DFT was established by Walter Kohnn (1923–2016) and Lu Jeu Sham. Its central focus is the electron density, ρ , rather than the wave function that is the focus of traditional ab initio methods. The "functional" part of the name comes from the fact that the energy of the molecule is a function of the electron density, and so may be written as $E(\rho)$. The electron density is itself a function of spatial position, \mathbf{r} , and in mathematics a function of a function is called a functional.

The Kohn–Sham equations of DFT are solved iteratively and self-consistently. First, one guesses the electron density, usually by making a superposition of the electron densities of the atoms making up the molecule. Then a quantity whose definition need not concern us, called an exchange-correlation energy , is calculated by assuming an approximate form for its dependence upon ρ . The simplest form, and the one most often used, is the local-density approximation (LDA), although there are variants in use of what is called the generalized gradient approximation (GGA). The third step is to solve the Kohn–Sham equations to give an initial set of orbitals. This set of orbitals is used to obtain a better approximation to the electron density. Finally, the process is repeated until both ρ and the exchange-correlation energy are constant, within some predetermined level of precision.

The main reason DFT methods are ignored in this book is that they have not been used to compute results accurate enough to be compared to experimental results from DTMS or IMS. Presumably this is because (Medvedev et al. 2017; Jacoby 2017) DFT gave increasingly more accurate results until about 2000 but since then

the errors have been growing due to their practitioners' focus on what are, from our point of view, extremely large molecules. The current state-of-the-art in using DFT to compute transport cross sections is given by Boschmans et al. (2016).

6.3 The Time-Independent Schrödinger Equation



The first suggestion that classical physics was not sufficient to explain the behavior of particles whose energy is partly due to speed and partly due to position was made in 1924 by Max Born (1882–1970). (Incidentally, this was the first time that the term quantum mechanics was used.) In the spring of 1925, Werner Heisenberg (1901–1976) developed the first reasonable approach to quantum mechanics, but in a form involving matrices (see Appendix A), which at that time were unfamiliar to chemists and most physicists. Later in 1925, Paul Adrien Maurice Dirac (1902–1984) developed a similar matrix system of quantum mechanics. Shortly afterwards, Erwin Schrödinger (1887–1961) developed what appeared at first sight to be an entirely new system of quantum mechanics and which, because of its use of the familiar concepts of waves, was much easier for most scientists to understand. Schrödinger later showed that his system was mathematically equivalent to the other systems.

There are several ways that may be used to determine the time-dependent Schrödinger equation governing the unknown wave function that represents a microscopic system of interest. None of these represent a rigorous derivation from a more fundamental equation, so whichever one is used must be viewed as leading to a postulate of quantum mechanics that is justified only by the fact that the Schrödinger equation serves as a good approximation to the systems of interest, particularly the ion-neutral systems of interest in this book.





Schrödinger

Landau

Lifshitz

The approach we shall take is described (Landau and Lifshitz 1965) by Lev Davidovich Landau (1908–1968) and Evgeny Mikhailovich Lifshitz (1915–1985). It is to start with the classical-mechanical expression for the total energy, E_{tot} , of the system and then replace the three components of the linear momentum vector, \mathbf{p} , and the total energy, E_{tot} , by differential operators acting on the unknown wave function, $\Psi(x, y, z, t)$. This so-called correspondence principle is

$$p_j \to \frac{h}{2\pi i} \frac{\partial}{\partial j} \qquad j = x, y, z$$
 (6.1)

and

$$E_{tot} \to \frac{ih}{2\pi} \frac{\partial}{\partial t},$$
 (6.2)

where h is Planck's constant (2014 CODATA value 6.626070040×10⁻³⁴ Js) and $i = \sqrt{-1}$ is the base of the imaginary numbers (see Appendix A). Note that these equations have a similarity to the algebraic equations that describe the Uncertainty Principle of Heisenberg, which are

$$\Delta p_j = \frac{h}{2\pi\Delta j} \qquad j = x, y, z \tag{6.3}$$

and

$$\Delta E = \frac{h}{2\pi \Delta t}.\tag{6.4}$$

From Newton's laws of motion (classical mechanics) we know that for a free particle (one not subject to any external forces),

$$E_{tot} = \frac{1}{2}mv^2 = \frac{p_x^2 + p_y^2 + p_z^2}{2m}.$$
 (6.5)

Hence the time-dependent Schrödinger equation for this system is

$$\frac{ih}{2\pi} \frac{\partial}{\partial t} \Psi(x, y, z, t) = \frac{1}{2m} \left(\frac{h}{2\pi i}\right)^2 \left(\frac{\partial^2}{\partial x^2} + \frac{\partial^2}{\partial y^2} + \frac{\partial^2}{\partial z^2}\right) \Psi(x, y, z, t). \quad (6.6)$$

This differential equation in four variables replaces the algebraic equations of classical mechanics.

In atomic and molecular systems, the electron is not free but is subject to forces described by Coulomb's law (see Sect. 1.3). These are due to its interactions with the nuclei and the other electrons that are present, and they are accounted for by adding a term involving the potential energy function. Thus

$$\frac{ih}{2\pi} \frac{\partial}{\partial t} \Psi(x, y, z, t) = \frac{1}{2m} \left(\frac{h}{2\pi i} \right)^2 \left(\frac{\partial^2}{\partial x^2} + \frac{\partial^2}{\partial y^2} + \frac{\partial^2}{\partial z^2} \right) \Psi(x, y, z, t) - eV(x, y, z, t)\Psi(x, y, z, t).$$
(6.7)

In this time-dependent Schrödinger equation it is assumed that the potential energy function per unit charge, V(x, y, z, t), is a known function of the position and time.

In the usual case where the potential energy function is time-independent, then the wave function can be written in the form

$$\Psi(x, y, z, t) = \psi(x, y, z) \exp\left(-2\pi i \widetilde{E}t/h\right). \tag{6.8}$$

Inserting this into (6.7), we find that the time-independent wave function, $\psi(x, y, z)$, must be determined by solving the time-independent Schrödinger equation (hereafter called the TISE),

$$\frac{1}{2m} \left(\frac{h}{2\pi i} \right)^2 \left(\frac{\partial^2}{\partial x^2} + \frac{\partial^2}{\partial y^2} + \frac{\partial^2}{\partial z^2} \right) \psi(x, y, z) - eV(x, y, z)\psi(x, y, z) \\
= \widetilde{E}\psi(x, y, z). \tag{6.9}$$

Here \widetilde{E} is the time-independent total energy; it should not be confused with the total energy of classical mechanics. To make the TISE easier to write, we use the Laplacian operator discussed in Appendix A and get

$$-\frac{h^2}{8\pi^2 m} \nabla^2 \psi(x, y, z) - eV(x, y, z)\psi(x, y, z) = \widetilde{E}\psi(x, y, z). \tag{6.10}$$

Many people write this equation in an even simpler form, by defining the Hamiltonian operator, named after William Rowan Hamilton (1805–1865), as

$$H = -\frac{h^2}{8\pi^2 m} \nabla^2 - eV(x, y, z), \tag{6.11}$$

so the TISE for a single moving particle becomes

$$H\psi(x, y, z) = \widetilde{E}\psi(x, y, z). \tag{6.12}$$

Note that the operator H acts upon the wave function $\psi(x, y, z)$ not only by multiplying it by constants but also by differentiating it.



Hamilton

Let us now assume that the nucleus of an atom is stationary and use it to define the origin of the coordinate system for each moving electron. It will be more convenient to use dimensionless atomic units (Landau and Lifshitz 1965), where Planck's constant is numerically equal to 2π and the electron mass, the proton charge, and Coulomb's constant $(1/4\pi\varepsilon_0)$ are numerically equal to one. Then when there are n electrons in an atom the Hamiltonian operator is

$$H = -\frac{1}{2} \sum_{i=1}^{n} \nabla_{i}^{2} - \sum_{i=1}^{n} \frac{\widetilde{Z}}{r_{i}} + \sum_{i=2}^{n} \sum_{j=1}^{n-1} \frac{1}{r_{ij}}.$$
 (6.13)

The first term has a Laplace operator for each of the moving electrons, the second term accounts for the Coulomb attractions between each electron and the nucleus of charge \widetilde{Z} , and the last term accounts for the Coulomb repulsions between the electrons. Correspondingly, the wave function depends on the position, \mathbf{r} , of each of the n electrons and can be represented as $\psi(\mathbf{r}^{(n)})$. Therefore the TISE is

$$H\psi(\mathbf{r}^{(n)}) = E\psi(\mathbf{r}^{(n)}). \tag{6.14}$$

Using atomic units has the additional value that the results of calculations do not change even when there are improvements in the values of the fundamental physical constants. Note in particular that the atomic units of length and energy are a_0 , the bohr (2014 CODATA value $0.52917721067 \times 10^{-10}$ m), and E_h , the hartree (2014 CODATA value $4.359744650 \times 10^{-18}$ J).



Oppenheimer

When an atomic ion interacts with a neutral atom, one ordinarily makes the Born–Oppenheimer approximation (Lewars 2003), named after Born and J. Robert Oppenheimer (1904–1967). Thus each nucleus is assumed to be stationary at a particular position, the TISE is solved for the moving electrons, and then the nuclei are moved to new positions and the process repeated. Mathematically, the approximation means that the TISE can be separated into an equation describing the electrons and another describing the nuclei. The latter can be recast as a classical-mechanical equation in terms of a potential energy surface (see Sect. 6.4), i.e. potential energy values as a function of the positions of the atoms in the molecule.

In atomic units, the Hamiltonian operator when there are n electrons and k nuclei in the Born–Oppenheimer approximation is

$$H = -\frac{1}{2} \sum_{i=1}^{n} \nabla_{i}^{2} - \sum_{i=1}^{n} \sum_{\vartheta}^{k} \frac{\widetilde{Z}_{\varphi}}{r_{i\varphi}} + \sum_{i=2}^{n} \sum_{j=1}^{n-1} \frac{1}{r_{ij}},$$
 (6.15)

while the TISE is still given by (6.14). Note that the ϑ index labels the nuclei. There are no terms involving repulsion between the nuclei since they cause a constant shift in the values of E and the calculations described below involve the interaction potential obtained by subtracting from the energy for a specific configuration of the nuclei the energy when the nuclei are all at infinite distance from one another. Usually, the interaction potential energy is a small number obtained by subtracting two large numbers, which will be shown later in this chapter to lead to problems.

For atoms or molecules, solution of the TISE is mathematically impossible unless \widetilde{E} takes on one of a set of discrete values that are connected by integers called quantum numbers. Thus, quantized energy and quantum numbers are an automatic consequence of the TISE and they do not have to be tacked onto the theory, as was the case in Bohr's theory of the atom. The particular values of \widetilde{E} for which the equation can be solved are called the eigenvalues (see Appendix A) of the TISE. Each solution (wave function) is an eigenfunction of the Hamiltonian operator and has a single eigenvalue (energy) associated with it (see Appendix A). However, several wave functions can have the same eigenvalue, a situation said to show degeneracy.

For a solution of the TISE to be physically meaningful, the eigenfunction must satisfy several conditions. One is that it must be single-valued (except for a sign), since the probability, $|\psi(\mathbf{r}^{(n)})|^2 d\mathbf{r}^{(n)}$, in any region, $d\mathbf{r}^{(n)}$, can have only one value. A second is that it must be finite in all regions of space; otherwise the probability would be infinite in some regions. A third is that the eigenfunction must be square-integrable, i.e., its absolute square should give a finite value when integrated over all space. Finally, if we get a number (call it c^{-2}) when the absolute square of the eigenfunction is integrated over all space, then we must be able to normalize the eigenfunction and talk about the square of $c\psi(\mathbf{r}^{(n)})$ as being the probability of finding the particle in the small region near the point $(\mathbf{r}^{(n)})$.

Although it is easy to write the TISE for any atom or molecule, explicit solutions are possible only for atoms with a single electron. This is because of the terms involving electron-electron repulsions, which make it impossible to perform a separation of variables and decompose the TISE into a series of one-dimensional differential equations. For many-electron atoms and molecules, it is therefore necessary to resort to approximations to the TISE that are solved to a specified accuracy on a modern computer.

6.4 Basis Functions for Solution of the TISE

6.4.1 Slater and Gaussian Orbitals

Since the TISE is a linear equation, the method of weighted residuals (see Appendix C) can be used to solve it once we decide what zero-order solution to use or, equivalently, what basis functions to employ. John Clarke Slater (1900–1976) introduced a set of basis functions in 1932 that are modified forms of the orbitals for the hydrogen atom, the modification being that they contain an effective nuclear charge rather than the actual charge. The Slater orbital corresponding to the usual n, l and m quantum numbers is written in spherical polar coordinates as

$$\psi_{n,l,m}(r,\theta,\phi) = N_S r^{n-1} \exp\left(-\frac{\zeta r}{a_0}\right) Y_l^m(\theta,\phi), \tag{6.16}$$

where $Y_l^m(\theta, \phi)$ is a spherical harmonic (see Appendix A) of the type that arises in solving the TISE for hydrogen atom and the orbital exponent, ζ , is dimensionless. The quantity N_S is a normalization factor, chosen so that

$$\int_{0}^{\infty} \int_{0}^{\pi} \int_{0}^{2\pi} \psi_{n,l,m}^{*}(r,\theta,\phi) \psi_{n,l,m}(r,\theta,\phi) r^{2} \sin(\theta) dr d\theta d\phi = 1.$$
 (6.17)

Equation (6.17) shows that using Slater orbitals is equivalent in the method of weighted residuals (see Appendix C) to setting the zero-order solution of the TISE equal to one.



Matrix elements of H involving Slater orbitals are extremely difficult to evaluate, even on a computer. Moreover, a theorem presented (Kato 1957) by Tosio Kato (1917–1999) shows that the electron density has a cusp as the electron approaches the nucleus, i.e. Slater orbitals and the wave function for real orbitals must become infinitely large as the electron-nucleus distance goes to zero.

Most of the computer programs of computational chemistry that are commercially available for solving the TISE are based on Gaussian orbitals (Lewars 2003). These functions do not have cusps, since they are of the form

$$\psi_{n,l,m}(r,\theta,\phi) = N_G r^{n-1} \exp\left(-\frac{\xi r^2}{a_0^2}\right) Y_l^m(\theta,\phi).$$
 (6.18)

Their advantage over Slater orbitals is that the product of two exponentials with squared distances can be expressed as a single exponent involving the square of a different distance, and hence so can an arbitrary number of s-type Gaussian functions (Besalú and Carbó-Dorca 2011). This means that large portions of the integrations involving H can be performed analytically when Gaussian orbitals are used, so that the computer packages can be programmed with essentially exact results that can be evaluated very rapidly. Their lack of a cusp at r=0 means, unfortunately, that it is usually necessary to include 3–6 times more Gaussian than Slater orbitals to obtain a similar level of accuracy.

6.4.2 Classification of Basis Sets by Size

Having decided upon the type of basis functions (Slater or Gaussian orbitals) and the locations for them (the nuclei and perhaps certain ghost locations where no nuclei are found), the most important factor in a computational chemistry calculation is the number of functions to use. The smallest number of functions is just enough to contain all the electrons in the molecule; this is a called a minimum basis set. The minimum basis set for hydrogen and helium is a single s-function. For lithium and beryllium, you need two s-functions. The pattern should be clear.

The next improvement in basis sets is ordinarily obtained by doubling the number, not just by adding one or two. A basis set with twice the minimum number of orbitals is said to be a double-zeta (DZ) basis. (The term "zeta" comes from the fact that the exponent of a Slater or Gaussian orbital contains an adjustable parameter that is usually denoted by ζ .) Doubling the number of basis functions allows for a much better description of the electron distributions in different directions, for example along and perpendicular to a line joining two nuclei.

Doubling the number of 1s functions used for carbon allows for a better description of the real 1s electrons. However, the 1s electrons are almost identical when the carbon atom is part of a molecule as when it is alone, so the improvement resulting from doubling the number of 1s functions is often minimal. Based on this empirical finding, a variation of the DZ basis was developed that only doubles the number of functions used for the valence electrons. Such a split DZ valence basis is then referred to as VDZ, indicating that only the valence orbitals are of double-zeta quality.

The next step in basis set size is triple zeta (TZ). Such a basis contains three times as many functions as the minimum basis. Again, it is often the case that only the number of valence orbitals is tripled, leading to a VTZ basis. Quadruple zeta (QZ), quintuple zeta (5Z) and sextuple zeta (6Z) basis sets are also used, but there are so many split-valence versions of these large basis sets that it is best to list explicitly the number of basis functions of each type, rather than resort to using only an acronym.

6.4.3 Polarization and Correlation in Basis Sets

One often needs to consider functions other than those corresponding to s and p orbitals. In the language of computational chemistry the d, f, g ... functions are denoted as polarization functions, because the use of such functions will allow changes from the symmetry restrictions imposed by the use of s and p orbitals. In the simplest case, the use of p-type functions will allow electrons to be polarized (have different properties along different directions in space), which is not possible using only s-type functions.

Adding a single set of polarization functions (for example, one set of three p-type functions in addition to the single s function for hydrogen or helium) to the DZ basis results in a "double zeta plus polarization" (DZP) basis. However, some researchers add a single set of polarization functions to every atom except hydrogen, on the grounds that doing so for hydrogen requires a huge amount of computing, while the hydrogen nuclei usually sit passively on the outside of the molecule and do not participate in chemical reactions or significantly affect the intermolecular potentials. Hence it is always best to check exactly what a particular author means when the DZP notation is used.

If two sets of polarization functions (with different exponents) are added to a TZ basis of s-type and p-type orbitals, the basis set is called a triple zeta plus double polarization (TZ2P) type. There are so many versions of these large basis sets in use that it is best to list explicitly the number of basis functions of each type.

The motion of real electrons is correlated, since they interact with each other because of their charges. One would therefore like to consider correlation when choosing basis sets to solve the TISE. Two main types of correlation have been identified.

- 1. In-out or radial correlation refers to the situation where one electron is close to, and the other far from, the nucleus.
- 2. Angular correlation refers to the situation where two electrons are in different places around the nucleus, but are still close enough to interact with each other.

To describe radial correlation, the basis set needs functions of the same type of angular momentum but with quite different ζ values. To describe angular correlation, the basis set needs functions of different types of angular momentum but with ζ values that have nearly the same value.

6.4.4 Balanced, Even- and Well-Tempered Basis Sets

Experience has shown that there is little value in violating the following rule of thumb: the number of functions of a given type should be less than the number used for the previous type, i.e. the type with angular momentum that is one unit smaller. When this rule is followed, the basis set is said to be balanced. Thus a 3s2p1d basis set is balanced, as is a 5s3p2d basis, but a 3s2p2d1f1g set is unbalanced because it is too heavily polarized (has too many functions of high angular momentum). Note that in computational chemistry 3s means three functions of s type, unlike the similar notation in quantum mechanics, which means n=3 and l=1 for an electron in an atom.

Determining the best values for the ζ used in a balanced set of either Slater or Gaussian orbitals is an example of a highly non-linear, least-squares problem (see Appendix A). Moreover, as the basis set becomes large, the functions become linearly dependent upon one another and the energy becomes a very flat function of the ζ values. Furthermore, it becomes difficult to distinguish local minima for the energy from the global minimum that is usually of interest. So what should we do to determine these values?

Careful analysis of the many basis sets that have been used for solving the TISE (Nagy and Jensen 2017) has revealed that the ratio between successive ζ values is approximately constant. If this ratio if assumed to be perfectly constant, then there are only two parameters that must be determined for each type of basis function (s-type, p-type, etc.). These two are the values of $\widetilde{\alpha}$ and $\widetilde{\beta}$ such that

$$\zeta_i = \widetilde{\alpha}\widetilde{\beta}^i, \tag{6.19}$$

where i=1 for the first functions of this type, i=2 for the second, etc. Basis sets constructed in this way are said to be even-tempered.

Even-tempered basis sets have the same ratio between the ζ values over the whole range of functions. For chemical considerations, it is usually preferable to cover the valence region better than the core. This may be achieved by using a "well-tempered" basis set of m functions of the same type in which the exponents are related by the equation

$$\zeta_{i} = \widetilde{\alpha}\widetilde{\beta}^{i-1} \left[1 - \widetilde{\gamma} \left(\frac{i}{m} \right) \widetilde{\beta}^{\delta} \right]. \tag{6.20}$$

Optimization of basis sets by determining the ζ values is not something the average user of a computational chemistry program needs to worry about. Optimized basis sets of many different sizes and qualities are built into the program or may be read by the program from tables supplied with the software package. The user "merely" has to select a suitable basis set.

6.4.5 Contracted Basis Sets

In computational chemistry, many of the functions in a basis set are primarily involved with describing the energetically important but chemically uninteresting core electrons. This fact is the foundation for the use of contracted basis sets. Consider, for example, a 10s2p basis set for carbon, which has 10 s-type functions and 2 sets of p-type functions; each p set has 3 functions, since each p orbital in an atom can have any one of three values for the magnetic quantum number. Having optimized the ten exponents for the s-type functions (by variation methods such as those described in the next section), suppose we find that six of the exponents are so large that they describe primarily 1s electrons, that two more are of intermediate size and hence describe 2s electrons when they are in the inner hump of the orbital, while the final two describe 2s electrons in the outer hump. We might decide to keep the coefficients in front of the first 6 s-type functions constant, thus describing a 1s orbital in carbon as a fixed linear combination of the six functions. We might similarly contract the remaining four functions into only two functions. We will have thus contracted the 10s2p set of "primitive" basis function into a "contracted" set that is described as 3s2p. The notation used is $(10s2p)\rightarrow (3s2p)$, or 10s2p/3s2p. Note that this notation does not tell how the contraction was done but only the number of primitive and contracted basis functions of each type.

Combining the full set of primitive Gaussian orbitals into a smaller set of functions by forming fixed linear combinations is known as basis set contraction. The resulting functions are known as contracted Gaussian orbitals. Warning: the previously introduced acronyms such as DZP, TZ2P, etc. refer to the number of contracted basis functions.

6.4.6 Pseudopotentials

As computer speed and storage capacity advanced, more and more electrons could be treated accurately using the basis functions discussed above and the calculation methods to be described below. Nevertheless, when atoms on the third row and below on the Periodic Table are of interest, either alone or as part of a molecule or part of an atomic ion-atom pair whose interaction governs the mobility, diffusion and reactions of interest in this book, it is still necessary to use approximations that make solving the TISE possible. One method for doing this is to employ a mixed quantum-classical approach, where the majority of the system is treated with Newton's laws of motion while a few parts are treated with quantum mechanics.

A mixed quantum-classical approach starts by making a distinction between the core and valence electrons in the system. Then one uses pseudopotential theory (Szasz 1985; Kahros and Schwartz 2013) to determine an effective potential that represents the interactions of the valence electrons with the group of core electrons. Many of the mixed quantum-classical schemes in use today employ the central-field (also called the frozen-core) approximation (Pilar 1968). The valence electrons are considered to be moving under the influence of an electric field that is created by the nucleus and the core electrons, without directly interacting with the individual charges in that "core". The approximation consists of neglecting the motion of the inner electrons, neglecting their individual interactions with the valence electrons, and thus assuming that the potential acting upon the valence electrons is static. Since the inner electrons completely fill their orbitals, by Unsőld's theorem (discussed in Appendix A) they create a spherical potential that is weaker than the potential due to the nucleus alone. The overall effect is that the inner electrons simply shield the valence electrons from feeling the full charge of the nucleus, the effective charge being reduced to some value that is smaller than the actual charge on the nucleus. We will return to the frozen-core approximation below.

Pseudopotentials are sometimes called effective core potentials (ECP). By ECP one usually implies that the pseudopotential has been optimized while taking relativistic effects into account. Although relativity is considered later in this chapter, it is worth noting that its effects are much larger on core electrons that are close to the nucleus than they are on valence electrons. Hence it is often the case that one can use an ECP in solving the TISE, without otherwise taking account of relativity.

It is beyond the scope of this book to discuss approaches that are being made (Kahros and Schwartz 2013) to use pseudopotentials that avoid the frozen-core approximation, particularly since such approaches are likely to have little influence on the calculation of interaction potentials between an ion and a neutral. Instead, we turn to the most commonly used method for solving the TISE, the variation method.

6.5 Variation Method

The variation method is based on choosing trial wave functions (i.e., basis functions) and varying the ζ parameters (and others that are discussed below) until a minimum energy is reached. To understand this method, suppose for a particular problem involving a single electron that we can solve the TISE exactly. This means that we know the eigenvalues (energies) for which a solution can be obtained, and that we know, for any particular energy, \widetilde{E} , a wave function, $\psi(x, y, z)$, that satisfies (6.12) with this value of \widetilde{E} . We can then multiply both sides of (6.12) by the complex conjugate of the wave function, $\psi^*(x, y, z)$, and integrate over all space. Because \widetilde{E} is a constant, we get

$$\int \psi^*(x, y, z) H \psi(x, y, z) \ dx \ dy \ dz$$

$$= \widetilde{E} \int \psi^*(x, y, z) \psi(x, y, z) \ dx \ dy \ dz. \tag{6.21}$$

The integral on the right-hand side of this equation is one if the wave function was normalized originally. The integral on the left-hand side is referred to as a diagonal matrix element of H, with the full matrix being obtained when the two wave functions in it are changed systematically.

Measurable physical properties are real, not complex. This can be shown mathematically to mean that the operators corresponding to measurable properties must always be Hermitian operators, i.e. they must satisfy the constraint,

$$\int \psi_j^*(x, y, z) H \psi_k(x, y, z) \, dx \, dy \, dz$$

$$= \int \psi_k(x, y, z) H^* \psi_j^*(x, y, z) \, dx \, dy \, dz, \quad (6.22)$$

where H^* indicates the complex conjugate of H. In terms of matrix elements, this means that H_{jk} must equal H_{kj}^* . It also means that the eigenfunctions corresponding to different eigenvalues (different values of the measurable property) are orthogonal functions, i.e. they satisfy the condition

$$\int \psi_j^*(x, y, z)\psi_k(x, y, z)dxdydz = 0 \qquad j \neq k.$$
 (6.23)

If two or more different eigenfunctions correspond to the same eigenvalue (a situation referred to as degeneracy), then the eigenfunctions may not be orthogonal, but it is always possible to take linear combinations of them and construct an equal number of functions that are orthogonal.

Now suppose that we do not know the exact solution of the TISE, but that instead $\psi(x, y, z)$ is a trial function obtained in some way to be specified later. We could use the trial function in the integrals in (6.21) and calculate a quantity, \widetilde{E} , with the

6.5 Variation Method 169

dimensions of energy. Since H is a Hermitian operator, mathematicians can prove rigorously that this calculated \widetilde{E} must always be either greater than or equal to the actual energy, with equality happening if and only if the trial function is exactly equal to the true wave function. Thus the calculated energy is an upper bound to the actual energy.

It should be noted that contracting a basis set will always increase the energy, since it results in a smaller number of parameters that can be changed in the variation method for solving the TISE. For the same reason, it also makes the basis set less flexible. However, the reduction in the amount of computer time needed to work with a contracted basis set may be great enough that the loss in accuracy can be tolerated (Nagy and Jensen 2017).

6.6 Electron Spin

Before we can proceed we must consider how electron spin can be incorporated into the TISE. Remember from general chemistry that the TISE can be related to the Periodic Table by imposing the condition that there are at most $2n^2$ electrons with principle quantum number n in an atom. It is easy to show from the rules governing the angular momentum, l, and magnetic, m, quantum numbers that arise from the solution of the TISE for H that the maximum number should be only n^2 . This suggests that somehow a factor of 2 is missing in the results based on the TISE. Similarly, the lowest energy line of the Balmer series in the emission spectrum of hydrogen atom (an electron with n=2 moving to a state with n=1) has been found, when looked at very carefully, to consist of two lines with wave lengths about 0.03 nm apart. In the middle 1920s a number of other experimental anomalies were discovered—the TISE is not correct, since the exact solution of this equation in this case does not agree with experiment!



In 1924, Wolfgang Pauli (1900–1958) suggested that the experimental anomalies noted above could be explained if electron spin is grafted onto the TISE. We will take up the details of how this is done shortly, but it suffices here to note that Pauli's

method means that a spin quantum number is assigned to each electron and that this fourth quantum number can have only one of two possible values: s = +1/2 or s = -1/2.

A bit of history is in order here. Ralph de Laer Kronig (1904–1995) was the first person to propose that the fourth quantum number was a spin number, but Kronig did not publish his proposal due to opposition by Pauli, who later changed his mind. In 1925, Samuel Abraham Goudsmit (1902–1978) and George Eugene Uhlenbeck (1900–1988) postulated that the electron had an internal angular momentum due to a spinning motion about an axis passing through its center of mass. They therefore introduced exactly the same quantum number as Kronig and Pauli.

The spin quantum number has no physical significance. After all, an electron is more like a wave than a particle when it is inside an atom, and the Uncertainty Principle greatly restricts our ability to find it, much less determine which way it is spinning. It seems ludicrous then to think that the electron is spinning in one of only two possible directions, east to west or west to east. Nevertheless, the use of the spin quantum number made the TISE come into better agreement with the experimental results for the hydrogen atom. The modified theory is in particularly good agreement with the 1921 results of Otto Stern (1888–1969) and Walther Gerlach (1889–1979), who studied how a beam of hydrogen atoms was split into two separate beams by a magnet.



Stern Gerlach

Since there is no classical counterpart to electron spin, it is impossible to express the spin operators or their eigenfunctions in terms of the dimensions of space and time. Instead, for a single electron we introduce a new coordinate, ξ_s , that defines the space in which the spin angular momentum operator, **S**, exists. Furthermore, we will introduce two eigenfunctions, $\alpha(\xi_s)$ and $\beta(\xi_s)$, such that

$$S_{z}\alpha(\xi_{s}) = \frac{1}{2} \left(\frac{h}{2\pi}\right) \alpha(\xi_{s}) \qquad S_{z}\beta(\xi_{s}) = -\frac{1}{2} \left(\frac{h}{2\pi}\right) \beta(\xi_{s})$$

$$S^{2}\alpha(\xi_{s}) = \frac{3}{4} \left(\frac{h}{2\pi}\right)^{2} \alpha(\xi_{s}) \qquad S^{2}\beta(\xi_{s}) = \frac{3}{4} \left(\frac{h}{2\pi}\right)^{2} \beta(\xi_{s}). \tag{6.24}$$

6.6 Electron Spin 171

It should be noted that the z axis here is arbitrary and only has significance if there is an external field that defines it. Furthermore, when integrated over all ξ_s , $\alpha(\xi_s)$ and $\beta(\xi_s)$ are orthonormal (see Appendix A).

Table 6.1 Relative ordering of the orbital energies

			1s
			2s
		2p	3s
		2p 3p	4s
	3d	4p 5p	5s
	4d	5p	6s
4f 5f	5d	6p	7s
5f	6d	7p	8s

Results obtained for multi-electron atoms from the TISE supplemented with electron spin can be rationalized with four simple rules and Table 6.1.

- 1. The relative ordering of the orbital energies usually follows the pattern in Table 6.1 (only the first 8 rows are shown). While this pattern is almost always appropriate for neutral atoms, it is only generally accurate for singly-charged ions, and can often give incorrect results for doubly- or triply-charged ions. In particular, while the 4s orbital is lower in energy than the 3d orbital (comes earlier when reading Table 6.1 in the usual left-to-right manner) for neutral atoms, the reverse is true for +2 and +3 ions.
- 2. The Pauli exclusion principle discussed below means that no two electrons can have all four quantum numbers the same.
- 3. The aufbau (German for "building up") principle is an approximation that means we can use a simple building-block approach to find the electron configuration in a multi-electron atom. Thus, electrons are added to orbitals in the order of increasing energy so long as the Pauli exclusion principle is obeyed. In general, each orbital is filled to capacity (two for an s orbital, 6 for a p orbital, etc.) before the next is started.
- 4. Hund's rules describes how orbitals of equal energy are filled. It was developed by Frederick Hermann Hund (1896–1997) and is discussed more fully in Appendix B. In general, the order of filling is such that as many electrons remain unpaired as possible and such that unpaired electrons have the same spin.



Hund

A rigorous formulation of the Pauli exclusion principle is based on symmetry arguments. Suppose there are two electrons in an atom that are together described by a wave function ψ and a probability density $\psi^*\psi = |\psi|^2$. If the two electrons swap places, there cannot possibly be a change in the electron probability density, so the swap changes ψ into either itself or its negative. In the first case we call the wave function symmetric for electron exchange, while in the second we call it antisymmetric. The experimental fact is that wave functions for electrons are always antisymmetric, so this is added to the postulates of quantum mechanics and the TISE.

Since spin-space is independent of the ordinary space of position and time, the total wave function for an electron can be written as a product of a spin part and a spatial part. Hence if the spatial part is symmetric then the spin part must be antisymmetric, and vice versa.

Consider two electrons, 1 and 2, in states that are each specified by four quantum numbers, i.e., (n_1, l_1, m_1, s_1) and (n_2, l_2, m_2, s_2) . An antisymmetric wave function for the pair would be

$$\psi = \psi_{n_1, l_1, m_1, s_1}(1)\psi_{n_2, l_2, m_2, s_2}(2) - \psi_{n_1, l_1, m_1, s_1}(2)\psi_{n_2, l_2, m_2, s_2}(1), \tag{6.25}$$

since if we exchange the labels 1 and 2 then ψ turns into $-\psi$. Suppose, however, that all four quantum numbers were the same for the two electrons. Then the subscripts are the same and $\psi=0$, i.e., the system cannot exist in this state. We conclude that the more rigorous statement of the Pauli exclusion principle reduces to the form given above.

Consideration of H_2 may help explain how the concept of electron spin is applied to molecules. According to the Pauli exclusion principle, the wave function for a system of electrons around two fixed nuclei (i.e., a system in which the Born–Oppenheimer approximation applies) must be anti-symmetric for the simultaneous exchange of the spatial and spin coordinates of any pair of electrons. If we omit the variables that indicate the dependence upon the positions of electrons 1 and 2, a symmetric wave function, ψ_S , must be multiplied by an anti-symmetric spin function and an antisymmetric wave function, ψ_A , be a symmetric spin function. For the pair of electrons in H_2 , we can set up four possible products of the spin functions for the two electrons. Omitting the variables ξ_S , they could be

6.6 Electron Spin 173

$$\alpha_1 \alpha_2 \quad \alpha_1 \beta_2 \quad \beta_1 \alpha_2 \quad \beta_1 \beta_2.$$
 (6.26)

Two of these are symmetric to exchange of the 1 and 2 labels, while the other two are neither symmetric nor anti-symmetric. We can, however, make linear combinations of them to get four other spin functions,

$$\alpha_1 \alpha_2 \quad \beta_1 \beta_2 \quad \alpha_1 \beta_2 + \beta_1 \alpha_2 \quad \alpha_1 \beta_2 - \beta_1 \alpha_2.$$
 (6.27)

The first three of these functions are symmetric to exchange of electrons, while the fourth one is anti-symmetric. We are thus led to four possible wave functions for the hydrogen molecule that include spin:

$$\psi(1) = \psi_A \alpha_1 \alpha_2 \tag{6.28}$$

$$\psi(2) = \psi_A \beta_1 \beta_2 \tag{6.29}$$

$$\psi(3) = \psi_A \left[\alpha_1 \beta_2 + \beta_1 \alpha_2 \right] \tag{6.30}$$

and

$$\psi(4) = \psi_S \left[\alpha_1 \beta_2 - \beta_1 \alpha_2 \right]. \tag{6.31}$$

Note that (6.28)–(6.30) form the so-called triplet state that is anti-bonding in H_2 . Equation (6.31) is the so-called singlet state that it is bonding.

6.7 Slater Determinants

The Pauli exclusion principle requires the true wave function of a multi-electron atom or molecule to change its algebraic sign when the coordinates (both spatial and spin) of any two electrons are interchanged. Hence the trial functions used in numerical solutions of the TISE should have this property as well. A simple way to satisfy this requirement is to use determinants (see Appendix A) to construct the trial functions from basis functions. A Slater determinant for *n* electrons has the form

$$\psi(\tau) = \frac{1}{\sqrt{n}} \begin{vmatrix} \psi_{1s}(1)\alpha(1) & \psi_{1s}(2)\alpha(2) & ... & \psi_{1s}(n)\alpha(n) \\ \psi_{1s}(1)\beta(1) & \psi_{1s}(2)\beta(2) & ... & \psi_{1s}(n)\beta(n) \\ \psi_{2s}(1)\alpha(1) & \psi_{2s}(2)\alpha(2) & ... & \psi_{2s}(n)\alpha(n) \\ ... & ... & ... & ... \end{vmatrix}$$
 (6.32)

Here $\psi_{1s}(n)\alpha(n)$ represents the product of a 1s basis set (a Slater or Gaussian orbital) for electron n and the α spin function (say for spin +1/2), etc. Thus, the n columns correspond to the n electrons, and the n rows correspond to the n lowest quantum states. Interchanging the coordinates of two electrons means interchanging two columns, which changes the sign of the determinant. The factor of $1/\sqrt{n}$ ensures

that the multi-dimensional wave function, $\psi(\tau)$, is normalized if each of the basis functions in the determinant is normalized.

Each term in the Slater determinant can be multiplied by a single adjustable parameter, if the normalization factor is adjusted appropriately. This gives a total of n such parameters for each of the n wave functions. Since each basis function has a ζ parameter, there are a total of 2n parameters in each of the n different wave function represented by the determinant. One keeps adjusting the 2n parameters until the calculated energy reaches its minimum value, at which point it is assumed (based on the variation principle) that the calculated energy is a good approximation to the true energy of that state of the atom. If all n states are used in the variation method, then the final values for all of the $2n^2$ coefficients make the linear combination of atomic orbitals (LCAO) represented by (6.32) a good approximation to the true set of n wave functions for this atom.

There are some problems with this technique. First, if there are too many adjustable parameters, the computer will spend a long time "wandering around in parameter space", as it constantly repeats the calculations with slightly different values. Second, it is possible that the computer will find a local minimum in parameter space, not the true minimum; in other words, continually getting values that change only in the last significant figure is not a guarantee that the answer is this accurate. Finally, the form of the basis functions (even- or well-tempered, contracted, etc.) often constrains the accuracy of the final results to an unacceptable degree; for more reliable results, a number of basis functions of different types should be employed.

It is easy to extend Slater determinants to molecules. All one must do is label each basis function with a symbol that indicates which location it is centered around. This greatly expands the size of the determinant in (6.32) and greatly increases the work involved in determining integrals such as those in (6.21). Conceptually, however, it makes no difference.

6.8 The Self-consistent-Field and Hartree–Fock Methods

An important method for dealing with molecules or with atoms containing multiple electrons is the self-consistent field (SCF) method. This method was introduced in 1928 by Douglas Rayner Hartree (1897–1958) and then improved by Vladimir Alexandrovich Fock (1898–1974). Technically, Hartree's method is the SCF method, but when spin is included it is the Hartree–Fock, or HF, method.

Treating an atom in either method starts with selection of individual orbitals for the electrons; e.g., ψ_{1s} , ψ_{2s} , etc., using either Slater or Gaussian functions given by (6.16) and (6.18), respectively. Any such orbital that is completely filled must have spherical symmetry, as a consequence of a theorem due to Albrecht Otto Johannes Unsőld (1905–1995) and discussed in Appendix A. If the outer orbital is not completely filled, then its electronic distribution can be averaged over all angles, which forces it to have spherical symmetry.







Unsőld

Hartree Fock

For molecules, one starts by specifying the molecular structure (the location of the nuclei) and then chooses individual molecular orbitals. Usually, the molecular orbitals are LCAO. Here, however, one must specify which nucleus each of the orbitals is centered around. In some case, orbitals are centered around locations where there are no nuclei; these are called ghost orbitals, and they are most often located at the center of a bond.

The second step starts by considering one particular electron in the potential field created by the nucleus around which it is centered, the other nuclei in their fixed positions, and the average electronic distribution of the OTHER electrons represented by the orbitals created in step one. The resulting spherical symmetry means that the TISE governing the chosen electron will be separable and spherical harmonics about the location of the selected electron will be the eigenfunctions of the angular terms in the TISE. One is left with a second-order, ordinary differential equation in one variable (the radius of the chosen electron) to solve numerically; this is much simpler than solving a partial differential equation in many variables. This results in a new, hopefully improved, wave function for the selected electron, one that can be substituted into the set of wave functions for the system, replacing the original orbital for the electron.

The second step is repeated for each of the electrons of interest, in an iterative procedure that stops only when there is no substantial change in the any of the orbitals.

The final step in the SCF method is to use the final set of orbitals in the variation method. In other words, adjustable coefficients are used to make the complete wave function a LCAO of the atomic orbitals obtained from repetition of step two, and the coefficients are changed so as to reach a minimum value for the energy.

With current computational chemistry programs, the steps are (Lewars 2003):

- 1. The user specifies the geometry of the molecule (i.e. the location of the nuclei and ghost orbitals, if any), the total charge, the electronic state of interest (e.g., singlet), the desired accuracy and the atomic basis set to be used. The latter is ordinarily done by selecting from one of the pre-programmed sets in common use.
- 2. The computer program calculates the kinetic energy, potential energy and overlap integrals, i.e. integrals that involve separate terms in the Hamiltonian operator.

- 3. The program constructs an overlap matrix from overlap integrals like the left-hand side of (6.23); it then determines the matrix that will diagonalize the overlap matrix.
- 4. The program calculates the initial "Fock" matrix using the kinetic energy and potential energy integrals and a guess (made by the program) of coefficients for the LCAO expression for the molecular orbitals.
- 5. The program uses the diagonalizing matrix from step 3 to transform the Fock matrix to a form based on an orthonormal set of functions derived from the original atom-centered and ghost basis functions.
- 6. The program diagonalizes the new Fock matrix to get the energies and the new coefficients for the LCAO expression.
- 7. The program uses the diagonalizing matrix from step 3 to back-transform the new coefficients so that they provide solutions to the original HF equations, complete with new energy values.
- 8. The program compares the new coefficients to the old ones, or it compares the new energies to the old ones. If the comparison does not meet accuracy standards set by the user, then the program returns to step 2. Otherwise, the program stops after printing all of the information that the user has requested.

6.9 Configuration Interaction

The HF method for solving the TISE gives the best (lowest) energy that can be obtained with a single-determinant wave function that is constructed from the chosen set of basis functions. Moreover, modern computers are so fast that they can compute these HF energies very rapidly, for any atom or for reasonably-sized molecules. Such energies are usually within 99% of the best values that could be obtained with a given set of basis functions. The problem is that even a 1% error in atomic units is much larger than can be tolerated if the results are to be compared to experiment. Hence much effort has been spent developing methods more accurate than HF.

The difference between the HF energy and the lowest possible energy obtained when a particular basis set is used in a variation solution of the TISE is called the electron correlation energy. Physically, the electron correlation energy corresponds to the motion of the electrons being correlated so that, on average, they are further apart than is described by the HF wave function.

It might be thought that the correlation between pairs of electrons belonging to the same molecular orbital would be the biggest part of electron correlation. This is not the case, however, since the number of electron pairs belonging to different molecular orbitals grows much faster (as the molecular size grows) than the number in the same orbitals. For example, consider the four valence orbitals for methane. There are four intra-orbital electron pairs of opposite spin (one pair for each CH bond), but there are $4 \times 3 = 12$ inter-orbital pairs of opposite spin and also 12 inter-orbital pairs of the same spin. A typical value for the intra-orbital pair correlation of a single bond is $80 \, \text{kJ/mole}$, while that of an inter-orbital pair is (if the two orbits are in adjacent

bonds) about 4 kJ/mole. Hence in methane the intra-orbital pair correlation energy is about 320 kJ/mole while the inter-orbital pair correlation energy is about 96 kJ/mole. In general, the two types of correlation energy are often comparable in magnitude.

The Slater determinate given in (6.32) has just enough basis functions to create enough wave functions to hold all of the electrons in an atom. The configuration interaction (CI) method involves adding one or more basis functions corresponding to excited electronic states of the system, states that do not ordinarily contain electrons. For example, in an investigation of sodium atom, which has a single valence electron in the 3s orbital, one might add functions that correspond to a 3p or 3d orbital. In general, adding more terms leads to closer approximations to the true energy, at the cost of increased computer time. The question that must be addressed for molecules is what additional functions to add and how to do so.

The how question is the easier one. In order to improve upon the HF results while still using the same basis set, the trial wave function must contain more than one Slater determinant. A general multi-determinant wave function can be written as

$$\psi = \widetilde{a}_0 \psi_{HF} + \sum_{i=0}^n \widetilde{a}_i \psi_i, \tag{6.33}$$

where ψ_{HF} is the Hartree–Fock determinant (wave function) and the ψ_i are excited Slater determinants that will be discussed in the next section. Since the HF energy is typically 99% of the total energy, \widetilde{a}_0 is close to 1 and the small contributions of the other determinants is reflected by the fact that their coefficients, \widetilde{a}_i , are found to be small after the variation method has been used to determine them.

A final general comment is that the number of basis functions in the Slater determinant limits the description of the molecular orbitals for the electrons, while the number of determinants limits the description of electron correlation energy. In addition, the mental picture of electrons residing in orbitals has to be abandoned when electron correlation is considered. Instead, one must use a mental picture that focuses on the electron density.

6.10 Excited Slater Determinants

Suppose we are interested in a system with n electrons and we want to use m > n basis functions. A Slater determinant for such a system is of dimension $n \times n$, since it has n/2 spatial orbitals and 2 spin functions for each (giving a total of n spin-orbitals). Solutions of the TISE with such a Slater determinant, based on m atomic orbitals for each wave function, will yield n/2 occupied molecular orbitals and m - n/2 unoccupied (virtual) orbitals. Note that this means there will always be more virtual than occupied molecular orbitals (except in the case of a minimum basis set, where there will be the same number of both types).

If we have solved the TISE with the Hartree–Fock method, then we clearly know all of the wave functions in the Slater determinant and all of the virtual molecular orbitals. By replacing molecular orbitals that are occupied with virtual orbitals, it is possible to generate from the Slater determinant a whole series of determinants. These are denoted by the number of occupied molecular orbitals that have been replaced by unoccupied ones, so we refer to the new determinants as Singles (S), Doubles (D), Triples (T), Quadruples (Q), etc. More about this will be given in the next section.

The total number of determinants that can be generated depends on the size of the basis set; the larger the basis set, the more virtual molecular orbitals there are and the more excited determinants that can be constructed. If all possible determinants in a given basis set are included, all of the electron correlation can be recovered, in principle. For an infinite basis set, this in principle means that the TISE can be solved exactly. Remember, however, that such an exact solution does not necessarily correspond to the experimental results, since the use of the Born–Oppenheimer approximation means that the nuclei have been assumed to be stationary. Moreover, the use of the TISE is itself an approximation, since it ignores the effects that are built into the Dirac equation and the even more involved equations that are described below.

6.11 More About Basis Sets

6.11.1 Correlation-Consistent and Complete Basis Sets

Simple basis sets of either Slater or Gaussian functions often do not lead to rapid convergence when electron correlation is taken into account. The most widely used basis sets that do converge rapidly in CI calculations are correlation-consistent (cc) basis functions that are optimized using CISD wave functions. Those developed by Thom H. Dunning, Jr. and coworkers are designed for converging post-HF calculations systematically to the complete basis set limit using empirical extrapolation techniques (Nagy and Jensen 2017). A bibliography that describes the development of the cc family of basis sets has been discussed by Peterson (2018a). Most of these basis sets now commonly found in software packages or can be downloaded from a repository (Peterson 2018b).

For first- and second-row atoms, the basis sets usually used are cc-pVXZ, which means a correlation-consistent, polarized valence basis set, with X = D indicating that a double zeta basis (usually of Gaussian orbitals) was used to start the process of constructing the cc basis set. Similarly, X = T, Q, .. indicates the use of basis sets that are triple zeta, quadrupole zeta, etc. It has been shown that the cc wave functions converge smoothly toward a basis set limit, said to be obtained in the complete basis set (CBS) limit sometimes indicated by setting $X = \infty$. As a reminder from

Appendix A, a basis set is said to be complete if an arbitrary function satisfying the same restrictions as the basis functions can be expanded in term of them (Pilar 1968).

A diffuse basis set of some angular momentum type (s, p, etc.) is actually a set of functions (1 for s, 3 for p, etc.) in which the ζ value is very small. This means that the orbital described by a diffuse basis set is much larger than a similar orbital of the same type. Diffuse functions are most often added for describing ions and longrange interactions such as Van der Waals forces, or to perform electronic excited-state calculations. When one set of diffuse functions is added for each type of orbital, the result is called an aug-cc basis set. As an example, a cc-pVDZ basis set for C is 3s2p1d, while an aug-cc-pVDZ basis is 4s3p2d.

Because of the way augmented basis sets are constructed, extrapolation towards the CBS limit can be accomplished easily for almost any property of interest. However, care must be taken when extrapolating energy differences, as the individual energy components converge at different rates. In particular, the Hartree–Fock energy converges exponentially, whereas the correlation energy converges polynomially.

For larger atoms, the cc basis sets can be augmented with further functions that describe core electron correlation. These core-valence sets (cc-pCVXZ, with C representing core) can be used to approach the exact solution to the all-electron problem, and they are necessary for accurate geometry and nuclear property calculations.

Weighted core-valence sets (cc-pwCVXZ, with wC representing weighted core) are also in use. The weighted sets aim to capture core-valence correlation, while neglecting most of core-core correlation, in order to yield accurate geometries with smaller cost than the cc-pCVXZ sets.

It should be clear that basis set improvements are a focus of research in computational chemistry. Unless you are intimately involved in such research, the most important thing to look for is an indication that the results you want to use have been computed with a large basis set that is approaching the CBS limit.

6.11.2 Frozen Core and Frozen Virtuals Approximations

For chemical reactions and for interactions between an ion and a neutral, the important things happen in the valence orbitals, with the core orbitals remaining almost constant. In many cases, therefore, we can focus attention on orbitals associated with the valence electrons. Limiting the number of Slater determinants to only those that can be generated by replacing valence orbitals with excited orbitals is a more precise definition of the frozen core approximation discussed above.

The frozen core approximation is not justified in terms of total energy, since the correlation of the core electrons gives a substantial contribution to the total energy. Instead, it is argued that the error made in the frozen core approximation is approximately constant and so can be ignored when computing energy differences (since the zero of energy is completely arbitrary). Another justification for the frozen core approximation is that the standard basis sets aren't really appropriate for calculating the correlation energy of core electrons. In order to represent the angular correla-

tion of core electrons, we must include higher angular momentum functions with approximately the same exponents as the s and p functions used for the core electrons. (Think of this as requiring 1p functions to allow for correlation of 1s electrons!) Hence, allowing excitations of the core electrons in a standard basis set does not really correlate them properly.

In some cases, the highest virtual orbitals (corresponding to anti-bonding combinations of the core electrons) are not allowed to be used in generating S, D, T or Q determinants; this is called the frozen virtuals approximation.

6.11.3 Basis Set Superposition Error

In quantum chemistry, calculations using finite basis sets are susceptible to basis set superposition error (BSSE). As the atoms of interacting molecules approach one another, their basis functions overlap. Each atom "borrows" functions from other nearby components, effectively increasing its basis set and improving the calculation of derived properties such as energy. If the total energy is minimized as a function of the system geometry, the short-range energies from the mixed basis sets are compared with the long-range energies from the unmixed sets, and this mismatch introduces an error.

Other than using infinite basis sets, two methods exist to eliminate the BSSE. The one most commonly used is the counterpoise method (CP). Here the BSSE is calculated by redoing all of the calculations using the mixed basis sets, and the error is then subtracted a posteriori from the uncorrected energy. (The mixed basis sets are realized by introducing basis set functions which have no electrons or protons.) The errors inherent in the CP correction of BSSE disappear more rapidly than the total value of BSSE in larger basis sets. Hence in most cases there is no need to go beyond the CP correction.

6.12 Electron Correlation Calculations

6.12.1 Overview

There are three main methods for calculating electron correlation: configuration interaction (CI), many-body perturbation theory (MBPT) and coupled-cluster (CC) methods. Here we will only discuss CI. To facilitate the notation, it is furthermore going to be assumed that the total number of electrons is even (technically, this is a restricted Hartree–Fock or RHF approach). Finally, it should be noted that, although the Slater determinants are composed of spin-orbitals, the Hamiltonian operator in the TISE is independent of spin, so the spin dependence of the determinants in the

CI method can be factored out; all we need to discuss is the spatial dependence of the integrals.

In CI, (6.33) indicates that the trial wave function is written as a linear combination of Slater determinants, with expansion coefficients determined by requiring that the energy should be a minimum when calculated by the variation method. It is also assumed that the molecular orbitals used to compute the S, D, T, ... excited Slater determinants are the virtual orbitals obtained from a HF calculation, and that they are kept fixed thereafter. The minimization of the energy must be constrained so that the total CI wave function is normalized, which is done by using Lagrange multipliers (see Appendix A). This means that the variation problem is transformed into solving a set of CI secular equations, which can be written in matrix form. The CI energy is the lowest eigenvalue of this matrix equation; the second lowest eigenvalue corresponds to the first excited state, etc.

The CI matrix elements can be evaluated by the same technique used in calculating the energy of a single determinant via the HF equations. This involves expanding the determinants into a sum of products of molecular orbitals and then expressing the CI matrix elements in terms of the matrix elements in the HF method. Fortunately, many of the CI matrix elements are equal to zero. For example, if two determinants have different total spin, then the corresponding matrix element is zero because the Hamiltonian operator does not contain spin. To take maximum advantage of this, linear combinations of the determinants are constructed so that they are proper spin eigenfunctions of H. Such linear combinations of determinants are called spinadapted configurations by some researchers and configurational state functions by others.

If the molecule contains symmetry, there are additional CI matrix elements that become zero. In particular, the Hamiltonian operator always belongs to the totally symmetric representation, so if two determinants belong to different irreducible representations, the CI matrix element is zero. This is why it is important to tell a computer program at the beginning what type of symmetry the molecule has (by telling it the multiplicity, the value of 2S+1, where S is the total spin quantum number).

Mathematicians have established that in the limit of large basis sets, all CI methods formally scale as m^5 , where m is the number of basis functions. To see what this implies, consider water with a DZP-type basis set of 24 functions. Allowing all possible excitations of the 10 electrons generates

$$\frac{24!}{10!(24-10)!} = 1,961,256 \tag{6.34}$$

S-type determinants, and a total of 451,681,256 determinants when all possible types are considered. The variation wave function thus contains roughly half a billion parameters, not including any ζ values in the Slater or Gaussian orbitals. This means that the number of entries in the CI matrix is of the order of the square of half a billion. Although a determination of the lowest eigenvalue of this problem can be made in a few hours on a modern computer, the result is only a single number and it is still

some 0.2 E_h (500 kJ/mole) larger than the experimental value! Full CI calculations are thus not a routine computational procedure for including electron correlation in anything except the smallest molecules.

6.12.2 Truncated Configuration Interaction

In order to develop a computationally tractable procedure, the number of excited Slater determinants in the CI expansion must be limited. Truncating the excitations at level 1 (CI with Singles, or CIS) does not give any improvement over the HF results, as all matrix elements between HF wave functions and singly excited determinants are zero. Thus the lowest CI level that gives an improvement over the HF result is CID (CI with Doubles). Since there are so many more doubly-excited determinants than singly-excited ones, it is routine to keep both in a CISD (CI with Singles and Doubles) calculation. In the large basis set limit, the CISD method scales as m^6 and it typically recovers 80-90% of the total correlation energy.

The next level in improvement is inclusion of the triply excited determinants, giving the CISDT method, which scales as m^8 . Taking into account quadruples gives the CISDTQ method, which scales as m^{10} . The CISDTQ method generally gives results close to the full CI, but even truncating the excitation at Quadruples produces so many configurations that it can be applied only to small molecules and only with small basis sets.

In order to calculate the total energies with a "chemical accuracy" of 4 kJ/mole, it is necessary to use large basis set and a large number of determinants. This is computationally feasible only for small molecules, where the state of the art is designated CISD(T), i.e. it considers all S and D replacements and a "non-perturbative" subset of the T replacements. For larger molecules, we must focus instead on calculating relative energies with errors that are as nearly constant as possible, so that the energy differences are given accurately.

6.12.3 Restricted and Unrestricted CI

The HF method we have been discussing applies only to closed-shell, ground-state molecules, i.e. to situations where all of the electrons are paired in orbitals of the lowest-possible energy. To show why this is a problem, consider the hydrogen molecule with one pair of bonding electrons. The RHF wave function for hydrogen is an equal mixture of ionic terms (where both electrons are near one or the other of the nuclei) and covalent terms. As the distance between the two nuclei increases toward infinity, the dissociation limit is 50% ionic and 50% covalent. However, we know that in the gas phase almost all bonds dissociate homolytically, so the ionic contribution should be nearly 0%. This means that the HF energy is much too high. Moreover, this is a general problem of RHF wave functions.

The wrong dissociation limit for RHF wave functions has several consequences:

- (1) The energy for stretched bonds is too high. In particular, activation energies for transition states are too high at the RHF level.
- (2) The excessively steep increase in energy as a function of the bond length causes the potential energy minimum to occur at too small a separation. Hence, equilibrium bond lengths are too small at the RHF level.
- (3) The excessively steep increase also causes the curvature of the potential energy surface near the minimum to be too great. Hence, RHF vibrational frequencies (particularly those describing bond stretching) are too high.
- (4) RHF wave functions are too ionic, and hence the dipole moments calculated from them are too large.

If a full CI calculation is carried out, the variation principle will lead to coefficients that minimize the effect of too much ionic character. Hence RHF procedures are not a problem with full CI. The problem is that so many Slater determinants become necessary that a full CI calculation is seldom possible.

The dissociation problem can also be avoided by using wave functions of the unrestricted Hartree–Fock (UHF) type. Here the molecular orbitals for the different spin-states of the electron are allowed to have different spatial dependences. This is done by using two spatial functions and writing the wave function for each electron as a linear combination of the two, with coefficients for the linear relationship that can be varied to minimize the total energy.

CI with UHF-type wave functions differs from that with RHF-type wave functions in several significant ways.

- The wave function will no longer have the exact spatial symmetry expected for the molecule.
- 2. The UHF energy will be lower than the RHF energy, simply because there are more parameters that can be varied.
- 3. The UHF wave function avoids the problem with too much ionic character, but only at the expense of including terms that are biradical (have two unpaired electrons). This is said to be a spin-contamination problem.

There are three strategies that have been advocated for removing spin contamination in a UHF approach to CI. They occur during the SCF procedure, after the SCF has converged, or after electron correlation has been added to the UHF solution. One way to do this (that applies with any of the strategies) is to interrupt the calculation, remove the biradical terms by forcing their variation coefficients to be zero, renormalize the wave function and resume the calculation. However, this projected UHF (or PUHF) procedure leads to artificial distortion of the potential energy surface and sometimes even to false minima. Furthermore, the derivatives of the PUHF energy are not continuous.

In summary, for closed-shell systems an RHF procedure is normally the preferred way to do CI. For open-shell systems, the UHF procedure is normally preferred. It is possible to use a procedure in which electrons occupy orbitals in pairs (as in

RHF) except for the unpaired electron or electrons that are "known" to exist in the molecule. Not only is this method more complicated, it is in a sense semi-empirical as well.

6.13 Multiconfiguration SCF

The multiconfiguration self-consistent field (MCSCF) method can be considered as a type of CI in which both the coefficients in front of the determinants and the coefficients used in the molecular orbitals are optimized by the variation method. The first iteration in MCSCF is simply HF. Since the number of MCSCF iterations required to reach convergence tends to increase with the number of configurations included, the size of the MCSCF wave function must be somewhat smaller than that used for CI calculations. Moreover, the MCSCF procedure is more likely than CI to converge on solutions where the energy is a local, not global, minimum.

The major problem with the MCSCF method is selecting the necessary configurations to include for the property of interest. One of the most popular approaches is the complete active space self-consistent field (CASSCF) method. Here the selection of configurations is done by partitioning the molecular orbitals into active and inactive spaces, where the active orbitals are typically some of the highest occupied and lowest unoccupied molecular orbitals from a HF calculation. Within the active space, a full CI is performed after the symmetry of the molecule is taken into account.

Which molecular orbitals to include in the active space is a decision that must be made each time a CASSCF procedure is used, based on considerations of the molecule and the properties of interest. A common notation is [n, m]-CASSCF, indicating that n electrons are distributed in all possible ways in m orbitals. Note, however, that this notation does not give all of the information about the calculation method.

As with the full CI method, CASSCF becomes unmanageable large even for quite small active spaces. There are a variety of restricted active space self-consistent field (RASSCF) methods that combine a full CI for a small number of the molecular orbitals in the active space with a CISD treatment of the others.

It should be noted that CASSCF and RASSCF methods inherently give an unbalanced description of molecules, since all of the electron correlation recovered is in the active space, with none in the inactive space or even between the two spaces. This is not a problem if all of the valence electrons are in the active space, but this is impossible except for small systems. In effect, if only some of the valence electrons are included in the active space, then these methods tend to overestimate the importance of biradical structures.

6.14 Multi-reference CI 185

6.14 Multi-reference CI

The CI methods considered so far have involved situations where excitations (whether S, D, T, Q or higher) have occurred only within a single determinant. This corresponds to having a HF-type wave function as the reference. However, it is also possible to use a MCSCF wave function as the reference. In this case, a CISD involves excitations of one or two electrons out of ALL the determinants that compose the MCSCF. The name for this method is multi-reference configuration interaction, and its acronym is MRCI.

Compared to the single reference (ordinary) CISD, the number of configurations used in MRCI is increased by a factor approximately equal to the number of configurations included in the MCSCF. This means that large-scale MRCI calculations can generate very accurate wave functions, but it also means that they are computationally very intensive.

Some researchers have used a state-selected MRCI method in which configurations are ignored if they lead to an "interaction" with some reference configurations that falls below a certain numerical threshold. Not only is this technique questionable because of the way an "interaction" is determined, but it also is unwise if your goal is to compare energies at different geometries. This is because the PES may become discontinuous at points where one or more of the configurations are suddenly ignored.

6.15 Potential Energy Surfaces

6.15.1 Basic Features

Equation (6.15) allows the TISE to be written explicitly for any molecule, assuming that the nuclei do not move from their assigned locations (the Born–Oppenheimer approximation). When there are two atoms, the only thing that matters is the separation, r, between the nuclei, and one can calculate the interaction potential energy curve, V(r), by subtracting the energy when $r \to \infty$ from the values at various r. For transport property calculations, however, one must be careful to make sure that the computational method being used evaluates the integrals that arise to high enough accuracy to make this subtraction of two large values yield small values that still have enough significant figures to make V(r) meaningful (Tuttle et al. 2015; Viehland and Yang 2015; Viehland et al. 2017).

When there are more than two atoms, there are many different inter-nuclear distances that can vary. Moreover, the angles between the various pairs of nuclei become important. Hence the potential energy becomes a function of many variables and it is said to be represented by an interaction potential energy surface (PES) in many dimensions (Lewars 2003). From now on, we will let PES stand for a true surface when several variables are involved or for a potential energy curve when the potential energy is a function only of r.

The concept of a PES apparently originated with the memoir of Rene Marcelin (1885–1914) that was published in 1915. It was not clear at that time, however, why it was the position of the nuclei that should determine the structure of a molecule rather than the positions of the electrons. This was clarified in 1927 by the Born–Oppenheimer approximation. After a gap of more than 15 years, the ideas of Marcelin were extended by Henry B. Eyring (1901–1981) and Michael Polanyi (1891–1976).





Eyring

Polanyi

Real molecules vibrate constantly, in accord with the Uncertainty Principle. Hence even in a diatomic molecule the nuclei must possess both kinetic and potential energies. This is usually represented on a PES by drawing a series of lines above each minimum of the surface, with each line representing the additional amount of vibrational energy that the molecule can have if the vibration of the bonded nuclei increases by one quantum number.

It should be clear that a real molecule never rests at a minimum on the PES. In fact, because it has vibrational energy it never actually moves on the PES that is constructed for the molecule. However, the effects of vibrational energy can usually be added separately from the effects of movement of the atoms along the PES, so it is customary to ignore vibration in initial considerations and to assume that molecules are "rigid". This is justified by noting that the amount of energy it takes to vibrationally excite a molecule from its ground state (v=0) is usually in excess of the thermal energy at 1000 K, so vibrational excitation seldom happens in the ion-neutral collisions of interest in this book.

There is yet another complication that must be mentioned, rotational motion. The energy difference between different rotational states of a molecule are usually small, equivalent to a temperature of 1–10 K. Therefore it is customary to treat molecules as if they are classical rigid rotors, i.e., as not vibrating at all when they have a vibrational quantum number v=0 and with so many rotational energy levels available that these can be treated with classical rather than quantum mechanics. More details about this can be found in most physical chemistry and introductory quantum mechanics texts.

6.15.2 Stationary Points

Among the main tasks of computational chemistry is the determination of the structure and energy of molecules, whether those molecules are stable or are transition structures (also called activated complexes) involved in chemical reactions. Consider the simplest possible chemical reaction, where a molecule changes from one stable form to another by going through a process that at each point requires the addition of the smallest amount of additional energy in order to move to the next point. The path that the molecule takes through the PES usually involves changes in many of the coordinates that we use when describing the molecule. Since the molecule always follows the lowest-energy path, however, it is possible to use only one coordinate, the so-called reaction coordinate, to describe its position along this one-dimensional path.

The initial and final positions of molecules undergoing the reaction just described are stable structures. This means that the PES obtained by plotting the potential energy for the system as a whole as a function of the reaction coordinate must have a minimum at both the initial and final positions. Somewhere between these positions there must be a maximum, which is called the transition structure. Ordinarily, chemists are interested in the arrangement of the atoms in the molecule when it is at either stable configuration or at the transition structure, i.e. when the potential energy is either a minimum or a maximum.

A stationary point on a PES is a point at which the surface is flat, i.e., parallel to the horizontal line corresponding to the single geometrical variable of interest. Mathematically, a stationary point is one at which the first partial derivative of the potential energy with respect to each geometrical variable is zero. Stable molecules exist at points on the PES where the potential energy is a minimum when approached from any direction; this requires that the second partial derivatives must all be positive. Transition structures, however, are saddle points, i.e., points where the potential energy is a maximum when approached from one particular direction (along the reaction coordinate) but a minimum when approached from any other direction. This means, mathematically, that the second derivative is negative along the reaction coordinate for a transition structure, but it is positive for all other directions.

Sometimes a PES has points where more than one second derivative with respect to a coordinate is negative. These are higher-order saddle points, but chemists usually refer to them as hilltops by analogy with the top of a hill, where you can go down by moving in several directions.

6.15.3 Geometry Optimization and Energy Minimization

Geometry optimization is the process of finding a stationary point on a PES. This means demonstrating that the point in question exists, calculating the values of all the independent variables that characterize the molecule at the stationary point, and deter-

mining the value of the potential energy function at the point. The more specialized process of finding a minimum point on a PES is usually called energy minimization.

Geometry optimizations are usually carried out by starting with an input structure (arrangement of the nuclei in the molecule) that is believed to resemble the desired stationary point. This plausible structure is submitted to a computer program that systematically changes the variables that characterize the geometry until it has found a stationary point. Obviously, the closer the input structure is to the correct answer, the faster the computer program will converge to the final answer. Finally, the curvature of the PES at the stationary point is calculated, and these second derivatives are used to determine whether the molecule is stable or in a transition structure.

The description above indicates why the optimized structure that one obtains with a computational chemistry program is the one whose geometry is closest on the PES to the input structure. This may be a local minimum, however. To be sure that this is a global minimum, one must search a PES by starting with several or many input structures.

Another problem with geometry optimization is that it is usually unclear (particularly when there are many variables characterizing a large collection of atoms) in which direction and how far to move in order to get closer to the stationary point. The most widely-used algorithm makes use of the first and second derivatives of the energy with respect to the geometric parameters, as illustrated below for a diatomic molecule with only one parameter, r.

If we assume that near a minimum the potential energy is a quadratic function of r, then

$$V(r) = V(\widetilde{r}) + \widetilde{k}(r - \widetilde{r})^{2}, \qquad (6.35)$$

where \tilde{r} is the true minimum and \tilde{k} is some unknown constant. The first and second derivatives of this function are

$$V'(r) = 2\widetilde{k}(r - \widetilde{r}) \tag{6.36}$$

and

$$V''(r) = 2\widetilde{k}. ag{6.37}$$

Then (6.36) can be rearranged and rewritten as

$$\widetilde{r} = r - \frac{V'(r)}{V''(r)}. ag{6.38}$$

For a diatomic molecule, we start with an input structure (a guess for r) and calculate the values of V(r), V'(r) and V''(r). The right-hand side of (6.38) is then used to estimate \tilde{r} . If \tilde{r} is not as close to r as the user desires, \tilde{r} is relabeled as r and the process is repeated until the changes in the estimates for r agree within some pre-specified value or percentage.

An extension of this method to molecules with more than two atoms has been developed using linear algebra (see Appendix A) and is incorporated into most if not all computational chemistry programs.

6.16 Maxwell's Equations in a Vacuum

It is necessary to incorporate relativity into quantum mechanics in order to go beyond the Schrődinger equations. We start with the differential forms of Maxwell's equations of electromagnetism for point charges in a vacuum. These equations in SI units are:

$$\nabla \cdot \mathbf{E} = \frac{\rho}{\varepsilon_0}$$
 (Gauss's Law for Electricity) (6.39)

$$\nabla \cdot \mathbf{B} = \mathbf{0}$$
 (Gauss's Law for Magnetism) (6.40)

$$\nabla \times \mathbf{E} = -\frac{\partial \mathbf{B}}{\partial t}$$
 (Faraday's Law of Induction) (6.41)

$$\nabla \times \mathbf{B} = \frac{1}{c^2} \left[\frac{\mathbf{j}}{\varepsilon_0} + \frac{\partial \mathbf{E}}{\partial t} \right]$$
 (Modification of Ampere's Law). (6.42)

Here ρ is the charge density, **j** is the current density vector, **E** is the electric field vector, **B** is the magnetic field vector and c is the speed of light in a vacuum.

Equations (6.39) and (6.40) describe the "sources" of the fields. The source for an electric field is the charge density on the right-hand side of (6.39). Equation (6.40) may be interpreted as a statement that isolated magnetic poles (magnetic monopoles) do not exist. Thus, the source for a magnetic field is not constant, but is instead related to the time dependence of the electric field as given by (6.42). Equation (6.41) shows that a change in a magnetic field produces an electric field; this is the principle behind the electrical circuitry in motors and generators. The fourth equation originally came from Ampere's Law, which indicates that, when a current passes through a circular loop of radius \tilde{R} , there is produced at the center of the loop (and normal to the plane of the loop) a magnetic field of strength $B = 2\pi i/c\tilde{R}$. Maxwell showed that this expression is inconsistent with the equation describing the conservation of charge, so he revised Ampere's Law to obtain (6.42).

As illustrated in Sect. 6.3, it is often more convenient to work in terms of field-related potentials rather than the fields themselves. To find such potentials, we start by noting from vector calculus (see Appendix A) that

$$\nabla \cdot (\nabla \times \mathbf{B}) = 0, \tag{6.43}$$

for any vector **B**. Therefore, if we define a vector potential, **A**, by requiring that

$$\mathbf{B} = \nabla \times \mathbf{A},\tag{6.44}$$

then (6.40) will automatically be satisfied, while (6.41) becomes

$$\nabla \mathbf{x} \left(\mathbf{E} + \frac{\partial}{\partial t} \mathbf{A} \right) = 0. \tag{6.45}$$

We know that for any scalar (see Appendix A), s,

$$\nabla \mathbf{x} \ (\nabla s) = 0. \tag{6.46}$$

Therefore (6.46) will automatically be satisfied if we define a scalar potential, V, by requiring that

$$\mathbf{E} + \frac{\partial}{\partial t} \mathbf{A} = q \nabla V. \tag{6.47}$$

The dependence of V upon position was indicated by using the notation V(x, y, z) in Sect. 6.3, but here it is left implicit. In (6.47), the charge is explicitly indicated (i.e., not included in V) in order to make it easy to distinguish between nuclei with positive q values and electrons, where q = -e. Therefore, V is the position-dependent, scalar potential per unit charge.

The definitions above of the vector and scalar potentials contain some ambiguity. For example, we can add any constant to V without changing the value of \mathbf{E} . In addition, we can add the gradient of any scalar quantity to \mathbf{A} without changing \mathbf{B} , although such a change in \mathbf{A} will require a corresponding change in V. The particular choice made for \mathbf{A} is referred to as the magnetic gauge and the particular choice for V is called the electric gauge. It should be noted that the gauge choices only influence the forms of the mathematical expressions; the physics and chemistry remain the same.



Poisson

The Coulomb magnetic gauge is obtained by requiring that whatever is needed is added to $\bf A$ in order to make

$$\nabla \cdot \mathbf{A} = 0 \tag{6.48}$$

The Coulomb electric gauge is obtained by requiring that whatever is needed is then added to V in order to fix the zero of energy to be the value when the charges are

infinitely far apart. With these choices, all four of Maxwell's equations are satisfied as long as the charge distribution satisfies Poisson's equation,

$$\nabla^2 V = -\frac{\rho}{\varepsilon_0}.\tag{6.49}$$

This equation was developed in 1813 by Siméon Denis Poisson (1781–1840).

Since the middle of the 20th century, it has been understood that Maxwell's equations are not exact. They are a classical field theory approximation to some aspects of a more fundamental theory called quantum electrodynamics. Even worse, some quantum-mechanical effects like quantum entanglement are completely missing from Maxwell's equations. Fortunately, deviations from Maxwell's equations are very small in phenomena that do not involve light, and hence can be ignored in this book.

6.17 The Dirac Equation

6.17.1 Introduction

Recall from Sect. 6.3 what happens when one starts with Newton's laws of motion for the total energy and makes the replacements of E_{tot} and ${\bf p}$ by operators according to the correspondence principle. We get the time-dependent Schrö dinger equation, which involves second derivatives with respect to the position variables but only first derivatives with respect to time. Clearly such an equation is inconsistent with the special theory of relativity, in which time and space are equivalent. The question addressed by Dirac is how to make quantum replacements in a way that is consistent with special relativity.

An electron must obey the relativistic equation

$$E^2 = c^2 \mathbf{p} \cdot \mathbf{p} + m^2 c^4. \tag{6.50}$$

This is the equation that reduces to Einstein's famous equation, $E = mc^2$, for the energy of a particle in its own rest frame (where $\mathbf{p} = 0$). If we add the scalar and vector potentials, the classical-mechanical equation describing the relativistic motion of an electron must be

$$(E + eV)^2 = c^2 \pi \cdot \pi + m^2 c^4, \tag{6.51}$$

where

$$\pi = \mathbf{p} + e\mathbf{A} \tag{6.52}$$

is called the kinetic momentum vector. Taking the square root of (6.51) gives

$$E + eV = c \left(\pi \cdot \pi + m^2 c^2 \right)^{1/2}. \tag{6.53}$$

What Dirac did that was new was to assume that the quantity inside the square root in (6.53) was a perfect square, i.e. he let

$$\pi \cdot \pi + m^2 c^2 = (\alpha \cdot \pi + \beta mc)^2. \tag{6.54}$$

Then he was able to write the classical-mechanical, relativistic equation as

$$E + eV = c\alpha (\mathbf{p} + e\mathbf{A}) + \beta mc^{2}. \tag{6.55}$$

Using the correspondence principle embodied in (6.1) and (6.2) to change from classical to quantum mechanics gives the Dirac equation for a particle,

$$\left(\frac{ih}{2\pi}\frac{\partial}{\partial t} + eV(x, y, z, t)\right)\Psi(x, y, z, t) = c\alpha \cdot \left(\frac{h}{2\pi i}\nabla + e\mathbf{A}\right)\Psi(x, y, z, t) + \beta mc^2\Psi(x, y, z, t). \tag{6.56}$$

Equation (6.56) involves first derivatives of both time and position, so it is consistent with special relativity. To make it practical, however, it is best to use quantities known as four vectors (see Appendix A) and then determine α and β . A four-vector has four components, the first along the x direction, the second along y, the third along z, and the fourth along t, the time direction. The equations of special relativity look simpler if we use the following four-vectors:

$$\overleftrightarrow{\mathbf{r}} = (x, y, z, ict) \tag{6.57}$$

$$\overrightarrow{\mathbf{p}} = \left(\frac{h}{2\pi i}\frac{\partial}{\partial x}, \frac{h}{2\pi i}\frac{\partial}{\partial y}, \frac{h}{2\pi i}\frac{\partial}{\partial z}, \frac{iE}{c}\right) \tag{6.58}$$

$$\stackrel{\longleftrightarrow}{\Box} = \left(\frac{\partial}{\partial x}, \frac{\partial}{\partial y}, \frac{\partial}{\partial z}, -\frac{i}{c} \frac{\partial}{\partial t}\right) \tag{6.59}$$

and

$$\overrightarrow{\alpha} = (\alpha_x, \alpha_y, \alpha_z, i).$$
 (6.60)

Then the Dirac equation may be written as

$$c \overleftrightarrow{\alpha} \cdot \left(\frac{ih}{2\pi} \overleftrightarrow{\Box} - eV(\overleftrightarrow{\mathbf{r}})\right) \Psi(\overleftrightarrow{\mathbf{r}}) = \beta mc^2 \Psi(\overleftrightarrow{\mathbf{r}}). \tag{6.61}$$

Now we turn to the determination of α and β , such that (6.54) is valid. If we expand the right-hand side of this equation and equate terms, we find that we must have

$$\alpha_i^2 = \beta^2 = 1 \tag{6.62}$$

$$\alpha_i \alpha_k = -\alpha_k \alpha_i \qquad j \neq k \tag{6.63}$$

and

$$\alpha_i \beta = -\beta \alpha_i \tag{6.64}$$

for j and k equal to x, y or z. Mathematicians have shown that these three equations cannot be satisfied by scalars or by tensors of order 2 or 3. The simplest way to satisfy them is with the following tensors of order 4 called the standard representation:

$$\alpha_{x} = \begin{bmatrix} 0 & 0 & 0 & 1 \\ 0 & 0 & 1 & 0 \\ 0 & 1 & 0 & 0 \\ 1 & 0 & 0 & 0 \end{bmatrix} \qquad \alpha_{y} = \begin{bmatrix} 0 & 0 & 0 & -i \\ 0 & 0 & i & 0 \\ 0 & -i & 0 & 0 \\ i & 0 & 0 & 0 \end{bmatrix}$$

$$\alpha_{z} = \begin{bmatrix} 0 & 0 & 1 & 0 \\ 0 & 0 & 0 & -1 \\ 1 & 0 & 0 & 0 \\ 0 & -1 & 0 & 0 \end{bmatrix} \qquad \beta = \begin{bmatrix} 1 & 0 & 0 & 0 \\ 0 & 1 & 0 & 0 \\ 0 & 0 & -1 & 0 \\ 0 & 0 & 0 & -1 \end{bmatrix}$$

$$(6.65)$$

The reader interested in knowing more about the Dirac equation, particularly how it can be extended to treat atoms and molecules, should consult the book by Dyall and Fægri (2007). Here we cite some general consequences of the Dirac equation without going into the details.

1. The quantity $c\alpha$ can be identified with the velocity operator, which means that

$$\stackrel{\longleftrightarrow}{\alpha} = \frac{\partial}{\partial t} \stackrel{\longleftrightarrow}{\mathbf{r}}.$$
 (6.66)

2. The quantity β is given by

$$\beta = \left(1 - \frac{v^2}{c^2}\right),\tag{6.67}$$

which is a familiar quantity from special relativity.

- 3. The probability density, $\Psi^2(\overrightarrow{\mathbf{r}})$, is time-independent when the electron is in a bound state.
- 4. When we study atoms and molecules using the Born–Oppenheimer approximation, the vector potential is zero, the scalar potential is the usual set of Coulomb potentials between the electrons and either the nuclei or the other electrons, and the motion of the electrons is governed by the time-independent Dirac equation (hereafter called TIDE) that may easily be obtained by making these changes in (6.56):

$$eV(x, y, z, t) \overrightarrow{\Psi}(x, y, z, t) = \frac{hc}{2\pi i} \nabla^{2} \overrightarrow{\Psi}(x, y, z, t) + m \left(c^{2} - v^{2}\right) \overrightarrow{\Psi}(x, y, z, t).$$
(6.68)

5. The appearance of tensors of order 4 in the TIDE means that the wave function must also have four components. However, only the usual variables (x, y, z and t) appear, and there is no need to invent a variable to describe some hypothetical spin-space.

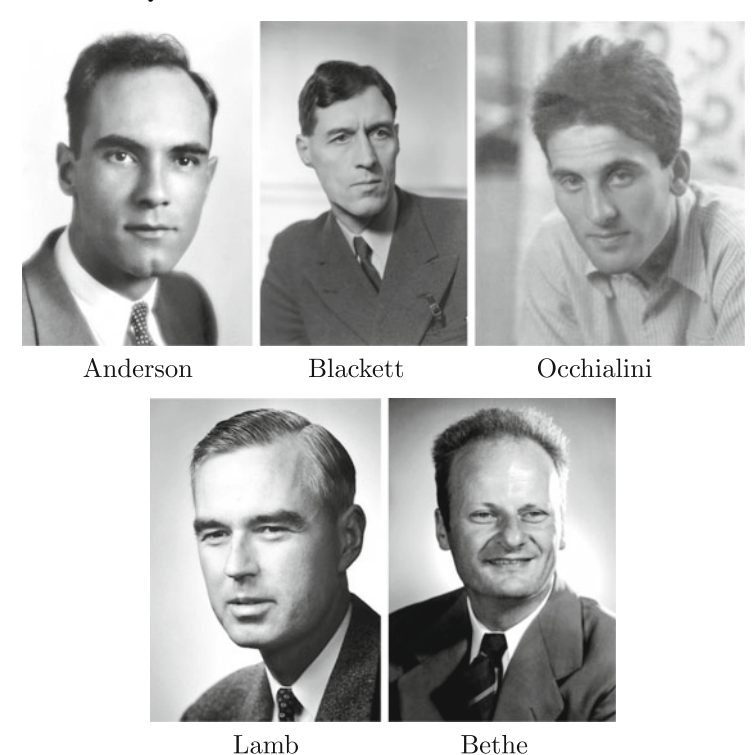
For a single electron, we have moved from a scalar function of three variables in non-relativistic quantum mechanics to a four-component vector function (called a 4-spinor) of four variables in relativistic quantum mechanics. Two of the components correspond to the s=1/2 situation when the TISE is supplemented with the concept of electron spin, while the other two correspond to s=-1/2. In each case, the two components are referred to as the large and small components; solutions with positive energies have large values for the large component, while solutions with negative energies (see below) have large values for the small component.

There are a number of things to note about the solution of the TIDE for the hydrogen atom (Dyall and Fægri 2007). Adding these to the list above gives

- 6. The Dirac *n* quantum number is called the principal quantum number. It may have any positive integer value, and it is the quantum number that principally determines the size and energy of an orbital; it is therefore essentially the same as the *n* quantum number in the TISE.
- 7. The Dirac l quantum number is called the azimuthal quantum number. It may have any integer value between 0 and n-1, and it is designated by the s, p, d, f, ... notation used for the Schrödinger l quantum number. However, it no longer represents the orbital angular momentum and it no longer determines the shape of the orbital.
- 8. The Dirac j quantum number is called the total angular momentum quantum number. It has the value obtained by taking the absolute value of l+1/2 or l-1/2, and it contributes to the orbital energy and shape. Note that j will always be half-integer.
- 9. The Dirac m quantum number is called the magnetic quantum number. It may have any half-integer value between -j and +j, while m and j together determine the orbital shape.
- 10. There is no spin quantum number. Although the electron interacts with external fields and is often casually referred to as if it were spinning, the TIDE does not contain a concept of the electron spinning about an axis through its center. This is gratifying, because otherwise the TIDE would be in conflict with the Uncertainty Principle, just like the TISE is.
- 11. The orbitals are shaped differently than those are described in such detail in general chemistry courses, which are based on the TISE.
- 12. There exists for the electron two sets of energy states, one of positive energy and one of negative energy. Dirac recognized that all observed electrons occupy the positive energy states. He postulated that the reason they cannot fall into the negative energy states is that all of these latter states are ordinarily occupied by electrons that we cannot observe. However, if we hit one of these hidden electrons with enough energy to move it into a positive energy state, we should be able to see an electron created while at the same time a "hole" is created in

the negative energy states. The hole should act like a particle of the same mass as an electron but of the opposite charge.

In 1930, Dirac predicted that an electron-positron pair could be created from pure energy (gamma rays or other kinds of light, for example), and that the collision of an electron with a positron would annihilate both leaving behind only energy. The positron was observed in 1932 by Carl David Anderson (1905–1991). Actually, Patrick Maynard Stuart Blackett (1897–1974) and Giuseppe Occhialini (1907–1993) had observed the same things as Anderson, but they published their results after Anderson. The positron or anti-electron is the first of a class of particles (or waves or wave-particles) known as "antimatter". Anti-protons and anti-neutrons, for example, were discovered in the 1950s. According to measurements in 1990, the proton and antiproton have the same mass within 1 part in 25 million; Dirac's theory predicts them to have exactly the same mass.



The final consequence of the TIDE is that the hydrogen spectrum is more accurately described than by the TISE, as it predicts the entire spectrum including the fine structure. However, in 1947 Willis Eugene Lamb, Jr. (1913–2008) and Robert Curtis Retherford (1912–1981) were able to show that two states of atomic hydrogen which should have the same energy according to the Dirac equation actually differ by about 2 parts per million. This very small shift, now called the Lamb shift, was approximately explained by Hans Albrecht Bethe (1906–2005), but could only be

completely described by a theory called quantum electrodynamics. QED was developed by Julian Seymour Schwinger (1918–1994), Sin-Itiro Tomonaga (1906–1979) and Richard Phillips Feynman (1918–1988), and it is even more elaborate than the Dirac equation. It is based on the idea that the wave function itself has to be quantized and has to obey the laws of special relativity. As an indication of the accuracy of this theory, it predicts that the Lamb shift causes the two lowest state of hydrogen to be split by $1057.860 \pm 0.009\,\mathrm{MHz}$, while the average of the best measured values is $1057.850 \pm 0.009\,\mathrm{MHz}$.



6.17.2 The Dirac-Fock Method

The assumption up to here has been that the nuclei involved in the ion-neutral systems of interest are points. Of course, this approximation is incorrect if one gets close enough to the nuclei, as can happen when one of the nuclei has a large number of protons and relativistic contractions bring the inner electrons much closer than usual to the nucleus. For this reason, the use of finite-size nuclear models in theoretical chemistry is becoming popular (Dyall and Fægri 2007). Apart from presenting a more physical model for the nuclear charge distribution than the usual point-charge model, the finite-size model also has important advantages in calculations that solve the Hartree–Fock equations. As a reminder of the relativistic aspect of the equations, one is said to be using the Dirac-Fock (DF) method of quantum mechanics.

In the usual HF and the DF methods, the expansion of the wave function in a basis set of finite size is preferably done using Gaussian orbitals, since multi-center integrals over Gaussian-type functions are more readily evaluated than integrals over Slater orbitals. This computational advantage outweighs the slower convergence of the atomic energy with the number of Gaussian basis functions. It remains, however, essential for computational feasibility to keep the number of basis functions employed as small as possible. Particularly in relativistic calculations for atoms low in the Periodic Table, a large number of basis functions is required to accurately represent the electron spinors in the core region. This slow convergence occurs when there is a weak singularity at the nucleus for the 1s and 2p spinors; it takes many

Gaussian-type functions to model this behavior and get an energy close to the DF limit.

As indicated previously, using an ECP usually implies that a pseudopotential has been optimized while taking into account the finite size of the nuclei. Hence such ECP account for one general aspect of relativistic effects on ion-neutral interaction potentials.

6.18 The Perturbation Method

Although most solutions of the TISE use the variation method, another solution method has long been used. This perturbation method will be shown below to lead to practical ways for solving the TIDE as well, so it is important to discuss it now.

The perturbation method starts with an exact or very accurate solution of the TISE for some similar but simpler problem than the one you are actually interested in. It then changes the solution in small ways so that it comes closer and closer to describing the real problem.

Suppose that the Hamiltonian operator for a similar problem is $H^{(0)}$ and that for this problem you know the values for the eigenvalues, $E^{(0)}$, and the corresponding wave functions, $\psi^{(0)}(\tau)$. Here τ stands for the four variables x, y, z and t. Because you know the Hamiltonian operator, H, for the real problem, you obviously know the perturbation operator, $H' = H - H^{(0)}$. Without going into the mathematical details, it can be shown that there is a systematic way of obtaining from H' successively better approximations to the eigenvalues and eigenfunctions of H. In first approximation, the eigenvalue, E_n , corresponding to the nth state of H is

$$E_n = E_n^{(0)} + \int \psi_n^{(0)*}(\tau) H' \psi_n^{(0)}(\tau) d\tau.$$
 (6.69)

Unfortunately, to go to the next higher approximation requires that you first calculate a new, more accurate set of eigenfunctions before you can calculate the new, more accurate eigenvalues, so such calculations quickly become difficult. This is why the perturbation method is seldom applied in solving the TISE.

6.19 Moller-Plesset Perturbation Method

When the perturbation method is applied to molecules that contain several or many nuclei, it is called many-body perturbation theory (MBPT). The type of MBPT we will discuss here is due to the work in 1934 of Christian Moller (1904–1980) and Milton Spinoza Plesset (1908–1991).

Moller–Plesset calculations are denoted as MP, and there is a hierarchy of calculations with increasing accuracy. The lowest acceptable level is MP2, since it is the

first level that goes beyond the HF method. The MP2 energy is the HF energy plus a correction term (a perturbation adjustment) that represents a lowering of energy brought about by allowing the electrons to avoid one another better than in the HF treatment. The perturbation correction is a purely electronic effect that is a sum of terms, each of which models the promotion of pairs of electrons from occupied to virtual molecular orbitals.

The reader interested in more details about MP calculations should consult the text by Lewars (2003).



6.20 Coupled Cluster Methods

The coupled cluster (CC) method was developed by Fritz Coester and Hermann G. Kümmel in the 1950s for studying nuclear physics phenomena. It became more frequently used after 1966, when Jiří Číž ek and Josef Paldus reformulated the method for electron correlation in atoms and molecules.

In retrospect, CC theory is the perturbative variant of the many electron theory (MET) of Oktay Sinanoğlu (1934–2015), which is the exact variation solution of the many electron problem. Because MET is somewhat difficult to perform computationally, the simpler CC theory is used more often in computational chemistry. It is a numerical technique used for calculations beyond the HF level, and it gives highly accurate results in comparison to experiment.

The essence of the CC method is to take the basic HF molecular orbitals and construct from them multi-electron wave functions using the exponential cluster operator to account for electron correlation. The reader interested in the details of this method is urged to consult the primary literature.

The restricted CC method, RCC, uses a RHF reference, so it is partially spin-restricted. The current state-of-the-art in computational chemistry is for ab initio calculations to be performed at the RCCSD(T) level, i.e. RCC with Singles, Doubles and non-perturbative Triples.

6.21 The Breit-Pauli Hamiltonian

The perturbation method most often used now in computational chemistry is based on the Breit–Pauli operator. The derivation of this operator using a perturbation method by Bethe and Edwin Ernest Salpeter (1924–2008) is discussed by Bethe and Salpeter (1951), Nicklass et al. (2000), and in Ch. 21 of Dyall and Fægri (2007).



Salpeter

The lowest-order relativistic corrections to the energy of a system can be calculated by using the Breit–Pauli operator or, for molecular systems, by an extension in which the relativistic Hamiltonian, H, is given in Sect. 13.A of Hirschfelder et al. (1964). Both account for relativistic effects through terms of order $1/c^2$ by using the dimensionless fine-structure constant (2014 CODATA value $7.2973525664 \times 10^{-3}$). Corrections of higher order cannot be obtained consistently by this approach, because the Hamiltonian is limited to systems containing nuclei with a small nuclear charge, $\widetilde{Z} < 137$ (approximately the fine-structure constant). However, this is not a practical limitation for most systems of interest in this book, since the valence electrons are shielded by the core electrons and the effective nuclear charge is not close to 137.

To include spin-orbit effects in an ion-neutral interaction potential, the procedure used by Tuttle et al. (2017) is recommended:

- Standard aug-cc-pwCVXZ basis sets (X = Q,5) are used for atoms from He-Ar. Small-core, relativistic ECPs are used to describe the innermost electrons in heavier atoms, with the valence electrons described with standard aug-cc-pwCVXZ-PP basis sets.
- The TISE is solved using the RCCSD(T) method.
- Interaction potential energies at each of 50–100 ion-neutral separations are counterpoise (CP) corrected to account for BSSE.
- The CP-corrected interaction potentials with X= Q and 5 are used as the unperturbed eigenvalues (see Appendix A) of the Breit-Pauli operator in a computational chemistry computer program that computes the CP-corrected interaction energies with spin-orbit effects included.
- The results at each separation are extrapolated to the CBS limit using the two-point (cubic) formula of Halkier et al. (1998, 1999).

It is beyond the scope of this book to give more details of spin-orbit (SO) calculations using relativistic Hamiltonians. The interested reader should consult Sec. 17.3 of Dyall and Fægri (2007), the papers by Nicklass et al. (2000) and Rasskazov et al. (2017), or the documentation for the computational chemistry computer programs that use them.

6.22 Transport Cross Sections

6.22.1 Classical Calculations

In the remainder of this chapter we assume that an accurate interaction potential energy curve, V(r), has been determined as a function of the atomic ion-atom separation, r, by accurate ab initio methods. The next step is to determine the set of transport cross sections that are defined by (1.22) and (1.23). These are classical-mechanical equations, but many years of experience indicate that quantum-mechanical calculations of the transport cross sections are necessary only for ion-neutral systems that involve resonant charge transfer. We will consider quantum calculations in the next subsection.

The $\overline{Q}^{(l)}(\varepsilon)$ are single-valued functions of the collision energy, ε , (also called the relative kinetic energy) for each integer value of l. Following Smith and Munn (1964) and O'Hara and Smith (1970), we adopt the condition that we must be able to specify a fractional error such that the final values of the $\overline{Q}^{(l)}(\varepsilon)$ are known to be correct within this relative accuracy. Calculation difficulties arise because of singularities (see Appendix A) at or near the endpoints of the intervals of integration in (1.22) and (1.23), particularly when ε , b and r are such that the colliding particles can orbit about one another indefinitely. These difficulties are further complicated by the phenomenon of multiple orbiting (Rainwater et al. 1982), where two or more sets of b and r values occur for a single ε . Finally, we are interested in using numerical rather than functional potentials, i.e., in the situation where V(r) is supplied as a tabulated set of points, (r, V), from ab initio calculations.

It is easy to write a computer program that makes use of (1.22) and (1.23) in a straightforward manner. Such programs can fail, often unexpectedly, when the quadrature procedures (see Appendix A) accidentally encounter a singularity, orbiting or multiple orbiting. For this reason a computer program named PC was developed (Danailov et al. 2008; Viehland and Chang 2010). PC is an improvement upon older computer programs (O'Hara and Smith 1970; Neufeld and Aziz 1972; Viehland 1982, 1984) because it uses a spline fit (see Appendix A) of the tabulated points to calculate the potential and its first and second derivatives at any separation. The spline fit is clamped so that it matches the asymptotically correct long-range potential at separations larger than those supplied by the user. It is also clamped at small separations so that it matches an inverse-power potential that agrees with the first

two points supplied by the user. Another improvement incorporated into PC is the way that it takes multiple orbiting into account.

Program PC works with tabulated interaction potentials for neutral rare-gas systems, for atomic ion-atom systems, and for systems where there is both a potential minimum and a long-range maximum. The latter type of potential can arise for molecular ion-neutral systems where all of the angles are fixed, as will be discussed in Chap. 8. Here, of course, we will focus on systems of the second type. For such systems, it is typical to determine 50–100 pairs of values, (r,V), covering separations from values of r large enough (30 a_0 or larger) that the potential smoothly matches the ion-induced dipole potential, and small enough that V is positive (i.e., the potential is repulsive) for at least the smallest three r. It is best if the potential at the shortest r is approximately one E_h , but it is not necessary to cover the potential minimum better than the other regions (unless one is also interested in calculating spectroscopic properties). Program PC will typically return transport cross sections accurate to 0.05% over collision energies from 1×10^{-9} to $1 E_h$.

In the last decade we have used program PC with high-quality, ab initio potentials for nearly 100 atomic ion-atom systems. To illustrate the results, consider $Ba^+(^2S_{1/2})$ in $Ar(^1S_0)$. The four accurate potentials that we will consider for this system did not take spin-orbit into account, and other relativistic effects were considered only through their influence on the ECP used for the core electrons in Ba. The potentials are those of:

- McGuirk et al. (2009), who used the CCSD(T) level of theory. They described the
 core electrons in Ba with a 46-electron ECP that included relativistic effects since
 it was optimized at the Dirac-Fock level (Lim et al. 2006). For the valence electrons
 in Ba they used a specially constructed basis set that was roughly equivalent to
 aug-cc-pV5Z. For Ar, they used the standard aug-cc-pV5Z basis set to describe
 all of the electrons. The full counterpoise correction was applied at each r in order
 to overcome bases set superposition error (BSSE).
- 2. Buchachenko and Viehland (2018), who made RCCSD(T) calculations with the 46-electron ECP description of Ba. For the valence electrons in Ba, they used an aug-cc-pwCV5Z basis set with additional ghost orbitals centered between the Ba and Ar nuclei. For Ar, they used an aug-cc-pV5Z basis set. All electrons except those in the Ba core were correlated. Counterpoise correction was made to overcome BSSE.
- 3. Buchachenko and Viehland (2018), who extrapolated results with aug-cc-pw-CVXZ basis sets using X = Q, T and S to the complete basis set limit, $X = \infty$. This is possible because ECP series are regular with respect to X; a mixed exponential-Gaussian function of X gave the best results.
- 4. Tuttle et al. (2018), who made RCCSD(T) calculations with an aug-cc-pCVXZ-PP basis set and a relativistic, small-core ECP for Ba, and an aug-cc-pwCVXZ basis set for Ar. Based primarily on a comparison of calculated spectroscopy values with experimental results, they state that "overall, the results from the present study and those of Buchachenko and Viehland (2018) may be regarded as being of a similar reliability."

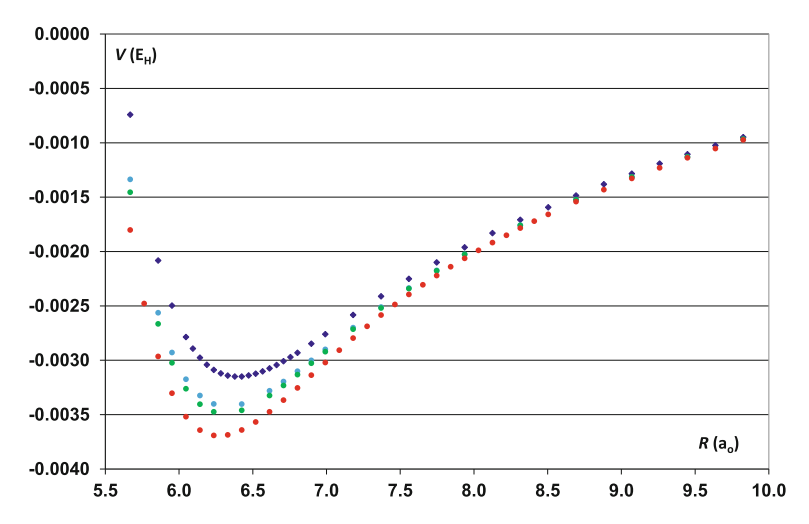


Fig. 6.1 Potential energies for $Ba^+(^2S_{1/2})$ interacting with $Ar(^1S_0)$. The upper, dark blue points are from McGuirk et al. (2009). The lower, light blue points are from Buchachenko and Viehland (2018), and their CBS values are given by the next lower, green points. The lowest, red points are from Tuttle et al. (2018)

The computational chemistry computer programs used to obtain these potentials require that the user specify the accuracy with which the integrals will be calculated when determining the matrix elements of the Hamiltonian operator, and the accuracy of the coefficients in the Slater determinants that are determined by iteration using the variation method. Usually, these are chosen so that the potential near the minimum in Fig. 6.1 is accurate within about 0.1 cm^{-1} or $5 \times 10^{-7} E_h$, in order to give accurate values of the spectroscopy parameters for the system. This means that errors in the fourth significant figure are acceptable near the potential minimum. Transport coefficients, however, are sensitive to the potential energy at larger separation when T_0 and E/n_0 are small.

In order to ensure that the ab initio potentials are highly accurate at intermediate and large separations, the potential values must be shifted by whatever small amount is needed to make the value at the largest r agree with the ion-induced interaction potential,

$$V(r) = -\frac{C_4}{r^4}. (6.70)$$

The value of C_4 in atomic units, \widehat{C}_4 , differs from the value of the neutral polarizability, $\widehat{\alpha}_0$, in cubic Angstrom by a factor of 0.2963694226 when the 2014 CODATA value of a_0 is used. Table 6.2 gives values of both quantities for the six rare gases, while Table 6.3 gives the largest separations used in the potentials for Ba⁺(2 S_{1/2}) in Ar(1 S₀) and the potential energy shifts needed to bring them into agreement with (6.70). The shift needed for the potential of McGuirk et al. (2009) is much greater than for the other three, indicating that it is probably the least accurate of the four potentials.

Atom	$\widehat{\alpha}_0$	\widehat{C}_4	$\widehat{\alpha}_0$ Source
Не	0.2050522	0.6918804	Lim and Schwerdfeger (2004)
Ne	0.39488	1.3324	Soldan et al. (2001)
Ar	1.6425	5.5421	Soldan et al. (2001)
Kr	2.4953	8.4196	Soldan et al. (2001)
Xe	4.044	13.645	Soldan et al. (2001)
Rn	5.102	17.215	Miller and Bederson (1989)

Table 6.2 Values of the polarizabilities in cubic Anstrom and the C4 coefficient in atomic units for the rare gases

Table 6.3 Energy shifts applied to ab initio potentials for $Ba^+(^2S_{1/2})$ in $Ar(^1S_0)$

r (a.u.)	Shift $(10^{-6} E_h)$	Potential Source
56.692	6.4783	McGuirk et al. (2009)
68.030	0.0022666	Buchachenko and Viehland (2018)
	0.0020470	CBS
37.795	-0.088924	Tuttle et al. (2018)

The momentum-transfer cross sections, $\overline{Q}^{(1)}(\varepsilon)$, calculated from the four potentials are shown in Fig. 6.2, in terms of the microscopic momentum-transfer collision frequency. As expected (McDaniel and Viehland 1984) for systems whose longrange potential varies as r^{-4} , e.g., for an ion-induced dipole interaction potential, the values of $\nu^{(1)}(\varepsilon)$ at low ε are constant. The structure in Fig. 6.2 near $\varepsilon=0.002$ E_h is real, as this is the maximum energy at which classical orbiting can occur. The minimum near 3×10^{-4} E_h is also real, as it corresponds to the region of the potential where the attractive and repulsive terms are about the same magnitude. This minimum leads to a mobility maximum (see Fig. 1.1) if the thermal energy is below the energy of the minimum and increasing E/n_0 leads to average kinetic energies above it. Note that the values of $\overline{v}^{(1)}(\varepsilon)$ obtained from potential 1 differ near 10^{-4} E_h from those obtained with the other potentials; this is consistent with the comment above that potential 1 is probably the least accurate of the four.

We will return to the $\text{Ba}^+(^2S_{1/2})\text{-Ar}(^1S_0)$ system later. Meanwhile it is worth noting that a graph like Fig. 6.2 is a useful tool in making a preliminary estimate of the quality of a given V(r). Wobbles like that shown in the figure for potential 1 have been found to signify unphysical oscillations in the potential, either because some of the calculated points, (r, V), are not accurate or because they are so far apart in r values that cubic-spline or other interpolation schemes give inaccurate results. The value of ε where such wobbles occur can also provide a clue to what part of V(r) is problematic.

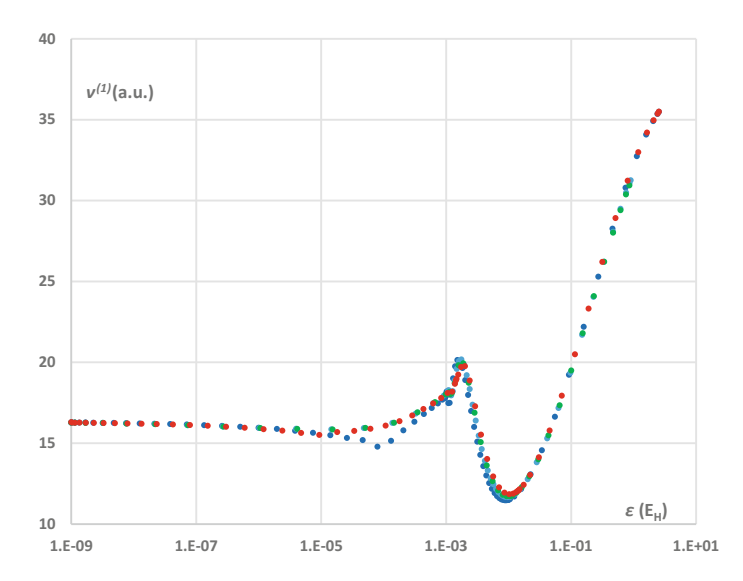


Fig. 6.2 Microscopic momentum-transfer collision frequency, $\overline{v}^{(1)}$, as a function of the collision energy, ε , for Ba⁺($^2S_{1/2}$) interacting with Ar(1S_0). The points are colored as in Fig. 6.1

6.22.2 Quantum Calculations

Viehland and Hurly (1996) made both classical and quantum calculations of the transport cross sections for $^{40}\mathrm{Ar}^+(^2\mathrm{P}_{3/2})$ in He($^1\mathrm{S}_0$), using the ab initio interaction potential of Carrington et al. (1995). The quantum values of the transport cross sections were calculated from phase shifts obtained with the computer program of Hurly et al. (1992) and formulas (Wood 1971; Mason and McDaniel 1988; Meeks et al. 1995) for the transport cross sections in terms of the phase shifts. For the momentum transfer cross section, the equation is

$$\overline{Q}^{(1)}(\varepsilon) = \frac{4\pi}{\widetilde{\kappa}^2} \sum_{l} (l+1) \sin^2 (\eta_l - \eta_{l+1}), \qquad (6.71)$$

where $\widetilde{\kappa}$ is the wave number of the relative motion of the ion-neutral pair. The phase shift, η_l , corresponding to the angular momentum quantum number, l, and the collision energy, ε , are obtained from quantum-mechanical calculations that are described in almost all textbooks for beginning courses in quantum mechanics.

Figure 6.3 compares the classical and quantum values for $\overline{Q}^{(1)}(\varepsilon)$ obtained by Viehland and Hurly (1996). The classical values were calculated from computer program MOBDIF (Viehland 1982, 1984), a predecessor of program PC discussed in the previous subsection. Although improved potentials and computer programs for calculating $\overline{Q}^{(1)}(\varepsilon)$ have been developed in the past twenty years, the 1996 calculations are accurate enough to show that classical-quantum differences can be ignored

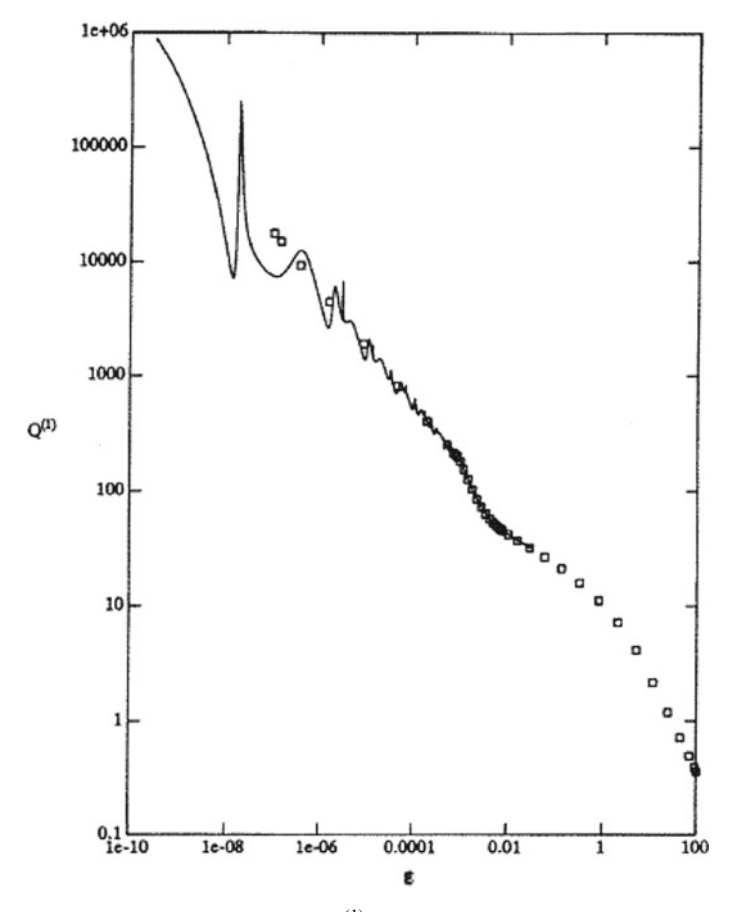


Fig. 6.3 Momentum-transfer cross section, $\overline{Q}^{(1)}$, for Ar⁺(2 S_{1/2}) in He(1 S₀), as a function of collision energy, ε . The curve is from quantum calculations and the squared from classical calculations

above about 10^{-4} E_h. Graphs similar to Fig. 6.3 have been obtained for $\overline{Q}^{(l)}(\varepsilon)$ with l indices from 2–5.

Averaging the transport cross sections over energy to get collision integrals will reduce the discrepancy between the classical and quantum values. Therefore, quantum-mechanical calculations are not necessary for theoretical determinations of the transport coefficients measured in DTMS and IMS apparatus, except for light atomic ions and atoms at extremely low T_0 and for systems that exhibit resonant charge transfer.

6.22.3 Resonant Charge Transfer

As discussed in Sect. 1.13, it has been known in principle since the 1930s how to calculate the transport cross sections for systems with resonant charge transfer (RCT) from quantum-mechanical phase shifts. Although numerical algorithms and computer resources have advanced tremendously since then, it remains difficult to make accurate calculations of the $\overline{Q}^{(l)}(\varepsilon)$ when RCT is involved. This is particularly the case when the energies probed in drift-tubes are large, due to high values of T_0 or E/n_0 , where a large number of phase shifts are involved, there can be modulo π errors (Wei and Le Roy 2006) in the calculation of phase shifts for large angular momentum numbers, and a large number of slightly different transport cross sections are needed in the kinetic theories discussed in Chap. 5. It is natural then to turn to a semi-classical treatment of the phase shifts.

A semi-classical picture of RCT was given by Holstein (1952). It indicates that RCT converts a glancing collision into an apparent head-on collision, thus making $\overline{Q}^{(1)}(\varepsilon)$ abnormally large compared to the viscosity cross section, $\overline{Q}^{(2)}(\varepsilon)$. Dalgarno (1958) gave a semi-classical description of RCT that showed that $\overline{Q}^{(1)}(\varepsilon)$ is approximately twice as large as the cross section for RCT, $Q_{RCT}(\varepsilon)$. After computers had advanced enough, Heiche and Mason (1970) used both quantum-mechanical and semi-classical techniques to calculate $Q_{RCT}(\varepsilon)$ and the first three $\overline{Q}^{(l)}(\varepsilon)$ for ${}^4\text{He}^+({}^2S_{1/2})$ in ${}^4\text{He}({}^1S_0)$. Their results showed that the semi-classical cross sections are quite accurate, particularly when one realizes that it is energy averages of the cross sections that govern the transport coefficients, and that averaging washes out most, but not all, of the structure in the quantum-mechanical cross sections. Sinha et al. (1979) showed that the residual differences make the quantum-mechanical mobilities for ${}^4\text{He}^+({}^2S_{1/2})$ in ${}^4\text{He}({}^1S_0)$ at room temperature smaller than the semi-classical values.

In DTMS and IMS experiments, there are basically only six atomic systems (not counting different isotopes) where RCT must be considered—the rare gas ions in their parent gases. Since the two nuclei are the same in such cases, each wave function must be either symmetric or antisymmetric with respect to interchange of the nuclei. These are referred to as g (gerade) and u (ungerade) potentials, respectively, and both must be considered simultaneously when evaluating the transport cross sections. For $^4\mathrm{He}^+(^2\mathrm{S}_{1/2})$ in $^4\mathrm{He}(^1\mathrm{S}_0)$, only one g-u pair is involved, but for the heavier rare gases three pairs must be considered. Fortunately, it follows from the assumption of a purely electrostatic Hamiltonian operator and the Born–Oppenheimer (BO) approximation that different g-u pairs of molecular states do not interact.

For ${}^4\text{He}_2^+$ in the ground state, the best PECs available in 2015 were those of Xie et al. (2005) and Tung et al. (2012). Because of technical problems with those potentials, new g-u potentials were determined by Viehland et al. (2016) using the CAS+MRCI method. A d-aug-cc-pVXZ basis set was used, with X = 6 and 7 extrapolated to the CBS limit. For r values below 1.51 a_0 , their potentials (and the previous ones) show unusual behavior assumed to be due to an avoided crossing with a higher

excited state. For calculating the ion transport coefficients, the potential was extrapolated to smaller separations using an inverse power potential that matches the first two points with $r > 1.51 \ a_0$; extrapolation is justified because this region of V(r) should have negligible effect on the transport and spectroscopic parameters of the system. The calculated values of the latter were in excellent agreement with the available experimental results.

Because they needed high precision in their calculations, Viehland et al. (2016) wrote a new Fortran computer program called QEx that extends the techniques in Viehland and Chang (2010) to a g-u pair of potentials for a system with RCT. The RCT, momentum-transfer and viscosity cross sections they obtained were in excellent agreement with those obtained from an earlier, less precise, computer program. They then used program GC (see below) to determine the transport coefficients for ${}^4\text{He}^+({}^2\text{S}_{1/2})$ in ${}^4\text{He}({}^1\text{S}_0)$ at temperatures where experimental results were available. Comparisons were also made with new experimental values obtained by Viehland et al. (2016). The new data agreed well with the theoretical ones, but it was concluded that only one set of previous data is reliable.

6.23 Gaseous Ion Transport Coefficients

6.23.1 Computer Program GC

Accurate, ab initio calculations of gaseous ion transport coefficients involve two main steps. First, the transport cross sections are calculated from the ab initio interaction potential, most often now by using program PC (see Sect. 6.22.1). Then the transport cross sections are used in one of the techniques discussed in Chap. 5 for solving the Boltzmann equation. Accurate results are now usually achieved by using the Gram–Charlier basis functions discussed in Sect. 5.9. The computer program called GC (Yousef et al. 2007; Danailov et al. 2008) uses the Gram–Charlier method, and it may be viewed as a specific implementation of the unified solution technique (Konovalov et al. 2017) for solving the Boltzmann equation for the case of electrons or atomic ions moving through atomic gases.

6.23.2 Field-Dependent Mobilities

Figure 6.4 compares standard mobilities, K_0 , calculated from computer program GC for 138 Ba⁺(2 S_{1/2}) in Ar(1 S₀) at 315 K with the experimental values of Penn et al. (1990) and Bastian et al. (1993). The theoretical values were obtained from the transport cross sections calculated for the four ab initio interaction potentials described in Sect. 6.22.1. It is clear that the potential of McGuirk et al. (2009) gives results that are too high, compared to experiment. This is consistent with our statement in

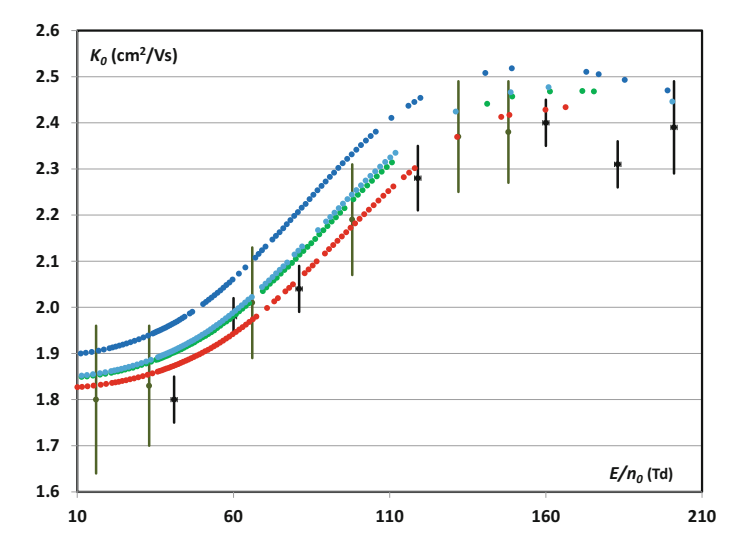


Fig. 6.4 Standard mobility, K_0 , as a function of the reduced field strength, E/n_0 , for ¹³⁸Ba⁺(2 S_{1/2}) in Ar(1 S₀) at 315 K. The color coding is the same as in Fig. 6.1. The black and gray points are from Penn et al. (1990) and Bastian et al. (1993), respectively. The black and gray lines represent the possible errors estimated by the experimenters

Sect. 6.22.1 about the accuracy of this potential. The other three potentials give K_0 values within the experimental error bars, but the most recent potential of Tuttle et al. (2018) matches the data most closely.

To date, theoretical mobilities have been calculated from ab initio atomic ion-atom interaction potential energies for 46 ions. When different charge states are included, the number becomes 61. It grows to 136 when different isotopes are included. When low-lying excited states are included along with the ground state, the number is above 200. Each of these state-specific ions can move through a gas made of the naturally-occuring mixture of the isotopes of one of the six rare gases. This gives more than 1200 combinations, many of which have several ab initio potentials available. Transport coefficients for each of the approximately 5000 cases are given at T_0 values of 100, 200, 300, 400 and 500 K (plus 4.35 K when the gas is He). Clearly there is now an immense database (LXCat 2018) available on the internet of theoretical values of gaseous ion mobilities and other transport coefficients. A smaller but still significant set of experimental values that cover a wide range of E/n_0 values is also included in the LXCat database (2018). The tables for both the theoretical and experimental values indicate the maximum percentage errors expected in various ranges of E/n_0 .

The periodic table in Fig. 6.5 is a guide to the theoretical gaseous ion transport data in the LXCat database (2018). A box that is completely filled indicates that the ion or ions indicated by the element symbol and the box color have been studied in 5 or 6 of the rare gases; Rn is sometimes omitted. A box that is partly filled indicates that the ion or ions have been studied (so far) in only a few of the rare gases; typically this

Н		Charge Rare Gases										Не					
Li	Ве	+1 -1 ±1 5 or 6: Filled +2 +1,+2 Some: Partly Filled +1,+3						В	С	N	0	F	Ne				
Na	Mg									Al	Si	Р	S	CI	Ar		
К	Ca	Sc	Ti	٧	Cr	Mn	Fe	Со	Ni	Cu	Zn	Ga	Ge	As	Se	Br	Kr
Rb	Sr	Υ	Zr	Nb	Мо	Tc	Ru	Rh	Pd	Ag	Cd	ln	Sn	Sb	Те	Ι	Xe
Cs	Ва	La	Hf	Та	W	Re	Os	lr	Pt	Au	Hg	TI	Pb	Bi	Po	At	Rn
Fr	Ra	Ac	Rf	Db	Sg	Bh	Hs	Mt	Ds	Rg	Ср	Nh	FI	Мс	Lv	Ts	Og
		Се	Pr	Nd	Pm	Sm	Eu	Gd	Tb	Dy	Но	Er	Tm	Yb	Lu		
		Th	Pa	U	Np	Pu	Am	Cm	Bk	Cf	Es	Fm	Md	No	Lr		

Fig. 6.5 Periodic table showing atomic ions for which gaseous ion mobilities have been calculated

means He-Ar only. Note that results have been calculated for ions of three elements (Rn, Fr and Ra) that do not have stable isotopes.

There are clearly many more atomic ion-rare gas systems that can be studied. Moreover, there are omissions that are surprising because the ions are important (for example, in the upper atmosphere), common, or easy to make. Figure 6.5 will need to be updated frequently in the years ahead.

6.23.3 Zero-Field Mobilities

A slight modification of computer program GC allows the zero-field mobilities, $K_0(0, T_0)$, to be calculated as a function of T_0 with the same accuracy and precision as the transport cross sections. The resulting computer program, named vary, has been used to add such values to the tables in the LXCat database (2018). These data can be used to assess the accuracy of various IMS techniques (see Chap. 2), assuming that they have been used to study atomic ions in a rare gas.

IMS measurements have been made of the zero-field mobilities of lanthanide ions in He at 295 K (Manard and Kemper 2017) and in Ar at 300 K (Laatiaoui et al. 2012). The values are compared in Table 6.4 with those calculated to an accuracy of 0.05% from the potentials of Buchachenko and Viehland (2014) that were labeled MWB. The theoretical calculations were repeated more recently, by shifting the potentials so that they matched the ion-induced dipole potential at the largest tabulated potentials (see above), which is why the values reported here differ slightly from the original ones. In the case of Gd, the theoretical values from 2014 are now believed to be

Ion	Neutral	$K_0(0) \text{ (cm}^2/\text{Vs)}$			
		Theory	Expt.		
¹⁵¹ Eu ⁺ (⁹ S ₄)	Не	18.289	18.4 ± 0.4		
$^{156}\text{Gd}^{+}(^{10}\text{D}_{5/2})$	Не	20.599	20.8 ± 0.5		
$^{174}\text{Yb}^{+}(^{2}\text{S}_{1/2})$	Не	19.159	19.5 ± 0.4		
$^{175}Lu^{+}(^{1}S_{0})$	Не	16.552	16.8 ± 0.4		
¹⁵¹ Eu ⁺ (⁹ S ₄)	Ar	1.9134	1.84 ± 0.03		
$^{156}\text{Gd}^{+}(^{10}\text{D}_{5/2})$	Ar	1.7376	1.69 ± 0.03		
$^{174}\text{Yb}^{+}(^{2}\text{S}_{1/2})$	Ar	1.8625	1.84 ± 0.03		

Table 6.4 Comparison of theoretical and experimental values of the zero-field mobility for lanthanide ions in rare gases

inaccurate for technical reasons, so the tabulated values are from recent work by Buchachenko and Viehland that has not yet been published.

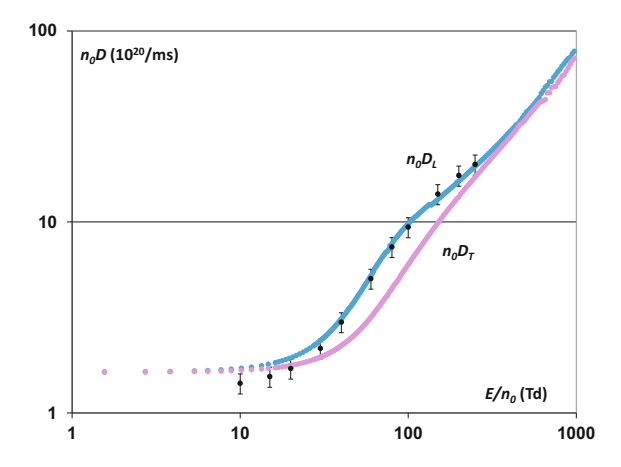
The experimental values in He are systematically higher than the theoretical values, although the error bars are large enough to encompass them. The experimental values in Ar are systematically lower and the error bars do not always include the theoretical values. This suggests that these and other IMS experimenters should use the techniques discussed in Sect. 2.2.9 to calibrate their instruments using atomic ions in rare gases, both to correct values already measured for molecular, biochemical or biological ions and to make sure that new measurements for such ions are as accurate as possible.

6.23.4 Diffusion Coefficients

Each of the theoretical files in the LXCat database (2018) containing field-dependent mobilities also contains ion diffusion coefficients parallel and perpendicular to the electric field, in the form of n_0D values. There are three labels used interchangeably for the parallel values: n_0D_z , n_0D_L or n_0D_{\parallel} . Similarly the perpendicular values are labeled n_0D_x , n_0D_T or n_0D_{\perp} .

The diffusion coefficients have not been measured as often as the mobility. One system that has been studied is ${}^{81}\text{Br}^{-}({}^{1}\text{S}_{0})$ in $\text{Ar}({}^{1}\text{S}_{0})$ at 300 K. Figure 6.6 compares the experimental values of Holleman et al. (1982) for $n_{0}D_{L}$ with theoretical values calculated with programs PC and GC by Buchachenko et al. (2006). The agreement is very good, given the rather large error bars estimated by the experimenters. As discussed in Sect. 2.4, it is difficult to determine accurate values for the diffusion coefficients, especially at large E/n_{0} . If values are needed for particular applications, it is recommended that one use the theoretical values in the LXCat database (2018).

Fig. 6.6 Products n_0D_L (blue) and n_0D_T (pink) for $^{81}\mathrm{Br}^-(^1\mathrm{S}_0)$ in $\mathrm{Ar}(^1\mathrm{S}_0)$ at 300 K, as functions of E/n_0 . The points are the smoothed values of n_0D_L from Holleman et al. (1982)



6.23.5 Other Transport Coefficients

The ion vdf for 138 Ba $^+(^2S_{1/2})$ in the rare gases have been probed (Dressler et al. 1988) by single-frequency laser-induced fluorescence (LIF) in a manner that has so far not been found possible with any other atomic ion-atom system. The laser beam propagates either along or perpendicular to the axis of the drift tube, i.e. parallel or perpendicular to the electric field. Doppler profiles of the drifting ions are obtained by scanning the laser frequency and plotting the LIF intensity as a function of the frequency shift. The signal-to-noise ratio is small, so rather long observation times are needed. Nevertheless, it is possible to obtain the ion drift velocity (and hence the standard mobility) from the measured frequency shift and the wavelength (in vacuum) of the transition between energy levels that is being probed.

In 1988 there was no other data for 138 Ba⁺(2 S_{1/2}) in He(1 S₀) to which the results of Dressler et al. (1988) could be compared. Since then, theoretical results have been calculated using computer programs PC and GC for the potential of McGuirk et al. (2009), those obtained by Buchachenko and Viehland (2014) with an aug-cc-pwCVXZ basis set and in the CBS limit, and the potential of Tuttle et al. (2018). Figure 6.7 compares the standard mobilities calculated from those potentials with the LIF values. The experimental values lie significantly below the theoretical values at all but the smallest values of E/n_0 . Nevertheless, the agreement is good, since the method used by Dressler et al. (1988) to obtain the standard mobilities is not performed in one of the traditional methods discussed in Chap. 2 and is subject to saturation of the laser beam and other optical phenomena such as optical pumping into metastable states (that are likely to have a smaller mobility).

Ion temperatures parallel and perpendicular to the field can be obtained from the full width at half maxima of the LIF intensities as a function of the frequency shifts. T_L values obtained by Dressler et al. (1988) are compared with more recent, theoretical values in Fig. 6.8. The agreement is good, although the experimental error bars are somewhat large. Note that the four potentials give ion temperatures that are

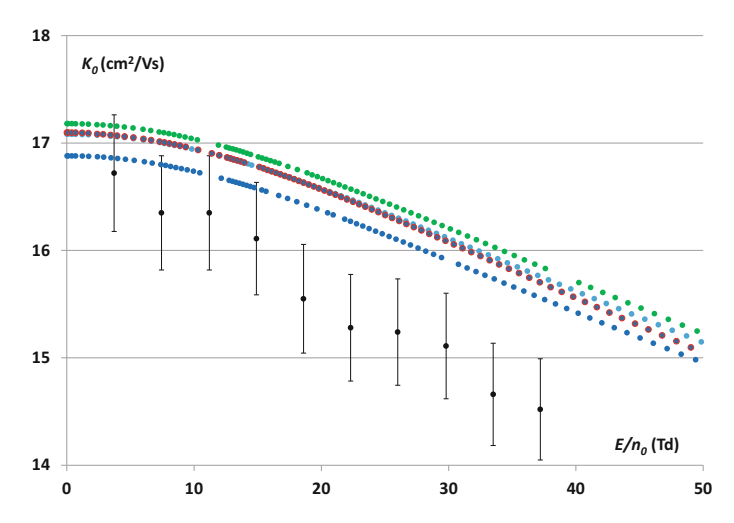


Fig. 6.7 Standard mobility, K_0 , as a function of the reduced field strength, E/n_0 , for ¹³⁸Ba⁺(2 S_{1/2}) in He(1 S₀) at 313 K. The color coding is the same as in Fig. 6.1. The black points are from Dressler et al. (1988). The black lines represent the possible errors estimated by the experimenters

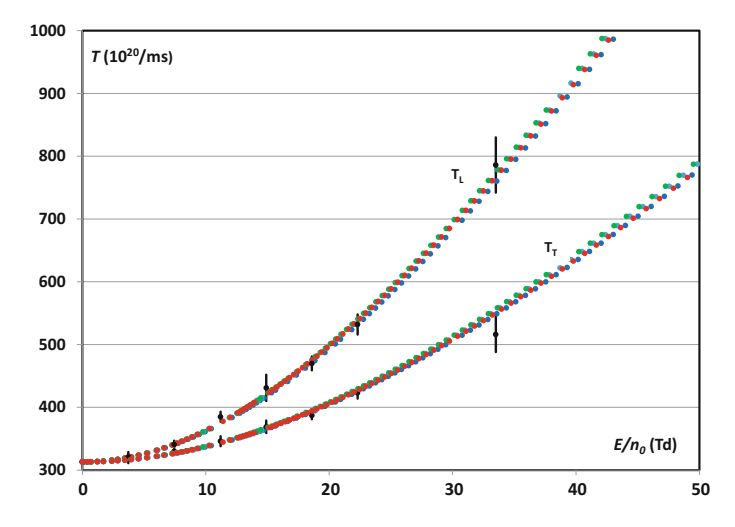


Fig. 6.8 Same as Fig. 6.7 but for the ion temperatures parallel and perpendicular to the field

very similar in value, so measured values of them cannot serve as good discriminators of ion-neutral interaction potentials.

The LXCat database (2018) contains tables of zero-field mobilities, $K_0(0)$, as a function of T_0 . It also contains tables of ten gaseous ion transport coefficients as functions of T_0 and E/n_0 for about 5000 ion-neutral combinations. Each of the field-dependent tables lists K_0 , n_0D_L , n_0D_T , T_L and T_T values. They also give values of the five deviation parameters defined in Sect. 5.9: the parallel skewness (α_L), the

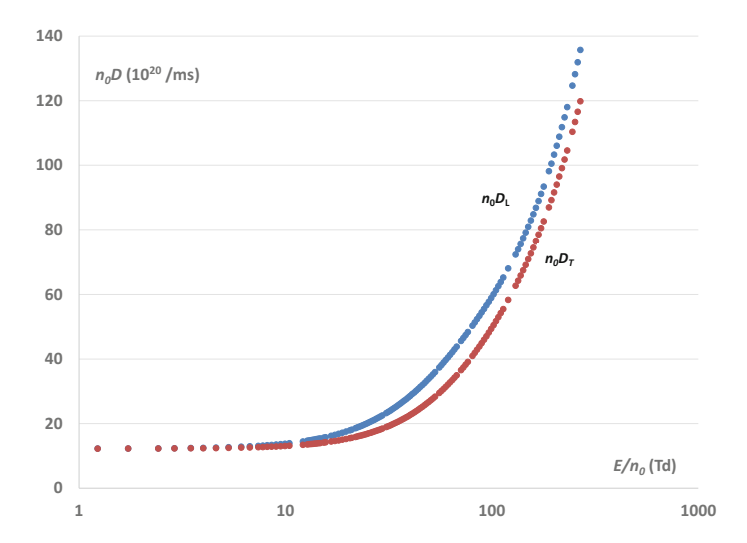


Fig. 6.9 Same as Fig. 6.7 but for the products of the gas number density and the ion diffusion coefficients parallel and perpendicular to the field

parallel excess kurtosis (β_L), the perpendicular excess kurtosis (β_T), the correlation coefficient (γ_1) between the parallel velocity and the perpendicular energy, and the correlation coefficient (γ_2) between the parallel and perpendicular energies.

Figure 6.9 shows the diffusion coefficients that correspond to the mobilities and ion temperatures in Figs. 6.7 and 6.8; for clarity of presentation, only the values calculated from the potential of Tuttle et al. (2018) are shown. Similar graphs at a variety of gas temperatures are shown in Figs. 1.2 and 1.3. Finally, an illustration of the field dependence of the other five transport properties will be shown in Chap. 7, where they are relevant to a discussion of gaseous ion reactions in drift tubes.

Subsequent work at Boulder (Penn et al. 1990; Bastian et al. 1993) resulted in experimental values for K_0 , T_L , T_T , α_L , β_L and β_T for 138 Ba $^+$ (2 S $_{1/2}$) in Ar(1 S $_0$) at 305 K. Comparisons were made in that work with theoretical values computed from an ion-neutral interaction potential inferred (Viehland and Hampt 1992) from the LIF data; since there were no ab initio potentials available, that was the best that could be done at that time. Improved potentials have been developed since that time, so here we will compare the LIF experimental values with those calculated from the CBS potential of Buchachenko and Viehland (2018) and the high quality, ab initio potential of Tuttle et al. (2018) for this system.

Figure 6.10 compares the experimental and theoretical mobilities at 305 K for 138 Ba $^+$ (2 S $_{1/2}$) in Ar(1 S $_0$). The agreement is excellent, with the exception of three values from Bastian et al. (1993) that appear to be in error based on a comparison with the other experimental values as well as the theoretical values. The agreement supports the accuracy of both the experimental measurements and the theoretical calculations based on computer programs PC and GC.

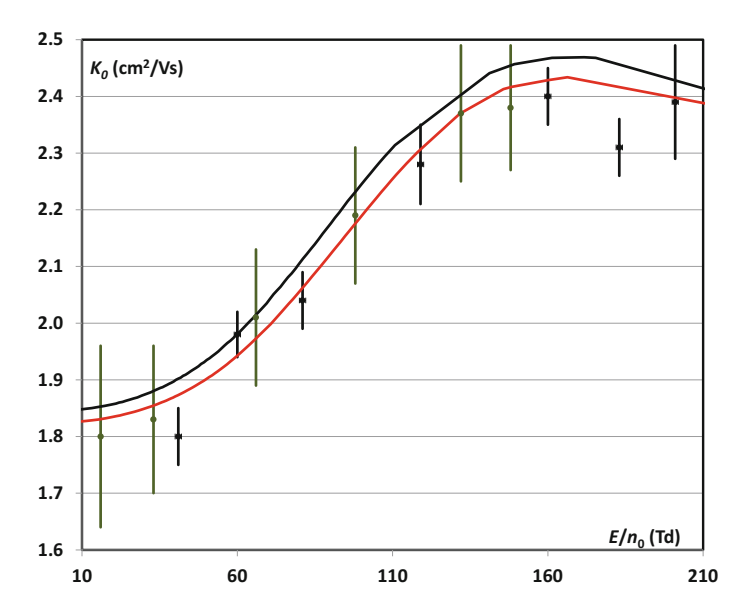


Fig. 6.10 Reduced mobility, K_0 , as a function of the reduced field strength, E/n_0 , for 138 Ba⁺(2 S_{1/2}) ions in Ar(1 S₀) at 305 K. The upper, black curve is calculated from the CBS potential of Buchachenko and Viehland (2018). The lower, red curve is calculated from the potential of Tuttle et al. (2018). The experimental points with large error bars are from Penn et al. (1990), while those with small ones are from Bastian et al. (1993)

Figure 6.11 compares the experimental and theoretical values of the ion temperatures for 138 Ba⁺(2 S_{1/2}) in Ar(1 S₀) at 305 K. The agreement is good, although it is better with the older data (Penn et al. 1990) than the new (Bastian et al. 1993). The two sets of theoretical values are extremely close, and they are probably more accurate than either set of experimental ion temperatures.

Penn et al. (1990) and Bastian et al. (1993) reported experimental values of a skewness parameter, δ_s , that is related to the Gram-Charlier skewness in Sect. 5.9 by the equation,

$$\delta_s = \alpha_I^{1/3}. (6.72)$$

Table 6.5 compares their values with those calculated for 138 Ba $^+(^2S_{1/2})$ in Ar(1S_0) at 305 K from the CBS potential of Buchachenko and Viehland (2018) and the potential of Tuttle et al. (2018). The agreement is excellent, especially considering the increased difficulty of the theoretical calculations (the error bars are larger than for the mobility, especially above 45 Td) and the difficulty of the measurements. Remember that these are the only experimental results for δ_s for any atomic ionatom system.

By making measurements with the laser parallel, perpendicular, and at a 45° angle to the electric field in the drift tube, Bastian et al. (1993) determined moments of the vdf at different angles for 138 Ba $^{+}$ (2 S_{1/2}) in Ar(1 S₀) at 305 K. These values

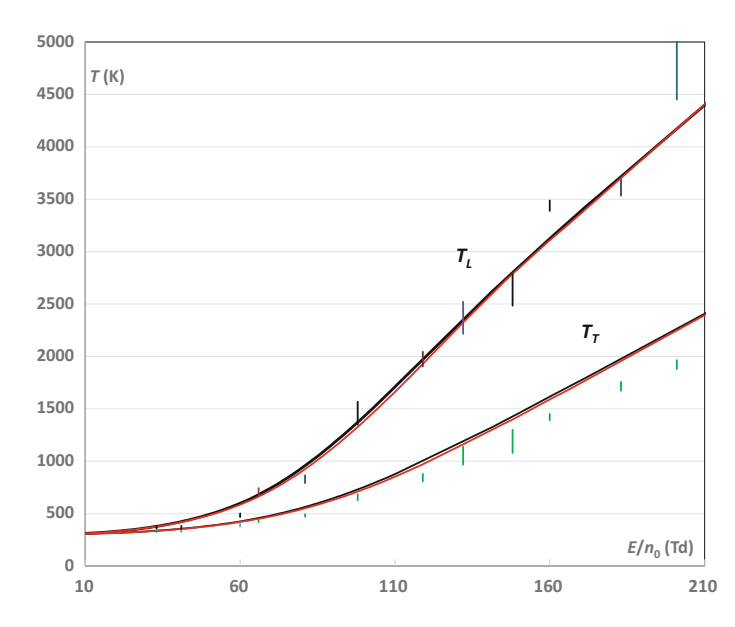


Fig. 6.11 Same as Fig. 6.10, for the ion temperatures parallel and perpendicular to the field

Table 6.5 Comparison of experimental and theoretical values of δ_s

E/n_0 (Td)	Experimental		Theoretical			
	Penn et al. (1990)	Bastian et al.	Buchachenko and	Tuttle et al.		
		(1993)	Viehland (2018)	(2018)		
0	0	0	0	0		
33		0.44 ± 0.08	0.4608 ± 0.0002	0.4512 ± 0.0002		
41	0.52 ± 0.02		0.5419 ± 0.0002	0.5323 ± 0.0002		
60	0.82 ± 0.02		0.7150 ± 0.0003	0.71 ± 0.04		
66		0.63 ± 0.07	0.76 ± 0.04	0.75 ± 0.04		
81	0.93 ± 0.03		0.85 ± 0.04	0.84 ± 0.04		
98		0.74 ± 0.07	0.88 ± 0.04	0.89 ± 0.04		
119	0.95 ± 0.03		0.87 ± 0.04	0.88 ± 0.04		
132		0.83 ± 0.08	0.86 ± 0.04	0.86 ± 0.04		
148		0.76 ± 0.10	0.83 ± 0.04	0.85 ± 0.04		
160	0.93 ± 0.03		0.82 ± 0.04	0.84 ± 0.04		
183	0.87 ± 0.03		0.82 ± 0.04	0.85 ± 0.04		
201	0.84 ± 0.08		0.83 ± 0.04	0.83 ± 0.04		

demonstrated that a positive correlation exists between the velocity components parallel and perpendicular to the field. In terms of the Gram-Charlier parameters in Sect. 5.9, this means $\gamma_2 > 0$. Although Bastian et al. (1993) claimed that this was the first experimental verification of the velocity component correlation in DTMS experiments, they were apparently not aware of the earlier work of Ong et al. (1992).

6.24 Summary

Gaseous ion transport coefficients can be calculated now with greater precision and accuracy than they can be measured, if the ion-neutral interaction potential supplied to programs PC and GC is highly accurate. In some cases, comparisons between theoretical and experimental values have indicated weakness in either V(r) or in the experimental data. However, in the majority of the cases, and particularly when the potentials are of recent vintage, the theoretical values fall within the experimental error bars, indicating that both V(r) and the experimental data are accurate.

We have indicated above that there are many atomic ion-atom systems that still need to be studied. This remains a task for the near future, but this work will be largely pedestrian. The big task that remains incomplete is the relationship between the fundamental PES for molecular ion-neutral systems and measured gaseous ion transport coefficients. Therefore, we will turn to molecular systems in Chap. 8, after first discussing drift-tube measurements of reaction rate coefficients.

References

M.J. Bastian, C.P. Lauenstein, V.M. Bierbaum, S.R. Leone, J. Chem. Phys. 98, 9496 (1993)

E. Besalú, R. Carbó-Dorca, J. Math. Chem. 49, 1769 (2011)

H. Bethe, E. Salpeter, Phys. Rev. 84, 1232 (1951)

J. Boschmans, S. Jacobs, J.P. Willisma, M. Palmer, K. Richardson, K. Giles, C. Lapthorn, W.A. Herrebout, F. Lemiere, F. Sobott, Analyst 141, 4044 (2016)

A.A. Buchachenko, J. Klos, M.M. Szczesniak, G. Chalsinski, B.R. Gray, T.G. Wright, E.L. Wood, L.A. Viehland, E. Qing, J. Chem. Phys. 125, 064305 (2006)

A.A. Buchachenko, L.A. Viehland, J. Chem. Phys. 140, 114309 (2014)

A.A. Buchachenko, L.A. Viehland, J. Chem. Phys. 148, 154304 (2018)

A. Carrington, C.A. Leach, A.J. Marr, A.M. Shaw, M.R. Viant, J.M. Hutson, M.M. Law, J. Chem. Phys. 102, 2379 (1995)

A. Dalgarno, Phil. Trans. Roy. Soc. A 250, 426 (1958)

D.M. Danailov, L.A. Viehland, R. Johnsen, T.G. Wright, A.S. Dickenson, J. Chem. Phys. 128, 134302 (2008)

R.A. Dressler, J.P.M. Beijers, H. Meyer, S.M. Penn, V.M. Bierbaum, S.R. Leone, J. Chem. Phys. 89, 4707 (1988)

K.G. Dyall, K. Fægri Jr, Introduction to Relativistic Quantum Chemistry (Oxford University Press, Oxford, 2007)

G. Heiche, E.A. Mason, J. Chem. Phys. 53, 4687 (1970)

References 217

A. Halkier, T. Helgaker, P. Jørgensen, W. Klopper, H. Koch, J. Olsen, A.K. Wilson, Chem. Phys. Lett. 286, 243 (1998)

- A. Halkier, T. Helgaker, P. Jørgensen, W. Klopper, H. Koch, J. Olsen, A.K. Wilson, Chem. Phys. Lett. 302, 437 (1999)
- J.O. Hirschfelder, C.F. Curtiss, R.B. Bird, Molecular Theory of Gases and Liquids (Wiley, New York, 1964)
- F.B. Holleman, W.M. Pope, F.L. Eisele, J.R. Twist, G.W. Neeley, M.G. Thackston, R.D. Chelf, E.W. McDaniel, J. Chem. Phys. **76**, 2106 (1982)
- T. Holstein, J. Phys. Chem. **56**, 832 (1952)
- J.J. Hurly, W.L. Taylor, F.R. Meeks, J. Chem. Phys. 96, 3775 (1992)
- M. Jacoby: Chem. Eng. News, Jan. 9, 2017, p. 5
- A. Kahros, B.J. Schwartz, J. Chem. Phys. 138, 054110 (2013)
- T. Kato, Commun. Pure Appl. Math. 10, 151 (1957)
- D.A. Konovalov, D.G. Cocks, R.D. White, Euro. Phys. J. D 71, 258 (2017)
- M. Laatiaoui, H. Backe, D. Habe, P. Kunz, W. Lauth, M. Sewtz, Eur. Phys. J. D 66, 232 (2012)
- L.D. Landau, E.M. Lifshitz, *Quantum Mechanics: Non-Relativistic Theory* (Pergamon Press, Oxford, 1965)
- E. Lewars, Computational Chemistry: Introduction to the Theory and Applications of Molecular and Quantum Mechanics (Kluwer Academic Publishers, Boston, 2003)
- I.S. Lim, P. Schwerdfeger, Phys. Rev. A 70, 062501 (2004)
- I.S. Lim, H. Stoll, P. Schwerdfeger, J. Chem. Phys. 124, 034107 (2006)
- LXCat database, https://fr.lxcat.net/data/set_type.php. Accessed Aug 2018 (2018)
- M.J. Manard, P.R. Kemper, Int. J. Mass Spectrom. 412, 14 (2017)
- E.A. Mason, E.W. McDaniel, Transport Properties of Ions in Gases (Wiley, New York, 1988)
- E.W. McDaniel, L.A. Viehland, Phys. Rep. 110, 333 (1984)
- M.F. McGuirk, L.A. Viehland, E.P.F. Lee, W.H. Breckenridge, C.D. Withers, A.M. Gardner, R.J. Plowright, T.G. Wright, J. Chem. Phys. 130, 194305 (2009)
- M.G. Medvedev, I.S. Bushmarinov, J. Sun, J.P. Perdew, K.A. Lyssenko, Science 355, 49 (2017)
- F.R. Meeks, T.J. Cleland, K.E. Hutchinson, W.L. Taylor, J. Chem. Phys. 100, 3813 (1994); errarata, J. Chem. Phys. 103, 1239 (1995)
- T. Miller, B. Bederson, Adv. At. Mol. Phys. 25, 37 (1989)
- B. Nagy, F. Jensen, in *Basis Sets in Quantum Chemistry*, in *Reviews in Computational chemistry Vol. 30*, ed by A. L. Parrill, K. B. Lipkowitz (Wiley, New York, 2017)
- P.D. Neufeld, R.A. Aziz, Comput. Phys. Commun. 3, 269 (1972)
- A. Nicklass, K.A. Peterson, A. Berning, H.-J. Werner, P.J. Knowles, J. Chem. Phys. 112, 5624 (2000)
- H. O'Hara, F.J. Smith, J. Comput. Phys. 5, 328 (1970)
- P.P. Ong, M.J. Hogan, K.Y. Lam, L.A. Viehland, Phys. Rev. A 45, 3997 (1992)
- S.M. Penn, J.P.M. Beijers, R.A. Dressler, V.M. Bierbaum, S.R. Leone, J. Chem. Phys. 93, 5118 (1990)
- K.A. Peterson, http://tyr0.chem.wsu.edu/~kipeters/basis-bib.html. Accessed Aug 2018 (2018a)
- K.A. Peterson, http://tyr0.chem.wsu.edu/~kipeters/basis.html. Accessed Aug 2018 (2018b)
- F.L. Pilar, Elementary Quantum Chemistry (McGraw Hill, New York, 1968)
- J.C. Rainwater, P.M. Holland, L. Biolsi, J. Chem. Phys. 77, 434 (1982)
- G. Rasskazov, M. Nairat, I. Magoulas, V.V. Lozovoy, P. Piecuch, M. Dantus, Chem. Phys. Lett. 683, 121 (2017)
- S. Sinha, S.L. Lin, J.N. Bardsley, J. Phys. B 12, 1613 (1979)
- F.J. Smith, R.J. Munn, J. Chem. Phys. 41, 3560 (1964)
- P. Soldan, E.F.P. Lee, T.G. Wright, Phys. Chem. Chem. Phys. 21, 4661 (2001)
- L. Szasz, Pseudopotential Theory of Atoms and Molecules (Wiley, New York, 1985)
- W.-C. Tung, M. Pavanello, L. Adamowicz, J. Chem. Phys. 136, 104309 (2012)
- W.D. Tuttle, R.L. Thorington, L.A. Viehland, T.G. Wright, Mol. Phys. 113, 3767 (2015)

- W.D. Tuttle, R.L. Thorington, L.A. Viehland, W.H. Breckenridge, T. G. Wright, Phil. Trans. Roy., Soc. A 376, 20170156 (2017)
- W.D. Tuttle, J.P. Harris, Y. Zheng, W.H. Breckenridge, T.G. Wright, J. Phys. Chem. A 122, 7679 (2018)
- L.A. Viehland, Chem. Phys. 70, 149 (1982)
- L.A. Viehland, Chem. Phys. 85, 291 (1984)
- L.A. Viehland, Y. Chang, Comp. Phys. Commun. 181, 1687 (2010)
- L.A. Viehland, D.S. Hampt, J. Chem. Phys. 97, 4964 (1992)
- L.A. Viehland, J.J. Hurly, J. Chem. Phys. 105, 11143 (1996)
- L.A. Viehland, C.-L. Yang, Mol. Phys. 113, 3874 (2015)
- L.A. Viehland, R. Johnsen, B.R. Gray, T.G. Wright, J. Chem. Phys. 144, 074306 (2016)
- L.A. Viehland, T. Skaist, C. Adhikari, W.F. Siems, Int. J. Ion Mobil. Spec. 20, 1 (2017)
- H. Wei, R.J. Le Roy, Mol. Phys. 104, 147 (2006)
- H.T. Wood, J. Chem. Phys. 54, 977 (1971)
- J. Xie, B. Poirier, G.I. Gellene, J. Chem. Phys. 122, 184310 (2005)
- A. Yousef, S. Shrestha, L.A. Viehland, E.P.F. Lee, B.R. Gray, V.L. Ayles, T.G. Wright, W.H. Breckenridge, J. Chem. Phys. 127, 154309 (2007)

Chapter 7 Reactions in Drift Tubes



7.1 Importance of Drift Tubes for Ion–Molecule Reactions

Ion-molecule reactions are an important part of chemistry, but their study covers such a wide range of things that a book the size of this one can only describe a small fraction of this research field. We focus on the range of kinetic energy from about 0.1 to 2 eV, equivalent to thermal energies from 1000 to 20,000 K. This range can best be studied by using a drift tube, either as a stand-alone device or in combination with a mass spectrometer and/or a flowing afterglow apparatus. The history of flowing afterglow experiments has been reviewed several times (Graul and Squires 1988; Bohme 2000; Bierbaum 2015) and will not be repeated here.

At collision energies below about 0.1 eV, there are many macroscopic techniques that can be used to study ion–neutral reactions. Most involve measuring the loss of reactant ions or the gain of productions as a function of temperature. Such experiments cannot be carried out above about 1000 K because the apparatus begins to soften and then melt.

At energies above about 2 eV, ion–neutral reactions can be studied by a variety of beam techniques in high vacuum. Such single-particle experiments cannot be carried out for ion–neutral reactions much below 2 eV because collisions of the ions with the walls of the apparatus build up static electricity that is sufficiently large that it influences the motion of the ions and makes it impossible to determine the actual energy of the gas-phase reactants.

In this chapter, we will consider ion—molecule reactions in drift tubes containing a trace amount of atomic ions moving through a dilute gas composed of a large amount of rare-gas atoms and a small amount of a single, reactive molecular neutral. Since the atoms are not affected by the small amounts of the reactive gas or the trace amount of the ions, they have a Maxwellian vdf, as given by (4.18) in terms of the velocity \mathbf{v}_j of the atoms of type j in the laboratory frame of reference. If we normalize this vdf to one when integrated over all velocities, rather than the number density of the neutral gas, then (4.18) can be replaced by

$$f_j(\mathbf{v}_j) = \left(\frac{m_j}{2\pi k_B T_0}\right)^{3/2} \exp\left(-\frac{m_j v_j^2}{2k_B T_0}\right).$$
 (7.1)

The small amount of reactive neutrals also has a Maxwellian vdf if we assume that the vibrational and electronic states of the molecules are at such high energies that these are not populated and that there are so many rotational states available that no specific rotational effects can be observed. Using an *R* subscript to refer to the reactive molecules means that

$$f_R(\mathbf{v}_R) = \left(\frac{m_R}{2\pi k_B T_0}\right)^{3/2} \exp\left(-\frac{m_R v_R^2}{2k_B T_0}\right).$$
 (7.2)

Both $f_j(\mathbf{v}_j)$ and $f_R(\mathbf{v}_R)$ have first moments equal to zero (the average velocities of both types of particles is zero because we assume that the gas is not moving) and second moments equal to the same temperature, T_0 .

The big problem with studying ion—molecule reactions in drift tubes is that the results are affected by the ion vdf that is generally unknown. For many years, it was necessary to make models of the ion vdf in order to interpret data from drift tubes about reactions. These were eventually replaced by Monte Carlo simulations, as discussed in Chap. 9, and by theoretical calculations of the ion vdf by solving the Boltzmann equation. We will focus on the latter in the rest of this chapter.

7.2 The Ion VDF

For Gaseous ion transport and reaction, the Boltzmann equation is linear (see Chap. 4) because there are so few ions present in a flow-drift tube that ion—ion interactions are completely negligible. The solution of this equation may therefore be based on the method of weighted residuals (Appendix C) in which it is assumed that the velocity distribution function (vdf) of the ions in the laboratory frame is equal in zeroth order to the Gram—Charlier (GC) ion vdf (see Chap. 5). This ion vdf is

$$f_{GC}(\mathbf{v}) = \left(\frac{m}{2\pi k_B T_\perp}\right) \left(\frac{m}{2\pi k_B T_\parallel}\right)^{1/2} \exp(-W_x^2 - W_y^2 - W_y^2)$$

$$\left[1 + \frac{\sqrt{2}}{6}\alpha_\parallel W_z(2W_z^2 - 3) + \frac{1}{24}(\beta_\parallel - 3)(4W_z^4 - 12W_z^2 + 3) + \frac{1}{24}(\beta_\perp - 3)(4W_x^4 + 4W_y^4 - 12W_x^2 - 12W_y^2 + 6) + \sqrt{2}\gamma_1(W_x^2 + W_y^2 - 1)W_z + (\gamma_2 - 1)(W_x^2 + W_y^2 - 1)\left(W_z^2 - \frac{1}{2}\right)\right], \quad (7.3)$$

7.2 The Ion VDF 221

where the dimensionless versions of the ion speeds in the laboratory frame of reference are

$$W_i = \left(\frac{m}{2k_B T_\perp}\right)^{1/2} v_{1i},\tag{7.4}$$

for i = x, y and

$$W_z = \left(\frac{m}{2k_B T_{\parallel}}\right)^{1/2} (v_z - v_d). \tag{7.5}$$

The other symbols are transport coefficients known as deviation parameters: α_{\parallel} , the skewness of the distribution along the field direction, β_{\parallel} and β_{\perp} , the excess kurtosis along and perpendicular to the field, and γ_1 , the correlation between ion energy perpendicular to the field and ion velocity parallel to the field, and γ_2 , the correlation between the parallel and perpendicular energies.

The GC ion vdf reduces to the three-temperature ion vdf given by (5.32) when we set $\alpha_{\parallel}=\gamma_1=0$, $\beta_{\parallel}=\beta_{\perp}=3$ and $\gamma_2=1$. This in turn reduces to the two-temperature ion vdf given by (5.23) when $T_{\parallel}=T_{\perp}$ and $v_d=0$. Finally, we get the one-temperature or Maxwellian ion vdf when T_{\parallel} and T_{\perp} are both equal to T_0 .

Below, we will show that the second-order rate coefficient for ion—neutral reactions is determined by the relative ion—neutral vdf. To obtain this vdf, we replace \mathbf{v}_R , in (7.2) and \mathbf{v}_1 in (7.3) with the relative and center-of-mass velocities, \mathbf{g} and \mathbf{G} , given by (3.5) and (3.6) (with the neutral gas subscripts 0 replaced by reactive gas subscripts R). Then the relative vdf is

$$f_{rel}(\mathbf{g}) = \int f_{GC}(\mathbf{v}(\mathbf{g}, \mathbf{G})) f_R(\mathbf{v}_R(\mathbf{g}, \mathbf{G})) d\mathbf{G}.$$
 (7.6)

There are two problems that immediately confront us. The first is that there is a displacement of the ion velocity along the electrostatic field in (7.5). The second is that an exponent involving $\mathbf{g} \cdot \mathbf{G}$ arises. To overcome both problems, we introduce changes of variables similar to those that were made in the appendix of Viehland and Mason (1978). Specifically,

$$\gamma_i = \left(\frac{\mu_R}{2k_B T_{eff,T}}\right)^{1/2} (v_i - v_{R,i}) \quad i = x, y,$$
(7.7)

$$\gamma_z = \left(\frac{\mu_R}{2k_B T_{eff,L}}\right)^{1/2} \left(v_z - v_d - v_{R,z}\right),\tag{7.8}$$

$$\chi_i = \left(\frac{m_R}{2d_T k_B T_0}\right)^{1/2} \left[(1 - d_T) v_i + d_T v_{R,i} \right] \quad i = x, y$$
 (7.9)

and

$$\chi_z = \left(\frac{m_R}{2d_L k_B T_0}\right)^{1/2} \left[(1 - d_L) \left(v_i - v_d \right) + d_L v_{R,z} \right]. \tag{7.10}$$

Here,

$$d_T = \frac{m_R T_T}{m_R T_T + m T_0},\tag{7.11}$$

$$d_L = \frac{m_R T_L}{m_R T_L + m T_0},\tag{7.12}$$

$$T_{eff,T} = \frac{m_R T_T + m T_0}{m_R + m},\tag{7.13}$$

and

$$T_{eff,L} = \frac{m_R T_L + m T_0}{m_R + m}. (7.14)$$

From the equations above, it can be shown after a considerable amount of tedious mathematics that

$$f_{rel}(\mathbf{g}) = \left(\frac{md_T}{2\pi k_B T_T}\right) \left(\frac{md_L}{2\pi k_B T_L}\right)^{1/2} \exp\left(-\gamma_x^2 - \gamma_y^2 - \gamma_z^2\right)$$

$$\times 1 + \frac{\sqrt{2}}{6} \alpha_{\parallel} d_L^{3/2} \left(2\gamma_z^2 - 3\right) \gamma_z + \frac{1}{24} (\beta_{\parallel} - 3) d_L^2 \left(4\gamma_z^4 - 12\gamma_z^2 + 3\right)$$

$$+ \frac{1}{24} (\beta_{\perp} - 3) d_T^2 \left(4\gamma_x^4 - 12\gamma_x^2 + 3 + 4\gamma_y^4 - 12\gamma_y^2 + 3\right)$$

$$+ \sqrt{2} \gamma_1 d_L^{1/2} d_T \left(\gamma_x^2 + \gamma_y^2 - 1\right) \gamma_z$$

$$+ (\gamma_2 - 1) d_L d_T \left(\gamma_x^2 + \gamma_y^2 - 1\right) \left(\gamma_z^{1/2} - \frac{1}{2}\right) \right\}. \tag{7.15}$$

This result is normalized such that

$$\int f_{rel}(\mathbf{g}) d\mathbf{g} = 1. \tag{7.16}$$

By changing the R subscripts to j, the relative vdf given here applies as well to the relative vdf between an ion and a molecule of buffer gas j when there is a gas mixture. By changing the subscripts to 0, (7.15) applies to an ion and a molecule of a pure gas.

It is almost impossible to visualize three-dimensional vdf in Cartesian coordinates. We can, however, take advantage of the uniform nature of the electrostatic field in a drift tube to switch from Cartesian coordinates to cylindrical-polar coordinates. Supplementary material to a paper by Viehland and Johnsen (2018) includes a spreadsheet called SS1 that allows one to visualize the ion vdf in cylindrical-polar

7.2 The Ion VDF 223

Fig. 7.1 Vdf for ${}^{16}{\rm O}^+({}^4{\rm S}_{3/2})$ ions in ${}^{40}{\rm Ar}({}^1{\rm S}_0)$ at 300 K and 0.04 Td

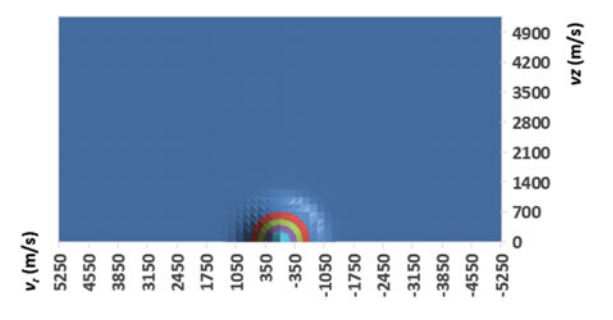
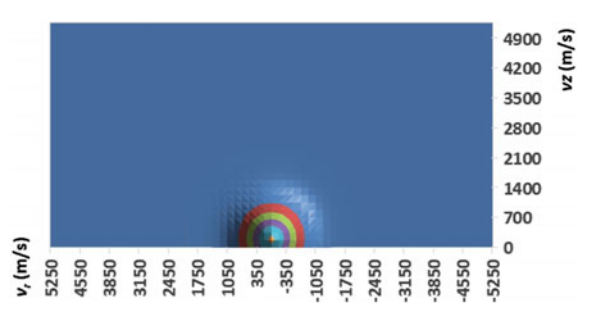


Fig. 7.2 Same as Fig. 7.1 at 25.10 Td

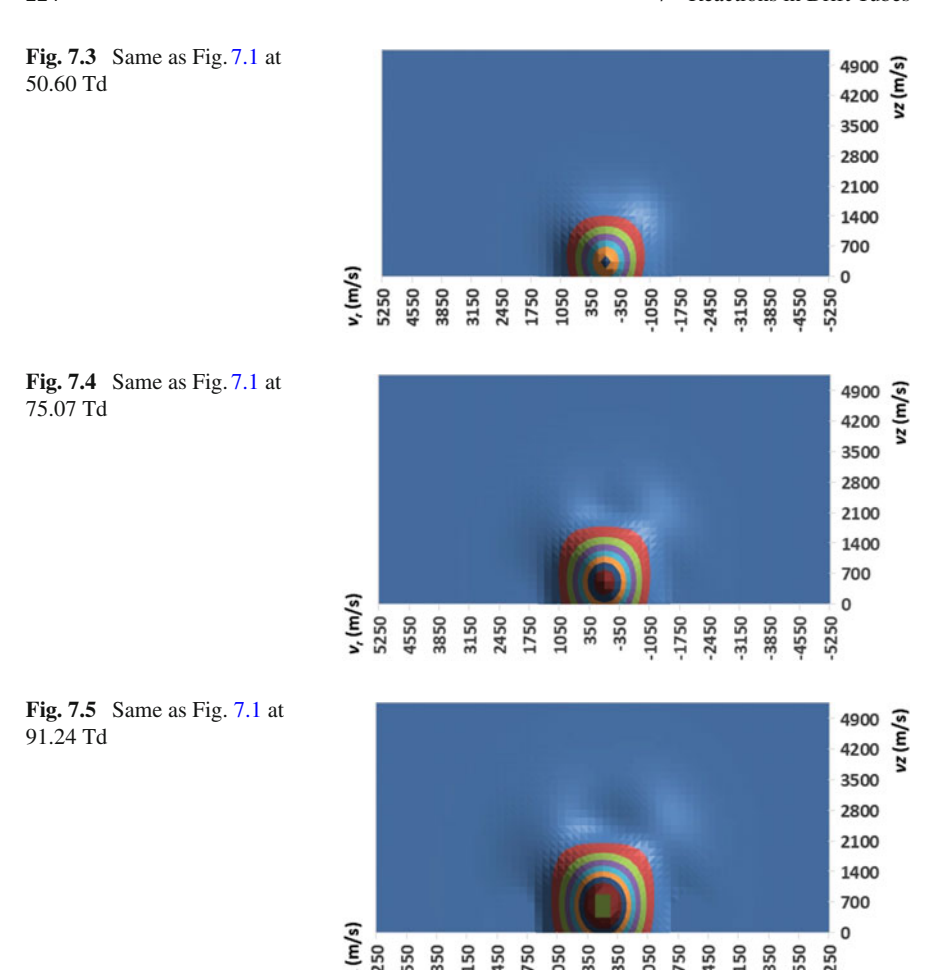


coordinates and another, called SS2, that is for the relative vdf. When they are opened, the spreadsheets have information in the first 11 columns of rows 5 and higher for $^{16}O^+(^4S_{3/2})$ interacting with He(1S_0). This information was computed as described in Chap. 6, using computer program PC to calculate the transport cross sections from the ab initio potential of Danailov et al. (2006), and then using computer program GC to calculate the transport coefficients from the transport cross sections. The ion vdf for $^{16}O^+(^4S_{3/2})$ ions in a naturally occurring mixture of He(1S_0) at 300 K isotopes has been shown as a function of E/n_0 by Viehland and Johnsen (2018), so here we shall focus on a different ion–neutral system, $^{16}O^+(^4S_{3/2})$ in the naturally occurring mixture of Ar(1S_0) isotopes.

Figure 7.1 shows contour plots at low E/n_0 along the v_z and v_r axes, where $v_r^2 = v_x^2 + v_y^2$. This is equivalent to a slice of the $v_x = v_y$ plane through a three-dimensional ion vdf that has spherical symmetry around $v_z = 0$, which is what is expected when the electric field is essentially negligible. A mental picture of the three-dimensional vdf can be obtained by rotating the image in Fig. 7.1 about the horizontal axis. Note that at small E/n_0 , nearly half of the ions are moving against the very weak electric field, i.e., have $v_z < 0$, and thus are not shown here.

Figure 7.2 shows that the spherical symmetry is disturbed at 25 Td. The center of the distribution has moved upward and fewer of the ions are moving against the field. Careful examination of this figure and the next two shows that there is a ridge developing parallel to the electric field, as predicted by Wannier (1953).

Figure 7.3 shows that at 50 Td there is a flattening of the distribution at high v_z . This is because the ions with high speed along the field direction are probing the



region where there are substantial deviations from the low-field values of $\alpha_{_{\parallel}}$, β_{\parallel} and β_{\perp} , γ_{1} and γ_{2} , while low-speed ions are still probing the low-field values of these deviation parameters.

Figures 7.4 and 7.5 show that the ridge is longer, and the deviation from spherical symmetry is more pronounced, as E/n_0 continues to increase. The distribution is pear-shaped, with the large end at high v_z , as predicted by Wannier (1953). These trends continue at even higher E/n_0 ; increases cause a gradual movement of the distribution upward and a gradual widening of the distribution in all directions, but no significant change in the pear shape. Moreover, the changes observed here are quite similar to those found (Viehland and Johnsen 2018) for $^{16}O^+(^4S_{3/2})$ ions moving through a naturally occurring mixture of $He(^1S_0)$ isotopes.

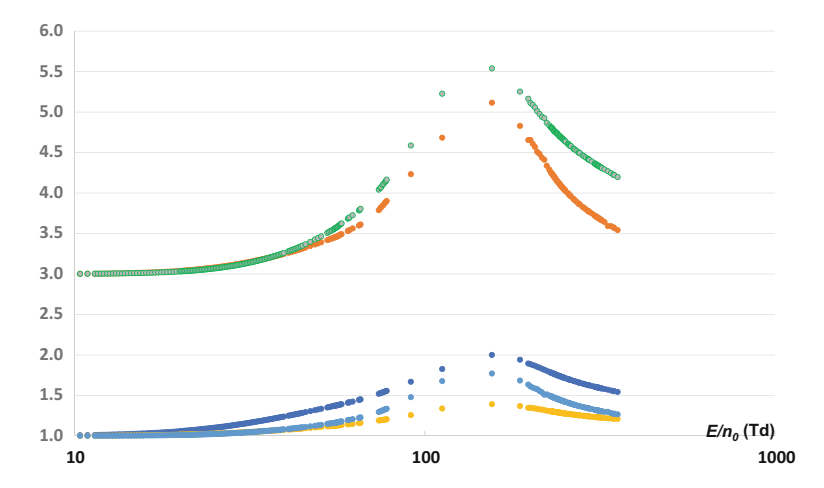


Fig. 7.6 Dimensionless deviation parameters for $^{16}O^+(^4S_{3/2})$ in $Ar(^1S_0)$ at 300 K. From bottom to top at large E/n_0 , they are $1+\gamma_1,\gamma_2,1+\alpha_\parallel,\beta_\perp$ and β_\parallel

Figure 7.6 shows the five deviation parameters as a function of E/n_0 for $^{16}\mathrm{O}^+(^4\mathrm{S}_{3/2})$ in $\mathrm{Ar}(^1\mathrm{S}_0)$ at 300 K. Below 100 Td, the values become significantly larger than their low-field limits. Note they become quite large near 200 Td, and then drop back as E/n_0 increases further. This happens at about the same E/n_0 when the gas is He, but in He those values of E/n_0 correspond to much higher average kinetic energies (because the ions are so light). This is why the GC calculations for $^{16}\mathrm{O}^+(^4\mathrm{S}_{3/2})$ in $\mathrm{Ar}(^1\mathrm{S}_0)$ converged more slowly than the corresponding calculations in He (Viehland and Johnsen 2018).

7.3 Reaction of ${}^{16}O^{+}({}^{4}S_{3/2})$ with $N_2(v=0)$

We are concerned with reaction (7.17), where the products can be in any state and the nitrogen reactant is in the ground electronic and vibration states but can occupy any one of a large number of rotational states. Below about 1 eV, this reaction is important in the Earth's atmosphere because it converts atomic oxygen ions (formed primarily from sunlight hitting oxygen atoms and oxygen-containing molecules) to molecular NO⁺ ions that recombine much more efficiently than oxygen ions with electrons. Early measurements (Fehsenfeld et al. 1965; Copsey et al. 1966; Warneck 1967) of the reaction rate coefficient for (7.17) were not in good agreement, probably due to the presence of faster reacting excited states of O⁺ and of N₂ molecules in higher vibrational states (Schmeltekopf et al. 1967). In addition, (7.17) is a very slow reaction at low relative kinetic energy between the reactants, which makes measurement of its rate coefficient difficult.

$$^{16}\text{O}^{+}(^{4}S_{3/2}) + \text{N}_{2}(v=0) \rightarrow \text{NO}^{+} + \text{N}$$
 (7.17)

Important steps forward in understanding reaction (7.17) were made by Albritton et al. (1977), Viehland and Mason (1977) and Lin and Bardsley (1977). Albritton et al. (1977) reported drift-tube results obtained with no more than 3% N₂ in He(1 S₀). This was still enough to produce a non-reactive loss of 16 O⁺(4 S_{3/2}), which the authors attributed to enhanced diffusion that had to be corrected for. On a positive note, Albritton et al. (1977) made measurements of R1 in both He(1 S₀) and Ar(1 S₀) gases in order to probe the effects of the ion vdf. They succeeded in deconvoluting the measured rate coefficients to derive $Q_R^*(\varepsilon_R)$, the reactive cross section as a function of energy, for reaction (7.17); it was consistent with the data in both He and Ar. This was done by assuming the accuracy of the ion vdf determined by Lin and Bardsley (1977) using Monte Carlo techniques (see Chap. 9) and a model for the 16 O⁺(4 S_{3/2}) interaction potentials with He(1 S₀) and Ar(1 S₀).

The paper of Viehland and Mason (1977) used the two-temperature kinetic theory (see Sect. 5.6) to convert measurements of $k(T_0, E/n_0)$ into values of $k(T_{eff})$. Essentially, they used the fundamental ion mobility equation, (1.45), with $\alpha_c = 0$ and Wannier's equation, (1.29). Wannier's equation was modified to account for the presence of both a reactive and non-reactive neutral, giving

$$\frac{3}{2}k_B T_{eff} = \frac{3}{2}k_B T_0 + \left(\frac{m_0 + m_1}{m_R + m_1}\right) \left(\frac{1}{2}m_R v_d^2\right) = K E_{cm}.$$
 (7.18)

This equation takes into account that reaction (7.17) depends upon the kinetic energy (KE_{cm}) in the center-of-mass frame of an ion and reacting neutral, while the ion speed is primarily dependent upon the relative kinetic energy between an ion and the atomic buffer gas that is present in much larger amount than the reactive neutral. Manipulating the data when naturally occurring mixtures of the isotopes of either $He(^1S_0)$ or $Ar(^1S_0)$ were used as the buffer gas gave consistent values for $k(T_{eff})$. This avoided the necessity of determining $Q_R^*(\varepsilon_R)$, but of course the reaction cross section could have been obtained by inverting the $k(T_{eff})$ data.

The reaction cross section presented by Albritton et al. (1977) on a log-log graph, as a function of the kinetic energy given by (7.18), became the accepted cross section for reaction (7.17). Two subsequent papers are worth noting. First, Hopper (1982) reported a theoretical cross section based on the questionable assumptions that N_2 was at 600 K and in a J=10 rotational state. His calculated cross section is significantly greater than that of Albritton et al. (1977) except near and above 2 eV. Second, Burley et al. (1987) reported guided ion beam mass spectrometry results on reaction R1 from 0.03 to 30 eV. They inverted their results to give $Q_R^*(\varepsilon_R)$, but this reaction cross section does not give $k(T_{eff})$ values with a minimum near $KE_{cm}=0.1$ eV. They also developed three models for the "true" cross section, and claimed that their model II is "probably the best estimate of the true cross section over the energy range examined". A functional form for this model is given by Viehland and Johnsen (2018). This model more nearly matches the drift-tube data at large KE_{cm} than does the accepted cross section, but there is still a large region of intermediate ε_R where

improvement is possible, perhaps because there was energy broadening due to the buildup of static electricity in the beam experiments.

To reexamine reaction (7.17), we start with (4.36). In terms of the relative distribution function defined by (7.6) and (7.15), the second-order rate coefficient for reactions between trace amounts of atomic ions and small amounts of reactive neutrals of type R, while both are immersed in a larger amount of a dilute gas, is

$$k_R = \int f_{rel}(\mathbf{g}) Q_R^*(\varepsilon_R) g dg, \qquad (7.19)$$

where

$$\varepsilon_R = \frac{1}{2}\mu_R g^2. \tag{7.20}$$

Note that this expression is independent of position and time, so it implicitly assumes that the electric field is uniform and static. A computer program named RR has been written in Fortran 90 by the author to evaluate k_R from tables of values of $Q_R^*(\varepsilon_R)$ and of the ten transport coefficients as a function of E/n_0 . This program uses (7.15) and (7.18); it is available from the author upon request.

In order to construct each of the three curves in Fig. 7.7, the transport coefficients in (7.15) were obtained from the LXCat (2017) database (Pitchford et al. 2017); they were placed in this database from calculations with computer programs PC and GC that started with an *ab initio* interaction potential (Danailov et al. 2006). The black curve that is the highest near 0.1 eV was computed using the $Q_R^*(\varepsilon_R)$ values in Fig. 6 of Burley et al. (1987). The red curve that is in the middle near 0.1 eV was determined using the functional form (Viehland and Johnsen 2018) of model II of Burley et al. (1987). Finally, the green curve was calculated using digitized values for the $Q_R^*(\varepsilon_R)$ shown graphically by Albritton et al. (1977). Figure 7.7 is a log-log plot because both Q_R^* and ε_R vary over orders of magnitude. This means that what appear to be small differences in Fig. 7.7 are actually highly significant. None of curves can be said to adequately represent the points that represent the values obtained by Albritton et al. (1977) using two-temperature kinetic theory to invert their measured values of the reaction rate coefficient.

The question that must now be addressed is the accuracy of the 2T calculations. Figure 7.8 shows the percentage difference of the 2T and 3T rate coefficients for reaction (7.17) from the GC values. Each was calculated for the naturally occurring mixture of $He(^1S_0)$ isotopes from the $O^+(^4S_{3/2})$ - $He(^1S_0)$ interaction potential of Danailov et al. (2006) and the reaction cross section from Fig. 9 of Albritton et al. (1977). The 2T results are in error by 30% at most kinetic energies, while a version of the 2T kinetic theory that includes velocity displacement along the field gives results in error by as much as 50%. The 3T results are better at high energies, but about the same below 0.5 eV. Compared to the 2T results, the 3T results indicate that asymmetry (different ion temperatures parallel and perpendicular to the electric field and a velocity displacement along the field) causes a noticeable change in the rate coefficient. Extending this comparison, the GC results indicate that another

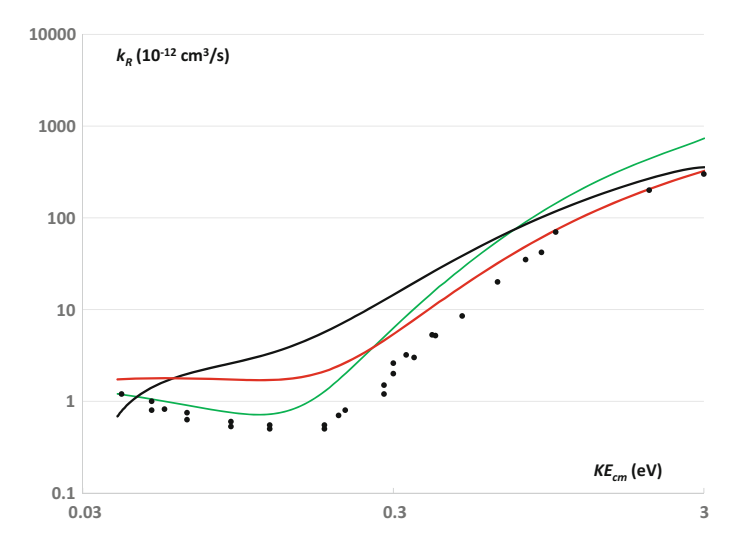
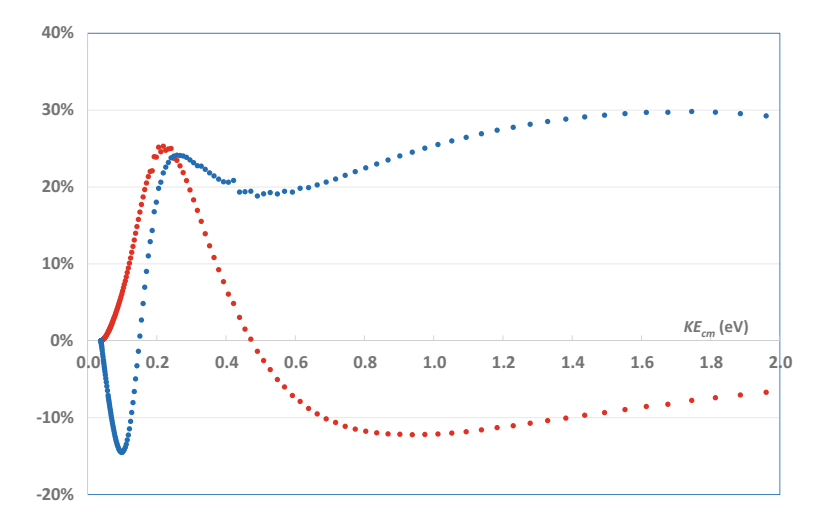


Fig. 7.7 Rate coefficient of reaction (7.17) in a He buffer gas, as a function of the relative kinetic energy in a $^{16}O^+(^4S_{3/2})+N_2(v=0)$ collision



 $\textbf{Fig. 7.8} \ \ \text{Percentage difference from the GC results of the 2T (blue points that are higher at high kinetic energy) and 3T (red, lower) results$

significant change arises when skewness, kurtosis, and correlation are included. Both kinds of effect must clearly be incorporated in order to infer a reaction cross section from the rate coefficient.

Viehland and Johnsen (2018) used the GC theory to infer the reaction cross section for reaction R1 from the measured values (Albritton et al. 1977) of the reaction rate coefficient and the interaction potential from Danailov et al. (2006). They started

229

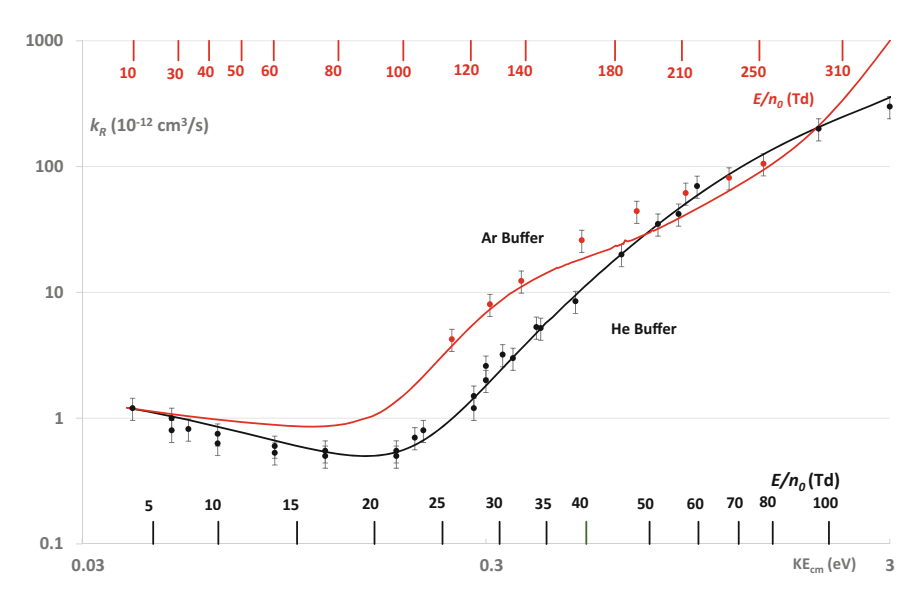


Fig. 7.9 Rate coefficient for reaction R1 in of $He(^1S_0)$ (black) and $Ar(^1S_0)$ (red), as a function of KE_{cm} . Both gases are at 300 K. The black vertical lines at the bottom indicate the value of E/n_0 when He is used. The red ones at the top are E/n_0 when Ar is used

from a tabulated version of the cross sections of Albritton et al. (1977) and iteratively modified the cross sections until the calculated and measured k_R values in the naturally occurring mixture of $He(^1S_0)$ isotopes at 300 K were in good agreement, as shown in Fig. 7.9. This figure also shows the results in the naturally occurring mixture of $Ar(^1S_0)$ isotopes at 300 K; these were calculated from the potential of Danailov et al. (2008). The agreement with the experimental values (Albritton et al. 1977) is excellent. This indicates that the new values of $Q_R^*(\varepsilon_R)$ tabulated by Viehland and Johnsen (2018) are more accurate than cross sections previously available. This, in turn, may have significant implications for models of the F-region of the upper atmosphere and in other applied areas of research.

7.4 Convergence Problems

The calculations reported in the previous section when the buffer gas was Ar were difficult because of poor convergence in computer program GC. Hence, this is an appropriate place to give the specifics of how this program works, and then the techniques that can be used to work around poor convergence.

As indicated in Sect. 5.9, the zero-order distribution function used in the Gram-Charlier approach involves eight parameters (indicated by decorations) that are supposed to be equal to the actual values (undecorated) of these eight quantities. This

means that they must be determined iteratively. As usual with iterative methods, this can take a considerable amount of computer time, especially if the initial guesses are not close to the final values.

Computer program GC is designed to work with user-specified values for T_0 , m_0 , m_1 , q, and the fractional accuracy with which the transport cross sections were calculated. It then starts at a very low E/n_0 value, where it is an excellent approximation that $\widetilde{v}_d = 0$, $\widetilde{T}_L = \widetilde{T}_T = T_0$, $\widetilde{\alpha}_L = \widetilde{\gamma}_1 = 0$, $\widetilde{\gamma}_2 = 1$, and $\widetilde{\beta}_L = \widetilde{\beta}_T = 3$. It then uses the method of weighted residuals (Appendix C) to refine these values, stopping when they have converged to the fractional accuracy of the cross sections. The converged values are assumed to be the values of the undecorated quantities, so program GC writes to a single line on the output file the values of E/n_0 , K_0 (calculated from v_d and E/n_0), T_L , T_T , n_0D_L , n_0D_T , α_L , β_L , β_T , γ_1 and γ_2 .

The program next makes a very small change to E/n_0 , uses the output values from the previous E/n_0 as the decorated quantities for this next reduced field strength, and repeats the calculations with the method of weighted residuals. This entire process is iterated as many times as it takes to reach the largest E/n_0 that is specified by the user. Typically at least 200 output lines are generated to cover the E/n_0 range from 0 to 1000 Td.

It is often found that, at some large enough value of E/n_0 , the calculations do not converge to the requested fractional accuracy by the time the method of weighted residuals reaches the largest possible value, which is determined by the size of the memory available in the computer being used. When this happens, the fractional accuracies are increased and the calculation resumed. If convergence is again not achieved, the fractional accuracies are again increased, etc. The convergence criteria for the mobility can be selected by the user of program GC, but ordinarily one starts with the precision of the transport coefficients and then goes through the sequence 0.5, 1.0, 1.5, and 2.0%. After program GC reaches 2.0%, all subsequent calculations are made without changing the convergence. It is up to the user to specify whether, in such cases, the values that have not converged are written to the output file with an * at the end of the line or, more often, no values at all are written to the output file.

When there are values of E/n_0 at which convergence is not achieved, one can make use of the more limited information provided by the converged values. However, estimates of the values in the unconverged region are written by computer program GC into a different output file, and the user may use them to make graphs of the transport coefficients as functions of E/n_0 in order to decide which, if any, of the values calculated at the 2.0% level should be ignored.

For $^{16}O^+(^4S_{3/2})$ ions in Ar, Viehland and Johnsen (2018) thought it important to overcome the convergence problems. They did this by restarting computer program GC from the value of E/n_0 where convergence was not achieved and then manually entering values for \tilde{v}_d , \tilde{T}_L , \tilde{T}_T , $\tilde{\alpha}_L$, $\tilde{\beta}_L$, $\tilde{\beta}_T$, $\tilde{\gamma}_1$ and $\tilde{\gamma}_2$. Since there are so many parameters, they frequently had to use a sequence of estimates for them before arriving at a set that leads to converged values when the method of weighted residuals is used in the highest approximation possible on the computer in use. Often, this overcame the problem only for a limited range of E/n_0 , and the manual entry had to

be repeated several times. This is certainly a tedious process, so it is not recommended in general. Nevertheless, Viehland and Johnsen (2018) were able to use it to obtain converged values of approximately the same accuracy in Ar as they obtained for $^{16}O^{+}(^{4}S_{3/2})$ ions in He. The agreement in Ar shown in Fig. 7.8 is not as good as in He, but it is satisfactory.

7.5 Summary

The use of drift tubes to study ion–neutral chemical reactions between 0.1 and 2 eV was common in the 1970s and early 1980s, but came to an abrupt halt. Part of the reason for this is that few of the reactions of importance have the extreme variation with kinetic energy as reaction (7.17); without such a variation, it is possible to interpolate between the low-energy results obtained with conventional, macroscopic experiments and the high-energy results obtained with beam or other microscopic experiments. Another part of the reason is that there was little demand for reaction cross sections more accurate than about 25%; it was believed that such accuracy had been achieved for such important reactions as (7.17).

The work of Viehland and Johnsen (2018) discussed in this chapter has shown that using the two-temperature expression for the ion vdf does not allow accurate reaction cross sections to be obtained from an inversion of reaction rate coefficients. The reactions of $O^+(^4S_{3/2})$ with O_2 and NO are as dependent upon kinetic energy as those with N_2 , so the values for $Q_R^*(\varepsilon_R)$ derived for those reactions from rate coefficient studies in drift tubes may have errors as large as 30–50%. In the near future, researchers should remeasure the rate coefficients in drift tubes for these and other ion–neutral reactions, and then analyze the new (and presumably more accurate) data in terms of the ion vdf used in GC methods for solving the Boltzmann equation. The new values of $Q_R^*(\varepsilon_R)$ may make important changes in models of the F-region of the Earth's ionosphere and in other situations where the kinetic energy is between 0.1 and 2 eV.

References

D.L. Albritton, I. Dotan, W. Lindinger, M. McFarland, J. Tellinghuisen, F.C. Fehsenfeld, J. Chem. Phys. 66, 410 (1977)

V.M. Bierbaum, Int. J. Mass Spectrom. **377**, 456 (2015)

D.K. Bohme, Int. J. Mass Spectrom. 200, 97 (2000)

J.D. Burley, K.M. Ervin, P.B. Armentrout, J. Chem. Phys. 86, 1944 (1987)

M.J. Copsey, D. Smith, J. Sayers, Planet. Space Sci. 14, 1047 (1966)

D.M. Danailov, R. Brothers, L.A. Viehland, R. Johnsen, T.G. Wright, E.P.F. Lee, J. Chem. Phys. 125, 084309 (2006)

D.M. Danailov, L.A. Viehland, R. Johnsen, T.G. Wright, A.S. Dickenson, J. Chem. Phys. 128, 134302 (2008)

- F.C. Fehsenfeld, A.L. Schmeltekopf, E.E. Ferguson, Planet. Space Sci. 13, 219 (1965)
- S.T. Graul, R.R. Squires, Mass Spectrom. Rev. 7, 263 (1988)
- D.G. Hopper, J. Chem. Phys. 77, 314 (1982)
- S.L. Lin, J.N. Bardsley, J. Chem. Phys. 66, 435 (1977)
- L.C. Pitchford, L.L. Alves, K. Bartschat, S.F. Biagi, M.C. Bordage, I. Bray, C.E. Brion, M.J. Brunger, L. Campbell, A. Chachereau, B. Chaudhury, L.G. Christophorou, E. Carbone, N.A. Dyatko, C.M. Franck, D.V. Fursa, R.K. Gangwar, V. Guerra, P. Haefliger, G.J.M. Hagelaar, A. Hoesl, Y. Itikawa, I.V. Kochetov, R.P. McEachran, W.L. Morgan, A.P. Napartovich, V. Puech, M. Rabie, L. Sharma, R. Srivastava, A.D. Stauffer, J. Tennyson, J. de Urquijo, J. van Dijk, L.A. Viehland, M.C. Zammit, O. Zatsarinny, S. Pancheshnyi, Plasma Proc. Polym. 14, 1600098 (2017)
- A.L. Schmeltekopf, F.C. Ferguson, G.I. Gilman, E.E. Ferguson, Planet. Space Sci. **15**, 401 (1967) L. A. Viehland database at www.lxcat.net (2017)
- L.A. Viehland, E.A. Mason, J. Chem. Phys. 66, 422 (1977)
- L.A. Viehland, E.A. Mason, Ann. Phys. (N.Y.) 110, 287 (1978)
- L.A. Viehland, R. Johnsen, J. Chem. Phys. 149, 074311 (2018)
- G.H. Wannier, Bell Syst. Tech. J. 32, 170 (1953)
- P. Warneck, Planet. Space Sci. 15, 1349 (1967)

Chapter 8 Kinetic Theory for Molecules



8.1 Basics

The Boltzmann equation discussed in Chap. 4 is the fundamental kinetic equation for the transport and reaction of atomic ions through atomic gases. Its generalization to molecules may be written in the form (Kagan and Maksimov 1961; Kagan and Afanas'ev 1961; Curtiss and Dahler 1963):

$$\frac{\partial f}{\partial t} + \mathbf{v} \cdot \nabla f + \mathbf{a}(\mathbf{r}, t) \cdot \nabla_{\mathbf{v}} f + [f, H_{int}] = Jf, \tag{8.1}$$

where the ion vdf, f, is implicitly a function of time (t), position (\mathbf{r}) , velocity (\mathbf{v}) and whatever internal variables may be needed to characterize the ion in phase space. In addition, ∇ is a gradient in physical space, $\nabla_{\mathbf{v}}$ is a gradient in velocity space, \mathbf{a} is the ion acceleration caused by an external electrostatic field, H_{int} is the internal Hamiltonian operator expressed in terms of the internal variables, and J is the collision operator discussed below. The square brackets indicate a commutator in quantum mechanics or a Poisson bracket in classical mechanics (see Appendix A).



Beenakker

In formulating explicit expressions for the collision operator, the time duration and extent of intermolecular interactions are ignored, as they were in Chap. 4 for the

Boltzmann equation for atomic ions in atoms. This has the necessary consequence that some of the possible terms in $[f, H_{int}]$ must also be ignored. The remaining terms are the source of the Senftleben–Beenakker effects (Senftleben 1965; Beenakker 1968; Moraal 1975) in which the transport properties of neutral, polyatomic gases are changed slightly when an external field is applied. Hermann Senftleben (1890–1975) observed these effects in paramagnetic molecules, while Joannes Josephus Maria Beenakker (1926–1998) observed them in diamagnetic molecules.

Electric field SB effects have not been observed for linear polyatomic molecules, presumably because the gases experience electrical breakdown at lower E than are needed to change the transport properties significantly. They are measurable but still small for more general molecules, and appear only when E is on the order of 100–400 V/cm (Borman et al. 1971), a factor of 100 larger than is usually used in drift tubes. Moreover, in drift-tube experiments, only the ions may exhibit electric SB effects. Since the ions are present only in trace amounts compared to n_0 , the value of E/n_0 at which SB effects can arise will be much larger than the values ordinarily used in DTMS, IMS, or the other techniques discussed in Chap. 2. Hence, we can drop the $[f, H_{int}]$ term in (8.1).

8.2 Quantum Collision Operators

On the microscopic level, a nonreactive collision between an ion in internal state α and a neutral molecule in internal state β is described by the differential cross section, $\sigma\left(\alpha\beta;\alpha'\beta';E_T\Omega\right)$, for scattering into new states α' and β' of the ion and neutral, respectively, given that the sum of the internal and relative kinetic energies is E_T and that the polar and azimuthal scattering angles in the center-of-mass frame are jointly denoted by Ω . The ions in a drift tube may be completely described on the microscopic level by a set of vdf, $f^{(\alpha)}(\mathbf{r}, \mathbf{v}, t)$, one for each internal state present in a region of space, \mathbf{r} , and with laboratory-frame velocity, \mathbf{v} , at time, t. Then, it was shown by Wang Chang et al. (1964) that (8.1) can be written without the $[f, H_{int}]$ term in a form similar to (5.1),

$$\left[\frac{\partial}{\partial t} + \mathbf{v} \cdot \nabla + \mathbf{a}(\mathbf{r}, \mathbf{t}) \cdot \nabla_{\mathbf{v}}\right] f^{(\alpha)}(\mathbf{r}, \mathbf{v}, t)$$

$$= \left[\sum_{j} n_{j} \mathfrak{J}_{j} - \sum_{R} n_{R} \mathfrak{J}_{R}\right] f^{(\alpha)}(\mathbf{r}, \mathbf{v}, t). \tag{8.2}$$

The nonreactive collision operator is a generalization of the atomic collision operator in (4.12), namely

$$\mathfrak{J}_{j} f^{(\alpha)}(\mathbf{r}, \mathbf{v}, t) = \sum_{\alpha'\beta_{0}\beta'_{0}} \iint \left[f^{(\alpha')}(\mathbf{r}, \mathbf{v}', t) F_{j}^{(\beta'_{0})}(\mathbf{v}'_{j}) - f^{(\alpha)}(\mathbf{r}, \mathbf{v}, t) F_{j}^{(\beta_{0})}(\mathbf{v}_{j}) \right] \\
\left| \mathbf{v} - \mathbf{v}_{j} \right| \sigma \left(\alpha\beta_{0}; \alpha'\beta'_{0}; E_{T}\Omega \right) d\Omega d\mathbf{v}_{j}, \tag{8.3}$$

where β_0 is the internal state of the neutral. In addition, the primes indicate postcollision quantities that are related to the pre-collision (unprimed) quantities by conservation of linear and angular momentum and of total energy, E_T , through $\sigma\left(\alpha\beta_0; \alpha'\beta'_0; E_T\Omega\right)$ and the scattering angles that are collectively represented by Ω . The reactive collision operator is similarly a generalization of (5.10),

$$\mathfrak{J}_R f^{(\alpha)}(\mathbf{r}, \mathbf{v}, t) = \sum_{\beta_R} \int f^{(\alpha)}(\mathbf{r}, \mathbf{v}, t) f_R^{(\beta_R)}(\mathbf{v}_R) |\mathbf{v} - \mathbf{v}_R| Q_R^*(\varepsilon_R) d\mathbf{v}_R.$$
(8.4)

Here, the reactive cross section, $Q_R^*(\varepsilon_R)$, is implicitly a function of the internal states α and β_R .



Waldmann

Equation (8.2) is a set of coupled, linear, and integro-differential equations for the various ion distribution functions. However, this equation is not strictly valid for molecules with degenerate internal states (such as rotation). In quantum work with most molecules, it is necessary to replace (8.2) by the equation (Waldmann 1957, 1958; Snider 1960) developed by Ludwig Waldmann (1913–1980) and Robert F. Snider, or by an even more elaborate (off the energy shell) kinetic equation due to Tip (1971a, b). However, evaluating the matrix elements of the collision operators that arise in any of these equations remains impossible in general situations, even 50 years after the equations were developed. Once must therefore turn to semiclassical kinetic equations.

8.3 Semiclassical Collision Operators

Wang Chang et al. (1964) presented a semiclassical kinetic theory (referred to as the WUB equation) for molecules that is analogous to a semiclassical kinetic theory for atomic particles. In that case, quantum-mechanical cross sections are used in the otherwise classical-mechanical Boltzmann equation discussed in Chap. 4. In the WUB equation, the state-specific cross sections are summed over final states and averaged over initial states. This avoids the incorrect assumption (see below) that time reversal of a collision results in an inverse collision. While theoretically satisfying, the semiclassical cross sections are almost as difficult to calculate for the WUB equation as are the quantum-mechanical cross sections for the equations described in Sect. 8.2. Hence, no applications to drift-tube experiments have been made using semiclassical kinetic theory.

It should be noted that Kuščer et al. (1981) found a correspondence between the quantum-mechanical, Waldmann–Snider equation and the semiclassical WUB equation. A strictly classical kinetic theory can be obtained from their equations by assuming that discrete quantities like rotational angular momentum are continuous. It is easier, however, to obtain a classical kinetic theory by entirely classical arguments, as described in the next sections.

8.4 Taxman's Classical Theory

Taxman (1958) was the first to develop a classical-mechanical kinetic equation for molecules, as an extension of the Boltzmann equation for atoms. This work was not pursued for many years, probably due both to his untimely death and to his argument that the existence of inverse collisions is unnecessary for the development of the theory.

Consider Fig. 8.1, which is based on the illustration by Tolman (1938) of collisions in two dimensions between a rigid circle and a rigid wedge, each with the same mass. The arrows in each portion of the figure show that the velocities of the two particles before (left side) and after (right side) the various types of collision are the same in magnitude but opposite in direction, so there is no total linear momentum of the system in any situation.

The top panel in Fig. 8.1 shows that before collision the left side of the wedge is not perpendicular to the pre-collision velocities. Therefore, the circle must bounce off at some angle in the second quadrant, as shown on the right, with the wedge going off in the fourth quadrant. Since the collision is shown causing the wedge to end up rotating clockwise, conservation of angular momentum means that the circle must end up rotating counterclockwise. The increase in rotational (internal) energy can only have occurred due to a decrease in kinetic energy, by conservation of total energy.

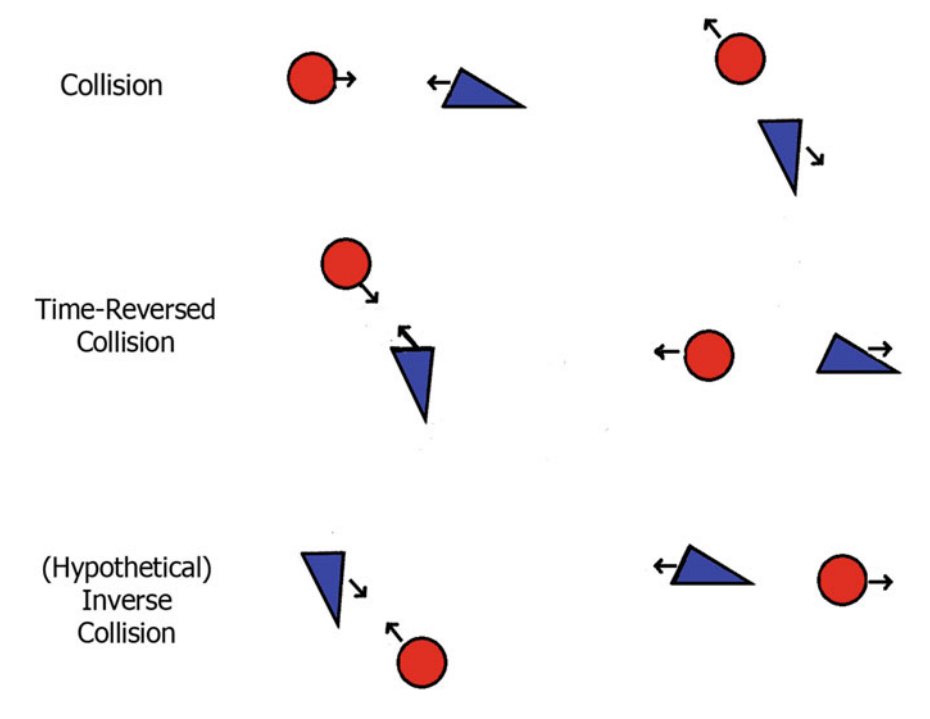


Fig. 8.1 Comparison of a collision between a rigid sphere and a rigid wedge with a time-reversed collision and an inverse collision

Time reversal leads to the reverse (sometimes called reciprocal) collision shown in the middle part of Fig. 8.1. Here, the particles start at the positions that they had at the end of the original collision, but their velocities are in directions that differ by 180° due to the time reversal. In order for the reverse collision to cause the circle to end up moving to the left and not rotating, it must cause the wedge to move to the right and stop rotating. As expected from Newton's laws of classical physics, the original collision, and the reverse collision are identical upon time reversal.

Now, we consider a hypothetical inverse collision in which the initial positions of the particles is inverted in comparison to their final positions at the end of the original collision. This is shown on the left in the bottom part of Fig. 8.1, where the initial velocities are the same as the final velocities in the original collision. However, the inversion in space cannot affect the internal state of either particle, so the wedge is still rotating clockwise and the circle counterclockwise. The inverse collision is supposed to lead to a final situation that is the inverse of the initial situation for the original collision, as shown in the right side of the bottom portion of Fig. 8.1. If the circle is moving to the right, conservation of linear momentum requires the wedge to move to the left with the same velocity, so this portion of the illustration is correct. However, it is possible for the wedge to end up in the orientation shown only if it is initially rotating counterclockwise; similarly, the sphere must have initially been

rotating clockwise if it is going to end up moving to the right with no rotation. This is a contradiction.

We have shown that the hypothesized inverse collision does not exist in a special case, so they cannot generally exist for molecules that obey Newton's laws of motion. On the other hand, inverse collisions do exist in semiclassical and quantum kinetic theory, even though there seems to be no way that they can arise from a classical-mechanical kinetic theory. They can vanish from a quantum-mechanical kinetic theory when passing to the classical limit, but only under special assumptions about the molecular symmetry point groups of the molecules (Borman et al. 1975). This still appears to be an unsolved problem in kinetic theory.

8.5 The Curtiss Equation for Gaseous Ion Transport

Curtiss (1981b) presented a classical-mechanical kinetic theory for non-vibrating (i.e., rigid rotor) diatomic molecules in their ground electronic states, a theory that does not assume that inverse collisions exist. This theory was generalized later to any type of polyatomic molecule (Curtiss 1992). Here, however, we will consider the original Curtiss equation that was used (Viehland 1986) to develop a classical kinetic theory of swarm experiments for diatomic ions and/or neutrals that do not contain hydrogen atoms. This theory assumes that:

- 1. The ions are present in trace amounts, so we need consider only a single type of ion
- 2. The electronic and vibrational levels of the ions and neutrals are at such high energies (compared to the ground states) that only the lowest levels are populated in swarm experiments.
- 3. The rotational levels of the ions and neutrals are so closely spaced that, in room temperature swarm experiments, there are so many rotational levels populated that the molecules can be treated as classical-mechanical rigid rotors. This assumption fails for molecules that include hydrogen atoms, so the Curtiss equation does not apply to them.

Assumptions 1–3 mean that the ions can be identified by their rotational angular momentum vector, \mathbf{J} , instead of the α superscript used in (8.2)–(8.4). Similarly, the nonreactive and reactive neutrals can be labeled with \mathbf{J}_j and \mathbf{J}_R , respectively. Then the Curtiss equation is

$$\left[\frac{\partial}{\partial t} + \mathbf{v} \cdot \nabla + \frac{q}{m} \mathbf{E} \cdot \nabla_{\mathbf{v}}\right] f(\mathbf{r}, \mathbf{v}, \mathbf{J}, t)
= \left[\sum_{j} n_{j} \mathfrak{J}_{j} - \sum_{R} n_{R} \mathfrak{J}_{R}\right] f(\mathbf{r}, \mathbf{v}, \mathbf{J}, t). \tag{8.5}$$

Note that

$$n_0 = \sum_{j} n_j \tag{8.6}$$

is the total number density of the neutral gas, and that the number densities are constrained so that

$$n(\mathbf{r}, t) << n_R << n_i \lesssim n_0.$$
 (8.7)

for any R and j.

The nonreactive collision operator is a specialization of (8.3),

$$\mathfrak{J}_{j}f(\mathbf{r}, \mathbf{v}, \mathbf{J}, t) = \iiint \left[f(\mathbf{r}, \mathbf{v}', \mathbf{J}', t) f_{j}(\mathbf{v}'_{j}, \mathbf{J}'_{j}) - f(\mathbf{r}, \mathbf{v}, \mathbf{J}, t) f_{j}(\mathbf{v}_{j}, \mathbf{J}_{j}) \right] |\mathbf{v} - \mathbf{v}_{j}| \ bdbd\Omega d\mathbf{v}_{j}d\mathbf{J}_{j}$$
(8.8)

Because the neutral gas is in equilibrium, its components have Maxwell–Boltzmann vdfs given by (3.19). When only the rotational degrees of freedom are important, this equation becomes

$$f_j(\mathbf{v}_j, \mathbf{J}_j) = \left(\frac{m_j}{2\pi k_B T_0}\right)^{3/2} \left(\frac{1}{4\pi I_j k_B T_0}\right) \exp\left(-\frac{m_j v_j^2}{2k_B T_0} - \frac{J_j^2}{2I_j k_B T_0}\right), \quad (8.9)$$

where I_j is the moment of inertia of neutral species j. Hence the only unknown is the ion vdf, $f(\mathbf{r}, \mathbf{v}, \mathbf{J}, t)$.

The reactive collision operator is a specialization of (8.4),

$$\mathfrak{J}_{R}f(\mathbf{r}, \mathbf{v}, \mathbf{J}, t) = \iint f(\mathbf{r}, \mathbf{v}, \mathbf{J}, t) f_{R}(\mathbf{v}_{R}, \mathbf{J}_{R}) \times |\mathbf{v} - \mathbf{v}_{R}| O_{D}^{*}(\varepsilon_{R}) d\mathbf{v}_{R} d\mathbf{J}_{R}.$$
(8.10)

Here, the reactive neutrals have the same Maxwell–Boltzmann distribution as in (8.9), with the j subscripts replaced by R. Note that the dependence of the total reaction cross section, Q_R^* (ε_R), upon the rotational angular momentum vectors and the scattering angles has been left implicit. This cross section will have to be obtained by theoretical methods outside the scope of kinetic theory.

There are thee more assumptions made when applying the Curtiss equation to gaseous ion mobility, diffusion, and reaction:

- 4. The transport properties of gaseous ions are governed by energy averages of both elastic and inelastic collision cross sections. The latter are much smaller than the former, usually amounting to no more than 10%, so slight errors due to a classical-mechanical treatment of the inelastic collisions are of little importance.
- 5. The timescale for the variation of the $n(\mathbf{r}, t)$ is much longer than that for all other ion properties. This means that we can neglect all time derivatives other than $\partial n/\partial t$. The physical justification of this assumption is that the ion momentum,

- energy, and other moments of the ion vdf can be dissipated locally by collisions with neutral molecules, but the ion mass can only change due to chemical reactions
- 6. The frequency of reactive ion—neutral encounters is orders of magnitude less than that for nonreactive collisions. Where necessary, this requirement can be satisfied by adding a large excess of a nonreactive buffer to the gas. This assumption is the justification for the above neglect of source terms compared to sink terms in the Curtiss equation.

8.6 Density-Gradient-Independent Moment Equations

Viehland (1981) used the rate equation of continuity, (5.12), to expand the ion number density in the Curtiss equation in powers of its gradients. In the rest of this chapter, we will not discuss diffusion coefficients or chemical reactions, so it is sufficient to assume that

$$f(\mathbf{r}, \mathbf{v}, \mathbf{J}, t) = n(\mathbf{r}, t) f(\mathbf{v}, \mathbf{J}). \tag{8.11}$$

The Curtiss equation for determining the density-gradient-independent ion vdf for rigid rotors then becomes (Viehland 1986)

$$\left[\frac{q}{m}\mathbf{E}\cdot\nabla_{\mathbf{v}} + \sum_{j} n_{j}\mathfrak{J}_{j}\right] f(\mathbf{v}, \mathbf{J}) = 0,$$
(8.12)

with

$$\mathfrak{J}_{j}f(\mathbf{v},\mathbf{J}) = \int \left[f(\mathbf{v},\mathbf{J}) f_{j}(v_{j},J_{j}) - f(\mathbf{v}',\mathbf{J}') f_{j}(v_{j}',J_{j}') \right] \times |\mathbf{v} - \mathbf{v}_{0}| \, b db d\mathbf{v}_{b} d\mathbf{J}_{b}.$$

Since this is a linear operator equation like the Boltzmann equation for atomic systems, its solution can be obtained by the method of weighted residuals (Appendix C), once we have decided upon the zero-order distribution to use with it.

8.7 Extension of the 2T Theory to Molecules

Experience indicates that the more closely the zero-order distribution in a method of weighted residuals (Appendix C) resembles the true ion vdf, the more quickly will the successive approximations to the transport coefficients converge. Since an electrostatic field can transfer energy into the rotational motion of an ion only indirectly,

by means of collisions, it should be reasonable to use a generalization of (5.23), the zero-order vdf in the two-temperature theory for atomic systems. Thus we assume that

$$f_0^{(2T)}(\mathbf{v}, \mathbf{J}) = \left(\frac{m}{2\pi k_B T_{kin}}\right)^{3/2} \left(\frac{1}{4\pi I k_B T_{int}}\right) \times \exp\left(-\frac{mv^2}{2k_B T_{kin}} - \frac{J^2}{2I k_B T_{int}}\right), \tag{8.13}$$

where I is the moment of inertia of the ions. The fact that the kinetic and internal ion temperatures, T_{kin} and T_{int} , in (8.13) differ and are not equal to T_0 is what keeps this from being a Maxwell–Boltzmann distribution function.

A complete set of basis functions that are orthonormal with respect to $f_0^{(2T)}(\mathbf{v}, \mathbf{J})$ has been constructed by Viehland (1986) based on previous results by Curtiss (1981a) and Kumar (1980a, b). (Corrections are given in Appendix A of Viehland and Kumar (1989).) They have been called (Viehland 1986) the Cartesian basis function and designated as B(km; pqst); there are six indices since they are obtained by coupling two vectors (one in velocity space and the other in rotational space) in three dimensions, each with three indices. With these functions, the density-gradient-independent Curtiss equation is

$$f(\mathbf{v}, \mathbf{J}) = f_0^{(2T)}(\mathbf{v}, \mathbf{J}) \sum_{k, m, p, q, s, t} f^{(2T)}(km; pqst) B(km; pqst);$$
(8.14)

the unknowns are the numbers $f^{(2T)}(km; pqst)$ that are equivalent to moments of $f(\mathbf{v}, \mathbf{J})$. Normalization requires

$$f^{(2T)}(00;000) = 2\pi^{-1/4}.$$
 (8.15)

Matrix elements of the collision operator in the Curtiss equation are defined in the 2T-like theory as

$$\begin{pmatrix} k' & p' & q' & s' & t' \\ k & p & q & s & t \end{pmatrix}^{(m')}$$
 (8.16)

Then the drift velocity is given by the expression

$$v_d = \frac{qE(1+\alpha_c)}{n_0 \begin{pmatrix} 1 & 0 & 0 & 0 \\ 1 & 0 & 0 & 0 & 0 \end{pmatrix}^{(0)}},$$
 (8.17)

where the correction factor, α_c is given by Viehland (1986) and called δ_1 . When the neutral gas is composed of only a single species, this result leads to a generalization to molecules of the fundamental ion mobility equation, (1.45), i.e.,

$$K_0 = \left(\frac{2\pi}{\mu k_B T_{eff}}\right)^{1/2} \frac{3q}{16N_0} \frac{1 + \alpha_c}{1 + \Delta_1} \frac{1}{\langle \gamma_z (\gamma_z - \gamma_z') \rangle},$$
 (8.18)

where the effective temperature is

$$T_{eff} = \frac{mT + m_0 T_{kin}}{m + m_0} \tag{8.19}$$

There are three ways that this result differs from (1.45). First, $\langle \gamma_z \ (\gamma_z - \gamma_z') \rangle$ is a generalization to rigid rotors of the classical-mechanical expression for $\Omega^{(1,1)}$ (T_{eff}). Second, the procedure for determining α_c is sufficiently different that one is not sure whether the values for it will be as small for molecules as it is for atoms (see Sect. 2.7.2) at low E/n_0 . Third, Δ_1 is a ratio of collision integrals (Viehland 1986) that vanishes when inverse collision are assumed to exist, and which therefore might be small (but not zero). From an experimental point of view, however, one can simply set

$$\Omega_{mol}^{(1,1)}\left(T_{0}, T_{eff}\right) = \left\langle \gamma_{z} \left(\gamma_{z} - \gamma_{z}'\right) \right\rangle \frac{1 + \Delta_{1}}{1 + \alpha_{c}}, \tag{8.20}$$

and leave it to theorists to try to compute this "effective momentum-transfer collision integral" for molecules from the right-hand side of (8.20).

8.8 Atomic Ions in Diatomic Gases

Calculations that are based on the Curtiss equation are necessary because it has been shown (Viehland 1988) that the spherical potential inferred from scattering data (Budenholzer et al. 1986) for $^{39}K^+(^1S_0)$ ions interacting with small molecules such as N_2 and CO fail to reproduce the gaseous ion transport data. Hence, the entire potential energy surface is important in understanding scattering and transport data for molecular systems, even when the molecules are small.

It became practical to carry out ab initio calculations based on the Curtiss equation after computer program MOBDIF was developed (Viehland and Kumar 1989). For atomic ions moving in diatomic gases, it requires classical-trajectory calculations (Dickinson and Lee 1985a,b) of a set of cross sections (Viehland 1992) defined by the equation,

$$\sigma^{(\lambda,v)}(\varepsilon,\varepsilon_{rot}) = \frac{1}{2\pi} \int_0^\infty db \ b \int_{-1}^1 d\cos(\chi) \int_0^{2\pi} d\phi_L \int_0^\pi d\phi_J \times \left[1 - \left(\frac{\varepsilon'}{\varepsilon}\right)^{\lambda/2} (\cos\theta)^{\lambda}\right] \left(\frac{\varepsilon'}{\varepsilon}\right)^v (\sin\theta)^{2v} . \tag{8.21}$$

Here, θ is the polar scattering angle that depends upon: ε' , the post-collision value of the ion kinetic energy, ε ; ε_{rot} , the pre-collision value of the rotational energy; b, the impact parameter; χ , the angle between \mathbf{J}_0 and the angular momentum, \mathbf{L} , of the ion–neutral relative motion; ϕ_J , the phase angle of \mathbf{J}_0 ; and ϕ_L , the phase angle of \mathbf{L} .

For ${}^7\text{Li}^+({}^1\text{S}_0)$ ions in $N_2(v=0)$, millions of classical trajectories had to be followed in order to obtain results for the cross sections defined by (8.21) that had converged to a precision of 1% and an accuracy of 2% (Viehland 1992). An important difference between such trajectories and those used for neutral systems is that an ion–neutral interaction potential falls off much more slowly at large separations than does a neutral-neutral interaction potential, i.e., as r^{-4} instead of r^{-6} . This means that the trajectories must be started with the ion and neutral much further apart than for two neutrals, and followed until they have collided and again are very far apart. Another difference is that the experimental data one is interested in comparing against usually stretches over much wider range of kinetic energy, since for ion–neutral systems one can easily change this by changing E/n_0 while for neutral systems one must change T_0 . Consequently, 10–100 times more trajectories must be used for ion–neutral systems, each lasting much longer in time due to the larger separations that must be probed.

The K_0 , n_0D_{\parallel} and n_0D_{\perp} values for $^7\text{Li}^+(^1S_0)$ ions in $N_2(v=0)$ at 300 K calculated (Viehland 1994) by using the classical-trajectory cross sections in computer program MOBDIF were stable within 0.55, 2.75, and 1.38%, respectively. These values differed by larger percentages than these from the experimental results of Selnaes et al. (1990), presumably because the ion–neutral interaction potential used to compute the cross sections was obtained from SCF calculations (Staemmler 1975) rather than one of the more accurate methods described in Chap. 6.

Grice et al. (1992) determined a MP4SDTQ/6-331+G(2df) potential for ${}^7\text{Li}^+({}^1\text{S}_0)$ ions in N₂(v = 0). This is a fourth-order Moller–Plesset calculations (see Sect. 6.19) that uses Singles, Double, Triples, and Quadruples to treat configuration interaction. The 6-331+G(2df) basis set of Gaussian functions is large, so the potential of Grice et al. (1992) is expected to be accurate. This potential was used by Viehland et al. (1992) to redetermine K_0 , n_0D_\parallel and n_0D_\perp values for ${}^7\text{Li}^+({}^1\text{S}_0)$ ions in N₂(v = 0) at 300 K. This time the theoretical and experimental values agreed within their mutual uncertainties.

Subsequently, a MP4SDTQ/6-331+G(2df) potential energy surface for ${}^7\text{Li}^+({}^1\text{S}_0)$ ions in CO(v = 0) was calculated (Grice et al. 1993a) and its angular components determined using a truncated expansion in Legendre polynomials. Millions of classical trajectories were again used (Grice et al. 1993b) to compute the transport cross sections to an accuracy of 1%. These were then used in computer program MOBDIF to give K_0 , n_0D_{\parallel} and n_0D_{\perp} values converged at low E/n_0 to 0.1, 0.25 and 0.25%, respectively. Estimates of the accuracy of the interaction potential, the cross sections and the MOBDIF calculations led to an overall theoretical error (Grice et al. 1993b) of no more than 6% at small E/n_0 , decreasing to below 3% at high E/n_0 . The values agreed with experiment (Satoh et al. 1988) for E/n_0 values below 100 Td. Inaccuracies in the theoretical transport coefficients at high E/n_0 suggested that the potential

energy surface is not accurate between about 6 and 10 bohr, which is consistent with the known properties of Moller–Plesset calculations at nonequilibrium geometries (Pople et al. 1987).

8.9 Diatomic Ions in Atomic Gases

Viehland and Dickinson (1995) used the Curtiss equation to develop equations for the transport coefficients of diatomic ions in atomic gases. Such work is more difficult than in the case of atomic ions in diatomic gases because one must explicitly take into account that increases in E/n_0 cause increases in both the kinetic and rotational energies (and hence temperatures) of the ions. The basis functions they used were modeled after those of Curtiss (1981a) but were modified in the manner of Kumar (1980a, b) in order to allow the ion kinetic and rotational temperatures to differ from T_0 . They were also modified as in the biMaxwellian approach of Ness and Viehland (1995), which allows for cases where there is partial ion runaway and two ion kinetic temperatures. Since the biMaxwellian approach has been replaced by the Gram–Charlier theory discussed in Sect. 5.9 and Chap. 6, we will not give further details about the theory used by Viehland and Dickinson (1995). The computer program based on this theory is named TRAJECK.

Computer program TRAJECK was used (Viehland et al. 1996) to determine the transport coefficients of ground-state $NO^+(v=0)$ ions in a gas composed of the naturally occurring mixture of the isotopes of $He(^{1}S_{0})$. They first constructed a MP4SDTQ/6-331+G(2df,p) potential energy surface, keeping the NO⁺ bond length fixed at 1.9392 a_0 , a value that they obtained with a HF calculation using the same basis set. Their potential values covered 42 ion-atom separations from 2.6 to 34 bohr (measured from the midpoint of the nuclei in NO⁺) at each of nine angles between the line connecting the N and O nuclei and the line connecting the midpoint of the ion to the center of the atom. In order to interpolate among the calculated interaction potential energies, they represented the potential with an expansion in Legendre polynomials. The functional form they obtained was extrapolated to larger separation using a cubic spline fit that was constrained to match the ion-induced dipole potential when the ion-atom separation became infinite. They also extrapolated it to smaller separation. From this potential, they calculated 118 different cross sections similar to those given in (8.16) and assumed another group of 61 cross sections to be so small as to be negligible. Finally, program TRAJECK was used to compute K_0 values that were in excellent agreement with the experimental values of Lindinger and Albritton (1975).

There are some problems with these results, however. First, the experimental mobilities had error bars of $\pm 7\%$, so the excellent agreement may be misleading. Second, the selection of which cross sections to compute and which ones to ignore was done ad hoc, and these cross sections cannot possibly give transport coefficients calculated in higher than second approximation of the solution of the Curtiss equation

by the method of weighted residuals. Third, the theoretical calculations covered only E/n_0 values from 0 to 25 Td, yet they still required nearly a year of computing time.

A MP4SDTQ/6-311++G(3df,2pd) calculation has been made (Maclagan et al. 1999) of the potential energy surface for CO^+ (v=0) ions interacting with $He(^1S_0)$. Calculations of the cross sections and transport coefficients from this PES were performed in a manner similar to that just described for NO^+ in $He(^1S_0)$. In this case, however, 1056 cross sections were calculated, enough to determine the first three approximations to the solution of the Curtiss equation by the method of weighted residuals. Numerous improvements were also made in computer program TRAJECK. The result is that it took several weeks of computer time to calculate the cross sections, and several more weeks to calculate the transport coefficients. Unfortunately, the calculations still could only cover a small range of E/n_0 , from 0 to 35 Td.

The computing problems just described were sufficiently large that no subsequent ab initio calculations were made for diatomic ion in atomic gases. Computers have advanced enough in the last 20 years that such calculations should be attempted again, but no one seems interested in doing this. Even if this is done, it is difficult to see how larger ion–neutral systems could be treated. This is because there would be a larger number of degrees of freedom that would have to be taken into account in ab initio calculations of the potential energy surfaces and more difficulty in interpolating and extrapolating among the PES values to determine, by classical-trajectory calculations, the larger number of transport cross sections as a function of many types of internal energy. A new approach must be developed in order to study larger ion–neutral systems.

8.10 Monchick-Mason Approximation

An approximate way to compute transport cross sections (and hence transport coefficients) for molecular systems was introduced long ago by Monchick and Mason (1961). In the Monchick–Mason approximation (MMA), inelastic collisions are ignored, the relative orientation between the colliding particles is fixed during the entire collision, and the transport cross sections are computed as if the collisions were between two atoms. The usual transport cross sections, $\overline{Q}^{(l)}(\varepsilon)$, are calculated from the interaction potential for many fixed orientation angles, and averaged to give effective cross sections. These are then used in equations for the transport coefficients obtained by solving the Boltzmann equation for atomic systems.

The physical reasoning behind the MMA is that the scattering angle in a collision is determined primarily by the forces between the particles when they are at the distance of closest approach. The colliding particles spend so little time at this distance that the orientation varies little during this portion of the collision. Hence, one may as well assume that throughout the collision the particles were always at the relative orientation present when they are at the distance of closest approach.

The accuracy of the MMA was difficult to assess in the 1960s, given the computational difficulties involved in making any other kind of calculation directly from ab initio potential energy surfaces. In the 1970s, theoretical attention turned to quantum-mechanical, close-coupling (McGuire 1974), and semiclassical (Neilsen and Gordon 1973a, b) calculations of cross sections for rotationally inelastic scattering. These were based on a formulation of scattering theory in the total angular momentum representation given by Arthurs and Dalgarno (1960). Since a large number of coupled equations arise in such approaches, many approximations were developed to reduce the computational effort that was required. It was discovered (Parker and Pack 1978) that the infinite-order sudden (IOS) approximation in quantum mechanics is equivalent to the MMA in classical mechanics. The IOS is equivalent to using both the energy-sudden approximation (Chang et al. 1983) and the centrifugal-sudden approximation (Thachuk and McCourt 1990, 1991).

By 1990, it was the accepted view (Gianturco et al. 1990; Heck et al. 1993, 1994) that the MMA gave results of moderate accuracy for the transport coefficients of neutral gases when the gas temperature was low, and that its accuracy improved as T_0 increased. Unfortunately, there were some gases, most notably CO (Heck et al. 1995), for which this was not true, for no reason that could be identified. This failure is one of the motivations that led to the BMM (beyond Monchick–Mason) approximation discussed in the next section.

Viehland (2001) applied the MMA to $CO^+(v=0)$ ions in $He(^1S^0)$, using a MP4SDTQ potential energy surface obtained with a 6-311++G(3df,3pd) basis set (Maclagan et al. 1999). The theoretical transport coefficients were accurate at room temperature for E/n_0 values above 30 Td. The experimental mobilities (Lindinger and Albritton 1975; Lauenstein et al. 1991) for this system had errors of up to 7%, so the discrepancies below 30 Td may not be significant. Assuming they are, Viehland (2001) suggested that they arose because the collisions were qualitatively different at angles where the potential well depth was larger than the average collision energy than at angles where it was smaller. This suggestion is supported by examination of the microscopic momentum-transfer collision frequencies, $\nu^{(1)}(\varepsilon)$, shown in Fig. 8.2; these were calculated from a modification (Gharibi et al. 2013) of the potential that corrected for basis set superposition error (BSSE). For the MMA to be appropriate, the curves should change rather smoothly with angles; the erratic behavior was another motivation for the BMM.

In recent, unpublished work by the author and colleagues at Chatham University, the transport coefficients of $NO^+(v=0)$ have been studied in the various rare gases from He to Xe. This work makes use of ab initio potential energy surfaces calculated by Orek et al. (2016) using an expanded and improved version of the CCSD(T) method with an expanded cc-pVTZ-PP basis set that was also augmented with bond functions; this is a high-quality calculation, so the interaction potentials should be highly accurate. For $NO^+(v=0)$ -He(1S_0) collisions, the $\nu^{(1)}(\varepsilon)$ calculated from the ab initio potential energy curves at various fixed angles are shown in Fig. 8.3.

It is obvious in Fig. 8.3 that the curves vary systematically with the fixed angle used in the calculations, much more so than in Fig. 8.2. This is especially true above $9.5 \times 10^{-4} a_0$, which corresponds to thermal energy at 300 K. Hence, the average

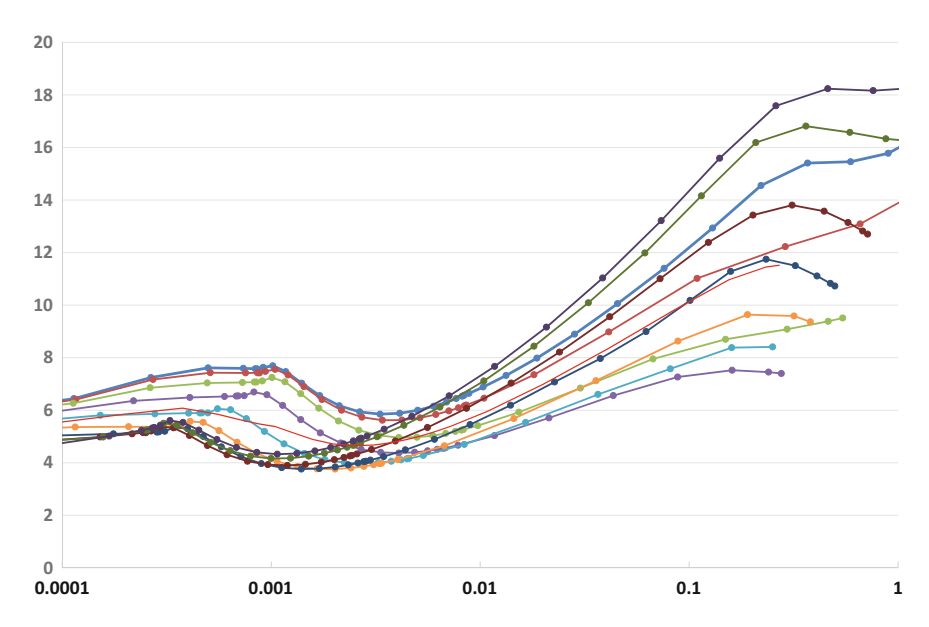


Fig. 8.2 Values of $\nu^{(1)}(\epsilon)$ for $CO^+(v=0)$ in $He(^1S_0)$, as a function of collision energy at fixed angles from $0^{\rm o}$ to $180^{\rm o}$ in steps of $20^{\rm o}$. The values are in atomic units. The thin red curve in the center is from the MMA average of the other curves

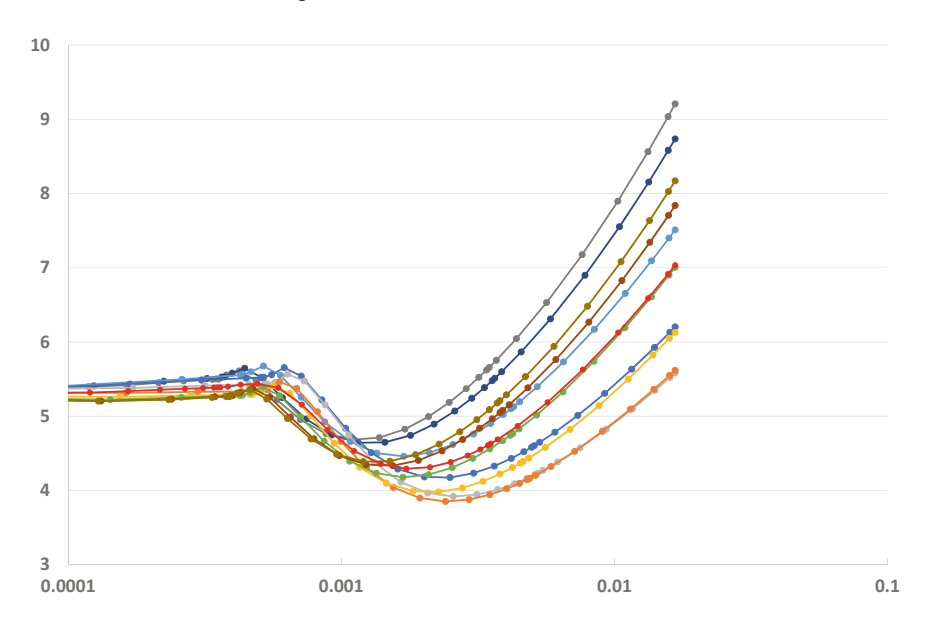


Fig. 8.3 Values of $\nu^{(1)}(\epsilon)$ for NO⁺(v = 0) in He(¹S₀), as a function of collision energy at fixed angles from 0° to 180° in steps of 10°. The values are in atomic units. The red curve in the center is from the MMA average of the curves

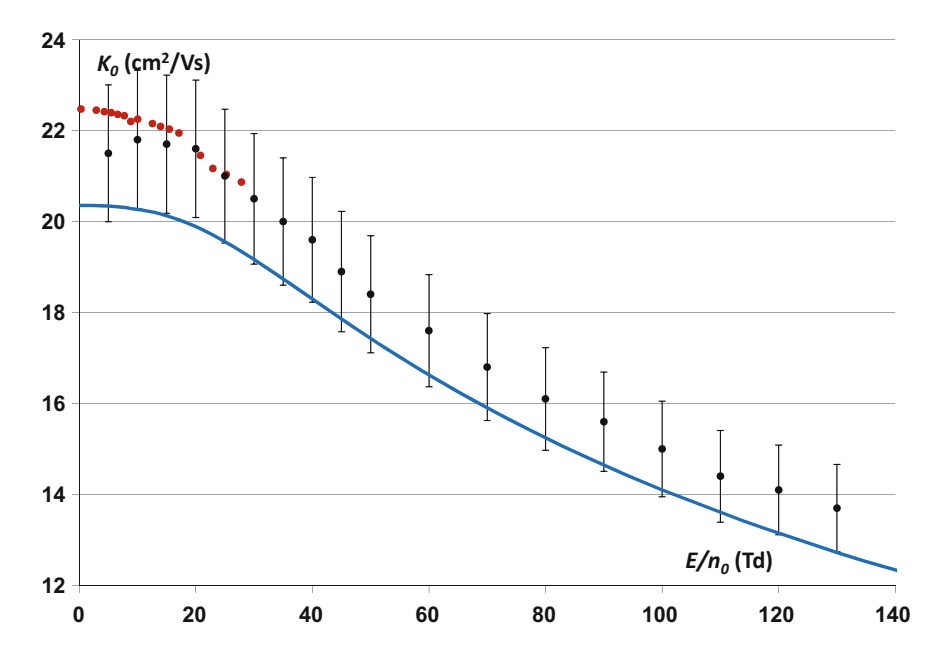


Fig. 8.4 Standard mobilities of NO⁺ in He at 300 K, as a function of E/n_0 . The red points were calculated from an old PES (Viehland et al. 1996), the blue curve was calculated from the PES of Orek et al. (2016), and the experimental data points (Ellis et al. 1977) are smoothed versions of data with an estimated accuracy of $\pm 7\%$

 $\nu^{(1)}(\varepsilon)$ computed by the MMA should be a good representation of the average of the values at the 19 separate angles, ranging from 0° to 180° in steps of 10°. Using these MMA cross sections in computer program GC gives the mobilities that are compared in Fig. 8.4 with experiment values (Ellis et al. 1976) that have rather large uncertainties, and with theoretical values calculated (Viehland et al. 1996) from an older potential energy surface that is expected to be less accurate than that of Orek et al. (2016). The old potential could not be used to compute mobilities for E/n_0 values above 30 Td, but at these low values the theoretical mobilities match the experimental ones quite well. The new PES, on the other hand, gives mobilities that lie on the lower end of the experimental error bars, for E/n_0 values from 0 to 130 Td.

There are three main possibilities for understanding the results in Fig. 8.4. One is that the experimental values are systematically high. A second, unlikely, possibility is that the old PES is more accurate than the new one. The final one is that the MMA is not accurate. To settle this issue, we have started making new measurements of the mobility of $NO^+(v=0)$ in the naturally occurring mixture of the isotopes of $He(^1S_0)$. If these turn out to be near the bottom of the error bars in Fig. 8.4, then the new potential and the use of the MMA are likely to be correct; therefore, the MMA can be used for molecular ions in atomic gases if the $\nu^{(1)}(\varepsilon)$ values are as

well behaved as in Fig. 8.3. If the new measurements are close to the old data, then it is likely (since the new potential is of very high quality) that the MMA cannot be used unless modified as discussed in the next section.

8.11 Beyond the MMA

The BMM (beyond Monchick–Mason) approximation was developed (Viehland and Chang 2012) for $^7\text{Li}^+(^1\text{S}_0)$ in $\text{H}_2(v=0)$, assuming that T_0 is high enough that enough rotational states are active that hydrogen may be treated as a rigid rotor. For such atomic ion-diatomic neutral systems, the ion–neutral interaction potential, $V(r,\theta)$, depends upon the separation, r, between the ion nucleus and the midpoint of the internuclear bond in the neutral, and upon the angle, θ , between the line connecting those two points and the line connecting the nuclei in the diatom. Since H_2 is homonuclear, θ needs to be varied only between 0° and 90° . At very large r, this potential must have the functional form (Mason and McDaniel 1988):

$$V(r,\theta) = \frac{C_3}{r^3} \left[3\cos^2(\theta) - 1 \right] - \frac{C_4}{r^4} \left(1 + \widehat{\kappa} \left[3\cos^2(\theta) - 1 \right] \right), \tag{8.22}$$

where the first term is the interaction between the charge of the ion and the permanent quadrupole of the neutral and the second is that between the ion and the induced dipole on the neutral. The quantity $\widehat{\kappa}$ measures the anisotropy of the ion-induced dipole potential. The important thing about (8.22) is that this potential varies as the inverse third power of the separation, except when $3\cos^2{(\theta)}=1$, or $\theta=55.74^\circ$. This causes the $\nu^{(1)}(\varepsilon)$ at different angles to have completely different behavior than in Figs. 8.2 and 8.3, as shown in Fig. 8.5.

At collision energies above $0.03 E_h$, the curves in Fig. 8.5 show a smooth trend with angle. This behavior is consistent with the MMA and with the general understanding that the repulsive wall of the interaction potential is qualitatively the same at all angles. Consequently, the BMM must reduce to the MMA at high energy.

At very low collision energies, the curves begin to differ greatly. This is because (8.22) shows that the long-range potential depends strongly upon the angle. Note that $\nu^{(1)}(\varepsilon)$ becomes independent of ε when $\theta=55^\circ$, as the discussion above indicates that it should be. Fortunately, these variations occur at energies so low, compared to thermal energy, that we do not need to explicitly incorporate their influence into the BMM.

The most striking feature of Fig. 8.5 is that the 19 curves come together at approximately $0.03~E_h$. Indeed, the angle with the lowest values of $\nu^{(1)}(\varepsilon)$ below $0.03~E_h$ has the highest values above this crossing point, and vice versa. The crossing point is about ten times higher in energy than the values indicated by the slanted line in Fig. 8.5. That line indicates the values of $\varepsilon_{\rm max}(\theta_i)$, the maximum energies at which classical orbiting can occur when θ is kept fixed at some value θ_i and the separation is varied.

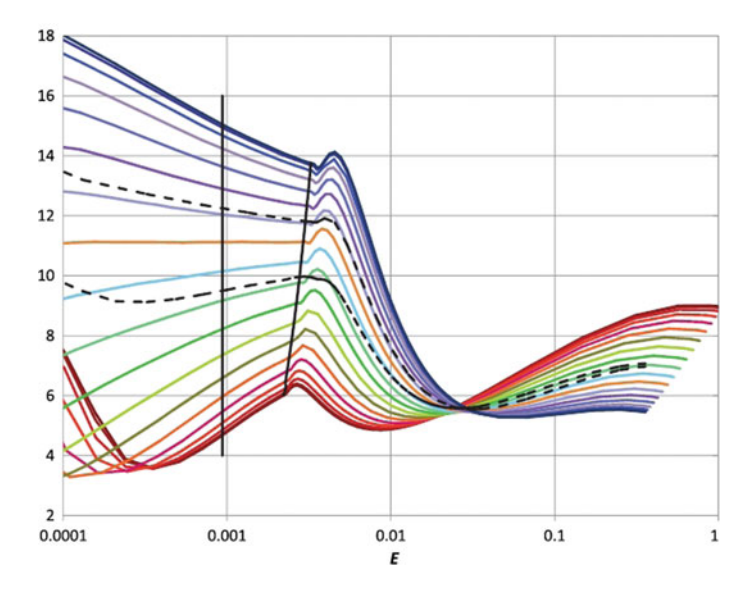


Fig. 8.5 Values of $\nu^{(1)}(\varepsilon)$ for ${}^7\text{Li}^+({}^1\text{S}_0)$ in $H_2(v=0)$, as a function of collision energy, ε , at fixed angles from 0° to 90° in steps of 5° . All quantities are in atomic units. The vertical line indicates thermal energy at 300 K

The considerations above suggested to Viehland and Chang (2012) that a BMM might involve a weighted average of the angle-dependent cross sections, namely

$$\overline{Q_{eff}}^{(l)}(\varepsilon) = \left[\sum_{i=0}^{n} w_i(\varepsilon, \theta_i) \overline{Q}^{(l)}(\varepsilon, \theta_i)\right] \left[\sum_{i=0}^{n} w_i(\varepsilon, \theta_i)\right]^{-1}.$$
 (8.23)

After some numerical experimentation, it was found that good results were obtained when the weighting factors were

$$w_i(\varepsilon, \theta_i) = 1 + 10 \left[\frac{\varepsilon_{\text{max}}(\theta_i)}{\varepsilon} \right] \sin(\theta_i).$$
 (8.24)

Various constants were tried in (8.24) in place of the 10 and the implicit powers of 1 for both the energy ratio and the sine, but the best results for the theoretical transport coefficients were obtained for ${}^{7}\text{Li}^{+}({}^{1}\text{S}_{0})$ in $H_{2}(v=0)$ with these numbers being 10, 1, and 1.

At large values of ε , the second term in (8.24) becomes negligible, and the BMM reduces to the MMA. At small ε , the first term becomes negligible and the weighting depends on θ_i . The factor of $\sin(\theta_i)$ gives more weight to the cross sections at large angle. For homonuclear diatomic gases, the calculations of the potential energy surface are arranged so that large angles correspond to θ_i near or equal to $\pi/2$, i.e., the ion is approaching the midpoint of the internuclear bond in the diatom. Thus,

low-energy collisions mean that a cation is moving toward the accessible electrons near the center of the bond with higher probability than it is moving toward the ends.

Calculations by Viehland and Chang (2012) showed that the BMM produced standard mobilities for ${}^7Li^+({}^1S_0)$ in ground-state $H_2(v=0)$ that were in much better agreement with experiment (Roeggen et al. 2002) than those obtained using the MMA. In both cases, the potential energy surface used was the potential of Roeggen et al. (2002), so the difference can only be due to the different approximations for determining the effective cross sections.

Gharibi et al. (2013) showed that the BMM also gave accurate mobilities for 23 Na $^{+}(^{1}S_{0})$ ions in H₂ at T_{0} =300 K with E/n_{0} between 0 and 250 Td when used with the RCCSD(T)/aug-cc-pVQZ interaction potential of Poad et al. (2008).

The values of $\nu^{(1)}(\varepsilon)$ in Fig. 8.2 do not vary as smoothly with angle as those in Fig. 8.3, but they are much better than those in Fig. 8.5. Therefore, Gharibi et al. (2013) applied both the MMA and the BMM to study ground-state $CO^+(v=0)$ ions in the naturally occurring mixture of the isotopes of $He(^1S_0)$. Neither gave good agreement with the smoothed experimental mobilities (Ellis et al. 1976) at 300 K. Good agreement was found when (8.24) was replaced with

$$w_i(\varepsilon, \theta_i) = \sin(\theta_i) \left(1 + 12.6 \left[\frac{\varepsilon_{\text{max}}(\theta_i)}{\varepsilon} \right] \right),$$
 (8.25)

leading to what they called the BMM2 approximation. In light of the findings above with $NO^+(v=0)$ in $He(^1S_0)$, it may turn out that the possible errors of $\pm 7\%$ in the experimental mobilities for $CO^+(v=0)$ in $He(^1S_0)$ accounted for the disagreement with the MMA results, and that the BMM2 is not needed. More research is clearly called for.

8.12 Future Calculations with the MMA and BMM

A strong argument in favor of continued research into the MMA and BMM is that such calculations could be extended with relative ease to considering larger molecules. To see this, suppose that an atomic ion–atom calculation of the transport cross sections takes an amount of computer time designated as o. With a present-day laptop, o is about 15 min, depending upon the number of tabulated points on the ion–neutral interaction potential that are supplied to computer program PC, the accuracy requested, etc. Experience indicates that it takes a time of approximately 4o for computer program GC to determine the transport coefficients at one value of T_0 over a wide range (approximately 0–1000 Td) of values of E/n_0 . Hence, it takes about 5o units of computer time to complete both calculations.

Now, consider a three-particle system for which the potential energy surface depends upon the ion-neutral separation and one internal degree of freedom. After the effective cross sections are computed, it still takes 40 units of time for program GC to calculate the transport coefficients. However, if there are nine angles (more

generally, values of the internal degree of freedom), it will take 9o units of time to compute the effective cross sections using the MMA or the BMM. The net time is still only 13o units of time, or $3.25 \, \text{h}$ if o is $15 \, \text{min}$. This is clearly feasible, especially given the many weeks or more required to use classical-trajectory calculations (see Sects. $8.8 \, \text{and} \, 8.9$).

Next, consider a four-particle system, such as the motion of a diatomic ion through a diatomic gas and assume that $9 \times 9 = 81$ values of the two internal degrees of freedom would need to be studied. This leads to (81 + 4)o units of time, or just less than one day. This too is feasible, considering that it would probably take much longer than this to compute the potential energy surface for two interacting diatoms.

Of course, the calculations rapidly become lengthy as the ion and neutral become larger, with more internal degrees of freedom. On the other hand, advances in computer speed (or switching from a laptop to a supercomputer cluster) can be expected to decrease the value of o. This will make possible nearly quantitative tests of potential energy surfaces for ion–neutral systems of chemical (but not biochemical or biological) interest. Until we get to that stage, we must resort to one of the methods discussed in Chap. 9.

References

```
A. Arthurs, A. Dalgarno, Prog. Roy. Soc. A 256, 540 (1960)
```

J.J.M. Beenakker, Festkorperprobleme 8, 276–310 (1968)

V.D. Borman, A.S. Bruev, B.I. Nikolaev, V.I. Troyan, Sov. Phys. JETP 33, 553 (1971)

V.D. Borman, A.S. Bruev, L.A. Maksimov, Sov. Phys. JETP 40, 472 (1975)

F.E. Budenholzer, E.A. Gislason, A.D. Jorgensen, Chem. Phys. 110, 171 (1986)

B. Chang, L. Eno, H. Rabitz, J. Chem. Phys. **78**, 3027 (1983)

C.F. Curtiss, J. Chem. Phys. 75, 376 (1981a)

C.F. Curtiss, J. Chem. Phys. 74, 6718 (1981b)

C.F. Curtiss, J. Chem. Phys. 97, 1416 (1992)

C.F. Curtiss, J.S. Dahler, J. Chem. Phys. 38, 2352 (1963)

A.S. Dickinson, M.S. Lee, J. Phys. B 18, 3987 (1985a)

A.S. Dickinson, M.S. Lee, J. Phys. B 18, 4177 (1985b)

H.W. Ellis, R.Y. Pai, E.W. McDaniel, E.A. Mason, L.A. Viehland, At. Data Nucl. Data Tables 17, 177 (1976)

M. Gharibi, L.A. Viehland, A. Abedi, A.H. Jalili, G. Afsahi, H. Behnejad, Mol. Phys. 111, 909 (2013)

F.A. Gianturco, M. Venanzi, A.S. Dickenson, J. Chem. Phys. 93, 5552 (1990)

S.T. Grice, P.W. Harland, R.J.A.R. Maclagan, Chem. Phys. **165**, 73 (1992)

S.T. Grice, P.W. Harland, R.J.A.R. Maclagan, J. Chem. Phys. 99, 7619 (1993a)

S.T. Grice, P.W. Harland, R.J.A.R. Maclagan, J. Chem. Phys. **99**, 7631 (1993b)

E.L. Heck, A.S. Dickinson, V. Vesovic, Chem. Phys. Lett. 204, 398 (1993)

E.L. Heck, A.S. Dickinson, V. Vesovic, Mol. Phys. 83, 907 (1994)

E.L. Heck, A.S. Dickinson, V. Vesovic, Chem. Phys. Lett. **240**, 151 (1995)

Y. Kagan, L. Maksimov, Sov. Phys. JETP 14, 604 (1961)

Y. Kagan, A.M. Afanas'ev, Sov. Phys. JETP 14, 1096 (1961)

K. Kumar, Australian J. Phys. 33, 449 (1980a)

K. Kumar, Australian J. Phys. 33, 469 (1980b)

References 253

- I. Kuščer, H.F.P. Knaap, J.J.M. Beenakker, Physica **108A**, 265 (1981)
- C.P. Lauenstein, M.J. Bastian, V.M. Bierbaum, S.M. Penn, S.R. Leone, J. Chem. Phys. 94, 7810 (1991)
- W. Lindinger, D.L. Albritton, J. Chem. Phys. **62**, 3517 (1975)
- R.G.A.R. Maclagan, L.A. Viehland, A.S. Dickinson, J. Phys. B 32, 4947 (1999)
- E.A. Mason, E.W. McDaniel, Transport Properties of Ions in Gases (Wiley, New York, 1988)
- P. McGuire, Chem. Phys. 4, 249 (1974)
- L. Monchick, E.A. Mason, J. Chem. Phys. 35, 1676 (1961)
- H. Moraal, Phys. Rep. 17, 225 (1975)
- W.B. Neilsen, R.G. Gordon, J. Chem. Phys. 58, 4131 (1973a)
- W.B. Neilsen, R.G. Gordon, J. Chem. Phys. **58**, 4149 (1973b)
- K.F. Ness, L.A. Viehland, Chem. Phys. 148, 255 (1990). Corrections are given in citation 6 of L.A. Viehland, A.S. Dickinson, Chem. Phys. 193, 255 (1995)
- C. Orek, J. Klos, F. Lique, N. Bulut, J. Chem. Phys. 144, 204303 (2016)
- G.A. Parker, R.T. Pack, J. Chem. Phys. 68, 1585 (1978)
- B.L.J. Poad, P.J. Wearne, E.J. Bieski, A.A. Buchachenko, D.I.G. Bennet, J. Klos, M.H. Alexander, J. Chem. Phys. 129, 184306 (2008)
- J.A. Pople, M. Head-Gordon, K. Raghavachari, J. Chem. Phys. 87, 5968 (1987)
- I. Roeggen, H.R. Skullerud, T.H. Lovaas, D.K. Dysthe, J. Phys. B 35, 1707 (2002)
- Y. Satoh, M. Takebe, K. Iinuma, J. Chem. Phys. 88, 3254 (1988)
- T.D. Selnaes, T.H. Lovaas, H.R. Skullerud, J. Phys. B 23, 2391 (1990)
- H. Senftleben, Ann. der Phys. 7, 273 (1965)
- R.F. Snider, J. Chem. Phys. 32, 1051 (1960)
- V. Staemmler, Chem. Phys. 7, 17 (1975)
- N. Taxman, Phys. Rev. **110**, 1235 (1958)
- M. Thachuk, F.R.W. McCourt, J. Chem. Phys. 93, 3931 (1990)
- M. Thachuk, F.R.W. McCourt, J. Chem. Phys. 95, 4112 (1991)
- A. Tip, Physica **52**, 493 (1971a)
- A. Tip, Physica **53**, 183 (1971b)
- R.C. Tolman, The Principles of Statistical Mechanics (Oxford University Press, London, 1938). Chap. 5
- L.A. Viehland, Gas-phase ion mobilities, ion-molecule reactions and interaction potentials., in *A Specialist Periodical Report: Mass Spectrometry*, vol. 6, ed. by R.A.W. Johnstone (London Chem. Soc., 1981) Chap. 3
- L.A. Viehland, Chem. Phys. 144, 552 (1988)
- L.A. Viehland, Chem. Phys. **101**, 1 (1986). Corrections in L.A. Viehland, K. Kumar, Chem. Phys. **131**, 295 (1989)
- L.A. Viehland, in *Status and Future Developments in Transport Properties, NATO Advanced Research Workshop*, ed. by W.A. Wakeham, A.S. Dickinson, F.R.W. McCourt, V. Vesovic (Kluwer Academic Publishers, Dordrecht, The Netherlands, 1992), p. 189
- L.A. Viehland, Physica Scripta T53, 53 (1994)
- L.A. Viehland, Comput. Phys. Comm. **142**, 7 (2001)
- L.A. Viehland, Y. Chang, Mol. Phys. 110, 259 (2012)
- L.A. Viehland, A.S. Dickinson, Chem. Phys. 193, 255 (1995)
- L.A. Viehland, K. Kumar, Chem. Phys. **131**, 295 (1989)
- L.A. Viehland, S.T. Grice, R.G.A.R. Maclagan, A.S. Dickinson, Chem. Phys. 165, 11 (1992)
- L.A. Viehland, A.S. Dickinson, R.G.A.R. Maclagan, Chem. Phys. 211, 1 (1996)
- L. Waldmann, Z. Naturforsch. **12a**, 660 (1957)
- L. Waldmann, Z. Naturforsch. 13a, 609 (1958)
- C.S. Wang Chang, G.E. Uhlenbeck, J. de Boer, in *Studies in Statistical Mechanics*, ed. by J. de Boer, G.E. Uhlenbeck (North-Holland, Amsterdam, 1964)

Chapter 9 Model Calculations for Molecules



9.1 Atomic Models of Molecular Systems

9.1.1 Maxwell Model

Models played an important part in understanding drift-tube experiments where atomic ions moved through atomic gases. Such models were crucial when computers were primitive, and were abandoned only when advances in quantum mechanics, kinetic theory, and computer hardware and software made it possible (see Chaps. 5 and 6) to make accurate, ab initio calculations. For molecules, we have not reached such an advanced position, as demonstrated in Chap. 8. Hence, we will begin this study of model calculations for molecular systems with atomic models that have been applied to molecular systems, without repeating any of the discussion in Sect. 2.8.3.

The simplest model for an ion-neutral system, whether one or both colliding particles is atomic or molecular, is that of the ion-induced dipole interaction potential, where V varies as r^{-4} . This is the famous Maxwell model of constant collision frequencies, although it is sometimes referred to as the polarization-limit model (Eiceman et al. 2014). It predicts that K_0 is a function only of T_0 , as shown in (1.20); in particular, K_0 does not change as E/n_0 increases. For modeling molecular systems, it is possible to treat K_0 as an adjustable parameter. This is seldom a useful model, however, since the ion mobility is usually not constant (except, of course, over small ranges of T_0 and E/n_0).

9.1.2 Rigid-Sphere Model

The next simplest model is that the ion–neutral interaction potential is like that describing the classical collision of rigid spheres. Then, the momentum-transfer collision integral is πd^2 and the fundamental ion mobility equation, (1.45), becomes

$$K_0\left(\frac{E}{n_0}, T_0\right) = \left(\frac{2\pi}{\mu_0 k_B T_{eff}}\right)^{1/2} \frac{3q}{16N_0} \frac{(1+\alpha_c)}{\pi d^2}.$$
 (9.1)

At high E/n_0 , the Wannier equation, (1.31), shows that the effective temperature is

$$T_{eff} = \frac{m_0 (1 + \beta_c)}{3k_B} \left[(E/n_0) N_0 K_0 \left(\frac{E}{n_0}, T_0 \right) \right]^2.$$
 (9.2)

Combining (1.4), (1.7), (9.1) and (9.2) gives

$$K_0\left(\frac{E}{n_0}, T_0\right) = \frac{1}{N_0} \left(\frac{6\pi}{m_0 \mu_0 (1 + \beta_c)}\right)^{1/4} \left(\frac{3q}{16} \frac{1 + \alpha_c}{\pi d^2}\right)^{1/2} \left(\frac{E}{n_0}\right)^{-1/2}.$$
 (9.3)

This is the well-known result that, for rigid spheres, the mobility decreases as $(E/n_0)^{1/2}$ at large E/n_0 .

For modeling purposes, a constant, low-field term can be added to (9.3). Making explicit once more the dependence of K_0 upon T_0 and E/n_0 , this gives

$$K_0\left(\frac{E}{n_0}, T_0\right) = K_0\left(0, T_0\right) \left[1 + \widetilde{\beta}_c \left(E/n_0\right)^{-1/2}\right],$$
 (9.4)

where $\widetilde{\beta}_c$ is a modeling parameter. This gives molecular modelers two quantities that can be adjusted to mimic the behavior of K_0 (E/n_0 , T_0). One problem with (9.4) is that is not clear for molecular ion–neutral systems how the low-field mobility should vary with temperature, i.e., what functional form to use for K_0 (0, T_0). Of course, this is not a problem if one is interested only in a single gas temperature, but then the other problems come into play. Real ion–neutral interaction potentials have both attractive and repulsive components, and having both of them is what causes a mobility maximum; such a maximum is impossible if (9.4) is used at fixed T_0 . In addition, experimental values of K_0 ($\frac{E}{n_0}$, T_0) at high E/n_0 ordinarily decrease smoothly with E/n_0 , but they do not vary as $(E/n_0)^{-1/2}$.

For light ions in heavy neutral gases (the Lorentz model), there is better way to add low-field corrections to (9.3). For this model of rigid spheres, it is possible to evaluate the mobility exactly, albeit it numerically (Hahn and Mason 1972). The results are in excellent agreement with the approximate equations from Sect. 5.2 of Mason and McDaniel (1988) that can be written as

$$v_d^* \left(1 + \frac{2}{3} v_d^{*2} \right)^{1/2} = \varepsilon^* \tag{9.5}$$

where

$$v_d^* = \left(\frac{m_0}{2k_B T_0}\right)^{1/2} v_d \tag{9.6}$$

and

$$\varepsilon^* = \left(\frac{m_1 + m_0}{m_1}\right)^{1/2} \frac{q(E/n_0)}{\sqrt{6k_B T_0 \left(\pi d^2\right)}}$$
(9.7)

After a moderate amount of algebra, these equations can be shown to give

$$K_0\left(\frac{E}{n_0}, T_0\right) = K_0(0, T_0) \left[\frac{\left\{1 + 2\widetilde{\beta}_c \left(E/n_0\right)^2\right\}^{1.2} - 1}{\widetilde{\beta}_c \left(E/n_0\right)^2}\right]^{1/2}, \tag{9.8}$$

where

$$\widetilde{\beta}_c = \frac{1}{24} \frac{m_1 + m_0}{m_1} \left(\frac{q}{k_B T_0 \left(\pi d^2 \right)} \right)^2. \tag{9.9}$$

For the purpose of molecular modeling, $\widetilde{\beta}_c$ and K_0 (0, T_0) can again be treated as adjustable parameters. Unfortunately, (9.8) has the same problems as (9.4). Moreover, the Lorentz model is not of much interest for modelers, who are primarily concerned with ions that are large and massive.

9.1.3 (n, 6, 4) Model

The (n, 6, 4) model of the interaction potential was introduced in order to overcome the problems with the rigid-sphere model. This model indicates that the potential energy is the following function of the ion–neutral separation:

$$V(r) = \frac{C_n}{r^n} - \frac{C_6}{r^6} - \frac{C_4}{r}. (9.10)$$

Although this model potential does not lead to analytical expressions for K_0 , tables of collision integrals have been published (Viehland et al. 1975) for it. Therefore, one can choose the four parameters in (9.10), look up $\overline{\Omega}^{(1,1)}(T_{eff})$ values at various effective temperatures, and use (1.31) and (1.45) to give the mobility at fixed T_0 as a function of E/n_0 . This process can be automated if computer program PC is used to generate the transport cross sections and a separate computer program (one called OMEGAS is available from the author) is used to compute the collision integrals from them. Of course, it would also be possible to use computer program GC along with the transport cross sections to compute values of the transport coefficients whose accuracy is primarily limited by the accuracy of the assumed V(r).

Choosing the four parameters in (9.10) is not completely random, because:

• The value of C_4 can be calculated exactly when the neutral is atomic, as shown in Table 6.2. Since the electric polarizability is known with moderate accuracy for

most molecular gases that one could use in a drift tube, C_4 can be estimated with reasonable accuracy even in such cases.

- The values of n and C_n govern the repulsive term in the potential. Usually, n is between 8 and 12, and this potential parameter makes K_0 vary as $(E/n_0)^{-1/2+2/n}$ at large E/n_0 . (Note that a rigid sphere potential would require $n = \infty$.) Once a value has been chosen for n, one can adjust the magnitude of the repulsion by changing C_n , based either on ab initio calculations of the potential energy surface at a few points for some approximation to the ion–neutral system of interest, or on the effect that such changes have upon the height of the mobility maximum.
- The inverse sixth power term accounts for the charge-induced quadrupole attraction and the London dispersion attraction between an ion and a neutral, both of which vary as r^{-6} . Although C_6 is seldom known as accurately as C_4 , methods have been developed (McDaniel and Mason 1973) for approximating it. The effect of adding this attractive term is illustrated by Viehland et al. (1975); it causes the height of the mobility maximum to decrease and can lead to a mobility minimum at intermediate E/n_0 . Note that changing C_6 might require a modeler to go back and make further changes in n or C_n .

If one chooses to set $C_6 = 0$, then this model is referred to as the Lennard-Jones (n, 4) model. If one sets $C_4 = 0$, then the potential reduces to the usual Lennard-Jones (n, 6) model of neutral–neutral interactions.

9.1.4 Core Models

The models above assume that the entire interaction potential can be described entirely in terms of r, the distance between the centers of mass of the ion and neutral. This is a good assumption for atomic systems, but it is often not a good model for molecular systems. A model that attempts to correct for this while still remaining simple is the (n, 4) core model,

$$V(r) = \frac{n\varepsilon_d}{3n - 12} \left[\frac{12}{n} \left(\frac{r_m - a}{r - a} \right)^n - 3 \left(\frac{r_m - a}{r - a} \right)^4 \right]. \tag{9.11}$$

Here, r_m is the separation at which the potential reaches its minimum value (i.e., r_m is the bond length), ε_d is the depth of the potential well (the value of -V when $r_m = r$) and a is the diameter of the core (so r must be larger than a in all circumstances). Nonzero values of a are assumed to account for the fact that the centers of attraction and repulsions are not the same as the centers of mass for molecular ions and neutrals.

The addition of a core to the (n, 4) model suppresses the height of the mobility maximum and, if a is large enough, can cause the standard mobility to be significantly lower than K_0 (0, 0), the polarization limit of the standard mobility that is given by (1.20). This effect differs from what is observed (Mason and McDaniel 1988) with an $(\infty, 4)$ potential because that model implicitly assumes that the charge is at the

center of the spherical ion whereas the (n, 4) core model assumes that it is spread evenly on the surface of the sphere of radius a.

The (12,4) core model has been shown to give good agreement with experimental mobilities (Patterson 1970) for several polyatomic anions in SF₆. To study such molecular systems with an (n, 4) core potential, one must choose values for n, ε_d , r_m and a; since C_4 can usually be estimated rather accurately (as described above), and n is usually between 8 and 12, only two of the parameters in this potential must be estimated by the modeler.

The use of a (n, 4) core potential for systems that show resonant charge transfer (e.g., He^+ in He) or ion transfer (e.g., He_2^+ in He) is discussed by Mason and McDaniel (1988).

It is straightforward to construct a (n, 6, 4) core potential based on the discussion of the (n, 6, 4) potential itself by Viehland et al. (1975). Thus,

$$V(r) = \frac{n\varepsilon_d}{(3+\gamma)n - 12(1+\gamma)} \left[\frac{12}{n} (1+\gamma) \left(\frac{r_m - a}{r - a} \right)^n - 4\gamma \left(\frac{r_m - a}{r - a} \right)^6 - 3(1-\gamma) \left(\frac{r_m - a}{r - a} \right)^4 \right]. \tag{9.12}$$

The new, dimensionless parameter in this equation, γ , ranges between 0 and 1 and measures the relative strengths of the r^{-6} and r^{-4} attractive interactions. When a=0, this equation becomes the same as (9.10) if we make the following identifications:

$$nC_n = 6C_6 r_m^{n-6} + 4C_4 r_m^{n-4}, (9.13)$$

$$\gamma = \left[1 + \frac{4}{3} \frac{C_4 r_m^2}{C_6}\right]^{-1} \tag{9.14}$$

and

$$\varepsilon_d = \frac{C_4 \left[3 + \gamma - 12 \left(1 + \gamma \right) / n \right]}{3r_w^4 \left(1 - \gamma \right)}.$$
 (9.15)

It would be easy to use computer program PC to determine the $\overline{Q}^{(l)}(\varepsilon)$ for the (n, 6, 4) core potential, and then to use computer program GC to compute the transport coefficients at a fixed value of T_0 as a function of E/n_0 . This has apparently not been done, presumably because attention has turned to the other methods described below. Another reason might be that such an approach would be better for a compact (almost spherical) polyatomic ion, whereas the ions that are now of the most interest are more like a chain (e.g., polymeric ions).

9.2 Site-Site Models

A common feature of the atomic models described in the previous section, and therefore a common weakness when they are used for molecular ions and neutrals, is that they assume two-body collisions between the ion and neutral or make approximate corrections for three-body effects. A different approach (Mesleh et al. 1996; Shvartsburg et al. 2001), and one that is probably better for long, chain-like molecules, is to assume that the center of each nucleus (each site) in a molecule influences the electrons around it in such a manner than the molecule can be described as a summation of site-site interaction potentials, i.e., interactions between the sites on the ion and the sites on the neutral.

The current state of such research is to use this procedure for a polyatomic ion as it is moves through a gas made of atoms. Then the interaction potential between the center of an atomic neutral and any site within the polyatomic ion can be assumed to be given by a Lennard-Jones (12, 6, 4) potential. The longest-ranged potential from each site can be combined as a vector sum, leading to the expression

$$V(x, y, z) = \sum_{i=1}^{N} \varepsilon_{i} \left[\left(\frac{r_{m,i}}{r_{i}} \right)^{12} - 2 \left(\frac{r_{m,i}}{r_{i}} \right)^{6} \right] - \frac{\alpha_{0}}{2} \left[\left(\sum_{i=1}^{n} \frac{q_{i} x_{i}}{r_{i}^{3}} \right)^{2} + \left(\sum_{i=1}^{n} \frac{q_{i} y_{i}}{r_{i}^{3}} \right)^{2} + \left(\sum_{i=1}^{n} \frac{q_{i} z_{i}}{r_{i}^{3}} \right)^{2} \right], \quad (9.16)$$

where x_i , y_i , and z_i are the Cartesian coordinates (with respect to a set of axes fixed at the center of the neutral atom) for the center of some nucleus within the ion, and $r_i^2 = x_i^2 + y_i^2 + z_i^2$. The constants ε_i and $r_{m,i}$ are the well depth and bond length for the (12,6) interaction—the first term in (9.16)—between the neutral atom and atom i within the polyatomic ion composed of N atoms, and q_i is the charge (which may be fractional) upon i. The electric polarizability of the neutral is α_0 .

If should be noted that the equivalent of (9.16) that is often given in the literature, for example, by Eq. (1.34) in Shvartsburg (2009), uses the zero-crossing points $(\sigma_i = 2^{1/6}r_{m,i})$ of the potentials in place of the bond lengths. Furthermore, it would be easy to use (9.12) to generalize (9.16) to a more elaborate site-site potential, one that included core effects, at the cost of having more parameters.

The positions (x_i, y_i, z_i) in (9.16) depend upon the distance between site i and the center of mass of the ion, as well as upon the separation between that center of mass and the nucleus of the atom at (0, 0, 0). The latter separation is what is meant by (x, y, z). The point is that one must know the positions (x_i, y_i, z_i) , the partial charges q_i , and the potential parameters, $r_{m,i}$, for each site before it is possible to use (9.16). This is a total of 5N parameters that must somehow be determined from limited mobility data, often with large experimental uncertainties. Although symmetry and other physical arguments can be used to reduce this number, it is a major limitation of site-site models.

9.2 Site-Site Models 261

The next problem with using site-site potentials is how to calculate $\Omega_{mol}^{(1,1)}(T_0, T_{eff})$. The kinetic theory in Sect. 8.7 indicates that the proper way is to use (8.20), but at present the calculation of the quantities on the right-hand side of that equation cannot be performed. Instead, Shvartsburg et al. (2001) decided to consider only low-field situations appropriate to IMS (so $T_{eff} = T_0$) and they assumed on ad hoc grounds that

$$\Omega_{mol}^{(1,1)}(T_0) = \frac{1}{8\pi^2} \int_0^{2\pi} d\theta_m \int_0^{\pi} d\phi_m \sin(\phi_m) \int_0^{2\pi} d\gamma_m \frac{\pi}{8} \left(\frac{\mu_0}{k_B T_0}\right)^3 \\
\times \int_0^{\infty} dg \exp\left(-\frac{\mu_0 g^2}{k_B T_0}\right) g^5 \int_0^{\infty} db \ 2b \left[1 - \cos\theta \left(\theta_m, \phi_m, \gamma_m, g, b\right)\right]. \tag{9.17}$$

Note the similarities and differences between this equation and (8.21). Here the translational kinetic energy (collision energy) is $\varepsilon = \mu_0 g^2/2$, where g is the relative speed between the colliding ion and neutral. Since (9.16) treats the potential energy surface as if the ions and neutrals were rigid rotors, the discrete nature of the internal energy states and rotational—translational coupling may be ignored. The collision geometry is defined by the three angles $(\theta_m, \phi_m, \gamma_m)$ whose volume element is $8\pi^2$. The constants before the integral over g, the exponential and the factor of g^5 can be justified in several manners, including the momentum-transfer theory in Chap. 3 that led to (3.32). The integral over the impact parameter, b, and the factor of 1-cos (θ) , where θ is the polar scattering angle, is the classical-mechanical version of the differential scattering cross section, as can be seen by comparing (3.17) and (3.18).

Evaluation of (9.17) requires classical trajectory calculations such as those described in Sects. 8.8 and 8.9 or additional approximations like those of Mesleh et al. (1996). What is missing in (9.17) is a factor of g'/g in front of the cosine term, as explained in Sect. 3.4.2. Presumably, Shvartsburg et al. (2001) left out this factor so that they could simplify (9.17) and then use a projection approximation (von Helden et al. 1993; Knapman et al. 2010). Therefore, the procedure used by Shvartsburg et al. (2001) greatly reduces the computational effort needed to calculate $\Omega_{mol}^{(1,1)}(T_0)$, which is the third problem with using site-site potentials. Others are that it ignores the details of the scattering process, not just the ratio of g'/g, and it cannot be used for molecules with concave surfaces that can cause some trajectories to lead to multiple scattering events.

The final problem is that there is no way that site-site potentials can be used to determine the correction term, α_c , and the ratio of collision integrals, Δ_1 , in (8.20). In short, for molecular ions and neutrals there is no known kinetic theory that gives the fundamental low-field ion mobility equation, (1.19), with (9.17) as the expression for the only collision integral that occurs. Hence, molecular modelers are trying to choose a moderate-to-large number of parameters for (9.16) that will model the PES for molecular ion–atom collisions and they are then computing, via (9.17), collision integrals that theory does not indicate are related to the experimental mobilities that

are measured. It is likely that good agreement with experiment is due more to the number of parameters that may be adjusted than it is to the inherent accuracy of site-site models. However, using the same fitting process for a homologous series of ions moving through the same neutral gas can be useful to an analytical chemist interested primarily in trendlines that aid the identification of the ions; this is an a posteriori argument that cannot help one understand the physical chemistry and chemical physics involved in DTMS and IMS studies.

One last comment. The site-site potential models the location of the charges in the ion, but it does not explicitly treat charges. It was concluded by Canzani et al. (2018) is that "not treating charge explicitly in calculations can result in large errors even for modestly charged ions".

9.3 Exact Hard Spheres Model

In order to account for multiple scattering when the molecular ions or neutral have concave surfaces, the exact hard spheres scattering (EHSS) model was introduced by Shvartsburg and Jarrold (1996). It is again assumed that the neutral is atomic, but now the molecular ion is assumed to be composed of a collection of hard (or rigid) spheres with positions and radii that can be chosen so as to fit experimental mobility data.

The complete neglect of attractive ion–neutral forces in the EHSS model makes this approach highly questionable. In addition, the repulsive forces at short separations between two nuclei vary with distance, r, more like $1/r^n$ with n between 8 and 12 than with $n = \infty$. Successful calculations with the EHSS method must therefore be attributed to coincidence and calibration factors, not to the correctness of the model. Only if the contributions from ion-induced dipole and other attractive forces decrease significantly with large molecules can this approach be justified. This has been shown in some recent calculations (Bleiholder et al. 2015; Canzani et al. 2018) but often not to the extent that one would call it "significant".

An improvement to the EHSS model was obtained by taking electron density distributions into account. This model (Shvartsburg et al. 2001) employs scattering on electron density isosurfaces. The ion cluster is represented by a surface defined numerically as a set of points in space where the calculated electron density has the same magnitude when calculated from density functional theory (DFT), with the value of this magnitude being used as an adjustable parameter. It appears (Shvartsburg et al. 2001) to be somewhat better than the EHSS model, although both ignore the ion-induced dipole potential that dominates the long-range forces between the ion and neutral. In addition, the comments in Sect. 6.2 about DFT must be kept in mind.

9.4 Early Monte Carlo Calculations

We now give up on potential models and focus on other types of calculations. The motion of an ion through a gas under the influence of an electrostatic field can be followed exactly if one knows the free times between each ion–neutral collision and both the scattering angles and energy loss (or gain) that results from each collision. This suggests that one might model gaseous ion transport by making simulations in which the free times, scattering angles and energy changes are randomly sampled from separate distributions that are supposed to correspond to a particular ion–neutral potential energy surface. Carrying out such sampling is defined as making a Monte Carlo (MC) calculation (Skullerud 1968; McIntosh 1974). Note that a MC calculation may be carried out for atomic or molecular systems, and without any reference to the Boltzmann equation or its generalizations in Chap. 8.

It has been known for many years that the main problem with MC calculations are how to determine the microscopic collision frequency that will be denoted here as $v(\varepsilon)$, by analogy with the microscopic collision frequency for momentum transfer,

$$\nu^{(1)}(\varepsilon) = \varepsilon^{1/2} \overline{Q}^{(1)}(\varepsilon). \tag{9.18}$$

One can, of course, adopt a model of a constant mean free path (the Maxwell model discussed in Sect. 9.1.1), in which case the MC method becomes simple and easy to implement (Wannier 1953). However, an electrostatic field causes an ion to continually accelerate during the time between collisions, so the true $v(\varepsilon)$ must vary as the ion moves from one collision to the next. To account for this, Skullerud (1968) introduced an improved MC method in which he used a model for $v(\varepsilon)$ that was constant over small intervals of ε , with each constant being greater than the actual value for any possible energy in the interval. He combined this with the null-collision assumption that some of the collisions result in no momentum transfer.

An extended null-collision method (Lin 1976; Lin and Bardsley 1978; Hennad et al. 1997) leads to a substantial reduction in the data size and computing time. Here, one makes the assumption that the future behavior of an ion is independent of its past, which defines a Markov process. As the ion moves between collisions, one generates a histogram for the ion vdf by computing the time that the velocity lies in each interval of the histogram. As the number of collisions increases, this histogram becomes the true ion vdf (Lin and Bardsley 1975). This work led to the papers (Albritton et al. 1977; Lin and Bardsley 1977) about $^{16}O^+(^4S_{3/2})$ reactions with $N_2(v=0)$ that were extensively discussed in Chap. 7.

Monte Carlo simulations of the behavior of electrons in H_2 have been reported (Hunter 1977; Davies et al. 1984). Discussion of these and more recent Monte Carlo studies with electrons is beyond the scope of this book. For the same reason, we will not discuss applications of Monte Carlo methods to such things as ion transport through glow discharge sheaths (Thompson et al. 1988). The key point is that MC calculations still are constrained by the difficulty in determining $\upsilon\left(\varepsilon\right)$ with good accuracy.

9.5 Molecular Dynamics Calculations

Molecular dynamics (MD) is another method for simulating the movement of ions through neutral gases. The ions and neutrals are allowed to interact for a fixed period of time, thereby giving a view of the dynamic evolution of the system. In the most common versions of MD, the trajectories of atoms and molecules are determined by numerically solving Newton's equations of motion for a system of interacting particles; the forces between the particles and their potential energies are often calculated using models of the interatomic potentials or molecular mechanics force fields. However, long MD simulations are mathematically ill-conditioned, generating cumulative errors in numerical integration that can be minimized with proper selection of algorithms and parameters, but not eliminated entirely.

Originally, MD calculations were too time-consuming to be practical for gaseous ion transport, since simulating the motion of trace amount of ions in a dilute gas means that much computer time can be spent following neutral-neutral interactions that are not crucial in determining the properties of the ions. An MD method for simulating DTMS and IMS experiments was developed by Koutselos (1995, 1996, 1997). The continuous dissipation to the neutrals of a part of the ion energy acquired from the electrostatic field is accomplished in his computer program through the use of so-called iconical interactions between the ions and images of the neutrals. The resulting ion mobilities, ion temperatures, and other transport coefficients compared well with available results derived from the 3T and Gram-Charlier calculations for $^{39}K^{+}(^{1}S_{0})$ ions in the naturally occurring mixtures of the isotopes of He($^{1}S_{0}$) and Ar(1S₀), and for ¹³⁸Ba⁺(2S_{1/2}) in naturally occurring mixtures of the isotopes of $Ar(^{1}S_{0})$. The advantage of this procedure is that it is more easily extended to more complicated ion-neutral systems (at the expense, of course, of increased computer time) and to moderately dense gases (Balla and Kostalos 2003). Its disadvantages are (1) obtaining mobilities accurate within about 5% requires large amounts of computer time, even for simple systems where the ions and neutrals are both atomic; and (2) investigating new values of T_0 , E/n_0 , or the ion mass (for a different isotope) requires a completely new calculation.

9.6 Recent Monte Carlo Calculations

An improved Monte Carlo method for studying gaseous ion transport of high E/n_0 was presented by Yousfi et al. (1998). This method overcomes the problem of ions that vanish, due to asymmetric charge transfer or electron detachment, by introducing fictitious ion creation processes. In effect, this is the inverse of the null-collision method discussed above.

The improved MC method was used (Chicheportiche et al. 2013) to study collision cross sections and ion transport coefficients for ${}^{4}\text{He}^{+}({}^{2}\text{S}_{1/2})$ in ${}^{4}\text{He}({}^{1}\text{S}^{0})$. A minor aspect of this work is that it used the PECs of Xie et al. (2005) and Tung et al. (2012),

rather than the newer set (Viehland et al., 2016) obtained using the CAS+MRCI method and discussed in Sect. 6.22.3. The important feature of this work is that it used quantum-mechanical methods to compute both the total and the momentum-transfer cross sections as functions of collision energy. Chicheportiche et al. (2013) found that the reduced mobilities at 300 K obtained with the same Monte Carlo computer program (Yousfi et al. 1998) using the different cross sections differed by about \pm 2% over the range of E/n_0 from 1 to 100 Td. Therefore, they inferred that it was sufficient to use $\overline{Q}^{(1)}(\varepsilon)$ rather than the total or differential scattering cross section (equivalently, to using $\nu^{(1)}(\varepsilon)$ rather than ν (ε)). This saves a factor of 20 in computer time and, more importantly, justifies using classical-mechanical values of $\overline{Q}^{(1)}(\varepsilon)$ for systems with heavier atoms. Note that classical-mechanical calculations of the total cross section are impossible due to divergences in the integrals involved in computing them, while quantum calculations for molecular ions and neutrals are extremely difficult even for small molecules.

The small difference between MC calculations with quantum-mechanical values of the total scattering cross section and classical-mechanical values of the momentum-transfer cross section is similar in size, and related to, the small difference between the first and higher approximations of kinetic theory. Remember that the low-field values of α_c were shown in Sect. 2.7.2 to be less than $\pm 0.6\%$, usually much less, for atomic ions in atomic gases. The MC calculations give indirect support to the usual assumption that α_c is small even at intermediate E/n_0 .

MC calculations for $\text{He}_2^+(\text{v=0})$ ions in the naturally occurring mixture of isotopes of $\text{He}(^1\text{S}_0)$ at 300 K have been reported (Chicheportiche et al. 2013). Quantum and semiclassical calculations were reported, along with calculations based on the IOS approximation . As discussed in Sect. 8.10, the latter is equivalent to a classical-mechanical calculation using the MMA. Unfortunately, Chicheportiche et al. (2013) used a rather crude model of the potential energy surface, one obtained from a diatomics-in-molecules calculation (Ellison 1963) into which they incorporated a method (Calvo et al. 2011) for including three-body interactions. This renders questionable the conclusions they reached by comparison of theoretical and experimental data, particularly since the latter (Ellis et al. 1976) cover E/n_0 values only up to 24 Td.

9.7 Software for Modeling Mobilities

The most widely used software for modeling the mobility of molecular ions in gases is MOBCAL (Jarrold 2018). This program was first developed in 1996 and has undergone several improvements since then. It can be used to calculate momentum-transfer collision integrals (called collision cross sections, CCD, in the program) from a set of atomic coordinates, using one of three different approaches.

1. The simplest and fastest calculation is the projection approximation (PA) that was described in Sect. 9.2. This calculates the CCD based on a hit/miss strategy

between the ion and the neutral atom with which it collides. Each particle is assumed to have a fixed interaction radius, so the geometrical cross sections are calculated for many two-dimensional snapshots covering the entire three-dimensional structure for a colliding ion and neutral. The overall CCD is taken as an average of these values.

- The second type of calculation uses the EHSS model to compute a CCD by modeling the atoms in a molecular ion as an array of overlapping hard spheres with radii equal to hard sphere collision distances.
- 3. The classical trajectory method (TM) uses a similar approach as for the EHSS, but with a site-site model of the interactions between an ion and a neutral atom. The TM is generally considered to give the best representation of the CCD, since it includes long-range attractive forces in modeling the ion–neutral interactions. However, the nature of these calculations means that the method is computationally difficult and therefore not applicable to large ions in MOBCAL.

A computer program named IMoS (Larriba and Hogan 2013a, b; Ouyang et al. 2013, Larriba-Andaluz and Hogan 2014) was tested by Shrivastav et al. (2017). It was shown to give mobilities within 1% of those given by MOBCAL when applied to the same 47 systems, using a mixture of the PA, EHSS and TM methods. This is the case even though there are major differences between the basic equations that are the bases of the two programs. IMoS is approximately 100 times faster than MOBCAL, due primarily to a more efficiently written algorithm and to parallelization of the code. This improved speed makes it possible to study ion mobilities in N_2 or air, not just He or other rare gases.

It has been stated (Knapman et al. 2010) that "when considering a comparison between theoretical collision cross sections [calculated by PA, EHSS, or CT methods] with experimental values for previously uncharacterized analytes, it is sometimes unclear which [of the three methods in the] MOBCAL program is the most appropriate to use." This statement summarizes many calculations in recent years, and it is true of IMoS as well. However, the very recent development (Zanotto et al. 2018) of a computer program named HPCCS implicitly makes this choice, because it uses only the TM method. It will be interesting to see in the next few years how MOBCAL, IMoS and HPCCS fare in additional head-to-head tests.

Let us assume for the moment that all three computer packages agree and give TM mobilities within 2% of the experimental values. While this would be great from some points of view, it would not overcome the arguments in Sect. 9.2 that the foundations of the calculations are shaky. The agreement might be due as much or more to the use of many adjustable parameters in site-site potentials (whose values can be "tuned" to force the computed mobilities to match experimental values that are often not as accurate as the experimenters claim) and to the focus upon only the zero-field mobilities of homologous series of ions in a limited number of gases. This is exactly what was found in the case of atomic ions in atomic gases, which is why model calculations for gaseous ion transport in such systems have been abandoned in favor of ab initio calculations of the type described in Chap. 6. Being able to make

ab initio calculations for molecular ion–neutral systems still lies many years in the future, so until then one should use the modeling software packages for practical purposes while, at the same time, remembering the limitations inherent in them.

References

- D.L. Albritton, I. Dotan, W. Lindinger, M. McFarland, J. Tellinghuisen, F.C. Fehsenfeld, J. Chem. Phys. 66, 410 (1977)
- G. Balla, A.D. Kostalos, J. Chem. Phys. 119, 11374 (2003)
- C. Bleiholder, N.R. Johnson, S. Contreras, T. Wyttenbach, M.T. Bowers, Anal. Chem. 87, 7196 (2015)
- F. Calvo, F.Y. Naumkin, D.J. Wales, J. Chem. Phys. 135, 124308 (2011)
- D. Canzani, K.J. Laszlo, M.F. Bush, J. Phys. Chem. A 122, 5625 (2018)
- A. Chicheportiche, B. Lepetit, M. Benhenni, F.X. Gadea, M. Yousfi, J. Phys. B 46, 065201 (2013a)
- A. Chicheportiche, M. Benhenni, M. Yousfi, B. Lepetit, R. Kalus, F.X. Gasea, Phys. Rev. E 88, 043104 (2013b)
- A.J. Davies, J. Dutton, C.J. Evans, A. Goodings, P.K. Stewart, J. Phys. D 17, 287 (1984)
- H.W. Ellis, R.Y. Pai, E.W. McDaniel, E.A. Mason, L.A. Viehland, At. Data Nucl. Data Tables 17, 177 (1976)
- F.O. Ellison, J. Am. Chem. Soc. 85, 3540 (1963)
- G.A. Eiceman, Z. Karpas, H.H. Hill Jr., Ion Mobility Spectrometry, 3rd edn. (CRC Press, Boca Raton, 2014)
- H. Hahn, E.A. Mason, Phys. Rev. A 6, 1573 (1972)
- A. Hennad, O. Eichwald, M. Yousfi, O. Lamroud, J. Phys. III (France) 7, 1877 (1997)
- S.R. Hunter, Aust. J. Phys. 30, 83 (1977)
- M.F. Jarrold, MOBCAL software at https://www.indiana.edu/~nano/software/ (Last modified June, 2000; accessed September, 2018)
- T.W. Knapman, J.T. Berryman, I. Campuzano, S.A. Harris, A.E. Ashcroft, Int. J. Mass Spectrom. **298**, 17 (2010)
- A.D. Koutselos, J. Chem. Phys. 102, 7216 (1995)
- A.D. Koutselos, J. Chem. Phys. 104, 8442 (1996)
- A.D. Koutselos, J. Chem. Phys. 106, 7117 (1997)
- C. Larriba, C.J. Hogan, J. Phys. Chem. A 117, 3887 (2013a)
- C. Larriba, C.J. Hogan, J. Comput. Phys. 251, 344 (2013b)
- C. Larriba-Andaluz, C.J. Hogan, J. Chem. Phys. **141**, 194107 (2014)
- S.L. Lin, Monte Carlo simulation of the ion motion in drift tubes. Ph.D. thesis, University of Pittsburgh, Pennsylvania, 1976
- S.L. Lin, J.N. Bardsley, J. Phys. B 8, L461 (1975)
- S.L. Lin, J.N. Bardsley, J. Chem. Phys. **66**, 435 (1977)
- S.L. Lin, J.N. Bardsley, Comput. Phys. Commun. 15, 161 (1978)
- A.I. McIntosh, Aust. J. Phys. 27, 59 (1974)
- E.A. Mason, H. Hahn, Phys. Rev. A 6, 1573 (1972)
- E.A. Mason, E.W. McDaniel, *Transport Properties of Ions in Gases* (Wiley, New York, 1988). Sec. 6–1
- E.W. McDaniel, E.A. Mason, *The Mobility and Diffusion of Ions in Gases* (Wiley, New York, 1973). Ch. 6
- M.F. Mesleh, J.M. Hunter, A.A. Shvartsburg, G.C. Shatz, M.F. Jarrold, J. Phys. Chem. A 100, 16082 (1996)
- H. Ouyang, C. Larriba-Andaluz, D.R. Oberreit, C.J. Hogan, J. Am. Soc. Mass Spectrom. 24, 1833 (2013)

- P.L. Patterson, J. Chem. Phys. 53, 696 (1970)
- V. Shrivastav, M. Nahin, C. J. Hogan, C. Larriba-Andaluz, J. Am. Soc. Mass Spectrom. 28, 1540 (2017)
- A.A. Shvartsburg, M.F. Jarrold, Chem. Phys. Lett. 261, 86 (1996)
- A.A. Shvartsburg, B. Liu, M.F. Jarrod, K.-M. Ho, J. Chem. Phys. 112, 4517 (2000)
- A.A. Shvartsburg, R.R. Hudgins, P. Dugourd, M.F. Jarrold, Chem. Soc. Rev. 30, 26 (2001)
- A.A. Shvartsburg, Differential Ion Mobility Spectrometry (CRC Press, Boca Raton, 2009)
- H.R. Skullerud, J. Phys. D 1, 1567 (1968)
- B.E. Thompson, H.H. Sawin, D.A. Fisher, J. Appl. Phys. 63, 2241 (1988)
- L.A. Viehland, E.A. Mason, W.F. Morrison, M.R. Flannery, At. Data Nucl. Data Tables 16, 495 (1975)
- G. von Helden, M.-T. Hsu, N. Gotts, M.T. Bowers, J. Phys. Chem. 97, 8182 (1993)
- G.H. Wannier, Bell Syst. Tech. J. 32, 170 (1953)
- M. Yousfi, A. Hennad, O. Eichwald, J. Appl. Phys. 84, 107 (1998)
- L. Zanotto, G. Heerdt, P.C.T. Souza, G. Araujo, M.S. Skaf, J. Comput. Chem. 39, 1675 (2018)

Chapter 10 Summary and Prognosis



Gaseous ion mobility, diffusion, and reaction have been studied by swarm techniques for about 120 years. As illustrated in Chap. 1, many important things have been discovered, including: the existence of electrons, ions, and isotopes; a verification of quantum mechanics by its use in distinguishing the mobilities of ${}^4\text{He}_2^+$ and ${}^4\text{He}^+({}^2\text{S}_{1/2})$ in ${}^4\text{He}({}^1\text{S}_0)$; the NTE equation relating the mobility and diffusion coefficient at low E/n_0 ; the tensorial rather than scalar nature of the diffusion coefficients; and the usefulness of DTMS for studying ion–neutral reactions at intermediate energies. So many of these discoveries happened so long ago that scientists often assume that there is little more to be done, despite the many experimental techniques that have been introduced in recent years. These are described in Chap. 2.

The fundamental ion mobility equation and its low-field limit play a significant role in theoretical descriptions of the transport of atomic ions in atomic gases. Chapter 3 obtains these equations, and the appropriate correction terms that arise for them, using algebra and physical insight. Chapters 4 and 5 obtain them from the Boltzmann equation that has been independently verified by its agreement with equilibrium statistical mechanics, and for nonequilibrium systems by its ability to connect experimental data for the transport coefficients of neutral gases with the fundamental forces that describe the atom—atom interactions.

There is only so far that one can go with analytical formulas. The last sections of Chap. 5 describe successive refinements in solving the Boltzmann equation by the method of weighted residuals (see Appendix C). This numerical method is appropriate because gaseous ion transport experiments are conducted with trace amounts of ions, so the Boltzmann equation contains no ion—ion interactions and hence is a linear equation.

Chapter 6 reviews the many steps necessary to make ab initio calculations of the ion mobility, diffusion, and other transport coefficients. This involves discussing many of the features of quantum mechanics, particularly those used in computational chemistry programs to determine atomic ion—atom interaction potentials. From such potentials, it is possible now to calculate the transport coefficients with more accuracy

than they can ordinarily be measured. As indicated by Fig. 6.5, more than half of the elements remain to be investigated, and this will take at least several years to complete. In addition, the accuracy of ab initio mobilities for atomic systems opens the possibility for researchers using DTMS and IMS to calibrate their apparatus by using them to study several such systems before moving on to the molecular systems that are presently of more interest.

Chapter 7 revisits the use of drift tubes to study ion—neutral reactions. The theory used in the late 1970s to analyze reaction data from swarm measurements appears not to have been as accurate as expected, at least for situations where the reaction cross section varies strongly with collision energy. The results in Chap. 7 should lead to the reexamination of many ion—neutral reactions that were once thought to be well understood. Such reexamination should involve new measurements and, perhaps more importantly, the use of more recent theories to interpret the data.

Our understanding of molecular ion—neutral systems is not nearly as advanced as for atomic systems. Chapter 8 shows that the only extension to molecules of the Boltzmann equation that is feasible to use in calculations is the Curtiss equation. Even then, it has proved practical to apply rigorous kinetic theory only to systems in which either the ion or the neutral is diatomic and the other is atomic. Much research is still needed into the kinetic theory of molecular systems, and many advances in computer hardware and software will probably be required. Meanwhile, there is hope that the BMM approximation will make possible accurate calculations of the transport properties for molecular systems of at least moderate size.

The use of models in understanding gaseous ion data, particularly the mobility, for molecular systems is described in Chap. 9. There are many aspects of such modeling that can be criticized, and this was done in Chap. 9. More important, however, is that such models can help analytical chemists understand the behavior of homologous series of ions, and thereby help them identify what ions are present in various gas samples that have been ionized. This is the reason why IMS has been combined so often in recent years with MS. Understanding the new data so obtained will be an exciting challenge for future research.

Appendix A: Dictionary of Mathematical Terms

Adjoint Operator has many, intricately connected definitions in various branches of mathematics. Hence we shall define it here only in a simple sense, for integrals in one dimension. Suppose a given operator O has an adjunct operator O^* . Then matrix elements of these operators formed from two functions must obey the relationship

$$\int \psi_1^*(x) O \psi_2(x) dx = \int \psi_2^*(x) O^* \psi_1(x) dx, \tag{A.1}$$

where the * on the functions indicates a complex conjugate (see below). Note that it is often a hard problem to determine O^* if all you know is O.

Associated Laguerre polynomials, $L_n^k(x)$, are a complete set of functions in onedimensional space, x. They are orthonormal on the interval $[0, \infty)$ with respect to the weighting function $x^k e^{-x}$. They are useful as basis functions because many integrals and derivatives of them are known in closed form, as are some interrelations when the order n or degree k changes (Gradshteyn and Ryzhik 1980).

Associated Legendre polynomials of degree l and order m, $P_l^{(m)}(x)$, are a complete set of functions in one-dimensional space, x. They are orthogonal on the interval [-1,1] with one as the weighting function. They are useful as basis functions because many integrals and derivatives of them are known in closed form, as are some interrelations when the order n or degree k changes (Gradshteyn and Ryzhik 1980). There are two sign conventions in common use, while some researchers normalize the $P_l^{(m)}(x)$ and others do not; in this book, we follow the practices of Hirschfelder et al. (1964).

Burnett functions are a complete set of functions in three-dimensional velocity space, \mathbf{v} , that are characterized by three indices, i.e., $\psi_{l,m,r}(\mathbf{v})$ They are defined by (5.21) in terms of associated Laguerre polynomials (also called Sonine polynomials) of v^2 , associated Legendre polynomials of the cosine of the polar angle of \mathbf{v} with respect to some space-fixed axis, and exponentials of the azimuthal angle of \mathbf{v} . They

are orthogonal when integrated over all velocities, i.e., the integral of two Burnett functions is zero unless the indices are the same on each. The normalization constant is given by (5.27).

Cartesian coordinates are descriptions of space that is defined by two or more mutually-orthogonal axes. In two dimensions, the coordinates are the familiar x and y of elementary mathematics courses. In three dimensions, the coordinates are usually designated x, y and z. Although the concept of Cartesian coordinates can be easily extended to as many dimensions as needed, there is no general agreement about the symbols to be used for them in such cases.

Commutator is a combination of two operators, O_1 and O_2 , in quantum mechanics that is in many ways equivalent to a Poisson bracket in classical mechanics. In particular,

$$[O_1, O_2] = O_1 O_2 - O_2 O_1. (A.2)$$

Complete set of functions is one that can be used to expand an arbitrary function (in the same space) in such a way that the difference between the function and its representation in the set of functions converges to zero in the limit where the number of expansion functions becomes infinite. See pp. 417–424 of Kaplan (1959) or any textbook of advanced calculus.

Complex conjugate of a complex number, a+ib, is one with the same real part but the negative of the imaginary part, i.e., a-ib where $i=\sqrt{-1}$ is the base of the imaginary numbers. By extension, the complex conjugate of any mathematical quantity (such as an operator) is obtained by leaving the real portions unchanged but changing the sign of the imaginary portions.

Cross product of two vectors is a binary operation on two independent vectors in three-dimensional space. If $C = A \times B$, then C is a vector that is perpendicular to both A and B and thus normal to the plane containing them. If A and B have the same direction (or the exact opposite direction from one another), or if either one has zero length, then C = 0. More generally, the Cartesian components of C are $C_x = A_y B_z - A_z B_y$, $C_y = -A_x B_z + A_z B_x$, and $C_z = A_x B_y - A_y B_x$.

Determinant is a value that can be computed from the elements of a square matrix (see below). In the case of a 2×2 matrix such as

$$\begin{bmatrix} a & b \\ c & d \end{bmatrix}, \tag{A.3}$$

the determinant is

$$\begin{vmatrix} a & b \\ c & d \end{vmatrix} = ad - bc. \tag{A.4}$$

Geometrically, a determinant can be viewed as the scaling factor of the linear transformation described by the matrix. See pp. 5–8 of Kaplan (1959) or any textbook of linear algebra.

Dot product is the same as scalar product (see below).

Dyadic (also known as a dyad) of a pair of vectors, **A** and **B** is the second-rank tensor **AB**. This means that the i-j element of the dyadic **AB**, is the product $A_i B_j$. The concept can easily be extended to a vector and a tensor, two tensors, etc.

Eigenfunction is the equivalent for functions as eigenvector (see below) is for more general mathematical objects (like determinants).

Eigenvalue (also known as characteristic value) of an operator O is an number λ obtained by using O on an eigenvector, f, and getting $Of = \lambda f$. There can be two or more functions that give the same eigenvalue when operated upon by O.

Eigenvector (also called eigenfunction) of an operator O is a quantity, f, that is returned intact when operated upon by O, except for a multiplicative factor, λ . Thus, $Of = \lambda f$. There is one and only one value of λ for a given eigenvector.

Factorial symbol is an! following a number, or an algebraic symbol representing a number. n! means the numerical value obtained by multiplying n by (n-1) and all progressively smaller integers down to 1. As an example, 3! is $3 \cdot 2 \cdot 1 = 6$. By definition, 0! = 1 and the factorial of any negative integer is zero.

Four vector has four components, the first along the x direction, the second along y, the third along z, and the fourth along ict, where $i = \sqrt{-1}$ is the base of the imaginary numbers, c is the speed of light in a vacuum, and t is the time.

Gamma function is an extension of the factorial symbol (see above) from integers to real numbers. The direct connection is that $\Gamma(n)=(n-1)!$ for integers. For real numbers, $\Gamma(x)=(x-1)\Gamma(x-1)$, so this relationship can be used to reduce the gamma function of any number greater than one to the range [0,1]. As an example, $\Gamma(3/2)=(1/2)\Gamma(1/2)=(1/2)\pi^{1/2}$. Although there is an analytical formula for $\Gamma(1/2)$, it is usually best to consult tables for other arguments between 0 and 1. See pp. 73–81 of Kaplan (1959).

Gauss' law from vector calculus is discussed in nearly every beginning, calculus-based course in physics. As illustrated by (A.13), one is interested in some flux that depends upon position, $\mathbf{j}(\mathbf{r})$. The net flow outward through an arbitrary, three-dimensional closed surface as $\int \mathbf{j}(\mathbf{r},t) \cdot d\widetilde{\mathbf{A}}$, where $d\widetilde{\mathbf{A}}$ is a vector, pointing outward, whose magnitude is the area of the infinitesimal surface being considered. Gauss' Law shows that this leakage may also be expressed as $\int \nabla \cdot \mathbf{j}(\mathbf{r}) d\widehat{V}_0$, where \widehat{V}_0 is the volume bounded by the surface.

Gradient vector is a three-dimensional vector whose components along the usual (x, y, z) Cartesian coordinates are the partial derivatives along those directions. In terms of the spatial unit vectors $(\widehat{x}, \widehat{y})$ and \widehat{z} , the gradient vector is defined by the equation,

$$\nabla = \widehat{x} \frac{\partial}{\partial x} + \widehat{y} \frac{\partial}{\partial y} + \widehat{z} \frac{\partial}{\partial z}.$$
 (A.5)

Hamiltonian function of a system is numerically equal to the total energy. When generalized coordinates, q_i , and the conjugate momenta, p_i , of the various degrees of freedom of the system are used,

$$H(q_i, p_i) = \sum_{i} p_i \frac{dq_i}{dt} - K + V, \tag{A.6}$$

where K is the sum of the kinetic energies of the individual particles and V is the potential energy function for the entire system. More information about how the Hamiltonian function is used in classical mechanics is given on pp. 36–39 of Hirschfelder et al. (1964).

Hamiltonian operator (sometimes simply called the Hamiltonian) is the quantum-mechanical equivalent of the Hamiltonian function in classical mechanics. It is the difference between the kinetic energy operator and the potential energy operator. One usually knows the classical expressions for the kinetic and potential energies in terms of positions and velocities, so the Hamiltonian operator can be obtained by using the correspondence principle of (6.1) and (6.2), while leaving the spatial coordinates unchanged.

Hermite polynomials are a complete set of functions in one-dimensional space, x. They are orthonormal on the interval $(-\infty, \infty)$ with respect to the weighting function $\exp(-x^2)$. They are useful as basis functions because many integrals and derivatives of them are known in closed form. (Gradshteyn and Ryzhik 1980). A product of three Hermite polynomials, one along each Cartesian axis, is a complete set of functions in three-dimensional space.

Imaginary numbers are proportional to the quantity $i = \sqrt{-1}$, the proportionality factor being a real number. An entire branch of mathematics is composed of the algebraic and other properties of imaginary numbers. Imaginary numbers have proven to be useful in many applied areas of science and engineering, including some of the sections of this book.

Integration by parts is represented by the one-dimensional formula

$$\int_{a}^{b} u(x)v'(x)dx = u(b)v(b) - u(a)v(a) - \int_{a}^{b} u'(x)v(x)dx.$$
 (A.7)

Lagrange multipliers are a means for finding the local maxima and minima of a function, subject to the condition that one or more other equations have to be satisfied exactly by the chosen values of the variables. More technically, Lagrange multipliers can be used to find the extrema of a multivariate function, $f(x_1, x_2, ..., x_n)$, subject to the constraint $g(x_1, x_2, ..., x_n) = 0$, as long as f and g have continuous first partial derivatives on the open set containing the curve $g(x_1, x_2, ..., x_n) = 0$, and as long as $\nabla g(x_1, x_2, ..., x_n) \neq 0$ at any point on the curve.

Laguerre polynomials are a complete set of functions in one-dimensional space, x. They are orthonormal on the interval $(-\infty, \infty)$ with respect to the weighting function $\exp(-x)$. They are useful as basis functions because many integrals and derivatives of them are known in closed form (Gradshteyn and Ryzhik 1980).

Laplace operator or Laplacian is a scalar operator that can be obtained by taking the scalar product of two gradient vectors. This operator makes it easy to represent the sum of three partial derivatives, one along each of the usual (x, y, z) Cartesian coordinates. Thus

$$\nabla^2 = \nabla \cdot \nabla = \frac{\partial^2}{\partial x^2} + \frac{\partial^2}{\partial y^2} + \frac{\partial^2}{\partial z^2}$$
 (A.8)

Least squares determination (linear) is the process of determining the parameters of a line (e.g. m and b in the equation y = mx + b) that best represents the dependent variable (y) as a function of the independent variable (x). The variants include ordinary (unweighted) and weighted least squares determinations, depending upon whether all regions of the independent variable are considered equally important or not. Numerical techniques for linear least squares determination usually involve inverting the matrix representing the normal equations, one for each value of the independent variable.

Least squares determination (nonlinear) is the process of determining the parameters that describe a nonlinear function of the independent variable that comes as close as possible to representing the given values of the dependent variable. Generally, one uses a computer program to make a non-linear least squares determination; the user must specify the functional form of interest and input the paired values of the independent and dependent variables.

Legendre polynomials, $P_l(x)$ are a subset of the associated Legendre polynomials, $P_l^{(m)}(x)$, obtained by setting m = 0.

Linear algebra is a branch of mathematics concerned with linear equations in which a dependent variable is expressed in terms of constants and first powers of one or more independent variables. The equations are represented in terms of matrices and determinants whose manipulations lead to solutions of the set of equations without specific indication of the variables involved. An undergraduate course in linear algebra is highly recommended for science and engineering majors, and elementary textbooks are commonly available.

Mathieu equation is a second order, ordinary differential equation (see below) that often arises in applied areas of science and engineering. It can be written as

$$\frac{\partial^2 u}{\partial x^2} + [a - 2q\cos(2x)] u = 0, \tag{A.9}$$

where a and q are constants and u is the unknown function whose dependence upon x is sought. This equation plays a fundamental role in many treatments of ion traps (March 2003).

Matrices are arrays of numbers that can be manipulated by the rules of linear algebra and then interpreted in terms of the numbers composing the final matrices. If there are n linear equations, each expressed in terms of the same m variables, then the set of equations can be written as a matrix with n rows and m columns. The final matrix obtained by operating on the initial matrix by a well-defined series of mathematical procedures can be back-translated into a new set of n equations. A particularly useful series of procedures is one that ends up with a diagonal matrix, one in which the only nonzero entries are along the main diagonal (from upper left to bottom right); when back-translated, one has a consistent solution of the original equations or can show that there is no solution or an infinite set of solutions. An undergraduate course in linear algebra is highly recommended for science and engineering majors, and elementary textbooks are commonly available.

Ordinary differential equation is a differential equation in which there is only one independent variable. Equation (A.7) is, for example, an ordinary differential equation of second order (since it involves a second derivative). An undergraduate course in ordinary differential equations is highly recommended for science and engineering majors, and elementary textbooks are commonly available.

Orthogonal functions are two functions (usually from a basis set) whose integral over all of the appropriate space is zero as long as the functions are different. An example is shown in (5.18), which includes a weighting function and the use of complex conjugation, neither of which is essential for orthonormal functions. Ordinarily, each of the functions in a basis set is orthogonal to all of the others.

Orthonormal functions are functions that are orthogonal (see above) and obey the constraint that the integral over all of the appropriate space of the product of the same two functions is one.

Partial derivatives occur when there are two or more independent variables and one takes the derivative with respect to one of them while keeping the other variable constant. When it is not immediately obvious which variable are being held constant, it is customary to write them explicitly. Thus the partial derivative of S with respect to X while Y is held constant is written as

$$\left(\frac{\partial S}{\partial x}\right)_{y}$$
. (A.10)

Partial derivatives are commonly encountered in courses about thermodynamics.

Partial differential equation is a differential equation in which there are two or more independent variables. Fick's second law, (1.16) is, for example, a partial differential equation of first order in time (since it involves a first derivative with respect to this independent variable) and second order in position (since it involves second derivatives with respect to \mathbf{r}). Ordinarily, courses in partial differential equations are given for science and engineering graduate students, so no knowledge of how to solve such equations is assumed in this book.

Poisson bracket is defined so as to simplify the equations of classical mechanics. Suppose some property, F, of a system depends explicitly on time, t. The total change of F with time following a path in phase space is

$$\frac{dF}{dt} = \frac{\partial F}{\partial t} + [F, H],\tag{A.11}$$

where H is the known Hamiltonian function (see above) of the generalized coordinates, q_i , and conjugate momenta, p_i , of the various degrees of freedom of the system, and where the Poisson bracket is

$$[F, H] = \sum_{i} \left(\frac{\partial F}{\partial q_{i}} \frac{\partial H}{\partial p_{i}} - \frac{\partial F}{\partial p_{i}} \frac{\partial H}{\partial q_{i}} \right). \tag{A.12}$$

The Poisson bracket in classical mechanics becomes a commutator in quantum mechanics.

Power series in a variable x is an infinite sum of the form

$$\sum_{i=0} c_i x^i, \tag{A.13}$$

where the c_i are constants.

Quadrature procedure is a numerical method for approximating an integral, the area under a curve in one dimension. The speed with which a particular quadrature procedure converges to an accurate value for the integral depends on the choice of the number of terms (N), the quadrature points (x_i) and the weights (c_i) such that

$$I = \int f(x)dx \approx \sum_{i=0}^{N} c_i x_i. \tag{A.14}$$

Different quadrature procedures are given different names. For example, the Curtis–Clenshaw method that is used in computer program PC is equivalent to an expansion of f(x) in terms of Chebyshev polynomials, so the quadrature points for a given value of N are the roots of a Chebyshev polynomial of order N and these roots are used to construct the corresponding weights.

Radius of convergence (R) is a term applied to a power series such as given in (A.11). For any power series, one of the following is true: (1) the series converges only for x = 0; (2) the series converges absolutely for all x; this means that $\sum_{i=0}^{\infty} c_i |x|^i$ is a finite number; or (3) the series converges absolutely for all x in the finite open interval (-R, R) and diverges if x < -R or x > R. Note that careful attention must be paid in case (3) to the points where |x| = R, since the series may converge absolutely, converge conditionally, or diverge.

Scalar is a quantity (number plus unit, if necessary) that has no dependence upon direction. It may be thought of as a tensor of rank 0.

Scalar product is a scalar that can be obtained from two vectors or two four-vectors by adding together the products obtained by multiplying the components along each direction. For vectors $\mathbf{A} = \widehat{x}A_x + \widehat{y}A_y + \widehat{z}A_z$ and $\mathbf{B} = \widehat{x}B_x + \widehat{y}B_y + \widehat{z}B_z$, the scalar product is

$$\mathbf{A} \cdot \mathbf{B} = A_x B_x + A_y B_y + A_z B_z. \tag{A.15}$$

For four-vectors $\mathbf{A} = \widehat{x}A_x + \widehat{y}A_y + \widehat{z}A_z + ictA_t$ and $\mathbf{B} = \widehat{x}B_x + \widehat{y}B_y + \widehat{z}B_z + ictB_t$, the scalar product is

$$\mathbf{A} \cdot \mathbf{B} = A_x B_x + A_y B_y + A_z B_z - c^2 t^2 A_t B_t. \tag{A.16}$$

Singularity in mathematics is a point at which a given mathematical object is not defined, or a point where it fails to be well-behaved in some particular way, such as integrability. An example of the first type is dividing by zero. An example of the

second type is where the endpoint of an integral is singular but the function may be approaching that endpoint in such a way that the integral converges; this is usually called an integrable singularity.

Spherical harmonics are the angular portion of the solution to the TISE for H atom in spherical coordinates. Care must be taken in identifying the notational convention being used, as mathematicians and physicists swap symbols the polar and azimuthal angles, and different researchers use different sign conventions for the Legendre polynomials that are implicitly part of the spherical harmonics. In this book we use the conventions of Hirschfelder et al. (1964).

Spline fit of a function, known at a series of points called knots, is its piecewise representation by polynomials between the knots. A cubic spline fit involves the use of polynomials of degree 3, with the values of the spline matching the values of the function at the knots and the values of the first and second derivatives at the polynomials forced to agree when the knots are approached from any direction. Spline interpolation is preferred to polynomial interpolation because it yields similar results but avoids wild oscillations between the knots.

Taylor series expansion in one dimension relates a function f(x) in a region near a particular value x=a as

$$f(x) = f(a) + \frac{1}{1!} \left[\frac{d}{dx} f(x) \right]_{x=a} + \frac{1}{2!} \left[\frac{d^2}{dx^2} f(x) \right]_{x=a} + \dots$$
 (A.17)

This definition can be extended to functions involving vectors or tensors of varying ranks.

Tensor of rank 0 is a scalar that is given this special name in order to emphasize its connection with tensors of higher rank.

Tensor of rank 1 is a vector (or four-vector) that is given this special name in order to emphasize its connection with tensors of higher rank.

Tensor of rank 2 is a quantity that in three-dimensional space has nine components, three along each of the two vectors from which it is constructed. Thus in three dimensions the dyadic (see above) formed from two vectors, $\mathbf{C} = \mathbf{AB}$, is a tensor of rank two whose components are

$$\mathbf{C} = A_x B_x \widehat{x} \widehat{x} + A_x B_y \widehat{x} \widehat{y} + \dots + A_z B_z \widehat{z} \widehat{z}. \tag{A.18}$$

Such a tensor is usually written as a matrix,

$$\mathbf{C} = \begin{bmatrix} A_x B_x & A_x B_y & A_x B_z \\ A_y B_x & A_y B_y & A_y B_z \\ A_z B_x & A_z B_y & A_z B_z \end{bmatrix}$$
(A.19)

These aspects of a tensor of rank 2 can be easily extended to four vectors, for which a tensor of rank 2 has 16 components.

Tensor of rank 3 is a quantity that in three-dimensional space has 27 components, three along each of the three vectors from which it is constructed. It is a straightforward generalization of the definition of a tensor of rank 2. This definition can be easily extended to four vectors, for which a tensor of rank 3 has 64 components.

Unit vector is a quantity of magnitude one that lies along a particular direction, usually the directions corresponding to the Cartesian axes in three-dimensional space. Unit vectors are indicated by \hat{x} is along the x direction, etc.

Unsöld's theorem states that a filled or half-filled subshell of atomic orbitals is spherically symmetric. For example, the nitrogen atom in its ground state has the configuration 1s² 2s² 2p³, and Hund's rule indicates that the three 2p electrons occupy different suborbitals; hence atomic nitrogen is spherically symmetric, within the limits of the TISE. The mathematical proof of Unsöld's theorem follows from the properties of the spherical harmonics.

Vector is a quantity in three-dimensional space that has three components, the first along the x direction, the second along y, the third along z.

Vector calculus is usually the third course in the undergraduate calculus sequence. It applies calculus operations such as differentiation and integration to quantities that either are vectors or are functions of vectors.

Appendix B: Notation for Ion States

A note about notation is in order, since it is sometimes possible to observe atomic ions in different electronic states. As an example, consider $^{16}O^+$ ions. The first superscript indicates that they have a mass number of 16, corresponding to the 8 protons that are in every oxygen nucleus plus 8 neutrons in this isotope; both types of nuclear particle have a mass close to one Dalton (Da, or g/mole). The chemical symbol is of course O for oxygen. The charge on the ion is indicated by the second superscript, i.e. +1, since the number is customarily omitted when it is 1; thus the ions have 7 electrons.

In the ground state, the electron configuration $1s^22s^22p^3$, where the sum of the superscripts is 7 because there are 7 electrons. Since the 2p orbitals can hold six electrons but there are only 3, the number of microstates is 6!/3!/(6-3)! = 20. Drawing the 20 orbital diagrams and sorting them by the value of the magnetic (mtype) quantum numbers (M_L and M_S for the components of the orbital and spin angular momenta, respectively) gives the following table:

An atomic D state has an orbital angular momentum quantum number $\widehat{L}=2$. It involves the 10 microstates in the two central columns of this table, each of which has a spin angular momentum quantum number of $\widehat{S}=1/2$ and a multiplicity $(2\widehat{S}+1)$ of 2. Removing this ${}^2\mathrm{D}$ electronic state thus gives

An atomic P state has $\widehat{L} = 1$. It involves the six microstates in the two central columns of the second table, each of which has $\widehat{S} = 1/2$ and a multiplicity of 2. Removing this 2P electronic state thus gives

The final table indicates an atomic S state with $\widehat{L} = 0$. It involves four microstates, each of which has $\widehat{S} = 3/2$ and a multiplicity of 4. Thus, we have accounted for all 20 microstates when we identify the electronic states as 2D , 2P and 4S .

Some researchers prefer to use non-relativistic term symbols, such as those just given. Real ions, however, experience relativistic effects, so full term symbols will always be used in this book for atomic ions. Since oxygen lies high on the Periodic Table, its electrons experience Russell-Saunders coupling. Therefore, each ion has a total angular momentum quantum number, J, that ranges from $|\underline{L} - S|$ to $\underline{L} + S$ and is indicated by a subscript. Taking Hund's rules into account leads to relativistic term symbols for $^{16}\mathrm{O}^+$ as $^2\mathrm{D}_{5/2}$, $^2\mathrm{D}_{3/2}$, $^2\mathrm{P}_{3/2}$, $^2\mathrm{P}_{1/2}$ and $^4\mathrm{S}_{3/2}$.

There is one question remaining. What is the order of energy for these five states of the oxygen cation? This question can by answered accurately only by looking at the energies calculated by solving the quantum-mechanical equations discussed in Chap. 6. However it can often be answered by Hund's rules:

- 1. For a given electron configuration, the term with the maximum multiplicity has the lowest energy. This means that for $^{16}\mathrm{O}^+$ the lowest energy state is the $^4\mathrm{S}_{3/2}$ state.
- 2. For a given multiplicity, the term with largest value of \widehat{L} has the lowest energy. This indicates that the 2D states will be lower in energy than the 2P states.
- 3. For states that differ only by their J values, there are two possibilities. If the outermost subshell is half-filled or less, then the lower the value of J, the lower the energy. If it is more than half-filled, then the higher the value of J, the lower the energy.

The 2p subshell in $^{16}O^+$ is half-filled, so in order of increasing energy its states are: $^4S_{3/2} \le ^2D_{3/2} \le ^2D_{5/2} \le ^2P_{1/2} \le ^2P_{1/2}$. If these ions are created with a large amount of energy, the five terms will be populated in the statistical ratio of 4:6:4:4:2

that come from the values of $2\hat{S} + 1$; the sum of these numbers corresponds to the 20 microstates when $^{16}O^+$ has the electron configuration $1s^22s^22p^3$. Of course, there are even higher energy levels that arise from excited electron configurations, but these are not available for studies with the experimental techniques described in this book.

Appendix C: Method of Weighted Residuals

To illustrate the method of weighted residuals for solving the TISE or any other linear equation, while keeping details to a minimum, suppose we are concerned with a one-dimensional equation of the form

$$Lf(x) = q(x). (C.1)$$

Here the function g(x) and the linear operator L are known for all values of x within some interval I. The problem is to solve this equation for f(x).

To use the method of weighted residuals, we first choose some trial functions, $T_i(x)$, defined for all i such that $0 \le i \le N - 1$. These trial functions are assumed to be sufficiently differentiable and well-behaved for all x contained in I. Then we assume that f(x) is well approximated by

$$f(x) = \sum_{i=0}^{N-1} f_i T_i(x).$$
 (C.2)

The problem thus has become one of determining the expansion coefficients, f_i , such that

$$\sum_{i=0}^{N-1} f_i L T_i(x) = g(x). \tag{C.3}$$

There is one constraint upon the choice of trial functions: they must be linearly independent, which means that no function in the collection can be represented as a linear combination of the others. This means, for example, that we can use $\sin^i(x)$ or $\sin(ix)$ as $T_i(x)$, but we cannot use $i\sin(x)$. As an aside, some guidance as to what trial functions can be used is usually obtained from a careful examination of the problem, as we shall illustrate in the next subsection.

The second step in the method of weighted residuals is to choose some weight functions, $A_i(x)$ for $0 \le j \le N - 1$, and require that each of the weighted residuals

$$R_{j} = \int A_{j}(x) \left[\sum_{i=0}^{N-1} f_{i} L T_{i}(x) - g(x) \right] dx$$
 (C.4)

be zero. The problem thus has become one of determining the expansion coefficients such that

$$\sum_{i=0}^{N-1} L_{j,i} f_i = g_j \quad 0 \le j \le N - 1, \tag{C.5}$$

where

$$L_{j,i} = \int A_j(x)LT_i(x)dx \tag{C.6}$$

and

$$g_j = \int A_j(x)g(x)dx. \tag{C.7}$$

There is again a subtle restriction: the weight functions must be linearly independent. Since the operator L is known, the function g(x) is known, and all of the functions $A_j(x)$ and $T_i(x)$ are known, the numbers $L_{j,i}$ and g_j can be calculated. Difficulties may arise in performing the necessary integrations, but with sufficient effort (and generally with the use of computer programs to evaluate them numerically) they CAN be calculated. This means that the N linear equations in N unknowns (the f_i) are algebraic equations, and we know that such equations CAN be solved, at least by using a computer. In practice, once a solution has been obtained with some chosen value for N, then the process is repeated using successively larger values of N until the particular answers of interest are constant within the number of significant figures of interest.

The generality of the method of weighted residuals is often not appreciated, and much effort has been spent in rediscovering the method in specific cases. For example, when the weight functions are powers of x, the method is known as a moment method (related to, but not to be confused with, what is called a moment method in this book). When the $A_j(x)$ and $T_i(x)$ are identical or are related by a simple constant, they are called basis functions and the method is known as the Galerkin method (Hildebrand 1956; Prenter 1975), after Boris Grigoryevich Galerkin (1871–1945) who used the method in a 1915 paper but referred to it as having been discovered by Walther Ritz (1878–1909). When L is a differential operator that is self-adjoint, the Galerkin method is equivalent to a somewhat simpler method called the Rayleigh–Ritz method, in acknowledgment of the contributions of John William Strutt, Lord Rayleigh (1842–1919). The method of weighted residuals is called a collocation or pseudo-spectral method when the trial and weighting functions are Dirac delta functions; there is a whole branch of mathematics devoted to the study of such generalized functions, but this book will not make use of them.







Galerkin

Ritz

Strutt

One more term is worth knowing. When the trial and weighting functions in a method of weighted residuals are the same, or differ only by trivial constants, then both sets of functions are referred to as basis functions.

References

- I.S. Gradshteyn, I.M. Ryzhik, Table of Integrals, Series, and Products (Academic Press, New York, 1980)
- J.O. Hirschfelder, C.F. Curtiss, R.B. Bird, Molecular Theory of Gases and Liquids (Wiley, New York, 1964). Corrected with Notes
- W. Kaplan, Advanced Calculus (Addison-Wesley, Reading, 1959)
- R.E. March, Ion traps, in *The Encyclopedia of Mass Spectrometry. Vol. 1. Theory and Ion Chemistry*, ed. by P.B. Armentrout (Elsevier, Amsterdam, 2003), pp. 144–158

A	Atmosphere
107 Ag ⁺ (1 S ₀), 20, 39, 57	chemistry, 2
$^{40}\text{Ar}^{+}(^{2}\text{P}_{3/2}), 204$	passive additive dispersion, 2
ab initio methods, 155, 156, 200	Atomic number, 31
Acceleration, 118, 125, 128, 233	Atomic units, 160, 161, 176
Activated complexes, 187	Aufbau principle, 171
Aerojet Rocketdyne, 4	Avogadro constant, 11
Aeronomy, 2	
Air, 74	
Aliasing method, 68	В
Al-Jazari	$^{11}B^{+}(^{1}S_{0}), 71$
abu al-'iz ibn isma'il ibn, 3	
Allis	¹³⁸ Ba ⁺ (² S _{1/2}), 72, 89, 211, 213, 214, 264 Ba ⁺ (² S _{1/2}), 201–203, 207
William Phelps, 34	138 Ba ²⁺ (1 S ₀), 72
Alpha function, 83	Bailey
Alpha particle, 31	Victor Albert, 26
Ambipolar diffusion, 37, 51	Barometer, 3
Anderson	Basis functions, 42, 127, 128, 132, 141, 166,
Carl David, 195	196
Angular correlation, 165	correlation-consistent (cc), 178
Angular momentum	Gram–Charlier, 207
quantum numbers, 165	multi-temperature, 139, 141, 147
Arrhenius	one-temperature, 133
Svante August, 15	two-temperature, 134, 136, 150
Arrival time distribution, 52, 59, 61, 62, 70	for molecules, 241
diffusion coefficient, 70	Basis set, 165, 169, 175, 178
full width at half maximum, 62	6-331+G(2df), 243
kurtosis, 62	aug-cc-pCVXZ-PP, 201
peak broadening, 69	aug-cc, 179
peak time, 61	aug-cc-pV5Z, 201
signal-to-noise ratio, 62	aug-cc-pwCV5Z, 201
skewness, 62, 65	aug-cc-pwCVXZ, 199, 201, 211
standard deviations if Gaussian, 62	aug-cc-pwCVXZ-PP, 199
Aston	augmented with bond functions, 246
Francis William, 30	balanced, 165
© Springer Nature Switzerland AG 2018	285

© Springer Nature Switzerland AG 2018 L. A. Viehland, *Gaseous Ion Mobility, Diffusion, and Reaction*, Springer Series on Atomic, Optical, and Plasma Physics 105, https://doi.org/10.1007/978-3-030-04494-7

cc-pVXZ, 178	124, 127, 128, 130–132, 134, 220,
contracted, 166, 169	233, 236, 240, 245, 263, 269, 270
core valence, 179	approximate derivation, 117
d-aug-cc-pVXZ, 206	formal form, 118
double-zeta, 164	generalization to molecules, 233
even-tempered, 165	quantum-mechanical, 46
expanded cc-pVTZ-PP, 246	solution methods
minimal, 163	biMaxwellian, 44, 128
mixed, 180	convergence problems, 44
plus double polarization, 164	Galerkin, 44
plus polarization, 164	Gram-Charlier, 44, 128
split valence, 164	Maxwellian, 124
terminology in computational chemistry,	multi-temperature, 139, 142
165	one-temperature, 42
terminology in quantum mechanics, 165	three-temperature, 44, 45, 128
triple zeta, 164	two-temperature, 42, 43, 45, 113,
•	135, 136
weighted-core valence, 179	unified solution technique, 207
well-tempered, 166	Wannier theory, 45
Basis set contraction, 169	streaming terms, 121, 122
Basis set superposition error (BSSE), 180,	Bond length, 73, 183
199, 201, 246	Bond stretching, 183
Battery, 8	Born
Beam techniques, 219	Max, 157, 161
Beenakker	Born-Oppenheimer approximation, 161,
Joannes Josephus Maria, 234	172, 178, 185, 186, 193, 206
Berti	Boundary conditions, 23, 34, 119, 131
Gasparo, 3	Breit–Pauli operator, 199
Bethe	Brown
Hans Albrecht, 195, 199	Sanborn Conner, 34
Beyond Monchick-Mason approximation,	Buffer gas, 43
see BMM	Burnett functions, 133, 134, 271
Bias voltage, 55, 59	
Biradicals, 183, 184	
Bird	C
Robert Byron, 117, 199	$^{35}\text{Cl}^{-}(^{1}\text{S}_{0}), 83$
Blackett	Canal rays, 12, 13, 30
Patrick Maynard Stuart, 195	Cannizzaro
Blanc	Stanislao, 10
A., 20	Carlisle
Blanc's law, 20, 30, 66, 68, 83, 146, 152	Anthony, 9
diffusion coefficients, 24	Cartesian coordinates, 272
extended to high E/n_0 , 67	CAS+MRCI method, 206, 265
BMM, 246, 249, 251, 270	Cathode rays, 11, 13, 14
Bohr	Cation
Niels Henrik David, 26	doubly charged, 73
Bohr (unit), 160	singly charged, 73
Bohr's theory of the atom, 161	Cavendish
Boltzmann	Henry, 7
Ludwig Edward, 117	CCSD(T) theory, 201
Boltzmann constant, 24, 129	CC with Singles, Doubles and non-iterative
Boltzmann equation, 29, 42, 44, 67, 76, 86,	Triples, CCSD(T), 246
88, 95, 96, 100, 103–105, 113, 117,	Central-field approximation, 167

Centrifugal-sudden approximation, 246	inelastic, 47, 114
Chang	irreducible
Cheng-shu Wang, 234	three- and multi-temperature, 140
Channeltron, 53	molecular, 85
Chapman	momentum-transfer, 24, 28, 33, 43, 76,
Sydney, 27, 28, 41	78, 103, 113
Charge	for molecular systems, 47, 103, 261,
conservation, 43	265
density, 189	normalization, 29
fundamental, 76	Collision operator, 233
point, 189	adjoint, 130
Charge number, 76	eigenfunctions, 134
Charge states, 208	instantaneous, 135
effects on mobility, 73, 74	Kramers–Moyal expansion, 44, 45
Charge-to-mass ratio, 15, 31, 53	linear, 120, 135
Charge transfer, 42	local, 135
resonant, 33, 35, 76	matrix elements
Charlier	Gram-Charlier, 143
Carl Vilhelm Ludwig, 141	multi-temperature, 140
Chemical bonds	three-temperature, 138
theory, 31	nonreactive
CI with Singles and Doubles, CISD, 182,	for atoms, 124, 129
184, 185	for molecules, 234, 239
CI with Singles, Double, Triples and	reactive, 121, 129
Quadruples, CISDTQ, 182	for molecules, 235, 239
CI with Singles, Doubles and non-iterative	self-adjoint, 130
Triples, CISD(T), 182	scalar, 120, 135, 144
CI with Singles, Doubles and Triples,	Collisions
CISDT, 182	archetype, 106, 108
Classical mechanics, 158, 167, 186, 246, 265	cooling, 110
Classical trajectory, 266	classification of, 105
Classical trajectory calculations, 242, 243,	cooling, 106, 110
245, 261	elastic, 99
Cold fusion, muon-catalyzed, 2	electron-neutral, 25
Collisional invariant, 122, 125, 131	heating, 106, 110
Collision cross section (CCD), see Colli-	in two dimensions, 236
sion integral, momentum-transfer, for	inelastic, 25, 46, 113, 114, 245
molecular systems	instantaneous, 104, 120
Collision energy, 35, 57, 58, 73, 200, 265	inverse, 130, 236–238
total, 100	ion-neutral, 16, 86, 87, 96, 234
Collision frequency, 97	ion-wall, 119, 219
effective, 88, 89	local, 105, 120
electron-neutral, 152	molecular ion-neutral, 245
microscopic momentum-transfer, 203,	reverse (reciprocal), 237
246, 248, 249	superelastic, 46
momentum-transfer, 37, 263, 265	three-body, 1, 118, 260
effective, 125	time-reversed, 236
Maxwell model, 147	two-body, 118, 260
multi-temperature, 148	Commutator, 233, 272
one-temperature, 146	Complete active space self-consistent field
two-temperature, 145	(CASSCF) method, 184
total or integral, 263, 265	Complete basis set (CBS) limit, 178, 179,
Collision integral, 205, 257	199, 201, 206, 211, 213

Complete basis set (CBS) method, 214	Coulomb's law, 7, 159
Complete set, 133, 241, 272	Counterpoise correction, 180, 199, 201
Complex conjugate, 272	Coupled-cluster (CC) method, 180, 198
Compressibility factor, 19, 55	Covalent terms in the wave function, 182
Computational chemistry, 164–166, 187,	Cowling
198	Thomas George, 41
computer programs, 163, 166, 175, 199,	Crookes
200, 202	William, 11
Computational chemistry calculations	Cross section
high accuracy in subtracting large num-	classical-mechanical expressions, 28
bers, 185	differential scattering, 33, 99, 102, 109
Computer program	113, 124, 234, 265
GC, 207, 211, 213, 216, 223, 227, 230,	energy-averaged (see collision integral)
248, 251, 257, 259	28
convergence problems, 229	for RCT, 206, 207
HPCCS, 266	integral for reaction, 130
IMoS, 266	molecular
ITSIM, 88	close-coupling calculations, 246
MOBCAL, 265, 266	rotationally-inelastic, 246
MOBDIF, 242, 243	semi-classical calculations, 246
OMEGAS, 257	momentum-transfer, 25, 26, 28, 97, 99
PC, 200, 201, 204, 207, 211, 213, 216,	100, 103, 203, 204, 206, 207, 265
223, 227, 251, 257, 259, 277	normalization, 29
QEx, 207	quantum-mechanical, 33
TRAJECK, 244, 245	reactive, 226, 227, 229
	reactive for molecular systems, 48, 239
vary, 209 Conductors, 6	semiclassical, 33
Configuration interaction (CI), 177, 180–	total, 265
182, 184, 185, 243	transport, 66, 148, 200, 206, 207, 223
	245
full, 183, 184	by classical calculations, 200, 204
matrix elements, 181	by MC calculations, 264
spin-adapted, 181	by quantum calculations, 200, 204
Conservation principles, 95	for molecular systems, 242–245
angular momentum, 236	viscosity, 206, 207
charge, 6	Current density vector, 189
energy, 96–98, 107, 120, 122, 235, 236	Curtiss
mass, 96, 118, 125, 131	Charles C., 117, 199
momentum, 96–98, 104, 107, 120, 235	Curtiss equation, 238–242, 244, 245, 270
Continuity	Curvature
equation of, 22, 118	of a PES, 188
rate equation of, 125	Cyclotron frequency, 86
Cook	Cyclotron line width, 86
William Richard Joseph, 28, 30	Cyclotron line width, 80
Core orbitals, 179	
Correction factor	
momentum-transfer, 112–114	D
Correlation coefficient, 97, 213, 216, 221	Davy
Correlation energy, 156, 176, 177, 179, 182	Humphry, 9
Correspondence principle, 158, 191	Definite proportions
Coulomb	law of, 10
Charles Augustin, 7	Degeneracy, 161, 168
electric gauge, 190	Dempster
magnetic gauge, 190	Arthur Jeffrey, 30

Density functional theory, 156, 262	DMS, 83
Density gradient expansion, 240	compensating voltage, 82
avoiding, 152	concentric-cylinder geometry, 82
Determinant, 272	definition, 82
Deuterium, 32	dispersion voltage, 82
Deviation parameters, 221, 224, 230	duty cycle, 82
Diatomics-in-molecules calculation, 265	higher order, 83, 84
Differential equation	history, 81
ordinary, 276	parallel plate geometry, 82
second order, 175	sensitivity, 82
partial, 175, 276	Doppler shift, 211
Differential IMS (see DMS), 82	Drift time, 59, 60
Differential mobility, 45	Drift tube, 17, 38, 51, 53, 55, 56, 69, 75, 84,
Diffusion, 15, 21, 44, 46, 70, 137	150, 211, 219, 220, 222, 234
ambipolar, 37, 51	cyclic, 86
anisotropic, 39	definition, 54
atmospheric, 2	electrodes, 85
cooling, 37	field-reversal experiments, 81
equation, 38, 39, 63, 65	injected-ion (see DTMS), 70
gaseous ion diffusion, 137	length, 55, 59, 81
tensor, 24, 38, 39	multi-wire, 2
tensor in magnetic fields, 40	picture of, 38
Hall component, 41	ping-pong experiments, 81, 86
longitudinal component, 41	selected ion, 54
transverse component, 41	selected-ion flow, 54
Diffusion coefficient, 21, 23, 38, 42, 114, 240	thermalization region, 55
neutral molecules, 24	Drift-tube mass spectrometer (DTMS), 4,
parallel to the field, 24, 34, 39, 62, 65,	52, 57, 60, 68, 72, 83, 141, 205, 206,
210	234, 270
perpendicular to the field, 24, 34, 39, 210	calibration, 59
Diffusion equation, see Fick's second law	definition, 38, 54, 70
Dilute gas, 1, 2, 43, 51, 55, 66	effects of gas temperature, 57
definition, 30, 118	Pittsburgh, 52, 56
Dimethyl methylphosphonate	reversible field (ping-pong), 54
proton-bound dimer, 79, 80	selected ion, 54
Dipole moment	variable temperature, 54
calculated by the RHF method, 183	Drift velocity, 16, 24, 26, 56
Dirac	electron, 37
delta function, 282	ion, 22, 39, 211
Paul Adrien Maurice, 157, 191, 192, 194,	laboratory frame, 122
195	reference frame of ion swarm, 122
Dirac equation, 178, 192, 193, 195, 196	Drift voltage, see Electromotive force (emf)
time-independent, 193	Druyvesteyn
Dirac-Fock equations, 196, 197	Mari Johan, 36
Dirac-Fock orbitals, 201	Du Fay
Discriminator, 53, 54	Charles Francis de Cisternay, 6
Dissimilar metals in contact, 8	Dunning
Dissociation limit, 183	Thom H., Jr., 178
Distance of closest approach, 245	Dyadic (dyad), 273
Distribution function	J (-J), - · ·
energy, 100	
ion, 118, 128	E
neutral, 119	151 Eu ⁺ (9 S ₄), 210
noutui, 11/	Lu (54), 210

ECP, 167, 197, 199, 201	Electron exchange
Effective core potential, see ECP	antisymmetric functions, 172
EHSS, 262, 266	symmetric functions, 172
Eigenfunction, 161, 168, 273	Electrophoresis
normalization, 162	gaseous, 70
of spin operators, 170	Electrospray ionization, 74, 83
Eigenvalue, 161, 168, 273	Emission spectrum
Eigenvector, 273	of hydrogen
Electric	Balmer series, 169
generator, 189	End effects, 16, 53, 56, 63, 80
Electrical	Energy
breakdown, 25, 69, 234	center-of-mass, 97, 98
charge, 1, 2, 5–9, 11, 12	field, 35, 36
conductivity, 15	internal, 99
discharge, 1, 4, 6, 13, 24	kinetic, 243
field, 55, 86	kinetic for molecular ions, 244
resistance, 16, 21	laboratory frame, 123
spark, 11	molecular, 187
Electrical force, 20	random ion motion, 35
Electric constant, 7	reference frame of ion swarm, 123
Electric gauge, 190	relative kinetic, 99
Coulomb, 190	rotational, 243, 261
Electricity	rotational for molecular ions, 244
animal. 8	thermal, 34, 36, 114, 127, 203
current, 7, 34	Energy dyadic, 123
one-fluid theory, 6	Energy exchange, 263
static, 5, 7, 219, 227	between translation and internal states,
two-fluid theory, 6	101
Electrochemistry, 10	Energy minimization on a PES, 188
Electrodes, 34	Energy partitioning, 66
Electromotive force (emf), 8, 55, 59, 69, 75	Energy shift
Electron, 2, 11, 14, 31, 33, 170	to give agreement with ion-induced
charge, 16	dipole potential, 202
core, 166, 167, 201	Energy-sudden approximation, 246
correlation, 178, 179, 183	Energy transfer
density, 156, 177	from an external field to an ion, 240
detachment, 42	Enskog
diffusion coefficients, 24, 39	David, 27, 28
discovery, 16	Equation of continuity, 152
drift velocity, 24, 26	Ergodic hypothesis, 1
mobility, 25	Exact hard-spheres scattering, see EHSS
runaway, 25	Exchange-correlation energy, 156
scattering, 36	Excited states, 177, 208
spin, 169, 171	determinants for, 178
in molecules, 172	Experimental restrictions, 51
spin function, 173	Experimental techniques, 51
spin space, 170	Explosives, 80
swarm, 24, 36	Eyring
transport in gases, 24	Henry B., 186
valence, 164, 167, 201	3
velocity distribution function, 36	
Electron correlation, 184, 198, 201	F
Electron density, 262	$^{19}F^{-}(^{1}S_{0}), 71$
Electron density, 202	1 (50), /1

Factorial symbol, 273	Franck–Hertz experiment, 2
False negative, 74	Franklin
False positive, 74	Benjamin, 6
minimizing, 74	Free diffusion, 2
Faraday	Free particle, 158
Michael, 9, 11	Free time between collisions, 263
Faraday constant, 11	Frozen core approximation, 167, 179
Faraday's law of induction, 189	Frozen virtuals approximation, 180
Faraday's laws of electrochemistry, 10	Functional (definition), 156
Feynman	Function of two variables, 56
Richard Phillips, 196	
Fick	
Adolf Eugen, 21, 38	G
Fick's first law, 21, 22, 38, 65	$^{156}\text{Gd}^+(^{10}\text{D}_{5/2}), 210$
Fick's second law, 22, 38, 40, 65	Gaede
Field	Wolfgang Max Paul, 4
ac, 34, 81, 86	Galerkin
dc, 55, 56, 69, 81, 82	Boris Grigoryevich, 282
electrostatic, 16, 30, 39, 54, 87, 127, 240,	method, 44, 282
263, 264	Galilei
uniform, 22, 53, 69, 141	Galileo, 3
external, 1, 128	Galvani
magnetic, 15, 30, 54, 87, 141	Luigi, 7–9
sources, 189	Galvanic cell, 8
time-dependent, 87	Gamma function, 37, 135, 273
asymmetric, 81–83	Gamma rays, 31
Field-asymmetric ion mobility spectrometry	Gas
(see DMS), 81	dilute, 219
Field theory, classical, 191	mixture, 66
Filled orbitals	transport coefficients, 66
spherical symmetry of, 174	number density, 1, 219
Fine-structure constant, 199	rarefied, 6
Flowing afterglow apparatus, 219	reactive neutral, 219
Fock	Gas constant, molar, 24
Vladimir Alexandrovich, 174	Gaseous electronics, 2
Force	Gas manifold, 52
at a distance, 7	Gas mixture, 20
drag, 86	Gate, 53, 55, 56, 59, 61, 62, 69
electrical, 7, 8, 86, 96	Gaussian (normal) distribution, 44, 61–64,
external, 118	128, 141
Force fields	Gaussian orbitals, 163–165, 173, 174, 178,
molecular-mechanics, 264	181, 196
Fourier transforms, 152	contracted, 166
Four vector, 192, 273	primitive, 166
for gradients, 192	Gauss' law, 273
for momentum, 192	Geissler
for position, 192	Heinrich, 4
Frame of reference	Generalized Einstein relations (GER), 45
Galilean transformations, 98	Generalized gradient approximation (GGA),
ion swarm, 123	156
laboratory, 122	Geometry optimization
Franck	on a PES, 187, 188
James, 2, 18	Gerlach

Walther, 170	laboratory frame, 123
Ghost orbitals, 163, 201	reference frame of ion swarm, 123
Gilbert	Heisenberg
William, 5	Werner, 157, 158
Global minimum, 184, 188	Helium ion
Glow-discharge sheaths, 263	diatomic, 33, 36
Goldstein	doubly charged, 31
Eugen, 13	singly charged, 31
Goudsmit	Hermite polynomials, 137, 152, 274
Samuel Abraham, 170	Hermitian operator, 169
Gradient, 273	definition, 168
in position, 118	Hershey
in time, 118	Allen Vincent, 30
in velocity, 118	Hertz
ion number density, 21, 22	Heinrich Rudolph, 2, 12
Graham	High accuracy
Thomas, 21	DTMS, 59
Gram	IMS, 79
Jorgen Pedersen, 141	IMS/MS, 79
Green's function technique, 152	Hilltops on a PES, 187
Ground state, 208	Hirschfelder
Guericke	Joseph Oakland, 117, 199
Otton von, 3	Hittorf
2 100-2 100-2, 0	Johann Wilhelm, 11
	Homologous series, 262
Н	Hot atom chemistry, 2
⁴ He(¹ S ⁰), 264	Hund
H ⁺ , 39	
$H_2^+, 31$	Frederick Hermann, 171
	Hund's rules, 171, 280
$H_3^+, 39$	Huxley
$^{4}\text{He}^{+}(^{2}\text{S}_{1/2}), 31, 33, 56, 61, 206, 207, 264$	Leonard George Holden, 19, 25, 40
⁴ He ₂ ⁺ , 33, 36	Hydradynamics 52
${}^{4}\text{He}^{2+}$, 31	Hydrodynamics, 52
$He_2^+(v=0), 265$	Hydrogen ion
Hall	diatomic, 31
Edwin Herbert, 41	monatomic (see proton), 31
Hamilton	
William Rowan, 159	
Hamiltonian function, 273, 276	I
Hamiltonian operator, 159–161, 175, 180,	Iconical interactions, 264
181, 197, 206, 274	Ideal gas equation, 19, 55
internal, 233	Imaginary numbers, 274
Harkins	Impact parameter, 28, 100, 106, 109, 119
William Draper, 32	120, 243, 261
Hartree	IMS, 57, 60, 68–70, 72, 74, 76, 79, 83, 96
Douglas Rayner, 174	141, 205, 206, 209, 210, 234, 270
Hartree (unit), 160	definition, 70, 82
Hartree-Fock (HF) method, 174, 176-179,	duty cycle, 84
182, 184, 196, 198	injected-ion (see DTMS), 70
restricted, 198	trapped ion, 85
Hassé	traveling wave, 84
Henry Ronald, 27, 28, 30	trend line, 77, 78
Heat flux, 132	IMS/MS, 75, 79, 270

Infinite-order sudden approximation, see IOS	molecular partition function, 48 number density, 2, 34, 51, 55, 219
Initial conditions, 23, 119	production, 24
Injection effects, 16, 53, 56, 63, 80	pulses, 54, 59, 61, 84, 85
Insulators, 6	runaway, 25
Interaction potential, 33, 42, 45, 73, 76, 161,	source, 53–55, 131
164	sources or sinks, 22, 23, 39, 119, 240
(12, 4) core model, 259	speed, 98
(12, 6, 4) model, 260	non-hydrodynamic contributions, 17
(n, 4) core model, 258, 259	swarm, 36
(n, 6, 4) core model, 259	thermometer, 85
(n, 6, 4) model, 257	transport in gases, 233
atomic ion-diatomic neutral, 249	transport through parent gas, 33
attractive terms, 78, 256, 258	trap, 2
convex-core model, 77	velocity, 16
curve, 206, 264	Ion cyclotron resonance (ICR), 86
for polyatomic systems, 73, 114	collision dominated, 87
g-u pairs, 206, 207	Fourier transform, 87
ion–neutral, 29, 36, 72, 75, 79, 81, 105,	Ion detector, 54
113, 120, 128, 199, 201, 212–214, 216,	Ion heating, 85
243	Ionic terms in the wave function, 182
ab initio, 202, 207, 208, 227	Ionization coefficient
relativistic effects, 197	Townsend's first, 25
ion-induced dipole, 27, 73, 78, 125, 201–	Townsend's second, 25
203, 249, 255, 262	Ion mobility, 55, 70
ion-quadrupole, 249	Ion mobility equation
Lennard-Jones (n, 4) model, 258	fundamental, 43, 95, 96, 112–114, 137,
Lennard-Jones (n, 6) model, 258	138, 146, 152
repulsive terms, 78, 256	correction factor, 43, 76, 80, 96
rigid spheres, 29, 78, 255, 257	fundamental low-field, 27, 30, 71, 80,
site-site, 260–262, 266	112, 113
surfaces for molecules, 75	correction factor, 76, 265
tabulated, 201	Ion mobility spectrometry, see IMS
three-body, 260, 265	Ion momentum
zero-crossing point, 260	change along the field, 96
Interaction potential energy	Ion pulse, 55
curve, 185, 200	Ion runaway
surface, 185–187	partial, 44, 137
Internal energy, 46, 97	Ion trap, 84, 139, 141
electronic, 113	linear, 89
rotation, 113	quadrupole, 87, 88, 147, 149
vibration, 113	IOS, 246, 265
Ion, 2, 14	Isoleucine, 83
biochemical, 75, 78, 83, 85, 210	Isotope, 30, 208, 223
biological, 75, 78, 83–85, 210	Isotropic scattering, 114
density gradient, 127	1 6
detector, 53, 55	
dissociation energy, 85	K
energy, 264	³⁹ K ⁺ (¹ S ₀), 67, 242, 264
ensemble, 122	Kaufmann
flux, 21, 22, 64, 122	Walter, 15
fragmentation, 85	Kinetic energy
molecular, 210	average, 203
*	<i>U</i> ,

average for trace ions, 127	Philipp von, 12
relative, 200	Leucine, 83
Kinetic momentum vector, 191	Lifshitz
Kinetic theory, 27–29, 70, 233, 255, 270	Evgeny Mikhailovich, 158
biMaxwellian, 137, 244	Light waves, 6
for molecules	Linear algebra, 275
with classical collision operators,	Linear combination of atomic orbitals
236, 238	(LCAO), 175
with quantum collision operators,	Loaded spheres, 79
234, 238	Local-density approximation (LDA), 156
with semi-classical collision opera-	Local minimum, 184, 188
tors, 236, 238	Loeb
Gram–Charlier, 114, 227, 244, 264	Leonard Benedict, 18, 27
Maxwell–Boltzmann, 23	Lorentz model, 256
multi-temperature, 139, 142	Loschmidt
quantum-classical correspondence, 124	Johann Joseph, 18
three-temperature, 114, 137, 264	Loschmidt's constant, 18
two-temperature, 101, 128	Low-field criterion, 35, 71, 73, 75, 81, 96
molecular theory, 241	LXCat database, 208–210, 212, 227
Kohn	
Walter, 156	
Kohn–Sham equation, 156	M
Kronig	Mack, Jr.
Ralph de Laer, 170	Edward, 24
Kurtosis, 98, 114, 213, 221	Magnetic gauge, 190 Coulomb, 190
	Magnetohydrodynamics, 1
L ¹⁷⁵ Lu ⁺ (¹ S ₀), 210	Many-body perturbation theory (MBPT), 180, 197
$^{7}\text{Li}^{+}(^{1}\text{S}_{0}), 65, 243, 249-251$	Many electron theory (MET), 198
Laguerre polynomials, 274	Markov process, 263
associated, 271	Mason
generalized, 133	Edward Allen, 30, 38, 42, 44, 46, 54
Lamb, Jr.	Mass
Willis Eugene, 195	eccentricity, 79
Lamb shift, 195, 196	gas, 2, 129
Landau	proton, 31
Lev Davidovich, 158	Mass fraction, 71, 97
Langevin	Mass ratio, 73
Paul, 18, 27, 28, 30	ion-neutral, 72
Lanthanide ions, 79, 209	Mass spectrograph, 30
Laplace operator (Laplacian), 274	Mass spectrometer, 2, 24, 30, 31, 38, 53–55,
Laser beam, 211	59, 70, 74, 219
saturation, 211	time-of-flight, 32, 74, 84
Laser-induced fluorescence, 211, 213	Mass-to-charge ratio, 31, 53
Lattey	Massey
Robert Tabor, 18	Harrie Stewart Wilson, 33
Least square determination	Mathieu equation, 88, 275
linear, 275	damped, 147
nonlinear, 275	Matrix, 275
Legendre polynomial, 28, 36, 243, 275	Matrix elements
associated, 271, 275	of the collision operator
Lenard	in the Curtiss equation, 241

of the Hamiltonian operator, 168, 202	tables, 17
Maxwell	temperature effects, 57
James Clerk, 29, 124, 189	tensor in magnetic fields, 40
Maxwell model, 124	Hall component, 41
of constant collision frequencies, 88,	longitudinal component, 41
125, 134, 136, 141, 147, 149, 255	transverse, 41
Maxwell's equation of change, 130	zero-field, 20, 209, 212, 258
Maxwell's equations, 191	Mohr
of electromagnetism, 189	Courtney Balthazar Oppenheim, 33
MC	Molecular dynamics, see MD
improved method, 264	Molecular dynamics simulation, 152
McDaniel	Molecular geometry, 175
Earl Wadsworth, 27, 38, 44, 46, 54	Molecular structure, 187
MD, 264	stable, 187
Mean free path, 119	transition, 187, 188
Mean-free-path theory, 29	Mole fraction of gas, 21, 66
Mean free time, 20	Moller–Plesset calculations, 197, 243, 244
Methane	Moment equations, 127, 130, 134, 136
valence orbitals, 176	Maxwell model
Microwave breakdown, 34	for ion velocity, 147
Millikan	multi-temperature
Robert Andrew, 16	for ion velocity, 148
Mixture, 69	of Maxwell, 130
gas, 24, 55	one-temperature, 134
MMA, 245, 246, 248, 250, 251, 265	for ion velocity, 146
Mobility, 16, 24, 26, 33, 42, 65, 84	two-temperature, 127, 135
ab initio calculations, 56, 60, 73, 81	for ion kinetic energy, 150
alkali ions, 32	for ion velocity, 145
calibrants, 80	Moment methods, 127, 128
dependence upon pressure, 18	disadvantage, 131
effects of emf, 58	equivalent to method of weighted resid-
effects of gas pressure, 58	uals, 133
effects of gas temperature	one-temperature, 127
correction for, 58	Moment of inertia, 239, 241
electron, 37	Moments
highly accurate, 59	of 2T basis functions, 136
imprecision, 61	of $f(\mathbf{r}, \mathbf{v}, t)$, 129
Langevin, 27	of the ion vdf, 98
low-field, 28	Momentum
maximum, 73, 203, 258	balance, 96
minimum, 258	gain, 56
of excited states, 211	linear, 99, 236
polarization, 27	change, 96, 102
quantum-mechanical, 33	loss, 56
relative values, 79	transfer, 86
SI unit, 16	Momentum-transfer coefficient, 111
standard, 18, 56, 71, 75, 76, 207, 211,	Momentum-transfer theory, 29, 45, 88, 95,
213	96, 261
correction to a common gas temper-	main weakness, 114
ature, 58	qualitative, 66, 95
dependence on T_0 and E/n_0 , 19, 20,	Monchick–Mason approximation, see
56	MMA
low-field, 56	Monte-Carlo methods, 42, 152, 226, 263

Monte-Carlo simulations, 220	reactive gas, 121
atomic systems, 42	
improved method	
with fictitious ion creation, 264	0
molecular systems, 42	¹⁶ O ⁺ (⁴ S _{3/2}), 223, 225, 226, 231, 263
null-collision method, 42, 263, 264	Ohm
extended, 263	George Simon, 16
of electrons in hydrogen, 263	Ohm's Law, 16
Moseley	Oppenheimer
Henry Gwyn-Jeffreys, 31	J. Robert, 161
Motor, electric, 189	Optical pumping, 211
Mott	Orbital energies
Neville Francis, 27	ordering, 171
Multichannel analyzer (MCA), 53-55, 59,	Orbitals, 174
61	atom-centered, 176
bin width, 61	ghost, 175, 176
Multiconfiguration self-consistent field	virtual, 177
(MCSCF) method, 184, 185	
configurations for, 184	Orbiting collisions, 200, 249
Multiplicity, 181	multiple, 200
Multi-reference configuration interaction	Orthogonal functions, 168, 276 definition, 168
(MRCI) method, 185	
state-selected, 185	Orthonormal functions, 241, 276
state selected, 100	Overlap matrix, 176
•	
N 14x+2p	P
$^{14}N^{+}(^{2}P_{3/2}), 39$	Partial derivative, 187, 276
N_2^{2+} , 39	second, 187
Negative differential conductivity, 67	Partition function, 100, 129
Nernst-Townsend-Einstein equation, see	Pascal
NTE equation	Blais, 3
Neutral	Pasteur
molecular partition function, 48	Louis, 9
polarizability, 28, 202	Path-integral methods, 152
Neutron, 32	Paul
transport, 2	Wolfgang, 87
Newton's laws of motion, 96, 120, 158, 167,	Pauli
191, 237, 238, 264	Wolfgang, 169, 170
collisional damping term, 88	Pauli exclusion principle, 171–173
Nicholson	Penning
William, 9	Frans Michel, 36
Non-hydrodynamic correction factors, 17	Periodic table, 167, 169, 208, 280
Non-vibrating molecules, 186	Perrin
Normalization, 174, 241	Jean-Baptiste, 14
Normalization constant, 133	Perturbation method, 197, 199
NTE equation, 23	Phase shift, 33, 204, 206
Nucleus	modulo π errors, 206
finite-size potential, 196	semiclassical, 206
point potential, 196	Phase space, 118, 121, 233
Number density	streaming motion, 120
gas, 1, 69, 97, 121, 129, 132	Photon, 6
gradient, 39, 52, 98, 105, 132	Physics
ion, 66, 69, 118, 129	atomic and molecular, 2

laser, 2 plasma, 67 Planck's constant, 158 Plasma, 1, 2, 34, 51, 70 processing, 2 weakly ionized, 2, 120, 127 Plasma chromatography (see IMS), 70 Plücker Julius, 11 Pohl Robert Wichard, 18 Poisson	for spatial moments, 152 Proton, 13, 31 Pseudopotentials, 197 Pulse generator, 53, 54 Pump diffusion, 4, 52, 53 mechanical, 4 mercury displacement, 4 suction, 2 turbomolecular, 4 vacuum, 3
Siméon Denis, 191 Poisson bracket, 233, 276 Poisson's equation, 191 Polanyi Michael, 186 Polarizability electric, 73 Polarization functions, 164 Polarization-limit model, 255 Positron, 195 Positron annihilation, 2 Potential energy at large separation, 202 electrical, 7, 159 minimum, 183	Q Quadrature procedure, 277 Quantum electrodynamics (QED), 191, 196 Quantum entanglement, 191 Quantum mechanics, 27, 33, 124, 157, 167, 172, 186, 191, 246, 255, 265, 277 Quantum number, 161, 172 angular momentum, 169, 204 azimuthal, 162, 194 magnetic, 162, 166, 169, 194 principle, 162, 169, 194 spin, 170, 194 total angular momentum, 194
Potential energy function, 45, 274	R
Potential energy operator, 274	Radial (in-out) correlation, 165
Potential energy surface (PES), 46, 183, 187, 188, 216, 242, 246, 248, 251, 258,	Radioactivity, 14
261, 263, 265	Radius of convergence, 20, 127, 128, 136,
cc-pVTZ-PP, 246	277
curvature, 183	Ramsauer
	Carl Wilhelm 26
molecular systems, 249	Carl Wilhelm, 26 Ramsauer–Townsend effect, 26
molecular systems, 249 MP4SDTQ/6-311++G(2df,p), 243, 244	Ramsauer-Townsend effect, 26
MP4SDTQ/6-311++G(2df,p), 243, 244 MP4SDTQ/6-311++G(3df,2p), 245	
MP4SDTQ/6-311++G(2df,p), 243, 244 MP4SDTQ/6-311++G(3df,2p), 245 MP4SDTQ/6-311++G(3df,3pd), 246	Ramsauer–Townsend effect, 26 Random walk, 105
MP4SDTQ/6-311++G(2df,p), 243, 244 MP4SDTQ/6-311++G(3df,2p), 245 MP4SDTQ/6-311++G(3df,3pd), 246 RCCSD(T)/aug-cc-pVQZ, 251	Ramsauer–Townsend effect, 26 Random walk, 105 Rare gas ions in their parent gases, 206
MP4SDTQ/6-311++G(2df,p), 243, 244 MP4SDTQ/6-311++G(3df,2p), 245 MP4SDTQ/6-311++G(3df,3pd), 246 RCCSD(T)/aug-cc-pVQZ, 251 Powell	Ramsauer–Townsend effect, 26 Random walk, 105 Rare gas ions in their parent gases, 206 Rate coefficient, 64, 70 ion–neutral, 63, 226, 227 ion–neutral reaction, 22, 43, 70
MP4SDTQ/6-311++G(2df,p), 243, 244 MP4SDTQ/6-311++G(3df,2p), 245 MP4SDTQ/6-311++G(3df,3pd), 246 RCCSD(T)/aug-cc-pVQZ, 251 Powell Cecil Frank, 32, 33	Ramsauer–Townsend effect, 26 Random walk, 105 Rare gas ions in their parent gases, 206 Rate coefficient, 64, 70 ion–neutral, 63, 226, 227 ion–neutral reaction, 22, 43, 70 thermal, 44
MP4SDTQ/6-311++G(2df,p), 243, 244 MP4SDTQ/6-311++G(3df,2p), 245 MP4SDTQ/6-311++G(3df,3pd), 246 RCCSD(T)/aug-cc-pVQZ, 251 Powell Cecil Frank, 32, 33 Power series, 277	Ramsauer–Townsend effect, 26 Random walk, 105 Rare gas ions in their parent gases, 206 Rate coefficient, 64, 70 ion–neutral, 63, 226, 227 ion–neutral reaction, 22, 43, 70 thermal, 44 molecular systems, 47
MP4SDTQ/6-311++G(2df,p), 243, 244 MP4SDTQ/6-311++G(3df,2p), 245 MP4SDTQ/6-311++G(3df,3pd), 246 RCCSD(T)/aug-cc-pVQZ, 251 Powell Cecil Frank, 32, 33 Power series, 277 divergence, 42	Ramsauer–Townsend effect, 26 Random walk, 105 Rare gas ions in their parent gases, 206 Rate coefficient, 64, 70 ion–neutral, 63, 226, 227 ion–neutral reaction, 22, 43, 70 thermal, 44 molecular systems, 47 second-order, 43, 131
MP4SDTQ/6-311++G(2df,p), 243, 244 MP4SDTQ/6-311++G(3df,2p), 245 MP4SDTQ/6-311++G(3df,3pd), 246 RCCSD(T)/aug-cc-pVQZ, 251 Powell Cecil Frank, 32, 33 Power series, 277 divergence, 42 Pressure	Ramsauer–Townsend effect, 26 Random walk, 105 Rare gas ions in their parent gases, 206 Rate coefficient, 64, 70 ion–neutral, 63, 226, 227 ion–neutral reaction, 22, 43, 70 thermal, 44 molecular systems, 47 second-order, 43, 131 RCCSD(T) method, 198, 199, 201
MP4SDTQ/6-311++G(2df,p), 243, 244 MP4SDTQ/6-311++G(3df,2p), 245 MP4SDTQ/6-311++G(3df,3pd), 246 RCCSD(T)/aug-cc-pVQZ, 251 Powell Cecil Frank, 32, 33 Power series, 277 divergence, 42 Pressure atmospheric, 3, 5, 27, 55, 69, 74, 83	Ramsauer–Townsend effect, 26 Random walk, 105 Rare gas ions in their parent gases, 206 Rate coefficient, 64, 70 ion–neutral, 63, 226, 227 ion–neutral reaction, 22, 43, 70 thermal, 44 molecular systems, 47 second-order, 43, 131 RCCSD(T) method, 198, 199, 201 Reaction coordinate, 187
MP4SDTQ/6-311++G(2df,p), 243, 244 MP4SDTQ/6-311++G(3df,2p), 245 MP4SDTQ/6-311++G(3df,3pd), 246 RCCSD(T)/aug-cc-pVQZ, 251 Powell Cecil Frank, 32, 33 Power series, 277 divergence, 42 Pressure atmospheric, 3, 5, 27, 55, 69, 74, 83 differential, 85	Ramsauer–Townsend effect, 26 Random walk, 105 Rare gas ions in their parent gases, 206 Rate coefficient, 64, 70 ion–neutral, 63, 226, 227 ion–neutral reaction, 22, 43, 70 thermal, 44 molecular systems, 47 second-order, 43, 131 RCCSD(T) method, 198, 199, 201 Reaction coordinate, 187 Reactions, 1, 30, 155
MP4SDTQ/6-311++G(2df,p), 243, 244 MP4SDTQ/6-311++G(3df,2p), 245 MP4SDTQ/6-311++G(3df,3pd), 246 RCCSD(T)/aug-cc-pVQZ, 251 Powell Cecil Frank, 32, 33 Power series, 277 divergence, 42 Pressure atmospheric, 3, 5, 27, 55, 69, 74, 83	Ramsauer–Townsend effect, 26 Random walk, 105 Rare gas ions in their parent gases, 206 Rate coefficient, 64, 70 ion–neutral, 63, 226, 227 ion–neutral reaction, 22, 43, 70 thermal, 44 molecular systems, 47 second-order, 43, 131 RCCSD(T) method, 198, 199, 201 Reaction coordinate, 187
MP4SDTQ/6-311++G(2df,p), 243, 244 MP4SDTQ/6-311++G(3df,2p), 245 MP4SDTQ/6-311++G(3df,3pd), 246 RCCSD(T)/aug-cc-pVQZ, 251 Powell Cecil Frank, 32, 33 Power series, 277 divergence, 42 Pressure atmospheric, 3, 5, 27, 55, 69, 74, 83 differential, 85 gas, 2, 4, 11, 18, 19, 25, 30, 52, 53, 58, 59, 83, 84, 86 Probability, 162	Ramsauer–Townsend effect, 26 Random walk, 105 Rare gas ions in their parent gases, 206 Rate coefficient, 64, 70 ion–neutral, 63, 226, 227 ion–neutral reaction, 22, 43, 70 thermal, 44 molecular systems, 47 second-order, 43, 131 RCCSD(T) method, 198, 199, 201 Reaction coordinate, 187 Reactions, 1, 30, 155 chemical, 18, 32, 34, 57, 120, 132, 164,
MP4SDTQ/6-311++G(2df,p), 243, 244 MP4SDTQ/6-311++G(3df,2p), 245 MP4SDTQ/6-311++G(3df,3pd), 246 RCCSD(T)/aug-cc-pVQZ, 251 Powell Cecil Frank, 32, 33 Power series, 277 divergence, 42 Pressure atmospheric, 3, 5, 27, 55, 69, 74, 83 differential, 85 gas, 2, 4, 11, 18, 19, 25, 30, 52, 53, 58, 59, 83, 84, 86 Probability, 162 Probability density, 172	Ramsauer–Townsend effect, 26 Random walk, 105 Rare gas ions in their parent gases, 206 Rate coefficient, 64, 70 ion–neutral, 63, 226, 227 ion–neutral reaction, 22, 43, 70 thermal, 44 molecular systems, 47 second-order, 43, 131 RCCSD(T) method, 198, 199, 201 Reaction coordinate, 187 Reactions, 1, 30, 155 chemical, 18, 32, 34, 57, 120, 132, 164, 240 clustering, 79 dissociation, 34
MP4SDTQ/6-311++G(2df,p), 243, 244 MP4SDTQ/6-311++G(3df,2p), 245 MP4SDTQ/6-311++G(3df,3pd), 246 RCCSD(T)/aug-cc-pVQZ, 251 Powell Cecil Frank, 32, 33 Power series, 277 divergence, 42 Pressure atmospheric, 3, 5, 27, 55, 69, 74, 83 differential, 85 gas, 2, 4, 11, 18, 19, 25, 30, 52, 53, 58, 59, 83, 84, 86 Probability, 162	Ramsauer–Townsend effect, 26 Random walk, 105 Rare gas ions in their parent gases, 206 Rate coefficient, 64, 70 ion–neutral, 63, 226, 227 ion–neutral reaction, 22, 43, 70 thermal, 44 molecular systems, 47 second-order, 43, 131 RCCSD(T) method, 198, 199, 201 Reaction coordinate, 187 Reactions, 1, 30, 155 chemical, 18, 32, 34, 57, 120, 132, 164, 240 clustering, 79

second order, 22, 63, 121	polar, 29, 99, 124, 234, 243
recombination, 18, 34	Scattering theory, 246
Reduced field strength, E/n_0 , 2, 19, 20, 23–	total angular momentum representation,
25, 34, 69	246
Reduced mass	Schrödinger
ion-neutral, 27, 28, 125, 147	Erwin, 157
ion–reactive neutral, 43	Schrödinger equation
Relativistic effects, 201	time-dependent, 157–159
Relativity, 34	time-independent (TISE), 159, 194
special theory of, 191, 192	Schuster
Resolution (see resolving power), 69	Franz Arthur Friedrich, 15
Resolving power, 69, 81, 82, 84–86	Schwinger
Resonant charge transfer (RCT), 200, 205,	Julian Seymour, 196
206	Self-consistent-field (SCF) method, 174,
Restricted active space self-consistent field	
(RASSCF) method, 184	183
	Semiconductor
Restricted coupled-cluster (RCC) method,	hot charge carriers, 2
198	Senftleben
Restricted Hartree–Fock (RHF) method,	Hermann, 234
180, 182–184	Senftleben–Beenakker effect, 234
Rigid circles, 236	electric field, 234
Rigid molecules, 186	Separation
Rigid rotor, 186, 238, 261	large enough to ignore ion-neutral inter-
Rigid spheres, 29, 78	actions, 119
Rigid wedges, 236	Sham
Ritz	Lu Jeu, 156
Walther, 282	Shutter, 53, 55, 56, 59, 61, 69, 84
Roentgen	Signal conditioner, 59
Wilhelm Konrad, 14	Signal-to-noise ratio, 71, 211
Rotation, 186	Singlet state, 173
excited states, 186	Singularity, 277
Runaway	Site-site model, see Interaction potential,
partial ion, 244	site-site
Rutherford	Size-to-charge ratio, 76
Ernst, 14–18	Skewness, 46, 98, 114, 212, 214, 221
	parameter, 214
	tensor of order three, 65
S	Slater
Saddle point	John Clarke, 162
on a PES, 187	Slater determinants, 173, 174, 177–181, 202
higher-order, 187	excited states, 177, 178, 181, 182
Salpeter	excited states from Doubles, 178, 243
Edwin Ernest, 199	excited states from Quadruples, 178, 243
Scalar, 277	excited states from Singles, 178, 243
Scalar (dot) product, 277	excited states from Triples, 178, 243
Scalar potential	Slater orbitals, 162–165, 173, 174, 178, 181,
definition for electromagnetism, 191	196
	Smooth spheres, 79
for electromagnetism, 190	
Scanning function, 82, 86	Sonine polynomial, 133
Scattering in 26	Space-charge effects, 1, 2, 55, 69, 120
isotropic, 36	Spatial gradients, 132
Scattering angle, 140, 235, 245, 263	Spectroscopic parameters, 207
azimuthal, 99, 124, 234	Spectroscopy, 45

foreign-gas perturber, 2	multi-temperature theory, 140
Speed	three-temperature theory, 138
average, 95, 104	two-temperature theory, 135, 242
drift, 96	gas, 2, 19, 42, 52, 57, 59, 98, 101, 121,
ion, 104, 105	127–129, 134, 137, 146, 243, 244, 246
average after collision, 105	above 400 K, 74
average before collision, 105	internal for molecular ions, 241
ion drift, 70	ion, 85, 98, 101, 127, 128, 134
relative, 97, 100, 130	internal, 47
root mean squared, 95	muti-directional, 139
thermal, 71, 105	parallel to the field, 44, 45, 137, 211,
effective, 102	214
Speed distribution function	perpendicular to the field, 44, 45, 137,
ion, 17	211, 214
Spherical harmonics, 134, 278	kinetic for molecular ions, 241, 244
Spin contamination, 183	
Spin operator, 170	molecular ions, 47
Spin-orbitals, 177	room, 57
Spin-orbit effects, 199	rotational for molecular ions, 244
Spin-orbit interactions, 201	tensor, 132
•	Temperature tensor
Spline fit, 278	laboratory frame, 123
clamped, 200 Standard representation of relativity, 103	reference frame of ion swarm, 123
Standard representation of relativity, 193	Tensor, 39
State functions, configurational, 181	irreducible algebra of, 136
Stationary point	of rank 0, 278
on a PES, 187, 188	of rank 1, 278
Stationary point on a PES, 187	of rank 2, 278
Statistical mechanics	of rank 3, 279
equilibirum, 122	unit, 279
Steady-state behavior, 96	Theoretical calculations
Stern	
Otto, 170	ab initio, 155
Stoney	philosophy, 155
George Johnstone, 10	approximate solutions of exact theo-
Structure factor	ries, 155
low-field, 76	exact solutions of approximate theo-
molecules, 77, 79	ries, 155
trend line, 77	Thermodynamics
Strutt	nonequilibrium, 40
John William (Lord Rayleigh), 282	Thomson
Swab test, 74	Joseph John, 14–16, 30
Swarm, 1, 2, 15, 21, 27, 37, 43, 47, 52, 117,	TIDE, 193–195, 197
122, 127, 128, 136	Time-correlation functions, 152
definition, 1	Time reversal, 237
experiments, 152	Time window, 54
experiments, 192	Tip equation, 235
	TISE, 159–161, 165, 167–169, 171–173,
T	175–178, 180, 185, 194, 195, 197,
Taylor series expansion, 278	199, 278, 279
Temperature	conditions upon solution, 162
effective, 35, 43, 85, 256	discrete solutions, 161
correction factor, 35, 43	for H atom, 169
ion–reactive neutral, 43	relationship to Periodic Table, 169

solution by method of weighted residu-	Unsöld's theorem, 167, 279
als, 162	Upper bound, 169
with electron spin, 169	Urey
Tizard	Harold Clayton, 32
Henry Thomas, 18	•
TM, see classical trajectory	
Tomonaga	V
Sin-Itiro, 196	Vacuum, 3
Torricelli	high, 219
Evangelista, 3	Valence orbitals, 179
Townsend	
John Sealy Edward, 16, 25, 26	Van de Graaff
Townsend (unit), 19	Robert Jemison, 32
	Variation method, 168, 175–177, 181, 184
Transient effects, 81, 83, 84, 96, 105	Variation principle, 174
Transition states, 183	Varley
Transition structure, 187	Cromwell Fleetwood, 11
Translation, 124	Vector, 279
treatment by classical mechanics, 34	Vector calculus, 279
Transport coefficients, 45, 46, 63–66, 138,	Vector potential
141, 152, 155, 156, 202, 205–208,	definition for electromagnetism, 189-
212, 216, 221, 223, 227, 230, 240,	191
243–246, 250, 251, 257, 259, 264	Velocity
ab initio calculations, 65, 72, 96, 155	cathode rays, 14
bulk, 120	center-of-mass, 97, 98
definition, 26	correlation coefficients, 216
flux, 120	dimensionless
for atomic ions in diatomic gases, 242	one-temperature, 133
for diatomic ions in atomic gases, 244	two-temperature, 134
for molecular systems, 245, 264	displacement, 221
neutral gases, 246	gas, 129
Transport properties	ion, 21, 88, 95, 97, 98
ab initio calculations, 59, 60, 62, 65	neutral, 97, 119
electron, 25	relative, 97, 119
ion, 25	post-collision, 99
molecular systems, 46	pre-collision, 99
relativistic effects, 34	three- and multi-temperature, 140
Trial function, 168, 173	Velocity distribution function (vdf)
Triplet state, 173	correlation coefficients, 45
Tritium, 32	displacement along the field, 44
Turning point, 29	electron, 36, 39
Tyndall	ion, 43, 100, 121, 127, 128, 133, 141,
Arthur Mannering, 18, 27, 32, 33, 75	211, 214, 220, 234, 240, 263
	Gram-Charlier, 220, 221
TI	Maxwellian, 221
U Historia ada	molecular, 233
Uhlenbeck	multi-temperature, 139, 142
George Eugene, 170	one-temperature, 221
Uncertainty principle, 158, 170, 186, 194	three-temperature, 137, 221
Unpaired electrons, 171	two-temperature, 221
Unrestricted Hartree–Fock (UHF) method,	zero-order, 133, 134, 241
183	kurtosis coefficients, 45
Unsöld	Maxwell–Boltzmann, 51, 100, 129, 239,
Albrecht Otto Johannes, 174	241

Maxwellian, 28, 51, 121, 129, 133, 219,	for multi-electron atom, 173
220	Hartree–Fock, 185
neutral, 121, 129	in molecular hydrogen, 172
normalization, 219	multi-determinant, 177
relative ion-neutral, 221	multi-dimensional, 174
skewness coefficient, 45	single-determinant, 176
tail, 44	time-dependent, 159
visualization, 222, 223	time-independent, 168
Vibration, 186	Wave length, 169
energy, 186	Wave number, 204
excited states, 186	Weighted residuals, 131, 132, 220, 230, 240,
quantum number, 186	245
Vibrational frequency	equivalent to a moment method, 133
from RHF calculation, 183	Well depth, 73
Virtual orbital, 177, 178, 180	Wiechert
Volta	Emil Johann, 15
Alessandro Giuseppe Antonio Anasta-	Wien
sio, 7–9	Wilhelm, 13
Voltaic pile (battery), 8, 9	WUB equation, 46, 236
Volume of gas, 2	solution methods
	two-temperature, 46
W	
Waldmann	X
Ludwig, 235	X-rays, 14, 15, 31
Waldmann-Snider equation, 46, 235, 236	A-lays, 14, 13, 31
Wannier	
Gregory Hugh, 34, 35, 38, 39, 45	
Wannier equation, 34, 136, 137, 152, 226,	Y
256	$^{1}_{174}\text{Yb}^{+}(^{2}\text{S}_{1/2}), 210$
Water vapor, 74	
Watson	
William, 6	${f Z}$
Wave function, 156, 157, 169, 172	Zeleny
antisymmetric, 172	John, 17
CISD, 178	Zeta values
for hydrogen molecule, 173, 182	in basis sets, 164, 165, 168, 178